Lawrence Berkeley National Laboratory

Lawrence Berkeley National Laboratory

Title

1ST. WORKSHOP ON ULTRA-RELATIVISTIC NUCLEAR COLLISIONS. MAY 21-24, 1979

Permalink

https://escholarship.org/uc/item/59z0z6p3

Author

Wenzel, W.

Publication Date

1979-05-01

Peer reviewed

eScholarship.org Powered by the California Digital Library
University of California

12
3/26/80

DR. 954

LBL-8957
UC-34C
CONF-7905107

MASTER

1st Workshop on Ultra-Relativistic Nuclear Collisions

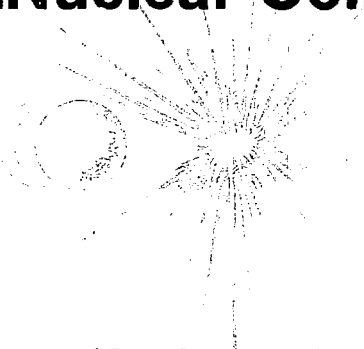

May 21-24, 1979

Lawrence Berkeley Laboratory
University of California

LBL-8957

Prepared for the U.S. Department of Energy under Contract W-7405-ENG-48

1st Workshop on Ultra-Relativistic Nuclear Collisions

May 21-24, 1979

SPONSORED BY

Lawrence Berkeley Laboratory
and
Gesellschaft für Schwerionenforschung

DISCLAIMER

This book was prepared as an account of work sponsored by an agency of the United States Government. Neither the United States Government nor any agency thereof, nor any of their employees, makes any warranty, express or implied, or assumes any legal liability or responsibility for the accuracy, completeness, or usefulness of any information, apparatus, product, or process disclosed, or represents that its use would not infringe privately owned rights. Reference herein to any specific commercial product, process, or service by trade name, trademark, manufacturer, or otherwise, does not necessarily constitute or imply its endorsement, recommendation, or favoring by the United States Government or any agency thereof. The views and opinions of authors expressed herein do not necessarily state or reflect those of the United States Government or any agency thereof.

FIRST WORKSHOP ON

ULTRA-RELATIVISTIC NUCLEAR COLLISIONS

CONTENTS

FOREWORD

The Workshop was held to explore the range of physical phenomena and processes that can be studied using beams of relativistic nuclei at energies > 10 GeV/nucleon, in both fixed target and colliding beam experiments. To do this, we brought together a group of scientists from around the world, whose interests spanned the spectrum of particle, nuclear and astro-physics, to discuss these problems. Neceasarily, a large part of the Workshop was devoted to reviewing what is presently known about high energy nucleon-nucleon and nucleon-nucleus collisions, before we could discuss the more complex nucleus-nucleus case.

The organizing committee, which planned this meeting, included Alan Axelrod, Rudolph Bock, Hans Gutbrod, Miklos Gyulassy (co-chairman), and Arthur M. Poskanzer. The Workshop would not have been possible without the hard work put in by Eileen Eiland, Maureen Jeung, and Peggy Little. Our many thanks go to them. Also, Cathy Webb has done an excellent job in editing these Proceedings.

Please note that only the invited talks are reproduced here. Although Dr. Gulamov was unable to attend, we are pleased that he was able to send his manuscript.

Lee S. Schroeder
Co-chairman of the
Organizing Committee

PROGRAM

First Workshop on Ultra-Relativistic Nuclear Collisions
21-24 May 1979

MONDAY, 21 May

Morning Session: Chairman, W. Wenzel (LBL)

1) T.Ferbel (Univ. of Rochester): "Coherent Processes and Multi-Particle Production in Hadron-Nucleus Collisions at High Energies"
2. A.Bialas (FNAL/Krakow): "Space-Time Structure of Hadronic Interactions via Hadron-Nucleus and Nucleus-Nucleus Collisions"

Afternoon Session: Chairman, C. Noack (LBL/Bremen)

1) M.Faessler (CERN/Heidelberg): "Inelastic Hadron-Nucleus Interactions at 30 and 37 GeV/c"
2) G.Yodh (NSF): "Cosmic Ray Data on High Energy Hadron-Nucleus and Nucleus-Nucleus Collisions"

TUESDAY, 22 May

Morning Session: Chairman, B. Povh (Heidelberg)

1) H.Frisch (Univ. of Chicago): "The Production of Systems with Large Mass or Large Momentum Transfer in Hadron-Nucleus Collisions"
2) D.Schramm (Univ. of Chicago): "Astrophysics Perspectives on High Energy Nucleus-Nucleus Collisions"

Afternoon Session: Chairman, J. Vary (Iowa State University)

1) K.G.Gulamov (Tashkent): "Critical Analysis of Models of Hadron-Nucleus Collisions"

Afternoon Short Talks:

1) S. Fredriksson (CERN): "Coherent Tube Model"
2) P. G. Rancoita (CERN/INFN): "Multiplicities in πA"
3) S. A. Chin (MIT): "Hyper-Strange Quark Droplets"
4) G. Yodh (NSF): "More Unusual Cosmic Ray Events"
5) Y. Karant (LBL): "Observables in A-A Collisions"

WEDNESDAY, 23 May

Morning Session: Chairman, H. Pugh (NSF)

1) H.Feshbach (MIT): "Nuclear Physics Perspectives on High-Energy Nuclear Collisions"
2) M.Albrow (CERN): "ISR Data"

Afternoon Session: Chairman, M. Gyulassy (LBL)

1) D.Gross (Princeton): "Vacuum Structure and QCD"

Afternoon Short Talks:

1) G. Zu Putlitz (GSI): "GSI Proposal"
2) H. Grunder (LBL): "VENUS Proposal"
3) J. Vary (Iowa State Univ.): "Coherent Production"
4) R. M. Weiner (Univ. of Marburg): "Mass Spectrum vs. Quark Phase"

THURSDAY, 24 May

Morning Session: Chairman, R. Stock (GSI)

1) W.Greiner (Univ. of Frankfurt): "Overview of Nuclear Collisions"
2) S.Brodsky (SLAC): "Parton Models, Hard Scattering and QCD"

PARTICIPANTS LIST

First Workshop on Ultra-Relativistic Nuclear Collisions
21-24 May 1979

Name	*Affiliation*
Albrow, Michael G.	Rutherford Laboratory/CERN
Aleklett, Kjell	LBL
Alonso, Carol T.	LLL
Axelrod, Alan	LBL
Baumgardt, Hans-Georg	University of Frankfurt
Bialas, A.	Fermilab
Bishop, Raymond F.	LBL
Bock, Rudolf	GSI
Bodmer, Arnold R.	Argonne National Laboratory
Brodsky, S.	SLAC
Carroll, Jim B.	LBL
Cerny, Joe	LBL
Chessin, Stephen A.	LBL
Chin, Siu A.	Massachusetts Inst. of Tech.
Das Gupta, Subal	McGill University
Faessler, Martin	CERN
Ferbel, T.	University of Rochester
Feshbach, Herman	Massachusetts Inst. of Tech.
Frankel, Kenneth A.	LBL
Fredriksson, Sverker	CERN
Friedlander, Erwin M.	LBL
Frisch, H. J.	University of Chicago
Gaga, Jorge V.	LBL
Greiner, Douglas E.	LBL
Greiner, Walter	University of Frankfurt
Gross, David	Princeton University
Grunder, Hermann A.	LBL
Gutbrod, Hans H.	LBL/GSI
Gyulassy, Miklos	LBL
Harris, John W.	LBL
Heckman, Harry H.	LBL
Hendrie, David L.	University of Maryland
Hernandez, Susana	LBL
Hofmann, Jurgen	University of Frankfurt
Huggett, R. W.	Louisiana State University
Huie, Arthur	U. C. Riverside
Hyde, Earl K.	LBL
Islam, M. M.	University of Connecticut

Name	*Affiliation*
Kapusta, Joseph I.	LBL
Karant, Yasha J.	LBL
Kauffmann, S. K.	LBL
Koike, Masahiro	LBL
Lee, Phyllis	University of Washington
Lindstrom, Peter	LBL
Lofgren, Edward J.	LBL
Loveland, Walter	Oregon State University
Lu, Jia-Jih	U. C. Riverside
Madansky, Leon	Johns Hopkins
Mahoney, Jeannette	LBL
Maier, Michael R.	GSI
Mallet-Lemaire, Marie-Claude	LBL
Mantzouranis, George	LBL
Maruhn, Joachim A.	University of Frankfurt
Mathews, Grant J.	LBL
Morrissey, David	LBL
Myers, William D.	LBL
Nagamiya, Shoji	LBL
Nagatani, K.	Texas A& M University
Nakai, Kozi	University of Tokyo
Noack, Cornelius	LBL/University of Bremen
Perez-Mendez, Victor	LBL
Poskanzer, Arthur M.	LBL
Povh, Bogdan	Max-Planck
Pugh, Howel G.	NSF
Rancoita, P. G.	CERN/INFN
Randrup, Jorgen	LBL
Redlich, Martin G.	LBL
Remaud, Bernard	LBL/University of Nantes
Remsberg, L. P.	Brookhaven National Laboratory
Ritter, Hans Georg	LBL/Marburg
Sandoval, Andres	LBL/Marburg
Sann, Hans	GSI
Sano, Mitsuo	Osaka University
Scharenberg, R. P.	Purdue University
Schimmerling, Walter	LBL
Schnetzer, Steve	LBL
Schramm, David N.	University of Chicago
Schroeder, Lee S.	LBL
Scott, David K.	LBL
Selph, Frank	LBL
Shida, Y.	University of Tokyo
Siemens, Philip J.	LBL
Steiner, Herbert	LBL

Name	*Affiliation*
Stelzer, Herbert	LBL/GSI
Stock, Reinhard	GSI
Stöcker, Horst	University of Frankfurt
Stokstad, Robert G.	Oak Ridge National Laboratory
Swiatecki, W. J.	LBL
Symons, James	LBL
Tanihata, Isao	LBL
Treuhaft, Robert	LBL
Van Bibber, Karl	LBL
Vary, James P.	Iowa State University
Weber, Christine	LBL
Webb, Catherine	LBL
Weiner, Richard M.	University of Marburg
Westfall, Gary D.	LBL
Wilson, Lance W.	LBL
Wohn, Fred K.	Iowa State University
Wolf, Kevin L.	Argonne National Laboratory
Yodh, Gaurang	NSF
Zisman, Michael S.	LBL
Zu Putlitz, G.	GSI

Coherent Processes and Multiparticle Production in Hadron-Nucleus Collisions at High Energies*

T. Ferbel

University of Rochester

Rochester, N.Y. 14627

We review basic phenomenology and currently available data on inclusive particle production and coherent inelastic processes on nuclear targets at energies of several hundred GeV.

*Research supported by the U. S. Department of Energy under contract No. EY-76-C-02-3065.

The use of nuclear targets in particle physics is generally regarded with a certain degree of suspicion. This is, of course, mainly due to the prejudices of our theoretical colleagues. Many hadronic production processes can be studied as effectively, and as unambiguously, using nuclei as with hydrogen targets. In addition, nuclei provide a number of unique physics opportunities that are not easily attainable in the case of "elementary" hydrogen. From nuclear targets we can learn, for example, about properties of hadrons at the time of their production, and examine the space-time development of hadronic processes; we can also use the nuclear Coulomb field to probe hadron-photon incident channels, and thereby measure radiative decay widths of unstable elementary particles.

Inelastic hadron-nucleus collisions can be divided into two broad categories. Namely, into coherent processes in which the nucleus remains intact (these are collisions that involve very little momentum transfer between the hadron and the nucleus); and into incoherent processes, which involve sizeable momentum transfers, in which both the hadron and nucleus break apart. In either case, subsequent to the initial collision, newly created hadronic matter propagates through the rest of the nucleus which then serves to sample the properties of the nascent hadronic system. In this lecture I will review the nomenclature, the data on high-energy collisions between hadrons and nuclei, and summarize what has been learned from such investigations.[1]

Coherent Reactions

From studies of electron-nucleus and hadron-nucleus elastic scattering it has been learned that nuclear radii can be expressed

approximately as $R \approx 1.1A^{1/3}$ Fm, where A is the nucleon number of the nucleus. Consequently, if an inelastic reaction is to take place in which the nucleus remains intact (in its ground state or in some low-lying excited state), the momentum transferred to the nucleus must be small. In fact, using the uncertainty principle, we expect momentum transfers (q) to be restricted to values corresponding to dimensions of $\gtrsim R$, namely, $q \lesssim \frac{\hbar c}{1.1A^{1/3}} \cong \frac{0.2}{A^{1/3}}$ GeV/c. If we assume that the distribution of nuclear matter can be represented by an absorbing disk of radius R, the diffraction pattern for coherent (non-flip) scattering from such a nucleus would be characterized by a shape of the form:[2] $\frac{d\sigma}{dq^2} \approx e^{-\frac{R^2}{4}\left(\frac{q}{\hbar c}\right)^2} \approx e^{-8A^{2/3}q^2}$. From this expression we see again that, for a reaction to proceed coherently, we must keep $q \lesssim \frac{0.3}{A^{1/3}}$ GeV/c, which is consistent with the previous restriction obtained for q.

Whereas the minimum value of the momentum transfer (q_o) for elastic scattering can be zero, this is not the case for inelastic production. To calculate q_o let us consider the coherent reaction

$$\pi + A \rightarrow \pi^* + A' \qquad (1)$$

where π^* is some excited hadronic state of rest mass M. The minimum value of q occurs, clearly, for production at 0°. Because the process is coherent, we expect the value of q_o to be small. Consequently, imposing energy conservation, we can ignore the kinetic energy of the recoiling nucleus and assume that the energy of the incident π will equal the energy of the π^*. In terms of the collinear momenta of the π and π^* in the laboratory frame we can write;

$$E_\pi = \sqrt{p^2 + m^2} = \sqrt{p^{*2} + M^2} = E_{\pi^*}$$

For production at 0°, the momentum transfer (p-p*) is just the minimum value of the momentum that must be imparted to the nucleus in the production of any π*. (For angles other than 0°, q has a contribution from a transverse as well as from this longitudinal component (q_o) to the momentum transfer.) Solving for $q_o = p - p^*$ at 0°, we obtain $q_o \approx \frac{M^2 - m^2}{2p}$. Here we have set $p \approx p^*$, assuming that $M \ll p^*$; this condition holds exceedingly well at high energies. In terms of the square of the four-momentum transfer (t), the minimum value of t is just q_o^2:

$$t_o \approx \left(\frac{M^2 - m^2}{2p}\right)^2$$

Consequently, we see that the higher the incident energy, the smaller becomes the value of t_o for producing a particular object of mass M, and the smaller, therefore, is the damping effect of the nuclear form factor on the process in question. In fact, if we require q_o to be far smaller than typical values of q that characterize coherent production, we can obtain the following restriction on the incident momentum:

$$p \gg 2(M^2 - m^2)A^{1/3}$$

Consequently, to produce a massive excited state of M ≃ 3 GeV on a lead nucleus requires incident momenta in excess of ∿100 GeV/c.

Before turning to the data, let us first discuss in somewhat more detail the kind of mechanisms that mediate coherent production. At high energies, the coherent conversion of an incident hadron into another hadron, or into a system of hadrons, is mediated either through the well understood process of Coulomb excitation or through the

not-so-well understood process of diffractive excitation.

Coulomb Excitation

Production in the Coulomb field of a nucleus of charge Z, (the reaction a + Z → b + Z) is calculable through a generalization of the Primakoff formula,[3] which in the high-energy limit yields (see Fig. 1):

$$\frac{d\sigma}{dm_b^2 dt} = \frac{\alpha Z^2}{\pi\eta} \frac{\sigma_\gamma(m_b^2)}{m_b^2 - m_a^2} \frac{t - t_o}{t^2} |F_{em}(t)|^2$$

where α is the fine-structure constant; η equals 1/2 if the incident particle is a photon, otherwise $\eta = 1$; m_a and m_b are the masses of the incident and the produced objects; $\sigma_\gamma(m_b^2)$ is the total cross section for the reaction $a + \gamma \to b$, at a γ-a center of mass energy $E_{cm} = m_b$; $F_{em}(t)$ is the electromagnetic form factor of the nucleus. When the final-state system b is a single particle of spin J_b, and of radiative width $\Gamma_\gamma(b \to a + \gamma)$, the expression for the cross section becomes:

$$\frac{d\sigma}{dt} = \frac{8\pi\alpha Z^2}{\eta} \frac{(2J_b + 1)}{(2J_a + 1)} \left(\frac{m_b}{m_b^2 - m_a^2}\right)^3 \Gamma_\gamma(b \to a + \gamma) \frac{t - t_o}{t^2} |F_{em}(t)|^2$$

Finally, if particle b is unstable, the above expression should be folded in with a Breit-Wigner term (normalized to unity), and Γ_γ replaced by a mass-dependent partial width that depends on the orbital waves present in the final-state decay products of particle b.

From the above formulae we see that electromagnetic production occurs largely at impact parameters corresponding to momentum transfers of several times q_o, namely, distances $\approx \frac{\hbar c}{2q_o} \approx \frac{0.2p}{M^2 - m^2}$. Thus, for an incident-pion

momentum of 200 GeV/c, and a produced mass of M ∿ 1 GeV, the impact parameter is typically ∿40 Fm. Because of this fact, inelastic production in the nuclear Coulomb field tends to be rather insensitive to the shape parameters that are used to describe the form factor.

Finally, because t_o decreases with increasing energy, the integrated cross section for Coulomb-excitation at fixed m_b increases with energy. This increase is quite rapid in the energy range in which q_o is comparable to values of q that are typical of nuclear radii ($q \sim \frac{0.2}{A^{1/3}}$); at sufficiently high energies the increase becomes logarithmic in incident laboratory momentum. Figure 1 displays the rough energy dependence of $\frac{d\sigma}{dt}$ expected for fixed m_b. Because cross sections for "exclusive" hadronic reactions (that is, for definite fully specified channels) do not increase with increasing energies, it is safe to speculate that, eventually, Coulomb excitation will dominate all coherent processes at small values of t.[4]

Diffractive Excitation

A number of years ago Good and Walker suggested that scattering of hadrons on nuclei might generate new coherently-produced states of hadronic matter.[5] To buttress their arguments, they provided the following analogy with scattering of polarized light. When light polarized along the $\hat{y}$ axis is passed through a polaroid rotated by 45° relative to $\hat{y}$, the transmitted wave (now polarized at 45°) contains, in effect, a $\hat{y}$ polarization as well as a generated polarization along $\hat{x}$. Good and Walker then argued that, just as the selective filtering of light can generate states orthogonal to the incident wave, so can the selective filtering in nuclei of the various

virtual states of a hadron cause a minor rearrangement of the incident wave to one that is closely related but orthogonal to the incident state. Although processes of this kind were observed and studied at low energies during the 1960's and are presently being investigated in the several-hundred GeV regime, there is at present still no fundamental theory for the diffractive excitation of hadrons. Optical models have been utilized to parameterize the features of coherent excitation, which are, in fact, very much akin to those for scattering of light from an absorbing disk.

Features of processes such as Reaction (1) can be summarized as follows: (1) There is very little energy dependence to the production cross section. (2) The observed angular distributions are peaked steeply at small angles, and have shapes that are characteristic of nuclear dimensions. (3) The internal structure of coherently produced hadronic states does not appear to differ in any essential way from the internal structure of the incident object; by this I mean that the isotopic spin (I) of the produced system is the same as that of the incident hadron (unlike the case of Coulomb excitation where both I=0 and I=1 exchanges are possible), as is the strangeness, G-parity, baryon number, etc. In fact, even the masses of the diffractively produced systems tend to peak at low values, close to the mass of the incident hadron. The only apparent change that occurs in the transition is an orbital excitation of the incident hadron, that is, only momentum is exchanged between hadron and nucleus. Thus for incident pseudoscalar mesons (spin-parity $J^P=0^-$), the excited states can have $J^P = 0^-, 1^+, 2^-$ etc. Such production processes are thought to be dominated by the exchange of vacuum quantum numbers, i.e., by the Pomeranchukon.[6]

In the context of an optical model, the cross section for processes

such as Reaction (1) can be written schematically as:

$$\frac{d\sigma}{dt} = |f_H(t) AF(t)|^2$$

where $f_H(t)$ is the amplitude for the reaction on a hydrogen target, and F(t) is the nuclear form factor convoluted with the absorption of the incident and outgoing system in nuclear matter. It has been customary in the past to parameterize the form factor using an eikonal approximation, and from the A-dependence of $\frac{d\sigma}{dt}$ to extract parameters of the optical model and interpret these in terms of physical cross sections for scattering of the unstable π^* systems on nucleons.[7] Although this program has met with a degree of success (particularly for photon induced reactions), the interpretation of the extracted cross sections is somewhat controversial. The difficulty stems from the classical treatment of the propagation of hadrons in nuclear material. That is, if time scales and distances involved in the production process are very large, then it may not be meaningful to separate initial production from the subsequent rescattering of the hadronic system within the nucleus. In fact, in the context of a Good-Walker model, it has been argued that independent of the detailed nature of the diffractively produced states, their attenuation properties should be essentially indistinguishable from those of the incident hadron.[8]

The closest thing that we have to a theory of diffractive excitation of hadrons is based on Drell-Hiida-Deck processes of the kind illustrated in Fig. 2. Models of this type have been utilized with some degree of success to interpret various aspects of the data.[9] The essential features of the model provide, through the propagators:

and through the "elastic" scattering of the virtual exchanged objects, steep t distributions and the kind of decay characteristics that are similar to those observed in the data. The predicted normalizations tend to be too high. It is felt, however, that additional absorption corrections might help bring agreement between theory and data.

Data on Coherent Production

To illustrate the experimental features of coherent production I will rely on data from the Rochester-Northwestern-Fermilab-SLAC Collaboration which has investigated neutron dissociation between 50 GeV/c and 300 GeV/c in the reaction:[10]

$$n + A \rightarrow (p\pi^-) + A \qquad (2)$$

the $(p\pi^-)$ system will, for convenience, be referred to as N^*. In addition, I will use the more recent results on meson dissociation from the Rochester-Minnesota-Fermilab Group.[11]

Figure 3 provides a dramatic illustration of the emergence of the importance of the Coulomb contribution to coherent production at high energies. (The data are shown in terms of the variable $t' = t - t_o$.) The $\Delta(1236)$ has a large radiative width, as a consequence of which the electromagnetic process dominates Reaction (2) at small t, even on a low-Z target such as Carbon.

The cross section for $\gamma n \rightarrow p\pi^-$ has been measured previously and the rise observed in $\frac{d\sigma}{dt}$ near t=0 in Fig. 3 is consistent with expectations from the Primakoff formula. (The rise does not correspond exactly to the $\frac{t'}{t^2}$ term because of experimental resolution.) The "background", which has the form exp(-75t), is substantially steeper than what might

have been expected for the angular distribution for diffractive production on a carbon nucleus. This increased steepness can be accommodated, however, in an optical model because the absorption of the inelastically produced hadron states at small impact parameters will result in an effective distribution for nuclear matter that will be ring-like in character. For a fixed nuclear radius, a ring provides a distribution that is far steeper than that from an absorbing disk of same size.[2]

Figure 4 shows typical fits to data of Reaction (2) that have been used to extract N*-nucleon total cross sections (σ_{N^*N}). The typical values of σ_{N^*N} are equal to or smaller than the known total N-N cross section of ∿40 mb. The sensitivity of the data to this parameter of the optical model (σ_{N^*N}) is indicated in the graph, as are the contributions from electromagnetic production. (Experimental resolution has also been folded into the calculations.) The measured coherent production cross section for fixed $M_{4\pi}$ rises somewhat with increasing energy, as expected from contributions due to the Primakoff formula.[10]

Figure 5 presents results of a measurement of the dissociation of π^- mesons into $\pi^-\pi^0$ systems. Because $\pi^-\pi^0$ systems can only be in $J^P = 1^-, 3^-, 5^-, \ldots$ states, they cannot be produced through the exchange of quantum numbers of the vacuum. Two-pion states can be produced, however, through photon exchange or through the exchange of mesons such as the $I=0, J^P=1^-$ ω^0. At 150 GeV/c the contribution from ω^0 exchange is expected to be small, and, because of the helicity-flip nature of the process, must vanish linearly with t at 0°. Strictly speaking, the Coulomb contribution also vanishes at 0° (except for a small "longitudinal" term, ignored in the Primakoff formula), but the peak of the cross section is at $t = 2t_0$, which for ρ^- production is at ∿10 μrad!

Using the Primakoff formula, and the data in Fig. 5, cross sections for the reaction $\gamma\pi^- \to \pi^-\pi^o$ can be obtained as a function of $\pi^-\pi^o$ mass. Alternately, radiative widths can be extracted for unstable resonances in the $\pi^-\pi^o$ system (e.g., ρ^-). The Rochester-Minnesota-Fermilab Collaboration has embarked on a series of experiments to measure radiative widths of vector and tensor mesons. Such measurements provide excellent tests of symmetry schemes and of quark models of elementary particles.[12] Table I provides the latest results from this series of experiments.

Although according to the prevailing orthodoxy pseudoscalar mesons cannot diffractively dissociate into two pseudoscalar particles, they can dissociate into three. A reaction of this kind that was studied at lower energies is:

$$\pi^- + A \to (\pi^-\pi^+\pi^-) + A'$$

The three-pion mass distribution for small values of t, at 150 GeV/c incident momentum, is shown in Fig.6.[11] The usual A_1 ($\pi^-\rho^o$ low-mass enhancement) at $\sim$1100 MeV, the analog of the $\sim$1300 MeV peak in the $p\pi^-$ system for Reaction (2), is observed in the data. There is, possibly, in addition, some structure near the $A_2(1310)$ resonance. Distributions in t for the low-mass region are shown for several target nuclei in Fig. 7. The rise in the cross section for $t \lesssim 0.0005$ GeV^2 is due to Coulomb production. This is the first experiment in which direct evidence has been found for the process $\gamma\pi^- \to \pi^-\pi^+\pi^-$. About half of the Coulomb signal is due to the A_2, but there is also a definite additional signal for the A_1 (the broad low-mass peak). Although this corresponds to first evidence of a finite $A_1\pi\gamma$ coupling, the data do not necessarily imply that the A_1 is therefore a resonance. This is because

non-resonant π-γ scattering could ostensibly provide such a signal (see the distinguishing graphs in Fig. 8). A spin-parity decomposition of the 3π system, through an Ascoli-type of analysis,[13] is underway to extract phase shifts as a function of mass at small t; this will hopefully provide information on the detailed nature of the signal.

The exponentials drawn in Fig. 7 are just to guide the eye. Again, for inelastic production, the slopes in t are larger than expected from the naive $\exp(-BA^{2/3}t)$ behavior. These slopes are smaller for dissociation for incident pions than for incident neutrons. For the Cu target, for example, the slope in Fig. 4 for neutron data is about 25% steeper than for the data in Fig. 7. This difference in slopes presumably reflects the fact that, at high energy, nuclei are not opaque to hadrons. Total π-Cu and n-Cu cross sections differ by similar factors.[14]

The last point I wish to discuss regarding coherent production is the attempt to understand the dynamics in the context of a Drell-Hiida-Deck (DHD) formalism. As with all things in strong interactions, the degree of success has been of a mixed nature. Osland, in trying to understand the transparency of nuclear matter (e.g., small values of σ_{N^*N}) from the viewpoint of DHD, has come to the conclusion that the model cannot provide the experimentally required transparency and consequently cannot be a major factor in coherent production.[15]

The most recent conclusions from the Rochester-Northwestern-Fermilab-SLAC experiment,[10] although in essential agreement with Osland that the DHD model has serious flaws, are that the model works surprisingly well for nuclear data. In fact, it appears that the model describes the nuclear data about as well as it described diffractive dissociation on a hydrogen target. Figure 9 displays the decay

polar-angle distributions of protons in the N* rest frame (quantization axis being given by the direction of the incident beam in the N* frame, i.e., θ is the polar angle in the Gottfried-Jackson frame). As might be expected, the decay spectra depend on the masses of the $(p\pi^-)$ systems. Higher masses correspond to larger internal momenta and consequently can provide systems having larger angular momenta. As I indicated previously, although the predictions of the unabsorbed model (Fig. 2, replacing incident proton p by nucleus A) yield far too high normalizations, the predicted shapes are in reasonable agreement with the data.

Figure 10 displays the dependence of t-distributions on the decay angles of the N*. A correlation between t and θ might certainly have been expected because, even for a fixed N* mass, different regions of θ correspond to differing contributions from the angular momentum states of the $p\pi^-$ systems, and therefore to differing amounts of helicity-flip contributions to the production amplitude. What is surprising is the unusually dramatic dependence of $d\sigma/dt$ on θ and especially the fact that the DHD model bears some semblance to reality. (I should point out that the Coulomb contribution in Fig. 10, as shown in Fig. 4, is restricted mainly to $t \lesssim 0.002$ GeV^2. Hence, the comparison of DHD with data should exclude that region of t.)

Inclusive Processes

Even more so than in the case of hydrogen, the variety of incoherent reactions on nuclear targets at high energy surely forms an innumerable set! It is therefore not surprising that the character of specific reaction channels is generally not regarded with great interest, but that rather the inclusive approach has been adopted in trying to ascertain

the nature of hadron production on nuclear targets. One crucial issue in this field pertains to the space-time development of hadronic processes. Measurements of inclusive hadron-nuclear collisions have been used to extract information on the constituent structure of hadrons, on cumulative or pseudo-coherent effects of nucleons within a nucleus, and on the dynamics of multiparticle production. Because the major part of this workshop is devoted to details of these subjects, I will spend the rest of this paper reviewing the more general ideas and just address the gross features of the data.

Nomenclature

Before proceeding to the data, it is worthwhile to define some of the terms that come up regularly in describing inclusive processes.[16] To start off, we must first define the invariant single-particle inclusive cross section. For the reaction

$$C + D \rightarrow G + \text{Anything}$$

the invariant differential cross section for emitting a particle G, of momentum $\vec{p}$ and energy E, into a Lorentz-invariant differential element of 4-momentum space d^3p/E, is defined as $d\sigma/(d^3p/E)$. If polarization can be ignored, the invariant cross section can depend only on the incident momentum, and on the longitudinal and transverse values of the momentum of particle G. Transverse momenta (p_T) of particles produced in hadronic reactions tend to be small, and essentially independent of incident energy. Two kinds of longitudinal-momentum (p_ℓ) variables have been found to be particularly useful in describing inclusive reactions. These are:
(1) The Feynman x variable, $x = p^*_\ell/E^*_T$, where p^*_ℓ is the longitudinal momentum of particle G and E^*_T is the total energy in the collision, both

expressed in the center of mass frame and (2) the rapidity variable $y = 1/2\ \ell n[(E + p_\ell)/(E - p_\ell)]$. The range of x is limited to between -1 and +1, while the allowed range of y values grows logarithmically with E_T^*.

Quite often, particularly when momentum measurements are not available, the pseudorapidity variable $\eta = -\ell n \tan(\theta/2)$ is used in place of y. Here θ is the production angle of particle G in the laboratory, and therefore $\tan\theta = \frac{p_T}{p_\ell}$. We can rewrite y in a manner analogous to that used for defining η: $y = -\ell n \tan(\phi/2)$, where ϕ is an angle defined by $\tan\phi = m_T/p_\ell$, and $m_T = (p_T^2 + m^2)^{\frac{1}{2}}$ is the "transverse" mass of a particle of mass m. Consequently, we see that the angles ϕ and θ, and therefore the rapidity and the pseudorapidity, approach each other only at large p_T. It is therefore important to distinguish results obtained for η and for y, particularly at small transverse momenta. (The x variable is also expressed at times in terms of laboratory momenta as $x = p_\ell/p_{in}$, where p_{in} is the incident momentum. This expression, clearly, holds only for large x.)

The invariant cross section can be written in terms of the x and y variables as follows:

$$\frac{Ed\sigma}{d^3p} = \frac{E}{\pi}\frac{d\sigma}{dp_\ell dp_T^2} = \frac{1}{\pi}\frac{d\sigma}{dydp_T^2} = \frac{E^*}{\pi p_{in}^*}\frac{d\sigma}{dxdp_T^2}$$

The multiplicity in some region of momentum space is defined as the inclusive cross section in that region divided by the total inelastic cross section. For example, the total inelastic multiplicity of particles G would be given by:

$$\langle n \rangle = \frac{1}{\sigma_{CD}} \int_{\substack{\text{all possible} \\ \text{momenta of G}}} E \frac{d\sigma}{d^3p} \cdot \frac{d^3p}{E} .$$

It is common to parameterize the dependence of inclusive differential cross sections on atomic mass in terms of the form A^{α}, where α may depend on both p_{ℓ} and p_T, as well as on p_{in}. Because inelastic hadron-nucleus total cross sections (σ_{hA}) increase with A approximately as $A^{0.7}$, the variation of the differential multiplicity can be expressed as $A^{\alpha-0.7}$. The multiplicity is independent of nuclear size for those regions of phase space where $\alpha = 0.7$. In addition to using α, another popular way of describing the A-dependence of inclusive cross sections or of multiplicities involves measurements normalized to data on hydrogen. In particular, the ratio of the inelastic charged-particle multiplicity in hadron-A collisions to that in hadron-p collisions is termed R_A, where R_A can be either the ratio of the integrated (total) multiplicities:

$$R_A = \frac{\langle n \rangle_{hA}}{\langle n \rangle_{hp}}$$

or a differential quantity, eg.,

$$R_A(\eta) \equiv r_A = \frac{\frac{1}{\sigma_{hA}} (d\sigma/d\eta)_{hA}}{\frac{1}{\sigma_{hp}} (d\sigma/d\eta)_{hp}}$$

Because the A^{α} parameterizations do not appear to extrapolate smoothly to hydrogen, it is sometimes difficult to relate, with precision, α to R_A.

Finally, a parameter that reflects the nuclear thickness, and at the same time takes account of the differing opacities for different

incident hadrons (h) is $\bar{\nu}$, defined as:

$$\nu = A\sigma_{hp}^{INEL}/\sigma_{hA}^{INEL}$$

$\bar{\nu}$ can be thought of as the average number of inelastic collisions that a projectile h would undergo in tranversing a nucleus A. (The value of $\bar{\nu}$ is $\simeq 0.65\ A^{0.31}$ for proton projectiles, and $\simeq 0.65\ A^{0.27}$ for pions.[17])

Data for Inclusive Production on Nuclei

One simple way to examine the kind of time scales that characterize hadronic reactions is through studying produced-particle multiplicities as a function of target material. If, for example, elementary hadron-hadron interaction times were short, that is, if the formed asymptotic states that we measure evolved on time scales of the order of nuclear tranversal times, then multiplicities on large nuclei would be expected to be far greater than on hydrogen. This is because an increase in multiplicity would result from multiple interactions of secondary particles produced within the nucleus. Such cascading would not be expected to be important at low incident momenta but should certainly occur at high energies, provided that characteristic collision times were $\lesssim 10^{-23}$ sec.

Figure 11 displays the ratio (R_{Em}) of the total inelastic charged-particle multiplicity in proton-emulsion collisions (average A $\sim$ 73) to that in pp collisions as a function of incident momentum.[18] From this compilation of data we see that, to $\sim$15% accuracy, R_{Em} does not exceed a value of $\sim$1.8, even for energies beyond several TeV. It appears, therefore, that there cannot be any substantial amount of cascading in nuclei. Thus, nuclei are rather transparent to the hadrons produced within nuclear

matter, which implies that hadronic time scales must be substantially longer than $\sim 10^{-23}$ sec.

The A-dependence of total charged-particle multiplicity has been measured recently by the MIT-Fermilab Group.[17] For p-A collisions in the several hundred GeV range of energies, for example, they obtain:

$$R_A = 0.72\ A^{0.23}$$

This result, again, confirms that there is very little intranuclear cascading. A number of alternate models have been suggested for explaining this nuclear transparency.[19] I will present just one simple hand-waving idea to indicate that such transparency is in keeping with what we know about multiparticle production processes at high energies.

There is a wealth of evidence suggesting that particles emitted in hadronic collisions are strongly correlated at production.[16] Such correlations stem partially from the presence of low-lying multiparticle resonances in the final states, but also from other dynamic clustering effects. Independent of the origin of such correlations, there is the phenomenological fact that multiparticle mass distributions peak at small values of invariant mass, and that these mass spectra have apparent widths that are comparable to the typical mass values.[20] Such a dynamic localization of masses can be translated into an uncertainty in the time scales for the production of these masses. If a typical hadronic cluster consists of about three pions, and if the effective mass of the cluster (M) is $\sim$ 1 GeV, then the time scale appropriate to the production (that is, for the full development) of such a cluster in the laboratory frame would be $\sim \frac{\gamma\hbar}{\Gamma}$. (For a total produced-particle multiplicity of $\sim$12, there will be, typically, 3-4 clusters per event.)

The values observed for Γ are about 1 GeV, and the Lorentz factor for the fastest clusters is about 50-200, in the several-hundred GeV domain of energies. Thus, on the basis of these simple arguments, characteristic production times would be expected to be $\sim 7 \times 10^{-23}$ sec, corresponding to hadron-formation distances of $\sim$ 20 Fm. Consequently, a cluster of particles created in a collision, can travel as a single unit of hadronic matter for distances of $\sim$20 Fm prior to breaking up into asymptotic remnants. Just from this picture alone (which does not nearly represent the whole story), we would therefore expect a drastic diminution in intranuclear cascading.

Having established the fact that interaction time scales in hadronic collisions at high energies are about an order of magnitude greater than traversal times, I would now like to proceed to certain interesting but more detailed features of the data. The energy dependence of the differential multiplicity for fixed $\bar{\nu}$, and the $\bar{\nu}$ dependence of the differential multiplicity, both as a function of η, are displayed in Fig. 12.[17] The energy variation is quite similar to that observed for reactions on hydrogen targets - this is, of course, not surprising because we noted already that R_{Em} hardly changes in this range of energies. In particular, the multiplicity (and the inclusive cross section) appears to be essentially independent of energy (it "scales") in the region of target fragmentation ($\eta \lesssim 1$), it is also independent of energy in the region of projectile fragmentation. The latter can be ascertained by examining $dN/d\eta$ in the rest frame of the incident projectile and not in the laboratory frame. This can be done simply by subtracting from η the quantity $\ell n(2p_{in}/m_{in})$ to take account of the boost from the lab frame to that of the projectile. Thus, to obtain the correct comparison,

the 50 GeV spectrum must be shifted left by ≃4.67 units of η, the 100 GeV spectrum by 5.36 and the 200 GeV spectrum 6.06. The resultant distributions are displayed in Fig.13.[17] The results for p-p data from the same experiment are shown as the solid curves on the distributions. From these results we conclude that the hypothesis of limiting fragmentation (HLF) is in substantial agreement with the data. (There is, nevertheless, good evidence for a small violation of HLF at high energies [21].)

The $\bar{\nu}$ dependence displayed in Fig. 12 indicates that the increase in multiplicity with increasing A occurs mainly for central ($y_{CM} \simeq 0$) and for backward production in the center of mass (region of target fragmentation). In the forward region of large η the production is essentially independent of nuclear size. Thus nuclei appear particularly transparent for forward rapidities (production of fast particles). This result is consistent in spirit with expectations from our trivial cluster model: The faster the produced particles the larger is the γ factor of the cluster and the longer the formation time scale and the less chance for cascading.

Figure 14 displays the results obtained from extracting α as a function of η. The data are again from the MIT-Fermilab experiment, to which the Rochester-Northwestern-Fermilab data on n-A collisions have been added for comparison.[22] (The neutron data are from a broad-band beam, whose average momentum is ∿ 300 GeV/c.) Again, there is observed the clear trend that substantial multiplication occurs mainly for low-energy secondaries. (The value of α = 0.69 for incident protons corresponds to no multiplication or, in other words, to "factorization" of inclusive cross sections on nuclei.)

Figure 15 illustrates an important point about inclusive nuclear data. Here I display, for positive-particle production in n-A collisions[22], the variation of the α parameter with η (same data as shown in Fig. 14 for $\eta < 8$), with y and with p_ℓ; in all cases the distributions have been integrated over p_T. The value of $\alpha = 0.69$ is also shown on the figure. It is clear that, particularly for rapidities $\gtrsim 6$, different conclusions may be reached regarding the question of particle multiplication in nuclear matter if the small but crucial differences between y and η are ignored. Using the more informative variables y and p_ℓ, which do not mix different regions of production the way η can, we see that α falls below 0.69 in the region of large particle momenta (projectile fragmentation). From Fig. 15 we can conclude that the multiplicity decreases with increasing A for $x \gtrsim 0.5$ (or for $y \gtrsim 6$). As it will surely be emphasized by the other speakers at this workshop, this kind of result is not consistent with the simplest kinds of models such as the Energy-Flux-Cascade, or single parton-chain exchange, or the single ladder multiperipheral model. More complicated contributions, e.g., multiple ladders, or cuts, are required to understand the attenuation of particles in nuclei in the forward direction. Our simple cluster picture would certainly allow for some attenuation in the forward direction; this is because the fastest cluster would be degraded somewhat in energy in its reinteraction within the nucleus.

The dramatic rise in α for $\eta \gtrsim 7$ can be attributed, at least partially, to contribution from coherent Coulomb production in the data. A similar effect has been noted by the Michigan Group for neutron production in p-A collisions (see Fig. 16).[23] At present, data at high

energies are not precise enough to confirm the possible presence of the exciting cumulative effects observed at the edges of phase space in collisions at lower energies.[24] I will therefore not comment on such phenomena at this time.

There is a weak p_T dependence to inclusive production on nuclear targets. This is displayed by the n-A data, integrated over p_ℓ, in Fig. 17.[22] The curves on the positive- and negative-particle data are drawn just to guide the eye. The small rise in α at small p_T^2 has been noted previously,[25] and the rise at large p_T^2, not so clear in these data, was discovered several years ago,[26] and will undoubtedly be interpreted in terms of hard-parton scattering later during this workshop.

A fascinating result obtained by the MIT-Fermilab group pertains to the projectile dependence of multiplicity.[27] This group has observed that multiplicity on nuclei becomes essentially independent of the nature of the projectile when data are examined as a function of $\bar{\nu}$ rather than of A. In Fig. 18 I have reproduced their differential measurements of $r(\eta)$ at 100 GeV/c, as a function of η for incident π^+, K^+ and p, all extrapolated to an equivalent target thickness of $\bar{\nu} = 3$. This lack of dependence of multiplicity on projectile implies that, subsequent to the initial collision, the rate for all secondary interactions is determined by the nature of the incident particle rather than by the many secondary pions produced in the first encounter. From a different vantage point (and probably a more incisive one) this result can also be interpreted to mean that the entire interaction on a nucleus takes place at one time - that is, several nucleons in the nucleus are hit by the same incident hadron (via its quark-parton chains) during the duration of the collision.[28] I might mention that this sort of picture can lead very naturally to a

small attenuation of the most energetic particles produced on nuclear targets. (Distribution of the incident energy among the simultaneous collisions of the projectile with several nucleons would yield such an effect.)

The results of Figs. 15 and 18, and other data, certainly point to the involvement of several nucleons in hadron-nucleus collisions. A question of immense importance is whether the hadron, in its simultaneous interaction with several nucleons in the nucleus, experiences a cumulative kind of collision (with a "coherent tube" or fluctuon)[24] or whether in effect the nucleons colliding with the projectile behave as independent entities. If the collision involves a pseudo-coherent process then the effective energy in the center of mass will be far larger than that for a projectile-nucleon collision at the same incident momentum. On the other hand, if the projectile interacts independently with several nucleons, then the energy per colliding nucleon will be smaller. I have examined data pertaining to this question but have not been able to reach a definite conclusion. I will present arguments for both interpretations and argue that new specific kinds of measurements can provide a clear answer to this fascinating problem.

The Seattle Group[29] has examined negative-particle production in π^-Ne reactions at 25 GeV and at 50 GeV. Figure 19 displays the correlation between $\langle N_-^{Pr} \rangle$, the average number of "produced" negative particles (using data for ≥ 2 negative tracks in the final state), and N_p, the number of identified protons in the final state. Yuldashev et al., interpreted these data assuming the validity of the coherent tube model (CTM)[30]; namely, they assumed that the collision occurs between the π^- and a coherent tube of nucleons located in the path of the π^-, and that the produced multiplicity is determined solely by the effective

energy in the center of mass of the beam and an effective mass (m_{eff}) of the coherent tube. Comparing known $\langle N_-^{Pr} \rangle$ from $\pi^- p$ data to $\langle N_-^{Pr} \rangle$ for Neon (for different values of N_p), they extracted a value of m_{eff} as a function of N_p. Their result, showing that $m_{eff} \sim (N_p + 1) m_{nucleon}$, is displayed at the bottom of Fig.19; this result is certainly consistent in spirit with expectations from the CTM.

In many respects h-A collisions do, in fact, resemble h-p collisions of higher energy. Figure 20, for example, shows how KNO multiplicity scaling, which holds in h-p collisions, also holds true in h-A collisions.[31] (It is interesting that the multiplicity spectrum even for neutrino-A collisions follows the KNO scaling form!) Other, more detailed, comparisons have been made of multiplicity distributions in $\pi^- p$ collisions at high energies with the distributions in $\pi^- A$ collisions (for a fixed value of N_p) at lower incident energies. Figure 21, also from ref.29, provides one such check of the CTM; charged-particle multiplicities for π^-Ne data at 50 GeV/c with N_p=2 are compared to $\pi^- p$ multiplicities at 147 GeV/c (corresponding, via the m_{eff} result from Fig. 19, to the proper CTM energy) and at 100 GeV/c. The multiplicity spectrum at 100 GeV/c clearly disagrees, while that at 147 GeV/c agrees with the π^-Ne data. These kinds of comparisons have demonstrated a remarkable similarity between low energy h-A interactions and higher energy h-p collisions, and displayed a surprising predictive power of the CTM.[32] In effect what such results suggest is that hadron-nucleus collisions are equivalent to hadron-hadron collisions shifted to higher energies. In addition, it appears that by changing N_p we can change the effective energy of the collision. Thus, the emulsion plate or a heavy-liquid bubble chamber can provide a way for fine-tuning energies for hadronic reactions. It is not clear to me how far a simple model such as the CTM can be pressed

for internal consistency. An important test can be provided through an extension of the analysis in Fig. 21 to include a comparison of rapidity spectra (dN/dy) in Ne for $N_p=2$ with data from π^-p interactions at 147 GeV/c.

Now I would like to turn to oft-neglected emulsion data to show that the more naive CTM ideas do not always work. Figure 22 displays a compilation[33] of $\langle n_s \rangle$, the average number of shower particles (lightly ionizing relativistic particles corresponding essentially to our previously defined $\langle n \rangle$), as a function of N_h, the number of heavily ionizing particles (mainly protons) observed in proton-emulsion collisions.[34] It has been known for some time that $\langle N_h \rangle$ (as well as the distribution of N_h) is essentially independent of energy ($\langle N_h \rangle \sim A^{2/3}$).[35] In increasing the incident energy from 200 GeV to 400 GeV the values of $\langle n_s \rangle$ appear to scale up by a factor 1.28 (independent of N_h). This is suggestively close to 1.18, the ratio of multiplicities on hydrogen at these two energies. Using these data I have tried to extract m_{eff} as a function of N_h for the three momenta $\geq$23 GeV/c. The disappointing results are shown in Fig. 23. Although there are some ambiguities in the comparison of $\langle n_s \rangle$ to $\langle n \rangle$,[34] as well as in the precise correlation between $\langle n_s \rangle$ and m_{eff} (and reading data points from miniscule graphs introduces some error), I do not believe that these uncertainties can in any way account for the gross variation of the cumulative m_{eff} with incident energy.

Taking the opposite ("incoherent") tack, I have also extracted in a rather crude manner an effective number of collisions as a function of N_h for the three sets of high-energy data in Fig. 22. The upper part of Fig. 23 displays the three sets of values of $\langle n_s \rangle$ in Fig. 22, each set divided by the value of $\langle n \rangle$ appropriate to pp collisions at the same incident momentum. (I have reduced each $\langle n \rangle$ by 1/2, to account for the

trivial difference in total charge between pA and pp incident channels.[34] Here the results are somewhat less dependent on incident energy. In fact, the value of $\langle n_s \rangle / \langle n \rangle$ appears to approach ~3 for large N_h; if this reflects the number of participating nucleons, then this result could be interpreted as suggesting the presence of 3 quarks in the proton.[36] The simplest interpretation of Fig. 23 would therefore be that models in which the projectile interacts with independent nucleons rather than with a fluctuon may be more in tune with the data. Judging from the comments at this workshop, the proponents of the CTM may be presently on the defensive; I suspect, nonetheless, that cumulative effects must be present in hadron-nucleus collisions (and, hopefully, not only the dullest kind, corresponding to multiple-scattering, Fermi motion, or electromagnetic effects). The only clear-cut conclusion I can come to at this time is that far more data, particularly with measurements of N_h, is crucial to settling the question of semi-coherence in inclusive production.

I have thus far dealt mainly with pion production, and I would like to end this part of my presentation with a brief summary of results pertaining to the production of more massive particles. To begin with, there is a surprising excess of energetic protons found in h-A and in neutrino-A collisions.[37] (Such an excess can be easily accommodated in the CTM[38].) The features of the production of the more massive hadrons, compared to pions, are that they appear to display a weaker dependence on p_T and greater attenuation (smaller α) at high rapidities.[22] A Michigan-Rutgers-Wisconsin Collaboration has studied K^o_s, Λ and $\bar{\Lambda}$ production in pA collisions.[34] Some of their extensive results are displayed in Figs. 24 and 25. These data indicate that, just as in the case of pion production, α decreases with increasing x and increases with increasing p_T (for fixed x, increasing the angle increases the value of α). Similar results on neutron production are available from the Michigan pA experiment.[23]

Finally, I wish to include in this review several results on jets or correlated multiparticle production. In a sense jets can be regarded as massive hadrons, and we would therefore expect such multiparticle systems to have properties akin to those observed for single hadrons. Figure 26 displays the α dependence of jet production as a function of p_T.[40] First, the rise of α beyond a value of $\alpha = 1$ with increasing p_T is similar to that observed for single hadrons,[26] as well as for dihadrons,[41] at large p_T. Finally, although the fact that at large p_T, p-induced jets display larger values of α than π-induced jets (more multiplication) might be argued as being consistent in spirit with the results of Fig. 18, that is, that the value of $\bar{\nu}$ is more relevant in multiplication than the value of A, the relative change of α with p_T is not so simple to understand. I will leave the interpretation of these and other large-p_T results to the other speakers at this workshop.

Acknowledgments

I thank L. Schroeder and the organizing committee for inviting me to participate in the Workshop. I also thank P. Slattery for helpful comments on this manuscript. Finally, I wish to acknowledge the co-operation of our students and my colleagues on Fermilab Experiment E272 in helping me compile the latest results on Coulomb excitation of mesons.

Table I

Recent Measurements of Radiative Widths

Process	Width (KeV)[+]
$\rho^- \to \pi^- \gamma$	50 ± 10
$K^*(890)^- \to K^- \gamma$	∿ 50
$A_2^- \to \pi^- \gamma$	∿450
$A_1^- \to \pi^- \gamma$	∿600

[+]All but the ρ^- values are quite preliminary and consequently no errors have been quoted for the observed processes. See Phys. Letts. 75B, No. 1 (1978) for previous measurements of such widths.

References

1. For recent reviews of the field and references see C. Halliwell, VII Int'l. Symp. on Multipart. Dyn. (Kayserberg 1977), R. Arnold et al, ed; and T. Ferbel, Int'l. Meet. on Front. of Phys. (Singapore 1978), K. K. Phau, ed. For a review of hadronic diffraction see U. Amaldi, M. Jacob and G. Matthiae, Ann. Rev. Nucl. Sci. 26, 385 (1976).
2. See, for example, B. Feld, Models of Elementary Particles, Ginn/Blaisdell (1969).
3. H. Primakoff, Phys. Rev. 81, 899 (1951). For a recent treatment and references to earlier work see G. Fäldt, Nucl. Phys. B3, 591 (1972).
4. This point has been stressed by G. Berlad et al., Ann. of Phys. 75, 461 (1973), and by Y. Nagashima and J. Rosen, University of Rochester Report UR-875-295 (1969).
5. M. Good and W. Walker, Phys. Rev. 120, 1857 (1960); E. L. Feinberg and I. Ia. Pomeranchuk, Suppl. Nuovo Cimento 3, 652 (1956).
6. For simplicity I am assuming the validity of the so-called Morrison rule: Phys. Rev. 165, 1699 (1968).
7. See K. Kolbig and B. Margolis, Nucl. Phys. B6, 85 (1968). Also, for a discussion of difficulties with this classical treatment see G. Fäldt and P. Osland, Nucl. Phys. B126, 221 (1977), and H. Miettinen and J. Pumplin, Phys. Rev. Lett. 42, 204 (1979).
8. W. Czyz, University of Virginia Preprint (1973).
9. See, for example, R. Cuttler and E. L. Berger, Phys. Rev. D15, 1903 (1977), and references given therein to other work of its kind.
10. W. Mollet et al., Phys. Rev. Lett. 39, 1646 (1977) and J. Biel et al., University of Rochester Preprint UR-690a (1979), to appear in Phys. Rev.
11. D. Berg et al., University of Rochester Preprint UR-677 (1978), and paper 34 submitted to the EPS Meeting (Geneva 1979).

12. See, for example, J. Babcock and J. Rosner, Phys. Rev. D14, 1286 (1976); R. L. Thews D17, 3038 (1978); A. Bohm and R. B. Teese, Phys. Rev. D18, 330 (1978).

13. See T. Roberts, Ph.D. Thesis, University of Illinois (1975).

14. See the compilation of W. Busza in Acta. Phys. Pol. B8, 333 (1977).

15. P. Osland, Harvard Preprint HUTP-78/B002 (1978).

16. For an introduction to inclusive reactions see H. Boggild and T. Ferbel, Ann. Rev. Nuc. Sci. 24, 451 (1974).

17. J. Elias et al., MIT/Fermilab Preprint (to appear in Phys. Rev); C. Young, Ph.D. Thesis, MIT (1977). I thank J. Elias for providing me an early copy of the Phys. Rev. article.

18. The data are taken from the previous compilation of A. Gurtu et al., Phys. Letts. 50B, 391 (1974), from reference 17, and from E. G. Boos et al., (Alma-Ata-Gatchina-Moscow-Tashkent Collaboration) Kazakh Academy Preprint HEPI 67-78 (1978).

19. See the various recent Proceedings of Symposia on Multiparticle Dynamics: Tutzing (1976), J. Benecke et al., eds; Kaysersberg (1977), R. Arnold et al., eds; Tabor (1978), V. Simak et al., eds.

20. P. Stix et al., Phys. Rev. D16, 558 (1977).

21. See R. Schindler et al., Phys. Rev. Letts. 33, 862 (1974) and Y. Takahashi, AIP Conf. Proc. 49 (1978), T. Gaisser, ed.

22. D. Chaney et al., University of Rochester Report UR-689 (to appear in P.R.) Similar results, but without momentum information, have been obtained for neutrons at ∿200 GeV. See D. L. Burke, Ph.D. Thesis, University of Michigan Report UM-HE 78-24 (1978).

23. M. R. Whalley et al., University of Michigan Preprint UMHE 78-46. I thank L. Jones for comments on this work. I might remark here that the kind of coherent effects noted in Figs. 15(a) and 16 are generally not observed in emulsion studies because, in the latter, coherent events are usually excluded from data on inelastic production channels. Some discrepancies between emulsion and counter experiments can probably be attributed to this difference in the definition of data samples.

24. See A. M. Baldin's report in Proc. of 19th Int'l. Conf. on High En. Phys. (Tokyo, 1978), S. Homma et al., eds.

25. D. Garbutt et al., Phys. Lett. 67B, 355 (1977). See also comments of J. Kuhn in Phys. Rev. D18, 338 (1978).

26. J. Cronin et al., Phys. Rev. D11, 3105 (1975).

27. J. Elias et al., Phys. Rev. Letts. 41, 285 (1978).

28. I thank S. Brodsky and A. Mueller for helpful clarifications of quark-parton and multi-Regge exchange ideas. For further discussion see S. Brodsky, J. Gunion and J. Kuhn, Phys. Rev. Letts. 39, 1120 (1977); A. Capella and A. Krzywicki, Phys. Letts. 67B, 84 (1977); J. Koplik and A. H. Mueller, Phys. Rev. D12, 3638 (1975).

29. B. Yuldashev et al., Acta Phys. Pol. B9, 513 (1978).

30. G. Berlad, A. Dar, G. Eilam, Phys. Rev. D13, 161 (1976). (See also S. Fredriksson's presentation at this Workshop.)

31. T. M. Burnett et al., AIP Conf. Proc. 45 (1978), R. S. Panvini and S. E. Czorna, eds. I thank H. Lubatti for a helpful correspondence, and for providing me with Figs. 19, 20 and 21.

32. See the comparisons of y-distributions between data for fixed N_p and predictions of the CTM in W. Yeager et al., Phys. Rev. D16, 1294 (1977).

33. The data are taken from A. Gurtu et al., and from E. Boos et al., loc. cit.

34. The reason that $\langle n \rangle$ in pp collisions is not exactly the same as $\langle n_s \rangle$ in pA reactions is because, in the latter case, some of the protons are absorbed into N_h. In addition, $\langle n \rangle$ in pp collisions is artificially larger than $\langle n_s \rangle$ in pA collisions because half of the interactions in nuclei occur on neutrons. When such threshold corrections are taken into account, the value of R_{Em} (Fig. 11) becomes essentially independent of energy for $p_{in} \gtrsim 10$ GeV/c. These subtleties are discussed in the excellent review of emulsion data by I. Otterlund in Acta Phys. Pol. B8, 119 (1977).

35. Hence N_h appears to reflect more the cross-sectional area of the nucleus rather than the number of nucleons in a tube that collide with the projectile. This is not completely consistent with the interpretation given to N_p in ref. 29. In the framework of the CTM the average number of interacting nucleons would be proportional to $A^{1/3}$. I must caution, however, that there is no simple relationship between the data in Fig. 19 ($\langle N_-^{Pr} \rangle$, N_p), and the data in Fig. 22 ($\langle n_s \rangle$, N_h).

36. Because of the uncertainty in $\langle n \rangle$ at energies beyond the ISR, I have not plotted $\langle n_s \rangle / \langle n \rangle$ for the largest N_h. There is nevertheless a trend for a decrease of the slope of this ratio with increasing N_h. See also the presentation of M. Faessler at this Workshop and the discussion of A. Bialas regarding simple quark models.

37. This has been emphasized by W. Yeager et al (ref. 32).

38. Private communication from A. Dar.

39. P. Skubic, Ph.D. Thesis, University of Michigan (1977), and K. Heller et al., Phys. Rev. D16, 2737 (1977).

40. C. Bromberg et al., Phys. Rev. Letts. 42, 1202 (1979)

41. D. A. Finley et al., Phys. Rev. Letts. 42, 1031 (1979) and R. L. McCarthy et al., Phys. Rev. Letts. 40, 213 (1978).

Figure Captions

1. Approximate energy dependence of t-distributions for electromagnetic conversion of a particle a to particle b. The curves correspond to values of t_o=0, 10^{-4} GeV^2, 2×10^{-4} GeV^2 and 5×10^{-4} GeV^2.
2. Drell-Hiida-Deck diagrams that contribute to neutron dissociation into ($p\pi^-$) systems. The symbol $\mathbb{P}$ represents Pomeranchukon exchange.
3. Mass and t' distributions of ($p\pi^-$) systems produced in the dissociation of neutrons on a carbon target.
4. (a) Differential cross section for neutron dissociation into $p\pi^-$ on copper, for 1.35 GeV < m < 1.45 GeV. (b) A-dependence of the cross section for the same mass range as in (a). The solid and dashed curves are based on calculations mentioned in the text. (Typical error bars are shown in the data points.)
5. Mass and t distributions of ($\pi^-\pi^o$) systems produced in the coherent (Coulomb) dissociation of π^- mesons on nuclear targets at 156 GeV/c.
6. Mass spectrum of ($\pi^-\pi^+\pi^-$) systems produced in the coherent dissociation of π^- mesons on nuclear targets at 156 GeV/c.
7. Distributions in t for ($\pi^-\pi^+\pi^-$) systems produced in the coherent dissociation of π^- mesons on nuclear targets at 156 GeV/c.
8. Possible non-resonant and resonant contributions to γ-π^- scattering near the mass of the A_1.
9. Gottfried-Jackson polar-angle distributions for the proton in the decay of ($p\pi^-$) systems produced coherently off Cu and C targets. The predictions of a DHD model (Fig. 2) are shown renormalized to the data at small masses. Magnitudes of the contributions from the three (interfering) terms in Fig. 2 are shown on the Cu results for 1.3 < M < 1.4 GeV.

10. Comparison of t'-distributions for the Cu data of Fig. 9 with the model of Fig. 2. (The theoretical predictions have been reduced by an arbitrary factor of 4.)

11. Ratio of produced particle multiplicity in emulsion to multiplicity in hydrogen for incident protons.

12. Dependence of differential multiplicity on incident momentum for proton projectiles for $\bar{\nu} = 2$, and the dependence of the multiplicity on $\bar{\nu}$ at 200 GeV for π^- projectiles.

13. Differential multiplicity in the projectile frame as a function of incident momentum for p-Pb, p-Cu and p-C data.

14. The dependence of α on pseudo-rapidity for 200 GeV pA data. Data for 300 GeV nA collisions (positive and negative particles) are shown for comparison.

15. Dependence of α on η, y and p_ℓ for positive particles produced in nA collisions at 300 GeV.

16. Dependence of α on x for neutron production in p-Pb and p-Be collisions at different laboratory angles.

17. Dependence of α on p_T^2 for positive and negative particles produced in nA collisions at 300 GeV.

18. Ratios of multiplicity for p, K^+ and π^+ beams for $\bar{\nu} = 3$ to multiplicity on hydrogen at 100 GeV.

19. Dependence of the average number of produced negative particles on the number of identified protons (N_p) in π^-Ne collisions. The extracted dependence of the effective target mass on N_p is shown at the bottom.

20. Distribution of KNO scaling variables for π^-p, π^-Ne, π^-C and ν-Ne collisions.

21. The ratio of the multiplicity distribution of negative particles in π^-Ne collisions with $N_p = 2$ at 50 GeV/c to those in (a) π^-p collisions at 147 GeV/c and (b) π^-p collisions at 100 GeV/c.

22. The average number of shower particles as a function of the number of heavily ionizing tracks in emulsions exposed to proton beams.

23. The extracted values of effective target mass and ratios R_{Em} for data in Fig. 22.

24. The dependence of α on x for K^o_s production in pA collisions at 300 GeV.

25. The dependence of α on x for Λ^o production in pA collisions at 300 GeV.

26. The dependence of α on p_T for the production of jets of hadrons at 200 GeV for hydrogen and aluminum targets.

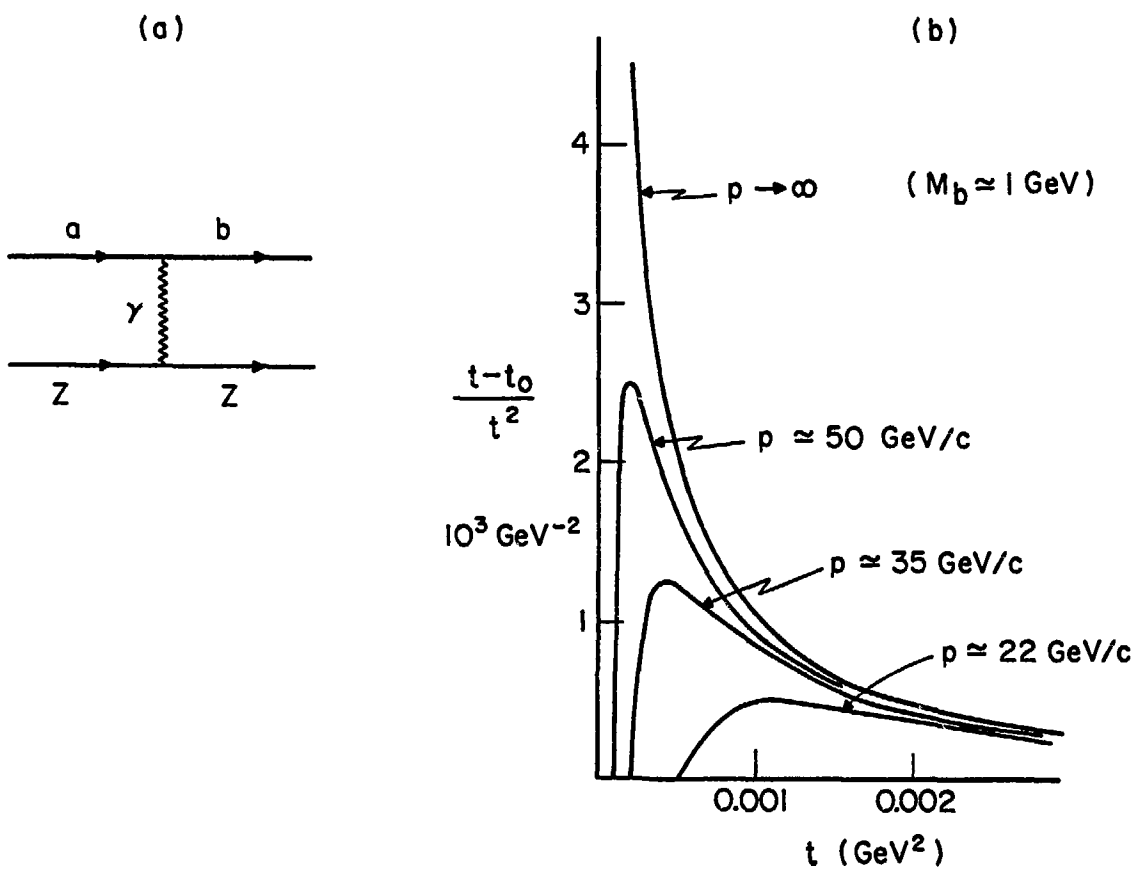
(a)
a
b
γ
Z
Z
(b)
4
3
2
1
$\frac{t-t_0}{t^2}$
10^3 GeV^{-2}
p → ∞
($M_b \simeq 1$ GeV)
p ≃ 50 GeV/c
p ≃ 35 GeV/c
p ≃ 22 GeV/c
0.001
0.002
t (GeV^2)

Fig. 1

(a) pion-exchange

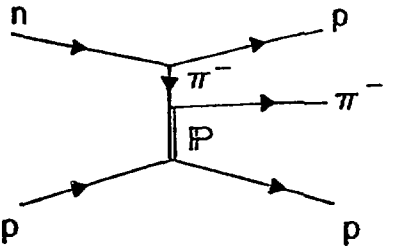

(b) proton-exchange

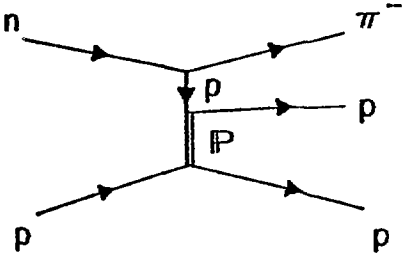

(c) neutron pole

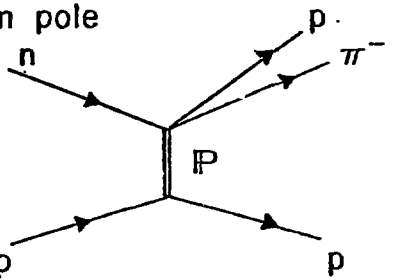

Fig. 2

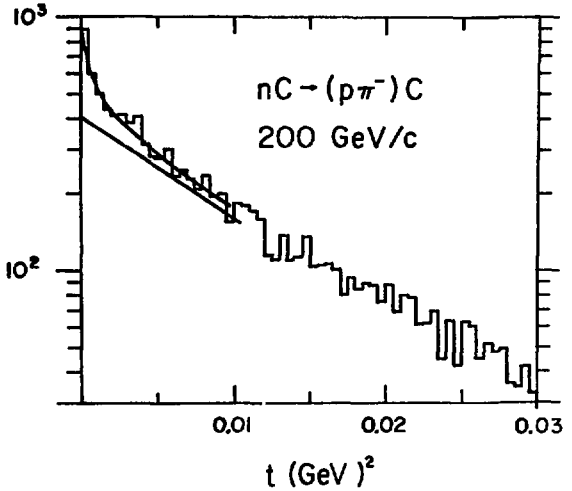
10^3
10^2
$nC \rightarrow (p\pi^-)C$
200 GeV/c
0.01
0.02
0.03
t (GeV)^2

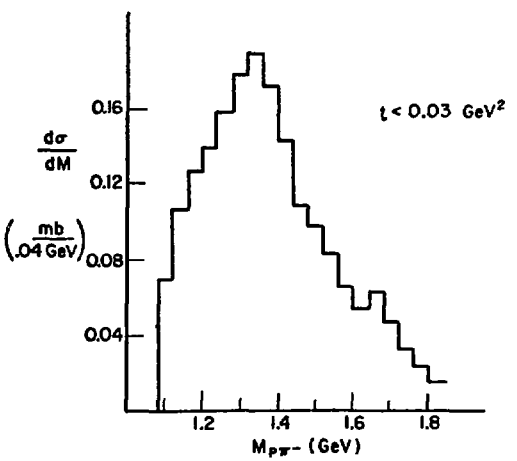
$\frac{d\sigma}{dM}$
$\left(\frac{mb}{.04\,GeV}\right)$
0.16
0.12
0.08
0.04
$t < 0.03$ GeV^2
1.2
1.4
1.6
1.8
$M_{p\pi^-}$ (GeV)

Fig. 3

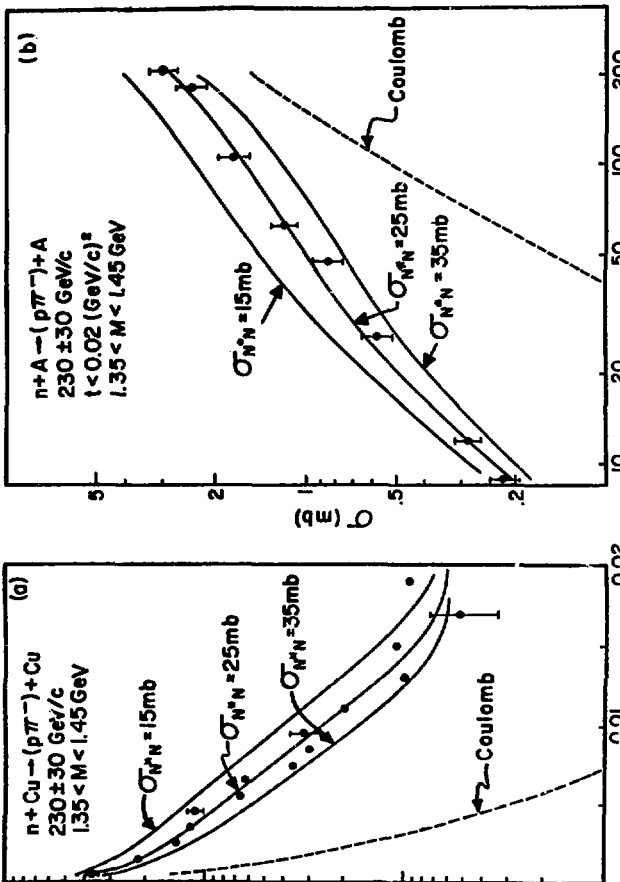
(a)
n+Cu→(pπ⁻)+Cu
230±30 GeV/c
1.35<M<1.45 GeV
σN*N=15mb
σN*N=25mb
σN*N=35mb
Coulomb
dσ/dt' (b/GeV²/c²)
0.10
0.01
0.01
0.02
t' (GeV/c)²
(b)
n+A→(pπ⁻)+A
230±30 GeV/c
t<0.02 (GeV/c)²
1.35<M<1.45 GeV
σN*N=15mb
σN*N=25mb
σN*N=35mb
Coulomb
σ (mb)
5
2
1
.5
.2
10
20
50
100
200
A

Fig. 4

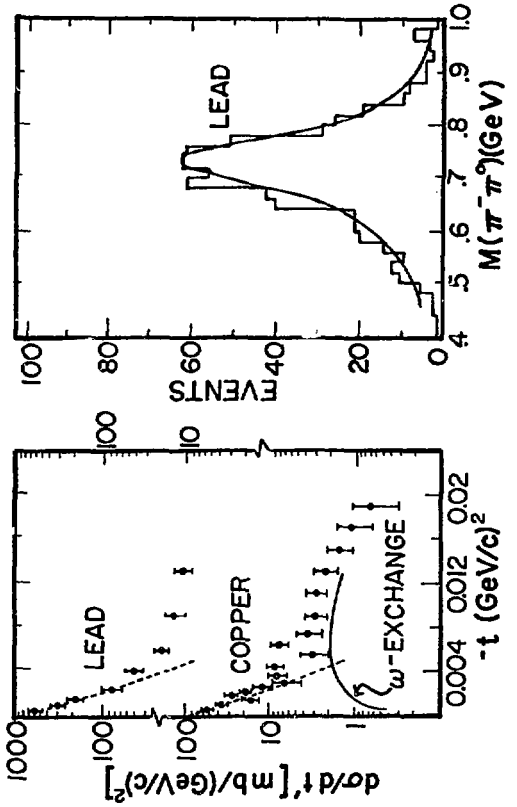
LEAD
COPPER
ω-EXCHANGE
dσ/dt' [mb/(GeV/c)²]
-t (GeV/c)²
EVENTS
LEAD
M(π⁻π⁰)(GeV)

Fig. 5

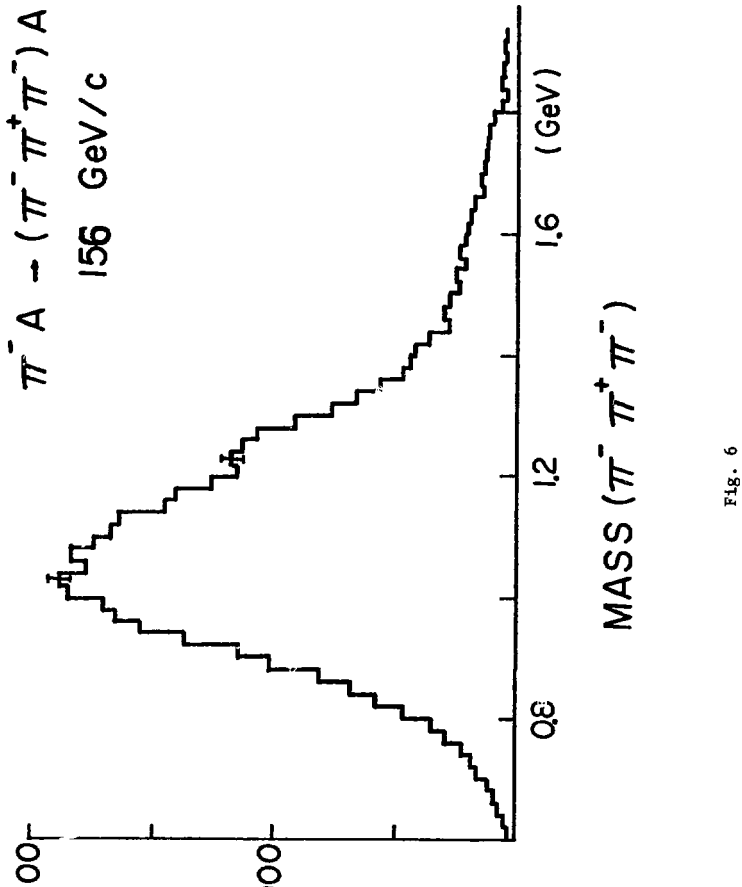

Fig. 6

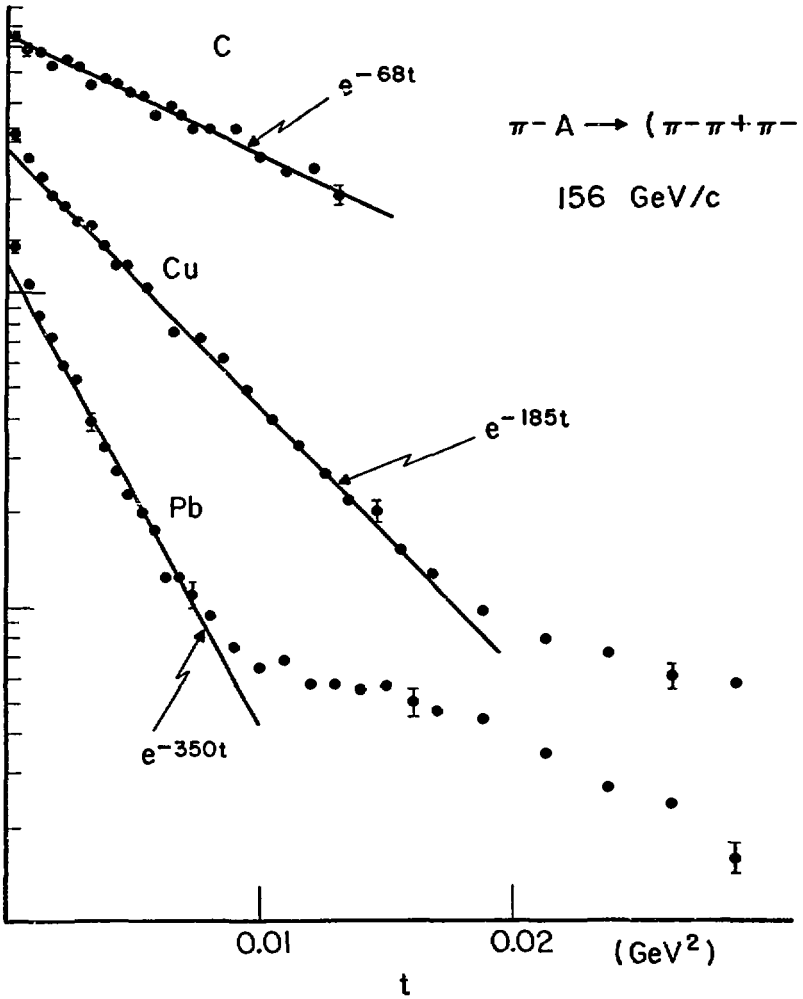

Fig. 7

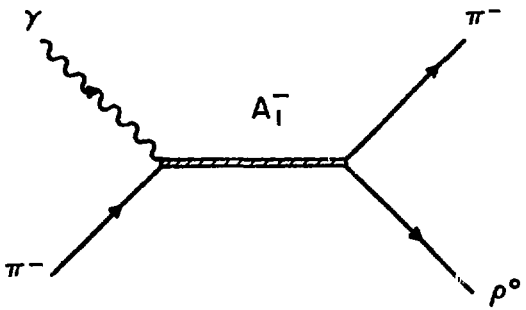

Resonant Process

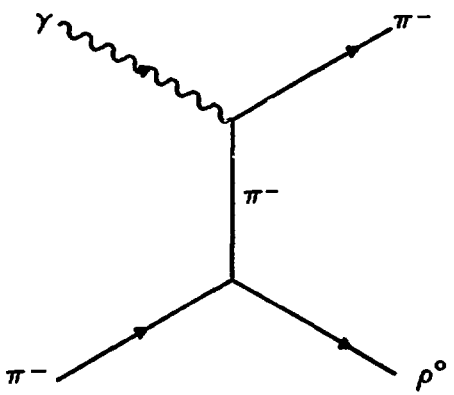

Non-Resonant Process

Fig. 8

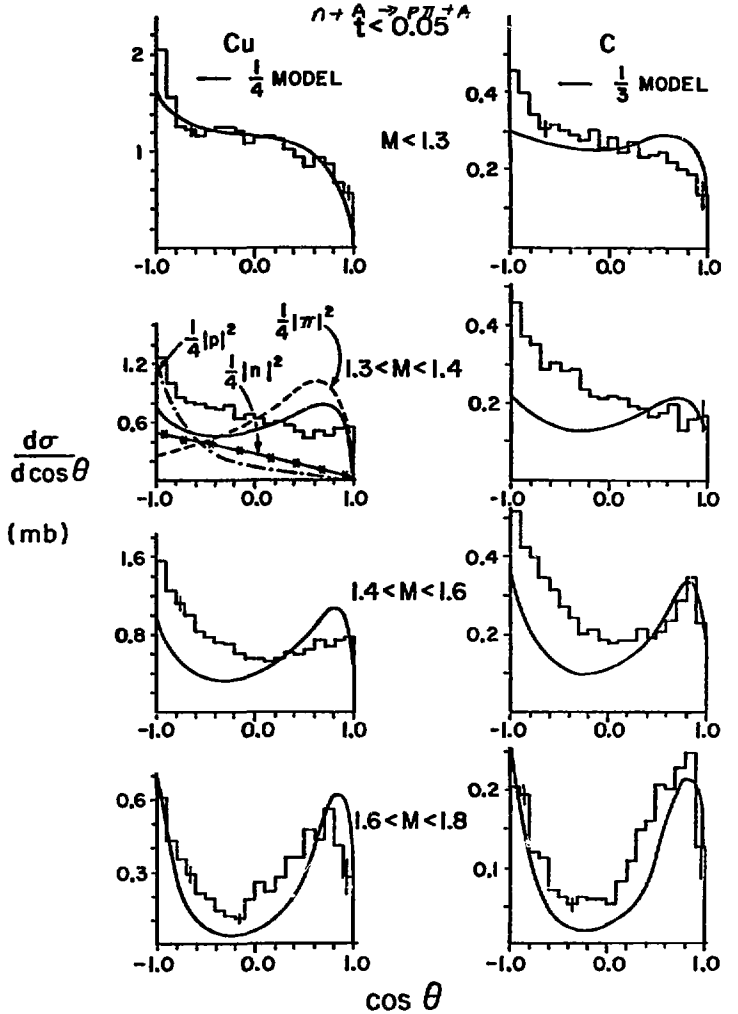
n + A → pπ + A
t < 0.05
Cu
C
¼ MODEL
⅓ MODEL
M < 1.3
1.3 < M < 1.4
1.4 < M < 1.6
1.6 < M < 1.8
¼|p|²
¼|n|²
¼|π|²
dσ/dcosθ
(mb)
cos θ

Fig. 9

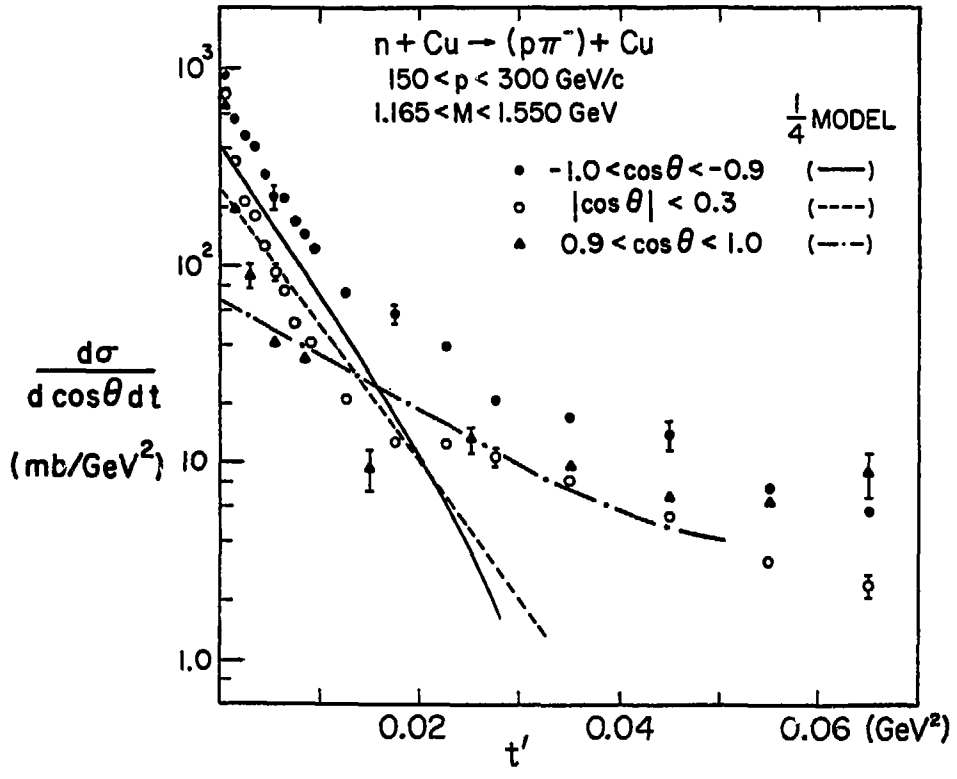
n + Cu → (pπ⁻) + Cu
150 < p < 300 GeV/c
1.165 < M < 1.550 GeV
1/4 MODEL
• -1.0 < cos θ < -0.9 (——)
○ |cos θ| < 0.3 (----)
▲ 0.9 < cos θ < 1.0 (—·—)
dσ / d cos θ dt
(mb/GeV²)
10³
10²
10
1.0
0.02
0.04
0.06 (GeV²)
t'

Fig. 10

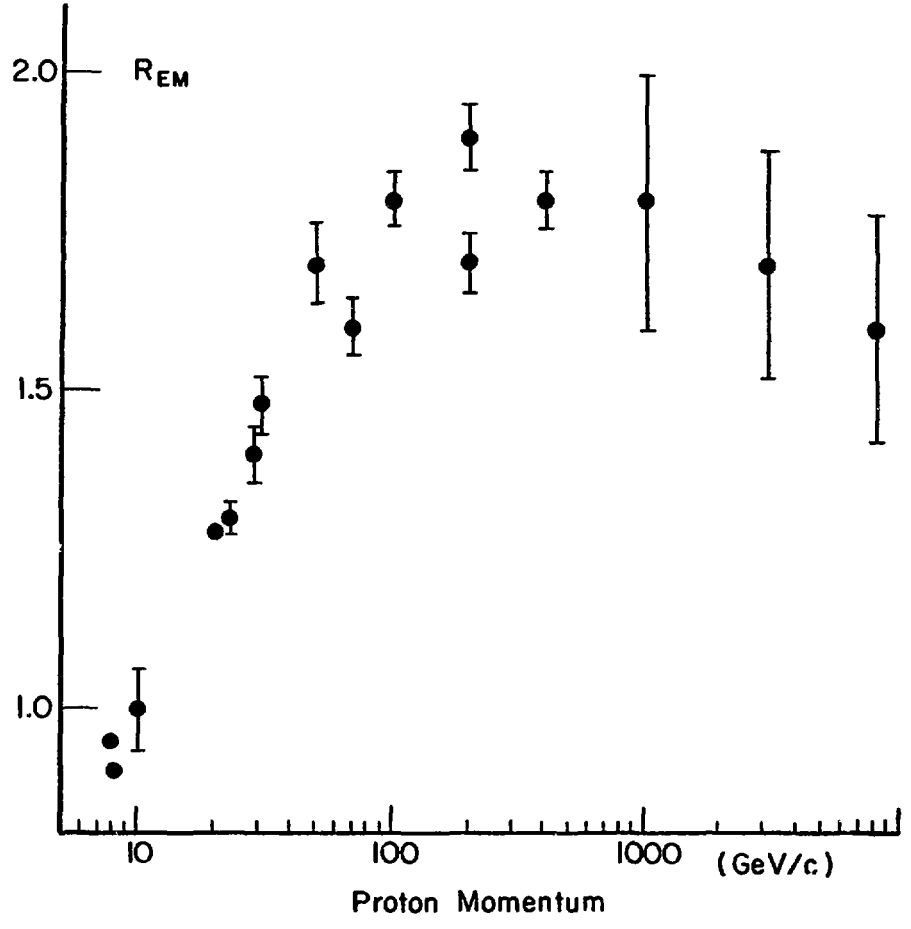

Fig. 11

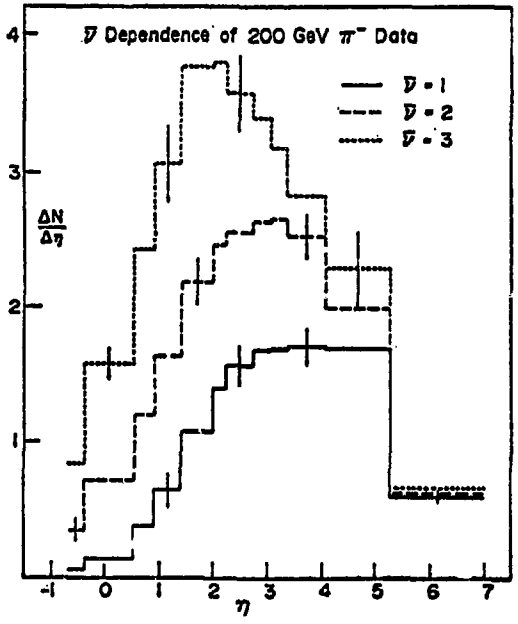
$\bar{\nu}$ Dependence of 200 GeV π^- Data
$\bar{\nu}$ = 1
$\bar{\nu}$ = 2
$\bar{\nu}$ = 3
$\frac{\Delta N}{\Delta \eta}$
η

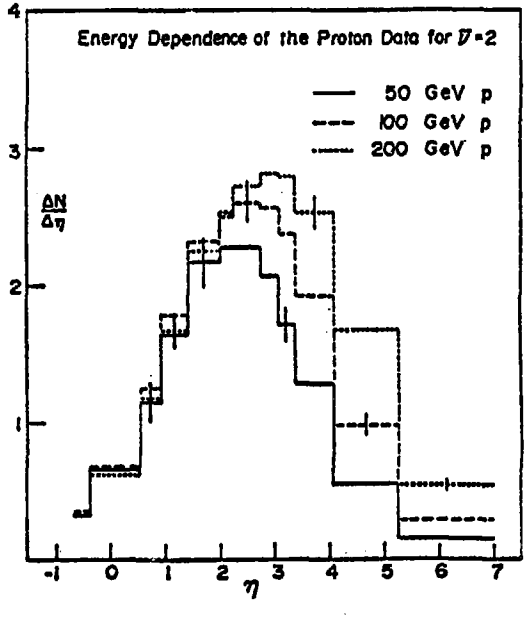
Energy Dependence of the Proton Data for $\bar{\nu}$=2
50 GeV p
100 GeV p
200 GeV p
$\frac{\Delta N}{\Delta \eta}$
η

Fig. 12

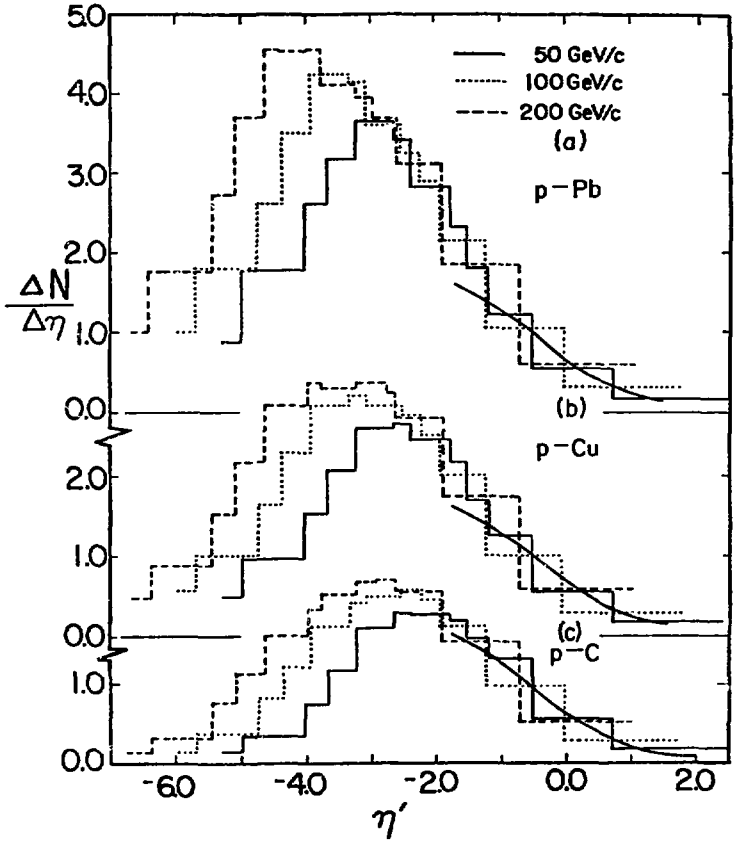
50 GeV/c
100 GeV/c
200 GeV/c
(a)
p−Pb
(b)
p−Cu
(c)
p−C
ΔN/Δη
η′
5.0
4.0
3.0
2.0
1.0
0.0
-6.0
-4.0
-2.0
0.0
2.0

Fig. 13

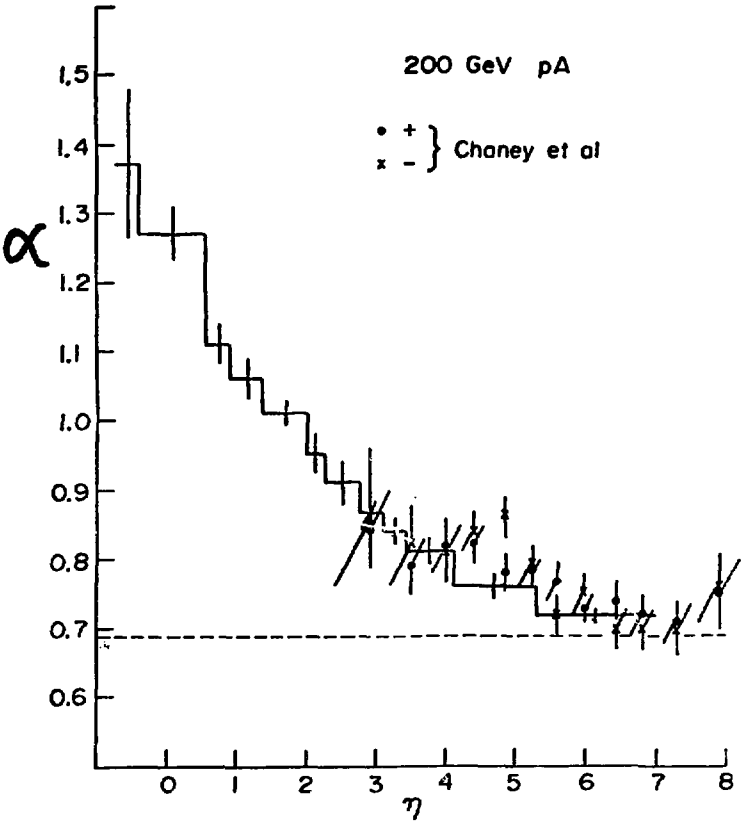

Fig. 14

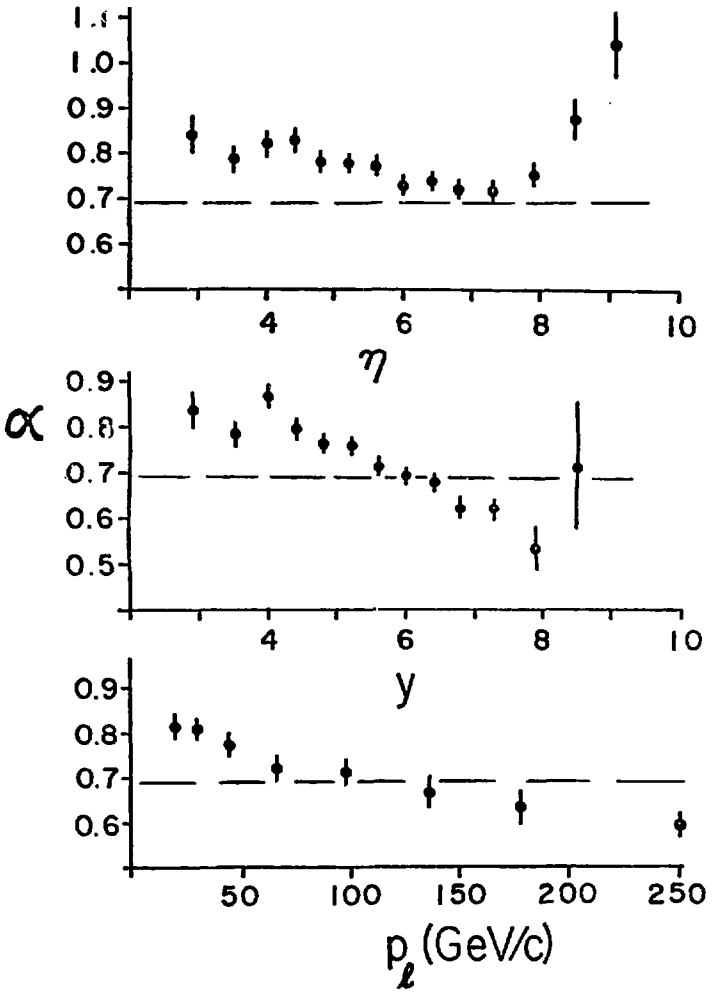
1.1
1.0
0.9
0.8
0.7
0.6
4
6
8
10
η
α
0.9
0.8
0.7
0.6
0.5
4
6
8
10
y
0.9
0.8
0.7
0.6
50
100
150
200
250
p_ℓ (GeV/c)

Fig. 15

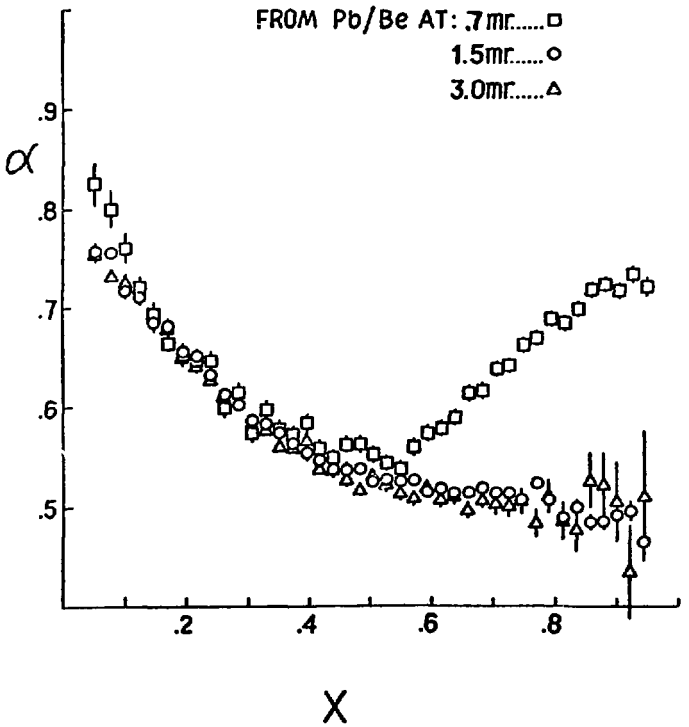

Fig. 16

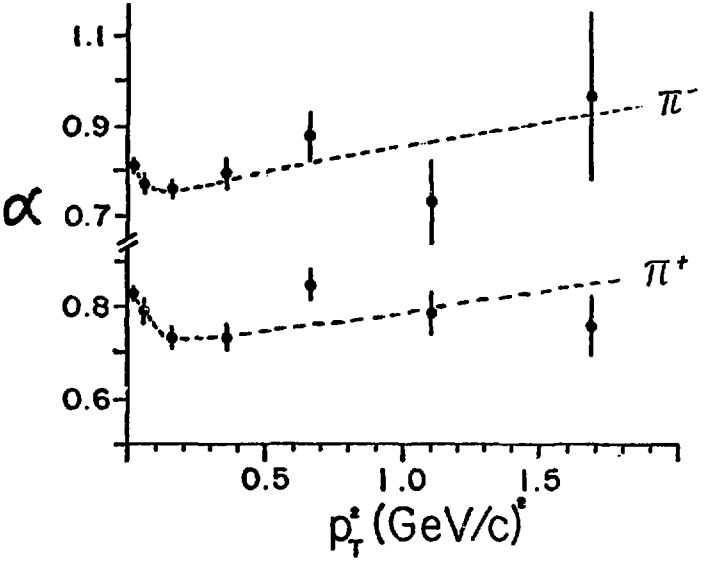

Fig. 17

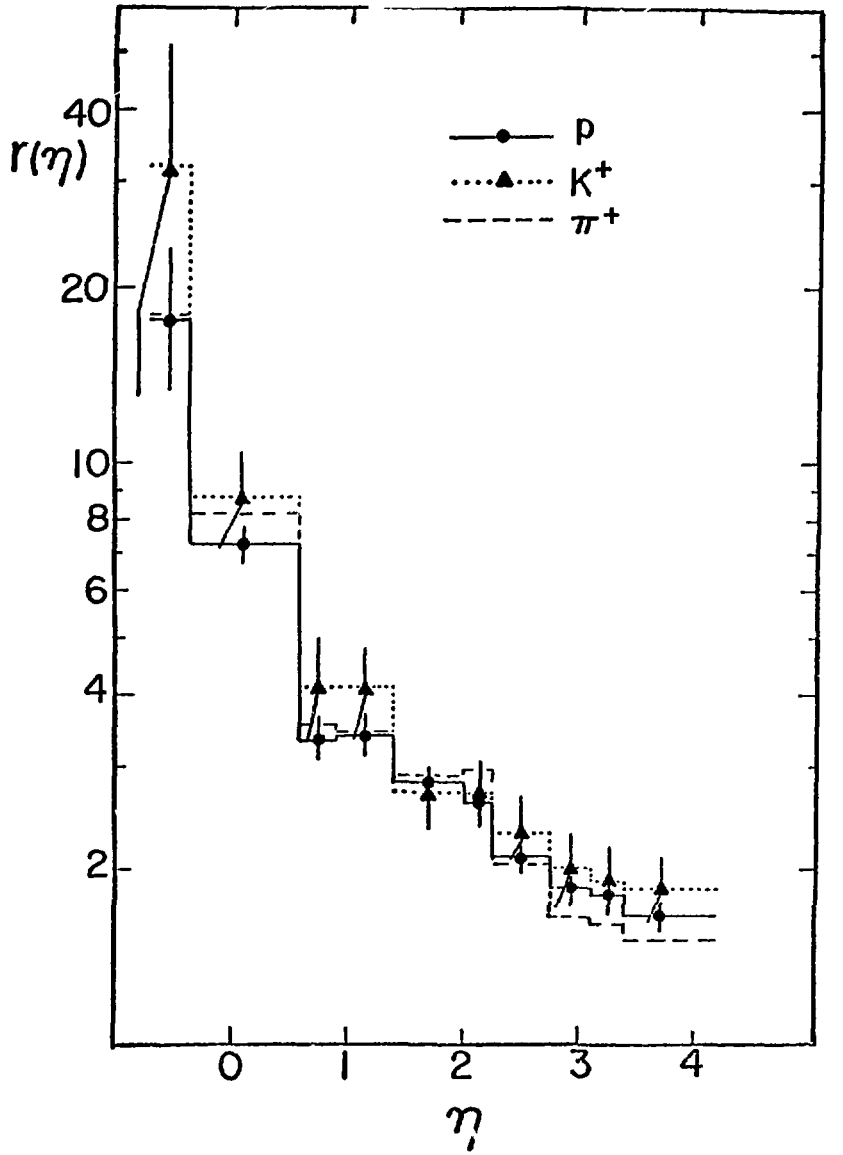

Fig. 18

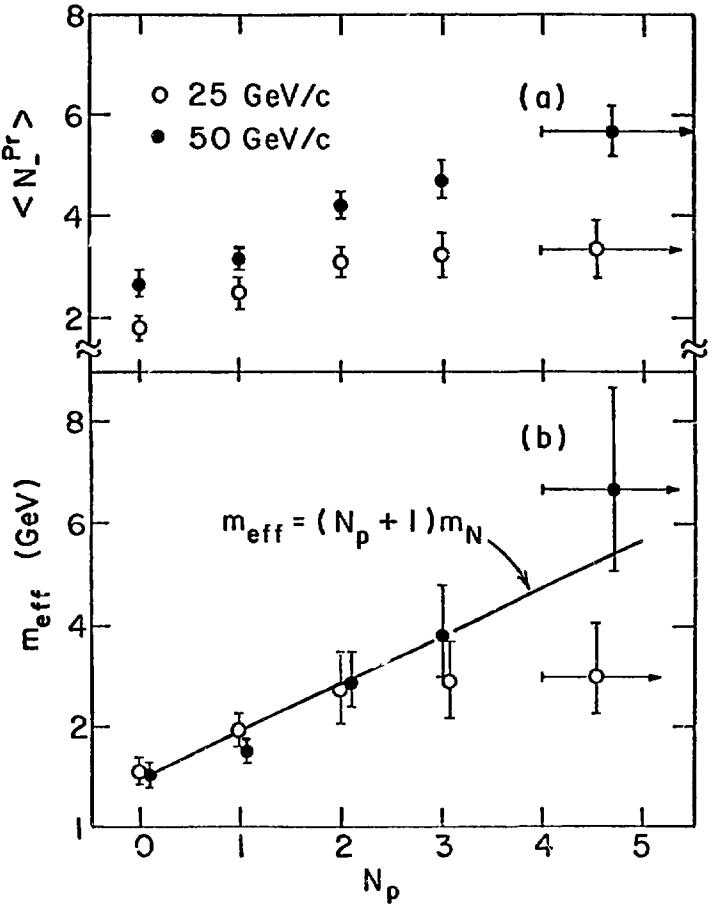

Fig. 19

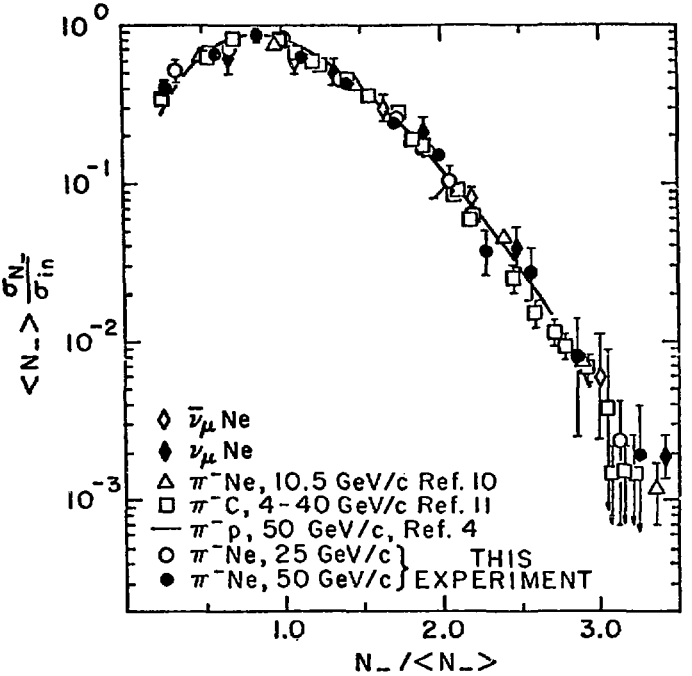
10^0
10^{-1}
10^{-2}
10^{-3}
$\frac{\sigma_{N_-}}{\sigma_{in}} < N_- >$
◊ $\bar{\nu}_\mu$ Ne
♦ ν_μ Ne
△ π^-Ne, 10.5 GeV/c Ref. 10
□ π^-C, 4-40 GeV/c Ref. 11
— π^-p, 50 GeV/c, Ref. 4
○ π^-Ne, 25 GeV/c } THIS
● π^-Ne, 50 GeV/c } EXPERIMENT
1.0
2.0
3.0
$N_- / < N_- >$

Fig. 20

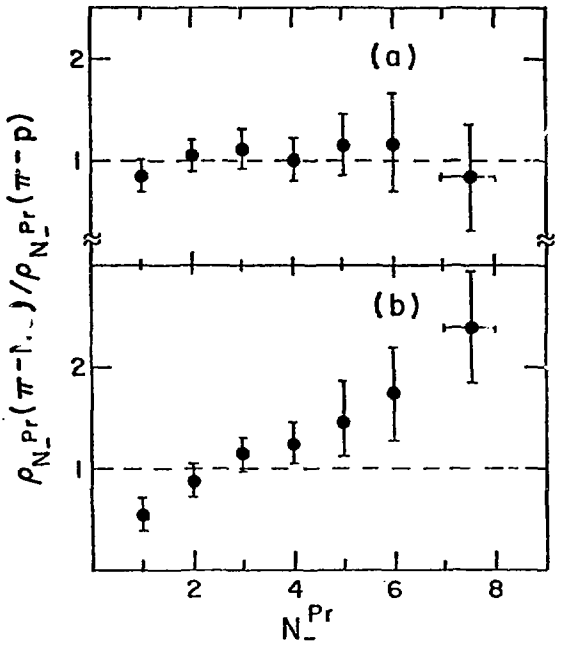

Fig. 21

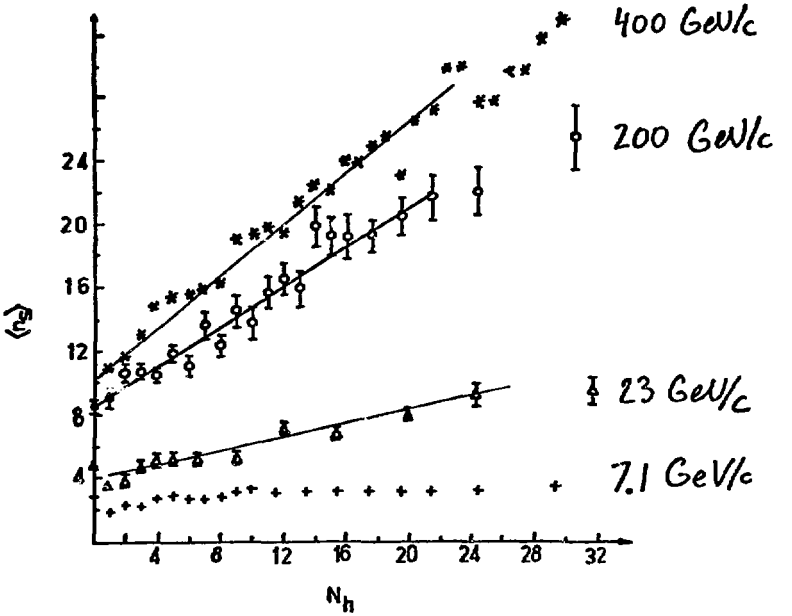
400 GeV/c
200 GeV/c
23 GeV/c
7.1 GeV/c
24
20
16
12
8
4
4
8
12
16
20
24
28
32
N_h

Fig. 22

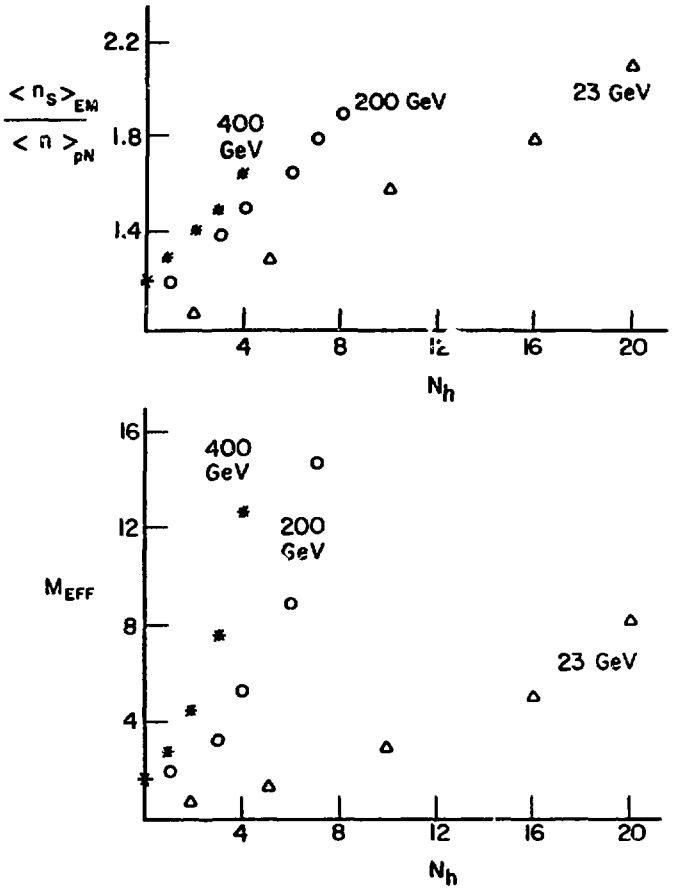
$\frac{\langle n_s \rangle_{EM}}{\langle n \rangle_{pN}}$
2.2
1.8
1.4
400 GeV
200 GeV
23 GeV
4
8
12
16
20
N_h
M_{EFF}
16
12
8
4
400 GeV
200 GeV
23 GeV
4
8
12
16
20
N_h

Fig. 23

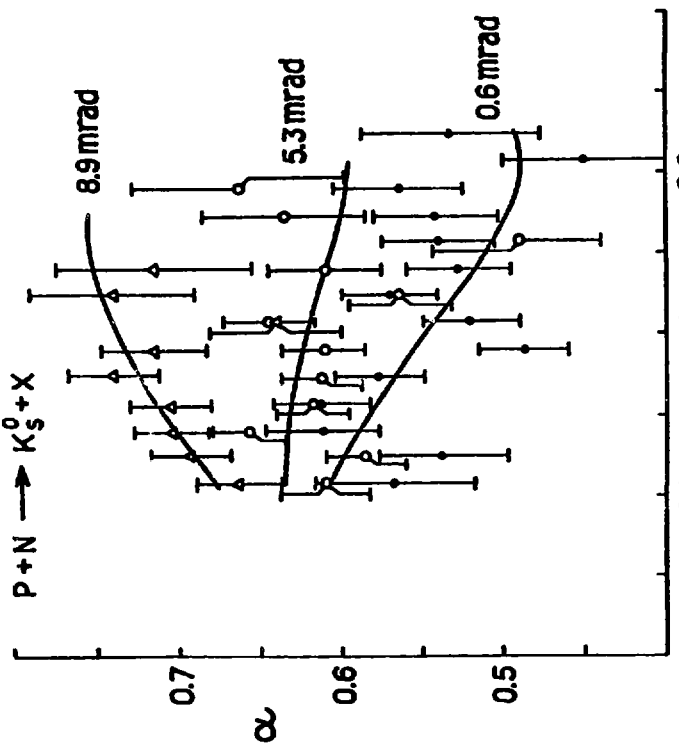

Fig. 24

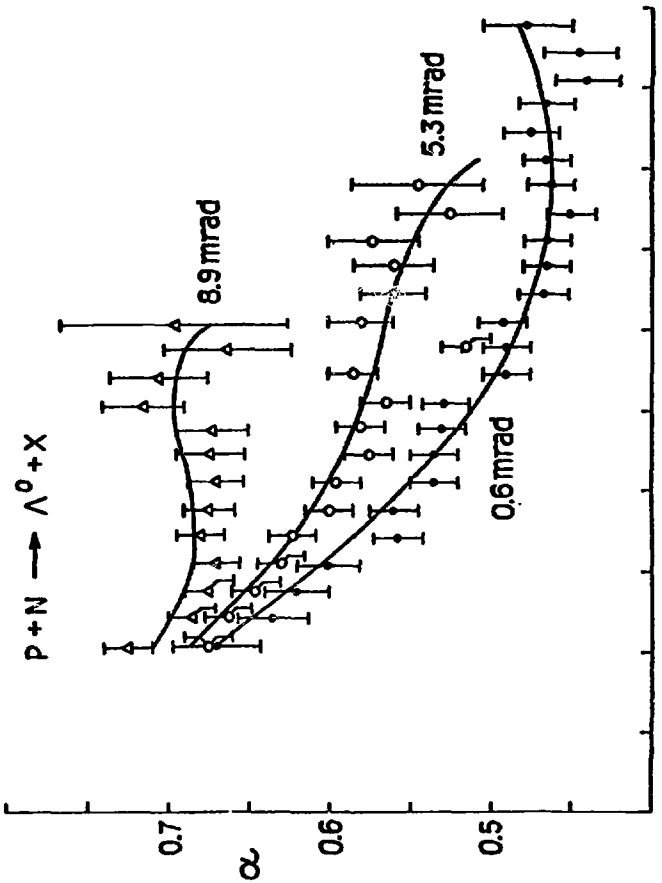

Fig. 25

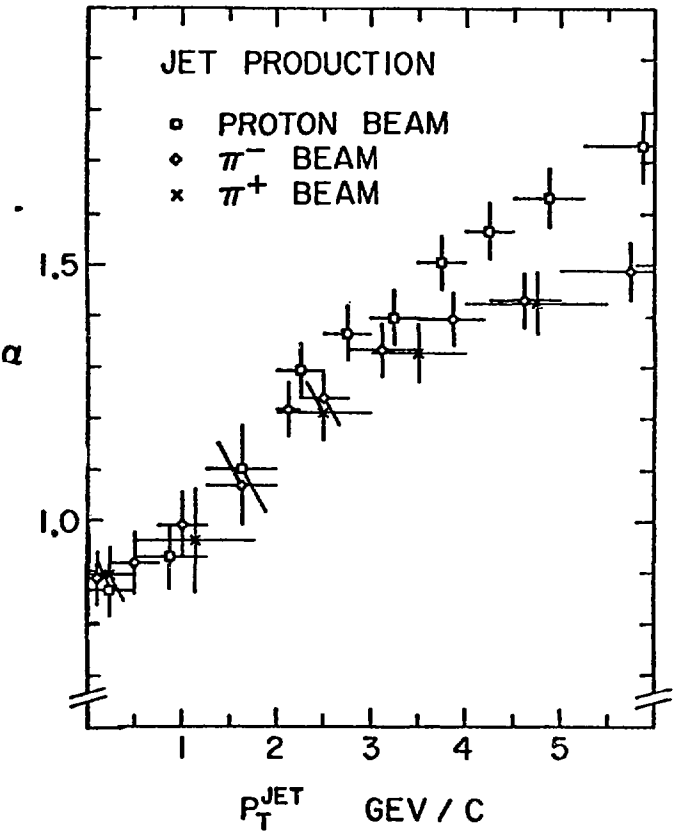
JET PRODUCTION
PROTON BEAM
π^- BEAM
π^+ BEAM
1.5
1.0
α
1
2
3
4
5
P_T^{JET} GEV / C

Fig. 26

Quark Model and High-Energy Nuclear Experiments

A. BIAŁAS
Fermi National Accelerator Laboratory, Batavia, Illinois 60510
and
Institute of Physics, Jagellonian University, Cracow, Poland

ABSTRACT

Theoretical aspects of the measurements of production of low transverse momentum secondaries in high-energy hadron-nucleus and nucleus-nucleus collisions are discussed. Applications of the quark model to those processes are discussed in some detail.

I. INTRODUCTION

As was recognized many years ago[1,2] and is now widely accepted, the interactions of high-energy hadrons with nuclear targets provide an opportunity to study the hadronic interactions at very short times. This possibility became particularly exciting, when the experimental discovery of the absence of intra-nuclear cascading of fast secondaries[2-5] indicated that hadronic physics at short distances is far different from what we normally see at macroscopic times. The detailed discussion of this phenomenon in terms of general principles of quantum mechnics and field theory was already presented in several review papers, including the classical one by Gottfried.[6-9] I shall not report the details here, but just indicate the main idea.

First, let me emphasize that the absence of intra-nuclear cascading of secondaries implies that the fast secondary hadrons are created outside of the nucleus. Indeed, were they present inside the nuclear matter, they would interact and induce cascade. This long-time character of "hadronization" can be interpreted as a consequence of uncertainty principle:[1,2,7,10,11] The minimal time necessary to emit a slow hadron is of the order $\tau_0 \gtrsim 1/E_0$, where $E_0 \gtrsim \sqrt{p_\perp^2+m^2}$ is the energy of this hadron. For an observer in laboratory frame this time becomes Lorentz-dilated and the hadron will show up after

$$t \gtrsim \cosh y \, \tau_0 \gtrsim \frac{E}{p_\perp^2+m^2} \qquad (1.1)$$

where y'E, p and μ are rapidity, energy, transverse momentum and mass of the hadron. t is very long for typical high-energy, low transverse momentum secondaries. Thus fast hadrons are created well outside the nucleus and, consequently, do not cascade.*

This argument shows that the absence of intra-nuclear cascading is a very natural phenomenon in any theory which contains uncertainty principle—in particular in any field theory.[1,2]

It should be stressed that the absence of intra-nuclear cascading is really of paramount practical importance for all discussions of interactions in nuclei, because it enables a relatively simple interpretation of the experiments and allows possible deductions about elementary hadronic interactions. With cascading present, it would be extremely difficult, if not impossible, to dig out the signal out of noise.

Since we know already that the hadrons are not present in the nucleus, we have to confront the next problem: what is the nature and properties of the intermediate state travelling through the nuclear matter. There is yet no final answer to this question. Actually, this is the "hot" issue at the moment and several different models are being considered.

---

*This argument implies also a very specific time-ordering of multiparticle production (slow particles are created earlier than fast ones). For discussion of this point see Refs. 12 and 13.

Most of the models[7,14-26] attempted to describe the existing nuclear data in terms of general properties of hadronic interactions, as derived from high-energy experiments. Thus, in a way, they try to omit the problem of the intermediate state and concentrate on those aspects of nuclear scattering which are independent, or weakly dependent on it. Those investigations showed that, indeed, the gross features of particle production from nuclei can be understood in terms of few parameters describing hadron-hadron inelastic collisions. They played an important role in finding regularities in the data. On the other hand, such a general description has necessarily a limited predictive power.*

Another approach, first considered by Goldhaber[27], and developed independently by several other groups[28-34] emphasizes the relation of the observed A-dependence of the spectra to the structure of the intermediate state which in turn is related to the structure of the incident high-energy hadron. This has the attractive feature that, if indeed such a relation is established, one may use the nuclear data for learning about the structure of high-energy hadrons. In the present talk I shall mostly concentrate on the recent investigations in this direction. I shall argue that, indeed, the nuclear experiments do provide interesting information on the structure of the incident high-energy hadrons.

---

*A notable exception is model of Ref. 22.

The intuitive picture which leads to this conclusion is as follows. The incident high-energy hadron can be viewed as a bound state of some numbers of constituents. Consider first its interaction with "elementary" say, proton, target (Fig. 1). In the "soft" — low momentum transfer — inelastic collision this hadronic bound state is destroyed. However, the nature and momentum distribution of hadronic constituents is not expected to change considerably just because the momentum transfer in the collision is small. Thus the constituents continue moving along the direction of the initial hadron, until they change into ordinary hadrons, with the lifetime

$$\tau(\gamma) = \gamma \tau_0 \qquad (1.2)$$

where γ is the Lorentz factor of the constituent and τ_0 a characteristice lifetime, as measured in rest frame of the constitutent.[12,13]

Consider now the same process happening inside the nuclear matter, as depicted in Fig. 2. In such a case the hadronic constituents move through the nuclear matter and can interact with it. This interaction implies the A-dependence of the process. Thus by measuring A-dependence of final spectra we can obtain information on interaction of hadronic constituents inside the nuclear matter and from that deduce their properties. The important parameter in the description of this final-state interaction is the constituent lifetime $\tau(\gamma)$ given by Eq. (1.2). Indeed, the argument presented here works only for constituents which $\tau(\gamma)$ is greater than nuclear

dimension, that is, the energetic constituents. The low-energy constituents have a big chance of decaying into hadrons inside the nucleus and consequently to induce some cascading phenomena inside the nuclear matter. Thus measurements of intra-nuclear cascading of slow secondaries can give information on lifetime of the hadronic constituents. This is an exciting possibility, but its discussion goes beyond the scope of the present paper.

It is worth it to emphasize that in such an approach the nucleus is treated as a part of apparatus — a kind of detector which (due to its extremely high time resolution), helps to observe phenomena non-accessible to ordinary detectors used in high-energy physics.* We are thus interested in details of nuclear structure only as far as they are necessary to understand the response of our detector. In most applications till now it seems justified to treat nucleus as a collection of quasi-independent nucleons. This description shall be used here.† It should be remembered, however, that, with increasing accuracy of the experiments it may be necessary to go beyond this approximation.

Let me add another remark which seems necessary to avoid misunderstanding. When I talk here about the "constituents"

---

*Indeed, the time resolution of a nucleus is of the order of average distance between nucleous $\sim$ 2fm $\sim 10^{-17}\mu$ sec! This fantastic time resolution is the main advantage of using nuclear targets.

†For other possibilities of treating the nucleus, see Ref. 35.

I do not necessarily mean "elementary constituents", like partons (although I would not like to exclude this possibility, as discussed in the last section). Indeed, the number and the nature of effective hadronic constituents, as seen in low-momentum transfer experiments may be actually very different from the elementary partons seen in deep inelastic processes. This is so because we are testing here hadrons on a very long-term scale compared to the one relevant to the large Q^2 phenomena. Thus we are sensitive to the soft interactions between the partons which may well build up important correlations, e.g., clustering effects. The possibility of uncovering such long-time correlations between partons is one of the attractions of the nuclear experiments at low momentum transfers.

The time available does not allow me to cover also another very exciting subject, namely large transfer processes in nuclear matter. Some aspects of this problem are discussed in Ref. 33 and in contribution of S. Brodsky to this meeting.

The structure of this talk is as follows. In the next section we describe results of a "measurement" of the number of independent high-energy constituents inside the incident energetic hadron.

In Section 3, various tests of the additive quark model are discussed. Nucleus-nucleus interactions are discussed in Sec. 4. In the last section, an attempt is made to interpret the obtained results in terms of the interactions of colored quarks and gluons.

II. MEASUREMENT OF THE EFFECTIVE NUMBER OF HADRONIC CONSTITUENTS

In this section, I shall discuss what the nuclear data can tell about the effective number of constituents contained in the incident hadron. In particular, I shall argue that: (a) the A-dependence of particle production in the central rapidity region is sensitive to the number of constituents in the incident hadron and (b) the data indicate that the effective number of constituents in nucleons and pions is equal to the number of constituent quarks in them, i.e., respectively 3 and 2.

The argument runs as follows.[28] Consider a hadron h made out of N_h independent constituents. The requirement of independence means that we do not like to consider as different the constituents which are strongly correlated to each other.* When hadron h scatters off the hydrogen target, some number (W_H) of these constituents (at least one) undergo inelastic collisions (Fig. 3a), and produce particles. We call them "wounded" constituents. Since the constituents are independent, the observed average multiplicity $\bar{n}_{hH}$ of the production process is

$$n_{hH}(y) = W_H \cdot n_W(y) \qquad (2.1)$$

where n_W is the multiplicity produced by one wounded constituent, and y is the rapidity of the observed hadron.

---

*This may be considered as a definition of a "constituent".

Consider now interaction of the hadron h with nucleus A. In this case the number of wounded constituents W_A may be substantially larger (Fig. 3b) because the hadron can interact with several nucleons in the target. Consequently, the average multiplicity $\bar{n}_{hA}$ in the production process with nuclear target

$$n_{hA}(y) = W_A \cdot n_W(y) \qquad (2.2)$$

is expected to be greater than $n_{hH}(y)$.

For the ratio $R_A(y) \equiv n_{hA}(y)/n_{hH}(y)$ we thus obtain

$$R_A(y) = \frac{W_A}{W_H} \quad . \qquad (2.3)$$

The derivation of this formula contains an implicit assumption that production of particles by one wounded constituent is approximately independent of the target. This seems to us a reasonable working hypothesis. Intuitively, it corresponds to the idea that the target can influence the production of only those particles which are created during the passage of the projectile through the target, i.e., only slow particles in the target fragmentation region. Since the bulk of the production in central rapidity region takes place long after the constituent passed through the target, there should be virtually no A-dependence in this region. However, we certainly do not expect the formula (2.3) to be valid in the target fragmentation region. For more detailed discussion of this assumption we refer the reader to the Ref. 27 and Sec. 5.

The right-hand side of the Eq. (2.5) can be expressed by the cross-sections of the constituent. We obtain[28,36]

$$W_A = \frac{N_h \sigma_{cA}}{\sigma_{hA}} \quad ; \quad W_H = \frac{N_h \sigma_{cH}}{\sigma_{hH}} \tag{2.4}$$

where σ's are inelastic, nondiffractive cross-sections. Using these formulae we obtain from (2.3)

$$R_A(y) = \sigma_{hH}\sigma_{cA}/\sigma_{hA}\sigma_{cH} = \nu_{hA}/\nu_{cA} \tag{2.5}$$

where ν_{hA} is the average number of collisions of the projectile h in the nucleus A:

$$\nu_h = A\, \sigma_{hH}/\sigma_{hA} \tag{2.6}$$

The only unknown parameter is now σ_{cH}, the inelastic cross-section of the hadronic constituent on hydrogen. However, we know that the hadron h is made of N_h constituents and thus we expect*

$$\sigma_{cH} \simeq \frac{1}{N_h}\, \sigma_{hH} \tag{2.7}$$

Using (2.4) we obtain immediately $w_H \simeq 1$. Furthermore, σ_{cA} can be calculated using (2.7) and the Glauber model formula

---

*This relation is only approximate. We have checked that the 10% correction to the formula (2.7) does not change the conclusion of this section. However, they may be not negligible if more detailed analysis of the data is attempted.

$$\sigma_{cA} = \int d^2b \; 1 - \left\{(1 - \sigma_{cH} D_A(b))^A\right\} \qquad (2.8)$$

where $D_A(b) = \int_{-\infty}^{\infty} \rho_A(b,z)\vec{dx}$ and $\rho(\vec{r})$ is the nuclear density. Consequently, we can calculate W_A and R_A in the central rapidity region.

In Fig. 4, the plot of R_A versus ν_{pA} is shown for incident nucleons for different values of number of constituents N_p. The inelastic nucleon-nucleon cross-section was taken 30 mb. The most striking feature one can see in this figure is that, for heavy nuclei, there is quite a dramatic dependence of predicted R_A on the assumed number of constituents N_p in the incident nucleon. It is just this strong N_p dependence which makes possible the determination of N_p from nuclear data. The data from Busza, et al.[35] are also shown in this figure. It is clear that they favor the choice $N_p = 3$, which coincides with the number of quarks inside the nucleon[38,39].

In Fig. 5 we are repeating the same exercise for pion beam. Again R_A is plotted versus $\nu_{\pi A}$ for different N_π. Although the data[5,38] are much more scarce than in the previous case, one can see a clear indication that $N_\pi = 2$, again coinciding with the number of quarks in the pion.

These results are very appealing, because they suggest that in the low momentum transfer phenomena the constituent quarks play the essential role. This could possibly be interpreted as evidence for strong cluster-like correlations between the wee partons and valence quarks. That is to say,

the wee gluons and $q\bar{q}$ pairs are not independent, but are clustering around the valence quarks. It should be noticed that such a picture was advocated on different grounds sometime ago by Leningrad group[40,41] and by Cabibbo et al.[41] Another possible interpretation is discussed in the last section.

One more remark may be in order here. All the conclusions we have reached about number of constituents are based on data on average multiplicities. Consequently, we can only say that on the average the number of constituents in hadron is equal to the number of quarks. To answer the problem of whether they are actually equal, it is necessary to analyze the multiplicity fluctuations which shall give information on dispersion of the distribution of number of constituents. No such investigation was carried out so far.

In the next section we shall consider the quark model in more detail and show that it gives many interesting predictions which may be tested in future experiments.

III. FURTHER CONSEQUENCES OF THE QUARK MODEL

A. Particle Production by Different Hadrons

Generalizing slightly the arguments of the preceding section and assuming that a wounded strange quark produces the same rapidity plateau as a wounded nonstrange quark*

*This assumption is supported by the experimental observation[43] that particle multiplicity in Kp interactions is similar to that in πp interactions.

one arrives at the following predictions for A-dependence of particle production by different beams:

$$\begin{aligned}
&\text{K beam} && R_A = \frac{\sigma_{QA}+\sigma_{\quad}}{\sigma_{KA}} \\
&\phi && R_A = \frac{2\sigma_{QA}}{\sigma_{\phi A}} \\
&\Sigma \ \& \ \Lambda && R_A = \frac{2\sigma_{QA}+\sigma_{SA}}{\sigma_{\Lambda A}} \\
&\Xi && R_A = \frac{(\sigma_{QA}+2\sigma_{SA})}{\sigma_{\Xi A}}
\end{aligned} \qquad (3.1)$$

where σ_{QA} and σ_{SA} are inelastic, non-diffractive cross-sections of non-strange and strange quarks. These predictions are plotted (together with those for proton and pion beams given in previous section) in Fig. 6 versus the so called "average number of collisions" ν_{hA} given by Eq. (2.6).

The inelastic cross-section of strange quark σ_{SH} was taken 4.5 mb [44] and generalization additivity rule (2.7) was used to calculate hadronic cross-sections from hydrogen. The nuclear inelastic cross-sections needed to calculate the number of wounded quarks were estimated from the Glauber model formula (2.6).

A characteristic feature seen in Fig. 6 is that the points cluster around the two well-separated lines, one for baryons and one for mesons. This again indicates that the only essential parameter is the number of constituents in the incident hadron. The measurements of particle production in central region by hyperon beams would be thus very useful for testing the ideas advocated here.

There is one particularly interesting case which is worth mentioning separately. If indeed the additivity rule works for Ξp cross-section, we expect $\sigma_{\Xi H} = \sigma_{QH} + \frac{1}{2}\sigma_{SH} \approx 19$mb. One notices that this is very close to the πp inelastic non-diffractive cross-section (∿20 mb). Thus we have two different projectiles with very similar cross-sections in hydrogen (and, consequently, also in nuclei). As seen from Fig. 6, however, the expected A-dependence of particle production is quite different in the two cases: the cascade baryon, having more constituents, should exhibit more A-dependence. This should be contrasted with predictions of the models which relate the A-dependence of particle production to the cross-section (or number of collisions) of the projectile.[18,22] Indeed, if the cross-section is the only relevant parameter, then A-dependence should be the same for Ξ and π beam. Thus the comparison of π and Ξ induced reactions in nuclei should provide a decisive test of the idea that the structure of the incident hadron is important for those phenomena. This observation is clearly much more general than a specific model we are exploring here.

B. Projectile Fragmentation Region

The results we were discussing until now are expected to be valid in the central region of rapidity. It is obviously quite important to analyze what happens outside of this region. Typical data showing projectile fragmentation region are shown in Fig. 7.[45]

Before further discussion, it is important to emphasize

that, whereas the results for the central region depend essentially only on the number of hadronic constituents, the projectile fragmentation region is much more sensitive to the details of the mechanism of the hadron formation. This gives more ambiguity in the predictions but, at the same time, provides opportunity of testing different mechanisms of the transition from hadronic constituents to hadrons.

Basically, two different approaches were considered: (a) decay and/or recombination of spectator quarks and (b) collective fragmentation model.

Let me now discuss their characteristic predictions.

(a) Spectator Quark Fragmentation Model

It was noted by Anisovich, et al.[31] that the important source of secondaries in projectile fragmentation region may be the decay of spectator constituent quarks which did not take part in the interaction (did not get wounded, in our language). This is because those spectator quarks have a tendency to be faster than the wounded ones (They do not lose energy for emitting secondaries in the central rapidity region.). If this is indeed the case, one immediately concludes that the number of particles produced in the projectile fragmentation region should be decreasing with increasing A. This is illustrated in Fig. 8.

An estimate of such effects in Ref. 31 was shown to agree with the data at 20 & 24 GeV.[16] A similar model was recently discussed in Ref. 47 where many additional relations were

derived and some of them compared successfully with the data.

If one assumes a specific model for spectator quark recombination functions, many predictions can be obtained. Nikolaev and collaborators[9,48] discussed this problem extensively using the quark recombination model[49] as a guideline.*

Actually, I feel that the situation in the fragmentation region is slightly more complicated than presented in Refs. 31, 47, 48. Since the quarks do not have fixed momentum, fast wounded quarks can contribute to particle production in the projectile fragmentation region, and one should consider both contributions.

For the incident mesons we can thus write simply

$$n_A(y) = w_A n_w(y) + (N_h - w_A) n_{sp}(y) \qquad (3.2)$$

where $N_h - w_A$ is the number of quarks which did not get

---

*Although most of the data was satisfactorily described by authors of Ref. 9,48, it seems that the new data of Ref. 50 give an evidence against the recombination model, as used by them. As noted by Nikolaev, et al.,[9,48] according to the recombination model, there should be a dramatic difference between the A-dependence of spectra for secondary particles which do have common quarks with the incident one and those which do not have common quarks; since the latter cannot be produced by recombination of spectator quarks, they should have always $R_A > 1$, i.e., their production should increase with increasing A. This prediction is strongly violated by data of Ref. 50 which shows identical A-dependence for Λ and $\bar{\Lambda}$ production (both having $R_A < 1$ for $x > .2$). Let me emphasize that the data of Ref. 50 do not contradict the general quark model formula, but only a simple recombination model for $n_{sp}(y)$ used in Refs. 9 and 48.

wounded and $\bar{n}_{sp}(y)$ is the multiplicity of secondaries produced by one such a spectator quark* Since w_A increased with A and $n_{sp}(y)$ is independent of A, this term must decrease with A. This is shown in Fig. 9.[51]

On the other hand, the first term in the R.H.S. of Eq. (3.2) increases with A, provided that, as we always assume, $n_w(y)$ is independent of A.[27,28] Since we do not know the exact form of $n_w(y)$ and $n_{sp}(y)$, it is not possible to predict exactly the A-dependence of the spectrum. However, it is interesting to observe that the Eq. (3.2) implies that the particle density is a linear function of the average number of wounded quarks:

$$n_A(y) = N_h\, n_{sp}(y) + w_A\left(n_w(y) - n_{sp}(y)\right) . \qquad (3.4)$$

Thus the spectator quark model suggests a very specific parametrization of A-dependence. It would be interesting to test this parametrization and use it for determining quark decay functions $n_w(y)$ and $n_{sp}(y)$.[51]

The formula (3.2) has many consequences for quantum numbers of the observed final particles. This is because the A-dependence of the spectra shall reflect $n_w(y)$ and $n_{sp}(y)$ which are expected to be different for different quarks and different detected particles. This should not affect the predictions of the model in the central rapidity region,

---

*For incident baryons the formula becomes more complicated, because it is necessary to account for the probability that two spectator quarks recombine to make one final baryon.[31,47] For more detailed discussion, see Ref. 51.

which is dominated by $n_w(y)$ and thus insensitive to quantum numbers of final particles. However, as we move towards the projectile fragmentation region the interesting effects may appear. The exact predictions depend on the form of the quark fragmentation functions $n_w(y)$ and $n_{sp}(y)$, and are therefore ambiguous. I would rather advocate using the experimental data in order to extract the quark decay functions and try to understand their systematics.[51]

(b) Collective Fragmentation Model

It is by no means obvious that the quarks contribute independently to the particle production in the projectile fragmentation region, as assumed in the spectator quark model. One may actually argue that, since they happen to be very close in phase-space, they may interact strongly before changing into hadrons, and therefore one cannot neglect the collective phenomena.* Such a point of view seems less attractive than the one advocated in Ref. 31, because it does not give so many specific predictions, at least as long as we cannot calculate these collective effects. It is, nevertheless, interesting to try to estimate what are the expectations from such a collective fragmentation model, in order to contrast them to the other one. This problem was discussed in Ref. 29.

---

*A simple example of the model which may lead to such a picture is the Low model of high-energy interaction of hadron bags.[52] In this model contribution to the projectile fragmentation region comes from the decay of the whole hadron bag and is not necessarily a sum of contributions from the individual quarks.

Since nothing is known about the collective phenomena in the fragmentation of the fast hadron, the authors of Ref. 29 took the extreme point of view, namely that in the fragmentation region all the memory of the quark structure is lost and the distribution of final particles is just governed by (longitudinal) phase space. Such a simplified approach can be motivated by the well-known fact that the observed spectra in hadron-hadron collisions are, to a large extent, determined by energy and momentum conservation laws.[53] In particular, the simple longitudinal phase-space (including cluster production and leading particles[54,55]) seems to be a very good description of bulk of hadronic production at small transverse momenta.

It was shown in Ref. 29 that, although the phase-space does not influence significantly the A-dependence of the spectra in the central region, it does modify it strongly in the fragmentation region of the projectile. As a matter of fact, the phase-space itself can explain a large part of the decrease of spectra with increasing A at high rapidities (see Fig. 7).

Qualitatively, it is rather straightforward to see that if the spectrum increases with increasing A in the central region, it must decrease in projectile fragmentation region.[56] Simply, since there are more particles produced in the central region, there is not enough energy left to produce very fast particles and the fragmentation decreases. A

typical result of the phase-space calculation[29] for A-dependence of the spectrum is shown in Fig. 10 for 300 GeV incident neutrons, together with data of Ref. 45. It is seen that there is only very little modification in the central region at this energy. It is also seen that the phase-space prediction follows the data quite closely in the projectile fragmentation region. This indicates that the fragmentation region is fairly well described by kinematic effects, provided the central region density is correctly chosen. It follows that it may not be easy to disentangle different mechanisms of particle production in this region, without detailed investigation of the quantum number correlations (the phase-space corrections are sensitive only to the masses of the produced particles and not to other quantum numbers).[29*]

C. Comparison With Other Models

Let me close this section with a few remarks about comparison of the quark model with some other models of particle production from nuclei.

a. The eikonal model predicts that for every projectile h

*This observation leads to a striking prediction that A-dependence of the spectra should be the same for particles and antiparticles. It is actually quite well confirmed by data for Λ and $\bar{\Lambda}$. I would like to thank K. Doroba for pointing out this data to me.

$$R_A = f(A)\ \nu_{hA}, \tag{3.5}$$

where f(A) is universal function of A, which does not depend on projectile h[18]. Although the Eq.(3.5) looks similar to our Eq.(2.5), it should be noted that their consequences are quite different. In Eq.(2.5) the coefficient $1/\nu_{cA}$ which multiplies ν_{hA} does depend on the nature of the projectile h (because the quark content may be different for different projectiles). This is an important point because, if Eq.(3.5) is applied to projectiles with very small cross sections on nucleons (e.g. heavy vector mesons), it implies* $f(A) \simeq 1$. Since f(A) does not depend on projectiles we recover the well-known result of the standard eikonal model

$$R_A = \nu_A, \tag{3.6}$$

which is in clear contradiction with the data, as seen e.g. in Fig. 3.

b. The model of Ref.24 expresses R_A as an integral over parton energy distribution. The authors calculated R_A for 200 GeV incident protons. It is plotted in Fig. 11, together with our calculation (Eq.2.5) for comparison. One sees that the results are close and differ substantially

*The condition $\sigma_{hH} \to 0$ implies $\nu_{hA} \to 1$, independently of A.

only at large A. At higher energies the model of Ref. 24 predicts further increase of R_A, so that the difference is expected to grow. The data at present[5] cannot clearly distinguish the two models, although the quark model seems slightly favored.

c. The model of Ref. 22 gives a simple formula for R_A.

$$R_A(y) = \bar{\nu}_{hA}(\tfrac{1}{2} - \tfrac{y}{Y}) + \{1 - (\tfrac{1}{2} - \tfrac{y}{Y})\bar{\nu}_{hA}\} \qquad (3.7)$$

where y is the cm. rapidity, and Y is the length of the central region at a given energy. To compare with the data, we integrated the formula (3.7) for $3 \leq y_{lab} \leq 4$ at 200 GeV incident momentum ($y_{lab} \simeq 3 + y_{cm}$). The results are sensitive to the choice of Y. In order to obtain agreement with the data Y has to be chosen $\lesssim 3$, which seems to be a little low, since the full length of the rapidity interval for pions at this energy exceeds 3 units. The results for Y=3 are plotted in Fig. 11.

D. Modified Cascade Model[25]

Finally, the results of the modified cascade model of Ref. 25 are plotted in Fig. 11. It is seen that they agree very well with the data of Ref. 5.

My general impression is that there is still much work to be done before one will be able to decide finally which model is the right one. At present the high energy data are rather scarce and no comprehensive critical comparison

with models was done. For more detailed discussion of different models, the reader is referred to Ref. 9.

IV. NUCLEUS-NUCLEUS INTERACTIONS

A. Central Rapidity Region

A good part of the argument of the previous sections can be generalized to include the nucleus-nucleus collisions.

Consider first the central rapidity region.[28] Let nucleus A be incident at high energy on a target. We first calculate the ratio $n_{AB}(y)/n_{AH}(y)$ of multiplicities when targets are nucleus B and hydrogen. According to the model of Ref. 28, this ratio is equal to the ratio of the number of wounded quarks in A for those two cases. Thus we have

$$\frac{n_{AB}(y)}{n_A(y)} = \frac{W_{AB}}{W_A} = \frac{N_A\sigma_{qB}}{\sigma_{AB}} : \frac{N_A\sigma_q}{\sigma_A} = \frac{\sigma_A\sigma_{qB}}{\sigma_{AB}\sigma_q} \tag{4.1}$$

where N_A is the total number of quarks in nucleus A; σ_q and σ_A are quark-nucleon and A-nucleon inelastic nondiffractive cross-sections. Using now Eq. (2.5) we obtain for the ratio $R_{AB}(y)$

$$R_{AB}^{\text{central}}(y) \equiv \frac{n_{AB}(y)}{n_{HH}(y)} = \frac{\sigma_H\sigma_{qA}\sigma_{qB}}{\sigma_{AB}\sigma_q^2} = \frac{\nu_{AB}}{\nu_{qA}\nu_{qB}} \tag{4.2}$$

there ν_{AB} is the total number of inelastic nucleon-nucleon collisions in A+B scattering

$$\nu_{AB} = \frac{AB\ \sigma_H}{\sigma_{AB}} \tag{4.3}$$

and ν_{qA}, ν_{qB} are number of collisions of quarks in A and B, given by Eq. (2.6). The numerical estimates of Eq. (4.2) are shown in Fig. 12 for different beams and target nuclei. It is seen that the results depend mainly on the product A,B. The most amazing feature seen in Fig. 12 are the large values of multiplicities which can be obtained in scattering of heavy nuclei. This indicates that the extrapolation one makes from nucleon-nucleus to nucleus-nucleus case is rather considerable. It would be indeed surprising if it would survive precise experimental tests.

Equation (4.2) was found to be compatible with cosmic ray data.[29] For comparison also the prediction from the model of Ref. 22 is plotted in Fig. 12. It is seen that the two models differ substantially only for collision of two very heavy nuclei.

The formula (4.2) is a generalization of Eq. (2.5) for nucleus-nucleus collisions. As Eq. (2.5), Eq. (4.2) is also expected to be valid in the central region of rapidity. This may mean very high energies, because at low energies the plateau is simply not present.

It is therefore of importance to analyze the projectile fragmentation region which most probably dominates the data at present energies. Unfortunately, this involves understanding of the processes of nuclear fragmentation and intra-nuclear cascading of slow secondaries (in nucleus rest frame), and thus appears to be fairly complicated.

No detailed discussion of this problem exists, therefore I shall restrict myself to few remarks.

B. Target Fragmentation Region

Consider first a special case of target fragmentation region in nucleon-nucleus collisions. A simple picture of multiple scattering inside nucleus suggests that multiplicity in this region should be approximately ν_{hA} times that in hydrogen. The possible cascading phenomena and Fermi motion effects[57] modify this simple prediction, but hopefully only in close neighborhood of the phase space limit. Indeed, in the region $y \lesssim 0 \lesssim 2$ the formula

$$n_A = \nu_{hA} n_H \tag{4.4}$$

works quite well,[5,38,58] supporting the picture of target nucleons interacting independently with the projectile.

If we follow the picture of the spectator fragmentation model, as described in the previous section, the general formula for multiplicity distribution in hadron-nucleus collisions should be written as*

$$n_A(y) = 2\nu_{hA} n_{sp}^{(-)}(y) + w_A n_w(y) + (3-w_A) n_{sp}^{(+)}(y) \tag{4.5}$$

where $n_{sp}^{(-)}(y)$ is the contribution from a spectator quark in the target and $n_{sp}^{(+)}$ is the contribution from a spectator quark in the beam. $n_w(y)$ is the contribution from wounded quarks. For y in the fragmentation region of the target this contribution is probably depending on A (proportional to ν_{qA}), so that the formula (4.4) is recovered in this region.

*To simplify our semi-quantitative discussion, we neglect the difference between decay of spectator quarks and diquarks. A more general formula can easily be written down.[51]

It should be stressed again that Eq. (4.5) probably underestimates the multiplicity in target fragmentation region, where cascading is expected to occur and where the data do indeed show multiplicity rising faster than ν_{hA}.[5] It is not clear to me at the moment what shall be the consequences of the internal motion inside the nucleus, but this effect can probably be estimated.[57]

We may ask now what is the proper generalization of the formula (4.5) for the target fragmentation in nucleus-nucleus collisions. As far as I can see, the most likely possibility is that multiplicity is proportional to the number of spectator quarks in wounded nucleons in the target. Thus we obtain for collision B + A

$$n_{AB}(y) = W_A^N(3-w_B)n_{sp}^{(-)}(y) + R_{AB}^{central}n_W(y) + \\ + W_B^N(3-w_A)n_{sp}^{(+)}(y) \qquad (4.6)$$

where W_A^N and W_B^N are numbers of wounded nucleons in A and B, respectively and $R_{AB}^{central}$ is given by Eq. (4.2). $n_{sp}^{(-)}$ is the contribution from a spectator quark in the target (A) and $n_{sp}^{(+)}$ that is beam (B) nucleus. Again, it should be pointed out that $n_W(y)$ may depend on A and B in the fragmentation regions, so no easy predictions are possible in general. Also the remarks about cascading phenomena and internal nuclear motion which I made before apply here as well.

With all of these caveats in mind, it is still interesting to see how the contribution from fragmentation region compares with that of central region, given by Eq. (4.2). Neglecting the central region we obtain

$$n_{AB}(y) \approx W_A^N(3-W_B)n_{sp}^{(-)}(y) + W_B^N(3-W_A)n_{sp}^{(+)}(y) \qquad (4.7)$$

If we assume that $n_{sp}^{(+)}(y)$ gives contribution only to forward hemisphere and $n_{sp}^{(-)}(y)$ only in backward hemisphere we obtain for integrated multiplicities

$$n_{AB} = \tfrac{1}{2}\{W_A^N(3-W_B) + W_B^N(3-W_A)\}n_H \qquad (4.8)$$

where n_H is multiplicity in proton-proton collision. The first term comes from the target (A) hemisphere and the second term from the beam (B) hemisphere. The ratio $R_{AB} \equiv n_{AB}/n_H$ obtained from Eq. (4.8) is plotted in Fig. 13. One sees that the obtained multiplicities are substantially lower than the ones from Eq. (4.2) (Fig. 12).* Thus, one expects ratio R_{AB} to increase with increasing energy, as the central region becomes more and more important.

V. OUTLOOK

I tried to argue in this talk that the constituent quark model provides a successful phenomenology of hadron-nucleus collisions at low momentum transfers. The natural next question is if this success can be understood in terms of a more fundamental theory. I shall close my lecture by some spectulations on this subject.

*If the diquark recombination into baryons is not neglected,[51] the obtained multiplicities are expected to be even lower than those seen in Fig. 13.

First let me emphasize again an important ingredient in our treatment of the quark model[27,28]: to obtain agreement with data it was necessary to assume that, in the central region of rapidity, radiation of particles from a "wounded" quark is independent of the target, i.e., of the number of scatterings it suffered from the target. This assumption looks fairly natural in the laboratory frame, where quark is fast and nucleus is at rest. Consider, however, the situation in the rest frame of the projectile.[28] In this frame, nucleus is bombarding the hadron with large energy and now quarks in the nucleus radiate final particles. If we like to be consistent we have to assume that total radiation from all quarks in the projectile nucleus which interacted with just one given quark in the hadron target is the same as from one quark. This is so because amount of radiation in the central region obviously cannot depend on the frame of reference we are choosing. When stated that way, this phenomenon is clearly much more difficult to understand. One possibility of understanding it is to notice that in the anti-laboratory frame the nucleus shrinks because of Lorentz contraction. Consequently, all constituen quarks which have the same impact parameter actually cannot be distinguished and behave as a single quark. The consequences of this effect were first described by Kanchelli[15], who argued that in such a case radiation is independent of the size of the target

*Kanchelli applied this argument to hadrons (not to quarks) and consequently obtained $R_A=1$ in the central region.

Another possibility, perhaps more attractive, is to observe that a similar phenomenon occurs if particle production at high energy is described by exchange of color gluons between colored quarks as suggested by Low.[52] In the Low model particle production occurs long after the exchange of gluons takes place and is caused by necessity to rearrange color in the final state so that two color octet states which move with high velocity in opposite directions do not show up as real particles. This amounts to breaking of the colored gluon "string" which connects the two octets (Fig. 14). The multiplicity of hadrons created in this way is likely to depend only on the amount of color in the "string", at least in the central region, not too close to the ends of the string. Now, the important point to observe is that in scattering from a single quark only two color exchanges are possible, independently of the number of scatterings: singlet and octet. Singlet exchange leads to diffractive interactions which we are not discussing here. This leaves us with unique possibility of octet exchange. Consequently, we indeed expect the same multiplicity created by one quark, independently of the number of times it scatters.

This argument requires the assumption that, if the two color strings are close to each other, they shall interact and collapse into one.* This seems to me a reasonable hypothesis

*The necessity of such self-interaction between "sparks" was already recognized in Ref. 27.

because the energy of one string is clearly smaller than two separate strings with the same color content.* Finally, let me add that in this picture the actual calculations may be quite involved, because the radiation must also depend on the (transverse) distance of the quarks inside the hadron (if the transverse distance between wounded quarks in the projectile is smaller than the range of interaction of the color tubes, those two quarks shall be seen as one object with (possibly) more complicated color content).

Although the picture presented here looks fairly natural in a theory of colored quarks and gluons, it should be realized that it indicates just the possibility and not yet a developed model. The main point (apart from obvious difficulties of applying QCD for low q^2 processes) is that in the Low model it is not trivial to calculate the number of wounded quarks: the model is formulated with amplitudes rather than probabilities—strong interferences between the amplitudes expected in small q^2 region destroy the naive probabilistic interpretation.† Thus more work should still be done on this problem before final conclusions are reached. I feel however that this is a very attractive possibility of understanding high-energy nuclear scattering and relating it to the fundamental theory of strong interactions.

---

*Other possibility was discussed by S. Brodsky at this meeting.

†I would like to thank Professor F. Low for an illuminating discussion about this point.

In conclusion, let me emphasize that, although the quark model of hadron nucleus interactions at high energies is far from being proven by existing experiments, it definitely provides an attractive possibility of interpretation of the data: (i) it gives many simple predictions, (ii) it allows the extraction from data of some interesting information about hadronic constituents and finally (iii) it gives a hope to relate the hadron-nucleus interactions to fundamental theory of hadrons. I feel that it is indeed worthwhile to undertake further investigations in this direction.

ACKNOWLEDGEMENTS

Most of the ideas presented here were worked out together with W. Czyż, to whom I am indebted for constant help and encouragement. I would like also to thank T. Ferbel, F. Low and L. Voyvodic for illuminating discussions. Finally, I thank M. Gyulassy and L. Schroeder for invitation to the meeting.

REFERENCES

[1]L.D. Landau and I. Ya. Pomeranchuk, Doklady Academii Nauk SSSR, 92 (1953) 535; ibid., 92 (1953) 735; E.L. Feinberg and I.Wa. Pomeranchuk, Nuovo Cimento Supl. 4 (1956) 652; E.L. Feinberg, Zh TEF 50 (1966) 502.

[2]For complete review and other references, see E.L. Feinberg, Physics Reports 5(1972) 237.

[3]M. Mięsowicz, Progr. of Elem. Particles and Cosmic Ray Physics X (1971) 128.

[4]T. Ferbel, invited talk at this workshop.

[5]W. Bugza, Acta Phys. Pol. B8 (1977) 333.

[6]K. Gottfried, Proc. of the V Int. Conf. on High Energy Physics and Nuclear Structure, Uppsala 1973.

[7]L. Stodolsky, Proc. of the VI Symp. of Multiparticle Dynamics, Oxford (1975), p. 577.

[8]G. A. Winbow, Proc. of the VII Symp. on Multiparticle Dynamics, Tutzing (1976), p. 153.

[9]N.N. Nik aev, A. Ya Ostapchuk and V.R. Zoller, CERN preprint Th. 2561 (1978).

[10]M. Mięsowicz, Proc. of VI Int. Conf on High Energy Phys., Weimar (1960), p. 429 and private communication.

[11]D.H. Perkins, Int. Conf on Theoretical Aspects of High Energy Phenomena, CERN, 1961 (CERN 61-22) p. 99.

[12]A.S. Goldhaber, Phys. Rev. Lett. 35 (1975) 748.

[13]J. Bjorken, Lectures at DESY Summer Institute (1975).

[14]K. Gottfried, Phys. Rev. Lett. 32 (1974) 957.

[15]O.V. Kanchelli, JETP Lett. 18 (1973) 469.

[16]V.N. Gribov, JETP 26 (1968) 414.

[17]V.A. Abramovskii, V.N. Gribov and O.V. Kanchelli, Sov. J. Nucl. Phys. 18 (1974) 308; A. Schwimmer, Nucl. Phys. 394 (1975) 445.

[18] L. Caneschi and A. Schwimmer, Nucl. Phys. B102 (1976) 381.

[19]J. Koplik and A.H. Mueller, Phys. Rev. D12 (1975) 3638.

[20]N.N. Nikolaev, Phys. Lett. B60 (1976) 363.

[21]G.V. Davidenko and N.N. Nikolaev, Yad. Fiz. 24 (1976) 772.

[22]S. Brodsky, J. Gunion and J. Kühn, Phys. Rev. Lett. 39 (1977) 1129.

[23]A. Capella and A.B. Kaidalov, Nucl. Phys. B111 (1976) 477.

[24]A. Capella and A. Krzywicki, Phys. Lett. B67 (1977) 84, Phys. Rev. D18 (1978) 3357.

[25]G. Białkowski, C.B. Chiu and D.M. Tow, Phys. Lett. 68B (1977) 451, Phys. Rev. D17 (1976) 862; M. Hossain and D.M. Tow, Austin preprint, January, 1979.

[26]L. Bertocchi and D. Treleani, J. Phys. G: Nucl Phys. 3 (1977) 147.

[27]A.S. Goldhaber, Phys. Rev. Lett. 33 (1974) 47. See also V.V. Anisovich, Phys. Lett. 57B (1975) 87.

[28]A. Białas, W. Czyż, W. Furmański, Acta Phys. Pol. 88 (1977) 585.

[29]A. Białas and W. Czyż, Cracow preprint, September 1978 (to be published in Acta Phys. Pol. B).

[30]N.N. Nikolaev, Phys. Lett. 70B (1977) 95.

[31]V.V. Anisovich, Yu. M. Shabelski and V.M. Shekhter, Nucl. Phys. B133 (1978) 477.

[32]N.N. Nikolaev and V.R. Zoller, CERN preprint, Th 2516 (July 1978).

[33]A. Białas, Fermilab preprint Pub-78/75-THY, September 1978, to be published in Proc. of the IX Multiparticle Symposium, Tabor (1978).

[34]W. Czyz, Proc. of the CERN School of Physics (1978).

[35]A. Berlad, et al., Phys. Rev. D13 (1976) 161; J. Dias de Deus, Nucl. Phys. B107, (1976) 146.

[36]A. Białas, M. Bleszynski, W. Czyż, Nucl. Phys. B111 (1976) 461.

[37]W. Busza, et al., Phys. Rev. Lett. 34, (1976) 836, and paper presented at the Tbilisi Conference (1976).

[38]C. Halliwell, Proc. of the VIII Symp. on Multiparticle Dynamics, Kaysersberg (1977), p. D-1.

[39]A. Białas, Paper presented at VIII Symp. on Multiparticle Dynamics, Kaysersberg (1977), (unpublished), see also V.V. Anisovich, F.G. Lepekhin and Yu. M. Shabelsky, Leningrad preprint (1977).

[40]E.M. Levin and L.L. Frankfurt, JETP Lett. 2 (1965) 105.

[41]V.V. Anisovich and V.M. Shekhter, Nucl. Phys. B55 (1973) 455.

[42]N. Cabbibo and R. Petronzio, Nucl. Phys. B137 (1978) 395, and references quoted there. See also R. Hwa, Oregon preprint (1979).

[43] V.V. Ammosov, et al., Nucl. Phys. B58 (1973) 77.

[44] A. Białas, W. Czyż, Nucl. Phys. B137 (1978) 359.

[45] D. Chaney, et al., Phys. Rev. Lett. 40 (1978) 71.

[46] J.V. Allaby, et al., CERN preprint 70-12 (1970).
T. Eichten, et al., Nucl. Phys. B44 (1972) 333.

[47] A. Dar and F. Takagi, Technion Preprint (1979).

[48] N.N. Nikolaev and S. Pokorski, Phys. Lett. 80B (1979) 290.

[49] For recent review, see L. Van Hove, invited talk at Int. Meeting on Frontier of Physics (Singapore 1978).

[50] P. Skubič, et al., Phys. Rev. D18 (1978) 3115.

[51] A. Białas and E. Białas, to be published.

[52] F.E. Low, Phys. Rev. D12 (1975) 163.

[53] L. Stodolsky, Phys. Rev. Lett. 28 (1972) 60.

[54] J. Benecke, A. Białas and A. Kotanski, Acta Phys. Pol. B8 (1977) 931.

[55] J. Benecke, A. Białas, E.H. De Groot, Phys. Lett. 57B (1975) 447.

[56] A. Białas and L. Stodolsky, Acta Phys. Pol. B7 (1976) 845.

[57] R. Blankenbecler and I.A. Schmidt, Phys. Rev. D16 (1977), 1318 and Proc. of VIII Colloquium on Multiparticle Dynamics, Kaysersberg (1977).

[58] D.L. Burke, et al., Phys. Rev. D19 (1979) 1616.

FIGURE CAPTIONS

Fig. 1 Low momentum transfer hadron-hadron collision.

Fig. 2 Low momentum transfer hadron-nucleus collision.

Fig. 3 Interaction of hadronic constituents in hydrogen and in nucleus.

Fig. 4 R_A from Eq. (2.3) plotted versus average number of collision ν_p of protons in nuclear data from Ref. 5. $\sigma_{pp} = 30$ mb.

Fig. 5 R_A from Eq. (2.3) plotter versus average number of collisions ν_π of pions in nuclear target. Data from Ref. 38. $\sigma_{\pi p} = 20$ mb.

Fig. 6 R_A for different projectiles calculated from Eqs. (2.3) and (3.1), plotted versus average number of collisions ν_h.

Fig. 7 Data from Ref. 45 showing A dependence of negative particle spectrum in the forward hemisphere for 300 GeV neutron-nucleus interactions. Line is the result of Eq. (2.3).

Fig. 8 Spectator quark contributions to the projectile fragmentation region.

Fig. 9 A-dependence of the spectator quarks contribution to particle production for pion and nucleon beam plotted versus atomic number of the target.

Fig. 10 Longitudinal phase space calculation[29] of the A-dependence of negatives spectrum for 300 GeV neutron-nucleus collisions. Data from Ref. 45.

Fig. 11 Comparison of different models of particle production. Data from Ref. 38.

Fig. 12 Central plateau density in nucleus-nucleus collisions at high energy, $\sigma_{pp} = 32.3$ mb.[5] Closed symbols—results from quark model, calculated from eq. (4.2), Ref. 28. For comparison also results from Ref. 22 are shown.

Fig. 13 Fragmentation density in nucleus-nucleus collisions at high energy, calculated from Eq. (4.8). $\sigma_{pp} = 32.3$ mb.[5]

Fig. 14 Particle production in high-energy interactions, according to model of Ref. 52.

LOW P_T PHENOMENA

Fig. 1

NUCLEUS AS DETECTOR OF HADRONIC CONSTITUENTS

TIME RESOLUTION: 10^{-17} μ sec

LOW P_T PHENOMENA

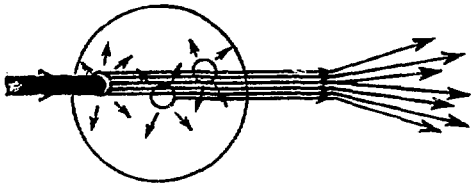

COLLECTIVE PARTON EFFECTS

Fig. 2

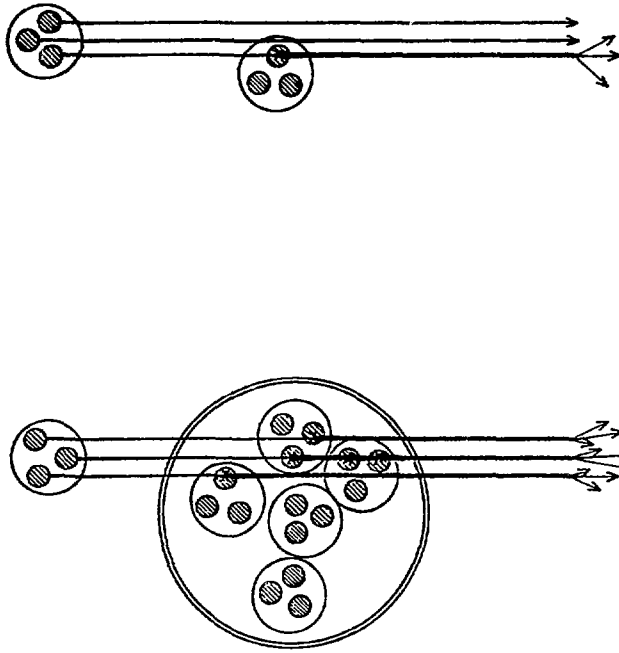

Fig. 3

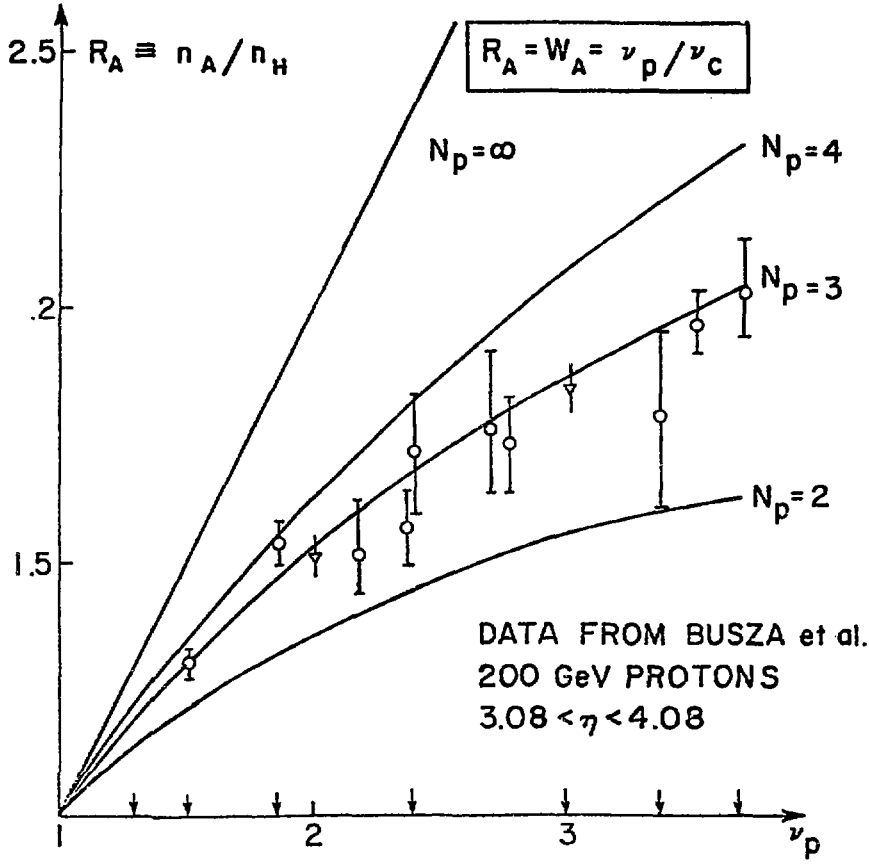
CONSTITUENT QUARK MODEL
NUCLEON BEAM
2.5
$R_A \equiv n_A / n_H$
$R_A = W_A = \nu_p / \nu_C$
$N_p = \infty$
$N_p = 4$
$N_p = 3$
$N_p = 2$
.2
1.5
DATA FROM BUSZA et al.
200 GeV PROTONS
$3.08 < \eta < 4.08$
1
2
3
ν_p

Fig. 4

CONSTITUENT QUARK MODEL

PION BEAM

$R_A = W_A = \nu_\pi \quad \nu_C$

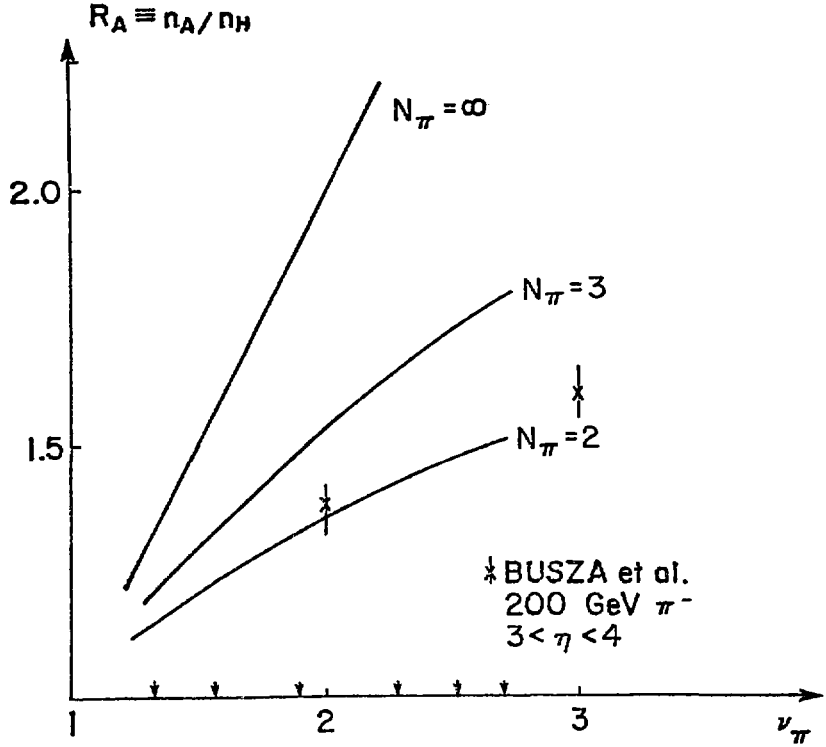

Fig. 5

CONSTITUENT QUARK MODEL

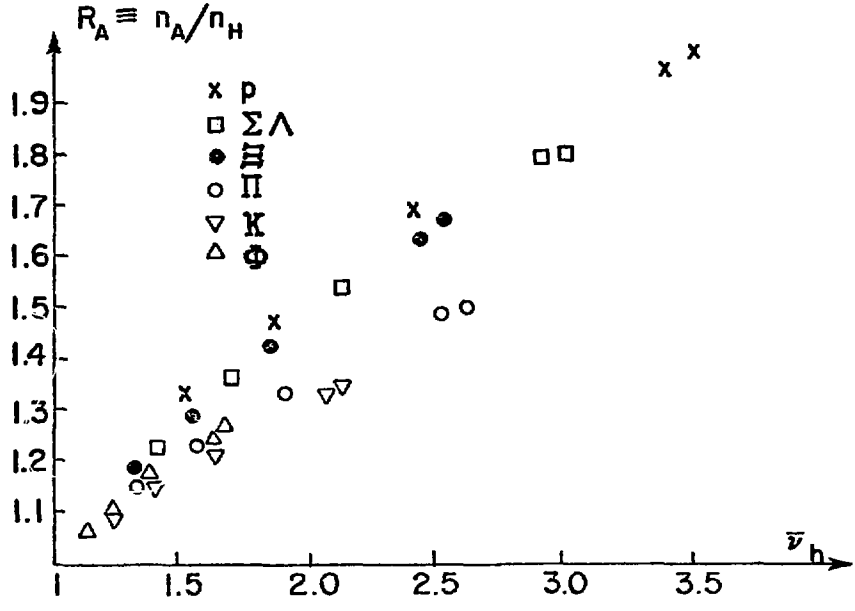

Fig. 6

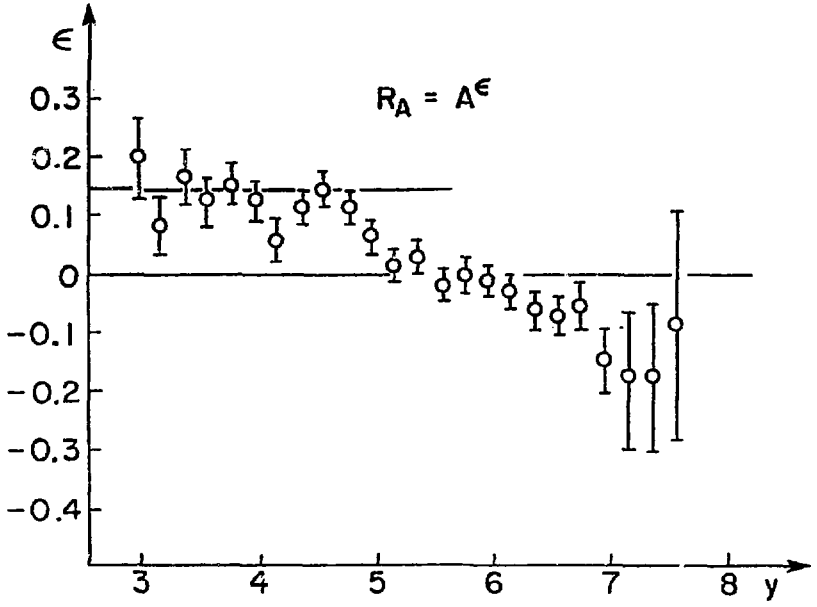

Fig. 7

PROJECTILE FRAGMENTATION REGION

ANISOVICH, SHABELSKY AND SHEKHTER N.P.B133 (1977)

N. NIKOLAEV, P.L. 70B (1977) 95.

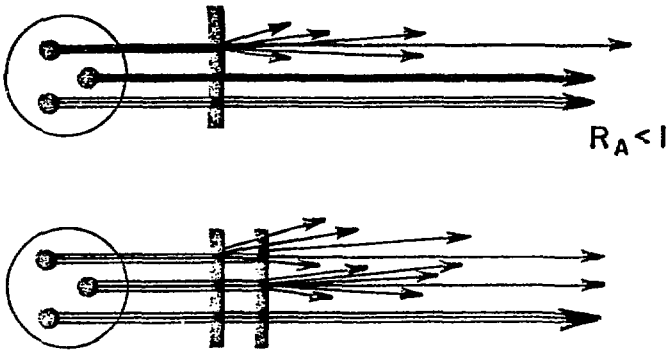

Fig. 8

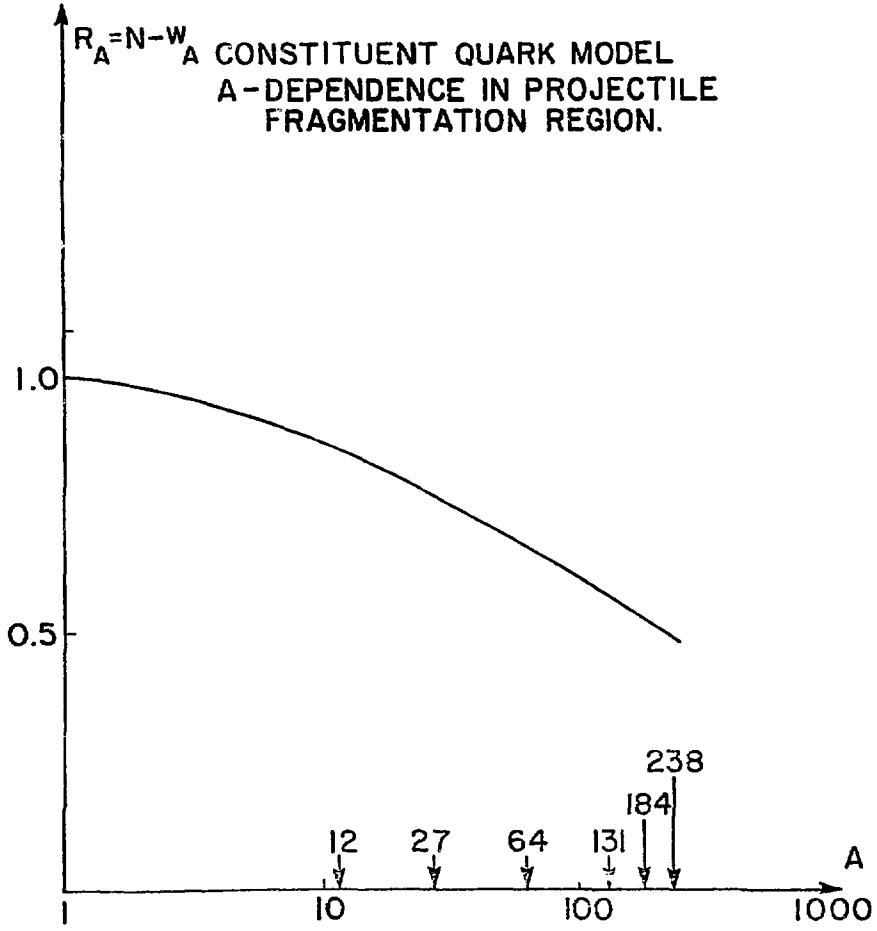
$R_A = N - W_A$ CONSTITUENT QUARK MODEL
A-DEPENDENCE IN PROJECTILE
FRAGMENTATION REGION.
1.0
0.5
12
27
64
131
184
238
A
1
10
100
1000

Fig. 9

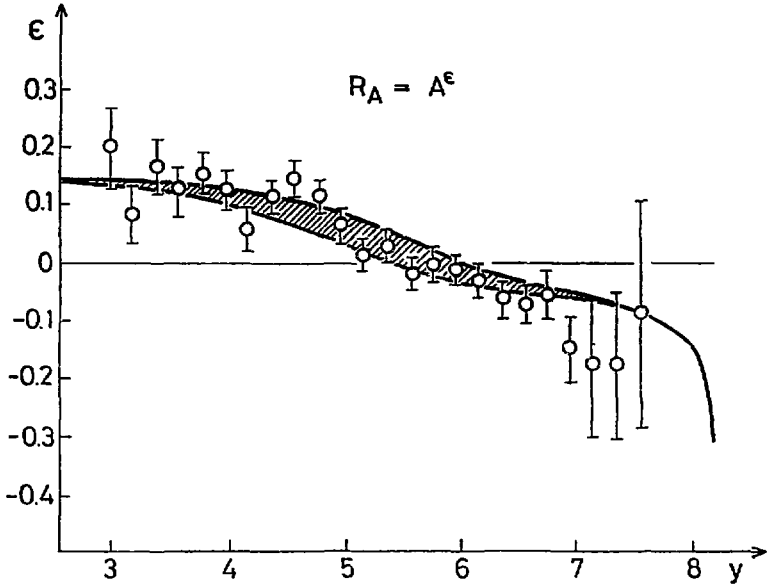

Fig. 10

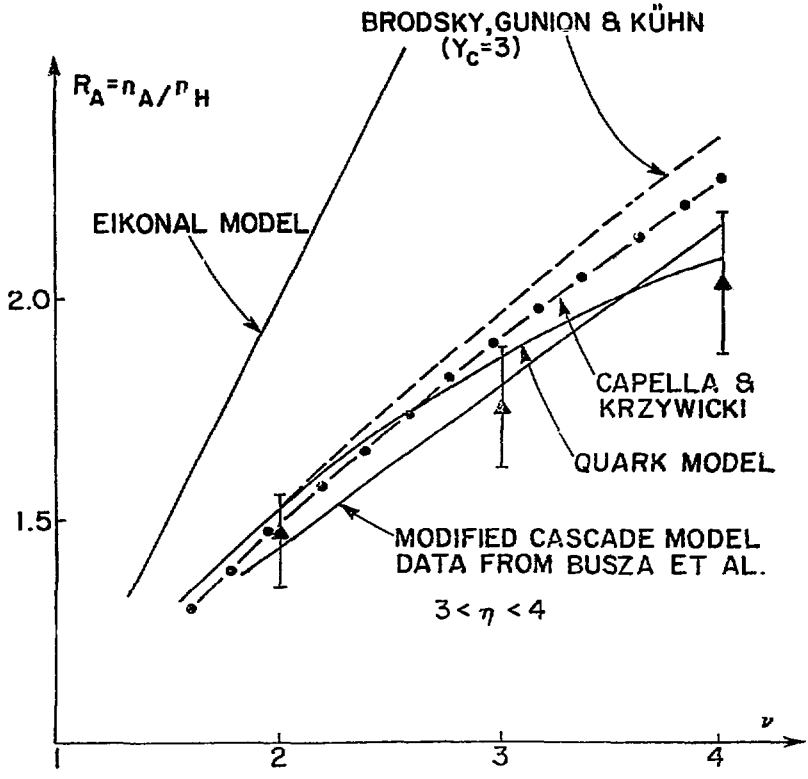
BRODSKY, GUNION & KÜHN
(Y_C=3)
$R_A = n_A/n_H$
EIKONAL MODEL
2.0
1.5
CAPELLA & KRZYWICKI
QUARK MODEL
MODIFIED CASCADE MODEL
DATA FROM BUSZA ET AL.
$3 < \eta < 4$
1
2
3
4
ν

Fig. 11

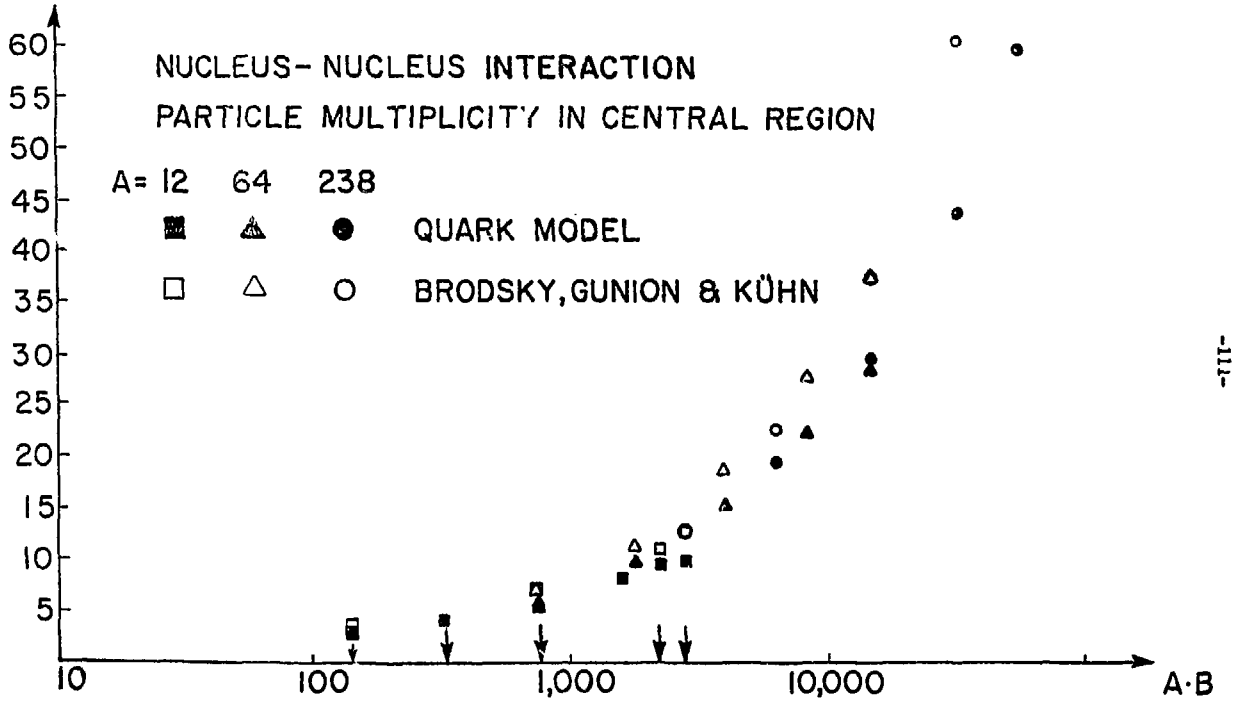
NUCLEUS- NUCLEUS INTERACTION
PARTICLE MULTIPLICITY IN CENTRAL REGION
A= 12 64 238
QUARK MODEL
BRODSKY, GUNION & KÜHN
60
55
50
45
40
35
30
25
20
15
10
5
10
100
1,000
10,000
A·B

Fig. 12

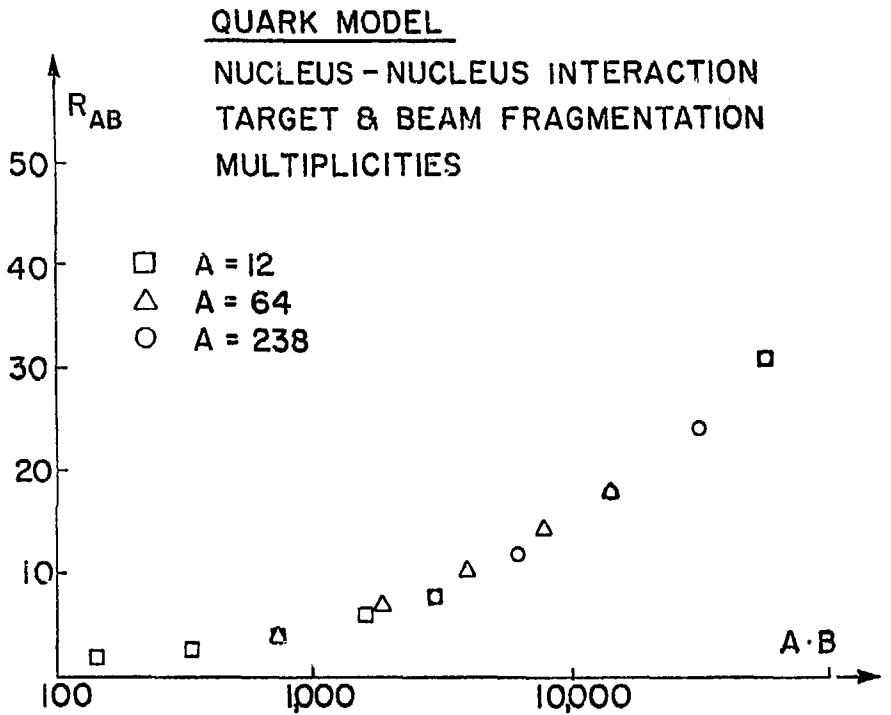
QUARK MODEL
NUCLEUS - NUCLEUS INTERACTION
TARGET & BEAM FRAGMENTATION
MULTIPLICITIES
R_{AB}
50
40
30
20
10
A = 12
A = 64
A = 238
100
1,000
10,000
A·B

Fig. 13

QUARK-QUARK INTERACTION BY EXCHANGE OF COLOUR GLUONS

(a) PROTON - PROTON INTERACTION

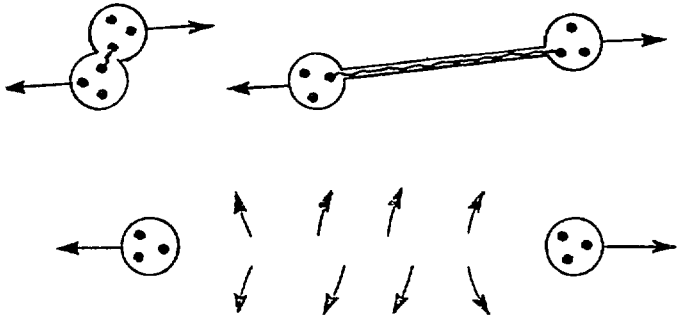

(b) PROTON - NUCLEUS INTERACTION

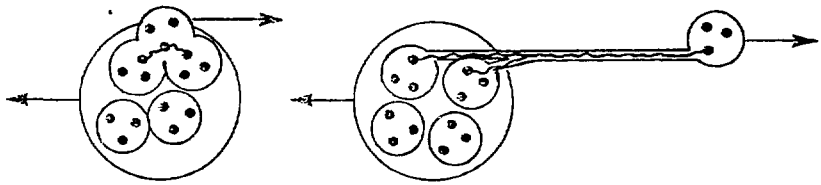

Fig. 14

MULTIPLICITY CORRELATIONS IN HIGH-ENERGY HADRON-NUCLEUS COLLISIONS

M.A. Faessler
Max-Planck-Institut für Kernphysik, Heidelberg, Germany

ABSTRACT

Inelastic hadron-nucleus interactions were measured at incoming momenta of 20 and 37 GeV/c at the CERN SPS. Angular and multiplicity distributions of relativistic particles were studied for different target nuclei and as a function of the multiplicity of knock-out nucleons. Possible implications of the experimental findings for theoretical models are discussed.

1. INTRODUCTION

One of the attractive properties of hadron-nucleus interactions at high energies is that they cannot be simply described in terms of more fundamental hadron-nucleon interactions[1]. The problem can neither be reduced to a multiple (coherent or incoherent) interaction of the incoming hadron with nucleons[2] nor to an equivalent single interaction with one nucleon at some shifted c.m. energy. We find rather that both aspects may be approximately valid in different phase-space regions of the outgoing particles. For the particles produced near to the projectile (hadron) rapidity "multiple collisions with nucleons" is not a meaningful notion, since their Lorentz-dilated formation time exceeds the propagation time through the nucleus[3]. Hence they see just a thicker target as compared to the proton target or a more massive "collective tube" of nucleons[4]. Seen from the target nucleus, however, several of its nucleons can be hit by the incoming hadron and all of these multiple collisions might contribute to the particles at rapidities close to the target nucleus rapidity.

The average inelastic hadron-nucleus interaction includes a large variety of different collisions -- from peripheral ones with a single surface nucleon to central ones with up to 6 nucleons being hit in a heavy nucleus. The number of nucleons being hit in the primary interaction represents a key parameter in hadron-nucleus interactions and the basic goal of the experiment described in this report[5] was to measure a few general aspects of particle production together with this parameter or at least a related quantity.

Previous knowledge gained in emulsion experiments provided the guidelines. In emulsions the tracks of charged particles are subdivided according to their ionization density. This division is not only appealing to the eye, but also corresponds to a relatively clean distinction of the underlying processes. The minimum ionizing tracks ("N_s", velocity $\beta > 0.7$) are dominantly pions produced in the interaction of the hadron with a row or tube of nucleons. The grey tracks ("N_g", $\beta < 0.7$) were found to be mainly nucleons (kinetic energies between 30 and 500 MeV); they, supposedly, are the products of a few-step intranuclear cascade started by the recoiling nucleons which have been hit in the primary interaction (Fig. 1). Finally, the black tracks are fragments with kinetic energies smaller than 30 MeV; they are the evaporation products of the heated-up nuclear fragments (multistep intranuclear cascade).

It was assumed in this experiment that it is the grey tracks which are most directly related to the number of nucleons involved in the primary interaction and therefore it was aimed to make a distinction between the emitted charged particles which is close to the distinction in emulsion between grey tracks and minimum ionizing particles[6].

2. APPARATUS

The detector measures charged tracks and distinguishes between slow and fast particles. The basic subunit of the apparatus is a counter consisting of a CsI(Tl) crystal, which is glued on a lucite light-guide (Fig. 2). The light signal produced in the CsI crystal is proportional to the energy loss. The lucite light-guide acts as a Čerenkov radiator if the velocity of the particle is bigger than $1/n_{lucite} = 0.7c$. (n_{lucite} is the refraction index of lucite). Thus the presence of a Čerenkov pulse signals a fast particle. Since the rise-time of the CsI signal is slower (20-30 nsec) than that of a Čerenkov pulse, a fast particle will trigger the discriminator somewhat earlier (about 6 nsec) than a slow particle (Fig. 3), and this time difference is used for the separation between fast and slow particles. A lower energy cut, around 30 MeV kinetic energy, is achieved automatically by absorption in the target and the material in front of the counters; therefore our slow particles are essentially the same as the grey tracks in emulsion.

The detector consists of 73 of these combined counters, covering 55% of the total solid angle, and of 55 counters of a lucite hodoscope, covering the forward cone of 13° opening angle (Fig. 4). In the forward hodoscope, which covers only 1% of the total solid angle, there was no distinction between fast and slow particles -- recoil nucleons are supposed to be mostly fast in this region. Each anode signal is given to a pattern, a Time-to-Digital converter and an Analog-to-Digital converter (energy loss). Figure 5 shows a plot of ADC versus TDC. The detector forms 12 rings of roughly equal size in pseudorapidity ($\eta = -\ln \tan \theta/2$) and is sufficiently fine grained such that not too high corrections are needed for multiple hits in one counter.

The beam was defined to a pencil beam of diameter 8 mm at the target by means of a combination of beam counters, and beam particles were identified with 2 threshold gas Čerenkov counters. The maximum energy of the beam was 40 GeV/c (S1 beam in the west hall of the CERN SPS). We ran at two energies, 37 and 20 GeV, mainly at negative polarity.

A minimum bias trigger asked for at least 2 charged particles away from the beam axis. Requiring only one track would have given too much accidental background, since we tried to measure at high beam intensity (up to 400,000 particles per sec). About 100,000 events were collected for each combination of energy, projectile and target mass. Targets used were C, Al, Cu, Ag, and Pb (and an empty target position). Data presented below are for incoming negative pions and kaons only; they behave quite similarly within the precision of the experiment. There are quantitative differences between $\bar{p}$ on the one hand and π^-, K^- on the other, but we have not extracted any physics yet from these differences. However, most of the qualitative discussion of the π^-, K^- data below applies to $\bar{p}$ projectiles as well.

3. RESULTS

We will discuss the following results of the experiment:

i) Target and energy dependence of multiplicities of the slow and fast particles. We find "limiting fragmentation" of the nuclear target -- both slow and fast particles at low pseudorapidities have energy-independent characteristics between 20 and 40 GeV.

ii) Target dependence of η-distribution of fast particles. We will present this in a form to allow easy comparison with theoretical predictions.

iii) Correlations between slow- and fast-particle multiplicities. Deviations from KNO scaling are observed if we plot the multiplicity distributions of fast particles as a function of the number N_g of observed slow particles (recoil nucleons). We will discuss the question of collectiveness of the row of nucleons hit in the primary collision.

iv) Pseudorapidity distributions of fast particles as a function of N_g (N_g interpreted as measure of the number of nucleons hit in the primary collision).

3.1 Target and energy dependence of slow and fast particles

In Fig. 6a the frequency distribution of events is shown for different targets as a function of the observed number of slow particles (N_g is the actually observed number, not corrected for solid-angle acceptance, etc.). The distributions are rapidly falling with increasing number of slow particles, the slopes getting less steep with increasing target mass. The distribution for $\bar{p}$ and Pb is also shown; it has the smallest slope. These distributions (together with their projectile dependence) can provide the basic input if one wants to establish a quantitative relation between the actually observed number of knock-out nucleons N_g and the corresponding average number of primarily (by the incoming hadron) hit target nucleons. While a calculation of the probability distribution $f(\nu)$ of the number ν of hit nucleons is straightforward (geometrical optics + Woods-Saxon density of nuclear matter) the calculation of the probability distribution $f(N_g)$ is more complicated, because assumptions about the intranuclear cascading of slow particles (Fig. 1) have to be made, which lead from one primarily hit nucleon to some distribution of N_g. A preliminary calculation has shown that for a heavy target like Pb one observed charged slow track in our experiment corresponds to about one primarily hit nucleon -- for not too high values of N_g.

The energy dependence of the multiplicity distribution of slow particles is shown in Fig. 7. The ratio of the distribution at 40 GeV/c to the one at 20 GeV/c is plotted versus N_g for the different targets. Constancy of the ratios means that the slopes in Fig. 6a stay the same between 20 and 40 GeV/c, and this is the case

to a remarkably high degree. The conclusion is that the characteristics of slow particles are energy *independent*.

In constrast to the slow particles the ratio for the fast particles increases, i.e. the probability of events with higher multiplicity N_s increases with increasing energy (Figs. 6b and 7b).

The energy independence of slow particles is not a proof, but a necessary condition for them to be interpreted as a measure of the number of nucleons involved in the primary interaction, since such a measure should depend on the energy at most via the energy dependence of the cross-section, i.e. weakly. In emulsion experiments the energy independence of grey tracks and black tracks has been shown over a much wider range of incoming energies (from ~ 20 to 1000 GeV). It is worth considering the energy independence of slow particles in a somewhat extended frame, since it is not an isolated effect. One knows that the number and distribution of pions at small laboratory rapidities is energy independent in pp as well as in pA collisions. (The same applies of course for the pions produced near the projectile rapidity, if one plots the rapidity distribution in the projectile rest frame.) See Fig. 8a showing the rapidity distribution of fast particles for different targets at 40 GeV and Fig. 8b showing the ratio of the rapidity distribution at 40 GeV to the one at 20 GeV. At low rapidities the ratio is equal to one (lowest bins have large systematic error from background correction; and for the Ag target the ratio deviates from 1.0 by 20%, probably because of insufficiently corrected background of low-N_s and low-N_g events).

This phenomenon is well known under the name "limiting fragmentation", and our measurements and earlier measurements in emulsions demonstrate that limiting fragmentation holds at all levels of the target fragmentation, for the "radiated" pions, for the knock-out nucleons from the slow intranuclear cascade, and for the black tracks emitted by the hot nuclear fragments. In other words: *the energy absorbed by the nuclear target reaches a limiting value*, independent of the incoming energy, apparently already at 20 GeV.

3.2 Target dependence of fast particles (pseudorapidity distributions)

A convenient parametrization for the inclusive cross-section of particles produced in hadron-nucleus interactions is

$$\frac{d^3\sigma(hA)}{dp^3/E} = A^{\beta(y,p_T)} \frac{d^3\sigma(hN)}{dp^3/E} \qquad (1)$$

where h = hadron, A = atomic mass number, N = nucleon. Since we did not measure the total inelastic cross-section or the transverse momentum p_T we rather used the pseudorapidity distribution $d\langle N_s(hA)\rangle/d\eta$ =

$$\frac{1}{\sigma_{inel}(hA)}\frac{d\sigma(hA)}{d\eta} = A^{\alpha(\eta)}\frac{1}{\sigma_{inel}(hN)}\frac{d\sigma(hN)}{d\eta} = \frac{\sigma(hN)}{\sigma(hA)}\int A^{\beta(p_T,\eta)}dp_T^2\frac{1}{\sigma(hN)}\frac{d^3\sigma(hN)}{dp^3/E} \quad (2)$$

The quantity $A^{\alpha(\eta)}$ could be called the "nuclear enhancement factor" (relative to the collision with one nucleon) or the "effective number of collisions". This quantity allows a comparison with theoretical models, which in general try to predict only the increase of multiplicity with increasing target mass relative to pp collisions which are assumed to be known. Figure 9 shows the power $\alpha(\eta)$ as extracted from the pseudorapidity distributions (Fig. 8). The power $\alpha(\eta)$ being about zero at large η means the effective number of collisions is there equal to one, independent of target size. The value of $\alpha(\eta)$ increases with decreasing η and passes the value $\langle\nu\rangle = A\,\sigma_{\pi N}/\sigma_{\pi A}$ (called by many authors the "average number of collisions in the nucleus"). This means that the effective number of nucleons involved in particle production is higher than the real number of nucleons and it shows that an intranuclear cascade is effective for the produced low-energetic particles. Qualitative agreement is found with several recent models[7]; but one has to say that our energies and the rapidity span of our distributions are still too low to rule out one or the other of the proposed models.

3.3 Correlations between multiplicities of slow and fast particles

The last two topics to be dealt with are correlations between fast and slow particles. We first consider multiplicity correlations. Figure 10 shows the frequency of events with a given pair (N_s, N_g) versus the number N_s of observed fast particles for a lead target, 40 GeV/c. Lines connect the data points with the same number of observed slow particles. Compare Fig. 6b, which shows the corresponding multiplicity distribution but integrated over N_g. (Recall that N_s and N_g are not corrected for solid angle, etc.) The curves in Fig. 10 indicate an increase of the mean N_s and a change of shape, with increasing N_g. The increase of the mean value $\langle N_s\rangle$ is shown in Fig. 11 for different targets and energies. (Here $\langle N_s\rangle$ is corrected for acceptance and multiple hits, etc.) A plateau is reached for the heavy targets. We do not know if the cause of the plateau is a limitation of the total energy available for particle production, e.g. the leading particle might lose its energy in a few subsequent collisions -- or, alternatively, a limitation of the number of collisions effective in particle production (maximum thickness of nucleus). I will not discuss this picture any further, since we can look at a more differentiated plot later (the pseudorapidity distributions of which $\langle N_s\rangle$ is nothing but the integral, as a function of N_g).

We can calculate the next higher moment of the distributions in Fig. 10, the mean dispersion of the multiplicity distributions as a function of N_g.

$$\langle D_s\rangle = \sqrt{\langle N_s^2\rangle - \langle N_s\rangle^2}\ . \quad (3)$$

In pp collisions the ratio $Z = \langle D_s \rangle / \langle N_s \rangle$ has been found to approach a constant value ~ 0.5 for higher energies [Malhotra[8]), this is called Wroblewski scaling today and is also a consequence of KNO scaling[9])]. Moreover, in hadron-nucleus interactions this ratio was found to obey the same scaling law[10]) and to have the same value ~ 0.5.

For the integrated (over N_g) multiplicity distribution we find as well that Z is approximately constant for different incoming energies and different targets. (See Fig. 12a, crosses. The scattering of the crosses is due to insufficiently corrected background at low N_s and low N_g.) In Fig. 12a the ratio Z is plotted versus $\langle N_s \rangle$, the corrected mean multiplicity which varies with energy and target. If we now increase $\langle N_s \rangle$ by increasing N_g (following the curves in Fig. 11), i.e. if we consider Z for different curves in Fig. 10, we obtain a remarkable *systematic decrease* of the ratio which is shown for the Pb targets at two energies in Fig. 12a. With our interpretation of N_g being a measure of the number of collisions, this consequently signifies a decrease of Z as a function of the ν nucleons participating in the primary interaction. Figure 12b shows that the parameter determining the decrease in fact is N_g, since as a function of N_g the two curves now fall approximately on top of each other. A decrease of Z is expected in models where part of the produced particles is due to statistically independent contributions[11]). Assume each collision contributes a statistically independent and equal amount of produced particles; then

$$\langle N_s \rangle_{hA} = \nu \langle N_s \rangle_{hN}$$

$$\langle D_s^2 \rangle_{hA} = \nu \langle D_s^2 \rangle_{hN} \, .$$

Therefore

$$Z_{hA} = \frac{\langle D_s \rangle}{\langle N_s \rangle} \propto 1/\sqrt{\nu} \, .$$

In most models only the particles produced in the target hemisphere result from independent multiple contributions by the nucleons hit in the primary collision, whereas the pions at high rapidities come from the decay of the projectile.

For a contrast, the coherent tube model predicts KNO scaling to hold for a hadron-nucleon-tube collision[12]), therefore Z should be a constant independent of the number of nucleons in the tube. Hence, at our energies, the coherent tube model seems to be in variance with the data, if there is a correlation between the number of nucleons in the tube and N_g.

3.4 Pseudorapidity distributions of fast particles as a function of N_g

Finally, we want to consider the pseudorapidity distribution as a function of N_g and incoming energy. (The differential multiplicities can obviously give more

insight into the mechanism at work than the total multiplicity (N_g).) The dominant impression from Fig. 13 is that the change with N_g, i.e. with the number ν of collisions, is quite different from the predictions of many models. They predict a clear separation of the rapidity distribution into two regions: one above a certain critical rapidity η_c, where no change with ν occurs, and the other below η_c, where the change with $\nu = \nu(N_g)$ should be linear. The critical rapidity η_c is predicted to depend only on the energy in some of these [e.g. Gottfried[2)]] and only on the size of the nucleus at given impact parameter in other models [e.g. Bertocchi[2)]]. What we observe is rather a separation into two regions, the upper part showing a depletion and the lower part showing an increase of the number of fast particles; the border η_c between the two regions depends both on the incoming energy and on the number of collisions. At first sight it may appear as if the main mechanism reflected in this behaviour is energy conservation and not dynamics. However, the pseudorapidity distributions could conserve energy in many other ways and we think that the particular way nature has chosen to conserve energy must tell us something about the dynamics. Many models claim to be true only at asymptotically high energies, where the effects of energy conservation should become invisible, and consequently none of these will be challenged by the present data. Although we feel that it is a long and painful road to approach the asymptotic energies, where theories become true, we are doing our best and will continue the experiment this summer at higher energies up to maybe 200 GeV.

REFERENCES AND FOOTNOTES

1) It would be justified to say that hadron-nucleus and nucleus-nucleus interactions are as fundamental as hadron-nucleon interactions. Matter densities of nuclei are about the same as those of nucleons, so using nuclear targets is equivalent to varying the size or thickness of the target hadron, which is a fundamental parameter of the interaction.

2) For inelastic interactions see, for instance:
K. Gottfried, *in* Proc. 5th Int. Conf. on High Energy Physics and Nuclear Structure, Uppsala, 1973 (Ed. G. Tibell) (North-Holland, Amsterdam, 1974), p. 79.
L. Bertocchi, *in* Proc. 6th Int. Conf. on High Energy Physics and Nuclear Structure, Santa Fe, 1975 (Ed. D.E. Nagle et al.) (AIP, New York, 1975), p. 238.
W. Busza, ibid., p. 211.
S.J. Brodsky et al., Phys. Rev. Lett. 39 (1977) 1120.
N.N. Nikolaev et al., Preprint CERN TH.2541 (1978).

Many articles and references to earlier work can be found in:
Proc. Topical Meeting on Multiparticle Production on Nuclei at Very High Energies, Trieste, 1976 (Eds. G. Bellini, L. Bertocchi and P.G. Rancoita) (IAEA-SMR 21, Trieste, 1977).

For elastic scattering, the simple Glauber theory needs corrections owing to the occurrence of inelastic intermediate states. See, for example:
G. Goggi et al., Phys. Lett. 77B (1978) 428;
G. Goggi et al., Phys. Lett. 77B (1978) 433;
G. Goggi et al., Phys. Lett. 79B (1978) 165;
G. Goggi et al., preprints CERN-EP/79-02, CERN-EP/79-03 (1979).
E. Jenkins et al., Proton-helium elastic scattering from 40 to 400 GeV, Report submitted to the 19th Int. Conf. on High Energy Physics, Tokyo, August 1978.

3) L. Landau and I. Pomeranchuk, Translated from Dokl. Akad. Nauk SSSR 92 (1953), 535 and 735, translations RT-530 and RT-864.
L. Stodolsky *in* Proc. 6th Int. Colloquium on Multiparticle reactions, Oxford, 1975 (Eds. C. Hong-Mo, R. Phillips and D. Roberts)(RL 75-143, Rutherford Lab., Chilton, Didcot, 1975), p. 577.

This seems to be contradicted by the parton model[6], where partons of the incoming hadron undergo several collisions, but this pseudocontradiction arises only from the microscopic description of the hadrons; different partons of one hadron may interact independently from each other. Nevertheless the hadron "decays" only after passing the target nucleus, and the resulting particle spectrum from this decay is equivalent to the one from a single collision of the same hadron at higher c.m. energy.

4) In the collective tube model this particular aspect is emphasized:
A. Dar, *in* Proc. Topical Meeting on High Energy Collisions involving Nuclei (Eds. G. Bellini, L. Bertocchi and P.G. Rancoita), Trieste, 1974 (Editrice Compositori, Bologna, 1975), p. 231.
S. Frederiksson, Nucl. Phys. B111 (1976) 167.

5) The experiment has been done by a Darmstadt-Heidelberg-Virginia-Warsaw Collaboration at CERN: M.A. Faessler, P. Gugelot, U. Lynen, J. Niewisch, B. Pietrzyk, B. Povh, H. Schroeder, T. Siemiarczuk and I.P. Zielinski.

6) It should be emphasized that the definition of the quantity, which we called key parameter ("number of hit nucleons" or "number of nucleons participating in the particle production") is rather model dependent. The relation between the observable quantity (the grey tracks) and the key parameter is model dependent, too. Eventually, it will turn out that the only meaningful quantity is the "effective number of collisions", which has different values in different phase-space regions of the outgoing particles. Nevertheless, we let ourselves be guided by the idea of such a key parameter.

7) S.J. Brodsky et al., Phys. Rev. Lett. 39 (1977) 1120.
N.N. Nikolaev and A.Ya. Ostapchuck, Preprint CERN TH.2575 (1978).

8) P.K. Malhotra, Nucl. Phys. A6 (1963) 559.

9) Z. Koba et al., Nucl. Phys. B40 (1972) 317.

10) W. Busza et al., Phys. Rev. Lett. 34 (1975) 839.

11) B. Andersson and I. Otterlund, Nucl. Phys. B88 (1975) 349.

12) A. Dar in Trieste Conference, 1976, see Ref. 2, p. 591.

Figure captions

Fig. 1 : a) The fast cascade of the incoming hadron.

b) The slow cascade of the recoil nucleons.

Fig. 2 : One combined counter unit of the detector.

Fig. 3 : The anode signal of a combined counter. The bottom part of the picture shows the beginning of the pulse on an expanded time scale.

Fig. 4 : The whole detector.
Top : layout of beam counter.
Bottom: the vertex detector.

Fig. 5 : ADC (energy loss in CsI) versus TDC (time) plot for one combined counter.

Fig. 6 : Frequency of events as a function of

a) the observed multiplicity of slow tracks N_g $[f(N_g)]$

b) the observed multiplicity of fast tracks N_s $[f(N_s)]$

for different targets, at 37.5 GeV/c.

Fig. 7 : a) Energy independence of the multiplicity distributions of Fig. 6 (slow particles). R is the ratio of the frequency $f(N_g)$ at 40 GeV/c to $f(N_g)$ at 20 GeV/c normalized to one at $N_g = 0$, for different targets.

b) Corresponding ratio for $f(N_s)$, the multiplicity distribution of fast particles, demonstrating their dependence on energy.

Fig. 8 : a) Pseudorapidity distribution of fast particles for different targets, at 37.5 GeV/c.

b) The ratio of these distributions (at 37.5 GeV/c) to those at 20 GeV/c.

Fig. 9 : a) The power of the nuclear enhancement factor s, Eq. (2), at 37.5 GeV/c and at 200 GeV (data taken from FNAL experiment, Halliwell et al., Trieste Conference, 1976, see Ref. 2).

b) Same at 20 GeV/c.

Fig. 10 : Frequency of events with N_s and N_g observed fast and slow tracks. Abscissa is N_s. Lines connect data points belonging to the same N_g. Only some of the data points are shown for sake of clarity. The vertical scale shows the number of events accumulated in this particular run.

Fig. 11 : Corrected mean multiplicities of fast particles versus number of observed slow particles for different targets at a) 37 GeV/c and b) 20 GeV/c incoming pion momentum.

Fig. 12 : The ratio $Z = \langle D_s \rangle / \langle N_s \rangle$ versus

a) $\langle N_s \rangle$, where $\langle N_s \rangle$ is a function of energy and target mass (crosses) or of energy and N_g (points connected by lines).

b) N_g.

Fig. 13 : Pseudorapidity distributions as a function of N_g for π^- on Pb at a) 20 GeV/c and b) 37 GeV/c.

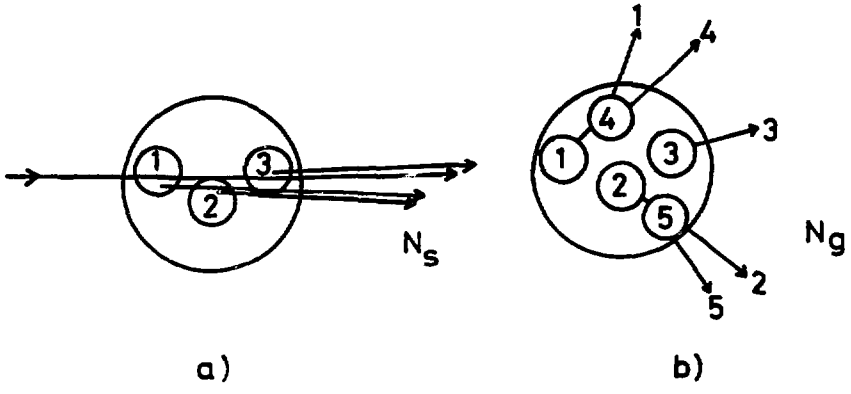

Fig. 1

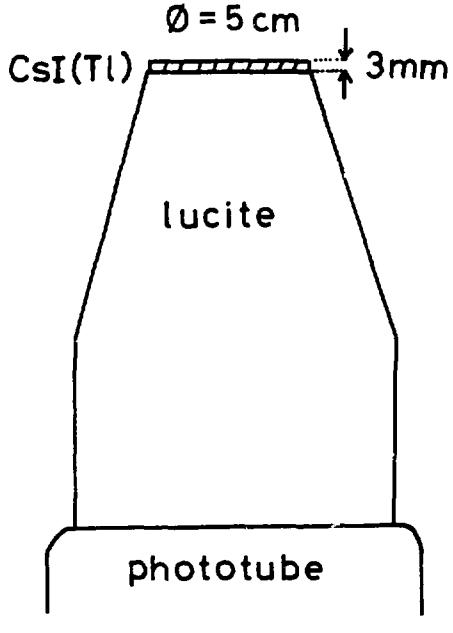

Fig. 2

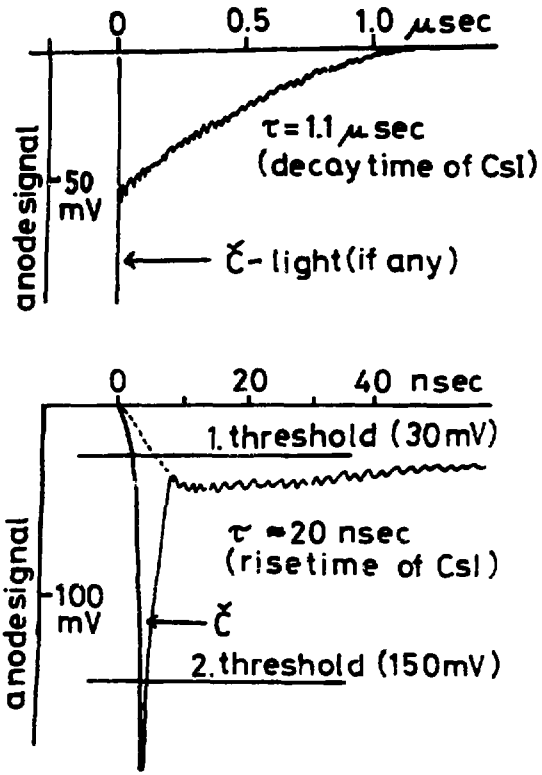
0
0.5
1.0 μsec
τ = 1.1 μsec
(decay time of CsI)
anode signal
50 mV
Č - light (if any)
0
20
40 nsec
1. threshold (30 mV)
τ ≈ 20 nsec
(rise time of CsI)
anode signal
100 mV
Č
2. threshold (150 mV)

Fig. 3

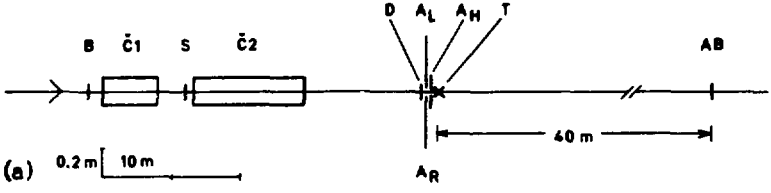
B
Č1
S
Č2
D
A_L
A_H
T
AB
40 m
A_R
(a)
0.2 m
10 m

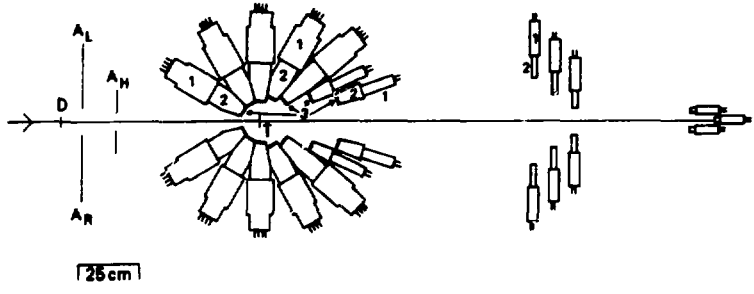
A_L
A_H
D
A_R
25cm
(b)
73 Cs I + Lucite counters
48 Lucite
7

Fig. 4

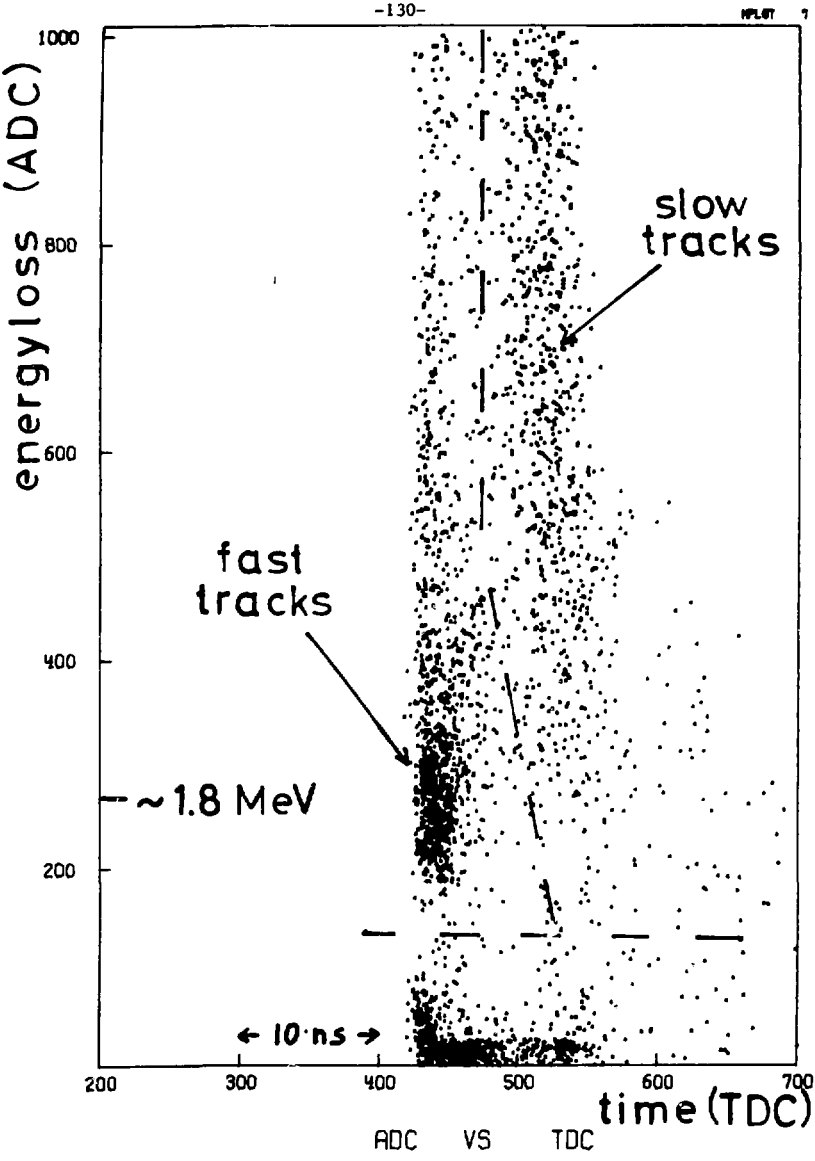
energyloss (ADC)
1000
800
600
400
200
slow tracks
fast tracks
~1.8 MeV
← 10 ns →
200
300
400
500
600
700
time (TDC)
ADC VS TDC

Fig. 5

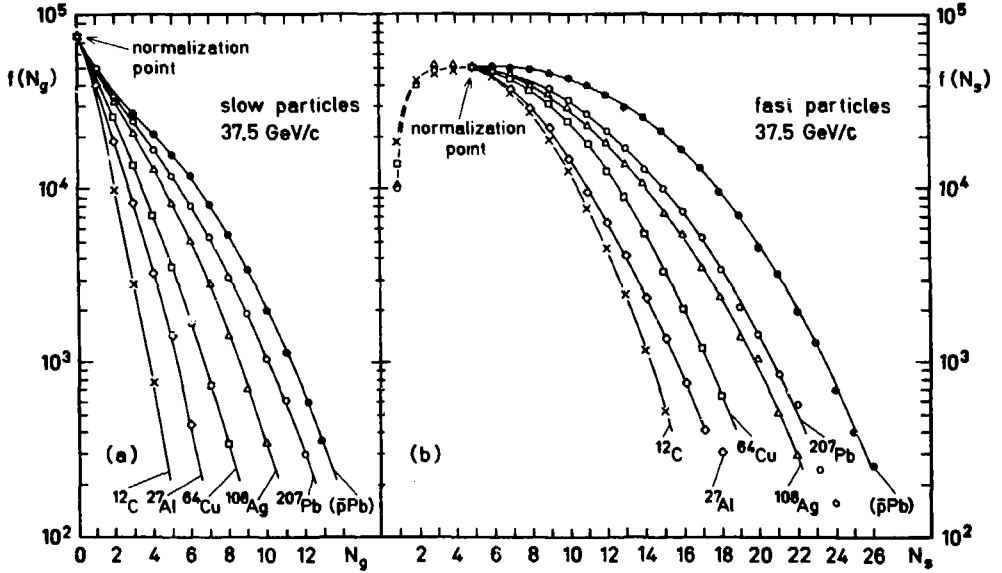
normalization point
slow particles
37.5 GeV/c
f(N_g)
(a)
12C 27Al 64Cu 108Ag 207Pb (p̄Pb)
N_g
normalization point
fast particles
37.5 GeV/c
f(N_s)
(b)
12C 27Al 64Cu 108Ag 207Pb (p̄Pb)
N_s

Fig. 6

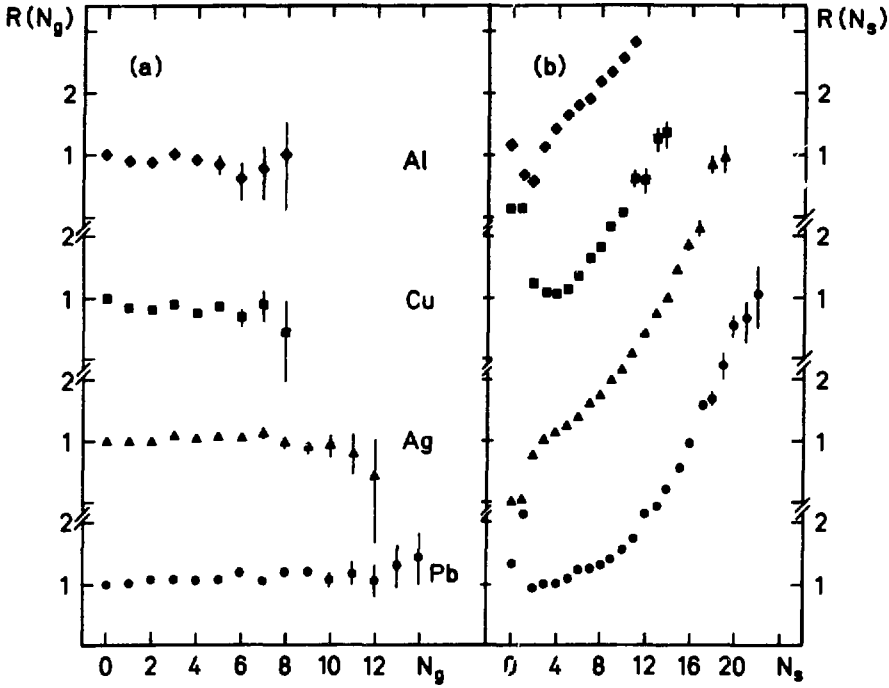

Fig. 7

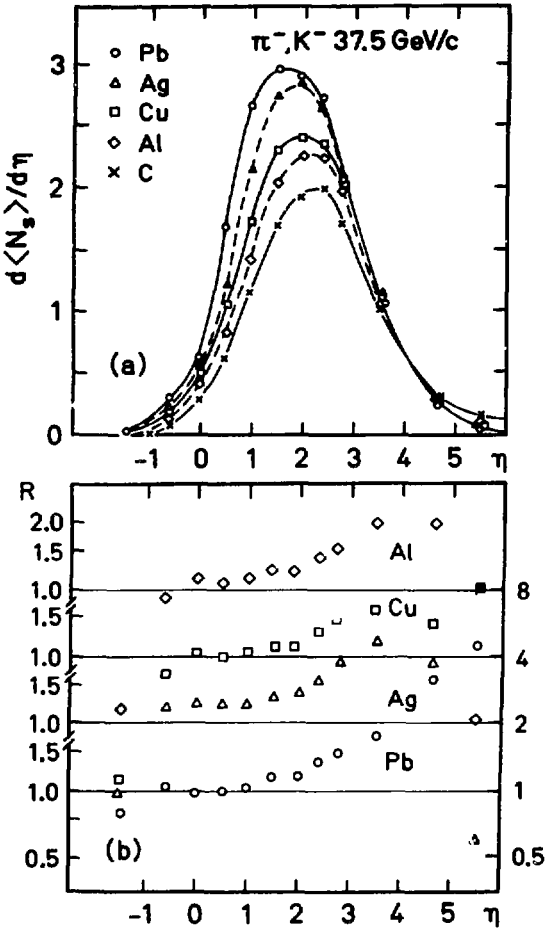

Fig. 8

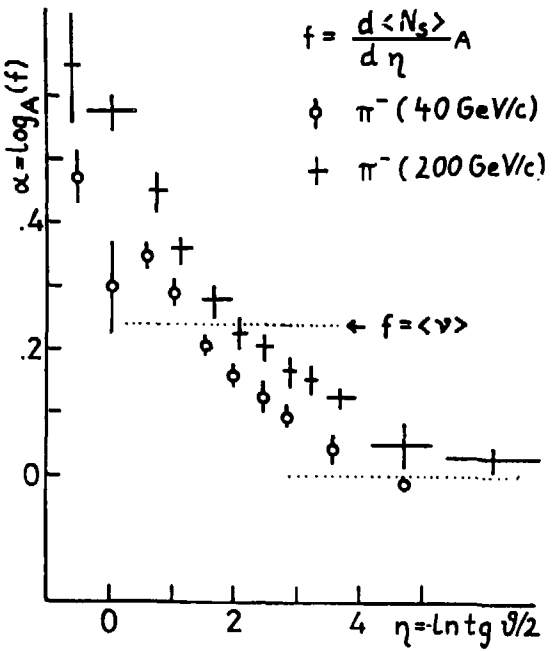
$f = \frac{d\langle N_s\rangle}{d\eta}_A$
π^- (40 GeV/c)
π^- (200 GeV/c)
$\alpha = \log_A(f)$
$f = \langle\nu\rangle$
.4
.2
0
0
2
4
$\eta = -\ln \operatorname{tg} \vartheta/2$

a)

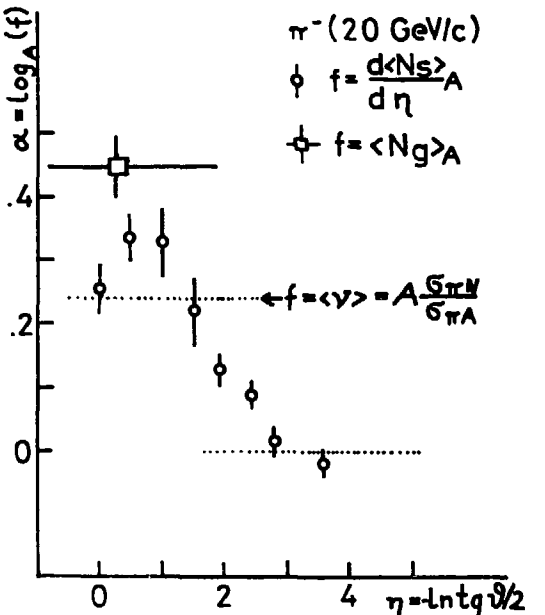
π^- (20 GeV/c)
$f = \frac{d\langle N_s\rangle}{d\eta}_A$
$f = \langle N_g\rangle_A$
$\alpha = \log_A(f)$
$f = \langle\nu\rangle = A\frac{\sigma_{\pi N}}{\sigma_{\pi A}}$
.4
.2
0
0
2
4
$\eta = -\ln \operatorname{tg} \vartheta/2$

b)

Fig. 9

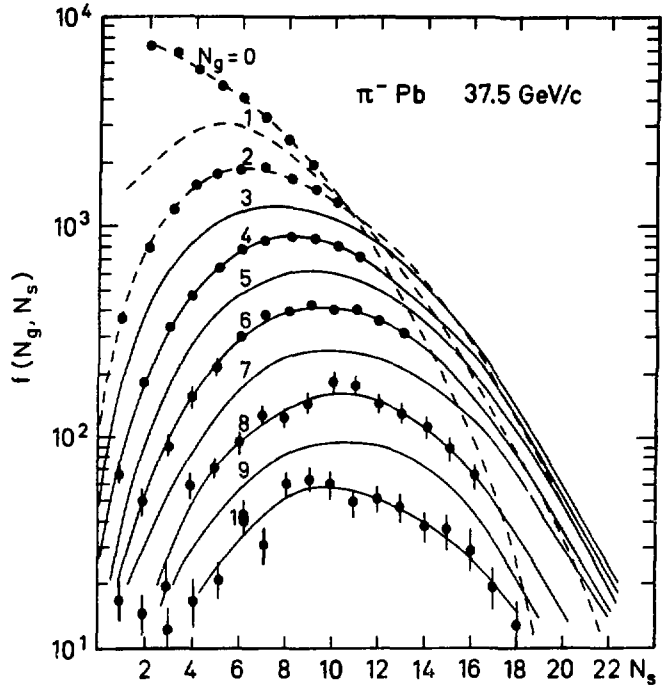
10^4
10^3
10^2
10^1
$f(N_g, N_s)$
$N_g = 0$
1
2
3
4
5
6
7
8
9
10
π^- Pb 37.5 GeV/c
2 4 6 8 10 12 14 16 18 20 22 N_s

Fig. 10

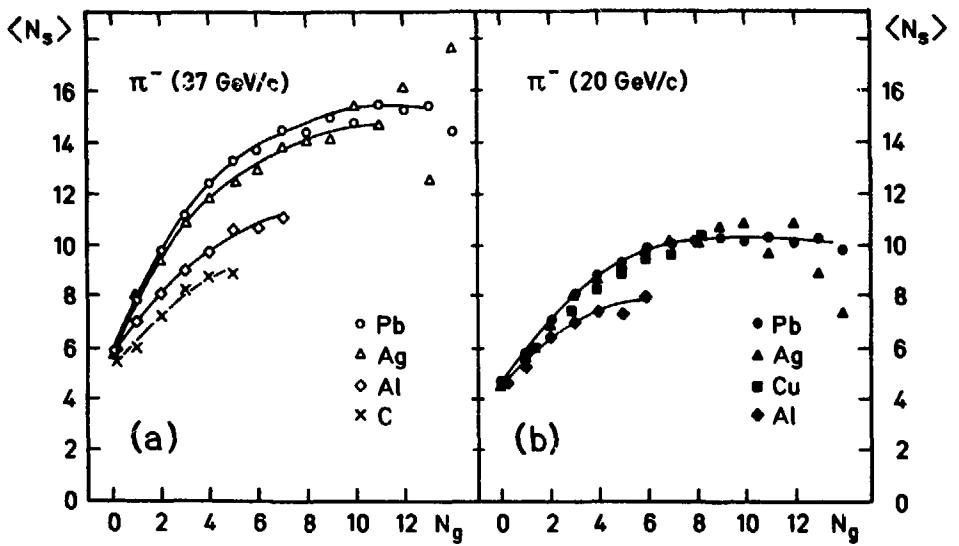

Fig. 11

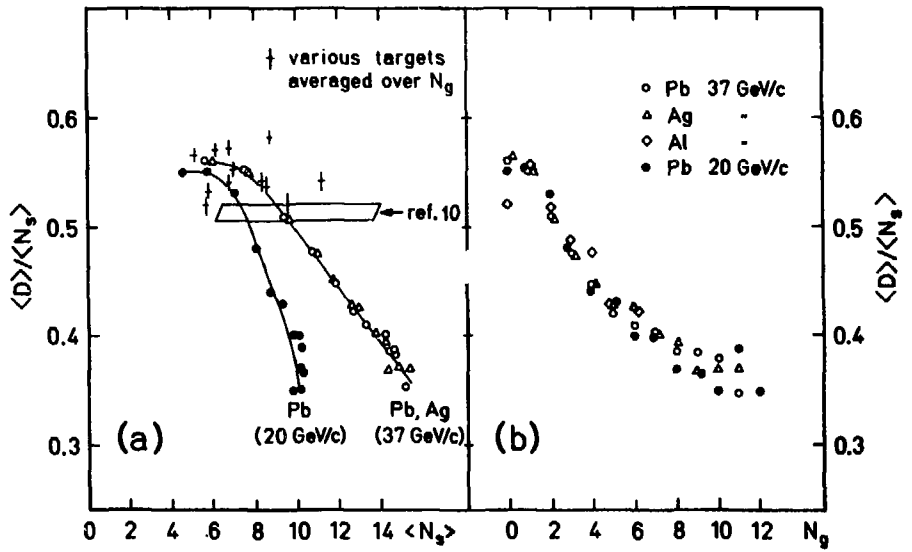
† various targets
averaged over N_g
ref. 10
Pb
(20 GeV/c)
Pb, Ag
(37 GeV/c)
(a)
(b)
Pb 37 GeV/c
Ag -
Al -
Pb 20 GeV/c
$\langle D \rangle / \langle N_s \rangle$
$\langle N_s \rangle$
N_g
0.6
0.5
0.4
0.3
0 2 4 6 8 10 12 14
0 2 4 6 8 10 12

Fig. 12

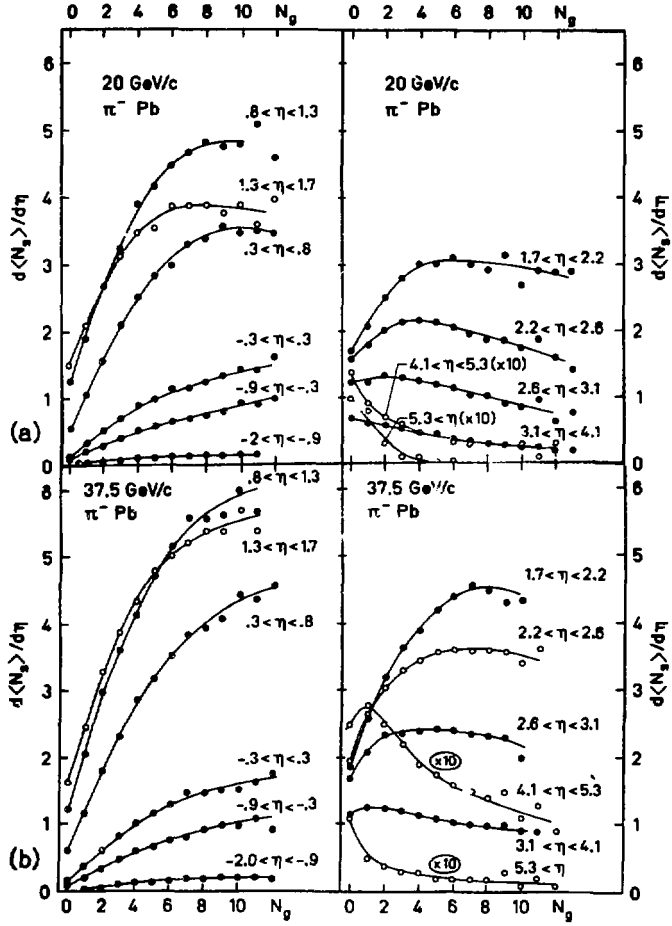
20 GeV/c
π⁻ Pb
.8<η<1.3
1.3<η<1.7
.3<η<.8
-.3<η<.3
-.9<η<-.3
-2<η<-.9
(a)
1.7<η<2.2
2.2<η<2.6
4.1<η<5.3(x10)
2.6<η<3.1
5.3<η(x10)
3.1<η<4.1
37.5 GeV/c
π⁻ Pb
.8<η<1.3
1.3<η<1.7
.3<η<.8
-.3<η<.3
-.9<η<-.3
-2.0<η<-.9
(b)
1.7<η<2.2
2.2<η<2.6
2.6<η<3.1
(x10)
4.1<η<5.3
3.1<η<4.1
(x10)
5.3<η
d⟨Ng⟩/dη
Ng
0 2 4 6 8 10

Fig. 13

COSMIC RAY DATA ON HIGH-ENERGY HADRON-NUCLEUS AND NUCLEUS-NUCLEUS COLLISIONS

G. B. Yodh[+]

National Science Foundation

Washington, D.C. 20150

The objective that I took upon myself is not to attempt to tell you all about what's known from cosmic rays about nucleus-nucleus interactions, but rather to concentrate on two aspects - (a) what part of cosmic ray physics immediately would benefit from having a 20 GeV per nucleon machine colliding with 20 GeV per nucleon and how it might be relevant to some cosmic ray questions and (b) to discuss some unusual cosmic ray events called Centauro events, which some of you have already heard about and I believe are the most exciting observations at high energies: in fact, one wonders whether 20 GeV on 20 GeV will be high enough to produce them.

For those of you who find that you'd like to read more about it, you can study the preceedings of the Bartol Conference, held last October, published as an AIP volume, entitled "Cosmic Rays and Particle Physics", where you will find papers by the original authors.

[+]On leave from the University of Maryland.

Cosmic Ray Beam:

Let me start by discussing some energy scales and then go on to discuss composition. If you have a 2 GeV per nucleon collider, we are talking about a total energy in cosmic ray laboratory of an incoming iron nucleus with a total energy of 448 GeV; with 20 GeV on 20 GeV we will be at 4.48×10^4 GeV for an iron nucleus. Isabelle which is 400 on 400 GeV P-P collider is equivalent to $3.2\ 10^5$ GeV in the laboratory; and if you want to go to 10^6 GeV with iron nuclei, you would want to build a collider where each beam energy is about 95 GeV per nucleon.

Next I will show you a composite figure for the cosmic ray spectrum from 10 GeV to 10^{10} GeV (Figure 1). What's plotted here is the integral spectrum of cosmic rays multiplied by $E^{1.5}$ in order to be able to put on the same scale an energy range going from 10 GeV to 10^{10} GeV (1). So if the integral spectrum is $E^{-1.5}$ you should get a straight line. The slanted lines going across give you lines of equal flux. For example, if you have 10^6 GeV energy per nucleus, then the flux of all particle entering the top of the atmosphere is 10^{-6} per meter square steradian, second. The total particle spectrum, up to the present, has been measured directly using satellites by Grigorov (2) in Russia; whose pioneering experiments used a large calorimeter, 2.7 interaction lengths deep, and you can see that it's a little steeper than $E^{-1.5}$. Above 10^6 GeV, all the experimental information comes from study of extensive air showers and we have information all the way out to 10^{11} GeV. Now, the two lines

marked p and Fe give you an indication relative composition of protons and iron in primary cosmic rays. Direct measurements to determine the primary cosmic rays sort of peter out at about 10^3 GeV just now. They were done in balloon experiments (3-6). Indirect measurements (7-11) in which you measure something on the Earth in an air shower and try to relate that to the primary composition, have been carried out above 10^3 GeV. Recent measurements of the Maryland group (11) indicate that the iron spectrum is such that when you multiply it by $E^{1.5}$ it will appear as increasing on this graph; in fact it is $E^{-1.36}$. The iron spectrum is flatter than the proton spectrum, whose spectral index is about -1.71 for the integral spectrum, and the two components cross over at something like 10^4 GeV; so if you do an experiment at the top of the atmosphere with emulsions, you can have a possibility of studying collisions of 10^6 GeV total energy iron nuclei with silver nuclei.

At about 10^7 GeV energy most of the particles are iron; although there are some other particles here, in fact it's 80% iron; 20% other nuclei. However, this means that whatever the source of iron, it must be such that there should be a cutoff beyond 10^7 GeV and I hope Dr. Schramm tells you what that signifies from the theoretical point of view. The Fly's Eye (12), which is a detector just going into operation in Utah will deal with energies starting from 10^7 GeV, and it is possible that Fly's Eye would be able to tell you the composition of primary cosmic rays at 10^9 GeV, whether they are protons or iron nuclei.

Now, how do colliding beam machines play a role in our understanding of cosmic rays? If you knew the properties of nuclear collisions, then the study of air showers, for example high energy muons and delayed hadrons, can be used to derive the primary composition; and these have immediate relevance on the theories of origin, acceleration and propagation of cosmic rays. If you consider still higher energies where there are no machines and you assume that nulcear physics doesn't change drastically, or if you assume that the composition doesn't change drastically, then study of air showers could tell you about origin of cosmic rays or about the properties of nucleus-nucleus collisions respectively. At 10^9 GeV, Fly's Eye can study the penetration of the first interaction point to measure nuclear cross sections at ultra-relativistic energies.

Let me go on to discuss the relevance to primary cosmic rays of knowing the nuclear physics, but before I do that let me describe what a typical experiment in cosmic rays involves. What we have coming in from the top of the atmosphere is an object called a nucleus (see Figure 2). It consists, we know, of nucleons, and it travels through the atmosphere, collides and leads to production of particles as it goes along. The model to describe this process which is generally used is what I would call the superposition model. It belongs to a class of independent constituent models, like one imagines when quarks are going thru a nucleus; here we have nucleons going through and colliding with other nucleons inside a nucleus. Protons with energy E_o can be compared to iron nuclei with energy E_o/A because they will make the same kind of

shower, with about the same total number of electrons. So, by observing something down below, some debris at the bottom of the atmosphere, we want to find out what's coming in; that's similar to deriving quark properties using independent constituent model of a proton by observing the crud coming out of the nucleus, it's a different kind of crud.

Now consider propagation, acceleration and origin of cosmic rays, I would like to briefly tell you what are the interesting questions and why this will be important.

First of all, what are the sources? Are they supernovae explosions? Or are there some other sources? How are they distributed? Are they distributed in the disk? Are there some local source like a nearby supernova? How do we study what is the nature of the sources?

Secondly, where does the acceleration take place? Does it take place in the source? There are many mechanisms for this to happen. One of the most popular ones for a few years was shock wave acceleration of cosmic rays in supernova explosions (13), or it could be electromagnetic accleration due to high magnetic fields like that which exists in many of the pulsars (14). You have 10^{12} gauss fields rotating rapidly and you can accelerate particles to as high an energy as you wish before they get out of it. Or it could be acceleration in the galaxy as was proposed originally by Fermi (15). Some cosmic rays are probably metagalactic in origin coming from outside the galaxy.

Now, the third question is: What is in between the source and where we receive the particles? And one way to find out what happens during the propagation is to ask how many secondary nuclei are produced by the fragmentations of the primary nuclei from the source which produces cosmic rays. It can be related to what is called containment time and one can try and find out something about the galactic magnetic fields and other things from studying abundance of secondary nuclei. In order to show you how these things are related and where accelerators play a role, I'll briefly discuss a specific model.

A favorite model at the moment is called the leaky box model of the origin and propagation of cosmic rays. I think it was first proposed by Scott and Chevalier (16), and of course many people have developed it. The present situation with experimental data is summarized by Ormes and Freier in a recent astrophysical journal article (17). What you assume is that whatever the sources are, they inject the cosmic rays spectra with the same index, γ_o, where the power law for the differential spectrum for many classes of acceleration models will be around 2.5. They assume, actually, 2.3 for the injection spectrum and their model assumes that electrons, protons, alphas, C, O, neon, magnesium, silicon and iron are all accelerated in the galaxy. It is an equilibrium model, so you can write down the equation that the rate of change of any species is given by the source strength plus all contributions from species with atomic weight greater that the particular species due to fragmentation. In the

steady state the observed flux for the ith species, J_i, can be related to the source strength Q_i and the fluxes of nuclei heavier than the ith species by:

$$J_i = \lambda_{eff} \left\{ \frac{Q_i}{a} + \sum{}' \left(J_j / \lambda_{ij} \right) \right\}$$

where

$$\frac{\lambda_{eff}}{a} = \left\{ \frac{1}{\tau_e} + \frac{1}{\tau_{int}} + \frac{1}{\tau_d} \right\}^{-1}$$

and

λ_{ij} = interaction length for species j giving rise to species i.

The three terms are escape time, interaction time and diffusion time. In steady state this is the equation and notice what you get is that observed fluxes of the ith element are primarily related to the source if the second term is neglected. For secondaries this term is the important one because $Q_i = 0$. So for primary nuclei, the spectrum that you see is equal to the spectrum of the source multiplied by a lambda effective. If the effective leakage length is energy-dependent function, then you will get a different observed slope than at the origin.

This equation indicates that there are a large number of parameters which go into the equation in order to relate the source composition to observes cosmic rays and, in general, if lambda effective is $E^{-\delta}$, then the observed slope is larger than the source slope. In fact, one finds the following: that the observed slope is steeper by about .4 in spectral index; so if the injected at 2.3 the slope should come at 2.7. And this model actually will say that all spectra at high enough energy, because of leakage dominates, will have the same spectral index. As pointed out earlier, in fact, that's not true; just to give you some idea, below 10^{15} electron volts, I showed you we have a varying composition with increasing importance of iron, the all particle spectrum being made up of two components, one varying at $E^{-2.7}$ and the other going at $E^{-2.3}$ approximately. There is very little anisotropy of cosmic rays observed at low energies but you can still accommodate apparently about 15% of local source which could account for the iron. So this sort of gives you, I hope, the flavor of what primary cosmic rays are like.

A 20 GeV by 20 GeV per nucleon machine would give us the parameters we need to really be sure of what is it that we can learn out of observing cosmic ray air showers about the primary composition. At higher energies I don't know yet what we will do, but it is an interesting question. To acquaint you with cosmic ray methods to study very high energy with air showers, I give a sample outline of how it is done.

Very High Energy Cosmic Ray Experiments

A typical cosmic experiment arrangement is shown in Figure 2. You start off, as I said, with something coming in which you don't know and then you decide you want to look for something so you put a little detector at sea level. Then you find when you do the experiment that you need to know more about what happens because you are trying to study what comes in and what happens in the first interactions and one detector won't do. So then you are ambitious and you build a larger detector, and so what we now have is a complete air shower detector on which most of the results are based. You have a series of detectors to detect electrons. In the shower, electrons are generated by gamma rays which in turn are generated by pi zeros in nuclear collisions or from decay and where you detect them they are spread out over a kilometer. To detect hadrons, we use calorimeters which measure their energy and their lateral spread and then underground we have muon detectors which are symbolically shown and way underground you have a high energy muon detector about 1 mile below the surface of the earth. From all this information you want to find several things: what is the primary energy, composition and what is the nature of high energy interactions. And if you are still more ambitious, you put in a detector called the "Fly's Eye" which looks at the nitrogen fluorescence from air showers and measures their longitudinal development.

The nuclear-electromagnetic shower starts near the top of the atmosphere, some 20 kilometers high. The overall transit time for particles moving

with the speed of light (photons, energetic electrons, high energy hadrons and muons) is of the order of 60 micro-seconds. The shower front, however, is well defined having a thickness of the order of 6 to 9 nano-seconds or 3 meters. Slow hadrons, low energy muons lag behind the shower front by time intervals from a few nano-seconds to hundreds of micro-seconds.

The Fly's Eye, which detects nitrogen flourescence from the air shower can only operate during dark hours, hence its efficiency is only 5%. However response functions of the Fly's Eye is a function which increases with energy, because the higher the energy of the shower, the farther away you can see; and therefore the geometrical factor increases more rapidly than the slope of the spectrum. This is true up to a certain energy and then it stops rising, the end then falls off because of light absorption in the air. At Dugway, where Fly's Eye is located, you can see up to 10 kilometers. (Dugway military base is where they store nerve gas (laughter) but it's a very comfortable spot.)

Now, let me tell you briefly how one tries to determine various properties of high energy interactions from cosmic rays indirectly. Indirect observations use a variety of methods: for instance measuring the ratio of positive to negative muons at high energies. High energy muons come from pion decay, and extreme high energy ones must come from very high up because the highest energy pions exists in the first few collisions. Also, the atmosphere is the thinnest in the first collisions so the

probability of decay is higher. So, most high energy muons come from the first few collisions and therefore measuring mu plus to mu minus ratio tells you two things. If you know the composition, it tells you something about the inclusive cross-section in the fragmentation region at very high energies. If you don't know the composition and want to find out the composition, you assume a scaling law based upon the accelerator data and calculate how many mu plus to mu minus there should be. It's quite sensitive to the difference between pion and kaon scaling functions for inclusive cross-sections from nuclei. If these functions are accurately measured at accelerators, cosmic ray physicists would be delighted!

Figure 3 shows experimental measurements of the muon charge ratio. The best data indicates a slight decrease in the ratio above 1 TeV. This is consistent with increasing fraction of iron in cosmic rays above 10 TeV (18).

Multiple muons at high energies are very sensitive of measurments of primary composition. There is now a new detector in Homestake mine, a goldmine which is still profitably operated; the price of gold is still going up in South Dakota (19). Ray Davis has his big detector for solar neutrinos and around the solar neutrino detector there was enough space to fill it up with muon detectors; water Cherenkov counters were installed which completely covered the tank all around and with an anti-coincidence shield on top. This detector, of the Pennsylvania group has an area of

200 sq. meters, is located at 1 mile depth and is being used to observe multiple muons. The average energy of the muons is 3 TeV. You measure the relative frequency of one, two and several muons arriving at this depth. The ratios of the frequencies depends critically on the primary mass, because we are riding on a steep spectrum. For a given total energy iron produces more muons than proton does, higher up in the atmosphere and these decay more easily. Using this, you can actually determine the composition.

Another technique of measuring the composition is to measure the total number of muons in a shower and the total number of electrons in a shower and determine their ratio (19, 20). This quantity is very sensitive to the primary composition. Experimental results are shown in Figure 4, where the average value for a total number of muons is compared with that of the total number of electrons. Monte-Carlo curves are also shown on the graph which shows two lines, a proton line and an iron line. A comparison of the curves with data requires substantial fraction of iron. If you knew the nuclear physics better you'd have much greater confidence in generating these curves and deriving primary composition.

Another parameter you can study is the shower maximum; how rapidly a shower builds up. If it's made up out of iron nuclei, you have many more nucleons to start the shower and a shower starts extremely rapidly compared to a shower started by a very high energy proton; and the difference in the rate of increase of the shower curve is a way you can

determine the primary composition. Figure 5 shows experimental data on location of the shower maximum (21). The maximum is about 150 g/cm^2 smaller in depth for iron primaries as compared to proton primaries. The data appears to favor iron primaries.

Similarly, you can study the fluctuations in the number of muons as a function of shower size which is shown in Figure 6 (22) and again here you can see that the data is somewhere in between what is expected for pure iron or pure protons. But I think it's clear that nobody can rule the presence of a lot of iron.

At this point we must reexamine figure 1 which shows the composite energy spectrum and remark that if the composition indicates the dominance of iron near 10^6 GeV, the steepening in the total cosmic ray spectrum requires that the iron spectrum must be cut off around 10^7 GeV. One possible way to terminate the iron spectrum is to suggest that iron nuclei are destroyed by photodisintegration in the source region. This would imply a sufficiently high temperature in the acceleration region, of the order of 1000^{o}C. Other possible mechanisms could be devised, but these must preferentially remove iron as the cosmic ray spectrum extends several orders beyond 10^7 GeV. Another remark is that if one is observing the source spectrum with iron around 10^6-10^7 GeV and if the source is local then one should observe some anistropy in the arrival direction of cosmic rays. The dilemma is that up to to about 10^6GeV the observed anistropy is small, less than 0.5%. This, however, may be due to

scattering by magnetic fields unless the source is very close. But it is true that after you get up to 10^{17} electron volts the anistropy increases to about 5, maybe even 10% before starting to decrease again when you go to extremely high energies. So the scenario right now is very interesting and quite complex.

The question of the nature of the most energetic cosmic rays is still open. Around 10^{11} GeV some tens of events have been detected by very large air shower detectors (Sidney array, Haverrah Park array and Yakutsk array). Fly's Eye detector may be able to address the question of their nature.

In the preceeding discussion, I have talked about iron as being the primary thing which is produced at the source. If that is a correct hypothesis, then protons and alphas must come from fragmentation of all of the heavier nuclei. In other words, they are all secondaries; maybe there are some primaries because there may be some sources which have protons dominance. But suppose we do not assume that, then is it possible t fit the data, within the uracies we have, with protons and alphas coming essentially from fragmentation of heavier nuclei through interstellar matter? This is a proposal made by Peters and Westgard (23) and they show that it is just feasable. So any information on the production rate of alphas and protons from high energy collisions would be extremely important to check theories of the origin of cosmic rays as the calculations are based on low energy accelerator data.

The other point I wanted to make with regard to very high energy nucleus-nucleus collisions is that there is a collection of cosmic ray events, which go up to about 30-40 GeV per nucleon. And there is a recent paper by Phyllis Frier and Jake Waddington which reports on a study of nuclear collisions around 15 GeV per nucleon, and you might be interested in looking at those events to see correlations they observe (24).

Unusual Events at 10^6 GeV

a) Detectors and Rates:

I go on to discuss individual events and tell you something about the Centauro events. I do it in two steps. I discuss the instrumental techniques that are used and first point out to you that if you analyze events called C-jets, jets where you know the location of the interaction, occurring in a block of wood or a block of iron, and if you compare them with events generated by Monte-Carlo techniques using scaling models that we know at lower energies you find no evidence of gross violation of scaling in the fragmentation region. Also, note that there is no information in the central region from cosmic ray data. If you go to higher energies, above 100 TeV, (between 100 and 500 TeV) you find unusual events called the Centauro events, which form a substantial fraction of the total number of events observed; and I want to show you why they are unusual and why they might provide interesting pointers for what to expect in the future. I won't discuss any of the interesting

phenomena that have been observed in other experiments. You can find a discussion of them in the Bartol proceedings and in a review paper I gave at Gif-sur-Yvette last summer (25).

I want to give you an idea of the kind of detectors you need. In Figure 7, I plot the size of a detector needed to get one event with a total energy greater than a thousand TeV. If you are at sea level, you need something like 10,000 sq. meters of detector. At Chacaltaya, which is at mountain altitude, you get one event per year in about 30-40 sq. meters. If you go into a satellite you can get one event with a detector with .1 to 1 sq. meters, depending on how long you can convince the government to keep it up there.

So, typical detectors to study high energy events need large collecting area, and different particles (protons, hadrons, muons and electrons) need different instruments to detect them. If the experimental technique uses nuclear emulsion chambers (which are used in balloons or satellites), they have to stay up about 1 sq. meter days to reach up to almost 100 TeV. The quantities measured by these detectors are charged particle energy, gamma ray energy; also the location of the interaction. The primary is usually seen in emulsion chambers which are flown. So, there's a great deal of advantage to fly such detectors; however, you can't reach much above 100 TeV. The error in charged particle energies is about 20%, the gamma ray energy is 10%, location is known to micrometers and as I said the primary is seen. On the mountain, however, one used x-ray nuclear

emulsion chambers whose sized vary from 40 to 1,000 meters square year, and you can obtain events up to several thousand TeV. The hadron jet energies are measured to 20%, gamma ray jets are measured to 20%, location of each jet is known to 1 to 10 microns; however, the primary particle and the point of interaction is usually not seen. You have to infer everything about the primary particle from the secondaries. In Table 1, I give a summary of properties of various detectors used in cosmic ray experiments.

Let us discuss one of these detectors (26) in terms of its structure and components; I will discuss the Mount Chacaltaya detector (Figure 8). The detector consists of two chambers (two cameras). The upper chamber which is 44.2 sq. meters consists of 10 cm. of lead or 20 radiation lengths, and there are layers of film immersed in between various layers of lead, a typical sandwich being 3 x-ray films and one 50 micron nuclear emulsion. The x-ray films are used to pick out the high energy events and the 50 micron nuclear emulsions are used to count the electrons in the jets. Of course you have to support the stack, so in addition to the absorber, which is 23 cm. of pitch, you have wood supports. The important thing about this detector is there is a big gap of 151 cm. of air between the chambers so as to be able to look at spreading of jets in the lower chamber. What you detect with such a chamber are the following kinds of events (Figures 9,10):

If you have a single, high energy photon impinging on the stack, you will get what is known as a gamma jet. The gamma jet, which is schematically shown is an electron-photon cascade; the figure indicates its development both laterally and longitudinally. Also shown is a jet; a C-jet. A C-jet is generated by an interaction in the absorber. And a typical C-jet would produce a gamma ray or a hadron which will make a collection of black spots in the lower film. A single hadron coming in sometimes can penetrate all the way down and produce a lead jet in the lower chamber. I'm going to first talk about events like these C-jet events in which there is nothing in the top chamber but there is something in the bottom chamber. I'll follow that with discussing A-jets, because all of the centauro events are the A-jet events.

There are two kinds of atmospheric jets you can get (Figure 10). One is called the gamma cascade. This cascade has a single gamma ray coming in; it multiplies and makes several sets of gamma rays and you get a collection of gamma rays which is called a cascade jet. Or you can get a hadronic interaction and you'll get in such hadronic interaction atmospheric gamma rays, pions, nucleons, some of them will make interactions in the absorber so you get a family of jets of different types giving a very complex structure which is called an A-jet.

A summary of event rates collected by various emulsion chambers and x-ray chambers is given in Table 2. Several hundred events with visible energies above 100 TeV have been detected up to now.

b) Selection of events:

What they do is to take their x-ray films and put them up against the light and look for black spots. A black spot is created if there is enough density of electrons per sq. micron, so as to develop sufficient grain density in the x-ray film. You need approximately .1 to 1 particles per sq. micron which corresponds to a density per sq. cm. of the order of 10^4, in order to make a black spot in those particular x-ray films. The reason they use the x-ray film is that they can expose it for a year without the x-ray films fogging up. Also the detection threshold is high (>TeV).

When they find the dark spots, they go to the nuclear emulsion and look at the nuclear emulsion and count the number of electrons. The number of electrons they see is proportional to the energy of the gamma ray. They do that as a function of depth and reconstruct the whole cascade. If a particular event starts deep down in the lead, then they say that it is a hadron. The chances for that being a gamma ray is very small. And that's how they identify which jets are due to hadrons and which are made by electrons or photons.

You can measure the direction of propagation. You can measure the cascade curve for each gamma ray, darkness as a function of thickness; and you can measure the separation of each of the gamma rays. You can also count tracks in the emulsion. When you do all that, you get a very

good measurement of the energy. The capability of hadron-photon separation is illustrated by a starting point distribution (Figure 11). This is the starting point distribution of cascades above 200 GeV, and those which start right away they call gamma rays and those which start beyond 8 r.d. they call hadrons. So they know how many are pions or nucleons - charged pions or nucleons or neutrons or anti-nucleons, and how many are gamma rays that are coming in in each one of those cascades. To check their identification they combine gamma rays in pairs (make marriages of gamma rays) and plot the gamma-gamma mass where they see pi-zero quite clearly.

c) Scaling in fragmentation region below 100 TeV:

Now, what can they measure? They can measure, therefore, the total energy of each of these black spots, each of the cascades. Let me just remark that if you require gamma rays to have the same azimuth and the same zenith to belong to the same family, you have no problem with any accidental coincidences, so that they really see families as a whole. There is a background of gamma rays but that's not what we are talking about. So, if you know the energy of each gamma ray and if you know the total energy, then you can calculate the fractional energy in each gamma ray for a family. The histogram of gamma ray energies is shown in Figure 12a for different energy events. These are all C-jets or jets which took place in the absorber. Energies are grouped between 7 and 10 TeV, 10 and 15 TeV, 15 and 40 TeV, and this is greater than 50 TeV. If you plot it as a fractional energy, you find that it scales (Figure 12b).

To investigate whether the observed fractional energy distribution is consistent with a continuation of scaling behavior characteristic of inclusive particle production at accelerator energies, a detailed Monte-Carlo calculation was done. This calculation incorporated biases introduced by the steep primary spectrum, selection criteria and experimental resolution (30). The scaling functions used were parametrized by e^{-Bx} where x is Feynman variable. In Figure 13, the shaded region indicates experimental spread while the different points represent Monte-Carlo results showing effects of varying scaling parameter B. One notices that the experiment is rather insensitive as a fine test of scaling but gross violations of scaling are definitely excluded.

So, up to a hundred TeV scaling holds, everything looks pretty good; so what are these unusual events? And the reason I want to mention them is of course we don't understand them. The unusual events, the Centauro events, have the following feature: That you have in those events, at production, something of the order of 100 hadrons, and no gamma rays. Now this is something which ordinary physics doesn't give, so that's why it's very exciting and so let me show you what such an event looks like.

d) Centauro event:

Here is the Centauro event that was seen (Figure 14). In the lower chamber one saw many, many jets with a lateral spread of only one cm. You measured the directions exactly and you found that the direction was

such that you should see something in the upper chamber. In the upper chamber they only saw about 6 or 7 jets, no more. And that brought the event to their attention because it was very unusual. Ordinarily, if you see so many jets in the lower chamber, you see many more in the upper chamber. So, it's the reverse situation; you see many more hadronic jets in the lower chamber but nothing in the upper. The trajectory traversed both the absorber and the wood support.

How does one reconstruct this event? What you do is first of all laboriously measure each one of these families, and notice here that close spaced clusters have been counted as one, basically, and that's because they are so close together that they cannot be due to two different hadrons coming from far above, the interaction must have taken place nearby.

Nobody knows where these crosses should be made. They are just artists guesswork. The only thing we know is that interaction took place somewhere in between the top and the bottom. Two of these jets penetrated enough that they could be lined up between the lower and upper chamber and one could measure the change in their relative separation. By measuring the relative separation you can find out where they came from. It was determined that they came from 50 meters above the target. Then, you can also measure the relative separation of individual jets as a function of depth in the lower chamber. When you do that, you can extrapolate backwards and ask where did they all come from? You assume

they came from the same point, when one calculates the point of origin it also comes out to be (50 $\pm$ 10) meters. That's the basis upon which this event is supposed to have taken place very nearby in the air. Also the one cm spread is an extremely small spread. Let me show you what the event looks like.

Figure 15 shows the development of the Centauro event in the chambers. The energies of individual jets are measured by counting electrons and determining the darkness of spots in the x-ray films.

Let me show you what the event looks like in Table 3. This is the first event and still the best event that they had. The number of identified lead jets and C-jets are 45. The number of nuclear active particles which should have gone all the way through without interacting was estimated to be 15. The number of lead jets identified in the upper chamber was only 5.

What do we see here? We see that the table gives you how many jets there are which they call gamma rays in the upper chamber and how many jets were in the lower chamber. Basically, look at the two numbers. There were 7 jets in the upper chamber and there were something of the order of 7, plus 29 plus 7 altogether in the lower chamber. Now, the total energy in the upper chamber was only 28 TeV; the total visible energy in the lower chamber was 202 TeV, the total visible energy is 230 TeV. If you assume that the amount of energy going into pi zeros

and therefore into gamma rays is about .2 of the total energy, then that would give 1700 TeV for the primary. But that is anybody's guess; nobody knows how to do it for these strange events, how to calculate the total energy; but it's a good estimate. Now, how do we calculate how many nucleons are incident upon the device? Well, the way they do it is by this particular method:

By using C-jets, they can determine the interaction length and the absorption length of each one of these high energy hadrons. Using that, they start from the bottom and plot an integral curve (31). If you have 7 jets, starting with 7 jets in the lower chamber, then go upwards and add the next set in the target layer and add the next set, and then you draw a curve through them based upon your knowledge of the interaction (Figure 16). You normalize that; and when you do that you can go all the way up to the interaction point. There should be about 65 nucleons or hadrons at the interaction point. Then there are some which miss at the bottom and we have to correct for that. That's how they find out how many hadrons are produced at the interaction. Now, given the fact that you have so many hadrons at production, if they were pions then you must have an equal number of pi plus, pi minus and pi zeros. The pi zeros will then decay and you can ask how many of them will make a jet, which is visible in the upper chamber. After you do that calculation, you find that you should have seen at least 15 gamma ray jets above threshold. In addition, you should have seen another 7 because the hadrons themselves will interact and produce secondary pi zeros. So you

should have seen a certian number of gamma ray jets in the upper chamber. And you saw none, that's why this is a really fantastic event. This fact is given in Table 4 which shows that the number of showers seen in the upper chamber was basically 7, the number of gamma rays and electrons incident upon the upper chamber was basically -4 because they had to correct this 7 for the number of lead jets that should have been in there.

The important point is that the number of gamma rays and electrons at production is negative or very small, while the total number of hadrons are of the order of 100.

Out of approximately 100 events, they have found 4 or 5 events in which you have an event with a large number of hadrons but very few gamma rays.

These are the Centauro events and in fact there is no explanation for these bacause they are mind boggling and contrary to conventional physics. I have a paper from Bjorken (32) in which he says that one possibility would be that these objects are primordial globs of colored quark matter. And it's a very interesting calculation, probably not true, but (laughter) certainly very entertaining. Now, if they are produced in the primordial situation, can they be produced in heavy ion collisions? That's an interesting question. And I think if these events are found by other groups. I would be very excited about the possibliities at extremely

high energies of making new kinds of matter. But of course it may not be the same matter as Bjorken proposes, it could be something else. Anyhow, the cross section for such processes is very large at these energies; and so even if it occurs occasionally on a 20 GeV on a 20 GeV machine you have the flux to hopefully see something, if such processes exist. Similarly, with $p\bar{p}$ colliders one might see them at Fermilab. Well, this is just tantalizing and very interesting to speculate upon. Whether they exist or not, however, I think what this tells us is that one should keep one's eyes open and that going to as high an energy as possible is the right thing to do.

Thank you.

References

1. A. M. Hillas, Proceedings of Conference on Cosmic Rays and Particle Physics-1978, edited by T. K. Gaisser, American Institute of Physics, Vol. 49, New York, 1979.

2. N. L. Grigorov et. al., Proceedings of 12th International Conference on Cosmic Rays, Hobart, 5, 1746, 1971.

3. M. J. Ryan, J. F. Ormes, V. K. Balasubrahmanian, Physical Review Letters, 28, 985, 1972.

4. V. K. Balasubrahmanian and J. F. Ormes, Ap. J., 186, 109, 1973.

5. E. Juliusson, Ap. J., 191, 331, 1974.

6. C. D. Orth, et. al., Ap. J., 226, 1147, 1978.

7. T. Kitamura et. al., Proceedings of 14th International Conference on Cosmic Rays, Munich, 6, 2024, 1975.

8. Allkofer et. al., Physical Review Letters, 41, 832, 1978.

9. T. K. Gaisser, R. J. Prothevoe and K. E. Turver, Review of Modern Physics, 50, 859, 1978...A rather complete summary of air shower data can be found in this paper.

10. S. C. Tonwar and B. V. Sreekantan, J. Physics, A4, 868, 1971; S. C. Tonwar et. al., Nuovo Cimento, 1, 531, 1971.

11. J. A. Goodman, R. W. Ellsworth, A. L. Ito, J. R. MacFall, F. Siohan, R. E. Streitmatter, S. C. Tonwar, P. R. Vishwanath and G. B. Yodh, Physical Review Letters, 42, 854, 1979, Physical Review, D19, 2572, 1979; and J. A. Goodman, Ph.D. Thesis, University of Maryland, 1978 (unpublished).

12. G. L. Cassiday, H. E. Bergeson, E. C. Loh, J. W. Elbert and D. Steck, A report on the Utah Fly's Eye, in Proceedings of Bartol Conference on Cosmic Rays and Particle Physics-1978, edited by T. K. Gaisser, AIP, vol. 49, 1979, page 417.

13. F. D. Kahn, Proceedings of 14th ICRC, vol. 11, 3566, 1975.

14. J. P. Ostriker and J. E. Gunn, Ap. J., 157, 1395, 1969 and Physics Review Letters, 22, 728, 1969.

15. C. J. Cesarsky, Proceedings of 15th International Conference on Cosmic Rays, vol. 10, 196, 1977.

16. J. S. Scott and R. A. Chevalier, Ap. J. Letters, 197, L5, 1975.

17. J. F. Ormes and P. Freier, Ap. J., 222, 471, 1978.

18. T. Kitamura, Rapportouer talk, 14th International Conference on Cosmic Rays, Munich, 11, 3925, 1975.

19. M. Deakyne, W. Frati, K. Lande, C. K. Lee and R. I. Steinberg, Proceedings of Bartol Conference on Cosmic Rays and Particle Physics-1978, edited by T. K. Gaisser, AIP publication, vol. 49, 1979, page 409.

20. G. B. Khristianson et. al., Proceedings of 12th International Conference on Cosmic Rays (Hobart), 6, 2097, 1971.

21. M. La Pointe et. al., Can. J. of Physics, 46, 568, 1968.

22. J. W. Elbert et. al., J. of Physics, G2, 971, 1976.

23. B. Peters and N. J. Westergaard, Astrophysics and Space Science, 48, 21, 1977 and I. L. Rasmussen and B. Peters, Nature, 258, 412, 1975.

24. P. S. Freier, Proceedings of Bartol Conference on Cosmic Rays and Particle Physics-1978, edited by T. K. Gaisser, AIP, vol. 49, page 87, 1979. Also papers submitted to the 16th ICRC, Kyoto, Japan, August 1979.

25. G. B. Yodh, High Energy Physics above 10 TeV-A Review, Talk presented at Gif-sur-Yvette French Summer School, September 1978, University of Maryland preprint PP No. 79127, to be published.

26. Brasil-Japan Emulsion chamber collaboration: J. Bellandi Filho et. al., Proceedings of Bartol Conference on Cosmic Rays and Particle Physics-1978, edited by T. K. Gaisser, AIP, 49, 317, 1979; Proceedings of 13th ICRC (Denver), 3, 2227, and 4, 2671, 1973; Proceedings of 14th ICRC (Munich), 7, 2393, 1975; M. Tamada Nuovo Cimento, 41B, 245, 1977; Proceedings of 15th ICRC (Plovdiv), 7, 208, 1977.

27. M. Akashi et. al.; E. C. experiment at Mount Fuji, Proceedings of Bartol Conference on Cosmic Rays and Particle Physics-1978, edited by T. K. Gaisser, AIP, 49, 334, 1979.

28. H. Sugimoto and Y. Sato, ibid, 126, 1979.

29. Anischenko et. al., Conference papers 13th ICRC (Denver), 3, 2228, 1973 and Pamir Collaboration Proceedings of 14th ICRC (Munich), 7, 2365, 23, 70 and 2374, 1975.

30. R. W. Ellsworth, G. B. Yodh and T. K. Gaisser, Proceedings of Bartol Conference on Cosmic Rays and Particle Physics-1978, edited by T. K. Gaisser, AIP, 49, 111, 1979.

31. A detailed discussion of this procedure can be found in "Unusual interactions above 100 TeV - A review" by G. B. Yodh, in the Proceedings of the Symposium on Prospects of Strong Interaction Physics at Isabelle, BNL report 1978.

32. J. D. Bjorken and L. D. McLerran, Proceedings of Bartol Conference on Cosmic Rays and Particle Physics-1978, edited by T. K. Gaisser, AIP, 49, 509, 1979.

Figure Captions

Figure 1: A composite representation of the integral spectrum of cosmic rays from 10 to 10^{11} GeV. Also shown are recent results for the composition below 10^{6} GeV. Diagonal lines are lines of constant intensity for the all particle spectrum.

Figure 2: Experimental arrangement for an air shower experiment at high energies.

Figure 3: Energy variation of charge ratio of single cosmic ray muons.

Figure 4: Average correlation between total number of muons and electrons in air showers.

Figure 5: Depth of shower maximum as a function of total energy.

Figure 6: Fluctuations in the number of muons as a function of energy (shower size).

Figure 7: Exposure factor for detecting one event per year at 1000 TeV.

Figure 8: Schematic of the Japan-Brasil emulsion chamber at Mount Chacaltaya (5200 m altitude).

Figure 9: Classification of individual jets.

Figure 10: Classification of families of jets.

Figure 11: Use of starting point distribution to separate hadron jets from electron-photon jets.

Figure 12a: Integral gamma-jet energy spectra for C-jets.

Figure 12b: Fractional gamma energy spectra for C-jets.

Figure 13: Fractional gamma energy spectra compared with Monte-Carlo calculations.

Figure 14: Artist's schematic of the first Centauro event.

Figure 15: Photomicrographs of the development of the Centauro event.

Figure 16: Integral curve for hadron survival used to estimate number of hadrons at production.

Tables

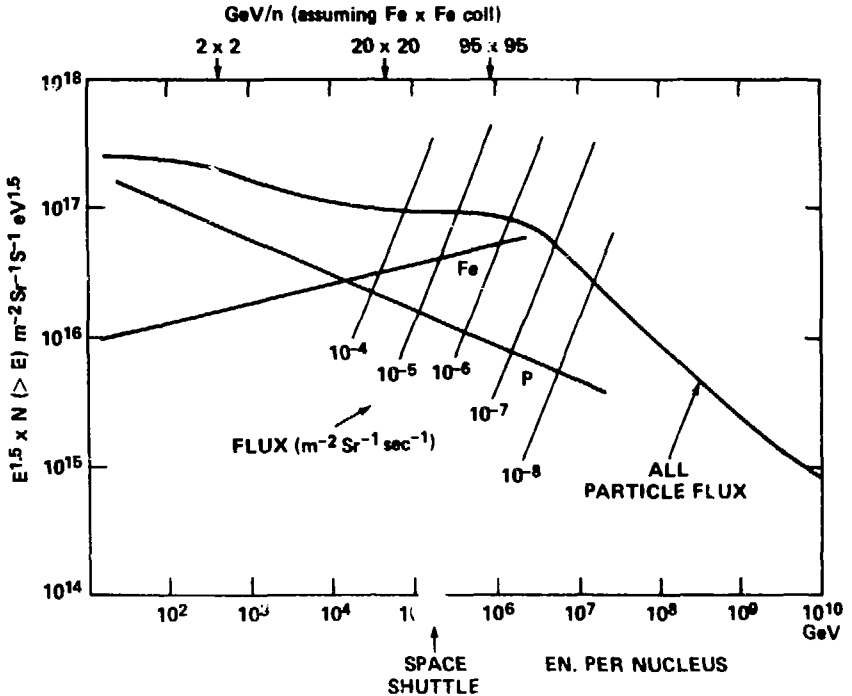
GeV/n (assuming Fe x Fe coll)
2 x 2
20 x 20
95 x 95
10^{18}
10^{17}
10^{16}
10^{15}
10^{14}
$E^{1.5} \times N\ (>E)\ m^{-2}Sr^{-1}S^{-1}\ eV^{1.5}$
Fe
P
10^{-4}
10^{-5}
10^{-6}
10^{-7}
10^{-8}
FLUX ($m^{-2}\,Sr^{-1}\,sec^{-1}$)
ALL
PARTICLE FLUX
10^{2}
10^{4}
10^{6}
10^{7}
10^{8}
10^{9}
10^{10}
GeV
SPACE
SHUTTLE
EN. PER NUCLEUS

Fig. 1

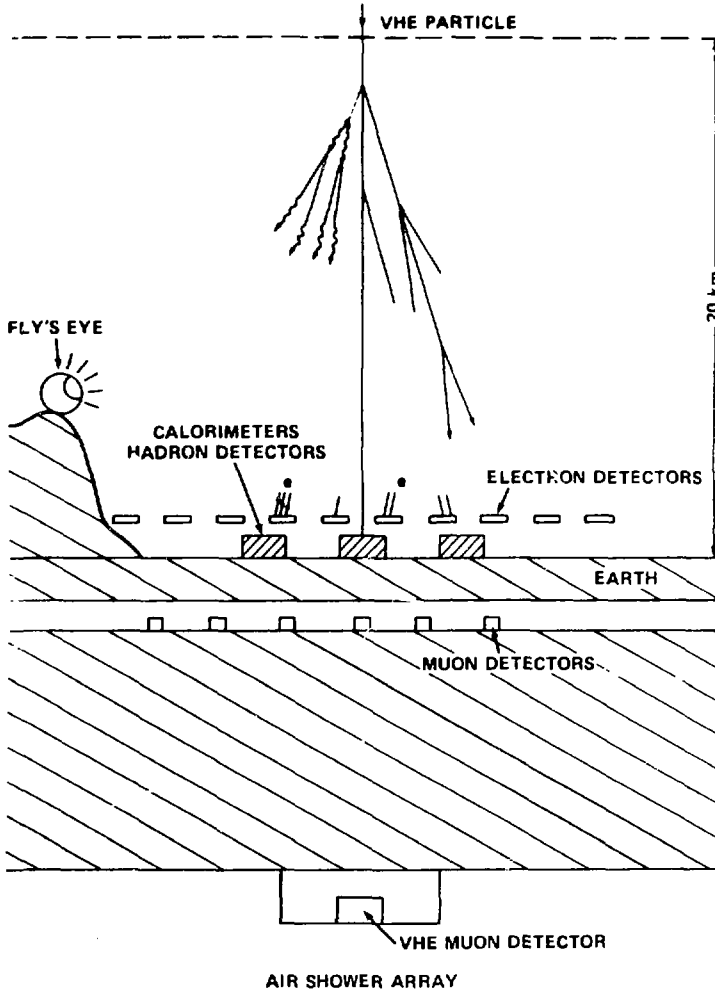
VHE PARTICLE
20 km
FLY'S EYE
CALORIMETERS
HADRON DETECTORS
ELECTRON DETECTORS
EARTH
MUON DETECTORS
VHE MUON DETECTOR
AIR SHOWER ARRAY

Fig. 2

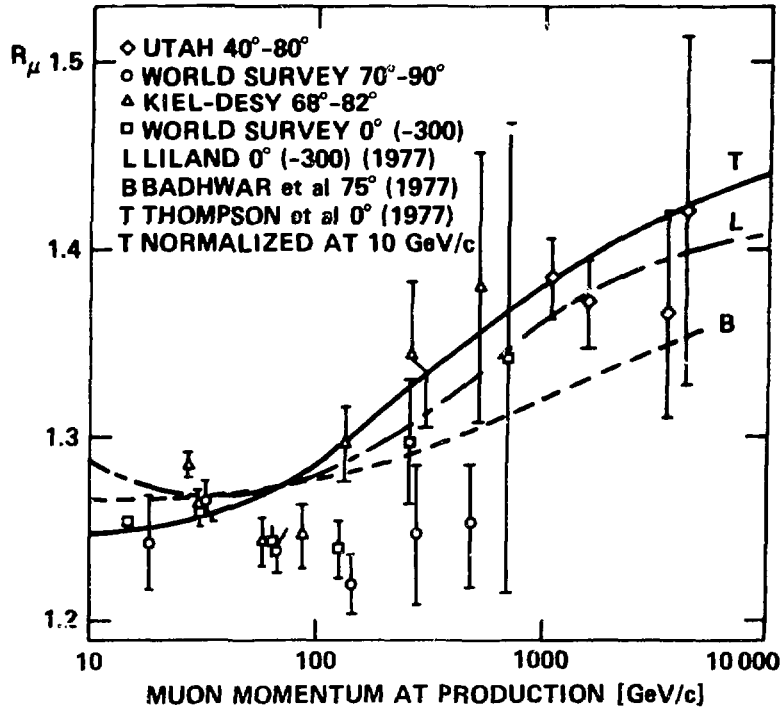
◇ UTAH 40°-80°
○ WORLD SURVEY 70°-90°
△ KIEL-DESY 68°-82°
□ WORLD SURVEY 0° (-300)
L LILAND 0° (-300) (1977)
B BADHWAR et al 75° (1977)
T THOMPSON et al 0° (1977)
T NORMALIZED AT 10 GeV/c
T
L
B
R_μ 1.5
1.4
1.3
1.2
10
100
1000
10 000
MUON MOMENTUM AT PRODUCTION [GeV/c]

Fig. 3

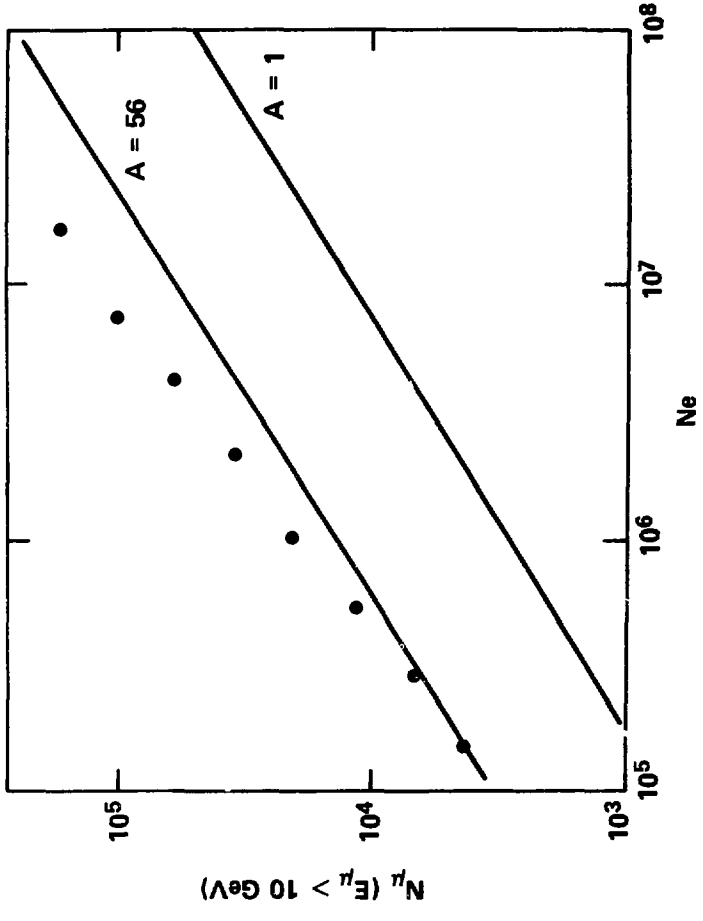

Fig. 4

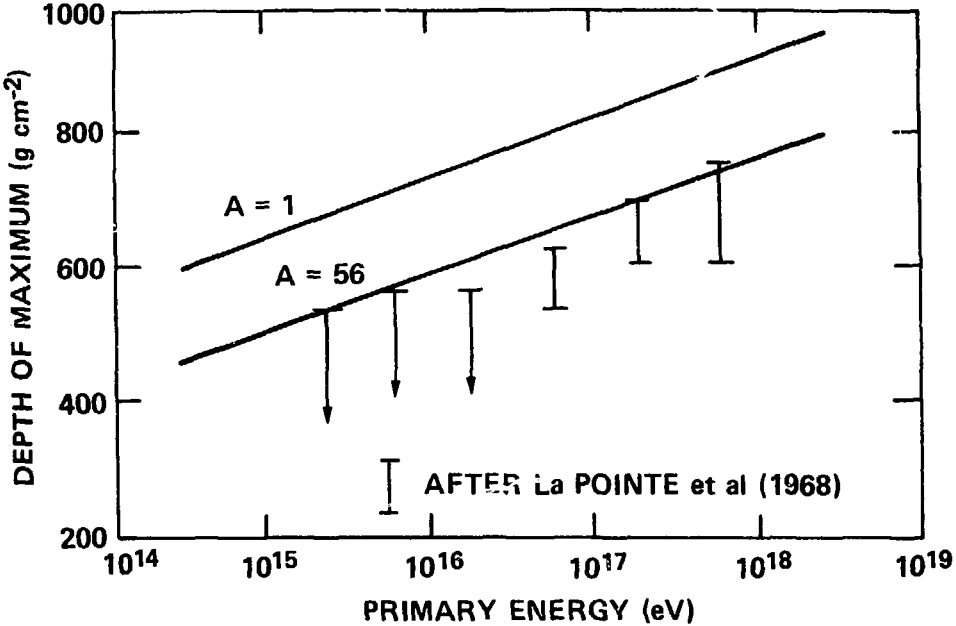
1000
800
600
400
200
DEPTH OF MAXIMUM (g cm^{-2})
A = 1
A = 56
AFTER La POINTE et al (1968)
10^{14}
10^{15}
10^{16}
10^{17}
10^{18}
10^{19}
PRIMARY ENERGY (eV)

Fig. 5

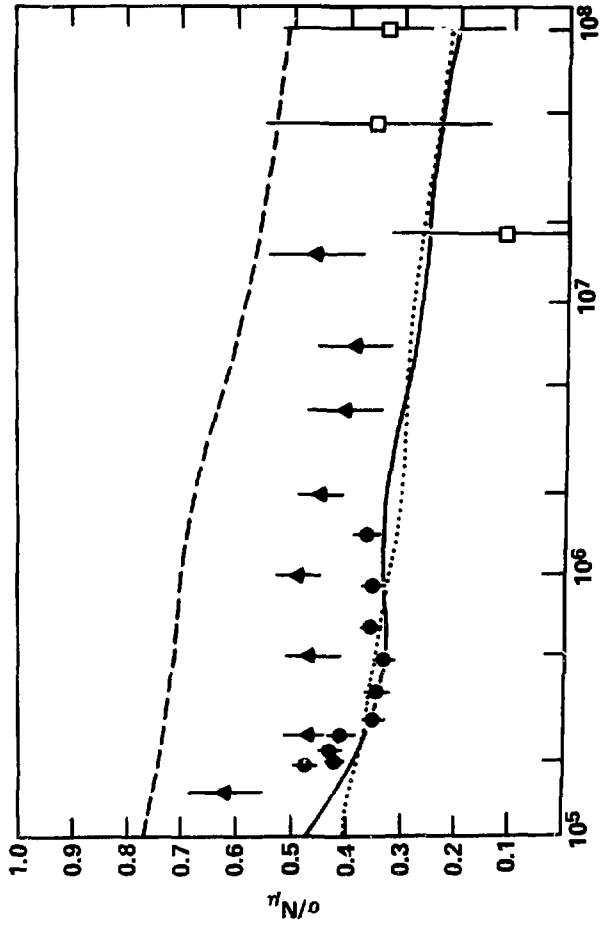

Fig. 6

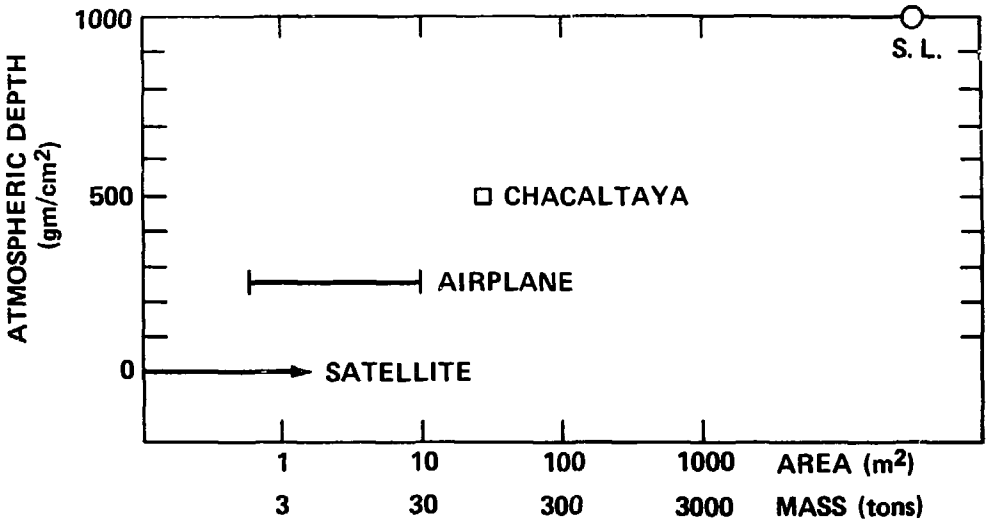
ATMOSPHERIC DEPTH (gm/cm²)
1000
500
0
S. L.
CHACALTAYA
AIRPLANE
SATELLITE
1
10
100
1000
AREA (m²)
3
30
300
3000
MASS (tons)

Fig. 7

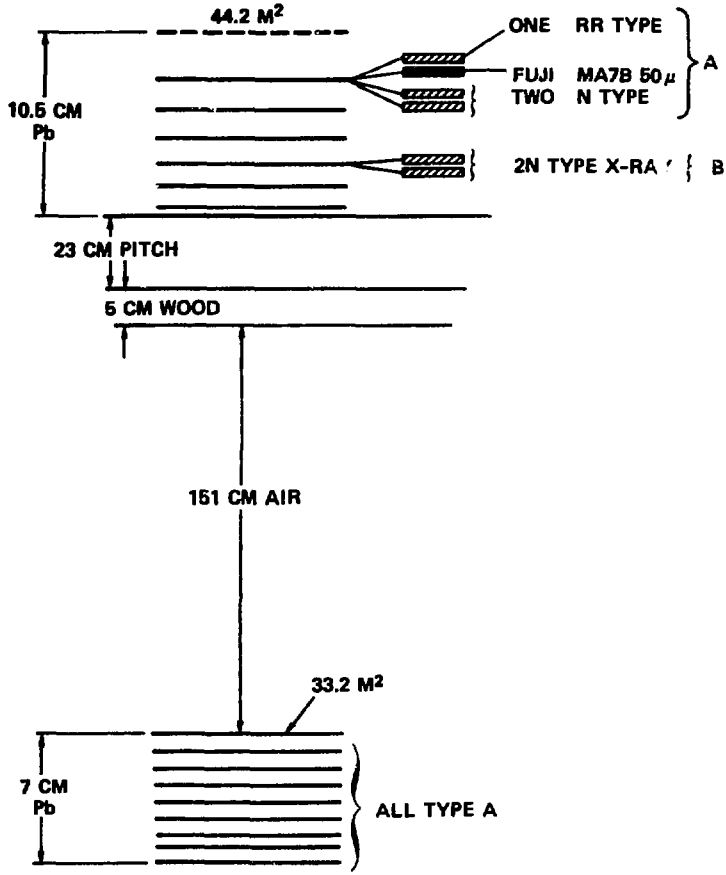

CHAMBER 17

Fig. 8

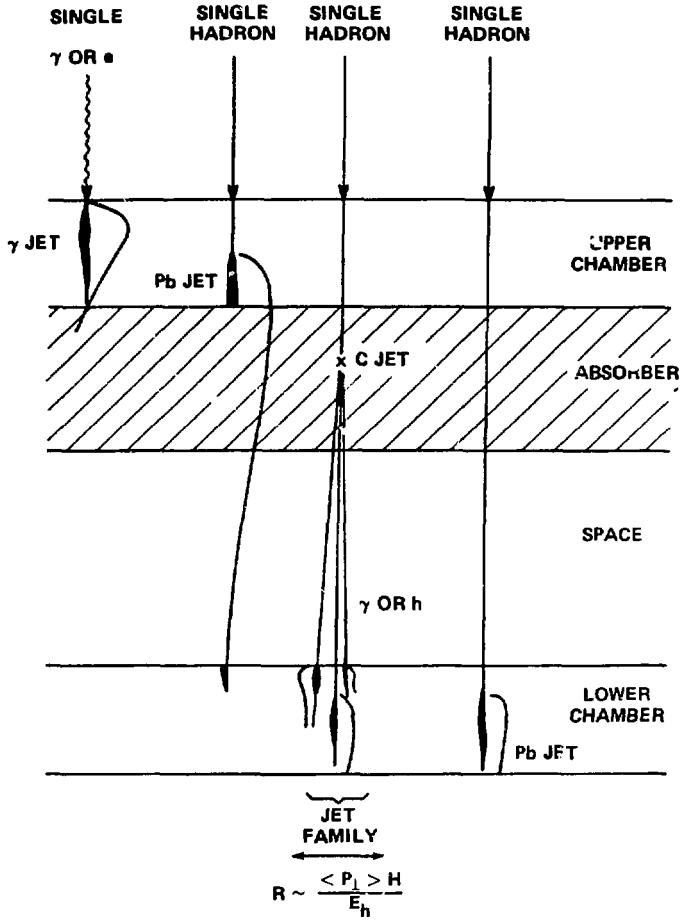
SINGLE
γ OR e
SINGLE
HADRON
SINGLE
HADRON
SINGLE
HADRON
γ JET
Pb JET
UPPER
CHAMBER
x C JET
ABSORBER
SPACE
γ OR h
LOWER
CHAMBER
Pb JET
JET
FAMILY
R ~ <P⊥> H / Eh

Fig. 9

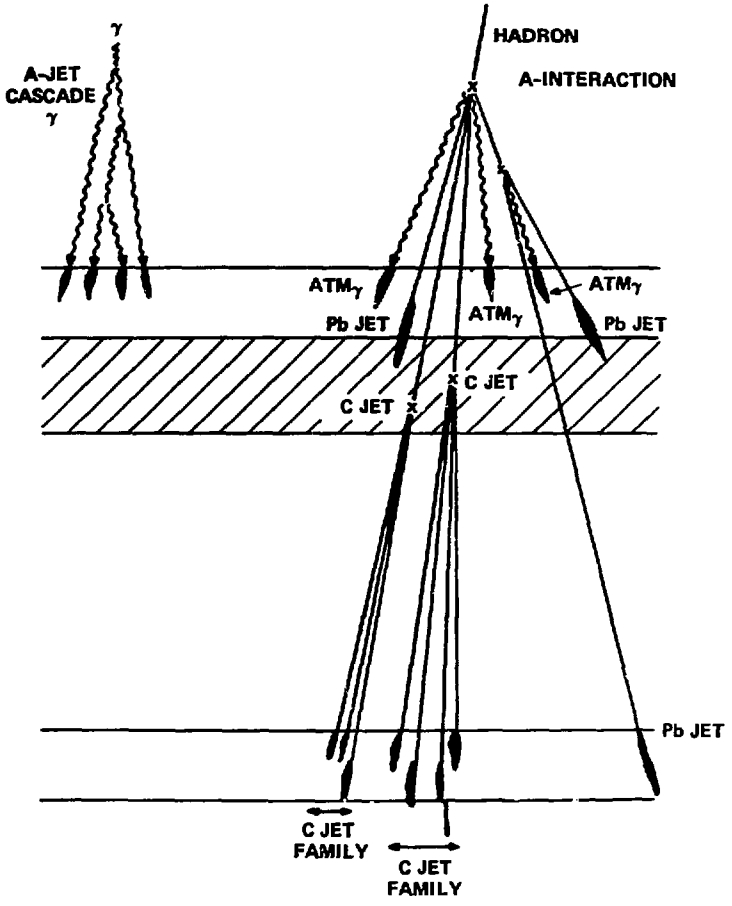
γ
A-JET
CASCADE
γ
HADRON
A-INTERACTION
ATMγ
ATMγ
ATMγ
Pb JET
Pb JET
C JET
C JET
Pb JET
C JET
FAMILY
C JET
FAMILY

Fig. 10

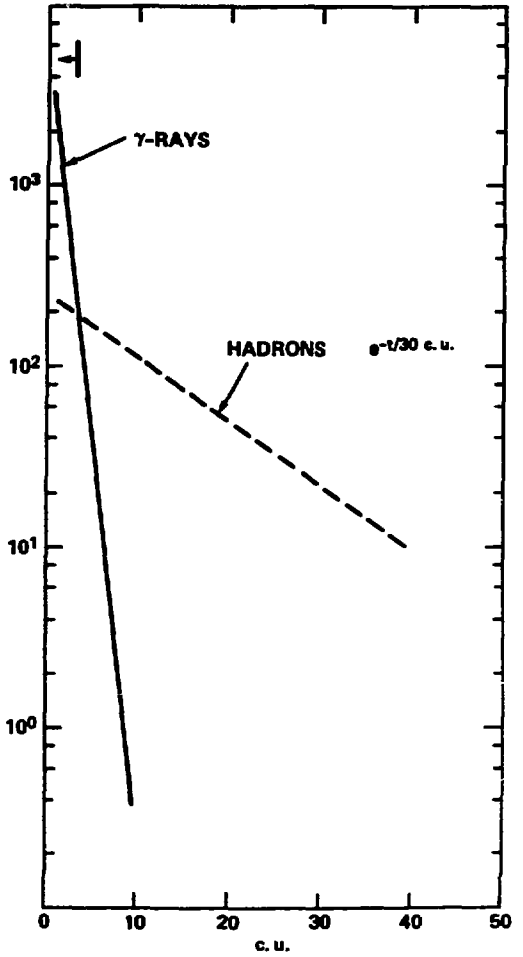

Fig. 11

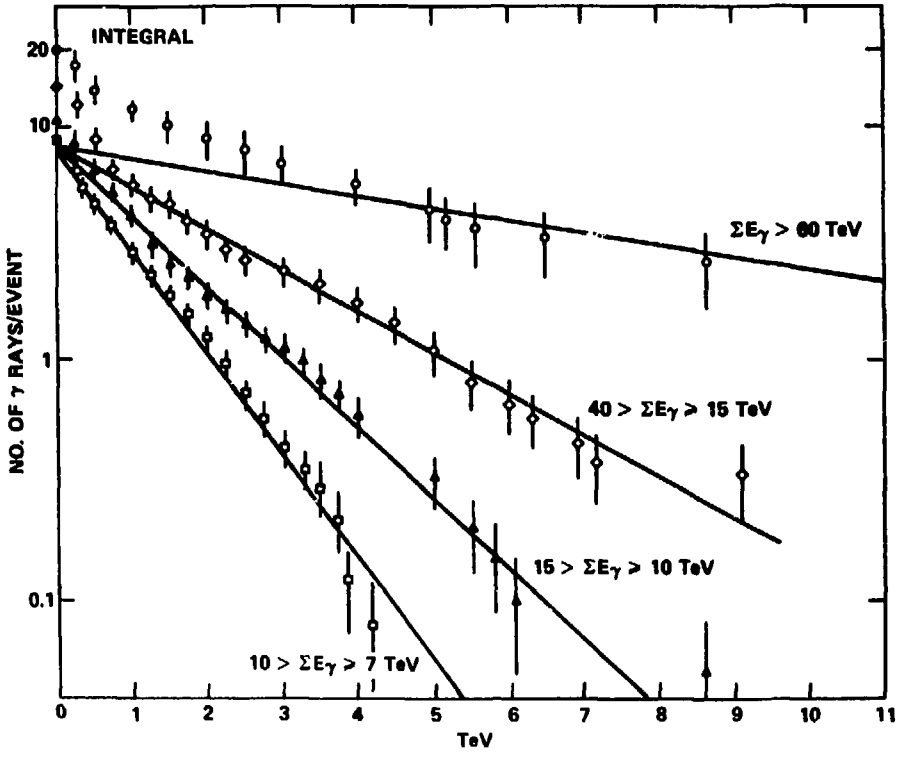
INTEGRAL
20
10
1
0.1
NO. OF γ RAYS/EVENT
ΣEγ > 60 TeV
40 > ΣEγ > 15 TeV
15 > ΣEγ > 10 TeV
10 > ΣEγ > 7 TeV
0
1
2
3
4
5
6
7
8
9
10
11
TeV

Fig. 12a

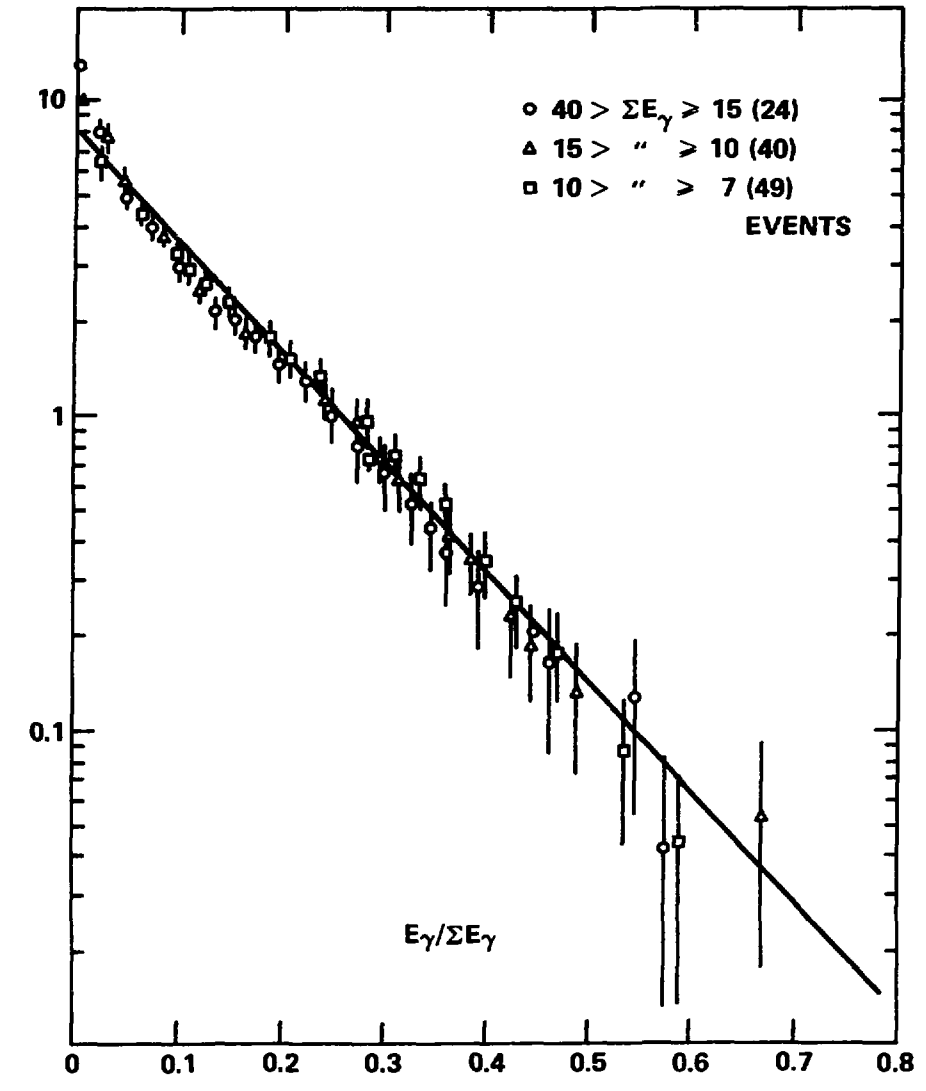
10
1
0.1
0
0.1
0.2
0.3
0.4
0.5
0.6
0.7
0.8
○ 40 > ΣEγ ≥ 15 (24)
△ 15 > " ≥ 10 (40)
□ 10 > " ≥ 7 (49)
EVENTS
Eγ/ΣEγ

Fig. 12b

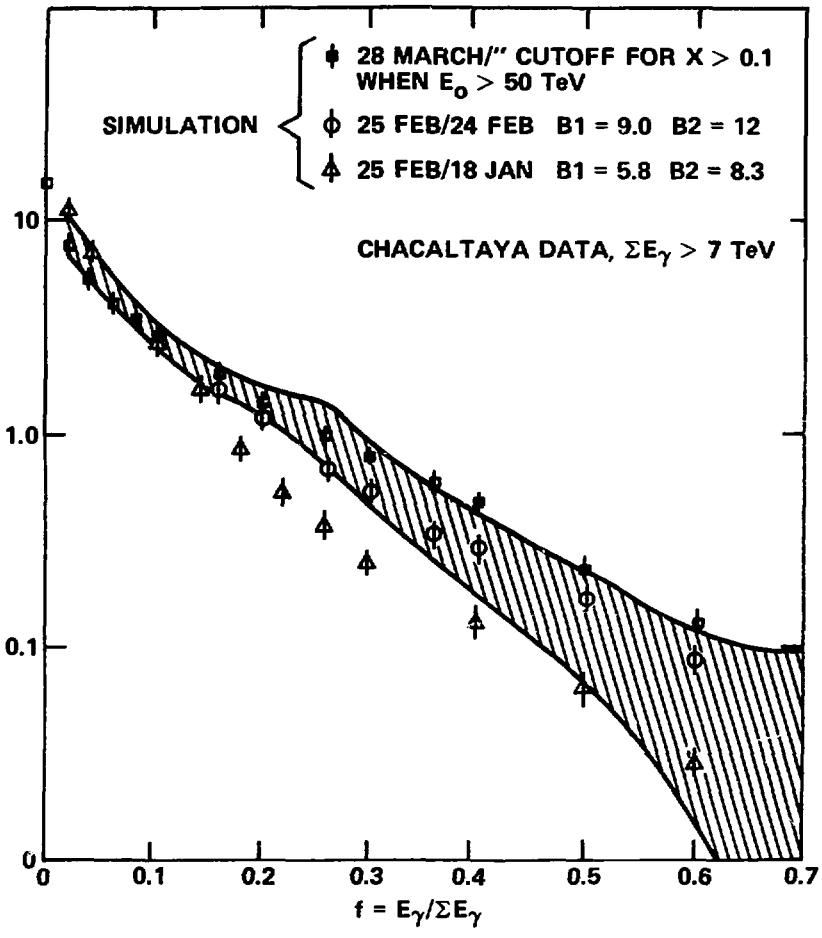
28 MARCH/" CUTOFF FOR X > 0.1
WHEN E_o > 50 TeV
SIMULATION
25 FEB/24 FEB B1 = 9.0 B2 = 12
25 FEB/18 JAN B1 = 5.8 B2 = 8.3
CHACALTAYA DATA, ΣE_γ > 7 TeV
10
1.0
0.1
0
0
0.1
0.2
0.3
0.4
0.5
0.6
0.7
f = $E_\gamma/\Sigma E_\gamma$

Fig. 13

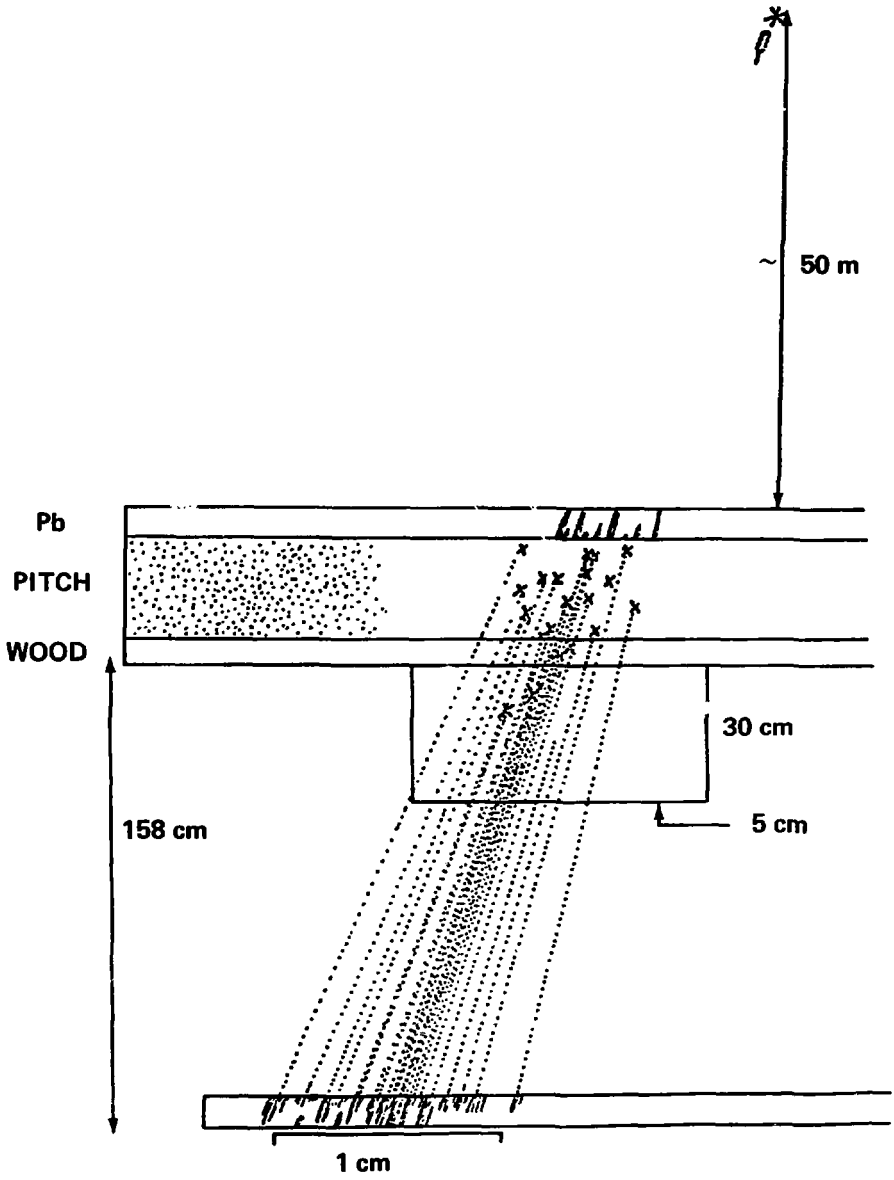

Figure 14

Centauro

Upper Chamber

Sup. 8 c.u.
N type X-ray film

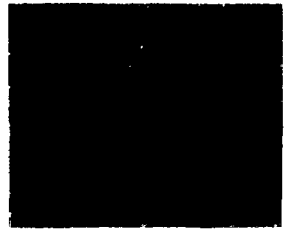

Sup. 12 c.u.
N type X-ray film

Lower Chamber

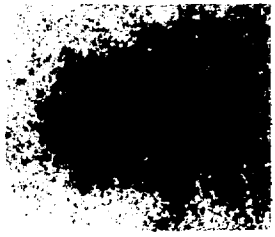

Inf. 8 c.u.
N type X-ray film

Inf. 10 c.u.
N type X-ray film

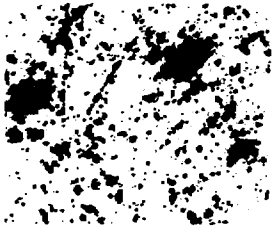

C-jet 4 c.u.
Emulsion

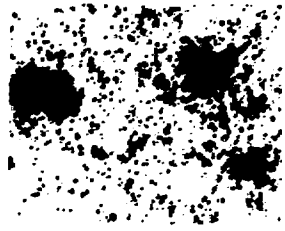

C-jet 6 c.u.
Emulsion

Fig. 15

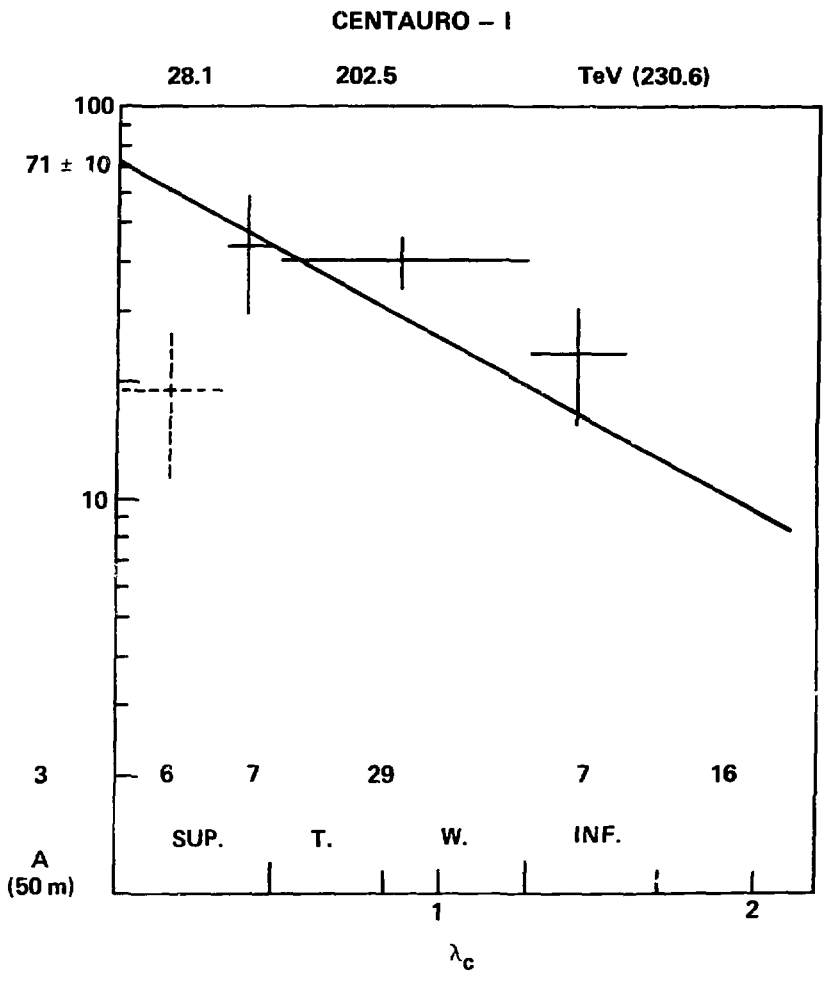
CENTAURO – I
28.1
202.5
TeV (230.6)
100
71 ± 10
10
3
6
7
29
7
16
SUP.
T.
W.
INF.
A
(50 m)
1
2
λ_c

Fig. 16

TABLE 1
STUDY OF INDIVIDUAL HIGH E EVENTS

Low flux needs large collecting area

Different particles need diff. instruments (e.g., -γ, h, μ, e)

Exp. Tech.	Quantity Meas.	How Well?
Nucl. emulsion chambers	Charged ptl energy γ-energy	± 20% M. S. ± 10% Cascade
Balloon, Satellite (Accelerators)	Location	~ 1μm
~ 1m^2 Days. < 100 Tev	Primary	Seen
X-ray, nucl. em. chambers Mt. Level.	Hadron-jets γ-jets	± 20% ± 20%
~ 100 ~ 1000m^2 yr	Location	1 to 10 μm
Up to ~ 1000 Tev	Primary	Not seen
Calorimeters Up to 1000 Tev.	Total energy of h Direction Location Primary	± 10% ± 1° ~ cm Sometimes

Other methods:

Shower cores → Ne_i, r_{ij}, Ne^T, $N_\mu{}^t$ . . . . . .

Multiple μs' → E_μ^{th}, r position-angle . . . . . .

TABLE 2

A NAIVE*SUMMARY OF EMULSION CHAMBER EVENT RATES WITH $\Sigma E\gamma > 100$ TeV

Experiment	Depth g/cm^2	Exposure Factor m^2, Sr, sec	No. of Events with $\Sigma E\gamma > 100$ TeV	Comments
1. Chacaltays				
CH-14	550	1×10^9	25	Only upper chamber exposed and completely scanned.
CH-15-16-17	550	4×10^9	100 (estimated)	Two Storey chamber with nuclear emulsion $E\gamma > 200$ GeV
2. Mt. Fuji [27]	650	1.7×10^{10}	80	Thin single layer EC with X-ray film only $E\gamma > 1.5$ TeV
3. Airplanes [28]	260	9×10^8	9	Two Stocey E. C. with nuclear Em. Complete scan. $E\gamma > 100$-300 GeV
4. Pamirs [29]	~600	3×10^{10} / 10^{10}	83 (reported)	Γ block only $E\gamma > 2$ TeV X-ray films only $\Gamma + H$ and $\Gamma + 3H$ $E_h > 5$ TeV

*Caution: Event selection criteria + steep spectrum = severe biases.

TABLE 3

MULTIPLICITY OF NUCLEAR-ACTIVE PARTICLES

Event No.	I	II	III	IV
Chamber No:	15	17	17	17
No. of identified Pb-jet and C-jets	45	32	37	38
No. of N. A. particles pentrated through	15	18	17	10
No. of Pb-jets (upper) left unidentified	5	16	9	10
No. of N. A. particles incident upon chamber	65	66	63	58
Estimated heighr of parent interaction (m)	50	80	230	500
Estimated number of A-jets	3	5	13	32
Multiplicity of N. A. particles at production	68	71	76	90

TABLE 4

MULTIPLICITY OF GAMMA-RAYS AND ELECTRONS

Event No:	I	II	III	IV
Chamber No:	15	17	17	17
No. of showers in upper chamber	7	14	42	76
No. of Pb-jets (identified plus expected)	11	25	25	25
No. of gamma-rays and electrons incident upon chamber	-4	-11	17	51
Estimated number of gamma-rays from A-jets	4	13	30	47
No. of gamma-rays and electrons at production	-8	-24*	-13*	4

*Location of Centauro II and III in the upper chamber are near an edge of the block, so that number of showers in the upper chamber may be underestimated because of detection loss.

The Production of Systems with Large Mass or Transverse Momentum in High Energy Hadron-Nucleus Collisions

H. Frisch

Physics Department and Enrico Fermi Institute, University of Chicago

In the past decade it has become clear that the hadrons (i.e., the strongly interacting particles such as the proton, neutron, π, K, etc.) are made of yet smaller objects. The key experiments which have made such a constituent picture so convincing have been of two kinds. First, the scattering of particles in collisions with large momentum transfer (e.g., the first deep inelastic electron scattering experiments at SLAC[1], and neutrino and muon scattering experiments[2] at Fermilab and CERN), have shown that for large space-like momentum transfers one 'sees' objects of a smaller scale inside the nucleon. Second, the discoveries of massive particles[3] (the J/ψ and the T) which are clearly interpretable as bound states of a new quark and its antiquark not only made the quarks real in our minds, but have more importantly led the way toward a theoretical unification of the strong, weak, and electromagnetic interactions.

Both deep inelastic scattering and the production of massive states such as the J and the T are rare processes. These processes are steeply falling spectra in the momentum transfer-squared ((q^2); read mass-squared in the particle production case). And both processes are greatly enhanced at a given value of q^2 by increases in the available energy of the collision. High energy physicists are therefore ever anxious to increase the energy available by building bigger fixed-target accelerators and by

building colliding beams .

Why are very high energy quark-quark collisions relevant to a symposium devoted to the possibilities inherent in a colliding beam accelerator designed to collide heavy nuclei on heavy nuclei? For the high-energy physicist, the question is whether or not the quarks in a fast-moving heavy nucleus have an increased chance of carrying more momentum than would be their share if the nucleons were independent. If in fact there were a non-negligible probability that one quark would be found with most of the momentum of the whole nucleus, then such a heavy-ion accelerator would be an immensely effective means of generating enormously high energy quark-quark collisions (and would, as far as I know, be the first working collective-effects accelerator). Such a concentration of the momentum of the whole nucleus among the quarks of one nucleon is one suggested explanation of the data I will show you.

The data I will discuss have to do both with the generation of particles at large momentum transfer and with the generation of systems with large mass in hadron-nucleus collisions. In the case of the large momentum transfer production, clear effects of collective action of the nucleons in the nucleus have been seen. In the large mass case, some of the data are conflicting. My strong belief is that, unfortunately, no collective effects exist which would help us in the way I outlined above to achieve ultra high energy quark-quark collisions. But as the interpretation of the observed effects is not clear, I will take the approach of laying the data out as clearly as I can, with particular emphasis on how the experiments are done for the benefit of experimentalists in the audience who may be

envisioning how to repeat such experiments on a new heavy ion accelerator. I hope that you will be able to judge for yourselves any possible payoffs in heavy-ion collisions of the type described above.

There are three types of hadron-nucleus experiments I will describe: 1) single particle production at large values of transverse momentum (p_T); 2) large mass hadron pair production; and 3) large mass dimuon production. Each of these is shown schematically in Figure 1.

Single Particle High p_T Measurements

It is a long-known fact that the spectrum in p_T of hadronic particle production is very steep. (p_T is the component of the momentum of the produced particle perpendicular to the beam--see Figure 1.) In Figure 2 the spectra of π^- production versus p_T in 200, 300, and 400 GeV proton-proton collisions is shown.[4] There are two noteworthy features: 1) the spectra are very steep in p_T, and 2) the cross-section at large p_T are energy dependent, rising with increasing energy.

Before discussing how these cross sections depend on the atomic weight of the target nucleus, I would like to give a brief description of the apapratus which made the measurements shown in Fig. 2 and which discovered the anomalous atomic weight dependence.[4] *The spectrometer of the Chicago-*Princeton collaboration is shown in Figure 3. The primary proton beam, of intensities of up to 10^{13} protons/pulse hits a target inside a heavily shielded target box. The targets are remotely controlled so that hydrogen (deuterium), beryllium, titanium, or tungsten (W) targets can be inserted easily in turn. The spectrometer is placed at 77 mrad to the incoming beam: this angle corresponds to 90° in the C.M. frame for 300 GeV protons. After 30 feet of steel collimation, quadrupole lenses focus

the secondaries. Bending magnets and four counter hodoscopes determine the momentum of the secondaries. Two 86'-long Cherenkov counters separate pions from kaons and protons. The experimenter defines a central value of p_T by setting a given current in the magnets: $\pi/K/p$ identification is done particle by particle at a given such setting. Figure 2 shows that results from this procedure can be obtained over 10 orders of magnitude in cross section!

Now what happens when different nuclei are used as targets? Figure 4 shows the relative production of π^- at a $\langle p_T \rangle \approx 3.82$ GeV for W, Ti, Be, D and H targets. The cross section per nucleus for each target has been divided by that of W, and plotted versus atomic weight. With the exception of the point for hydrogen, all of the nuclei lie along a straight line on the log-log plot. This implies that a parameterization of $\sigma(A) \approx A^{\alpha}$ is at least a good parameterization (it should not be confused with a theory--in fact, while the A^{α} provides a good χ^2 fit to these points, so does a sum of terms such as $C_1A^{2/3} + C_2A^1 + C_3A^{4/3}$).

Figure 5 shows the power α of the effective atomic weight dependence for both π^+ and π^- production versus p_T. The lines are the same on both plots (and are to guide the eye) to facilitate the comparison of π^+ and π^- production. The interesting fact is that in both cases the power α in the effective A-dependence grows to be greater than 1, reaching about 1.12 to 1.14. The errors shown include both systematics and statistics. It is clear that 1.0 is excluded.

What does α greater than 1 imply? The total cross section grows with A approximately as $A^{0.7}$, close to the value of $A^{2/3}$ which one would expect from the area of a black disc. For a transparent disc (these are

rare collisions at high p_T, after all) one might expect only the volume of the nucleus would matter, in which case $A^{1.0}$ would be expected. An A-dependence of $A^{1.14}$ requires that the nucleons act collectively.

There are two main classes of mechanism which could produce such a collective effect. The first is multiple collisions of a constituent of the projectile proton.[5] For example, a hard collision in which a large momentum transfer is imparted to a constituent might be followed by a second almost elastic collision which increases the angle (and hence the p_T) of the constituent. This mechanisms would allow the probing of the passage of 'bare' constituents through hadronic matter: i.e., collision on nuclear targets could be used as a tool for investigating short-time and short-distance behavior in hadronic matter of the constituent. A second type of collective mechanism is a change in the sharing of momentum among all the quarks in the nucleon, with the consequent increase in probability that one quark can carry a substantial fraction of the momentum of the whole nucleus. This has been suggested by many people, especially Afek, Berlad, Dar, and Eilam[6], and Krzywicki.[7] (Fermi motion, which is just such an effect, is not large enough to account for the data.[8])

The Chicago-Princeton experiment also measures the relative production of kaons and protons to pions with its Cherenkov counters in a fashion which is quite free of systematic errors. Figure 6 shows a typical plot of the ratio of proton to π^+ and anti-proton to π^- production versus p_T for hydrogen, beryllium, and tungsten targets. The cross sections rise with atomic weight A. Figure 7 shows that (except for hydrogen) the ratios can also be parameterized as $A^{\Delta\alpha}$, where $\Delta\alpha$ is the difference in the powers of α for the two particle types.[9]

This difference in powers is shown in Figure 8 for proton and π^+,

and $\bar{p}$ and π^-. One sees that proton and antiproton production is even stronger with atomic weight than that of pions, reaching values of 1.3 or greater at large values of p_T. (One should note that it would take 880 independent nucleons to equal the production from a W nucleus at $\alpha = 1.3$.) Figure 9 shows a similar plot for the K^+/π^+ and K^-/π^- ratios. Here, however, K^+ is seen to behave as does π^+, but K^- has a much stronger A-dependence than the π^-.

A summary of the results on A-dependence for the six particle types is given in Figure 10. In each case a collective effect (i.e., α greater than 1) is seen. Is this in fact due to the energy dependence of the cross section (see Fig. 2) and a significant effect as discussed above? Or is it a multiple scattering of some 'bare' object which doesn't feel the nuclear absorption (the absorption would greatly diminish rather than enhance the production of any produced object which acts like a normal hadron in nuclear material--remember any significant degradation of momentum is a degradation of p_T, and the spectrum in p_T is very steep--cf. Fig. 2).

These Chicago-Princeton results have been confirmed and extended in several experiments. Table I lists the later experiments. All are in good agreement, and the effect seems to persist down to AGS energies ($\sqrt{s}$ = 7 GeV).

Double-Arm Measurements

The A-dependence of the production of systems whose mass is a substantial fraction of the available energy of a single nucleon-nucleon collision is a sensitive test of certain types of collective effects. In particular, models in which constituents of one nucleon can share the momentum of the whole nucleus tend to predict large increases in the

Table I

Other Single-arm 'High p_T' Experiments

Acronyms	Reference	$\sqrt{s}$	p_T	Targets	Comments
MIT/BNL	Becker et al., PRL 37, 1731 (1976)	7.43 GeV	0.75-2.25	Be, Ti, W	Over this limited p_T range agrees with our data
Imp. College, Rochester, Rutgers	Barbutt et al., Phys Lett 67B, 355 (1977)	9.68-22.7	0.2-2.35	C, W	Ditto-- 10% change in over this s range
SUNY, Columbia, Fermilab	McCarthy et al., PRL 40, 213 (1978)	27.4	1.8-4.3	Be, W	Agrees-- double arm data
Purdue, U. of Mich., Fermilab	Finley et al., PRL 42, 1026 (1979)	27.4	1-2.8	Be, Pb	Ditto-- double arm data

cross-sections for large mass events. We will see that this is particularly striking in the production of muon pairs by the Drell-Yan mechanism (discussed in the third section) in proton-proton collisions, as the cross-section is normally regulated by the difficulty in finding an antiquark with a large momentum fraction of the protons' momentum. The predictions are much less clear for hadron pair production, however.

The first measurements of two hadrons produced with a large (>4 GeV) mass for the pair were made by a SUNY-Columbia-Fermilab collaboration. The process is shown schematically in Figure 1. Both particles are measured at angles which are close to 90° in the center-of-momentum frame in a proton-proton collision. The spectrometer used, shown in Figure 11, measures the p_T of each particle with multi-wire-proportional chambers and a bending magnet in each arm. Cherenkov counters give particle identification.

The two measured variables are the respective values of p_T in each arm, p_{T1} and p_{T2} (see Fig. 1). It is, however, the sum and difference of the two which seem physically the most meaningful. The sum, $p_{T1} + p_{T2}$, is the invariant mass for symmetric decays, and the difference is the p_T of the pair (considered as the parent object).[11]

Figure 12 shows the spectrum (plotted as a double invariant cross section) for a pair of charged hadrons with total charge zero plotted versus the mass of the pair divided by the total available energy. The spectra are seen to be very steep, and the shape is almost the same for the three beam energies when plotted against this scaling variable.

Figure 13 shows the spectra plotted against the other variable for the pair, the p_T difference of the two particles, p_T'. The data have

been binned into different mass intervals; for each case, however, the spectra are quite flat compared to the single particle case (see Fig. 2).

Now how does the production of these rare pairs of hadrons depend on the atomic weight of the target nucleus? Data were taken on beryllium and platinum targets. The production per nucleus was fitted to the form A^{α} as before. Figure 14(a) shows the results of these fits for α as a function of the mass of the pair (for all pairs of oppositely charged particles, integrated over all values of the transverse momentum of the pair p_T'). We see that α is consistent with a value of 1.0, implying that each nucleon in the whole volume of the nucleus is contributing independently.

The dependence of the power α on the variable p_T' (the difference in the transverse momentum of the particles in the pair) is shown in Figure 14(b). In this case α increases with p_T', especially for very large pair invariant masses. Values of α for single particle production as measured by this experiment and the Chicago-Princeton experiment discussed in the previous section are shown for comparison. The values for pair production are seen to be even larger than those for single particle production. Table II shows the powers of α derived for the different particle types for two regions of the variable p_T'.

To summarize the data of the SUNY-Fermilab collaboration:

1) no anomalous A-dependence is seen in the production of large-mass pairs as a function of the mass of the pair, over the region $4.8 < m_{pair} < 8.8$ GeV. The data are consistent with an $A^{1.0}$ behavior, which is reasonable for a rare process.

Table II

	π^-	K^-	$\bar{p}$	h^-
π^+	0.99 ± 0.03	1.05 ± 0.09	1.29 ± 0.14	1.00 ± 0.03
	1.08 ± 0.11	1.37 ± 0.46	-	1.12 ± 0.08
K^+	0.98 ± 0.09	1.33 ± 0.17	-	1.05 ± 0.05
	-	-	-	1.24 ± 0.22
p	1.11 ± 0.07	1.58 ± 0.21	1.37 ± 0.13	1.16 ± 0.05
	-	-	-	1.14 ± 0.19
h^+	1.00 ± 0.02	1.11 ± 0.06	1.17 ± 0.07	1.01 ± 0.02
	1.15 ± 0.06	1.52 ± 0.20	1.41 ± 0.43	1.18 ± 0.04

The power α of the A dependence of the invariant dihadron production cross section is given as a function of particle species for $p_t < 2.1$ GeV/c (upper value) and for $p_t > 2.1$ GeV/c (lower value in each box). h^+ denotes all positive hadrons, h^- all negative hadrons.

2) An anomalous A-dependence is seen for those rare events produced when the pair has a large value of the net transverse momentum p_T.

3) The pairs involving heavy particles K and p tend to have larger values of α ($p\bar{p}$ has an especially large value, for example).

This, so far, does not seem clear as to what it implies for the production mechanisms, but at least seems clear-cut experimentally. Unfortunately, an experiment performed some time after this one tends to make the picture less rather than more clear.

The apparatus and list of authors of the Purdue-Michigan-Fermilab collaboration[12] is shown in Figure 15. The apparatus is somewhat similar to the one of the SB-F-C collaboration just described above; it has a somewhat larger acceptance but a much lower intensity beam. The experiment did not have the sensitivity to reach as high values of mass or transverse momentum as the previous experiment[13], stopping at values of mass just where the SB-F-C experiment begins.

In Figure 16 are shown the values of single particle A-dependence power α as measured by this experiment, as well as those of the CP and SBFC collaborations. All three experiments agree remarkably well.

However, in Figure 17 the power α for pair production is shown versus the sum of the transverse momenta of the two particles in the pair (for symmetric decays, remember, this is the mass of the pair). The data start with $\alpha \sim 1.1$ at a mass of just above 2 GeV, and α rises to be 1.2 or so at a mass of almost 5 GeV. The SBFC data, also shown, while they do not overlap in mass range and hence cannot rigorously conflict, show no sign of this rising trend.

The values of α versus the difference of the transverse momenta as measured by the PMF collaboration are shown in Figure 18. There is no strong sign of the rise in α observed by the SBFC group (compare the righthand-most plot of the PMF collaboration, in which α is 1.2 over the range $0 < p_T' < 2$ GeV/c, with Figure 14b.

Finally, how does the PMF atomic-weight dependence for pairs involving kaons and protons compare with that measured by SBFC? Figure 19 is a compendium from which the relative values of α can be derived for the various kinds of pairs. Shown are the fractions of time a given type of particle is observed for a given type of trigger particle. For example, the upper left hand plot shows that the fraction of time a positive hadron in a pair is a proton when the other particle is an antiproton is greater on a beryllium target than on a lead target. This implies that α is smaller (!) for $p\bar{p}$ pairs than for, say $\pi^{\pm}$ pairs, in direct contradiction to the SBFC results.

To summarize the data of the PSM collaboration:

1) An anomalous A dependence <u>is</u> seen in the production of large-mass pairs as a function of the mass of the pair, over the region $2.4 < m_{pair} < 4.8$ GeV. The effective power rises from 1.09 to 1.2.
2) An anomalous A dependence is seen at large mass, but it does not depend strongly on the variable p_T.
3) The pairs involving kaons and protons tend to have smaller values of α(especially $p\bar{p}$).

Every one of the conclusions is contradictory to those derived from the SBFC data in the higher mass region.

So little fundamental has emerged from the study of hadron pair production by hadron-nucleus collisions. The experimental data seem contradictory, and there exist no clean predictions as to what one would expect in any case.

Happily there is a much clearer situation both experimentally and theoretically in the production of muon pairs by hadrons. It is now well established experimentally that this process is dominated by a process called the Drell-Yan process[14] in which an antiquark inside one nucleon annihilates a quark inside another nucleon. This process, as well as the definitions of the relevant kinematic variables is shown in Figure 1.

A list of the dimuon experiments from which I will present results is given in Table III. The first of these experiments, by the Fermilab-Columbia-Hawaii-Illinois collaboration (FCHI),[15] utilized a large spectrometer built in the wide-band photon beam at Fermilab. For dimuon production, however, the group removed a long deuterium filter used to purify the beam of neutrons, and studied the muon pairs produced by neutron interactions in their target.

The results of the FCHI experiment are shown in Figure 20. The power of the atomic weight dependence (called γ instead of α by these authors) is shown versus mass in Fig. 20b for muon pairs which are not made by the production of strongly interacting resonances. The power is seen to rise steeply from values of 0.6 or so to about 0.9 at dimuon masses in the several GeV range.

In fact, one would expect $\alpha = 1.0$ from the folklore of the quark model if the mechanism for production of the muon pairs is the Drell-Yan mechanism. Quarks with substantial momentum are expected to interact only

Table III

Relevant Di-muon Experiments

Institutions	Reference	$\sqrt{s}$ including particle	Targets	$m_{\mu\mu}$	α	Comments
Fermilab, Columbia, Hawaii, Illinois	M. Binkley et al., PRL 37, 571 (1976)	~24.5 GeV neutrons	Be, Al, Cu, Pb	.75 (ρ,W) to 3.1 (ψ)	.62±.03 .93±.04	Rises with mass
Chicago-Princeton (I)	D. Antreasyan et al., PRL 39, 906 (1977)	27.4 GeV (p)	Be, Cu	9 GeV	1.03 ± 0.10	First high mass (τ~0.3) measurement
SUNY, Fermilab, Columbia	D.M. Kaplan et al., PRL 40, 435 (1978)	27.4 GeV (p)	Be, Pt	5-12 GeV	0.97 ± .05	
Chicago, Illinois, Princeton	K.J. Anderson et al., PRL 42, 944 (1979)	20.5 GeV π^- (p)	C, Cu, W	1-7 GeV	1.12 ± .05	Rises with mass up to $m_{\mu\mu}$~3

weakly in matter, and here the cross section should scale with the number of quarks, i.e. as $A^{1.0}$. The fact that the data does rise with increasing mass (and thus in the Drell-Yan model increasing momentum of the quarks) is hopeful.

Now if there did exist a component of the quark distribution which shared the momentum of the whole nucleus as suggested by Krzywicki and others, one would expect a large enhancement in the dimuon production on heavy nuclei. The first experiment to measure α for very high mass (~9 GeV) dimuon production was the Chicago-Princeton collaboration discussed in Part I, who modified their apparatus in a dirty way to add another arm. The result they measured was $\alpha = 1.03 \pm .10$. This result ruled out simple collective effects of the type suggested by Krzywicki.

The SB-F-C collaboration,[16] with the much more sophisticated apparatus previously shown in Fig. 15, has improved the CP results on α for high mass dimuon production by protons, obtaining the value $\alpha = 0.97 \pm .05$. This is in excellent agreement with the prediction of $\alpha = 1.0$.

The situation with dimuon production by pions is less clear. A Chicago-Illinois-Princeton collaboration,[17] using the large Chicago cyclotron spectrometer at Fermilab (Figure 21) has measured for both incoming pions and protons. Figure 22 shows their data for incoming pions. They find $\alpha = 1.12 \pm .05$. Their data for an incoming proton beam is shown in Fig. 23 with the SB-F-C data. The proton data are consistent with $\alpha = 1$. It is possible that the pion data really imply that α is different from 1.0 and that some new effect is operating. I think it is more likely that α is 1 for pions as well.

I would like to divide my conclusions into two types: 1) facts, and 2) thoughts and hypotheses.

Facts

1) The single particle high p_T production data show a 'collective effect.' For $\bar{p}$ production a tungsten nucleus has the equivalent cross section of 1500 independent nucleons (!).

2) The double arm data seem inconsistent. At least one experiment is wrong, or something very funny is going on.

3) The dimuon production data is consistent with an atomic weight dependence of $A^{1.0}$ after an initial rise in α at low mass.

Random Thoughts and Hypotheses (with apologies to anybody who feels proprietary toward any of them)

1) Most of the cross sections discussed above are steep functions of mass or the effective C.M. energy p_T. They are thus very sensitive to any process which can change any of these variables: For example: a) multiple collisions of constituents;
b) components of the nucleus with high lateral momentum;
c) large mass components of the nucleus.

2) 'Fast' quarks don't interact strongly with the quarks in the nucleus, so there is little absorption. The $A^{2/3}$ dependence comes from the slow ones, but A^1 is the 'natural dependence of processes with large mass or p_T. (See G.R. Farrar, Ref. 5.)

3) At smaller p_T or smaller mass (less than several GeV) α is less than 1. This 'turn-on' may be governed by how fast the quarks are.

4) For single particle production at high p_T, the effect can be explained by multiple collisions of the quarks. All attempts to explain it by letting secondary hadrons be formed in the nucleus fail, because of the attenuation inside the nucleus.

So how does all this relate to the question of whether or not to build a machine to collide nuclei on nuclei? I feel that, while we don't yet have a quantitative description of what goes on in hadron-nucleus collisions, all facts seem consistent with a picture in which large mass or large momentum transfer collisions are governed by the scattering or annihilation of objects much smaller than a nucleon. There seems to be no evidence for the kind of collective effect in which one constituent shares the momentum of many nucleons. Hence the high energy physics of searching for yet higher mass states or yet 'harder' collisions will probably not benefit from very high energy nuclear-nuclear collisions. But as Neils Bohr said, "It is very hard to predict, especially the future!"

I would like to thank David Finley for help and discussion.

References

1. E.D. Bloom et al., Phys Rev Lett 23, 930 (1969), M. Breidenbach et al., Phys Rev Lett 23, 935 (1969).
2. See, for example: W.R. Francis and T.B.W.J. Kirk, Physics Reports 54, 307 (1979); P. Musset and J.P. Vialle, Physics Reports 39, 1 (1978); B.C. Barish, Physics Reports 39, 279 (1978).
3. J.J. Aubert et al., Phys Rev Lett 33, 1404 (1974); J.E. Augustin et al., Phys Rev Lett 33, 1406 (1974); S.W. Herb et al., Phys Rev Lett 39, 252 (1977).
4. J.W. Cronin et al., Phys Rev D11, 3105 (1975); D. Antreasyan et al., Phys. Rev D19, 764 (1979).
5. J. Pumplin and E. Yen, Phys Rev D11, 1812 (1975); G.R. Farrar, Physics Letters 56B, 185 (1975); J.H. Kuhn, Phys Rev D13, 2948 (1976); A. Krzywicki, J. Engels, B. Petersson, and U. Sukhatme, Physics Letters 85B, 497 (1979).
6. Y. Afek, G. Berlad, A. Dar, and G. Eilam, Technion PH-77-52.
7. A. Krzywicki, Phys Rev D14, 152 (1976).
8. This has been shown by many people: for example, me (private communication); S. Fredriksson, Nucl. Physics B94, 337 (1975); J. Kuhn, Phys Rev D13, 2948 (1976).
9. For example, if the cross section for proton production is parameterized as $A^{\alpha p}$, and that for pion production as $A^{\alpha \pi}$, then the ratio will obviously behave as $A^{\alpha p}/A^{\alpha \pi} = A^{\Delta \alpha}$ where $\Delta \alpha = \alpha p - \alpha \pi$.
10. H. Jöstlein et al., Phys Rev D20, 53 (1979). Figures 11 through 14 and Table II are either from this reference or from the Ph.D. thesis of Randall Jay Fisk (Stony Brook, Aug., 1978).

11. The SB-F-C group calls the sum of the transverse momenta m', and the difference p_T'. To remain consistent with their figures, I will adopt their notation. The variables m' and p_T' are sometimes called p_S (for sum) and p_D (for difference) by the PFM group (see Figures 17 and 18).

12. D. Finley et al., PRL 42, 1031 (1979) and the thesis of David Finley (Purdue, 1978).

13. This should not be held against the authors--the experiment was designed to find hadronically produced charm: A-dependence was a (necessary) by-product.

14. S.D. Drell and T.M. Yan, Phys Rev Lett 25, 316 (1970). See also C.S. Lam and Wu-ki Tung, Phys Rev D18, 2447 (1978).

15. M. Binkley et al., Phys Rev Lett 37, 571 (1976).

16. D.M. Kaplan et al., Phys Rev Lett 40, 435 (1978).

17. K.J. Anderson et al., PRL 42, 944 (1979).

Figure Captions

1. Schematic representations of each of the three processes discussed in the talk. The variables p_T ($p\perp$), is the component of the transverse momentum perpendicular to the beam. For the pair experiments, the mass of the pair m is approximately the sum of the individual transverse momentum, and the p_T of the pair is the difference.
2. The spectra for π^- production versus p_T in 200, 300, and 400 GeV proton-proton collisions.
3. The single-arm spectrometer of the Chicago-Princeton collaboration.
4. The relative production of π^- per nucleus at transverse momentum of 3.8 GeV for tungsten (W), titanium (Ti), beryllium (Be), deuterium (D) and hydrogen (H) targets. The cross section per nucleus has been normalized to the cross section per W nucleus. The line shows a fit of the form A^{α} to all of the points except hydrogen. The error bars include systematic errors.
5. The power α for π^- and π^+ production on nuclei derived from fits of the type shown in Figure 4. Note that the scale is split--the upper half is for π^- production, and the lower half is for π^+. The lines are drawn only to guide the eye, and are the same curve to show the similarity of π^+ and π^- atomic weight dependence.
6. The relative production of protons (antiprotons) to that of pions for proton-proton, proton-beryllium and proton-tungsten targets. The increasing production of the heavier particles with atomic weight is clear at large values of the transverse momentum.
7. A plot of the particle ratios versus atomic weight A at a p_T of 3.85 GeV/c. The lines are fits (excluding hydrogen) of the form $A^{\Delta\alpha(p_T)}$.

8. The values of the difference $\alpha_p - \alpha_\pi$ derived from the particle ratios, versus p_T at 300 GeV/c. The lines are drawn to guide the eye.

9. The values of the difference $\alpha_K - \alpha_\pi$ derived from the particle ratios, versus p_T at 400 GeV/c. The lines are drawn to guide the eye.

10. The power α of the A dependence of the invariant cross section versus p_T for the production of hadrons by 400-GeV protons; (a) π^+, (b) π^-, (c) K^+, (d) K^-, (e) p, and (f) $\bar{p}$. Unless indicated, the errors are smaller than or equal to the size of the points.

11. The double-arm spectrometer of the SB-C-F collaboration.

12. The cross-section for producing a pair of hadrons. The cross section is plotted versus the scaling variable $X_t = m'/\sqrt{s}$, where m' is the mass of the pair, and $\sqrt{s}$ is the total energy in the center of mass.

13. The cross section for producing a pair of hadrons at a value of p_T', the difference in the two transverse momenta. The data have been separated into intervals of mass.

14. a) The power α of the atomic weight dependence versus the mass (actually the sum of the transverse momenta) of the pair. Note that the data are consistent with a value of 1.0.

    b) The power α of the atomic weight dependence versus the p_T of the pair. The single arm results of the SBCF and CP collaborations are also plotted.

15. The double-arm spectrometer of the Purdue-Michigan-Fermilab collaboration.

16. The values for α for single particle production as measured by both double-arm experiments and the CP collaboration.

17. The power α for pair production as measured by the PMF collaboration versus mass. The SB-F-C measurements are also shown.

18. The values of α for pair production as measured by the PMF collaboration versus the p_T of the pair. Remember p_S is the sum of the transverse momenta of the two hadrons, and is close to the mass of the pair.

19. This nigh-incomprehensible plot shows the fraction each type of particle subsumes when the other arm detects the trigger particle listed on the ordinate. For example, the top left plot shows the fraction of time a positive hadron is a proton for p, K^+, π^+, $\bar{p}$, K^-, and π^- triggers, for both beryllium and lead targets.

20. The power α (here called γ by the authors) as measured by the FCHI collaboration for dimuon production by neutrons: a) is for the strongly-produced resonances ρ and ω, and the J, b) is for non-resonant pairs.

21. The Chicago cyclotron spectrometer used in the CIP experiments on dimuon production.

22. The values for α for dimuon production by incident pions as measured by the CIP collaboration.

23. The values for α for diumon production by incident protons. Also shown are the SB-F-C measurements.

HIGH MASS OR HIGH $P_\perp$

I. SINGLE PARTICLE HIGH $P_\perp$ MEASUREMENTS

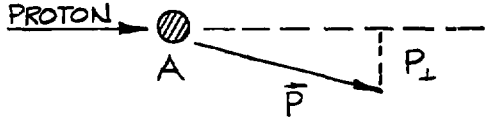

II. DOUBLE ARM MEASUREMENTS

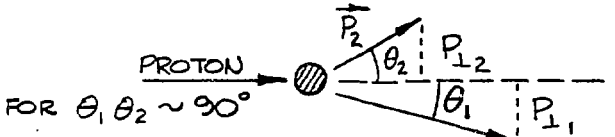

III. DIMUON PRODUCTION

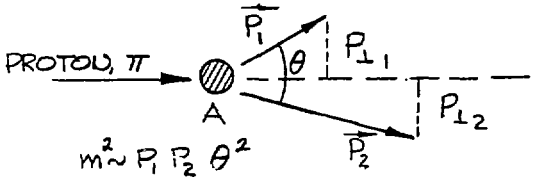

Figure 1

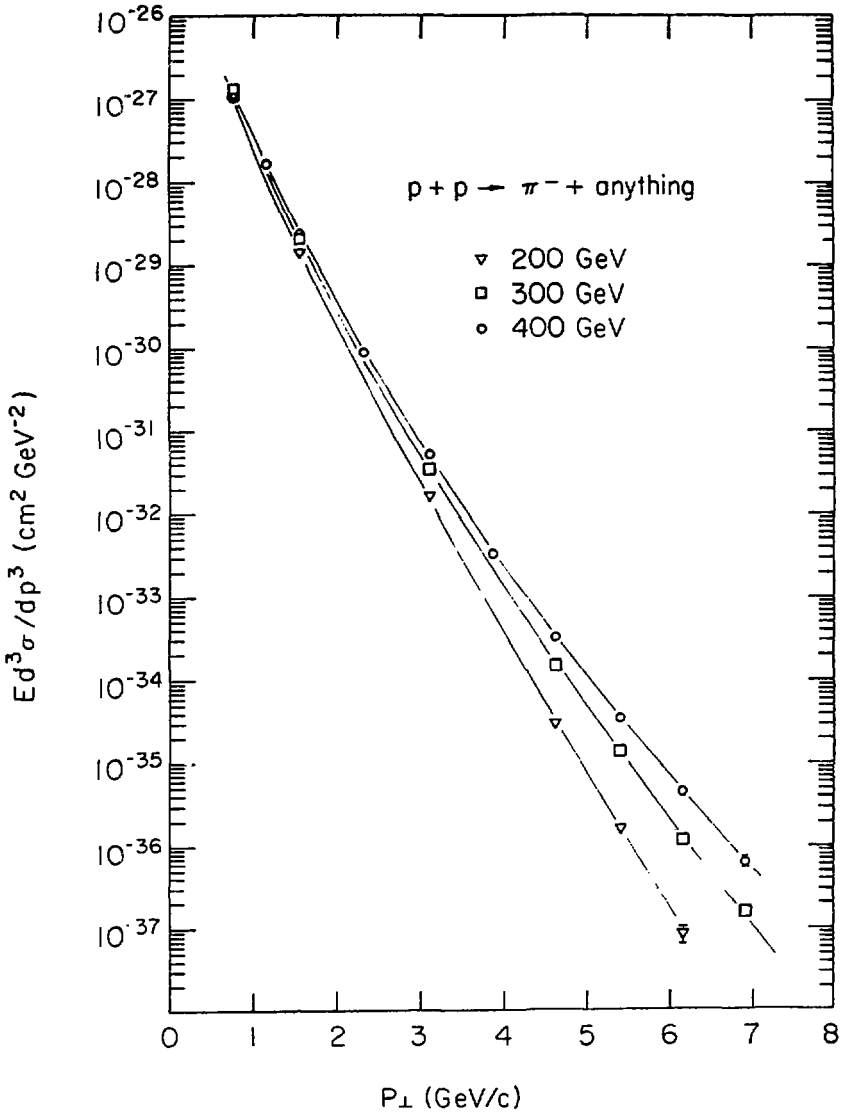
10^{-26}
10^{-27}
10^{-28}
10^{-29}
10^{-30}
10^{-31}
10^{-32}
10^{-33}
10^{-34}
10^{-35}
10^{-36}
10^{-37}
$Ed^3\sigma/dp^3$ (cm^2 GeV^{-2})
$p + p \rightarrow \pi^- +$ anything
200 GeV
300 GeV
400 GeV
0
1
2
3
4
5
6
7
8
$P_\perp$ (GeV/c)

Figure 2

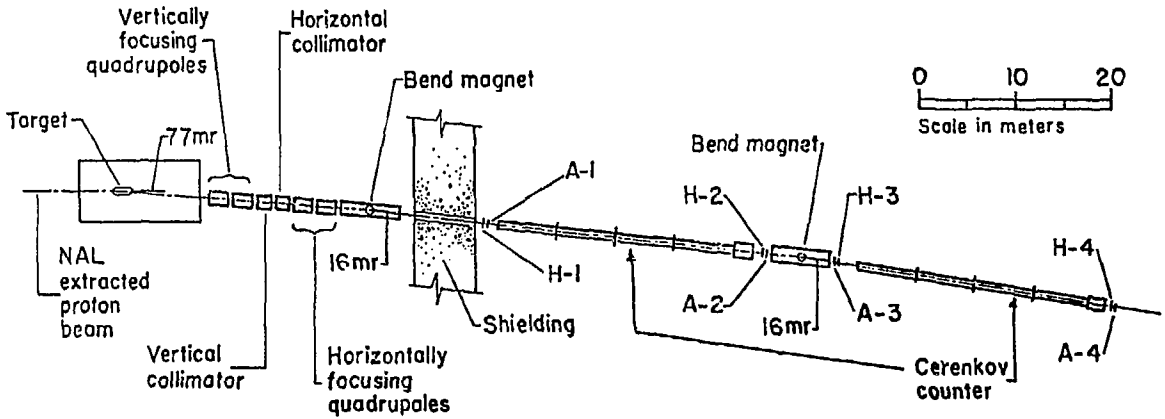

J. W. Cronin, H. J. Frisch, and M. J. Shochet

The Enrico Fermi Institute

University of Chicago, Chicago, Illinois 60637

and

J. P. Boymond, P. A. Piroué, and R. L. Sumner

Department of Physics, Joseph Henry Laboratories

Princeton University, Princeton, New Jersey 08540

Figure 3

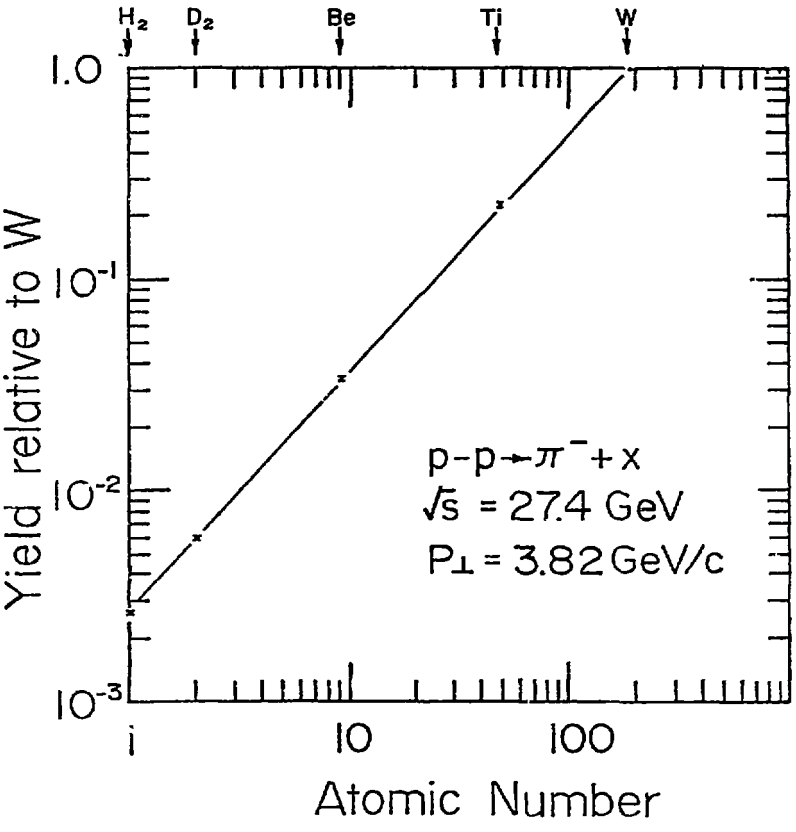
H2
D2
Be
Ti
W
1.0
10-1
10-2
10-3
Yield relative to W
p-p→π⁻+X
√s = 27.4 GeV
P⊥ = 3.82 GeV/c
1
10
100
Atomic Number

Figure 4

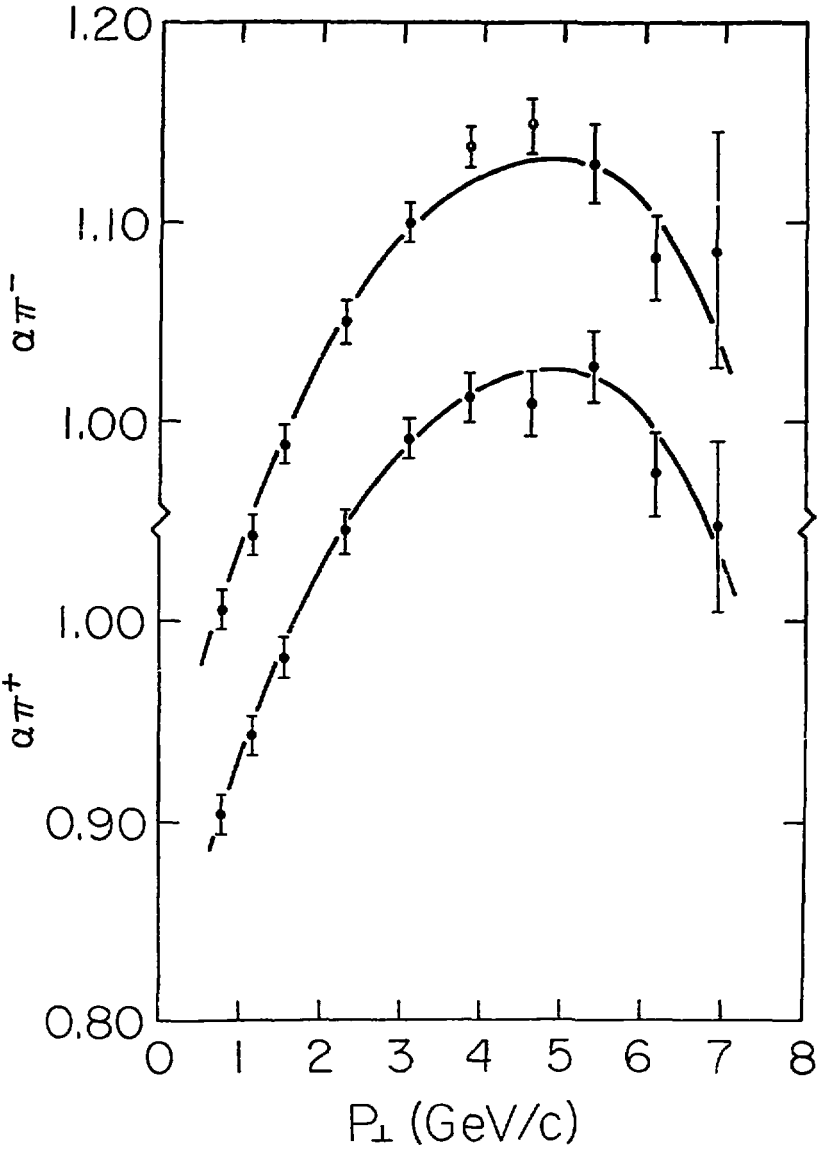
1.20
1.10
1.00
1.00
0.90
0.80
α_{π^-}
α_{π^+}
0
1
2
3
4
5
6
7
8
$P_\perp$ (GeV/c)

Figure 5

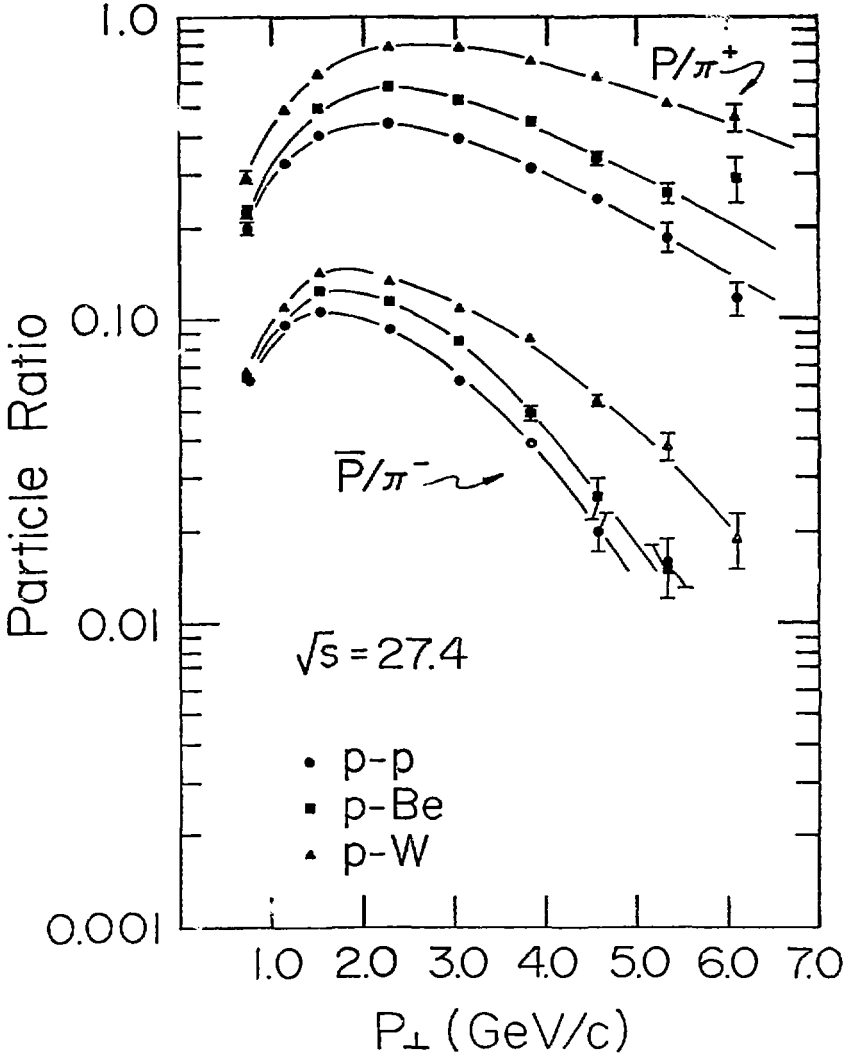
1.0
0.10
0.01
0.001
Particle Ratio
P/π+
P̄/π−
√s = 27.4
• p-p
▪ p-Be
▲ p-W
1.0 2.0 3.0 4.0 5.0 6.0 7.0
P⊥ (GeV/c)

Figure 6

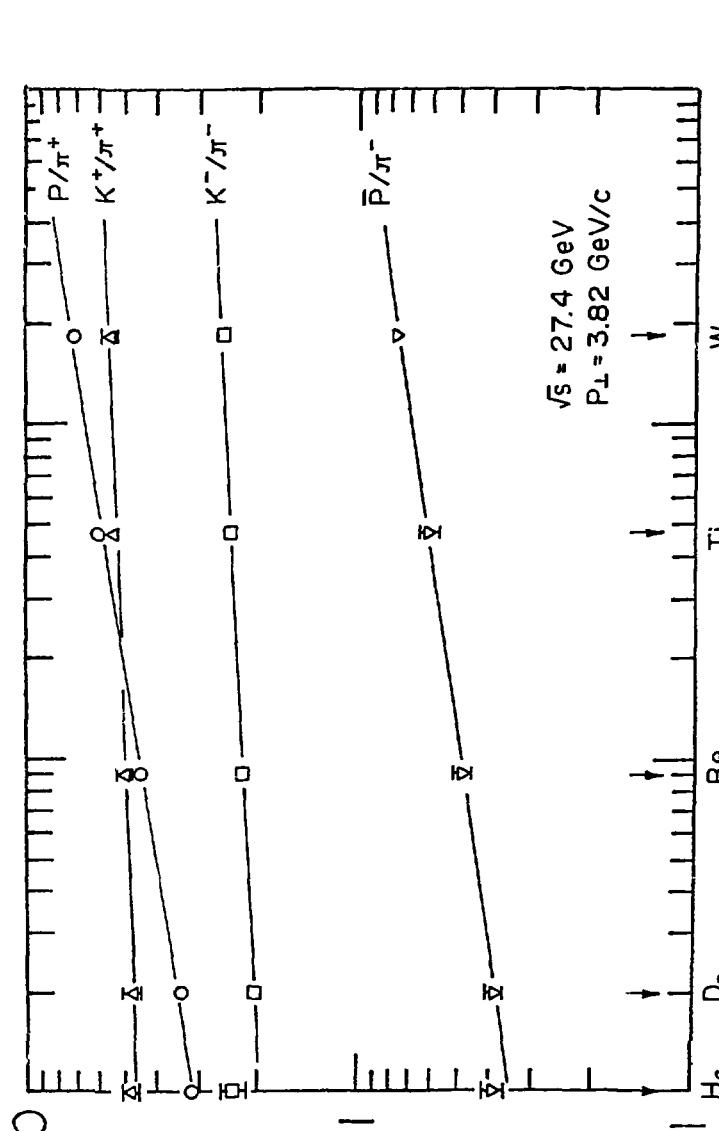
P/π+
K+/π+
K-/π-
P̄/π-
√s = 27.4 GeV
P⊥ = 3.82 GeV/c
H2
D2
Be
Ti
W
1.0
10
100
Atomic Number
Particle Ratio
.01
.1
1.0

Figure 7

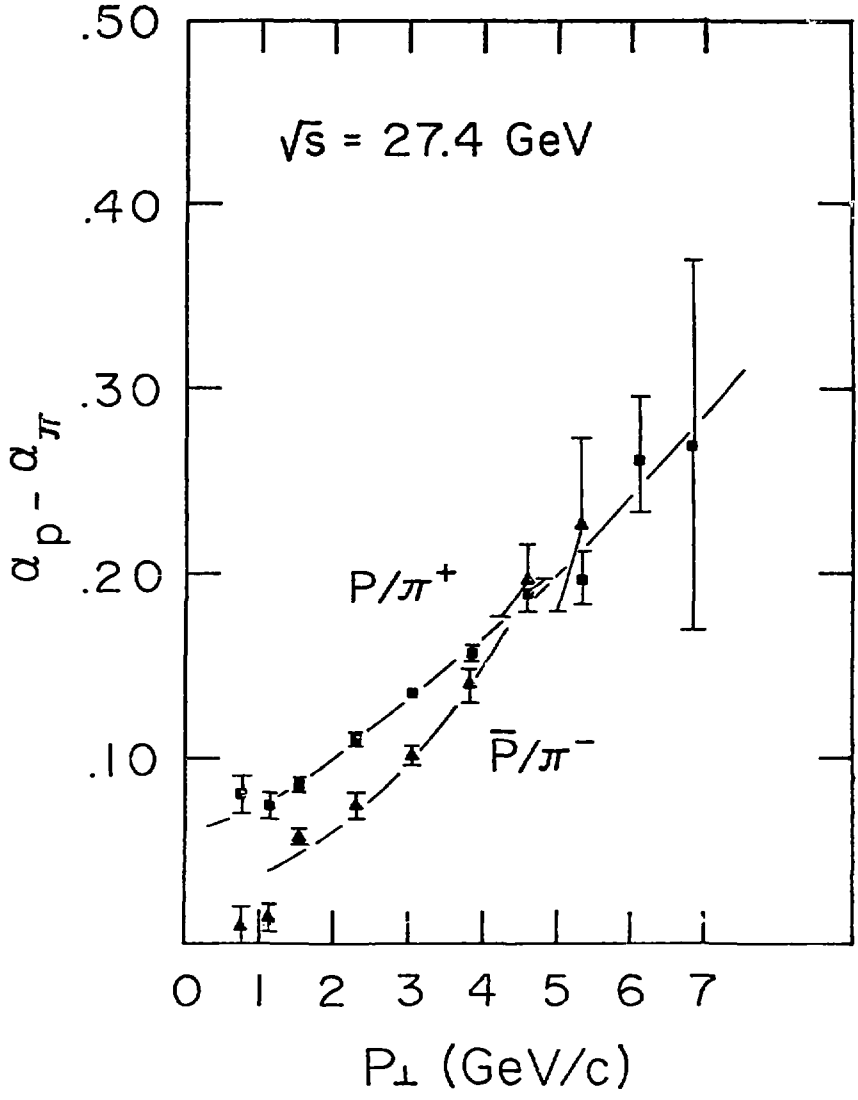
.50
.40
.30
.20
.10
$\sqrt{s}$ = 27.4 GeV
$\alpha_p - \alpha_\pi$
P/π^+
$\bar{P}/\pi^-$
0 1 2 3 4 5 6 7
$P_\perp$ (GeV/c)

Figure 8

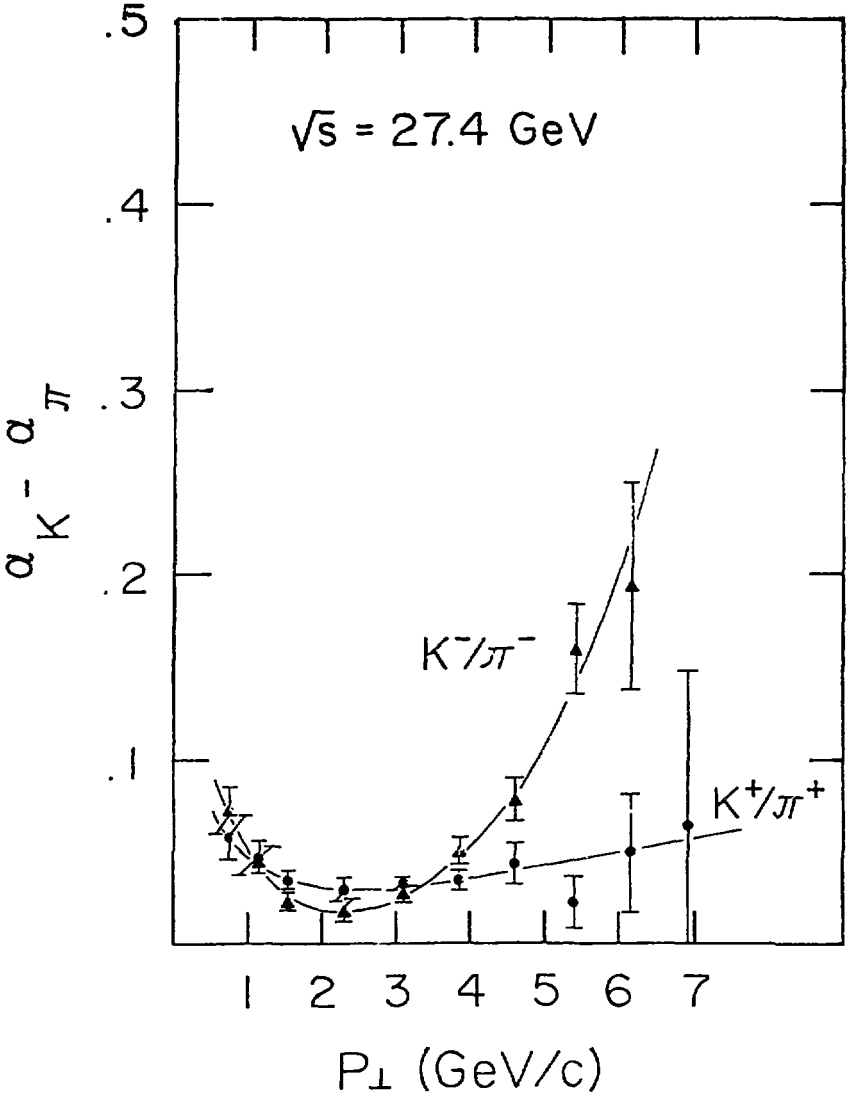
.5
.4
.3
.2
.1
$\alpha_K - \alpha_\pi$
$\sqrt{s}$ = 27.4 GeV
K^-/π^-
K^+/π^+
1
2
3
4
5
6
7
$P_\perp$ (GeV/c)

Figure 9

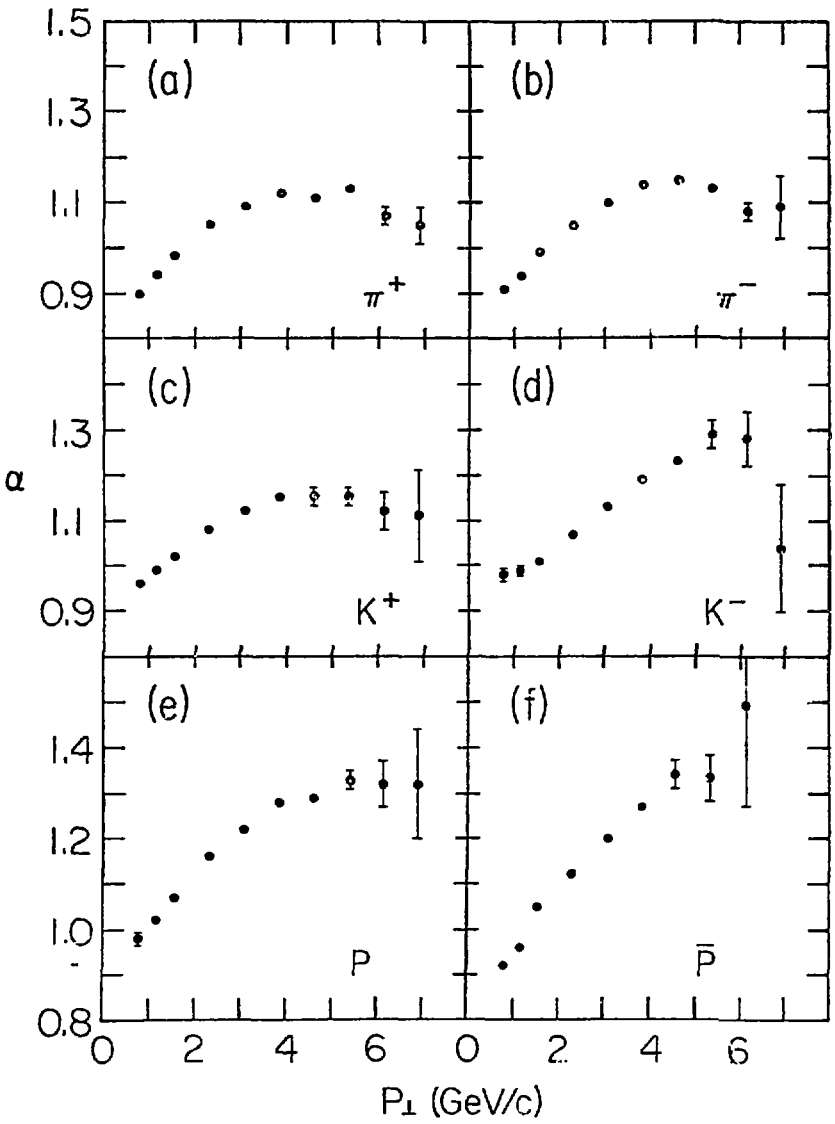

Figure 10

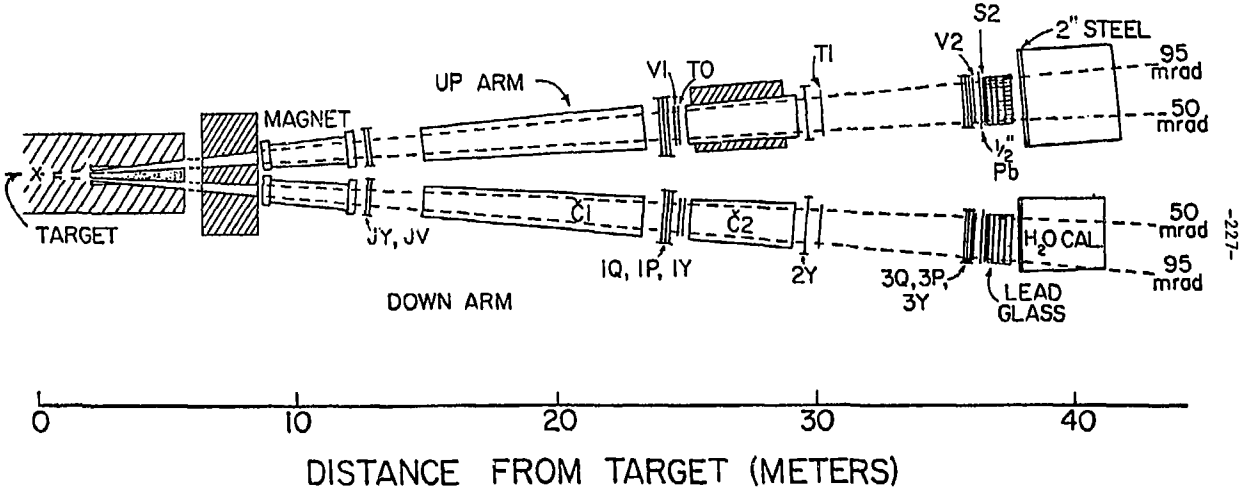
THE APPARATUS (TOP VIEW)
S2
2" STEEL
V2
95 mrad
50 mrad
UP ARM
V1
T0
T1
MAGNET
½" Pb
TARGET
JY, JV
C1
C2
50 mrad
H2O CAL
95 mrad
1Q, 1P, 1Y
2Y
3Q, 3P, 3Y
LEAD GLASS
DOWN ARM
0
10
20
30
40
DISTANCE FROM TARGET (METERS)

Figure 11

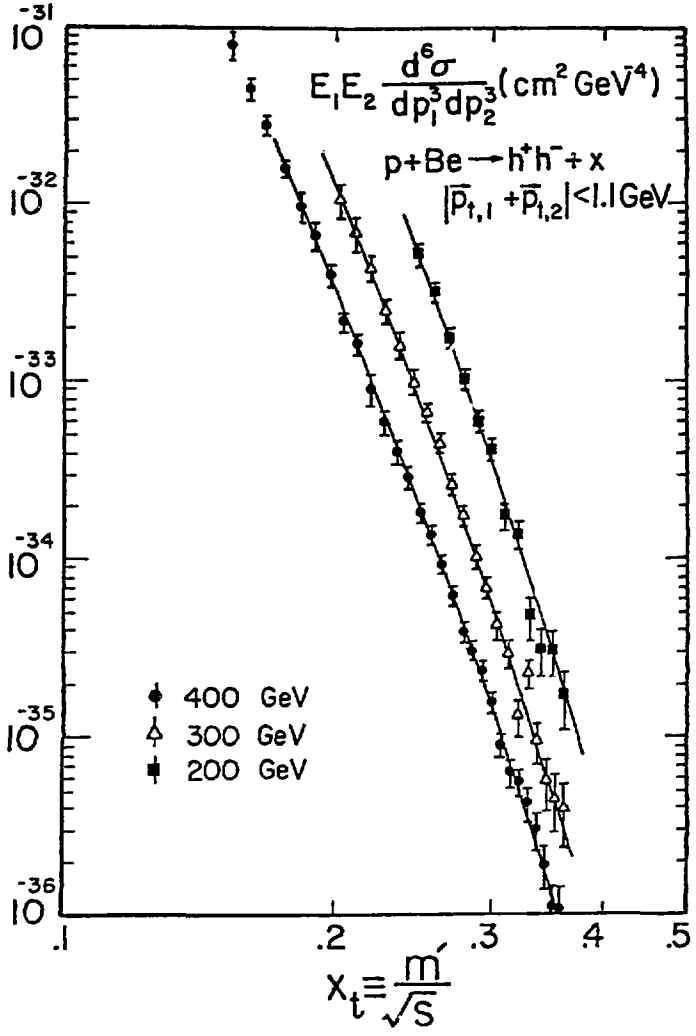
$E_1E_2\frac{d^6\sigma}{dp_1^3dp_2^3}(cm^2\,GeV^{-4})$
$p+Be\rightarrow h^+h^-+x$
$|\vec{p}_{t,1}+\vec{p}_{t,2}|<1.1\,GeV$
400 GeV
300 GeV
200 GeV
10^{-31}
10^{-32}
10^{-33}
10^{-34}
10^{-35}
10^{-36}
.1
.2
.3
.4
.5
$x_t\equiv\frac{m'}{\sqrt{s}}$

Figure 12

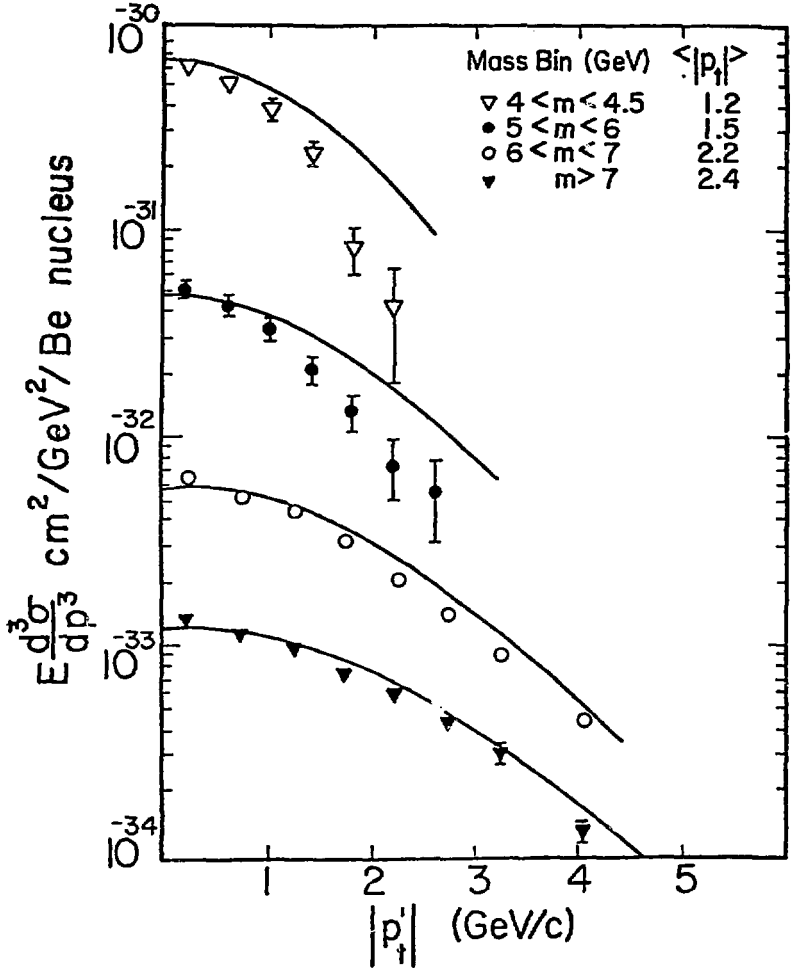
Mass Bin (GeV)
<|p_t|>
▽ 4 < m < 4.5 1.2
● 5 < m < 6 1.5
○ 6 < m < 7 2.2
▼ m > 7 2.4
E d³σ/dp³ cm²/GeV²/Be nucleus
10⁻³⁰
10⁻³¹
10⁻³²
10⁻³³
10⁻³⁴
1
2
3
4
5
|p'_t| (GeV/c)

Figure 13

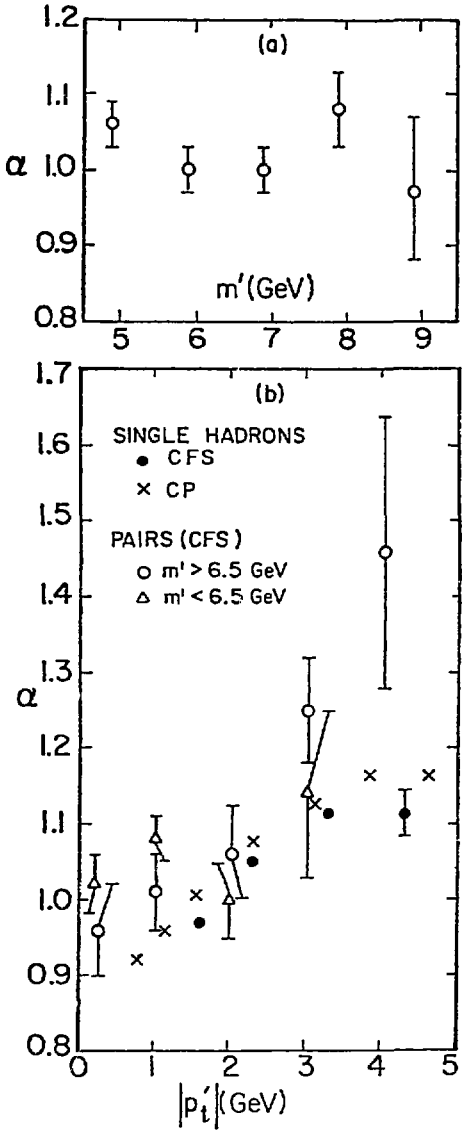
(a)
α
m'(GeV)
(b)
SINGLE HADRONS
● CFS
× CP
PAIRS (CFS)
○ m' > 6.5 GeV
△ m' < 6.5 GeV
α
|p_t'| (GeV)

Figure 14

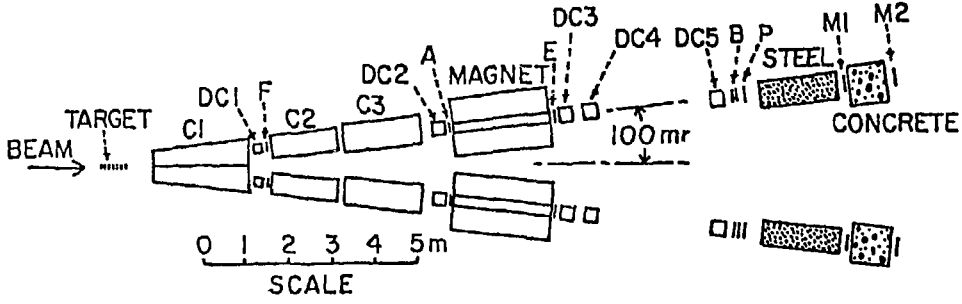

C: CHERENKOV COUNTER
DC: DRIFT CHAMBER
F,A,E,B,P,M: SCINTILLATION COUNTERS

D.A. Finley, W.R. Ditzler, O.E. Johnson, F.J. Loeffler, and E. Shibata
Purdue University, West Lafayette, Indiana
and
C.W. Akerloff, P. Alley, R. Fabrizio, D. Koltick, D.I. Meyer, and R. Thun
University of Michigan, Ann Arbor, Michigan
and
D. Bintinger, R.L. Loveless, R.A. Lundy, K.C. Stanfield, and D.D. Yovanovitch
Fermi National Accelerator Laboratory, Batavia, Illinois

Figure 15

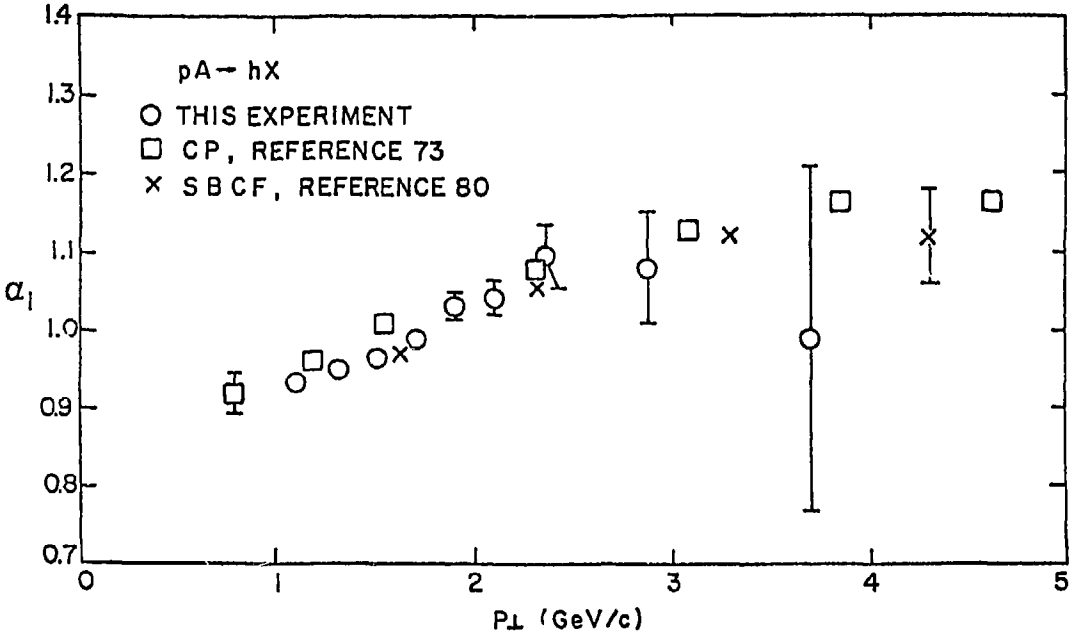
pA → hX
THIS EXPERIMENT
CP, REFERENCE 73
SBCF, REFERENCE 80
α_1
$P_\perp$ (GeV/c)
1.4
1.3
1.2
1.1
1.0
0.9
0.8
0.7
0
1
2
3
4
5

Figure 16

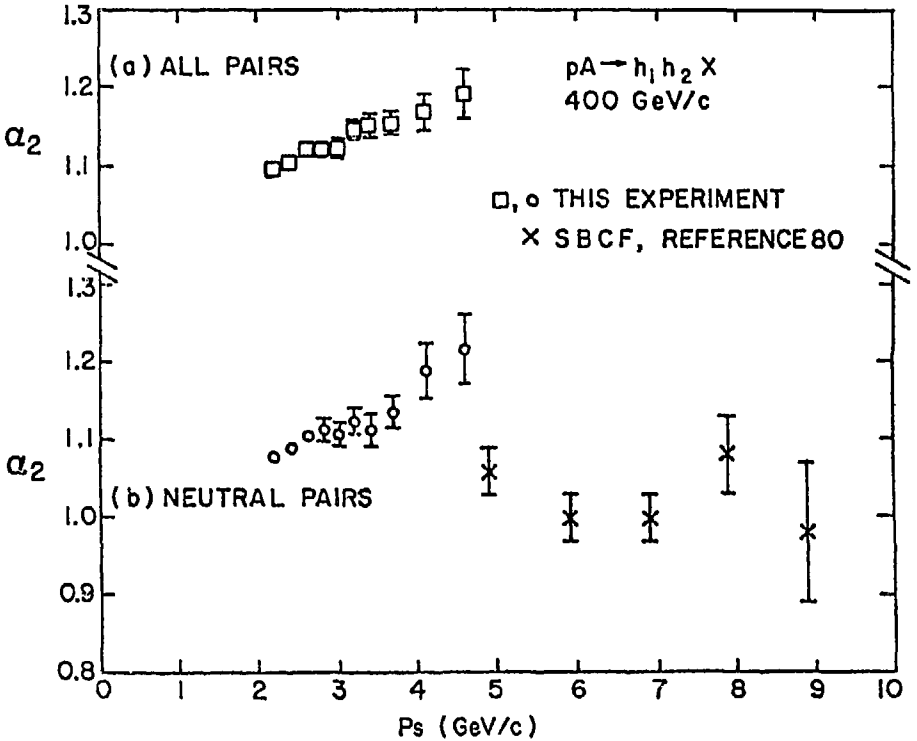
(a) ALL PAIRS
pA → h1 h2 X
400 GeV/c
□, o THIS EXPERIMENT
× SBCF, REFERENCE 80
(b) NEUTRAL PAIRS
α2
α2
Ps (GeV/c)
1.3
1.2
1.1
1.0
0.9
0.8
0
1
2
3
4
5
6
7
8
9
10

Figure 17

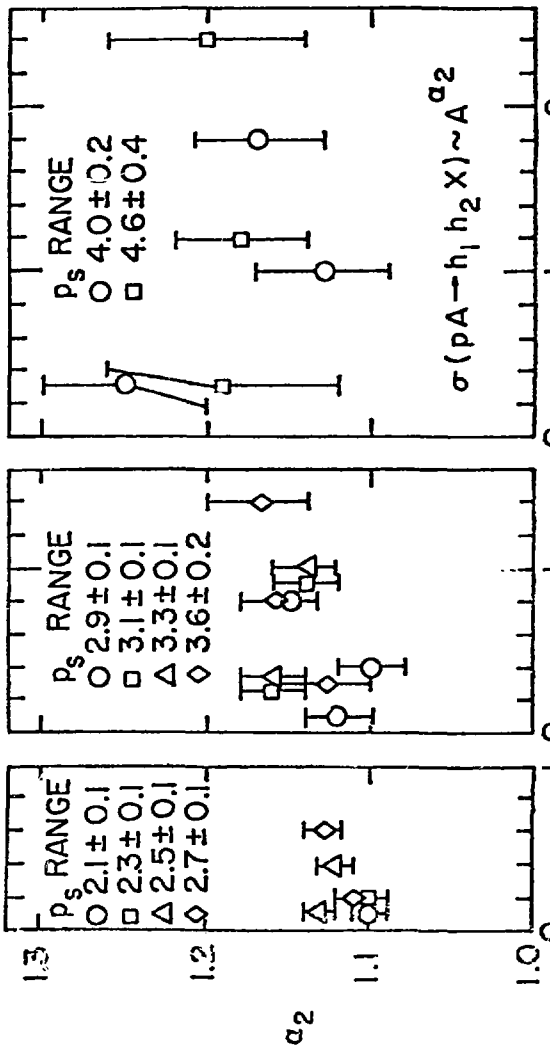
p_s RANGE
○ 2.1±0.1
□ 2.3±0.1
△ 2.5±0.1
◇ 2.7±0.1
p_s RANGE
○ 2.9±0.1
□ 3.1±0.1
△ 3.3±0.1
◇ 3.6±0.2
p_s RANGE
○ 4.0±0.2
□ 4.6±0.4
$\sigma(pA \to h_1 h_2 X) \sim A^{\alpha_2}$
α_2
1.3
1.2
1.1
1.0
0
1
0
1
2
p_D (GeV/c)

Figure 18

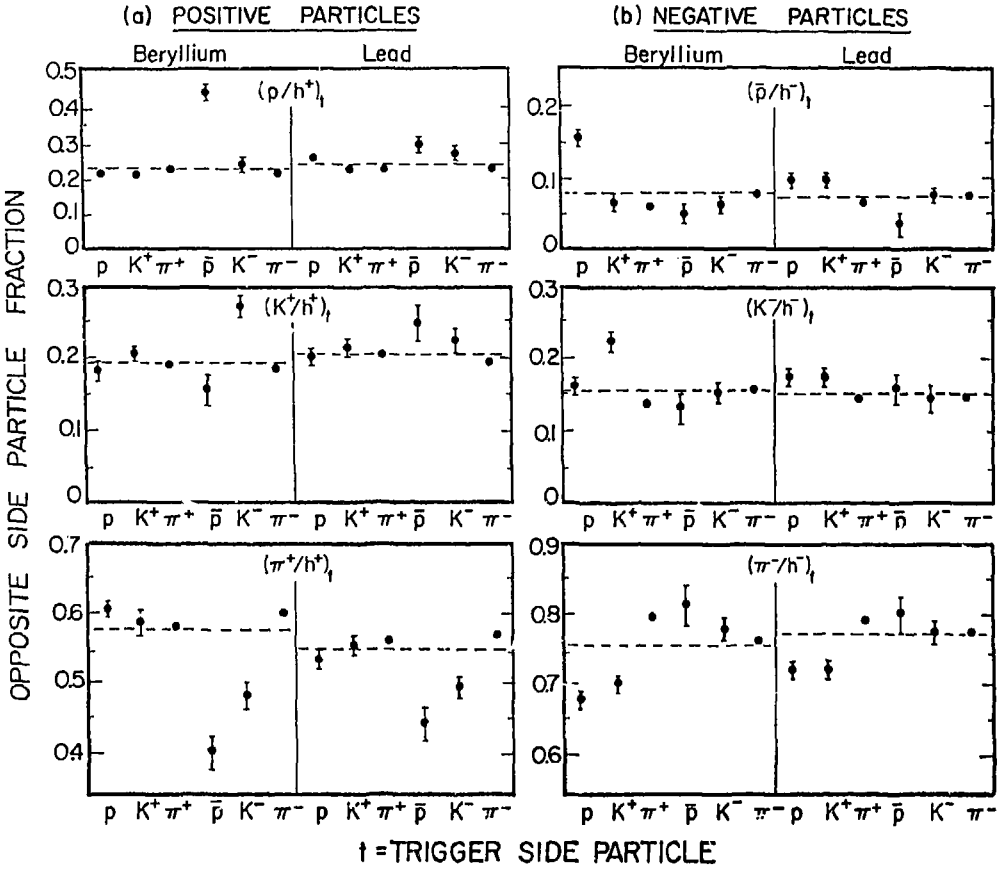
(a) POSITIVE PARTICLES
(b) NEGATIVE PARTICLES
Beryllium
Lead
$(p/h^+)_t$
$(\bar{p}/h^-)_t$
$(K^+/h^+)_t$
$(K^-/h^-)_t$
$(\pi^+/h^+)_t$
$(\pi^-/h^-)_t$
p K^+ π^+ $\bar{p}$ K^- π^-
OPPOSITE SIDE PARTICLE FRACTION
t = TRIGGER SIDE PARTICLE

Figure 19

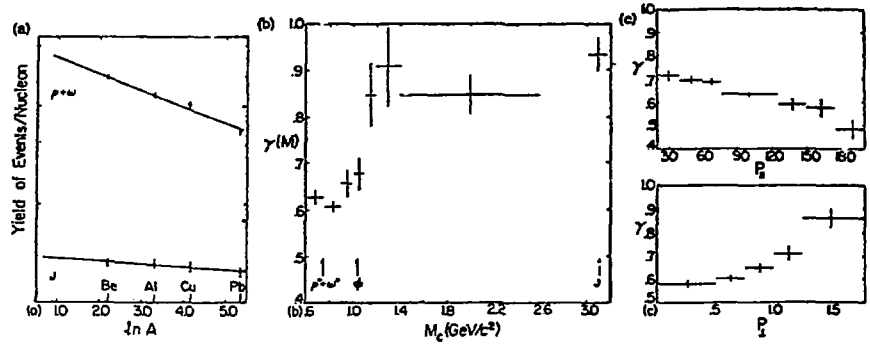

(a) A dependence of yields of $\rho+\omega$ and J. Straight lines are least-squares fits to the data. Error bars are statistical only. (b) A dependence of the dilepton yield as a function of mass; cross-section per nucleus proportional to $A^{\gamma(m)}$. Vertical bars are statistical errors from least-squares fits. (c) A dependence of the dilepton yield in the $\rho+\omega$ mass region as a function of $p_\parallel$ and $p_\perp$ of the pair.

Figure 20

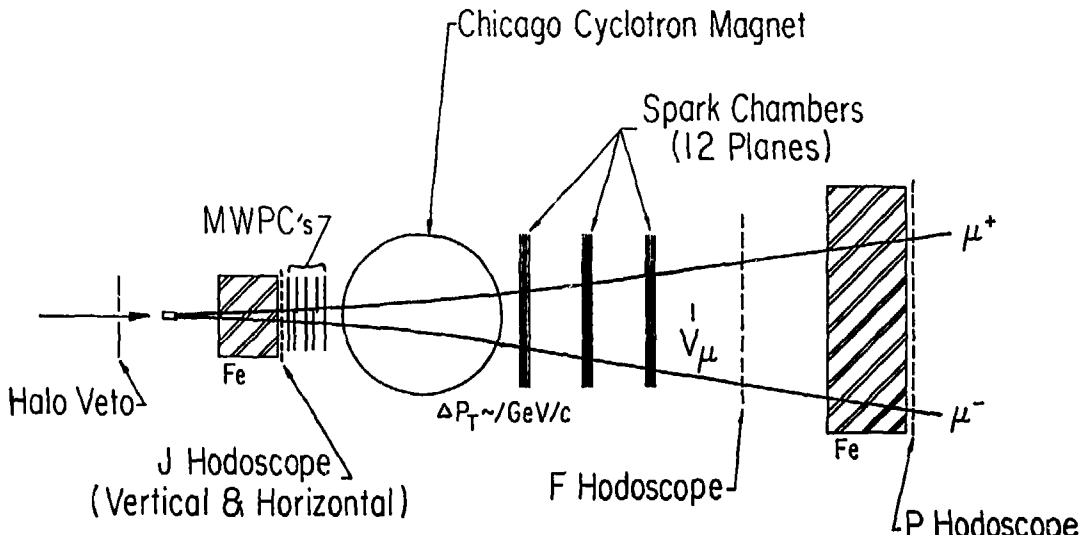

G. E. Hogan, K. J. Anderson, R. N. Coleman,[a] K. P. Karhi, K. T. McDonald,
C. B. Newman, J. E. Pilcher, E. I. Rosenberg, G. H. Sanders,[b]
A. J. S. Smith, and J. J. Thaler
Enrico Fermi Institute, University of Chicago, Chicago, Illinois 60637, and University of Illinois, Urbana, Illinois 61801, and Joseph Henry Laboratories, Princeton University, Princeton, New Jersey 08540

Figure 21

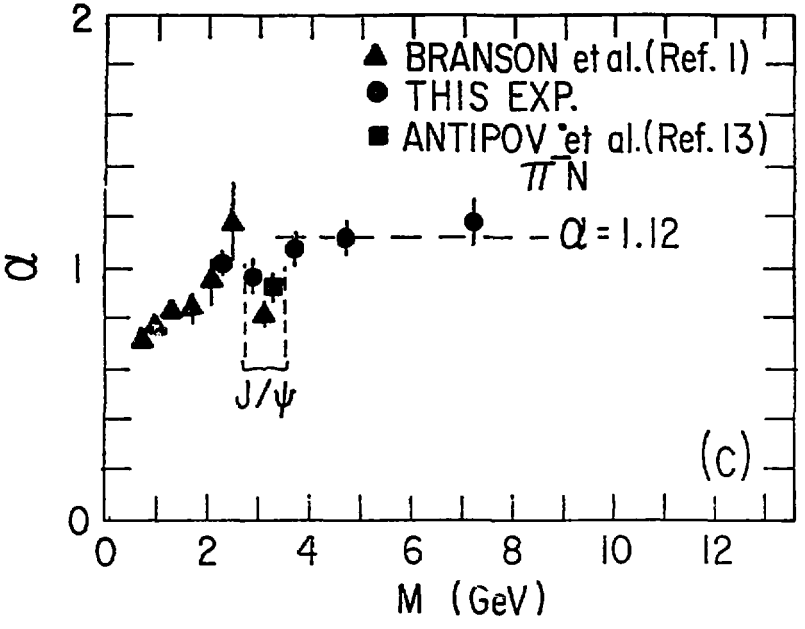
BRANSON et al.(Ref. 1)
THIS EXP.
ANTIPOV et al.(Ref. 13)
$\pi^- N$
$\alpha = 1.12$
J/ψ
(c)
α
M (GeV)
0
1
2
0
2
4
6
8
10
12

Figure 22

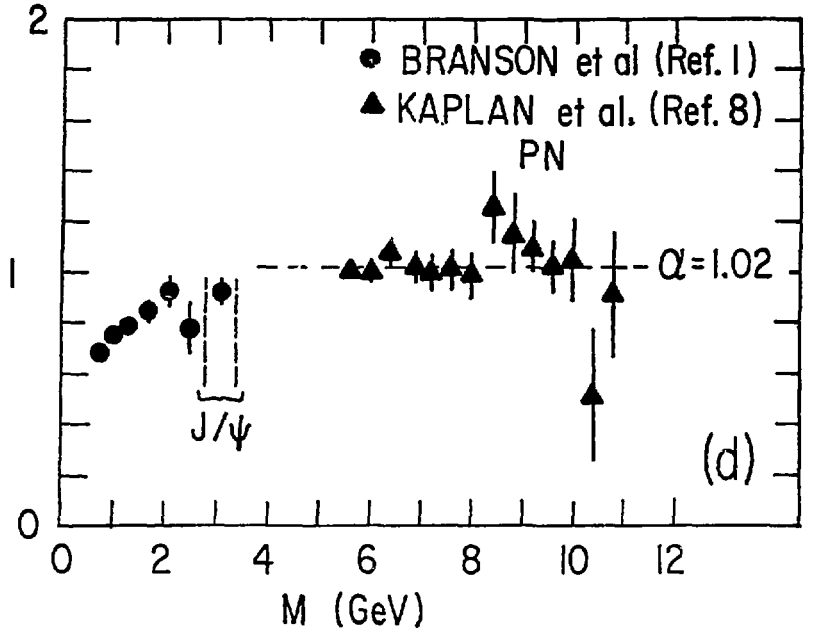
2
1
0
BRANSON et al (Ref. 1)
KAPLAN et al. (Ref. 8)
PN
α=1.02
J/ψ
(d)
0
2
4
6
8
10
12
M (GeV)

Figure 23

ASTROPHYSICS PERSPECTIVES ON HIGH-ENERGY NUCLEUS-NUCLEUS COLLISIONS

D.N. Schramm, Matt Crawford and Keith A. Olive
University of Chicago

The purpose of this talk is to review various implications of high energy heavy ion collisions on astrophysics problems. The possible implications fall into four specific astrophysics problems:

1. cosmic ray propagation and calibration studies
2. equation of state of neutron star matter and the maximum mass of a neutron star
3. equation of state of collapsing stellar matter and the origin of black holes, neutron stars and supernovae
4. the quark-hadron phase transition in the early universe and the possible role it may play in generating fluctuations in the universe.

This talk will not present a detailed set of references on each topic but will instead try to present a discursive overview with referencing primarily to reviews rather than to primary source material. The first problem mentioned above is already an on-going program at LBL and, as such, does not need to be expanded upon here. The point is that heavy ion reactions at high energies can duplicate those reactions which take place in interstellar space as cosmic rays propagate from their sources to their detection near earth. Thus understanding these reactions can enable cosmic ray physicists to have a better chance of removing propagation effects and determine the implied source composition. This in turn can be used to understand the origin of the cosmic rays and the detailed nature of the sources. Another related

application is the use of high energy heavy ion accelerators to calibrate the cosmic ray detection equipment which is to be flown in satellites, balloons, etc. Such calibrations are an absolute necessity for interpreting results of isotopic composition experiments. John Simpson is currently preparing a detailed review of the subject of the isotopic composition of cosmic rays and the roles of both spallative studies and calibration will be explicity developed and referenced there. This problem will primarily be concentrated on the latter three subjects. There will be a section dealing with cold neutron matter and its equation of state. This problem has long been central to the study of neutron stars and has not yet been resolved in a satisfactory manner. By probing nuclear matter at high energies and at densities much greater than nuclear density one could learn something about this equation of state. For further details on this subject see ref. 2.and references therein.

The next section will discuss the related but different problem of the equation of state of hot, dense nuclear matter. This is relevant to collapsing stellar matter and the problem of forming a neutron star or a black hole and ejecting the outer part of the star in a supernova explosion. Aspects of this problem are reviewed by Lattimer and Brown[3] and Freedman, Schramm and Tubbs[4].

Another section will discuss the relevance of heavy-ion physics on two current problems in the early universe: the spectrum of particles produced by the quark-hadron phase transition and the possible generation of pre-galactic density fluctuations by this same transition. It is expected that the spectrum of particles produced in relativistic heavy ion collisions may be related to that produced in the early

universe. This spectrum may have features indicative of the quark matter phase. The density fluctuations might result from the details of the color force between quarks.

Maximum Mass of Neutron Stars

The maximum mass of neutron stars is an important question in resolving the existence of black holes. For example let's look at Cygnus X-1 which is a compact object. It's known to be a compact object since it's emitting x-rays, and it's in a binary system so we can get estimates of its mass. We determine that its mass is much larger than the probable maximum mass of a neutron star, and therefore the indication is that in Cygnus X-1 there is a black hole. The key point, however, is whether it is truly more massive than any neutron star could be. If one could make a massive neutron star, one could explain the observation. Thus it is very important to know what is the maximum mass of neutron stars in order to establish the existence of black holes.

The well known Oppenheimer-Volkov limit from the late 1930's, which uses non-interacting point neutrons gives a maximum mass of 0.7 solar masses. However, we know from x-ray binaries (for example, the work of Joss and Rappaport) that there are x-ray binary stars that contain neutron stars with masses of the order of 1.5 solar masses. So we do know that neutron stars exist with masses significantly bigger than the Oppenheimer-Volkov mass. We clearly must worry about the nucleon-nucleon interaction, as of course would be expected. In fact, from the x-ray observations any equation of state that yields a maximum mass less than 1.5 solar masses is outlawed. The equation

of state must have a sufficiently repulsive core to enable the maximum mass to be greater than 1.5 solar masses.

Another question is, as long as one has the maximum mass for a neutron star greater than 1.5, can one really tell anything more about it from observations? It may be that all neutron stars actually form with a mass of 1.5 because of stellar evolution and nuclear physics has nothing to do with it. If the maximum mass that can be supported by nuclear matter is 1.5 solar massesor greater, and if stellar evolution always produces 1.5 solar mass neutron stars, then one really is not able to probe what is the true maximum mass from observations of the stars. To know anything about that, one would have to try to attack it from the fundamental nucleon-nucleon interaction point of view rather than with the astrophysical observations metioned above. The best current calculations using state-of-the-art physics give a maximum mass for neutron stars of about 2 solar masses (see review by Gordon Baym and Chris Pethick).

When one examines the structure of a neutron star, the outer surface is a crust of iron, which has the maximum binding energy per nucleon. The crust consists of free nuclei and electrons. Toward the inner part of the crust, one starts to get some neutronization. As one moves further in, the neutrons and protons become a liquid, possibly even a superfluid, in the mantle region of a neutron star. The critical factor that affects this maximum mass is the equation of state in the very central regions. In the central region one is getting to 5 to 10 times nuclear density. Various hypotheses have been advanced. For example, people have worried about pion condensations and how that may affect the equation of state. They have also worried about the

superfluidity of the neutron-proton fluid and the effect of hyperonic matter on the equation of state as the Fermi potential gets sufficiently high so that the neutron plus pion systems are driven into various hyperons (Δ's, Λ's, Σ's) and how that affects the equation of state. The actual formation of a solid neutron lattice is another possibility that people have considered. This question has really not been resolved and is still being debated. If one could probe these very dense states in heavy ion collisions, one might be able to get some indications of what is occurring here. There's also the question of whether there would ever be a high enough density in the center of a neutron star, to create quark matter, Lee-Wick matter or some density isomer. It seems unlikely that it would be dense enough for quark matter, because for quark matter to be produced one needs densities of 10^{16} gm/cm^3. The central densities in all the typical calculations are never much above 10^{15} gm/cm^3. Therefore, it is probably true that with a neutron star one cannot really probe the quark matter situation. It should also be remembered that quarks do seem to interact like point particles and thus their maximum mass would be more like the 0.7 $M_\odot$ Oppenheimer-Volkov mass than the 2 $M_\odot$ neutron star maximum mass. Therefore any collapsing star with a mass greater than the neutron star mass would not be stopped at the quark star state.

Black Hole and Neutron Star Formation and Supernovae

We will now discuss the mechanisms for making a neutron star. A star starts out its evolution as hydrogen, the hydrogen then burns to form a helium core. At the temperatures of burning hydrogen, helium is inert so the helium core begins to collapse until its central temperature is sufficiently high that it can burn. It will then burn to carbon. For a massive star this sequence goes until there is an iron core surrounded by burning shells of ^{28}Si, ^{16}O, ^{20}Ne, ^{12}C, ^{4}He and H. There are actually other alpha particle nuclei mixed in as well, those listed are the primary ones. This work has been done by a number of people with the current state-of-the-art calculation being that of Tom Weaver, Stan Woosley and Art Zimmerman[5] at Livermore.

The previous scenario applies for any star bigger than about 8 ± 2 solar masses. Lower mass stars end up having their evolution stopped long before they form this complete onion skin model, because a core is developed that is supported by degenerate electron pressure and not able to collapse further. What limits the size of the core is the Chandrasekhar mass (1.4 solar masses), the amount of mass that can be supported by degenerate electrons. Because of mass loss and other details, the lowest mass star that will complete the sequence going all the way to a 1.4 solar masses Fe-Ni core has about 8 solar masses. Once more than 1.4 solar masses of silicon have burned the electron pressure no longer is able to support the core and it will begin to collapse. Unlike all the previous stages of collapse there is now no thermonuclear energy available to halt the collapse. Therefore, this is the final configuration before some sort of catastrophic event will happen to the star.

The density of the central region, iron-nickel core, is about 10^{10} gm/cm^3 at the start of core collapse. The densities drop off with the silicon shell, oxygen shell, and so on being at significantly lower densities. The more massive stars will tend to have much more material in the oxygen, neon, and carbon zones, whereas the lower mass stars (nearer the 8 solar masses boundary) will have very thin oxygen, neon and carbon zones and a larger fraction of its material in the helium zone. This is the reason why the more massive star will tend to eject large amounts of heavy elements when it blows up, whereas a lower mass star, although it's making some heavy elements, has a relatively small fraction of heavy elements other than helium, and therefore will eject primarily helium and its hydrogen envelope. Thus there is a gradient in the amount of heavy elements ejected in these different stars. While different mass stars all made heavy elements and will eject them in a supernova explosion, they will do so in relatively different ratios.

We have the following scenario for the future of the iron-nickel core: Since there is no further nuclear energy available to prevent the collapse, the iron is not able to stop the star's collapse like the previous nuclear burning stages were able to do. The silicon burning has added to the mass of the iron core so that it is above 1.4 solar masses, and degenerate electron pressure can no longer support it. We also have sufficiently high density so that the Fermi energy is above the threshold for electron capture. This means electrons are being captured by protons, neutronizing the material. In fact, it's not the free protons but the complex nuclei that are undergoing electron capture, and emitting neutrinos. Electron capture is pulling away the electrons which were providing the pressure support, thus

decreasing the pressure support making the collapse go even faster. The temperature is also sufficiently high to permit electron-positron pair annihilation and related processes, producing neutrinos. The density is so high that photons cannot escape. Although there is a constant interchange of electron-positron annihilation to photons, the photons are trapped, but every now and then by the ratio of the weak to electromagnetic interaction, a neutrino pair is produced. Because of the effect of the neutral current, all types of neutrino pairs, not just electron neutrino pairs are produced. These neutrinos do escape, at least in the first stages of this collapse. As a result, the star is being cooled and the pressure is further reduced.

Another fact to be taken into account is that at these temperatures iron is excited. This point is one that Gerry Brown, Jim Lattimer and Hans Bethe have recently been emphasizing. A few years ago it was thought that a lot of energy goes into photodisintegration rather than excitation in which case the iron would break down into free neutrons and protons. In fact, what probably occurs is just nuclear excitation. Because of cooling, the temperature does not seem to be high enough to completely break down the iron. Instead, there is nuclear excitation of the iron.

One aspect of this process is that the free nucleon gas is not there to stop the collapse. If the iron was broken down into free neutrons the free neutron gas would have $\gamma = 5/3$ as opposed to the electron gas which has $\gamma = 4/3$. In that case the collapse would be stopped because the pressure would get stiffer. Now we recognize that the nucleons stay in complex nuclei, and since there are very few complex nuclei since the nucleons are then in bundles of 60, the

pressure is still always dominated by the electron pressure, which is a $\gamma = 4/3$ relativistic gas. This is true until the iron starts to actually bump into other iron nuclei. Thus there is a soft equation of state all the way down to nuclear densities. For this reason it is thought that we should now focus on what happens at and above nuclear densities, as far as the future of the problem is concerned. Whereas just a few years ago we thought the collapse would stop long before nuclear densities.

Following the hydrodynamic situation in different zones of a star (a number of people have done these calculations, including Jim Wilson and Dave Arnett), one sees zones collapsing until a transition from densities much less than nuclear densities where the pressure is dominated by leptons, both the electrons and the neutrinos and a soft equation of state, until the density surpasses nuclear density and nucleon-nucleon interactions begin. At this point, $\gamma > 4/3$, and there is a sudden stiffening, as Bethe, Brown, Applegate, and Lattimer have pointed out. Because of the sudden stiffening of the equation of state, the material then feels a bounce.

Now, depending upon what is bouncing, whether it's a whole core bouncing with new material falling in on the core that bounces off of the stable core, or whether it's a core oscillating, one gets various scenarios, and that all depends on the equation of state. One may get a core bounce and a shock wave that propagates so that as it moves out it eventually starts to steepen and drive off the outer material while allowing the inner material to fall down to become a neutron star. In such a scenario there is some sort of mass cut between the material that gets shocked and ejected and the material that falls in to make a neutron star.

High energy heavy ion experiments will hopefully probe the compressibility of nuclear matter at densities beyond that of normal nuclei. These are regions which effect the hydrodynamic bounce and determine whether or not mass is ejected and whether one forms a neutron star or a black hole.

In addition to the direct effects of the nuclear equation of state there is also a dependence on the neutrinos. They are the dominant way in which energy is emitted from the star. The neutrinos are trapped above $\sim 10^{12}$ gm/cm^3, that is they have to diffuse out rather than stream out. The neutrinos that diffuse out may actually help eject matter. They may cause a pressure build-up and help eject the outer layers. However because there's so much uncertainty in the equation of state, it's not clear what role the neutrinos really play. It is apparent that at the present time uncertainties in the equation of state are much bigger than uncertainties in the neutrino interaction physics and, as a result, changes in the equation of state can dominate the effects much more than the slight difference obtained from neutrino pressure or non-pressure.

Neutrinos provide another interesting observable which may have a feedback back on the system. This is the neutrino photosphere. By taking cross-sections and typical energies one finds that the neutrinos may stream out freely from the photosphere at densities below 10^{11} gm/cm^3. At densities from 10^{11} - 10^{12} gm/cm^3 the neutrinos start to scatter and above 10^{12}gm/cm^3 they are completely trapped. In order for the star to collapse to a neutron star, 10^{53} ergs of gravitational binding energy must be released. This energy must be carried off in the form of neutrinos. Perhaps some of the energy

might be released in the form of gravitational radiation if you have non-spherical modes. However, even in calculations that maximize the gravitational energy, you never get more that 1% of the binding energy off in gravitational radiation. The bulk of it always comes off in neutrinos.

These energetic arguments concern the binding energy of the neutron star, 10^{53} ergs, that has to escape to make a neutron star. The energy of a supernova is only 10^{51} ergs. The dynamics, from looking at the mass motion, is only a percent of this total binding energy. Therefore, one's only tapping onto a very small fraction of the binding energy to make the supernova outburst. We also know that 10^{57} electron neutrinos must escape: The star starts out with roughly half protons and almost all those protons are eventually going to become neutrons. Thus 10^{57} electron capture neutrinos must escape which is about 10^{52} ergs. But remember, 10^{52} is still only 10% of total binding energy, so the bulk of the binding energy is really going to come off in neutrino pairs, not only electron-neutrino pairs but also muon-neutrino pairs, tau-neutrino pairs, etc.

There are detectors now operating, in particular the Ken Lande detector in the Homestake goldmine which is about 500 cubic meters of water, capable of seeing 10 MeV neutrino from even a 10^{52} erg event anyplace in our galaxy. If a collapse did occur in our galaxy, Lande should be able to see it and get the neutrino signature which might give us more information on the nuclear equation of state. It is even conceivable that the neutrino spectrum from neutron star formation will differ from that produced in black hole formation since the black hole may trap the neutrinos before they diffuse out.

The Early Universe

It is fairly certain that the universe started out hot and dense. This idea is supported in several ways.

The first observation suggesting an expanding universe was the discovery by Hubble of the recession of galaxies. The 3K background radiation discovered by Penzias and Wilson tells us that the universe once had a temperature $\geq 10^5$ K, the temperature at which photons decouple from matter. In fact, this radiation was predicted by George Gamov as a necessity of the occurrence of nuclear reactions in the early universe. From that argument alone one knows that the temperature was probably greater than 10^9 K. In fact, the nuclear reactions and the radiation are very closely coupled arguments. They can be made more quantitative by noting that the present helium abundance of about 25% by mass throughout the universe shows that the big bang nucleosynthesis model is very sucessful. We know not only that nuclear reactions occurred, but we also have a quantitative understanding of the reactions that did occur, and that understanding goes back to temperatures of 10^{10} K. Since there is no other way of understanding why one-fourth of the mass of the universe is in helium if it did not come out of the big bang we are fairly confident that the universe was at one time hotter that 10^{10} K.

Having reasonably assured ourselves that the Universe has evolved from a very hot and dense era, the next question we may ask is: at what point in our extrapolation to higher temperatures and densities do we encouter a physically different state of matter than we have explored, to date, in the laboratory. Such a transition will occur when hadrons merge to form a soup of quarks and gluons. We expect

such a stage to have occurred due to the finite size of hadrons. At very high densities, hadrons begin to overlap and eventually lose meaning as individual particles. We may then refer to the universe as being a quark-gluon fluid. It is expected that this transition occurs when the total number density of hadrons is $\gtrsim$ 10 n_o ($n_o = 0.17/fm^3$).

Wagoner and Steigman have argued that the transition must have occurred at a temperature between $170 \leq T_c \leq 360$ MeV, where T_c is the condensation temperature for quarks going into hadrons. These arguments are based solely on 1) the physical size of hadrons and their geometry and 2) the QCD potential at very short distances. If we further assume that the transition in the early universe took place adiabatically and as a second order phase transition, the condensation temperature is found to be 207 MeV, which is consistent with the arguments of Wagoner and Steigman. This temperature corresponds to a number density of $\simeq$ 13 for hadrons.

The assumption that the transition occurs as a second order phase transition is not unreasonable for the early universe, however as we will see, when one considers the transition occurring in a heavy ion collision this assumption is no longer valid. In the early universe, we expect the transition to have occurred gradually and reversibly in addition to requiring that the total entropy remain constant throughout the transition. Furthermore we have neglected the baryonic chemical potential, since $n_B - n_{\bar{B}} / n_\gamma \simeq 10^{-9}$, where $n_{B,\bar{B},\gamma}$ are the number densitites of baryons, antibaryons and photons respectively. This point will be made clear in discussing the transition in heavy ion collisions, where we can no longer neglect the baryonic

chemical potential.

Having determined the condensation temperature, T_c, it is now possible to predict the spectrum of hadrons which emerges from the condensation of quarks into hadrons as the universe expands. It should be noted that of the six quarks, u, d, s, c, b, t only u, d and s were of sufficient abundance at this time in the universe to generate hadrons. Due to their mass and the low condensation temperature the abundances of c, b, t are greatly reduced by a Boltzman factor $\exp[-m_Q/kT_c]$. Thus we expect only hadrons composed of u, d, s quarks to sppear in the spectrum.

The hadron spectrum following the transition is found by examining the total number density of hadrons at T_c. The most abundant particles emerging from the transition and their relative percent abundances are: nucleons (3.6), Δ (1232) (4.9), π 15.0, ρ (770) (7.5), K (495) (8.1), K^* (892) (6.5). The large abundances of Δ, ρ and K^* are mainly due to their statistical weight. As the universe continues to cool, however, these particles will annihilate and decay leaving only the lighter hadrons present. For example, within 20 μ sec after the transition the abundance of pions is already 50%. As the temperature drops further, the pions will disappear leaving only a very small amount of nucleons. (This is due to the small excess of baryons over antibaryons, otherwise the entire hadron spectrum would have disappeared when $T \lesssim$ 50 MeV.)

A heavy ion collision experiment can be proposed to test this model of the quark-hadron transition. Such an experiment may in fact yield a signature for quark matter. Using the nuclear fireball model[6,7,8] for heavy ion collisions, it is expected that a region of quark matter

may exist temporarily in a collision of sufficiently high energy.

However, there are two major differences between the transition in the Big Bang and a heavy ion collision. These are: 1) the net baryon number of the system and 2) the effect of surface radiation in the fireball[9,10]. As we have said, the net baryon number in the Big Bang is quite negligible, while in a heavy ion collision this is no longer the case. For a typical collision of ^{20}Ne on uranium, the net baryon number $N_B \simeq 60$ compared to a total number of particles in the fireball of about 400. Thus in computing the spectrum of hadrons formed in the transition the baryon chemical potential must be considered. The effect of surface radiation is not quite as obvious. In the Big Bang it is obviously not relevant since one has a near infinite fluid. For our purposes we will neglect this correction as it should not affect the qualitative existence of a quark signature.

Because of the large net baryon number in the fireball, we can no longer assume a second-order phase transition. This point can be made obvious by examining the total entropy of the system. In general the entropy is given by

$$S = V \frac{dP}{dT} - N \frac{d\mu}{dT}$$

where V, P, N, μ represent the volume, pressure, number of particles and the chemical potential of the system. Since the chemical potential of the quark and hadron phases have different dependences on the temperature, one might expect a chage in the entropy (a latent heat) during the transition.

The signature of the quark matter is found by examining the spectrum of hadrons emerging from the collision at various energies (or fireball temperatures). If a transition occurs, there should be no difference in the spectrum at temperatures greater than T_c. Since we do not expect to see any isolated quarks in the spectrum, the fireball will always cool down to the condensation temperature before any particles appear in the spectrum (neglecting surface effects). Thus the spectrum as a function of the fireball temperature should remain constant at temperatures greater than T_c.

If no transition occurs, the ratio of antibaryons to baryons in the spectrum should approach unity as the fireball temperature is increased. In addition, the relative abundance of pions should steadily decrease. The reason for these effects is simply that at higher temperatures, more baryon particle-antiparticle pairs will be produced and will eventually overshadow the net number of baryons. The relative number of pions seen will decrease, since more of the higher resonance mesons will be produced. Thus by comparing the ratio of antinucleons to nucleons and abundances of pions at various energies, one should be able to determine whether or not a transition occurred.

For a ^{20}Ne on uranium collision, it is found that a fireball temperature of at least 180 MeV, corresponding to an incoming laboratory energy of about 11 GeV/nucleon, is necessary to reach the quark phase. It is hoped that such laboratory energies may be produced in heavy ion accelerators which are now being planned, in order to further confirm the existenceof quark matter and to obtain a greater understanding of the Big Bang model of the early universe.

Another current problem in cosmology is the question, where do

galaxies come from? In fact we know that on very large scales, the universe appears to be very homogeneous and isotropic. The average density of the universe is someplace between 10^{-31} and 10^{-30} gm/cm^3. Yet the local average density if 1 gm/cm^3; so it's clear that the universe is not completely homogeneous and isotropic; there are large variations in density. And the question is why? Why did we have these fluctuations that ended up producing stars, galaxies, planets, people, etc. To make galaxies, one needs some sort of fluctuation, and it has to be of sufficient amplitude to become gravitationally bound so that that fluctuation remains even though the universe is expanding to lower densities.

The fluctuations must be bound at a particular time. The reason is this: the universe is dominated by radiation early in its history, gravitational contraction cannot occur. Galaxies cannot form. So the universe had to have a fluctuation that had grown in amplitude sufficiently to make a bound fluctuation after the universe was no longer radiation dominated, and also after recombination, after the time the photons freely propagated. We do know that the 3° radiation is relatively uniform and isotropic, so sometime after that recombination there had to have been a fluctuation of the matter density that was sufficient to be a bound fluctuation. The question is, where do these fluctuations come from? What is their origin? What some people have done in trying to make galxies is to assume some sort of arbitrary spectrum of primordial fluctuations coming out of the big bang singularity. A major goal of other people has been to find a mechanism for the production of these fluctuations after the singularity. One such process we are very interested in is this quark-hadron phase

transition. Could what happens at the phase transition be of a nature that might stimulate clustering of some sort, some sort of fluctuation?

Remember this phase transition is from a quark soup to lower densities at which hadrons are formed. Current ideas on quark confinement tell us that the quark-quark color interaction is stronger the farther apart the quarks are. Therefore as 3 quarks are removed from the quark soup to make a baryon, it may be that this lower quark density site is maximally unstable to further hadron condensation. In addition, the removing of a triplet of quarks reduces the Debye-color screening of the remaining quarks in the vicinity and thus enables those particular quarks to have longer range interactions. It thus seems that the quark-hadron phase transition may be unstable to the growth of density fluctuations.

Could this kind of fluctuation that occurs here lead to clustering of any kind? Is this unstable to seeds stimulating the transition locally rather than uniformly passing to the hadron state? This question of what goes on during the transition is very critical, and one hopes that this might be able to answer the galaxy formation question. (It may be very wishful thinking.) When one is doing a heavy ion experiment, going to very high energies, one is traversing this transition both ways because one is starting with hadrons, banging them together into a quark soup temporarily, and then they re-emerge. There is an important difference between the early universe and the heavy nucleus collisions. In the early universe, the transition region is unbounded, while in a heavy nucleus collision there is a central region that may be quark soup but there's also a region where the quark interactions may proceed quite differently. This transition

problem is a difficult one but an important one.

One other possible effect of the quark-hadron phase transition is the generation of entropy as a result of the quarks possibly radiating some binding energy as they condense into hadrons. Lasher[11] has utilized this to try to generate the entire entropy per baryon of the universe. We personally feel his mechanism requires an unphysically large separation of quarks prior to condensation and is thus unreasonable, however there nevertheless may be some smaller amount of free enrgy so generated with the bulk still coming from the hot initial early universe conditions.

Summary

In summary let us repeat that the use of ultra-high energy, heavy ion collisions may probe nuclear matter properties above nuclear matter densities; and such knowledge is fundamental to the understanding of neutron stars, supernovae, and the big bang; and it may even be related to the origin of galaxies and perhaps the origin of the entropy of the universe.

This work was supported in part by NSF grant AST 78-20402 and NASA grant NSG 7212 and K.O.'s Fannie and John Hertz Foundation Fellowship.

References

1. Simpson, J. Ann. Rev. Nuc. Part. Sci 31 (1981) in preparation.

2. Baym, G. and Pethick, C. Ann. Rev. Astron. and Astrophys. (1978).

3. Lattimer, J. and Brown, G. Ann. Rev. Nuc. and Part. Sci. 30 (1980).

4. Freedman, D., Schramm, D.N. and Tubbs, D. Ann. Rev. Nuc. Sci. 27, 167 (1977).

5. Weaver, T. and Woosley, S. Ann. Rev. Nuc. and Part. Sci. 31 (1981) in preparation.

6. Westfall, G.D., et al 1976 Phys. Rev. Lett. 37, 1202.

7. Mekjian, A.Z., 1978 Phys. Rev. C.17, 1051.

8. Mekjian, A.Z., 1978 Nuc. Phys. A.312, 491.

9. Olive, K.A., 1979, Proc. Neutrino '79, Bergen, Norway.

10. Olive, K.A., 1979, submitted to Phys. Lett. B.

11. Lasher, G., 1979 Bull. Am. Astron. Soc.

NUCLEAR PHYSICS PERSPECTIVES ON HIGH-ENERGY NUCLEAR COLLISIONS*

Herman Feshbach
Massachusetts Institute of Technology

My crystal ball is not sufficiently clear for me to predict the nuclear effects which will play a dominant role when ultra-relativistic heavy ions collide with nuclei. New and unexpected effects will surely occur but whether these will reveal new and striking information regarding the structure of nuclei and their interaction is of course not certain. Whatever they may be, it is essential that we understand the effects we can predict now so that the unusual will become more clearly visible, in this way increasing the signal to noise ratio. It is thus important to identify the sources of "noise" and to evaluate their consequences carefully.

In this talk I shall consider two such classes of phenomena. In the first the prediction of heavy ion reactions in terms of the reactions induced by a single nucleon will be considered. The deviation of such a prediction from experiment would indicate the presence of new phenomena which are present because of the structure of the incident heavy ion. It would tell us that it is not possible to regard the latter as a simple collection of nucleons which "happen to be travelling together".

Suppose the $\mathcal{J}$ matrix for a nucleon-nuclear reaction is given by $\mathcal{J}_{nT}(\vec{k}|\vec{k}')$ where $\vec{k}'$ is the momentum of the incident nucleon and $\vec{k}$ represents the momenta and other variables required to describe the emitted system. Moreover suppose that the incident projectile consists of a set of nucleons whose momentum distribution relative to the projectile center of mass

*This work is supported in part through funds provided by the U.S. DEPARTMENT OF ENERGY(DOE) under contract EY-76-C-02-3069.

is $\rho_p(\kappa)$. Then the J matrix for the projectile-nucleon collision $J_{pT}(\vec{k}\ \vec{k}_p)$ where $\vec{k}_p$ is the momentum of the projectile is given approximately by

$$J'_{pT}(\vec{k}|\vec{k}_p) \simeq A_p \int d\vec{x}\ \rho_p(\vec{x}) J_{nT}(\vec{k}|\vec{x}+\vec{k}_p) \qquad (1)$$

In most applications J_{nT} is taken as closely as possible from experimental data. This expression assumes that the incident projectile is just a collection of incident nucleons. It will fail if correlations in the projectile before and after the collision are important. If there is any domain where it is correct it would be for relatively small energy and momentum changes.

An expression similar to Eq. (1) but valid in another domain can be developed by going to the projectile frame of reference in which the incident system is the target. In this frame one can in complete parallel to Eq. (1) write

$$J''_{pT} \simeq A_T \int d\vec{x}\ \rho_T(\vec{x}) J_{pn}(\vec{k}|\vec{x}+\vec{k}_T) \qquad (2)$$

where J_{pn} is the nucleon-projectile J matrix. Small energy losses and small momentum changes in the projectile frame will of course transform to a domain which differs from that in which Eq. (1) is possible valid.

Essentially the above method has been used at relativistic energies by Papp et al.[1] to predict pion production while Shaeffer et al.[2] and Viollier[3] have used the method for

elastic and inelastic alpha particle scattering by nuclei. Corrections to Eq. (1) and Eq. (2) have been derived[4], but need evaluation. Cascade calculations[5] which have also been moderately successful refer the the nucleon-nucleus collision back to the nucleon-nucleon collision.

With this background, we turn to the ultra-relativistic domain and ask what is known with regard to the proton-nuclear collision. As we shall see the phenomena which have been demonstrated so far are unexpected and unusual. In Figure 1 the average energy of a Sr fragment formed in a p+U collision is plotted as a function of the proton energy[6]. We see that as the proton energy increases the fragment energy decreases, eventually approaching an asymptotic constant value after about 10 GeV. This is the opposite of what happens at lower energies. The angular distribution[7] is similarly anomalous. As indicated by Figure 2, giving the ratio of the forward (F) to backward production the angular distribution becomes increasingly peaked as the proton energy increases up to roughly 3 GeV. Beyond that energy the angular distribution becomes more isotropic, F/B approaching unity at Fermi Lab energies. More detail is provided by the experiments of Remsberg and Perry[8] for 28 GeV protons colliding with U or Au. As can be seen from Figure 3, the angular distribution is rather flat with a maximum in the laboratory frame at about 70°.

These experimental results strongly imply that in the collision of the incident proton with the target nucleon energy

and momentum are being transferred to the nuclear degrees of freedom in increasingly smaller amounts as the proton energy increases possibly tending to constant values at sufficiently high energies. Rather, and this is of course a guess, it is the internal degrees of freedom of the nucleon that are excited by the collision and that excitation is only partially transferred to the nucleons of the target in the form of kinetic energy.

Another phenomenon, which has been discussed extensively at this meeting, with a conclusion identical to that given just above, has been observed at large proton energies. It is by no means assured that it and those given above have identical cause, that of hadron excitation. But as a tentative hypothesis we shall assume that to be the case. I refer to the measurement of multiplicity of high energy ($v/c>0.7$) charge particle production. Some typical data[9] are shown in Figure 4 and in Table I[10]. These measurements demonstrate that the number of such particles increases very slowly with increasing mass number. No cascading is indicated showing that little energy is deposited inside the nucleus. Empirically the multiplicity ratio, R, of the multiplicity in a collision of a hadron with a nucleus to that of a collision with hydrogen is given by

$$R = 1 + \tfrac{1}{2}(\nu - 1) \qquad (3)$$

where ν is the mean number of collisions of the incident hadron.

The current explanation (see for example Gottfried[11]) begins with the presumption that upon the collision of the incident hadron with a nucleon of the target nucleus, both are excited. The wave function for the system can then be decomposed into a linear combination of states each with its own lifetime τ_0 for decay into the hadrons and a number of secondary particles, generally pions. This lifetime is given in the rest frame. In the laboratory frame, the lifetime is $(E/m)\tau_0$ where E is the kinetic energy of the system with lifetime τ_0 as formed in the collision and m is its rest mass.

Because of this time dilatation, the lifetime of the excited hadron in the laboratory may be so long that it does not decay inside the nucleus but outside the nucleus. Naturally these external decays are more likely to be associated with the fast, that is, leading hadron.

The critical length is the mean free path, λ, of the incident hadron. If $c\tau$ is greater than λ, the excited hadron will not have decayed before it has its second collision, upon which the decay will be halted and the excited hadron state will be reconstituted. Under these circumstances, $c\tau>\lambda$ then, the excited hadron will pass through the nucleus without decaying, emitting a number of pions, for example, after it has left the nucleus. Equation (3) can be obtained if one assumes that on each collision a component which decays outside the nucleus is generated with average energy E^α with multiplicity $\log E^\alpha$ with $\alpha=\frac{1}{4}$.

A rough value of the hadron energy at which this phenomenon becomes dominant is estimated as follows. We assume that the excited system is at rest in the center of mass frame of the incident proton and target nucleus nucleon. Taking the mass to be the proton mass, then the excited hadron energy, $\bar{E}$, is

$$\bar{E}/m \simeq \sqrt{E_{Lab}/2m} \tag{4}$$

and the corresponding laboratory lifetime, $\bar{\tau}$, is

$$\bar{\tau} = \sqrt{E_{Lab}/2m}\ \tau_0 \tag{5}$$

The critical value of E_{Lab} is determined by the inequality

$$c\bar{\tau} > \lambda$$

Placing $c\tau_0$ equal to 1 fm and λ equal to 2 fm yields E_{Lab} equal to 7.5 Gev, which is the correct order of magnitude. This result is suggestive only. It indicates that the explanation of the phenomena picture in Figures 1,2,3 may be the same as that used to explain the multiplicity ratio R. Obviously much more work has to be done to confirm this possiblity. A more detailed quantitative theory must be developed, and many more experiments are needed.

The question may be asked as to the impact on the target nucleus. The transverse momentum transfer is thought to be small[12]. Elastic scattering experiments indicate values of the order of 300 MeV/c. The longitudinal momentum transfer in elastic scattering is consequently also small. If this were the case in production reactions as well, the incident nucleon in

its passage through the nucleus would transfer roughly 100 MeV to each nucleon it encounters so that the collision with the nucleus would be relatively gentle. A rough estimate of the longitudinal momentum transfer indicates it to be between .500 GeV/c to 1.0 GeV/c. However there are models that do not follow the Gottfried description. These predict that the incident nucleon would drill a hole through the target nucleus. Clearly we need some experiments to settle this issue.

A second class of predictable reactions are those generated by peripheral collisions. Peripheral collisions generally involve the action of the "fringing" Coulomb and nuclear field of the target on the projectile or vice versa. The cross-section for Coulomb induced peripheral reactions is given by the Coulomb Weiszäcker-Williams result:

$$\sigma = \int \sigma_\gamma(\omega)\, n(\omega)\, d\omega \tag{6}$$

$$n(\omega) = \frac{2}{\pi}(Z\alpha)^2 \frac{1}{\omega} \tag{7}$$

In these formulas $n(\omega)$ is the number of equivalent photons with frequency between ω and $\omega+d\omega$, $\sigma_\gamma(\omega)$ is the cross-section for a reaction denoted by the subscript γ induced by a photon of energy $\hbar\omega$. This Coulomb effect has been observed in the production of protons in the collision of relativistic heavy ion with nuclei[12]. In deriving (6) and (7) it is assumed that the projectile moves in a straight line along the incident direction. It is also assumed that the interaction is weak.

The nuclear peripheral collision is evaluated using the nucleon Weiszäcker-Williams method[14]. In this theory the straight line motion is assumed and the perturbation, the long range part of the nucleon-nucleus interaction, is taken to be weak. Clearly this can only be accurate in the fringing field. The formula analogous to Eq. (6) is

$$\sigma_T = \left(\frac{2\pi}{k}\right)^2 \int \rho_\beta \, d\varepsilon_\beta \, d\vec{k} \, d\omega \, |F_p(-\vec{k}, -\omega/v)|^2 \, |F_T(\vec{k}, \omega/v)|^2 \, \delta(\omega - \omega_{\beta i}) \quad (8)$$

where

$$F_T = \langle \psi_\beta | \sum_\tau e^{i\vec{q}\cdot\vec{\xi}_\tau} | \psi_o \rangle , \quad \vec{q} = (\vec{k}, \omega/v) \quad (9)$$

In this expression the target makes a transition from the ground state to state β, the energy transfer is ω $(=\omega_{\beta i})$, the longitudinal momentum transfer ω/v, where v is the velocity of the projectile, $\vec{k}$ is the transverse momentum transfer. The variables $\vec{\xi}_T$ are the coordinates of the target nucleons. The density of states β is ρ_β. The quantity $|F_T|^2$ plays a role similar to that of σ_γ in Eq. (6). In the case considered in Eq. (9) it is the nuclear field of the projectile which induces transitions in the target. Of course the reverse in which the field of the target induces transitions in the projectile must also be considered as is the case in Ref. [13]. The quantity F_p depends upon the mechanism involved. When the nuclear field is generated by the nucleon-nucleon potential, V_{NN}, the projec-

tile factor F_p is

$$F_p = \frac{1}{2\pi v} V_{NN}(\vec{k}, \omega/v)\, \rho_p(-\vec{k}, -\omega/\gamma v) \tag{10}$$

where ρ_p is the Fourier transform of the proje ile density, and γ is the relativistic factor $(1-v^2/c^2)^{-\frac{1}{2}}$. Its presence is a consequence of the Lorentz contraction of the relativistic projectile.

Of course a variety of states β can be excited by the effective interaction $\sum_T e^{i\vec{q}\cdot\vec{\zeta}_T}$. An important point is that the effect of the properties of the projectile on that excitation can be factored out as shown by Eq. (10). In Ref. [14] the process involved is two particle absorption of the momentum $\vec{q}$ and energy $\hbar\omega$. Another process of general interest is the excitation of collective modes. In the adiabatic approximation F_T becomes a matrix element between the ground state and a collective mode designated by $|\alpha'\rangle$ of the operator

$$\hat{F}_T = \int d\vec{x}\, \rho(\vec{x}, \alpha)\, e^{i\vec{q}\cdot\vec{x}} \tag{11}$$

so that

$$F_T = \langle \alpha' | F_T | \alpha \rangle$$

As a final example consider pion production. In that case the V_{NN} of Eq. (10) must be replaced by a nucleon-nucleon-pion field $V_{NN\pi}$. To simplify the discussion we consider a spin independent $V_{NN\pi}$:

$$V_{NN\pi} = \sum_{p,\tau} t_\tau^{(-)} t_p^{(+)} \mathcal{J}(\vec{r} + \vec{\xi}_\tau - \vec{\xi}_\pi ;\ \vec{r} - \vec{\xi}_p + \vec{\xi}_\pi) \tag{12}$$

where t^+ and t^- are isospin operators. Coherent pion production will occur if the transition of the projectile is to the isobar analog of its ground state. The latter wave function is given by

$$|A\rangle = \frac{T^{(+)}}{\sqrt{N_p - Z_p}} |\chi_o\rangle \tag{13}$$

where

$$T^{(+)} = \sum_p t_p^{(+)}$$

Then the relevant matrix element can be evaluated:

$$\langle A | t_\alpha^{(+)} | \chi_o \rangle = \left[(N_p - Z_p)^{1/2} / A_p \right] \rho_p \tag{14}$$

The product $V_{NN}\rho_p$ in Eq. (10) is replaced

$$V_{NN}\rho_p \longrightarrow \tilde{\mathcal{J}}\left[\tfrac{1}{2}(\vec{k} - \vec{k}_{\pi\tau}),\ \tfrac{1}{2}\left(\tfrac{\omega}{v} - k_{\pi\lambda}\right);\ \tfrac{1}{2}(\vec{k} + \vec{k}_{\pi\tau}),\ \tfrac{1}{2}\left(\tfrac{\omega}{v} + k_{\pi\lambda}\right)\right]$$

$$\times \rho_p\left[\tfrac{1}{2}(\vec{k} - \vec{k}_{\pi\tau}),\ \tfrac{1}{2\gamma}\left(\tfrac{\omega}{v} - k_{\pi\lambda}\right)\right] \tag{15}$$

where the pion momentum $\vec{k}_\pi$, has the transverse component $\vec{k}_{\pi\perp}$ and the longitudinal component $k_{\pi\lambda}$. $\tilde{\mathcal{J}}$ is the Fourier transform of $\mathcal{J}$.

The matrix element F_T of Eq. (9) is replaced by

$$F_T = \langle \psi_\beta | \sum_\tau t_\tau^{(-)} \exp(-i\vec{q}\cdot\vec{\xi}_\tau) | \psi_o \rangle \tag{16}$$

where

$$\vec{q} = \left\{ \tfrac{1}{2}(\vec{k} + \vec{k}_{\pi\tau}), \tfrac{1}{2}\left(\tfrac{\omega}{v} + k_{\pi\lambda}\right) \right\} \qquad (17)$$

Single nucleon absorption is probably the main mechanism.

Expressions given by Eq. (15) and Eq. (16) include, of course, the production of pions via Δ formation in the projectile.

It should be remarked once more that the above describes the coherent production of pions by the projectile. Coherent production by the target can be obtained by using the projectile frame and interchanging the projectile and target coordinates in the preceding discussion.

References

[1] J. Papp, J. Jaros, L. Schroeder, J. Staples, H. Steiner, A. Wagner and J. Wise, Phys. Rev. Lett. 34 (1975) 601.

[2] V. Layly and R. Schaeffer, "High Energy Apha Scattering on Nuclei", Saclay preprint.

[3] R. Viollier, to be published in Annals of Physics.

[4] H. Feshbach, Les Houches Session 30, Nuclear Physics with Heavy Ions and Mesons, R. Balian and G. Ripka, Eds., North Holland (Amsterdam) 1978, p. 378.

[5] J.D. Stevenson, Phys. Rev. Lett. 41 (1978) 1702.

[6] Ø. Scheidemann and N.T. Porile,Phys. Rev. C14 (1976) 1534.

[7] Ø. Scheidemann and N.T. Porile,Phys. Rev. C14 (1976) 1534.

[8] L.M. Remsberg and D.G. Perry, Phys. Rev. Lett. 35 (1975) 361.

[9] W. Busza, Multiparticle Production in High Energy Hadron-Nucleus Collisions, Proc. High Energy Physics and Nuclear Structure, D.E. Nagle, A.S. Goldhaber, C.K. Hargrove, R.L. Burman and B.G. Storm, Eds., (American Institute of Physics, New York, 1975).

[10] J.E. Elias, W. Busza, C. Halliwell, D. Luckey, L. Votta and C. Young, Phys. Rev. Lett. 41 (1978) 285.

[11] K. Gottfried, Phys. Rev. Lett. 32 (1974) 957; F. Low and K. Gottfried, Phys. Rev. D17 (1978) 2487.

[12] Fermilab Single Arm Spectrometer Group, Phys. Rev. Lett. 35 (1975) 1195.

[13] D.E. Greiner, P.J. Lindstrom and F.S. Beiser, Phys. Rev. 28 (1972) 926. See also B. Cork, Fragmentation of Relativistic Nuclei, Proc. High Energy Physics and Nuclear Structure, D.E. Nagle, A.S. Goldhaber, C.K. Hargrove, R.L. Burman and B.G. Storm, Eds., (American Institute of Physics, New York 1975).

[14] H. Feshbach and M. Zabek, Ann. Phys. 107 (1977) 110.

Figure Captions

Figure 1: Energy dependence of the ranges of Sc nuclides produced when protons of energy E_p are incident on a ^{238}U nucleus. From Ref. [7].

Figure 2: Ratio of forward (F) to backward (B) production as a function of the incident proton energy E_p. The target is ^{238}U. From Ref. [7].

Figure 3: Angular distribution of Flourine fragments produced when uranium is irradiated by 28 GeV protons in the laboratory frame. From Ref. [8].

Figure 4: Angular dependence of the ratio of the multiplicity with indicated target nuclei, to the multiplicity with a hydrogen target. The variables, $\bar{\nu}$, is the average thickness of the nucleus in units of the mean path of the incident projectile. From Ref. [9].

TABLE CAPTION

Table I: The average multiplicities of relativistic charged particles produced in 100 GeV/c hadron-nucleon collisions. From Ref. [10].

TABLE I

Target	Projectile	Average Multiplicity
C	π^+	7.86±0.15
	K^+	6.92±0.33
	p	7.72±0.16
Cu	π^+	10.29±0.26
	K^+	8.89±1.10
	p	11.00±0.32
Pb	π^+	13.21±0.30
	K^+	12.92±0.79
	p	14.75±0.38
U	π^+	14.57±0.39
	K^+	12.93±1.33
	p	15.94±0.50
Hydrogen (bubble chamber)	π^+	6.62±0.07
	K^+	6.65±0.31
	p	6.37±0.06

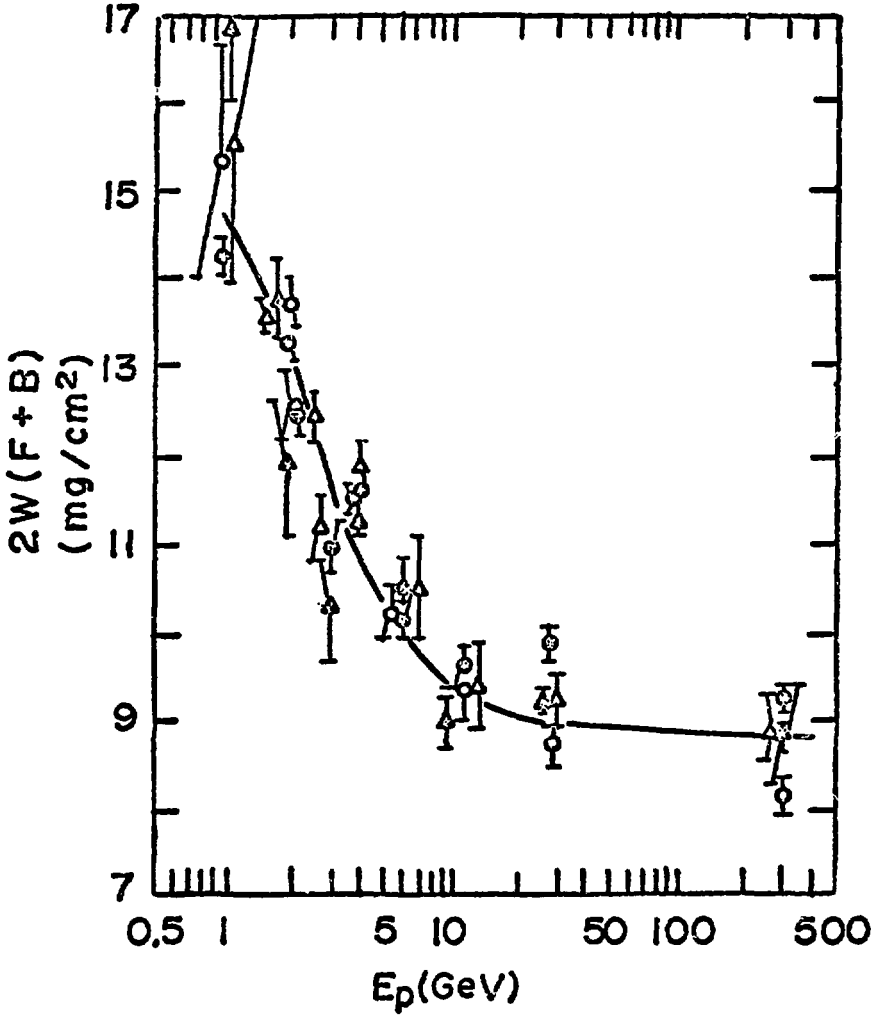

Fig. 1

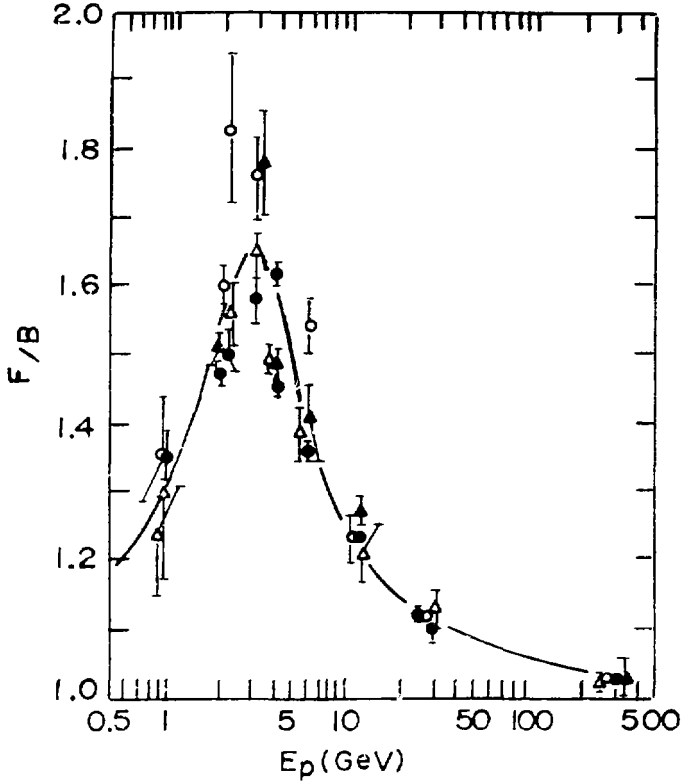

Fig. 2

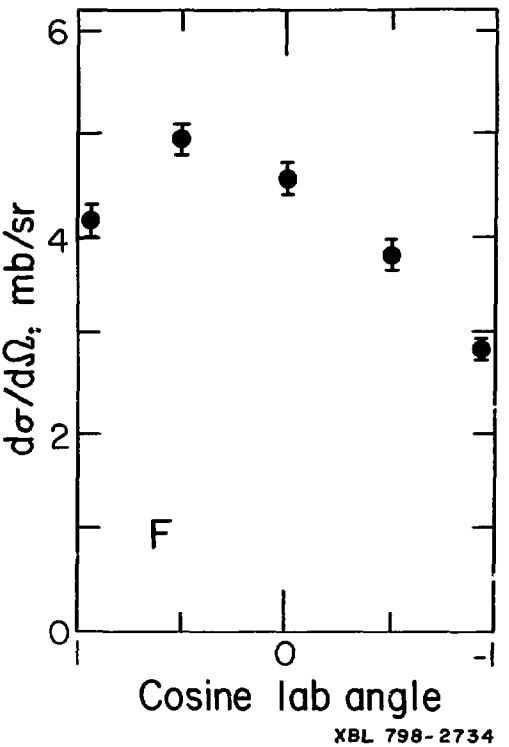

Fig. 3

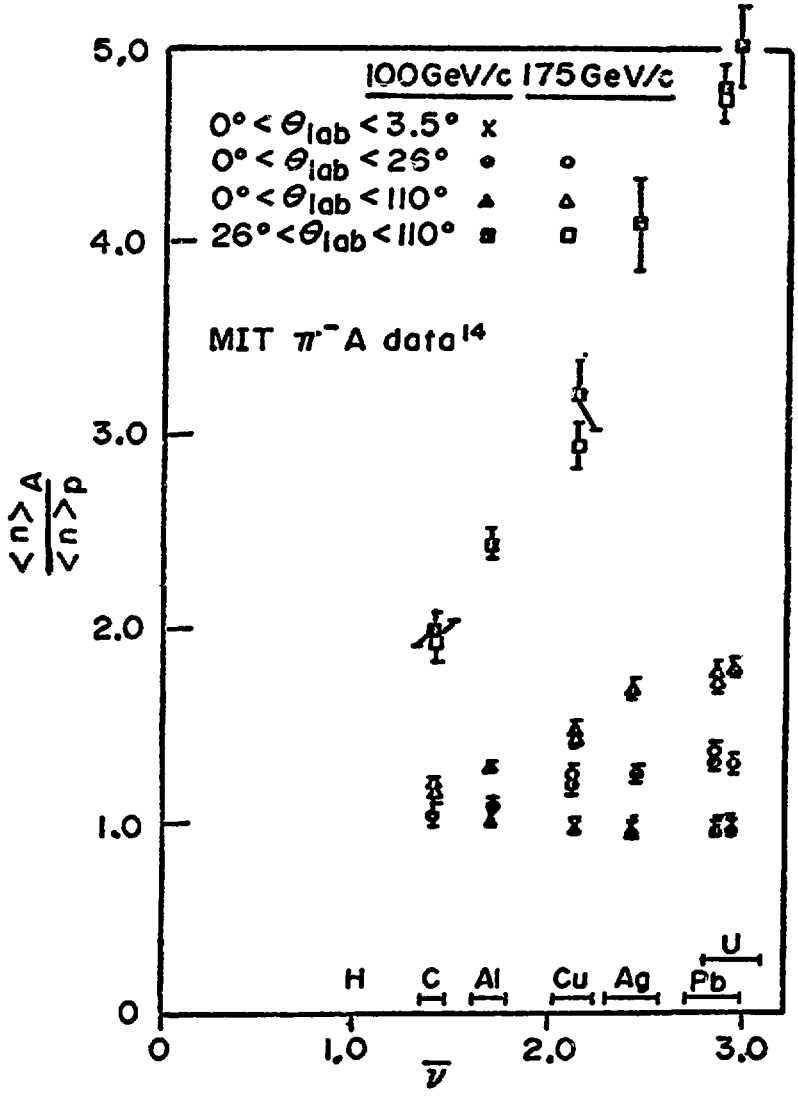
100GeV/c 175GeV/c
0° < θlab < 3.5°
0° < θlab < 26°
0° < θlab < 110°
26° < θlab < 110°
MIT π⁻A data[14]
<n>A / <n>p
ν̄
H
C
Al
Cu
Ag
Pb
U
0
1.0
2.0
3.0
4.0
5.0

Fig. 4

HIGH p_T TRANSVERSE MOMENTUM PHYSICS AT THE CERN ISR

M. G. Albrow
Rutherford Laboratory and CERN

THE INTERSECTING STORAGE RINGS

Since 1971 the Intersecting Storage Rings (ISR) at CERN have provided the highest collision energies available for laboratory study. Two interlaced rings (See Fig. 1), with a diameter in the order of 300 m, store proton beams of energies between 11.4 GeV/c and 31.4 GeV/c and currents up to about 30 amps. The total center-of-mass collision energy, $\sqrt{s}$, in the range 22.8 to 62.8 GeV would require a laboratory beam in the energy range of 280 to 2100 GeV on a stationary target. Seven of the eight intersection regions can be used for experiments. The luminosity L (event rate per unit cross section, per collision region) is $\sim 2 \times 10^{31}$ $cm^{-2} sec^{-1}$ at the higher energies, giving about $8\ 10^5$ interactions per second, the total cross section for proton-proton collisions being in the order of 40 mbarn in this energy range. Typically about 8 hours is spent on tuning the machine and injecting and stacking beams from the CERN proton synchrotron (PS). Stable beam runs then last for 40-60 hours with very little loss of luminosity.

Deuterons have been injected and stored in the ISR and both p-d and d-d collisions studied. We plan to store α-particles next year, for short p-α or α-α runs, but the luminosity is expected to be smaller (a few x 10^{29} $cm^{-2} sec^{-1}$ and a few x 10^{28} $cm^{-2} sec^{-1}$, respectively). This appears to be limited by the non-optimized source, the ISR itself being capable of storing high currents of such particles.

INTRODUCTION TO HIGH TRANSVERSE MOMENTA

In the 1960's (before the CERN ISR, SPS, and FNAL became operational) it was generally believed that multiparticle production in hadron collisions had the characteristic that the produced particles were exponentially damped in transverse momentum p_T relative to the collision axis. This was understood as being due to the transverse dimensions of the hadron in the order of 10^{-13} cm and unchanging with energy producing particles with a conjugate transverse momentum in the order of 200-300 MeV/c. This rule of thumb still does hold true for the vast majority of particles at the ISR. A "typical event" was seen as consisting of two "jets" of hadrons, with limited p_T relative to the jet axis and with longitudinal momentum components, p_L, along that axis which grow in proportion to $\sqrt{s}$. This latter property is known as Feynman scaling. Nevertheless, it was pointed out in a classic paper by Berman, Bjorken, and Kogut[1] (BBK) in 1971 that if hadrons contain point-like constituents (partons, now considered as both quarks and gluons) they should occasionally scatter through large angles. The scattering must take place at least through the electromagnetic interaction if the parton model were to explain deep-inelastic electron scattering data. It should also take place through the strong interaction, which could not be calculated at that time but for which we now have a theory: quantum chromodynamics (QCD). BBK speculated that the scattered partons would dissociate into "jets" of hadrons, and that the resulting spectra should have the form p_T^{-4} in a scale-free theory. At about this time Blankenbecler, Brodsky, and Gunion[2] also predicted important high p_T particle production (constituent Interchange Model, CIM).

SINGLE PARTICLE SPECTRA

The following year early data from the ISR[3,4,5] showed that for $p_T \gtrsim 2$ GeV/c the produced particle spectra deviate upwards from the exponential low p_T behavior, and more so as the collision energy increases. Since that time there has been great activity in this field, especially at the ISR which is well suited because of its very high center-of-mass energy, among other things. Experimentally we measure the inclusive single particle spectra:

$$E \frac{d\sigma}{d^3p} (p_T, y, \sqrt{s}) \text{ for } p + p \to c + \text{anything}$$

where c is a produced hadron of transverse momentum p_T and longitudinal rapidity y,

$$y = 1/2 \ln \left\{ \frac{E+p_L}{E-p_L} \right\} = \tanh^{-1} \beta_L \quad .$$

Other useful forms for the differential production cross-section are:

$$E \frac{d\sigma}{d^3p} = \frac{E}{p^2} \frac{d^2\sigma}{dpd\Omega} = \frac{1}{\pi} \frac{d}{dydp_T^2} = \frac{E}{\pi} \frac{d}{dp_L dp_T^2} \quad .$$

Figure 2 shows a compilation of ISR data[6,7,8] on pion production near 90^0 in the c.m.s. The π^0 spectra extend out at present to higher p_T values (~12 GeV/c, conjugate to $\lesssim 2 \times 10^{-15}$ cm) than the charged π spectra, due to the relatively large coverage obtainable with lead-glass or shower counter detectors. The spectra extend over 12 orders of magnitude in cross-section! Note the break from the low p_T exponential behavior to a more gentle form, similar to an inverse power fall-off. However, these recent high p_T data disagree by a rather large factor (~4) at high p_T. This discrepancy is not yet understood, being larger than the errors quoted by the groups. For these types of detectors,

a thorough understanding of the calibration, resolution, and linearity is crucial (though not easy) when measuring a sharply falling spectrum.

Now in a hard scattering model the cross section is given effectively by a convolution of two factors: the first has the basic form $1/p_T^n$ and represents the scattering cross section for two constituents (partons) through an angle such that each acquires a transverse momentum p_T; the second is a function only of x, f(x), where x is the fractional momentum of the constituent in the initial proton, and represents the "parton flux factor". Because the magnitude of the parton momentum does not change in the collision, one can, for large angle scattering, use instead $x_T = p_T/p_{beam} = 2p_T/\sqrt{s}$. Thus we expect a form:

$$E\frac{d\sigma}{d^3p} = A \cdot \frac{1}{p_T^n} \cdot f(x_T) \quad .$$

(The fact that the scattered parton decays to produce the observed hadron does not change this form if the decay distribution is scale invariant, i.e., if it does not depend on the parton momentum.)

Data up to $p_T \sim 6$-8 GeV/c were all consistent with the above form but the power n was close to 8 rather than to the scale-invariant expectation of 4. The model of Blankenbecler, Brodsky, and Gunion (CIM) explained this as due to the presence of meson constituents interacting via quark exchange. It is perfectly reasonable that if a proton consists <u>basically</u> (and as seen by a high momentum probe) of quarks, gluons, and a sea of quark-antiquark pairs, closely bound q-q pairs will exist and act as mesonic constituents. At still higher p_T a p_T^{-4} term due to q-q scattering, if present, will overtake a p_T^{-8} term and become dominant eventually. Thus the power n should decrease and become more like 4. In QCD, however, we do not have a scale invariant

theory--the proton structure function, the strong q-q coupling α's, and the parton decay function all depend on the four momentum transfer (Q^2) of the collision. The "raison d'etre" of the scaling power 4 has disappeared except as an asymptotic limit.

From the data the power is determined by comparing the cross-section at the same value of $x_T = \frac{2p_T}{\sqrt{s}}$ at two values of s.

$$E\frac{d\sigma}{d^3p} = A\frac{1}{p_T^n} f(x_T) = A\frac{1}{(\sqrt{s})^n} g(x_T) \qquad \therefore n = 2 \ln\left\{\frac{E\frac{d\sigma}{d^3p}(s_1)}{E\frac{d\sigma}{d^3p}(s_2)}\right\} \Big/ \ln\left(\frac{s_2}{s_1}\right)$$

Figure 3 shows the results of an analysis of this type using the data of Fig. 1 (along with similar data at another energy). Despite the disagreement between the CERN-Columbia-Oxford Rockefeller group[6] data and that from the Athens-Brookhaven-CERN-Syracuse[7] both agree that the power falls from its previous value of 8 to something closer to 5 for large x_T ($x_T \gtrsim 0.3$). We should be cautious because of the above mentioned disagreements--but it is clearly a very interesting trend. Another word of caution--at these high values of p_T, a π^0 gives two photon showers which overlap in the detector, due to the limited spatial resolution. Thus what is measured may be not just π^0 but also single high p_T photons, if such are produced. Some recent preliminary results from the ABCS group, using retracted liquid Argon shower counters of good spatial resolution, show what they believe to be evidence for single γ production at high p_T. They generally can resolve the two γ's from a π^0 up to $p_T \sim 8$ GeV/c in this experiment. Figure 4 shows the resulting γ/π^0 ratio as a function of p_T after

subtracting a background calculated with a Monte Carlo program which assumes only π^0 production with merging of the two photon showers and other effects which could take a single γ. The experiment shows a γ/π^0 ratio which rises from essentially zero below 3 GeV/c to ~40% at $p_T \sim 8$ GeV/c. The experiment is presently being repeated. Single photons are expected in the "standard models" (e.g. QCD) from several diagrams, of which in pp collisions the dominant one seems to be gluon + quark → photon + quark. This diagram should be smaller by nearly two orders of magnitude ($\alpha em/\alpha s$) compared with gluon + quark → gluon + quark, however, when it happens the photon can emerge intact at high p_T whereas the gluon would disintegrate into pions of much lower p_T. Because the pion p_T spectrum falls steeply one can easily recover the factor 10^2 lost in the coupling constants, and may expect ratios of γ/π in the order of unity by ~10 GeV/c. In principle this effect can give a handle on the essentially unknown gluon distributions in the proton.

Before moving on from single particle spectra I should mention particles other than π's and γ's. The spectra of $K^{\pm}$, p, and $\bar{p}$ have only been measured up to $p_T \sim 6$ GeV/c at the ISR, and there has been nothing new for a few years on this subject. At Fermilab the Chicago-Princeton group measured these particles out to $p_T \sim 7$ GeV/c (Fig. 5). There are some interesting effects, for example, the π^+/π^- ratio rises from 1 at low p_T to $\gtrsim 2$, presumably as the valence quarks become more important relative to the sea quarks and gluons (there are two u's to form a π^+ and only one d to form a π^-). This effect still has to be seen at the ISR, it is perhaps a function only of x_T. Also

heavy particles become relatively abundant compared with the situation at low p_T, e.g., $K^+/\pi^+ \sim 0.5$. High p_T should give a favorable (signal: background) situation in searching for new heavy particles, e.g., charmed hadrons. A major new high p_T experiment is being istalled now at the ISR (CERN-Copenhagen-Lund-Rutherford collaboration) and an early project will be to measure the spectra of $K^{\pm}$, p, $\bar{p}$ beyond 10 GeV/c in p_T.

CORRELATIONS AND EVENT STRUCTURE

The next step in complexity beyond single particle spectra is to look at two particle correlations, i.e., to measure the relative probability of finding two particles in specified regions of phase space compared with what one would expect if the particles were produced independently. The Correlation Function can be defined in various ways, for example:

$$R(y_1,y_2,p_{T_1},p_{T_2},\phi_1-\phi_2,\sqrt{s}) = \sigma_{inel}\left\{\frac{\frac{d\sigma}{dy_1 dp_{T_1} d\phi_1 dy_2 dp_{T_2} d\phi_2}}{\frac{d\sigma}{dy_1 dp_{T_1} d\phi_1}\frac{d\sigma}{dy_2 dp_{T_2} d\phi_2}}\right\} - 1.$$

This equation looks rather complicated and does indeed contain many independent variables. To keep the data manageable one generally keeps one particle (the trigger particle) fixed at $y = 0$, $\phi = 0$, $4 < p_T$ 5 GeV/c, and looks at the distribution (in y,ϕ,p_T) of the associated particles produced in these high p_T events. Then simply:

$$R + 1 = \frac{\text{mean track density for high } P_T \text{ event}}{\text{mean track density for typical inelastic event}}.$$

The final step in complexity is to attempt to look more globally at the structure of the events containing high p_T particles, for example, do they contain the famous jets proposed in BBK's paper? In this phase one tries in the experiment to detect as many of the produced particles in the event as possible. This requires larger angular coverage, generally with wire chamber detectors in a magnetic field, and the experiments become large and complex. Then one has to use imagination and ingenuity to extract meaningful and comprehensive results from the data! Three body correlation functions are sometimes used but the number of independent variables is almost unmanageable. Other methods are often based heavily on a model (or preconceived notion) so that they may suffer from a lack of objectivity. Nevertheless we now have a model that fits in its main features a wide body of data and is no longer very controversial. This model is indeed based on constituent scattering with subsequent jet-like decay of the scattered constituents, much as in the early BBK prediction. Before moving on to this very large subject of correlations with high p_T particles and event structure, it would be appropriate to describe the main apparatus that has been used.

EXPERIMENTAL DETECTORS

One of the most important instruments so far used at the ISR in this field is the Split Field Magnet detector (SFM), shown in Fig. 6. The magnetic field is unfortunately complicated, having a vertical dipole field downstream and a quadrupole field at large angles. The magnet gaps are filled with proportional wire chambers (~70,000 wires). Three different approaches to the problem of triggering on high p_T

particles have been used (see Fig. 7): (1) a lead-glass array to trigger on high p_T π^0's (CERN group); (2) a straight-track requirement in the SFM proportional chambers at $\theta \sim 20^0$ or $\theta \sim 45^0$ (CERN-College de France-Heidelberg-Karlsruhe); and (3) a single charged particle magnetic spectrometer at $\theta = 90^0$ (British-French-Scandinavian). A new experiment with an improved SFM detector and external devices is presently running (see Figs. 8,9). These experiments have had the best global coverage of phase space yet achieved, especially in rapidity y (or polar angle θ). Other recently completed experiments include a double arm spectrometer of the CERN-Saclay-Zurich experiment (Fig. 10) with picture frame dipole magnets backed by Pb glass, and the experiment of Athens-Brookhaven-CERN-Syracuse (Fig. 11) using thinner foil transition radiation detectors with liquid argon calorimeters. Both of these had limited coverage (2 steradians can be called limited!) in rapidity and azimuth. Complete azimuthal coverage was at last obtained in the superconducting solenoid of the CERN-Columbia-Oxford-Rockefeller group (Fig. 12) although even they are restricted to triggering around the horizontal plane with lead glass arrays. The latter three experiments were largely motivated by the fashionable search for high mass electron pairs.

The future should see a great deal of new high p_T physics from the Axial Field Spectrometer presently being installed (CERN-Copenhagen-Lund-Rutherford collaboration). The apparatus is shown in Fig. 13. It consists of a dipole magnet with a field parallel to the beams and azimuthally symmetric, like a solenoid with the coil condensed into a pair of Helmholtz coils on the pole pieces. The return yoke is beneath. A central cylindrical drift chamber has 42 layers of wires

parallel to the beam axis arranged in 86 sectors of 4^0 in azimuth ϕ. Each wire gives a precise (200μ) transverse coordinate, a coarse (~8 mm) longitudinal coordinate from change division along the wire, and a pulse height ($\partial E/\partial x$) measurement. The latter will be used for identification of low momentum particles. One steradian ($\Delta\phi = 45^0$, $45^0 < \theta < 135^0$) will be instrumented with external proportional chambers and Cerenkov counters (aerogel, 4-atmosphere freon, and 1-atmosphere freon) for triggering on and identifying high p_T hadrons. The rest of the azimuth ($\Delta\phi = 270^0$, later $\Delta\phi = 360^0$ with the Cerenkov arm displaced) will be covered with a uranium-scintillator sandwich calorimeter. Apart from detecting neutrals and measuring their energy, the latter will enable a trigger on hadronic jets instead of single high p_T particles. Very high transverse momenta ($p_T \gtrsim 20$ GeV/c) should be reached with jet triggers.

GENERAL FEATURES OF EVENT STRUCTURE

It is difficult to summarize the wealth of data that has emerged from ISR studies of high p_T event structure in the last few years. A good place to start is with the distribution in azimuth ϕ of the particles associated with a high p_T trigger particle. This is shown in the form of a correlation in Fig. 14 from Ref. 9. The particle density in high p_T events is higher than in normal events (in the central region), and this excess divides naturally into an azimuthal region <u>towards</u> the trigger particle ($|\phi-\phi_{trig}| \lesssim 45^0$) and a broad region <u>away</u> from the trigger particle ($|\phi-\phi_{trig}| \lesssim 90^0$), as seen in Fig. 14. First let us study in more detail the region towards the trigger by summarizing a few features of the event structure:

1. Close to the high p_T trigger particle (in rapidity y and azimuth ϕ) there is a positive correlation, i.e., there are more particles found in this region than there would be if the trigger particle was absent.
2. The strength of the correlation increases both as the p_T of the trigger particle is increased (see Fig. 15) and as the p_T of the associated particle is increased. Equivalently, the mean p_T of these close particles is greater than in normal inelastic events, and grows with p_T (trigger).
3. If the trigger particle is charged, a close high p_T particle is very likely to have the opposite charge (see Fig. 15).
4. The extension of this feature (which bears all the expected features of a jet containing the trigger particle) is typically $\pm 30^0$ in ϕ and ± 0.5 units of rapidity. (Fig. 16 shows the rapidity difference distribution $|\Delta y|$ between pairs of high p_T particles on the towards side, one being the trigger particle Note that if there is no preferred direction around the trigger particle of the associated particles (circular jets) the ϕ extension in radians should equal the rapidity extension, which appears to be the case.
5. Despite this positive "towards" correlation, very frequently when one triggers on a high p_T particle one does not see (on an event-by-event basis) an associated jet. For example with 4 GeV/c $< p_T$(trig) $<$ 8 Gev/c at y = 0, about 80% of the triggers have no associated charged particle with $P_T > 0.8$ GeV/c, $y < 1$ and $\Delta\phi < 30^0$. This effect is perfectly well understood

qualitatively, and is called trigger bias. Simply stated, a jet of 5 GeV/c giving 80% of its energy to one particle is more likely than a jet of 8 GeV/c giving 50% of its energy to one particle. This is because of the steeply falling p_T spectrum of jets; thus a 4 GeV/c particle generally arises from a jet having not much more (on average ~10% more) transverse momentum. Quantitatively, however, it seems that models producing only multiparticle jets do not agree with the strength of the effect. If (as in the CIM) high p_T mesons can be produced singly, agreement is easily obtained.

I now turn to the azimuthal side away from the trigger particle. Some general features are:

6. There is a broad enhancement in the particle density on the away side when one averages over events (see Fig. 17). Unlike the towards side correlation it covers a large part of the rapidity range available (±4 at the ISR). It extends over ~90^o in ϕ, centered on the direction opposite the trigger.
7. The strength of this positive correlation also grows with p_T (trigger) and p_T of the associated particles. Equivalently, the mean p_T of the away side particles is higher than in normal inelastic events and grows with p_T (trigger).
8. There is no observable dependence on the polar angle θ of the high p_T trigger.

From the above observations, resulting from just two-particle correlation studies, one cannot distinguish whether the away side structure on an event-by-event basis is like a jet that jumps about

in rapidity from event to event, or is like a broad fan, for example. To learn more we must effectively study three-particle correlations, although that may not be obvious from the way in which I shall present the conclusions!

9. Look for the track on the away side that has the highest p_T. If the p_T of that track is reasonably high, then study the particles near to it in phase space. Now all of the statements (1 to 5) above become true if you replace the word "trigger" with the phrase "highest p_T away side"!
10. One can also select those away-side particles that have a moderately high p_T ($p_T > 0.8$ Gev/c) and look at the distribution of rapidity differences Δy between them. There is a strong peak with $\Delta y \lesssim 0.5$, as shown in Fig. 18, much above a randomized distribution obtained by using the same sample of tracks but combining a track from one event with a track from a different event.

The conclusion generally made from observations like these is that on the away side a single jet is generally present but that its rapidity varies from event to event, so that the two-particle correlation function shows only a broad smear in y. Its azimuth, however, is roughly (within $\sim 10^0$ for $p_T(\text{trig}) > 5$ GeV) opposite in azimuth to the trigger particle. Both features are readily understandable in a parton collision model. The former arises of course because the c.m. frame of the proton-proton collision is not that of the parton-parton collision, as the partons each have a longitudinal momentum distribution within the proton. The latter may arise partly from

the fact that the trigger particle is not identical to the trigger side jet in all cases, and may have a different ϕ. Another factor is that partons have some intrinsic small transverse momentum themselves before they collide, which may be out of the trigger plane. This intrinsic parton transverse momentum is, however, more likely to be mainly in the trigger plane and indeed pointing in the trigger direction. This is another, slightly more subtle, trigger bias effect, which has at least two consequences. One is that the forward particles (the beam fragments) generally recoil somewhat against the trigger p_T. The mean recoil per particle is (Ref.10) ~80 MeV/c, rising to ~300 MeV/c if the forward fragment has x near to one (in which case there must be very few forward fragments.) This recoil also results in an azimuthal non-uniformity of the forward fragments, as shown in Fig. 19 for two regions of Feynman x ($x=2p_L/\sqrt{s}$) and two values of p_{trig} (Ref. 10). The second consequence is the away side jet will not completely balance the p_T of the trigger side jet, which makes it less evident than it would otherwise be.

It is now generally believed that most high p_T events actually do consist of something like four jets of hadrons: two in the beam directions resulting from fragmentation of the spectator constituents and two high p_T jets. However, most of the events studied up to now at the ISR do not show this structure clearly for various reasons: (1) one triggers on a single high p_T particle and this biases the towards-side jet strongly, especially if occasionally single particle jets are present as in the BBG model[2]; (2) The away jet has a reduced p_T as explained above; (3) the p_T range studied is not really very

high, for much of the data being below ~5 GeV/c; (4) often only the charged particles are seen, with π^0 over a limited aperture in some experiments. What is evidently needed is to trigger directly on hadronic jets, to detect neutral hadrons as well as charged particles, and to go to higher values of p_T, say $\gtrsim$ 10 GeV/c.

Despite these limitations it has been possible to study to what extent the high p_T jets resemble the jets observed in e^+e^- collisions (at SPEAR and DORIS) which are believed to be due to fragmenting quarks. To first order much similarity is observed. Given a fragmenting quark of momentum P, what is the distribution of fractional momenta $z = p/P$ of the resulting hadrons (momentum p)? In e^+e^- collisions dn/dz is a steeply falling distribution, approximately exponential with little dependence on p, i.e., it scales. In pp collisions one can approximate the variable Z with $x_E = p_x/p_{trig}$ (where the trigger is along the negative x axis). The distribution, shown in Fig. 20, is very similar to that seen in e^+e^-, especially when one takes into account the slightly different variables used. The extent to which this distribution scales can be seen in Fig. 21, where slices at fixed x_E are plotted versus p_{trig}.

The transverse momentum components of the away-side jet particles relative to the jet axis are somewhat more difficult to study. First the jet axis must be found, which requires seeing all the charged and neutral particles and knowing which are jet members and which are background. Instead it has become common practice to measure the distribution of the momentum component out of the plane defined by the trigger particle and the beams, called p_{out}. The mean value

of this quantity is found (see Fig. 22) to rise with x_E. This is something like a seagull effect and has also been seen in e^+e^- jets. Apparently the jets have almost a conical rather than a cylindrical structure in phase space. At fixed x_E, $\langle|p_{out}|\rangle$ also rises with the total jet momentum. Much more work needs to be done in this direction to establish similarities and/or differences with e^+e^- jets and to understand the features observed in terms of theory.

NUCLEAR COLLISIONS

I have said nothing so far about the relevance of heavy ion collisions in high p_T physics. There has been no work done at the ISR with anything other than p-p, except for some brief measurements of low p_T and diffractive processes with p-d and d-d. Next year there should be some short runs with p-α and α-α collisions, but because of the limited luminosity and running time the p_T range reached will be limited to a few GeV/c. H. Frisch has described the very interesting results from FNAL on p-A collisions. It is likely that studies of event structure with "4π" detectors would teach us much about the mechanisms responsible for the anomalous enhancement of high p_T production in nuclei. Do the forward/backward jets show large recoils, as might be the case if transverse Fermi-motion effects were important? Are multiple jets observed, as might be the case if multiple scattering is responsible? What can we learn about the space-time development of a hadronic jet? Does a scattered quark behave immediately as a group of hadrons or a single object? Note that the latter two questions could also be well studied in deep inelastic lepton-nucleus collisions, where the scattered quark has a well known momentum and/or flavors.

Presumably the best argument at this time for high p_T studies in nucleus-nucleus collisions is that it is completely unknown territory, and surprises are to be expected. Experience from the ISR leads one to make the following recommendations: (1) A large solid angle coverage by detectors is very important, both to reach the highest p_T values and to study event structure; (2) Neutral hadron (π^0 but also K^0,n...) detection is desirable in addition to the charged hadrons; (3) One should aim at the ability to trigger on hadron jets via a large energy deposition in a limited solid angle; (4) It would be useful to see the beam fragments in the forward and backward directions in addition; and (5) The machine luminosity and energy should both be as high as possible. L $\sim 10^{30}$ $cm^{-2}sec^{-1}$ and E $\sim$10 GeV/nucleon are perhaps the minimum values needed to get to reasonable p_T values ($\gtrsim$ 5 GeV/c must be the aim).

CONCLUSIONS

Essentially all data presently available is compatible with a model involving hard scattering between proton constituents. Probably several types of constituents are needed: quarks, antiquarks, gluons, and at lower p_T possibly also mesons. The experiments need as complete information about the event as possible, and hence become large and complex. The theory is not particularly simple either. However, by combining theory and experiment we are learning about the types of proton constituents and their distributions (both transverse and longitudinal components), their hard interactions (scattering cross-sections) and their materialization into hadronic jets. It is consequently a rich and important field of study.

ACKNOWLEDGEMENTS

I would like to thank my colleagues in the British-French-Scandinavian collaboration for an enjoyable experiment at the ISR especially Norman McCubbin for some help with this talk. I apologize to other high p_T groups at the ISR for showing less of their data than I should have; essentially all the features I have illustrated have been seen by all the groups.

REFERENCES

(1) S.M. Berman, J.D. Bjorken, and J.B. Kogut. Phys.Rev. D4, 3388 (1971).

(2) R. Blankenbecler, S.J. Brodsky and J.F. Gunion, Phys.Rev. D6 2652 (1972).

(3) B. Alper et al., Phys.Lett. 44B, 521 (1973).

(4) M. Banner et al., Phys.Lett. 44B, 537 (1973).

(5) F.W. Busser et al., Phys.Lett. 46B, 471 (1973).

(6) A.L.S. Angelis et al. (C.C.O.R. Collaboration), Phys.Lett 79B 505 (1978).

(7) C. Kourkoumelis et al., (A.B.C.S. Collaboration) CERN Rept. EP 7929, Submitted to Phys.Lett B.

(8) A.G. Clarke et al., (C.S.Z. Collaboration), Phys.Lett. 74B, 267 (1978).

(9) M.G. Albrow et al., Nucl.Phys. B145, 305 (1978).

(10) H.G. Albrow et al., Nucl.Phys. B145, 461 (1978).

FIGURE CAPTIONS

Fig. 1. Layout of the CERN Intersecting Storage Rings showing the injection system and the eight beam crossing regions I1-I8.

Fig. 2. Compilation of ISR data on production at large angles, showing the change from exponential p_T dependence at low p_T to a much flatter high p_T component.

Fig. 3. The exponent n of the expression $E\frac{d\sigma}{d^3p} = A\ p_T^{-n}\ f(x_T)$ versus x_T as measured by the CCOR and ABCS groups for π^0 production at large angles.

Fig. 4. Preliminary rsults from the ABCS group for the ratio of direct photon to π^0 production, versus p_T. Known backgrounds have been subtracted.

Fig. 5. Data from the Chicago-Princeton group at FNAL on particle production ratios in pp collisions at large angles, versus x_T.

Fig. 6. Cut away view of the Split Field Magnet detector at the ISR. The upper pole and half of the MWPC detectors have been removed for clarity.

Fig. 7. Schematic plan view of some high p_T SFM experiments. The 90^o spectrometer of the BFS group is shown in detail, with a bending magnet, two gas Cerenkov counters, scintillator hodoscopes, and spark chambers. One of the four trigger roads of the CCHK group, and the lead glass array of the CERN R412 group, are indicated.

Fig. 8. The present configuration of the SFM for the Annecy-CERN-College de France-Heidelberg-Karlsruhe-Warsaw experiment R416. The

SFM vacuum chamber and MSPC system have been improved. Additional external detectors include Cerenkov counters (1,2) and time-of-flight hodoscopes (5).

Fig. 9. A view of the SFM experiment R416 shown schematically in Fig. 8. The two beam lines can be seen behind the experiment.

Fig. 10. Cut-away view of one arm of the two-arm spectrometer CSZ experiment.

Fig. 11. Cross-section of the ABCS experiment, consisting of four modules containing lithium foil transition radiation detectors (for electron identification) and liquid argon/proportional strip chamber calorimeters.

Fig. 12. End-on and plan views of the CCOR experiment, consisting of a superconducting solenoid, cylindrical drift chambers, scintillator hodoscopes, and two walls of Pb-glass counters.

Fig. 13. End-on and plan views of the CCLR experiment (R807) currently being installed. A one-steradian Cerenkov arm on the left identifies high p_T hadrons, and a large uranium-scintillator calorimeter is used for the study of hadronic jets.

Fig. 14. Azimuthal distribution of the charged particle density in the central region ($|y| < 0.5$, $p_T > 0.5$ GeV/c) relative to that of normal events, for two values of trigger p_T of order 0.8 GeV/c and 3.4 GeV/c.

Fig. 15. Values of the correlation between the trigger particle (π^+) of specified p_{trig} at y = 0, and same-side associated particles of specified charge, with $p_T > 1$ GeV/c, versus y.

16. Distribution of rapidity difference $|\Delta y|$ between the trigger particle (with $4 > p_T$ 8 GeV/c) and other same-side charged particles with $p_T > 0.8$ GeV/c, $\Delta\phi \lesssim 30^0$. About 20% of these trigger particles have an associated charged particle with $|\Delta y| < 1$ and $p_T > 0.8$ GeV/c.

Fig. 17. Values of the correlation between the trigger particle of specified p_{trig} at y = 0, and away-side associated particles with $p_T > 0.5$ GeV/c, versus y.

Fig. 18. Distribution of rapidity differences $|\Delta y|$ between pairs of away-side charged particles, each of which has $p_T > 0.8$ GeV/c. The event sample is 915 events with $4 < p_{trig} < 8$ GeV/c. The randomized distribution is obtained by taking the tracks of the previous distribution and randomly pairing them. About 25% of these events have an observed pair with $|\Delta y| < 0.75$, p_{T_1} and $p_{T_2} > 0.8$ GeV/c.

Fig. 19. Correlation R versus azimuth ϕ for forward beam fragments of specified charge and Feynman $x(=p_L/p_{beam})$, with a trigger particle at x = 0, $\phi = 180^0$. The cut $p_T > 0.2$ GeV/c has been applied.

Fig. 20. Distribution of charged particles in x_E for various values of $p_{trig} > 3$ GeV/c. The cuts $|y| < 1$ and $p_{out} < 0.5$ GeV/c have been applied, where p_{out} is the momentum component out of the plane defined by the beams and the trigger particle (BFS).

Fig. 21. Apparent approach to scaling of the away-side jet in terms of the variable $x_E = p_x/p_{trig}$ (the trigger is along the -x axis at 90^0 polar angle in the c.m. system). For $p_{trig} > 3$ GeV/c the value of $\frac{1}{N_{trig}} \frac{dn}{dx_E}$ becomes roughly independent of p_{trig} for $x_E \gtrsim 0.3$ (BFS collaboration).

Fig. 22. Mean values of p_{out} versus x_E for various large values of p_{trig} (CCOR collaboration). The trigger particle is a π^0.

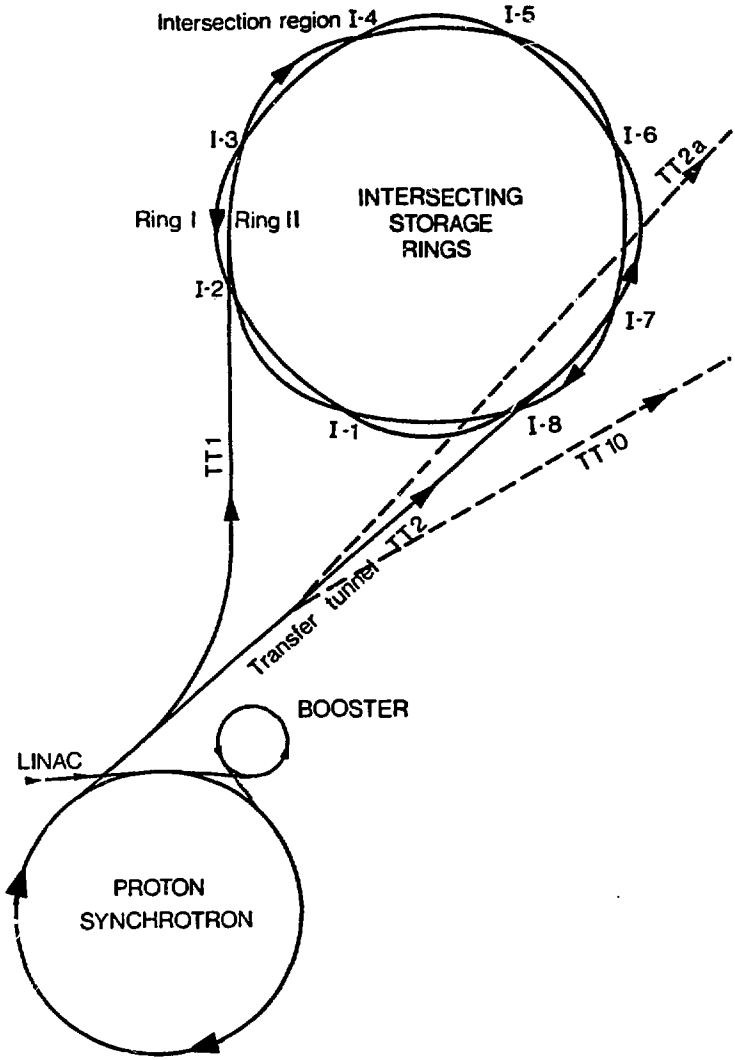
Intersection region I-4
I-5
I-3
I-6
TT2a
Ring I
Ring II
INTERSECTING
STORAGE
RINGS
I-2
I-7
I-1
I-8
TT10
TT1
TT2
Transfer tunnel
BOOSTER
LINAC
PROTON
SYNCHROTRON

Fig. 1

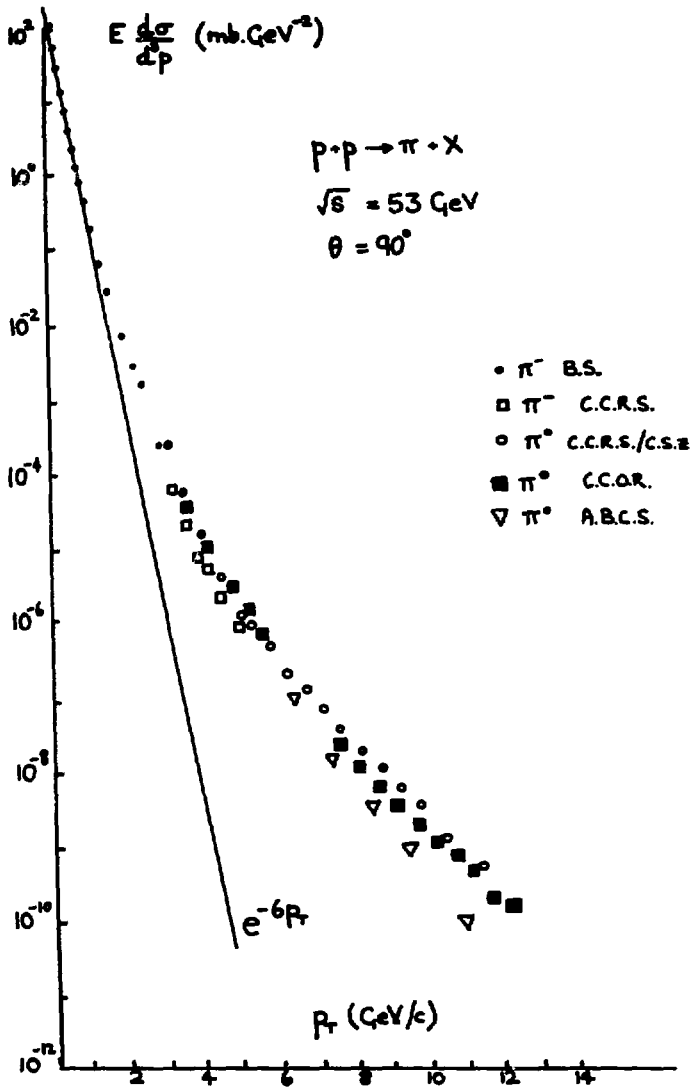
$E\frac{d\sigma}{d^3p}$ (mb.GeV^{-2})
$p+p \rightarrow \pi + X$
$\sqrt{s}$ = 53 GeV
θ = 90°
π^- B.S.
π^- C.C.R.S.
π° C.C.R.S./C.S.I.S.
π° C.C.O.R.
π° A.B.C.S.
e^{-6p_T}
p_T (GeV/c)
10^{2}
10^{0}
10^{-2}
10^{-4}
10^{-6}
10^{-8}
10^{-10}
10^{-12}
2
4
6
8
10
12
14

Fig. 2

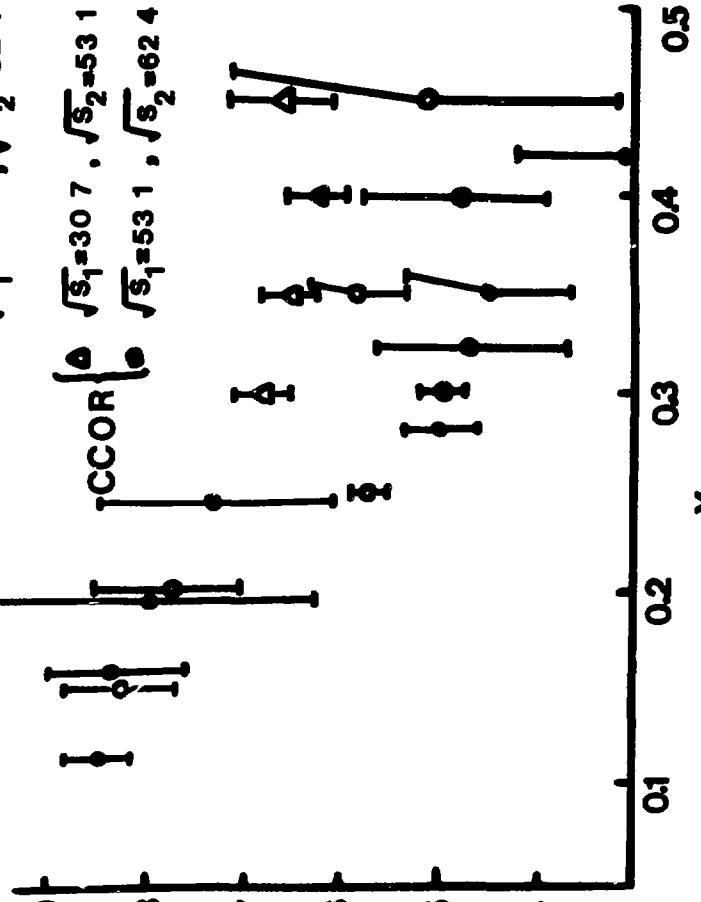
ABCS • $\sqrt{s_1}$=53 7 , $\sqrt{s_2}$=62 4
CCOR $\sqrt{s_1}$=30 7 , $\sqrt{s_2}$=53 1
$\sqrt{s_1}$=53 1 , $\sqrt{s_2}$=62 4
n
9
8
7
6
5
4
0.1
0.2
0.3
0.4
0.5
X_T

Fig. 3

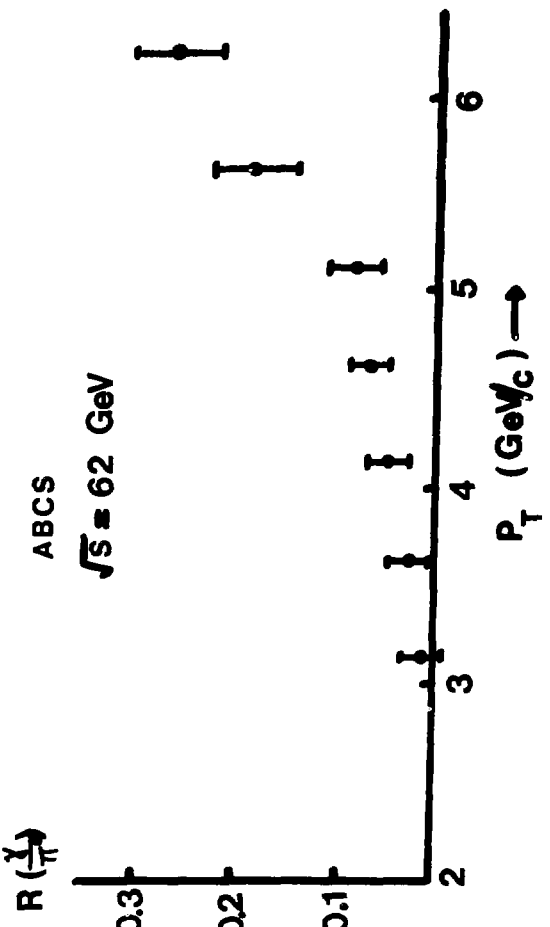

Fig. 4

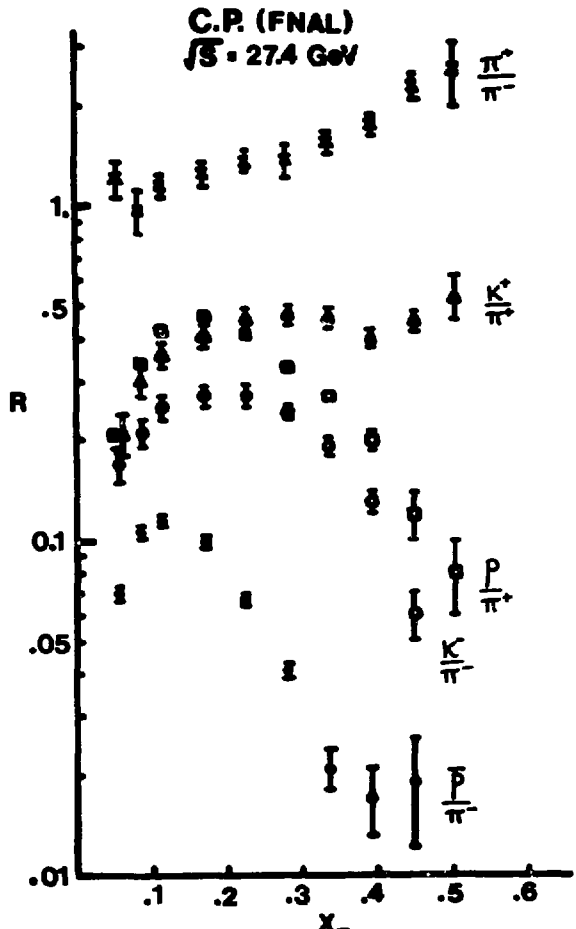
C.P. (FNAL)
√S = 27.4 GeV
R
1.
.5
0.1
.05
.01
.1
.2
.3
.4
.5
.6
X_T
$\frac{\pi^+}{\pi^-}$
$\frac{K^+}{\pi^+}$
$\frac{p}{\pi^+}$
$\frac{K^-}{\pi^-}$
$\frac{\bar{p}}{\pi^-}$

Fig. 5

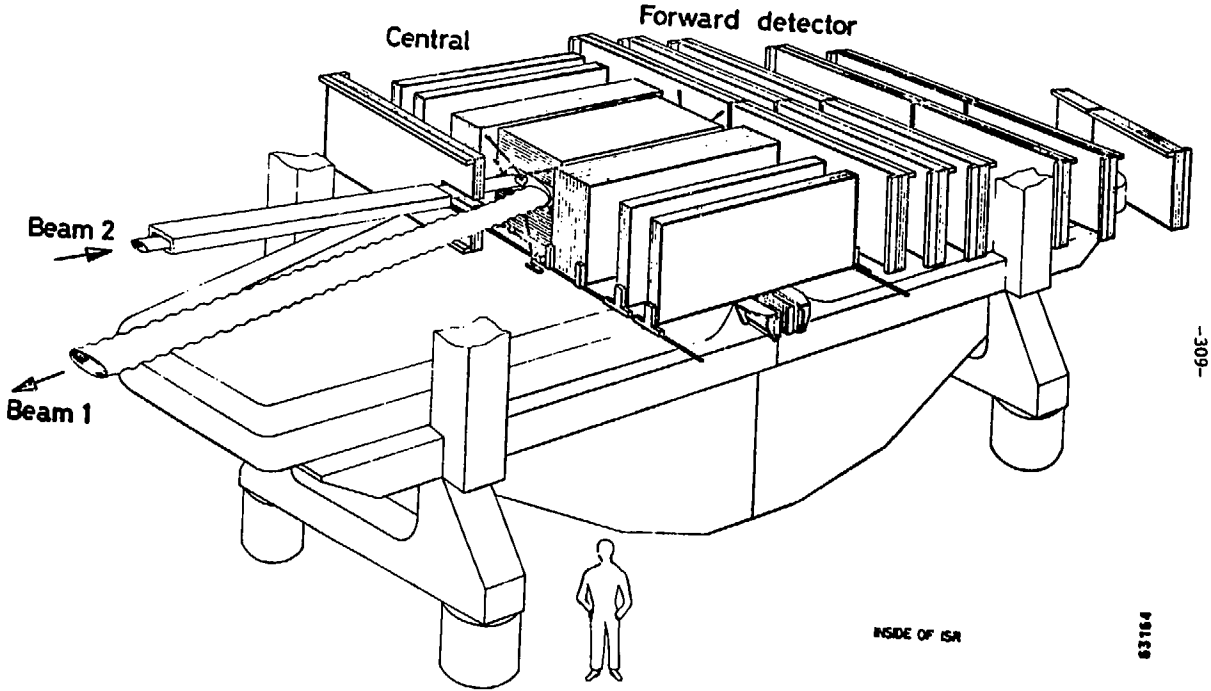

Fig. 6

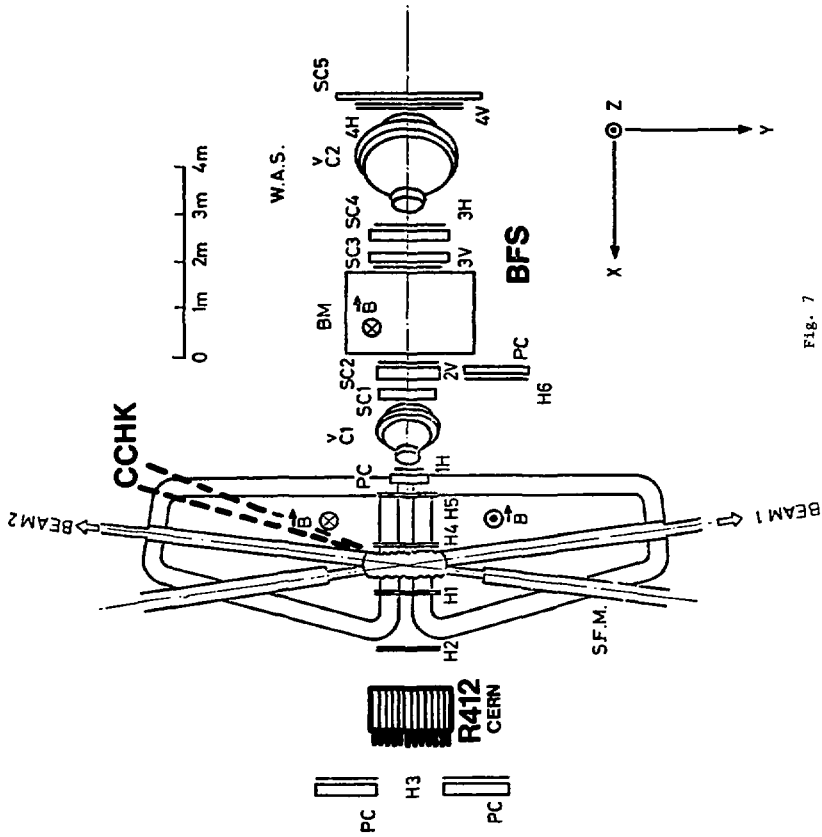
CCHK
BEAM 2
BEAM 1
PC
1H
H4 H5
H1
H2
S.F.M.
R412
CERN
H3
PC
PC
C1
SC1
SC2
2V
H6
BM
B
SC3 SC4
3V
3H
BFS
W.A.S.
C2
4H
SC5
4V
0 1m 2m 3m 4m
Z
Y
X

Fig. 7

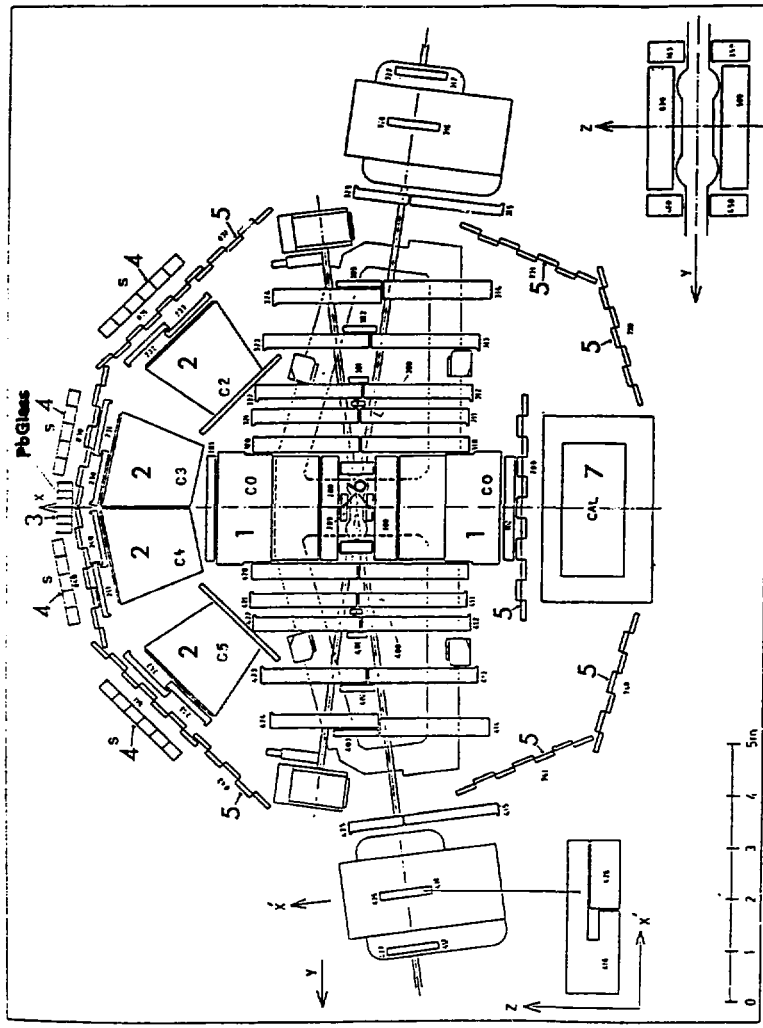

Fig. 8

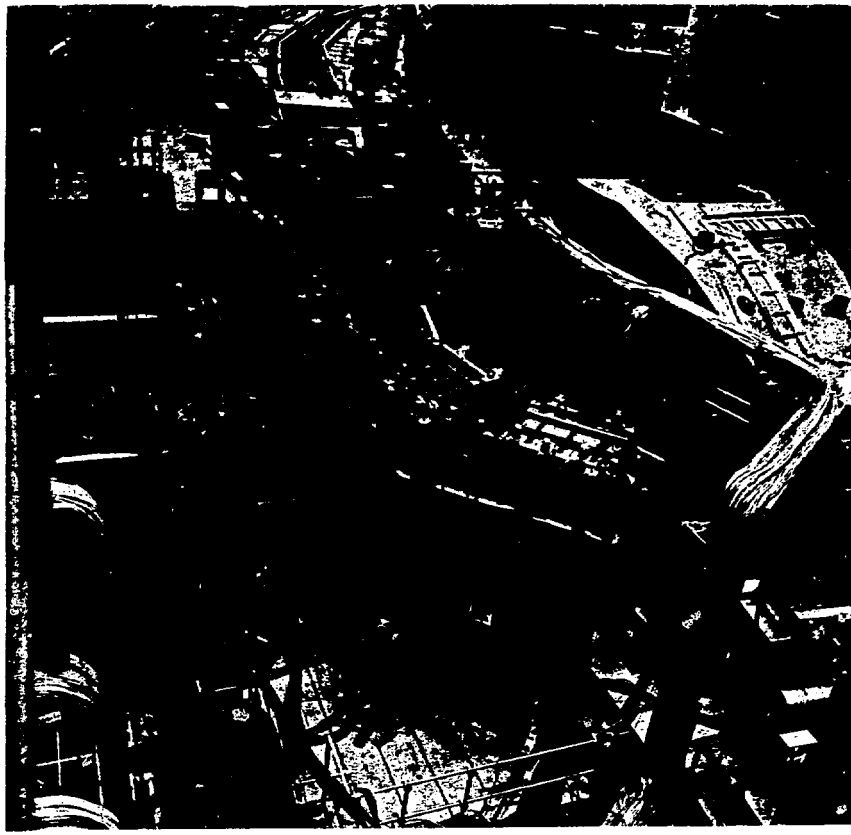

Fig. 9

CSZ

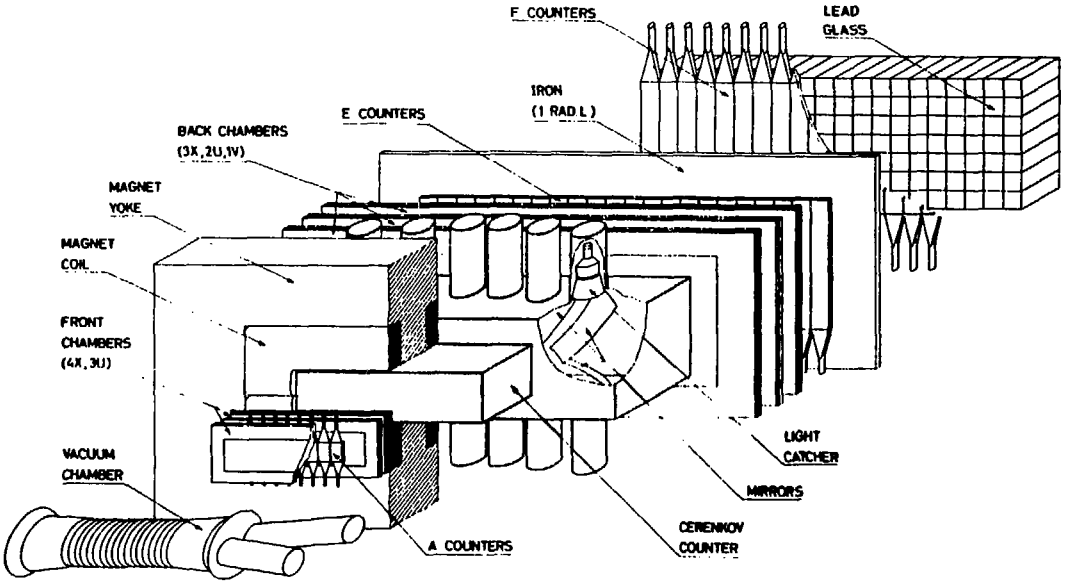
F COUNTERS
LEAD GLASS
IRON (1 RAD.L)
E COUNTERS
BACK CHAMBERS (3X,2U,1V)
MAGNET YOKE
MAGNET COIL
FRONT CHAMBERS (4X,3U)
VACUUM CHAMBER
LIGHT CATCHER
MIRRORS
CERENKOV COUNTER
A COUNTERS

Fig. 10

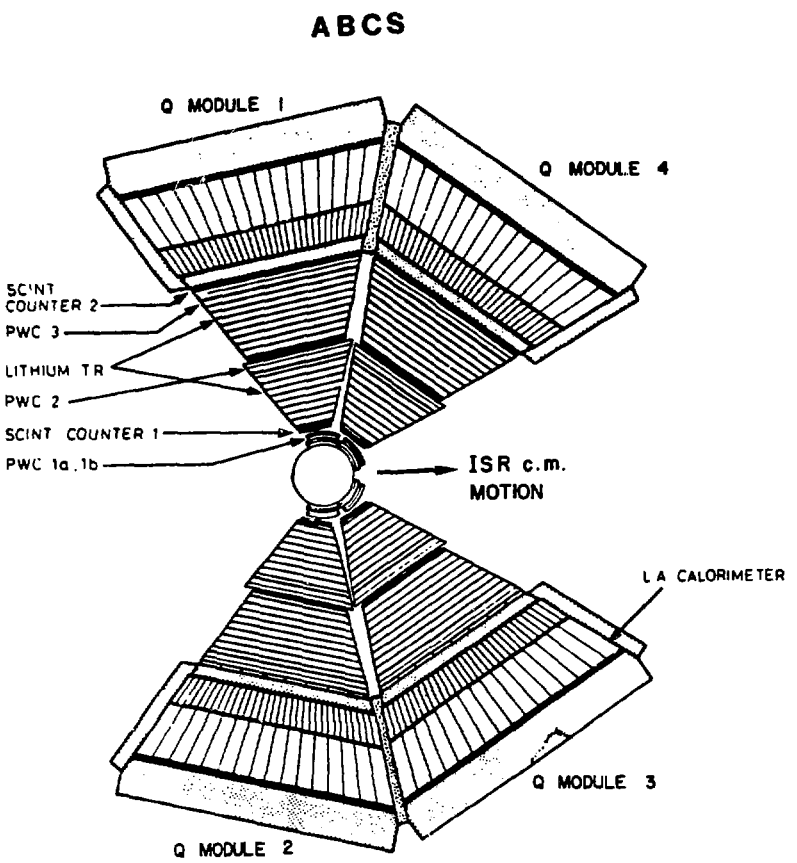
ABCS
Q MODULE 1
Q MODULE 4
SCINT COUNTER 2
PWC 3
LITHIUM TR
PWC 2
SCINT COUNTER 1
PWC 1a, 1b
ISR c.m. MOTION
L A CALORIMETER
Q MODULE 3
Q MODULE 2

Fig. 11

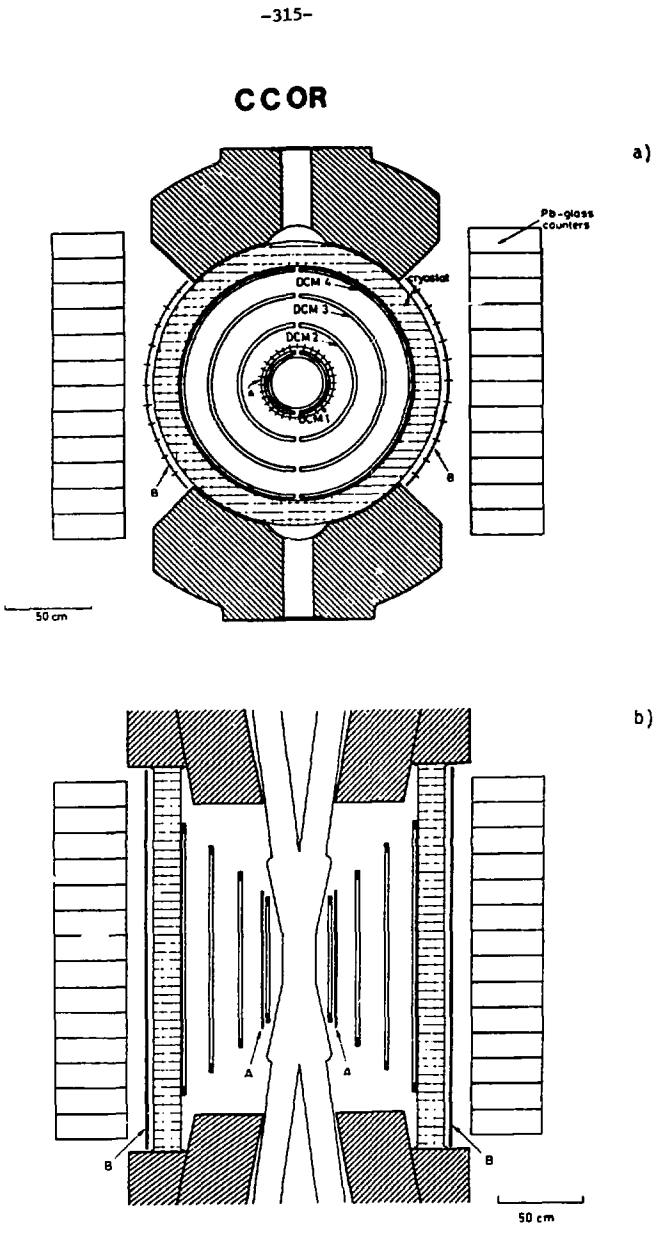
CCOR
a)
Pb-glass counters
cryostat
DCM 4
DCM 3
DCM 2
DCM 1
B
B
50 cm
b)
A
A
B
B
50 cm

Fig. 12

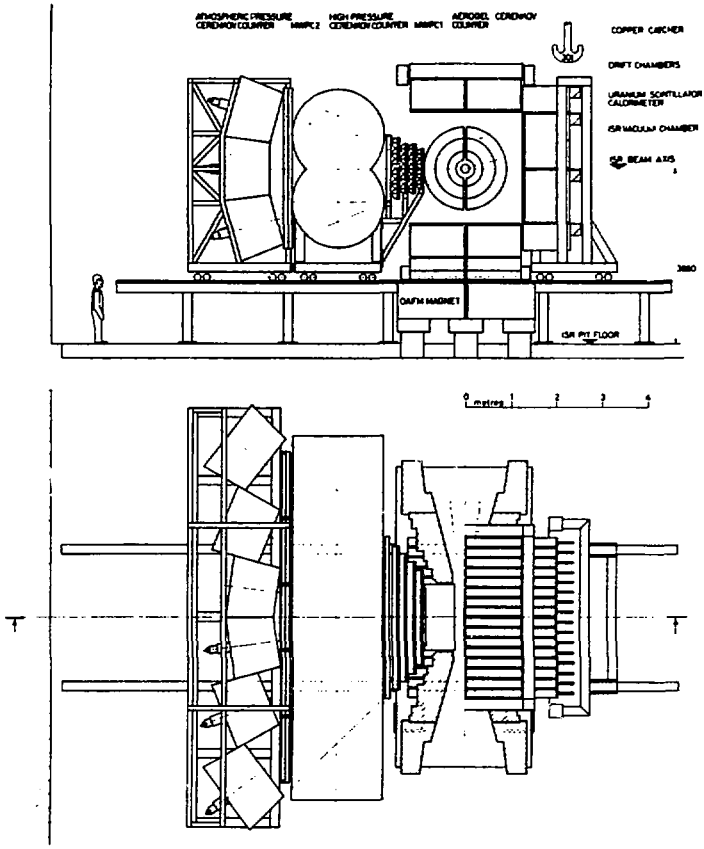
ATMOSPHERIC PRESSURE CERENKOV COUNTER
MWPC 2
HIGH PRESSURE CERENKOV COUNTER
MWPC 1
AEROGEL CERENKOV COUNTER
COPPER CATCHER
DRIFT CHAMBERS
URANIUM SCINTILLATOR CALORIMETER
ISR VACUUM CHAMBER
ISR BEAM AXIS
OMEGA MAGNET
ISR PIT FLOOR
metres

Fig. 13

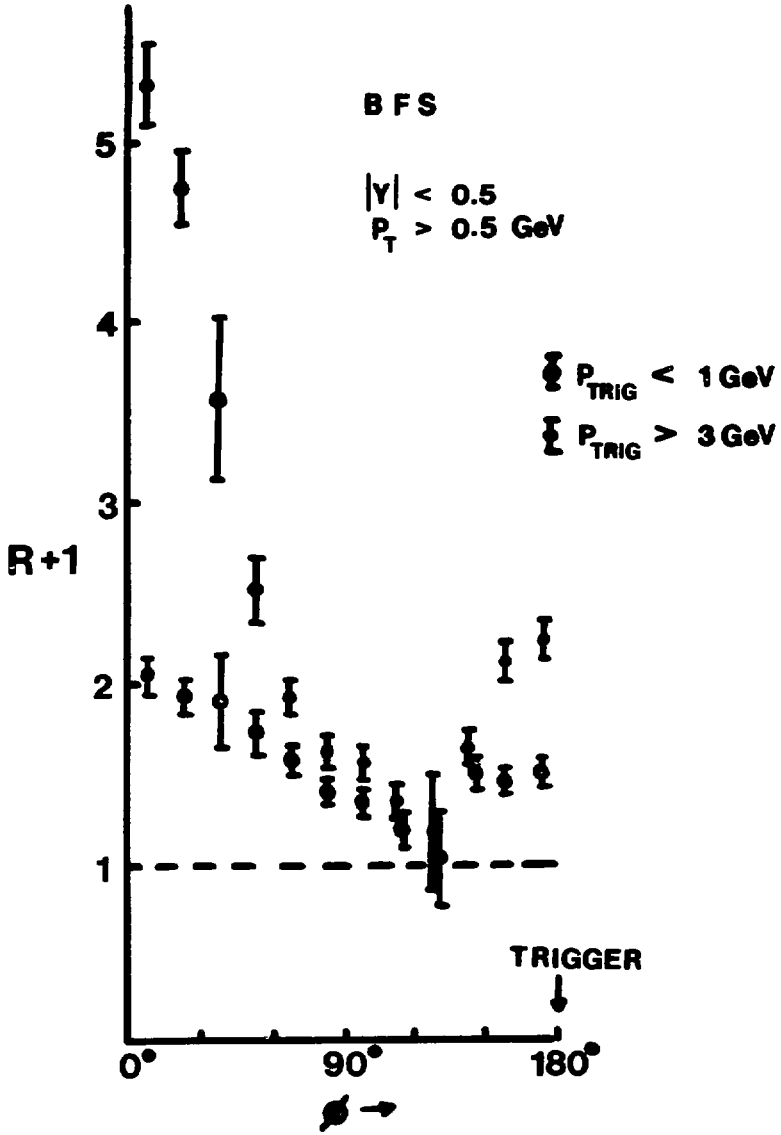
BFS
|Y| < 0.5
P_T > 0.5 GeV
P_TRIG < 1 GeV
P_TRIG > 3 GeV
R+1
5
4
3
2
1
TRIGGER
0°
90°
180°
φ

Fig. 14

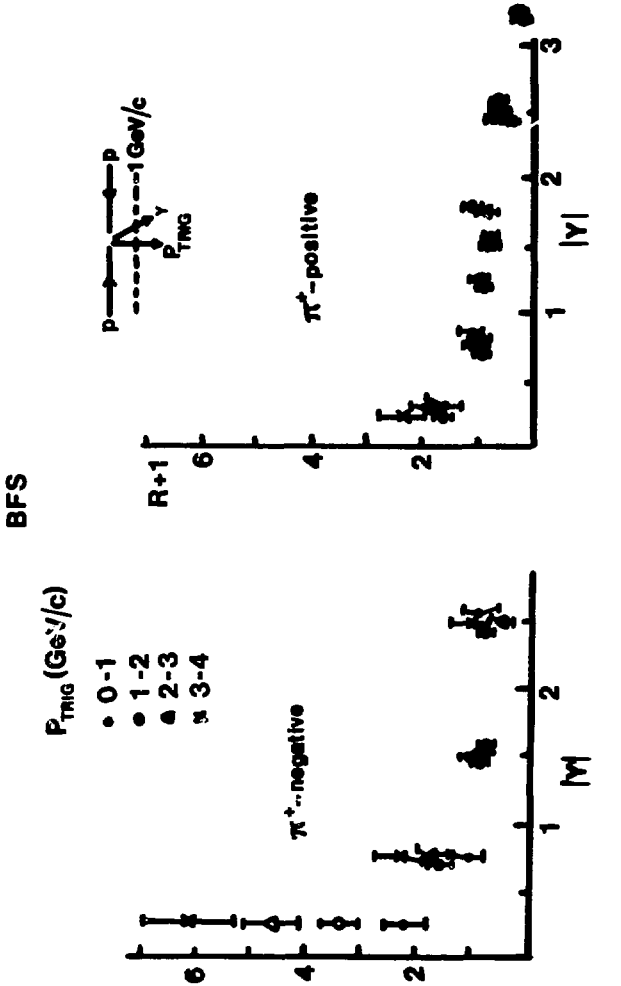
BFS
P_{TRIG} (GeV/c)
• 0-1
• 1-2
• 2-3
• 3-4
π^+-negative
π^+-positive
R+1
|Y|
p
p
1 GeV/c
P_{TRIG}
Y

Fig. 15

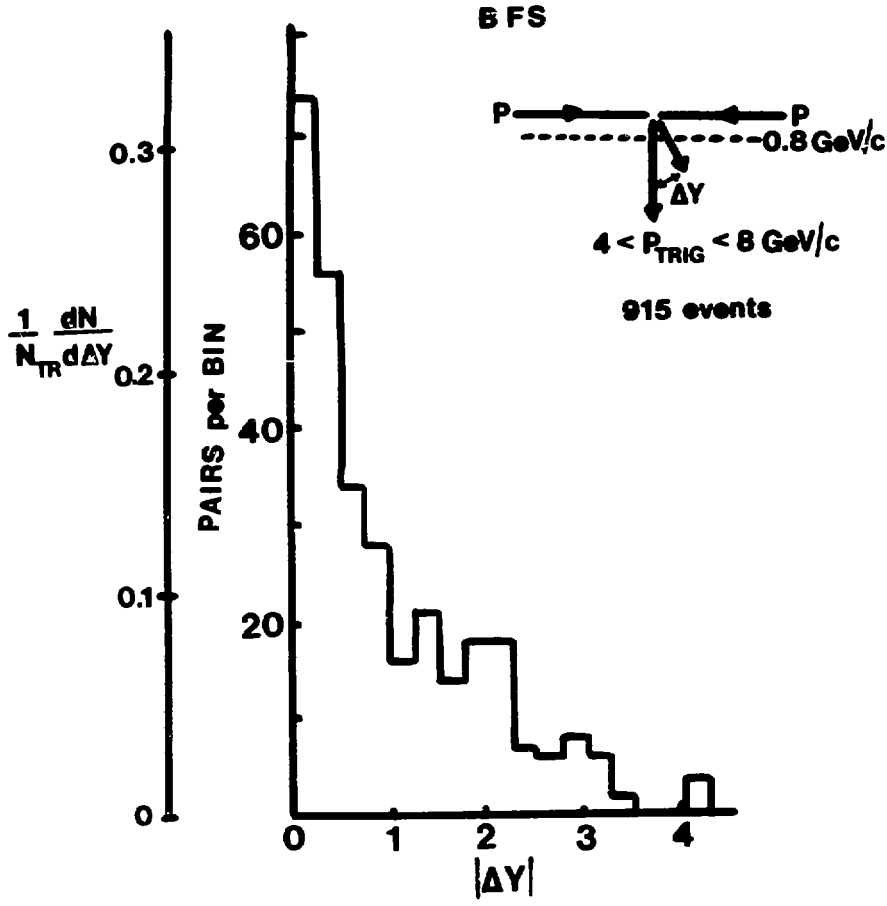
B FS
P
P
0.8 GeV/c
ΔY
4 < P_TRIG < 8 GeV/c
915 events
1/N_TR dN/dΔY
0.3
0.2
0.1
0
PAIRS per BIN
60
40
20
0
1
2
3
4
|ΔY|

Fig. 16

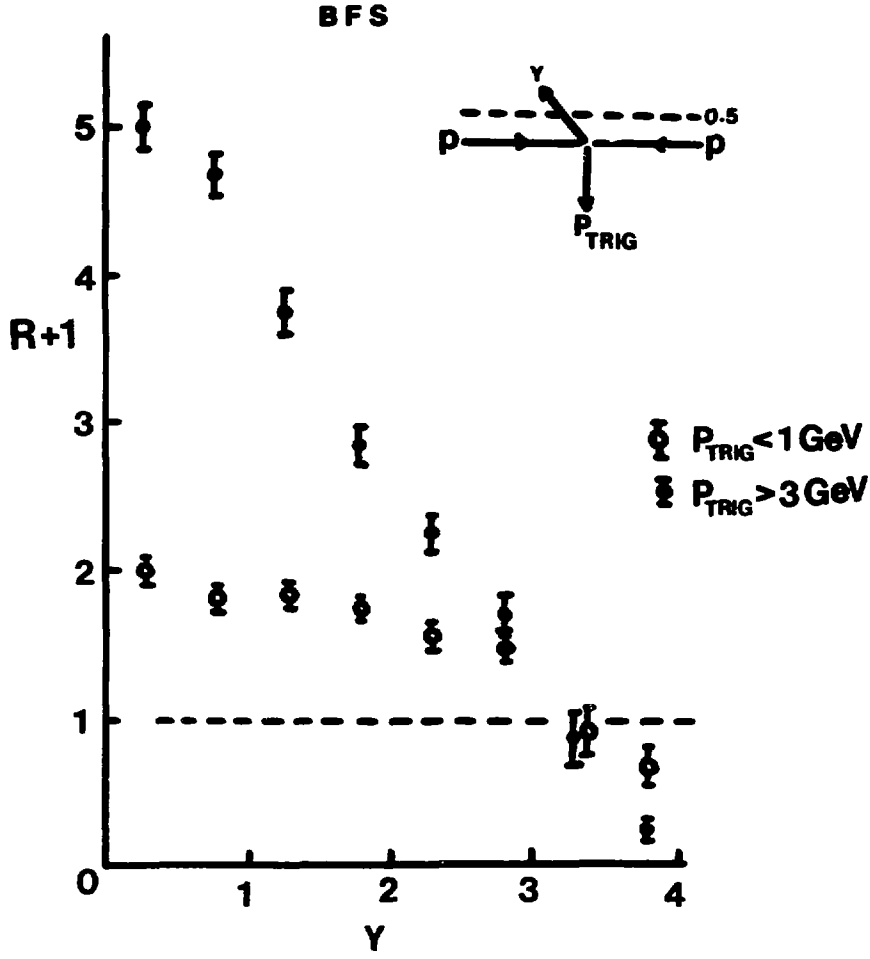

Fig. 17

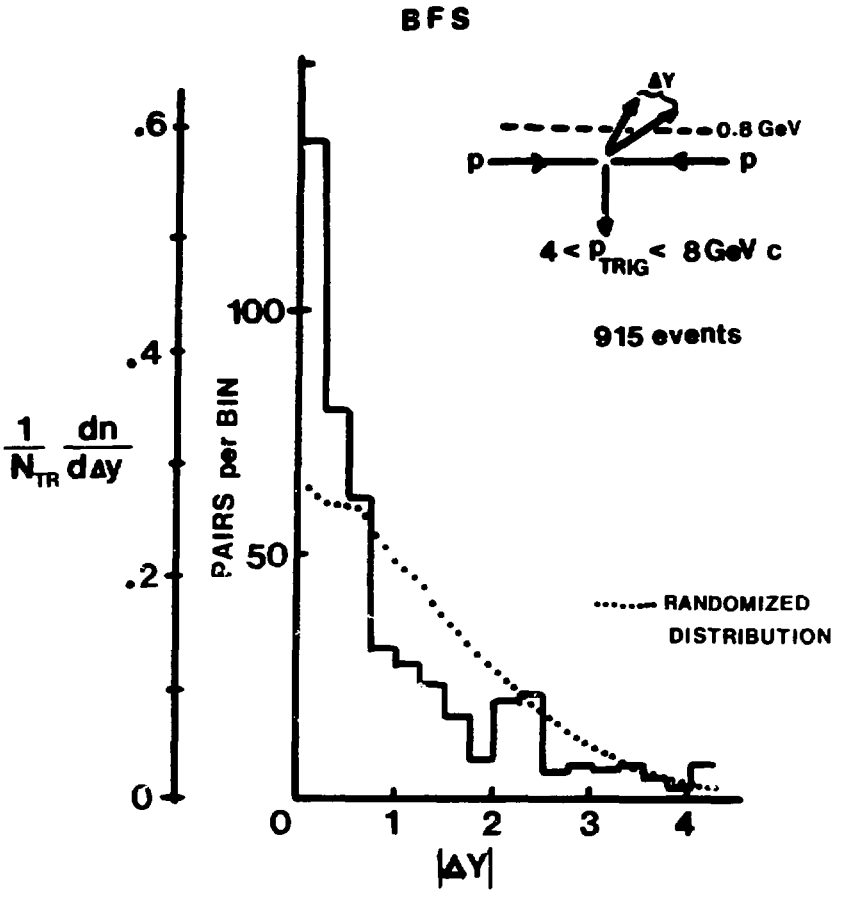
BFS
ΔY
0.8 GeV
p
p
4 < p_TRIG < 8 GeV c
915 events
1/N_TR dn/dΔy
PAIRS per BIN
100
50
.6
.4
.2
0
0
1
2
3
4
|ΔY|
RANDOMIZED
DISTRIBUTION

Fig. 18

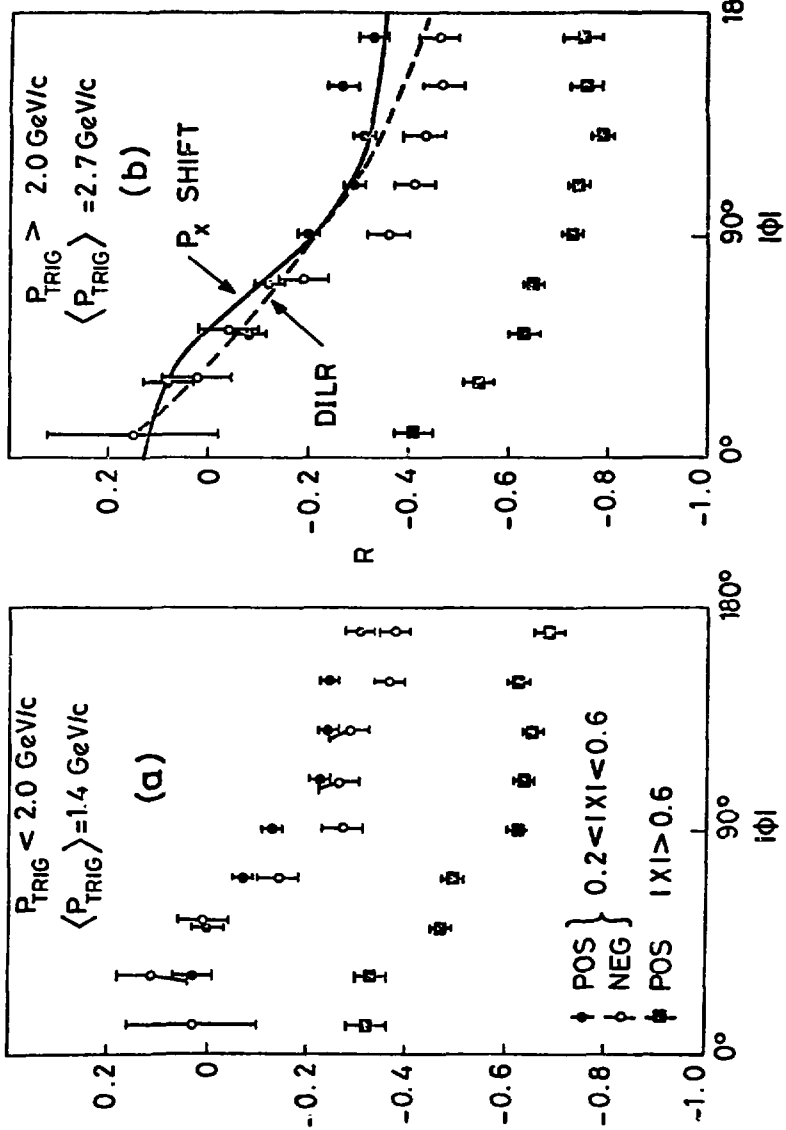
P_{TRIG} < 2.0 GeV/c
$\langle P_{TRIG} \rangle$ = 1.4 GeV/c
(a)
POS
NEG
0.2<|X|<0.6
POS |X|>0.6
R
|Φ|
0°
90°
180°
0.2
0
-0.2
-0.4
-0.6
-0.8
-1.0
P_{TRIG} > 2.0 GeV/c
$\langle P_{TRIG} \rangle$ = 2.7 GeV/c
(b)
P_x SHIFT
DILR

Fig. 19

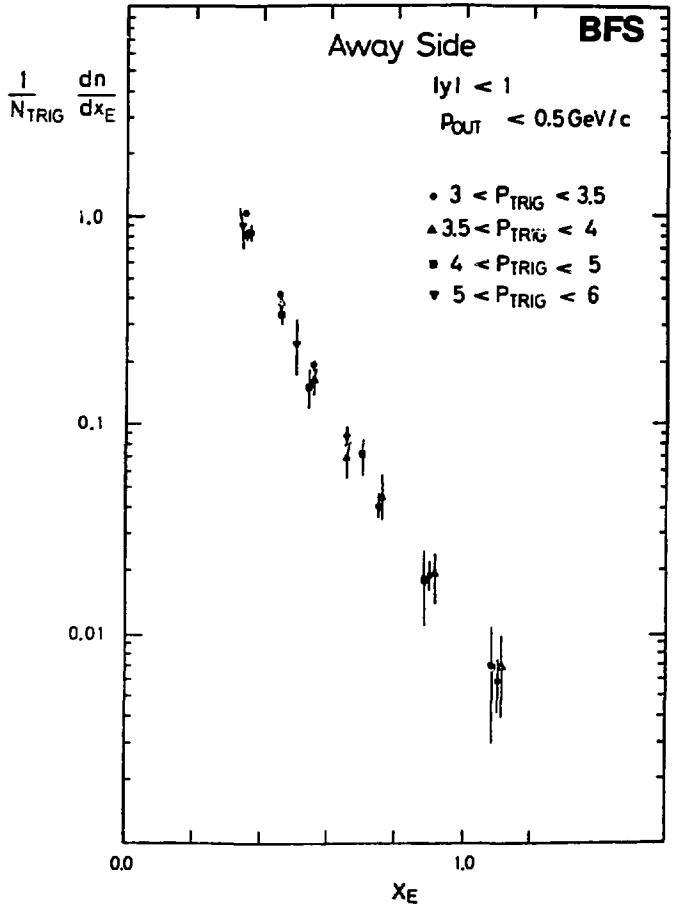
BFS
Away Side
|y| < 1
P_{OUT} < 0.5 GeV/c
• 3 < P_{TRIG} < 3.5
▲ 3.5 < P_{TRIG} < 4
■ 4 < P_{TRIG} < 5
▼ 5 < P_{TRIG} < 6
$\frac{1}{N_{TRIG}} \frac{dn}{dx_E}$
1.0
0.1
0.01
0.0
1.0
x_E

Fig. 20

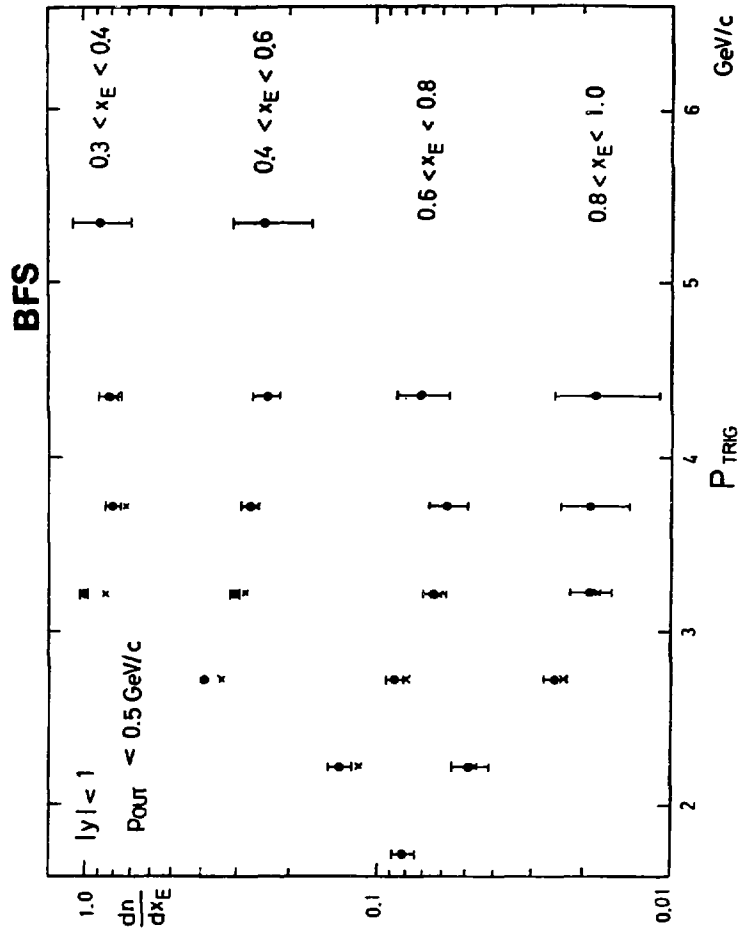
BFS
|y| < 1
p_{OUT} < 0.5 GeV/c
0.3 < x_E < 0.4
0.4 < x_E < 0.6
0.6 < x_E < 0.8
0.8 < x_E < 1.0
$\frac{1}{N_{TRIG}} \frac{dn}{dx_E}$
1.0
0.1
0.01
2
3
4
5
6
P_{TRIG}
GeV/c

Fig. 21

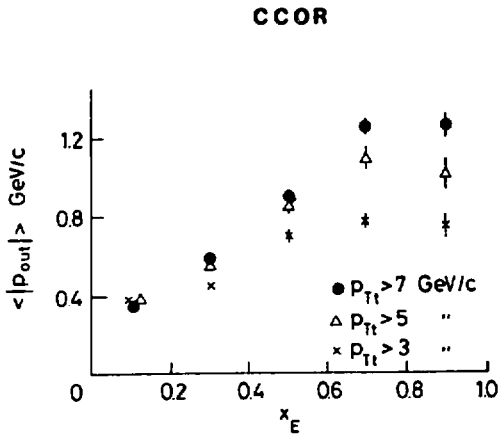

Fig. 22

VACUUM STRUCTURE AND QCD

D. Gross (Princeton)

Many of you are probably asking yourselves the question, "What has the structure of the vacuum according to QCD have to do with heavy ion collisions?" The basic answer to that question is that most of us working in particle physics today are convinced that QCD is the fundamental theory of the strong interactions that eventually will enable us to calculate all the properties of hadrons including nuclear physics as a special case. Thus QCD is clearly relevant to the phenomena that one might observe in heavy ion machines. I think, in fact, that the interaction between elementary particle physics and nuclear physics is likely to increase in the coming years as the fundamental theory of hadronic matter develops. At present one is clearly far from the goal of predicting the Rosenfeld tables from the Lagrangian of QCD, although some progress, which I will report on here, has been made in that direction. Now any microscopic theory of hadrons that is able to discuss the hadronic matter that one finds in nuclei should also be able to describe hadronic matter in unusual environments where the temperature and/or the baryon number density are different from those that one encounters inside ordinary nuclei. Any experiment that has the hope of exploring matter in these unusual environments should be encouraged since it will provide tests of the theory in domains where one has little experimental information. Heavy ion machines appear to be the only hope of exploring matter at high densities in the laboratory. It is of course not clear, as has been emphasized by many of the speakers at this meeting, that in heavy ion collisions

high density states will be produced. Furthermore even if a particle theorist hands you the equation of state of hadronic matter, it will be a difficult task to relate that to quantities which one can measure in the laboratory. These are matters that I will not discuss at all; they represent very difficult problems. However, there is obviously some finite chance of being able to observe, for example, hadronic matter at high densities using heavy ion machines and, if so one, will have a very nice test of any fundamental microscopic theory of hadrons, and in particular of QCD.

What I shall do in this talk is to briefly remind you what QCD is, and discuss some of the dynamical issues which face the particle theorists who are attempting to solve this theory. In particular, I shall focus on the problems that arise in attempting to discuss the structure of low lying hadrons, say nucleons, starting with a color gauge theory of quarks. Then I will review the picture of hadronic structure, which has been developed by Callan, Dashen, and myself in the last few years. In this picture we claim to see the qualitative features of hadronic structure emerge in a direct way from first principles. Finally I shall discuss the relevance of our emerging understanding of the structure of hadrons to the question of what hadronic matter, i.e., nuclear or quark matter, might look like at high densities.

First let me remind you briefly what QCD is and why we believe that it describes the strong interactions. QCD is a color gauge theory of quarks. The fundamental constituents of hadrons, we believe, are spin one-half quarks which come in a variety of flavors, five of which have been "observed" to date. These quarks have a strange mass spectrum

which we must take from experiment. This spectrum has nothing to do with the strong interactions and is presumably produced by a unified theory which includes the flavor interactions which connect quarks of different flavors. For the purposes of discussing low lying hadrons, and nucleons in particular, we are only interested in the so-called light quarks which, for reasons that are not understood, have light masses compared to the nucleon mass scale. Therefore their physics is approximately invariant under a chiral $SU_3 \times SU_3$ global symmetry group. The strong interactions themselves are generated, we believe, by colored color gluons which mediate a local SU_3 color gauge group and are flavor-blind, i.e., do not see the flavors which distinguish the different quarks except insofar as they have different masses. The strong interaction coupling constant, $\alpha_s = g_s^2/4\pi$, that characterizes the strong interactions at a scale of the hadronic mass, is roughly equal to a third. This, then, is the theory. It is described by the Lagrangian

$$L = -\frac{1}{4} F^{\alpha}_{\mu\nu} F^{\mu\nu}_{\alpha} + \sum_{i=1}^{F} \bar{\psi}_i [i\phi(A) - m_i]\psi_i \quad . \tag{1}$$

In principle we have good reasons to believe that this is the fundamental theory of the strong interactions from which, by using ordinary relativistic quantum mechanics, one could deduce all the properties of hadrons.

The most compelling reason to believe in the theory is its ability to explain the observed, simple, short distance structure of hadrons in terms of almost non-interacting massless quarks. This phenomenon of asymptotic freedom tells us something about this theory, which in this respect is unique among all possible four-dimensional relativistic

quantum field theories. The coupling that characterizes the interactions of the quarks (which as in any quantum field theory is a function of the length scale at which one is carrying out one's observations) vanishes at short distances or large momenta logarithmically.

$$\frac{1}{x(p)} = \frac{g^2(p)}{8\pi^2} \underset{p\to\infty}{\approx} \frac{1}{11\ell n(p/\ )} \quad . \tag{2}$$

This is relevant to experiments that involve the propagation of quarks over short distances and for short times. Of particular importance, both historically and as a way of testing the theory, is the process of deep inelastic scattering of leptons off nucleons. There in the "scaling limit" one has a photon of large energy and large momentum transfer interacting with nucleons, and one thus can obtain an instantaneous snapshot of the structure of the nucleon. In this way one can see the fundamental constituents over short distances and short times. It is these experiments that enable us to see the quarks and the gluons directly; to deduce their existence and their quantum numbers; to confirm, or historically to deduce, the nature of the quark gluon interaction; and to measure the effective coupling constant that characterizes the coupling of the gluons to quarks as a function of the momentum transfer to the quarks. It is these experiments which have confirmed our belief that QCD is the fundamental theory of the strong interactions.

The use of asymptotic freedom has been developed enormously in the last few years. It has been used to deduce the short distance properties of QCD and thus to predict the behavior of the interactions of hadrons at large energies and momentum transfers in terms of the almost free quarks with weak gluon corrections by using ordinary perturbation theory.

The methods one uses here are straightforward and provide us with many ways of testing the theory.

The problems that one encounters, however, in trying to turn this Lagrangian into a theory of hadrons reside not in the short distance regime where the effective coupling is very small but in a distance regime which is at least the size of a hadron. Clearly the coupling cannot be arbitrarily small here. In fact we believe that the coupling becomes very big at large distances, and that is responsible for the fact that the quarks are confined in color singlet hadronic bound states and cannot be pulled out of the hadron. Thus, although the theory originated in the attempt to explain the simple behavior that quarks exhibit at short distances, the solution of the theory, in particular the description of hadrons within the theory, requires going beyond the asymptotically free regime.

There are two major problems that must be dealt with in describing hadrons as bound states of quarks in QCD. One normally thinks of confinement as the major problem; however, an equally difficult and important problem is that of chiral symmetry breaking. As I remarked above, the light up, down, and strange quarks which make up nucleons (particularly the up and down quarks) are very light compared to the typical hadronic mass scale. Furthermore, we believe that it is a very good approximation, as good as isotopic spin symmetry, to neglect the masses of the light quarks, which results in invariance of the strong interactions under a chiral SU_2 or SU_3 global symmetry. That is the basis of chiral symmetry, the notion of PCAC, and the interpretation of the pion as the Nambu-Goldstone mode of a chirally asymmetric vacuum

in which there is a non-vanishing expectation value for the quark mass operator. The quarks thereby acquire a dynamical constituent mass from the dynamical symmetry breaking of this chiral symmetry. Spontaneous chiral symmetry breaking is a mechanism which theorists are quite comfortable with because they have many models which mimic such behavior--thus it is not mysterious. However, it is very hard in a theory like QCD to produce in a quantitative fashion the dynamical breaking of chiral symmetry. It is absolutely necessary to do so in order to understand the proton and the neutron. In the absence of this symmetry breaking they would be members of parity degenerate multiplets or masses. They clearly are not. In fact, we think that the dynamics of light quark states, such as the nucleon, is governed to a large extent by the mechanism of chiral symmetry breaking and not of color confinement. As I will briefly summarize, in our picture of QCD we find that the structure of the vacuum is such that it indeed breaks chiral symmetry and generates a large quark mass. The normal QCD vacuum, therefore, is a state in which quarks would have a large energy due to their dynamical mass. The energetics is such that when quarks are inserted into such a vacuum they will prefer to live in a different vacuum phase where they behave as massless objects, in order to construct a state of a given baryon number.

This picture is somewhat similar to the picture of so-called abnormal nuclear matter according to Lee and Wick, where these objects were not quarks but nucleons themselves; and of course it is very similar to the M.I.T. bag model. In fact to zeroth order our picture is almost identical to the M.I.T. bag model. Here the light quarks are confined

to a bag of simple and perturbative, dilute vacuum phase immersed in the normal vacuum which expels the quarks by producing a very large mass for the quark outside the bag. The light hadrons, which are built out of light quarks, are simply free quarks rattling around inside this bubble, so that their kinetic pressure balances the outside vacuum pressure. This model, if one includes gluon corrections, gives a very nice description of the static properties of light hadrons.

All of this demonstrates that the understanding of the mechanism of chiral symmetry breaking is quite crucial for understanding the properties of light hadrons.

Now, in addition, there is the question of color confinement and the colored interactions of quarks. These are also important in understanding the properites of light hadrons, although less so than chiral symmetry breaking. They are certainly important in understanding the dynamics of heavier quarks and in determining whether one can ultimately produce quarks if one hits a hadron with large energies. Normally the way one poses the question of confinement is to ask what the interaction energy of separated quarks is. One imagines very heavy quarks which one can insert into the vacuum with a fixed separation. Since they're heavy they don't move, and one calculates the energy of that state as a function of the quark anti-quark separation. In a confining theory this energy must approach infinity as one separates the quarks, otherwise one could clearly produce asymptotic quark states. One believes, in fact, that the energy will increase linearly with the separation of the quarks.

Again, at least in our picture of QCD, the mechanism that will

lead to this linear increase in energy is due to the confining, now color confining, properties of the QCD vacuum which acts like a anti-dielectric medium. The vacuum fluctuations that we can treat by semi-classical methods have the effect of making the dielectric constant of this medium very small. The result is that the ordinary QCD vacuum expels the electric (non-Abelian) flux that must go from one quark to the other quark; simply because the energy is inversely proportional to the dielectric constant. It is the strong anti-screening effects of the vacuum fluctuations in QCD that give rise to this small dielectric constant and confine the flux to a region of simple, dilute perturbative vacuum phase in which the dielectric constant is 1. Creating this abnormal phase will cost some energy per unit volume and leads to an interaction energy proportional to the length of the produced flux tube as one separates the quarks. To zeroth approximation this is simply the M.I.T. heavy quark bag model, which can be used in principle to discuss the properties of very heavy quark bound states such as charmonium and the like.

Next I will give an overall view of the dynamics of QCD. QCD is a very difficult theory to solve, partly due to the fact that it is such an ambitious theory. A gauge theory, by virtue of the large symmetry involved, contains only one free parameter which characterizes the strength of the interactions, namely the gauge coupling g. The theory also contains the masses of the quarks as parameters, but as I argued before, the light quark masses can be neglected in describing the properties of light hadrons. Thus, the theory essentially contains only one dimensionless parameter and no dimensional parameters. If the theory

produces sensible physical states, the phenomena of "dimensional transmutation" will necessarily take place. The coupling constant in such a theory only has meaning when we introduce a characteristic length scale at which we define the coupling characterizing the interactions and will vary as one varies this length scale. However, if the theory produces, as we believe it will, a physical state such as the proton and we measure the coupling at a physical length corresponding to the radius of the proton, for example, then this coupling constant will be not an arbitrary parameter but a calculable number. Thus, QCD contains no adjustable parameters except for the arbitrary units of time, mass, and distance that one must always introduce in any theory. For that reason, one potentially has an extraordinarily predictive theory. But on the other hand, one also has an extraordinarily difficult task to predict anything because there are no parameters which one can adjust. In particular there are no small parameters with which one can expand the theory. Normally calculations within the framework of field theory or ordinary quantum mechanics utilize an expansion in some interaction strength. In the case of QCD the interaction strength varies as one varies the scale of the phenomena one is discussing. Therefore, it is no surprise that any method of calculation for QCD is bound to work only for a limited domain of scale sizes. Furthermore, one expects different physics to occur when one looks at the phenomena in QCD at different scale sizes, short distances, or large distances.

The simplest region to probe (because of asymptotic freedom) and indeed the only region where we can really quantitatively test the theory, is that found in experiments which probe phenomena which

occur at distances short compared to the typical size of a hadron. Then we are guaranteed that the effective coupling is small and we can use ordinary perturbation theory. The inverse coupling constant x, which is $2\pi/\alpha_s = \frac{8\pi^2}{g^2}$, increases logarithmically as one decreases the scale size of the phenomena being observed. One is thereby guaranteed to get away with using ordinary perturbation theory, i.e. summing, Feynman diagrams, to calculate anything. In particular if we wish to describe the structure of the ground state, as seen in experiments which probe the ground state wave function at short distances, what we will see will be a vacuum characterized by small oscillations about vanishing field strengths. These harmonic modes, which are normally called quarks and gluons, interact with weak anharmonic interactions and can be treated by performing an asymptotic expansion in the weak coupling which characterizes the couplings of these harmonic modes. That is the simple picture obtained at short distances. It clearly cannot describe hadrons which will never appear to any order of perturbation theory. There is another very simple picture of QCD which one finds if one goes to very large distances. Then, if one is describing the structure of the ground state over distances which are very large compared to the size of the hadron, it is reasonable to approximate the theory by a lattice theory. This is useful since one can then use it to perform strong coupling approximations to the theory, since at large distances we believe that the coupling increases quite rapidly. These investigations of the theory have been performed using lattice approximations and expanding in powers of the inverse coupling. Again the physics is quite simple. The fluctuations of the vacuum are now

not harmonic modes around a zero field background, but rather random unitary matrices (which are defined for each link on the lattice). The physics is that of strings of electric flux between external colored sources or quarks.

This description of the theory at large distances has confinement built into it with a linear interaction energy between external quark sources, and unlike the very coherent Gaussian fluctuations of the vacuum, one has total chaos here. Any field configuration is equally likely and it is the total randomization over all possible fluctuating gauge fields which disorders the theory completely and leads to the confinement of color. Now, the trouble is that the physics that generates hadronic bound states lies somewhere in between these two regions. That is why the theory is difficult to treat. The size of the hadron is presumably where the coupling is neither weak nor strong.

We can try to approach the region where hadrons are formed by working our way out of the perturbative region or by trying to work our way down (say in a lattice theory) from the strong coupling region. Unfortunately, these two descriptions use different languages and the problem of proving confinement is to show that within the same theoretical framework one can get from strong to weak coupling. A separate question is what the physics is like in intermediate regions and whether one can calculate the properties of hadrons. Our work has concentrated on moving out of the perturbative region by going beyond ordinary perturbative expansions in the coupling constant. At larger distances one has, in addition to perturbative corrections to free field theory behavior, semi-classical weak coupling corrections

which are non-perturbative. In fact these are the fluctuations that turn out to be important as one increases the coupling slightly from the very weak coupling region. They are tunneling fluctuations which have to do with the fact that the QCD potential looks like a periodic potential, and in addition to Gaussian harmonic fluctuations around each well, there are important tunneling fluctuations. These tunneling fluctuations are proportional to $\frac{1}{g^{12}}e^{-1/g^2}$ but are big compared to perturbative fluctuations in a region where one can still use semi-classical methods and begin to explore interesting non-perturbative dynamics. What we find is that the physics generated by such fluctuations begins to produce, as one moves out in distance, the physics that is required to produce the hadrons we see. Namely, these fluctuations give rise to mechanisms that break chiral symmetry, generate large quark masses, and strongly anti-screen color, which causes the dielectric constant of the vacuum to decrease and thus the self energy of quark anti-quark pairs to increase greatly.

On the other hand, the methods that we use break down at some scale size due to the increase in coupling. It is still an open question and a matter of controversy whether, in order to get to the strong coupling regime and have a complete description of QCD, one will have to consider weird objects such as vortices, monopoles, merons, and many other configurations or vacuum fluctuations to explain the disordering or confining of color. We actually believe that the weak coupling, semi-classical regime and the strong coupling regime essentially overlap and that there is no gap in between. The same fluctuations that can be used to describe the physics at a distance where one begins to self-consistently produce hadrons also produces a strong coupling theory. One can then describe

the large scale structure of the QCD vacuum by using strong coupling techniques. Our picture of structure of the vacuum in QCD therefore consists of two components: one that can be described by semi-classical or WKB weak coupling methods, and the other component which describes larger scale fluctuations that can be described by chaotic, completely random fluctuations of the gauge field. For the purposes of discussing hadrons, these random fluctuations have little influence on the physics that goes on at lower scale sizes.

I certainly don't have time to discuss this picture in detail. I will, however, describe very briefly how we develop the vacuum structure of QCD, from the weak coupling point of view.

A few years ago, due to the discovery of the instanton, it was realized that the "potential" in QCD is periodic. Since one can show that the barrier between the different wells is finite, one knows on general quantum mechanical grounds that the ground state will not consist of localized Gaussian wave packets about each well but rather of a superposition of such packets, and that one will have a kind of Bloch wave description of the vacuum. It is possible to discuss tunneling, as you know from ordinary quantum mechanics, as long as $\hbar$, or the magnitude of the anharmonic couplings is sufficiently small by means of the WKB approximation. Our investigation started by exploring the dynamics that arise due to these tunneling fluctuations in QCD. It is very useful to develop WKB methods in field theory by considering the Euclidian time history of the vacuum or the propagator in imaginary time. According to Feynman this can be written as a sum over all possible field configurations, or time histories of the gauge field, weighted by the classical action. The

semi-classical or WKB approximation consists of approximating the sum over all time histories by those which are saddle points of the integration, namely solutions of the classical equations of motion in imaginary time. That is a method which generalizes the WKB method to systems with an in-finite number of degrees of freedom. It also yields a very simple analog picture in which you regard the time history of the vacuum as the spatial configuration of a four dimensional gas. The localized tunneling events occur at some point in space and time and are characterized by an orientation in group space and a definite scale size. The vacuum-to-vacuum amplitude can then be regarded as the partition function of a gas of objects, i.e., tunneling events or instantons in four spatial dimensions. To the extent that they don't interfere with each other they behave as a free gas with a given activity. In this perfect gas approximation, where one neglects the interference between different tunneling events, one simply has a four-dimensional gas of objects with a density of tunneling events of size ρ given by

$$D(\rho) = \text{const.}\ x^6\ (\rho)\ e^{-x(\rho)}$$

$$x(\rho) = \frac{8\pi^2}{g^2(\rho)} \approx 11\ \ell n 1/(\rho\Lambda) \qquad (3)$$

This contains the typical tunneling barrier penetration factor of $\exp(-\frac{1}{g^2})$, except that in QCD the coupling constant varies with the size of the tunneling event. This density is guaranteed to be very small for small scale size instantons, since $x \to \infty$ as $\rho \to 0$, but will increase, and thus the tunneling events will become more numerous and closer together, as one considers larger scale sizes. If one

considers arbitrarily large scale sizes one will have arbitrarily large couplings; and the semi-classical approximation, valid for small couplings, will break down. So once again we will try to describe the structure of the ground state constructed by WKB methods up to some scale size at which the methods break down.

To characterize the influence of such tunnelings we might ask what is the faction of space time occupied by instantons or what is the net probability that there will be a tunneling event? This is given by $f(\rho)$ which includes all instantons up to some scale size ρ_c.

$$F(\rho_c) = \pi^2 \int_0^{\rho_c} \frac{d\rho}{\rho} D(\rho) \tag{4}$$

The physical effects of instantons will become large when f begins to be of order one. One finds that f increases rapidly as one goes from weak coupling at short distances to scale sizes where the coupling is of order 1/25. So, even for distances where ordinary perturbation theory would lead you to believe nothing much is happening, you find a strong change in the wave function of the vacuum which now mainly consists of tunneling fluctuations and not the Gaussian fluctuations you see in ordinary perturbation theory.

We then attempt to describe the structure of that part of the vacuum wave function that knows about gauge fields which vary over a scale size of less than ρ_c. That will give a rough description of the time history of the vacuum as a rather dense gas of instantons where the vacuum mainly consists of these tunneling fluctuations and the vacuum wave function is strongly localized on these instanton-like fields which exist during the tunneling event.

What is the physics of the vacuum on the scale size of ρ_c? Do we begin to see quarks binding into hadrons when we look at the vacuum over this scale size? The first thing we investigate is the question of chiral symmetry breaking. Here the instantons play two roles. First, they kinematically solve an old problem which occurs in any quark theory of reducing the apparent U(3) axial symmetry to SU(3). This is a result of a kinematical property of tunneling, having to do with the topological properties of instantons, which I will not discuss here. From our point of view, the important dynamical feature of instantons is that these fluctuations generate a mechanism for dynamical symmetry breaking of chiral SU(3), a non-vanishing quark mass, and a composite pion even if the light quark masses were set equal to zero. In fact, if one considers the propagation of light quarks in the QCD vacuum which contains these tunneling fluctuations, one finds that a right handed light quark, after a tunneling has taken place, has become left handed. If one had but one flavor of quark then these tunneling events would look exactly as though a mass term was added to the theory. As the quarks propagate everytime a tunneling takes place, they switch their chirality, exactly as if there was a perturbative mass term. One can, then, for one flavor, quite simply calculate the dynamically generated, momentum dependent mass of the quarks. One finds

$$m(p^2) = 2\pi^2 \int \frac{d\rho}{\rho^2} D(\rho)\ F^2(p\rho) \tag{5}$$

where F is a known function that can be easily calculated by solving the Dirac equation in the presence of an instanton field. The main feature of such a calculation is that one does generate a quark mass

that is strongly momentum-dependent. This means that at very large momenta or short distances the dynamical mass generation turns off rapidly and the quarks behave as massless objects. As one goes to larger distances or smaller momenta, one generates a quark mass of order $2/\rho_c$. Thus, on the scale size of ρ_c the quarks will begin to propagate as if they have a mass of order $1/\rho_c$. The treatment of this chiral symmetry breaking in the real world, where we have at least 2 light quarks, is much more complicated. An adequate treatment of this mass generation has not yet been developed. However, crudely speaking, the physics is exactly the same as in the case of one flavor. At the scale length where we can describe the vacuum as a dense gas of instantons, the quarks begin to acquire a mass which is typical of that scale length. We estimate a mass of something like 1 to 2 GeV per quark, at this scale length. This of course is not the mass of a physical quark, which presumably will be infinite, but rather the mass which characterizes the propagation of a quark for momenta of order $1/\rho_c$.

This will lead to something like the light M.I.T. bag model, although here the real existence of phases in equilibrium has not been established quantitatively. If we describe the vacuum as this dense gas of instantons in which quarks would have a large mass of order of a few GeV and then demand that we have say a nucleon, i.e., a baryon number-one state, consisting of 3 quarks, it will be energetically favorable to create a bubble of perturbative, dilute vacuum phase in which instantons don't exist. It costs some amount of energy per unit volume to create such a phase, i.e., to construct a trial wave function for such a state which excludes tunneling in some region,

however the quarks inside such a perturbative phase behave as massless, weakly interacting fermions. We believe that this produces a description of light hadrons which, to zero approximation, is simply a bubble of quarks confined in a dilute perturbative phase, since outside the bubble they would have a very large mass produced by instantons. If one adds the color interactions of the quarks and incorporates the color-confining properties of the QCD vacuum, one in fact ends up with the M.I.T. bag model, to first approximation. In addition, since one has not destroyed chiral symmetry by hand, the theory will contain a Nambu-Goldstone composite pion. One can eventually calculate this pion, which couples to the quark degrees of freedom inside the bag.

This picture then allows one to relate the bag constant, i.e., the energy density of the QCD vacuum which can be calculated in terms of the instanton gas, to the only dimensional parameter we have, the arbitrary renormalization scale length. Thus, via the M.I.T.-like phenomenology Λ can be related to the radius of the hadron and we can determine the value of $1/\rho_c$ in terms of GeV. We find, in what so far is a very crude treatment, that the numbers are consistent with bag model phenomenology and with the values of the couplings that emerge from tests of asymptotic freedom.

The other important problem in QCD is that of color confinement. I shall briefly describe the effects of instantons on color confinement. The main effect of instantons is the anti-screening of color. One can explore this effect by exploring the effect on heavy quarks of the instanton tunneling fluctuations. One finds a strong coupling constant renormalization due to instantons. There is a very simple

way to understand this effect. In the analog instanton gas the instantons have a natural interpretation as permanent magnetic dipoles. One can interpret the anti-screening effect which rescales the coupling between the quarks by an enormous factor as simply the paramagnetic permeability of the vacuum due to these instanton fluctuations. They typically change the coupling from weak coupling to strong coupling. In fact once one gets up to the scale size where these fluctuations begin to fill the vacuum, one sees a coupling at larger scale sizes of order one. At half the critical scale size the coupling is very weak and one can make calculations using WKB methods, but as one doubles the scale size of the phenomena one is investigating, it becomes very strong. One can quite reliably and quantitatively discuss the possibility of a phase transition, i.e., the possibility that when static (massive) quarks are put into such a vacuum they will prefer to live in a phase where these fluctuations are not present simply because those fluctuations decrease the dielectric constant and thus increase the energy of such a state enormously. One can discuss in some detail the equation of state of QCD in the presence of color fields created by quarks and including the physics of the fluctuations up to ρ_c. One finds that there are two phases of the system which can exist in equilibrium in the presence of color fields produced by the quarks with very different densities of instantons and very different coupling constants.

That leads us to deduce the bag model of hadrons—what we would call a heavy quark bag. Again, one puts heavy quarks into the vacuum, the quarks sit there and propagate in time and one calculates their energy as a function of separation. We find that in the presence

of the electric fields created by the quarks, the electric fields bore holes in the dense instanton QCD vacuum outside and create a bag or flux tube. Inside one has a dilute, perturbative, trivial phase which is in equilibrium with a dense strongly anti-screening phase outside the bag. The electric field cannot penetrate the dense phase which has a vanishing dielectric constant. This produces to first approximation the M.I.T. bag model for heavy quark system. It allows us to estimate the transverse dimensions of a flux tube, relate that to the Regge slope parameter and to estimate the size of such a bag. Furthermore by relating these parameters to the size of the fluctuations from which we're building this dense vacuum we show that it makes sense to discuss a bag of this scale size. This phenomenon of color confinement is less relevant to light quark bound states, nucleons in particular, where they are less important than the dynamics of chiral symmetry breaking and quark mass generation.

Finally, I shall discuss what all of this might imply regarding quark matter at high densities. There are many discussions of what might happen at high quark densities based on ideas which are certainly correct in QCD. The first of such discussions, initiated by Collins and Perry, was simply based on the observation that in an asymptotically free theory, baryon density plays the role of an infrared cutoff. By dialing up the density, one can guarantee that the effective coupling will become arbitrarily small. Thus the density plays the same role as momentum transfer in deep inelastic scattering and guarantees, on general grounds, that at sufficiently high baryon density, the stable form of matter will be quark matter. This will be a relativistic

gas of weakly interacting almost massless quarks, described by the following energy density which one can calculate straightforwardly in perturbation theory.

$$\varepsilon_0 = \frac{3}{4\pi^2}(p_u^4+\ldots)\left[1+\frac{2\alpha_s}{3\pi}+\frac{\alpha_s^2}{3\pi^2}(8.66+1.9\ \ell n\ \frac{\alpha_s}{\pi})+\ldots\right] \qquad (6)$$

$$\alpha_s = \frac{g^2(pf)}{4\pi} \qquad \text{Pressure} = \frac{1}{3}\varepsilon$$

This simple equation of state is guaranteed by asymptotic freedom. Now, of course, this tells us nothing about where the phase transition from hadronic to quark matter might occur, i.e., at what density and what kind of phase transition occurs. Most of the more detailed discussion in the literature is based on the bag model, which I've argued will emerge to first approximation in QCD. One simply adds to the perturbative treatment of QCD at short distances, valid for very large baryon densities, the energy density B of the vacuum (i.e., of what we would call the dilute vacuum phase).

$$\varepsilon = \varepsilon_0 + B$$
$$P = 1/3\ (\varepsilon - 4B) \qquad (7)$$

This treatment is consistent with our picture of QCD. Namely, at large densities the coupling is turned off. Therefore, the mechanism that non-perturbatively creates this large negative energy density in the vacuum state has been also turned off, and we have to add the missing energy B to the perturbative vacuum energy. This leads to an equation of state which has the possibility of producing self-balanced states. In fact one has to be careful if one is not

to conclude that quark matter is more stable than nuclear matter. The calculations that are performed are essentially the same calculations that one does within the bag model to show that the deuteron is a bound state of a neutron and a proton and not a six quark bag. However, the calculation is very sensitive to the strength of the gluon interaction inside the bag. It is only the gluon-induced spin-splitting interactions that render self-bound quark matter unstable and give it a binding energy per nucleon of a few hundred MeV.

Of greater interest, since such self-bound metastable quark matter bags are unlikely to be experimentally observable, is the possible phase transition, at large densities, from nuclear matter to quark matter. Again, estimates vary enormously. They depend very much on the exact value of the bag parameters, and even more on how one describes nuclear matter at such high densities. Simple estimates, using the bag mod' and nuclear matter extrapolations, indicate that the transition occurs at something like 10 times nuclear density and thus might be relevant to a description of states that could possibly be produced in heavy ion collisions. From my reading of the literature I conclude that the problem is very tricky. The calculations are extraordinarily sensitive to both nuclear physics as well as to the parameters of the bag model. Furthermore, there are many questions that can be raised, some of which are related to the remark of Gordon Baym that in the bag model nuclei are so big they appear, even at ordinary nuclear densities, to almost overlap. One might therefore expect at intermediate densities of hadronic matter something like a percolation phase transition where quarks in one bag can be connected via a path

in the nucleus to quarks in another bag. It is hard, however, to see what would distinguish such a phase from ordinary nuclear matter. There is also the concern voiced by Gerry Brown and collaborators that such big hadron bags might invalidate the standard description of nuclear matter, since it is hard to use the usual ideas about particle exchange in a nucleus made up of almost overlapping bags. They also argue that, if you believe in our picture of QCD, where pions exist outside the bag in the ordinary vacuum, the pion external pressure will in fact cause the M.I.T. bag model to collapse to a small bag, which is not one fermi in radius but rather 1/5 of a fermi, and that actually hadrons are small bags.

So, what does QCD have to say about a transition from nuclear to quark matter? Clearly, in our picture, to first approximation, the bag model is qualitatively correct. Thus there should be such a transition at roughly 8 times nuclear density. The factor of eight is equivalent to changing the fermi momentum by a factor of 2, or decreasing the scale that is being investigated by a factor of 2. It is just this factor of 2 that we believe takes us from very strong to very weak coupling, from instantons generating large quark masses and large couplings to simple perturbative physics. So, qualitatively we would expect a phase transition at this point. However, from a quantitative point of view it is clear that at present we are still far from being able to do much better than the crude bag model in a reliable way. There is no reason within the framework of the bag model to believe that the bag constant, the value of α's, or the mass of the quarks do not depend on the baryon density, as when one extrapolates

from nuclear density to 8 times nuclear density. In our picture they surely do depend on the density. Namely, as one goes from what is obtained at very high density, where one has a relativistic-like quark gas to nuclear matter at nuclear densities, one must include in between the non-perturbative effects which generate hadrons from quarks. These non-perturbative effects, which we would say can be well described on the scale size of a hadron by instanton fluctuations, will depend on the density. They are in fact turned off at large density, but as we decrease the density they will be more likely to occur. That will mean that the bag constant will be a function of the density. In fact it will decrease as we increase the baryon density. Also the coupling constant will increase because of the anti-screening effect of the increasingly likely instantons. Thus the properties of quark matter, as we decrease the density, will be quantitatively quite different from what one would calculate by simply extrapolating bag model parameters. These quantitative issues can be already dealt with, at least at high enough density, since one will then have very low instanton densities and that's just where our methods are most reliable. It will be much harder to treat the region of the phase transition.

There is also the possibility of interesting qualitative physics at moderate densities due to the chiral properties of the QCD vacuum. Let us try to imagine how nucleons nucleate out of a relativistic-like quark gas. In our picture this occurs in the following way: As you decrease the density, the likelihood of having tunneling fluctuations will increase. This will have two effects. They will increase the

coupling in this normal vacuum phase, and at some stage they will increase the mass of the quark. There will be a critical density at which chiral symmetry breaking will first appar, the quark will begin to develop a dynamical mass and a Nambu-Goldstone boson (the pion) will appear. These effects eventually cause the quarks to nucleate in dilute vacuum bags, because they don't like to live in this medium in which they interact strongly and where they have a large mass. But before we get to the phase transition, it might very well be that quark matter does not consist of light quarks but rather of medium light quarks, and that pions appear and are present in quark matter. This of course would have significant effects on the behavior of quark matter in this intermediate density region. I have no idea whether chiral symmetry breaking occurs or whether there is first a transition to nuclear matter. In any case, it is clear that the quantitative description of the intermediate region is going to be quite different than that one would get simply by using density-independent parameters within the bag model.

I should also note that in QCD "abnormal nuclear matter" simply doesn't exist. Nucleons are not point-like objects that get their mass through the interaction with a sigma field. They are made out of quarks, which indeed get their mass through a dynamical mechanism of chiral symmetry breaking; but they are already inside a mass bag in which they are light. Abnormal nuclear matter in a sense is simply the same state that we've been describing here as quark matter.

Another subject that has been investigated within QCD, both from the strong coupling lattice point of view and from the point of view

of our semi-classical treatment of the vacuum is the effect of increased temperature on hadronic matter. Here one can argue that for temperatures of order several hundred MeV there is a phase transition to an unconfined phase. However, it is not at all clear that this is relevant to the physics of heavy ion collisions, since it seems doubtful that there is enough time available in such collisions to establish thermodynamic equilibrium.

In conclusion, I have tried to present a treatment of QCD which leads to a consistent description of hadrons. At the moment this is still a very approximate description of hadrons, in which we can, at best, calculate to within perhaps a factor of 2; but at least our treatment involves no arbitrary cutoffs or free parameters. The picture, very crudely, is that of a two-phase description of hadrons. Quarks live in a bubble of dilute, trivial, perturbative vacuum in which they are light, almost massless, and weakly interacting. The bubble is in equilibrium with the normal QCD vacuum phase in which one has fluctuations which are on a scale size of roughly half the hadronic scale size due to tunneling fluctuations, and on larger scale sizes totally random fluctuations, which give rise to large quark masses and large couplings. To first approximation this picture leads to the M.I.T. bag model (although there are some differences). To do better than the M.I.T. bag model, one must match the weak coupling description we have of the wave function of the vacuum with the strong coupling description of the vacuum that one has larger scale sizes. This picture for quark and nuclear matter implies that in first approximation we should expect the physics suggested on the basis of the bag model and perturbation

theory to be qualitatively correct. Surely at high enough densities, there will be a transition to quark matter (although I don't think that one can calculate at the moment where the transition takes place). There will also be metastable quark matter states with roughly nuclear density. If one includes strange quarks, some of these states might live for a long time and actually be observed. To do better than the first approximation, and calculate reliably the equation of state of QCD, one must include the density dependence of the non-perturbative physics that gives rise to hadrons. We can begin to do that, I think, in a reliable fashion for high densities, and there exists the interesting possibility that there is intriguing physics in between very high density and nuclear density related to the chiral properties of hadronic matter.

INDICATION FOR THE FORMATION OF STRONGLY COMPRESSED NUCLEAR MATTER IN RELATIVISTIC HEAVY ION COLLISIONS*

H. Stöcker, J.Hofmann, J.A. Maruhn, and W. Greiner

Institut für Theoretische Physik der Johann Wolfgang Goethe-Universität, Frankfurt am Main, Germany

ABSTRACT

In the present paper we develop the essential theoretical tools for the treatment of the dynamics of High Energy Heavy Ion Collisions. We study the influence of the nuclear equation of state and discuss the new phenomena connected with phase transitions in nucleer matter (pion condensation). Furthermore we investigate the possibility of a transition from nuclear to quark matter in High Energy Heavy Ion Collisions. In this context we discuss exoctic phenomena like strongly bound pionic states, limiting temperatures, and exotic nuclei.

KEYWORDS

High Energy Heavy Ion Collisions, compression, shock waves, nuclear fluid dynamics, pion condensation, density isomers, quark matter.

1. INTRODUCTION

One of the most exciting motivations for the high energy heavy ion physicist is the possibility to study the nuclear equation of state at high densities, temperatures and pressures (Scheid, 1968; Chapline. 1973; Scheid, 1974; Scheid, 1974a; Wong,1974; Heinz, 1978), as well as the search for phase transitions into abnormal superdense states of matter like pion condensates (Migdal,1972; Brown,1975; Brown,1976; Migdal,1978; Campbell,1975), density isomers (Lee,1974), and quark matter (Collins, 1975; Baym,1976; Keister,1976).
We will concentrate on the following topics:
First we discuss the semi-validity of the nuclear fluid dynamical model which we use later on to describe high energy nuclear collisions. Then the nuclear equation of state is discussed, together with the compressibility, phase transitions like pion condensates and density isomers and the baryon-quark matter.

*Supported by Bundesministerium für Forschung und Technologie (BMFT), and by the Gesellschaft für Schwerionenforschung (GSI).

By comparing the results of the hydrodynamical approach with a number of recent experiments we will discuss the circumstantial evidence for the occurrence of strong compression effects (shock waves) and high thermal excitation. Finally we speculate about the phenomena which may occur at very high energies.

2. APPLICABILITY OF THE HYDRODYNAMICAL APPROACH

For the applicability of the fluid dynamical concepts it has to be ensured that fast equilibration and thermalization of the incident momentum and energy occurs in high energy heavy ion collisions, and that the mean free path (more precisely: the longitudinal momentum decay length) over the typical dimension, L, of the system is small $\lambda/L \ll 1$.
The mean free path λ is given by

$$\lambda = \frac{1}{\sigma \cdot \rho}$$

where σ is the total nucleon-nucleon scattering cross section and ρ is the actual nuclear density. For normal nuclear density ρ_o and a free n-n scattering cross section $\sigma_{NN} \sim 30$ mb at high energies, the mean free path is $\lambda \sim 2$fm, which is not too small against the nuclear dimensions L~10fm (Scheid,1968; 1974; 1974a).

High relative momenta between nuclei, signifying no overlap in phase space, as well as the large longitudinal momentum decay length calculated from the free n-n scattering cross section were interpreted as a complete transparency for the two nuclei at high energies and as a death for compression (shock) waves at energies above 1 GeV/n (Sobel,1975). However, in the "formation flight" of ensembles of nucleons, collective scattering phenomena (Gyulassy,1977; Ruck,1976) and compression effects can not be neglected, so that the scattering cross section and the density can be modified drastically leading to a decrease of the mean free path

$$\lambda = 1.4 \frac{\sigma_{NN}}{\sigma_{coll}} \cdot \frac{\rho_o}{\rho} \quad \text{fm} \quad .$$

Pions and pionic waves produced in inelastic nucleon collisions via the creation and decay of nuclear isobars (Hofmann,1976) (nucleon resonances) in processes of the type

$$N + N \rightarrow N + N^* \rightarrow N + \pi + N \rightarrow N^* + N \rightarrow \ \ldots$$

and via pionic bremsstrahlung (Vasak,1979) may lead to rapid randomization of longitudinal momentum and energy, and thus to a short mean free path and to generation of shock waves.

Another important process for randomization is the critical scattering of nucleons in the vicinity of a phase transition point (Gyulassy,1977). This is in analogy to the critical opalescence, which is characterized by the great enhancement of the scattering cross section of light near a liquid-gas phase transition, or of the critical scattering of neutrons in ferromagnets near the Curie point (Stanley, 1971) or - as the last example - the critical scattering appearing in two colliding plasma beams: When the drift velocity of the two plasmas exceeds a critical value, unstable plasmon modes appear, resulting in a growth of strong electric fields, which greatly reduce the penetration depth of the two plasmon beams in comparison to values estimated from free two-body collisions.

Thus, the vicinity of a phase transition - e.g. the onset of pion condenstion or gluon condensation is expected to be marked by the occurrence of critical nucleon-nucleon scattering, i.e. a large enhancement (a factor of 2-4 for pion condensation) of the density-dependent n-n cross section (Gyulassy,1977; Ruck,1976).

Together with the doubling of the nuclear density due to the overlap of nuclear matter the mean free path can then reduce by a factor of 4-8 or more to

$$\lambda \lesssim 0.4 \text{ fm}$$

This would mean that even at bombarding energies above one GeV/n nuclei do not become transparent to each other: On the contrary, very violent collisions can be expected. One should keep in mind, however, that nucleus-nucleus collisions are a quantum meachanical process. Hence - in the sense of quantum mechanical fluctuations - under the same initial conditions processes with violent randomization (i.e. the occurrence of pronounced shock waves) may occur as well as processes with less pronounced interaction. It is a formidable experimental task to separate the former from the latter.

Indeed, recent experiments (which we discuss later) show that up to lab-energies of 4 GeV/n a considerable part ($\sim$ 30%) of the total cross section are violent events with high multiplicities and large momentum transfer.

3. THE EQUATION OF MOTION

The most complete representation of nuclear hydrodynamics is given for the non-relativistic case by the Navier-Stokes equations, where the nuclear viscosity and thermal conductivity are included as well as a realistic treatment of the nuclear binding and surface via the Coulomb- and Yukawa potential (Wong, 1977; Maruhn, 1977; Stöcker, 1979). The equations of motion express the conservation of particle number

$$\frac{\partial \rho}{\partial t} + \nabla \cdot (\rho \vec{v}) = 0 \tag{1}$$

momentum

$$\frac{\partial (\rho_m v)}{\partial t} + \nabla (m \rho \vec{v} \cdot \vec{v}) = -\nabla \overleftrightarrow{S} - \rho \nabla V \tag{2}$$

and - energy

$$\frac{\partial (\rho E)}{\partial t} + \nabla (\rho E v) = \nabla (\kappa \nabla T) - \nabla (\overleftrightarrow{S} \cdot \vec{v}) - \rho v \cdot \nabla V \tag{3}$$

where $\overleftrightarrow{S}$ a Newtonian form has been assumed. The potential, which allows a realistic treatment of the nuclear binding and surface is a sum of the Coulomb potential determined via the Poisson-equation

$$\nabla^2 V_c(\vec{r}) = -4\pi \left(\frac{Ze}{A}\right)^2 \rho(\vec{r}) \tag{4}$$

and a Yukawa potential V_y given by

$$(\nabla^2 - \alpha^2) V_y(\vec{r}) = -4\pi\beta \rho(\vec{r}) \quad . \tag{5}$$

The Yukawa force allows for a smoothed nuclear surface - a realistic surface thickness can be obtained e.g. with the parameters $\alpha = 2.1$ fm^{-1} and $\beta = -280$ MeV fm corresponding to a nuclear surface energy coefficient

$$\eta = 2\pi \frac{\beta}{\alpha^4} \sim 90 \text{ MeV fm}^5 \tag{6}$$

Up to now, three-dimensional nuclear fluid dynamical calculations have only been performed using the Euler equations, i.e. the equations of motion for an ideal - i.e. non-viscous and non-thermo-conducting fluid (eq. (1),(2),(3) with η, K=0).

(Stöcker,1979). The above equations describe fluid dynamical processes completely. However, it is often advantageous to gain more insight into the physical processes by solving more simplified, schematic models, which can be solved (at least to some extent) analytically. In this case another set of equations is applied in the more schematic treatment of the fluid-dynamical description of high energy heavy ion collisions, namely the shock equations:

Shock waves have to be clearly distinguished from sound waves. In contrast to sound waves, shock waves are connected with a strong, density dependent mass flow with a flow velocity v_f. The shock front itself propagates with the shock velocity $v_s > v_f$ and does also depend strongly on the compression amplitude (Baumgardt,1975). Shock waves are non-linear phenomena - for large amplitudes $\rho >> \rho_o$ both v_s and v_f tend to the velocity of light (see Fig. 1), while for small perturbations $\rho \sim \rho_o$ they approach the linear limit of sound waves. Shock waves imply a large entropy production: The matter flow through the shock front is highly irreversible, it is not only connected with strong compression, but also with large thermal excitation (Hofmann,1976; Stöcker,1977,1977a,1978).

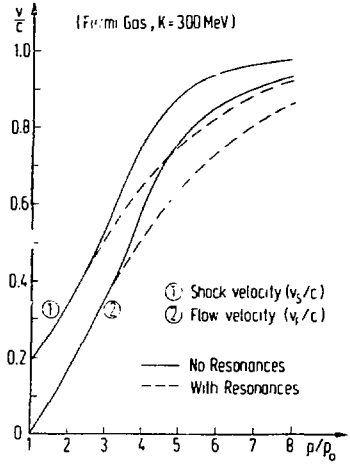

Fig. 1. shows the strong dependence of the shock velocity v_s and the flow velocity of v_f on the compression.

The shock calculations have to be viewed as an idealization assuming a zero width of the shock front together with the discontinuous jump of the state variables(e.g. ρ,T,e,p). However, the comparison of the nuclear shock wave calculations with the result of the full Navier Stokes calculations (Stöcker,1979b) show that the resulting compression rates and temperatures are very similar, although in the Navier Stokes calculations the compression front is smeared out over 1-2 fm due to the viscosity. Such a width seems to be rather realistic, as the width of a shock front is approximately given by 2-3 mean free path, which can be less than half a fermi in high energy nuclear collisions. For a large nuclear transparency, the shock front width may be of the order of the nuclear radius. However, no indication for transparency has been found in the high energy experiments up to now.

The relativistic shock equations (Baumgärtel,1975) can be derived from the continuity of the

$$\begin{aligned} &\text{particle flux density} && [j^o] = [\rho\, u_x] = 0 \\ &\text{energy flux density} && [T_{ox}] = [i\, u_o u_x] = 0 \\ &\text{and momentum flux density} && [T_{xx}] = [i\, u_x^2 + p] = 0 \end{aligned} \tag{7}$$

where [ ] denotes the jump of the respective variable across the shock front, and x gives the direction normal to the shock front as seen from the shock front's rest frame.

Eliminating the velocities u_x from the continuity equations yields the relativistic shock equation

$$\frac{i_o^2}{\rho_o^2} - \frac{i^2}{\rho^2} + (p-p_o)\left(\frac{i_o}{\rho_o^2} - \frac{i}{\rho^2}\right) = 0 \tag{8}$$

which gives an unique connection between the free enthalpy i, pressure p, and density ρ within the respective rest frame of the matter (subscript o stands for the undisturbed matter in front of the shock wave, quantities without subscript refer to matter in the compressed state). When we insert $i = \rho W + p$ and $i_o = \rho_o W_o$ the equation

$$W^2 - W_o^2 + p\left(\frac{W}{\rho} - \frac{W_o}{\rho_o}\right) = 0 \tag{9}$$

is obtained. Here $W(\rho,T)$ is the energy density functional, which characterizes the nuclear equation of state. It will be discussed in the next section. Neglecting pions and resonances and regarding the pure nucleon fluid only, the relation $p_T = \alpha\rho\, E_T$ obtained in the next section can be used to obtain a quadratic equation in E_T, which can be solved in terms of the nucleon density ρ analytically. E_T is the temperature-dependent part of $W(\rho,T)$.

For the non-relativistic case $\alpha = \frac{2}{3}$, the temperature is easily calculated from

$$T = \left(\frac{2\, E_T\, \rho^{2/3}}{8}\right)^{1/2} \tag{10}$$

It is important to note that the thermal energy of the nucleon gas does not depend on the gas ansatz for E_T, but only on the relation $p_T = \frac{2}{3}\rho\, E_T$. Thus this equation is also valid for a classical ideal gas, whereas the temperature in the compressed matter depends drastically on the gas ansatz $T = \frac{2}{3} E_T$ for the classical gas. (see Fig. 2).

The inclusion of pions and resonances demands for an numerical iterative solution of the shock equation, as the pressure is now more complicated.

The shock velocities v_s and v_f can be determined by the continuity of the energy and momentum flux density. From the relative velocities of the matter with respect to the shock front, the relative matter flow velocity v_f is obtained by covariant summation (see Figs. 1 and 3).

$$\begin{aligned} \frac{v_s}{c} &= \left\{ \frac{p\, w\, \rho}{(w_\rho - w_o\rho_o)(w_o\rho_o + p)} \right\}^{1/2} \\ \frac{v_f}{c} &= \left\{ \frac{p(\rho w - \rho_o w_o)}{\rho w\, (p + \rho_o w_o)} \right\}^{1/2} \end{aligned} \tag{11}$$

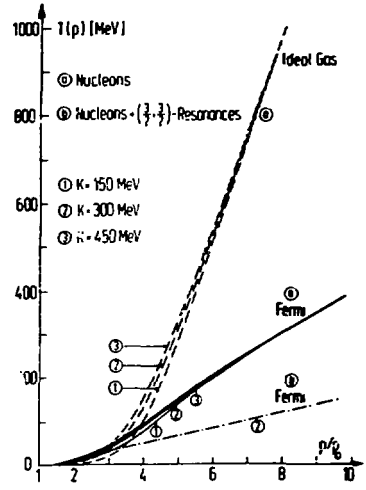

Fig. 2. The density dependence of the temperature T is shown for different equations of state and compression constants K.

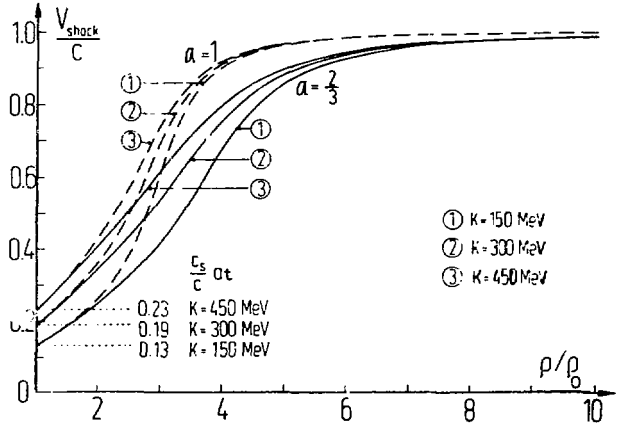

Fig. 3. The dependence of the shock velocity on the compression constant is shown.

A one dimensional relativistic shock model

A simple illustration model can be constructed to calculate the shock compression and -temperature in the central collision of two heavy nuclei as a function of the bombarding energy (Baumgardt,1975; Stöcker,1978). This model assumes the compressed fluid to be at rest in the center-of-momentum system (equal velocity frame). Three-dimensional fluid dynamical calculations show that this requirement is fulfilled fairly well for non-ps ipheral collisions of heavy nuclei near the collision axis: A sort of stationary compression stage develops. That means, that practically all of the incident kinetic energy is transformed into internal energy (compression and excitation).

As v_f denotes the relative velocity from the laboratory to the shocked matter in the c-M frame, the lab energy is given by

$$E_{LAB} = \left[(1- (\frac{v_p}{c})^2)^{-1/2} - 1 \right] W_o \qquad (12)$$

where $v_f = \frac{2v_f}{1+(v_{f/c})^2}$ denotes the projectile velocity.

Though this model will, due to the lack of kinetic energy of the compressed matter and due to the outflow of matter perpendicular to the collision axis (as compared to three dimensional calculations), give too large values for compression and temperatures as function of the bombarding energy, it is sufficiently good to give a rather quantitative overview about the expected compression and thermal excitation. The influence of the beam energy and the nuclear equation of state (e.g. different compressibility constants) and the importance of resonance and pion production on the collision dynamics can be studied rather nicely at very low cost - the integration of the full three dimensional fluid model actually is not yet possible with the inclusion of resonances. The results of this model calculations are presented in section 7.

4. THE NUCLEAR EQUATION OF STATE

Usually one starts with the energy per nucleon $W(\rho,T)$ for which we use the ansatz

$$W(\rho,T) = M_o c^2 + E_c(\rho) + E_T(\rho,T) \qquad (1)$$

for purely nucleonic fluid. Here $M_o c^2$ is the nucleon's rest energy, $E_c(\rho,T=0)$ phenomenologically reflects the nuclear binding energy, the Fermi energy, the hard (soft) core and the exchange parts of the nuclear forces. For $E_c(\rho)$ one usually uses a power expansion in the density as obtained in nuclear matter calculations. We will use a parabolic expansion known from the extended liquid drop model (Scheid, 1969)

$$E_c(\rho) = \frac{K_o}{18 \rho_o} (\rho - \rho_o)^2 + B_o \qquad (2)$$

where $B_o = -16$ MeV and $K_o = 200$ MeV is the nuclear compression constant.

Secondary minima (density isomers) are represented by a similar ansatz with different ρ_1, K_1, B_1. For the thermal energy, the simplest ansatz is the classical ideal gas $E_T = 3/2\ T$. (See Fig. 4).

We will also use the Fermigas expansion

$$E_T(\rho,T) = \frac{a}{2} \rho^{-2/3} T^2 = \frac{\sigma^2}{2a} \rho^{2/3} = E_T(\rho,\sigma) \qquad (3)$$

where we used the standard thermodynamical relations

$$T = \frac{\partial W}{\partial \sigma}\Big|_{\rho} = \frac{\sigma}{\beta}\ \rho^{2/3} \quad , \quad \beta = \left(\frac{g\pi}{6}\right)^{2/3}\ \frac{mc^2}{(\hbar c)} \quad , \tag{4}$$

σ being the nucleon's specific entropy.

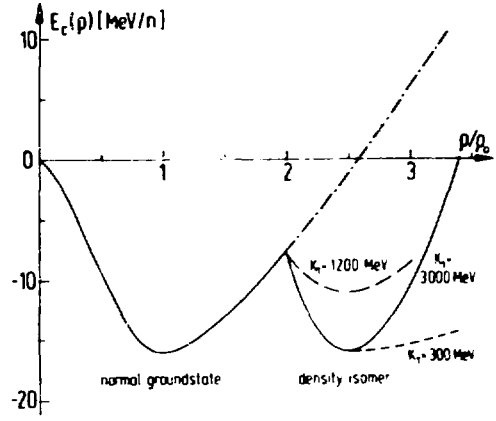

Fig. 4 The compression energy with the various possibilities for a density isomer is shown.

At high temperatures, the production of resonances becomes important (Hofmann, 1976). The resonance excitation is treated thermodynamically, where the following approximations have been used. As practically nothing is known about the nucleon - N^* and N^* - N^* interactions, we assume that the N^* interaction does also only depend on the total baryon density. Therefore the compression energy $E_c(\rho)$ is unchanged, ρ being now the baryon number density. The first difference is the thermal excitation energy of the isobars. Using the free Fermi gas expansion as above the thermal energy of a resonance with mass $m_i c^2$ is given by

$$E_{T_i} = \frac{1}{2}\,\beta_i\ \rho_i^{-2/3}\ T^2 \tag{5}$$

where

$$\beta_i = (\tau_i/6^{\pi})^{2/3}\ \frac{m_i c^2}{\hbar c}$$

and ρ_i is the density of the i-th resonance phase.

The resonances can be viewed as excited nucleons (resonance pair production is not important at the above temperatures). A Boltzmann distribution for the excitation probability of the i-th resonance has been assumed. Ensuring baryon number conservation, one obtains the partitions

$$\lambda_i = \frac{\tau_i\ e^{E_{i/T}}}{\Sigma\ \tau_k\ e^{-E_k/T}} \tag{6}$$

where $$\lambda_i = \frac{g_i}{g_n} = \frac{(2\ \text{Spin}\ (i) + 1) \cdot (2\ \text{Isospin}\ (i)+1)}{4}$$

is the statistical weight factor of the i-th resonance, and $E_i = (m_i - m_o)\, c^2$ is the energy necessary for the resonance excitation.

The density of the i-th phase is then given by

$$\rho_i = \lambda_i \rho \tag{7}$$

and the total energy density $e = \rho W$ is given as the sum over the energy densities of all phases

$$e = \sum_i e_i = \sum_i \rho_i W_i . \tag{8}$$

As all baryons are assumed to interact only via $E_c(\rho)$, the energy per resonance i is

$$W_i = m_i c^2 + E_c + E_{T_i} \tag{9}$$

which corresponds to a mean energy per nucleon

$$W(\rho,T) = m_o c^2 + E_c + \sum_i \lambda_i (E_{T_i} + E_i) \tag{10}$$

where the mean thermal energy per baryon is

$$E_T = \sum_i \lambda_i E_{T_i} \tag{11}$$

and

$$\Delta M c^2 = \sum_i \lambda_i E_i \tag{12}$$

is the mean additional rest mass due to the occupation of the resonances with $m_i > m_o$. The inclusion of a free pion gas (Stöcker,1978) with energy

$$E_\pi = \frac{g_\pi}{e^{\frac{m_\pi c^2 - \mu_\pi}{T}} - 1} \cdot m_\pi c^2 + \frac{4\pi\, g_\pi}{(hc)^3 (2\pi)^3} V \int_{m_\pi c^2}^{\infty} \frac{d\epsilon\, \epsilon^2 \sqrt{\epsilon^2 - m^2}}{e^{\frac{\epsilon - \mu}{T}} - 1} \tag{13}$$

is of little importance at lower temperatures because most of the pions stem from the decay of the Δ resonance only. The direct production of pions due to thermal nucleon-nucleon collisions has also been studied, but will be reported elsewhere (Stöcker,1979a).

The pressure is evaluated from the relation

$$p = -\left(\frac{\partial E}{\partial V}\right)_s = \rho^2 \left.\frac{\partial W(\rho,T)}{\partial \rho}\right|_s . \tag{14}$$

Taking the pure nucleon gas only, we immediately obtain

$$p = p_c + p_T = \rho^2 \frac{dE_c}{d\rho} + \rho^2 \frac{\partial E_T(\rho,\sigma)}{\partial \rho}\Big|_\sigma \quad . \tag{15}$$

For the compression energy we obtain the compression pressure

$$p_c = \frac{K_o}{18\rho_o} (\rho^2 - \rho_o^2) \quad . \tag{16}$$

The thermal pressure of the Fermi gas is given by

$$p_T = \frac{1}{3} B^{-1} \sigma^2 \rho^{5/3} = \frac{1}{3} B \rho^{1/3} T^2 \tag{17}$$

which leads to the relation

$$p_T = \frac{2}{3} \rho E_T \quad . \tag{18}$$

This relation, however, is not only valid for the low temperature limit, but also for the zero temperature Fermi gas and, non-relativistically, for any finite temperature. This relation is, in fact, also valid for a classical ideal gas as can be seen directly from $p V = N k T_k$ which is equivalent to $p = \rho \cdot T$ and with $E_T = 3/2 \; T$ one has $p = 2/3 \; \rho \; E_T$.

For an ultra-relativistic gas ($\varepsilon/m \gg 1$) the analogous relation $p_T = 1/3 \; \rho \; E_T$ holds again as well for a classical as a Fermi gas (even for $T_F = 0$). Therefore one has in this case $E_T = 3T$.

Knowing the pressure and the energy density $\varepsilon = \rho \, W$ we can calculate the sound velocity in nuclear matter

$$c_s/c = \left(\frac{\partial p}{\partial \varepsilon}\right)^{1/2}\Big|_\sigma \tag{19}$$

which for groundstate nuclear matter ($\rho = \rho_o$, $T = 0$) is connected directly to the compression constant (see Fig. 3)

$$K_o = 9 \rho_o^2 \frac{\partial^2 E_c}{\partial \rho^2}\Big|_{\rho_o} \tag{20}$$

via $$c_s/c = \left\{ \frac{K_o}{9W_o} \right\}^{1/2} \sim 0.1 - 0.2$$

5. PHASE TRANSITION OF NUCLEAR MATTER IN HIGH ENERGY HEAVY ION COLLISIONS

One of the most intriguing motivations for investigating relativistic heavy ion collisions is the possibility that phase transitions occur in highly dense nuclear matter, which eventually can lead to stable, abnormally dense nuclei called density isomers. A lot of theoretical investigations on this subject have been undertaken: Feenberg (1945) and Primakoff discussed the possibility of a transition of normal nuclear matter into a superdense "collapsed" tightly bound nucleus, with a total mass close to zero and therefore with enormous binding energies. They argued that this phase transition may occur due to strong nuclear tensor forces or short-range attractive many-body forces. The collapsed state should be separated from the normal ground state by a large potential barrier, which practically prevents the transition into the new state of matter. They also mentioned at first the possibility of collapsed transuranic (i.e. superheavy) nuclei, and briefly

discussed highly deformed states and very large spin states. 20 years later Ne'eman (1974) considered a similar effect: The existence of an attractive inner part in the hard-core nucleon-nucleon interaction may lead to the appearance of strongly bound dense nuclei.

Independently of both former ideas, Bodmer (1971) proposed to look for collapsed light nuclei with large baryon numbers, behaving like new elementary particles. He suggested that these objects may consist of a dense system of tightly bound quarks, so that a soft repulsive core might be responsible for their existence. A series of publications were initiated by Migdal (1972) when he proposed the formation of abnormal nuclear states due to pion condensation. Theoretically, the onset of pion condensation is often described as the decay of the Hartree-Fock ground state into ordered zero frequency (i.e. zero energy) particle-hole states carrying pionic quantum numbers. In the new phase at high density the ground state nuclear matter consists of nucleons forming a spin-isospin lattice (Irvine, 1975). This phenomenon may also be interpreted as a phase transition from the nuclear liquid to a nuclear spin-isospin crystal. Or in other words, the phase transition to the abnormal state takes place as a strong collective pion mode appearing above a critical density $\rho_c \gtrsim \rho_o$ with the pion field acquiring a finite ground state expectation value. The pion condensate leads to a lowering of the total energy per nucleon with respect to normal nuclear matter. This is due to the strong, attractive p-wave pion-nucleon interaction. Later on it was found that the inclusion of nuclear correlations and the effects of pion s-waves and $\Delta(3/2,3/2)$ interactions shifts the critical density ρ_c, at which the normal ground state of nuclear matter decays into the spin-isospin ordered system, to higher densities $\rho_c \gtrsim 1.5\ \rho_o$ (Migdal, 1972; Brown, 1975, 1976; Migdal, 1978).

It is very essential to note that the perturbation expansion and therefore the RPA approximation completely break down if the system undergoes a phase transition. We therefore propose a method which allows the possibility of a phase transition and which is capable of allowing calculations beyond the phase transition point. (Mattuck, 1968).

In the following we will use the effective particle-hole interaction of Migdal (Migdal, 1967):

$$\left(\frac{d\rho}{dc_F}\right)_{\rho=\rho_o} \qquad U = f_o + f_o' \vec{\tau}_1\cdot\vec{\tau}_2 + g_o \vec{\sigma}_1\cdot\vec{\sigma}_2 + g_o' \vec{\tau}_1\cdot\vec{\tau}_2 \vec{\sigma}_1\cdot\vec{\sigma}_2 \qquad (1)$$

In the momentum independent limit we use, this interaction corresponds to a zero range force in ordinary space. The constants f_o, f_o', g_o, g_o' can be calculated from elementary processes (π,ρ,ω ..... exchange). (Anastasio, 1977).

Furthermore we define the nucleon propagator as

$$G(\vec{1},\omega) = \frac{1}{4}\left[g(\vec{1},\omega) + \vec{\sigma}\cdot \vec{S}(\vec{1},\omega) + \vec{\tau}\cdot\vec{T}(\vec{1},\omega) + (\vec{\tau}\cdot\vec{T}(\vec{1},\omega))(\vec{\sigma}\cdot\vec{S}(\vec{1},\omega)) \right] \qquad (2)$$

where $g(\vec{1},\omega)$, $\vec{S}(\vec{1},\omega)$, $\vec{T}(\vec{1},\omega)$ are functions which have to be determined self-consistently from the Dyson equation

$$G(\vec{1},\omega) = \left[G_o^{-1} - \Sigma_{HF} \right]^{-1} \qquad (3)$$

where $G_o^{-1} = \omega - (\varepsilon_k - \mu) + i\delta$ is the free propagator with $\varepsilon_k = \frac{k^2}{2m}$ and the chemical potential μ. Σ_{HF} is the self-energy in Hartree-Fock approximation, i.e.

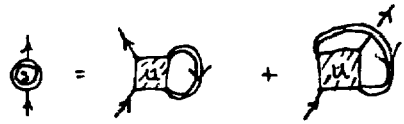

(4)

The direct part is given by

$$\Sigma_{dir} = -i \int \frac{d^3 \vec{l}}{(2\pi)^3} \frac{d\omega}{2\pi} \, tr \, [U \, G \, (\vec{l},\omega)] \, e^{-i\omega o^-} \tag{5}$$

It has to be stressed at this point that denotes the full propagator which is a matrix in spin-isospin space; it has diagonal elements which do not change spin or isospin but in addition has off-diagonal elements which describe spin or isospin flip. The off-diagonal elements vanish in the normal phase and are non-zero after the phase transition. This is the reason why the HF approximation does not break down in the condensed phase in our method.

As the observables e.g. ρ (particle density) and $\vec{I}$ (spin density) are given by

$$\begin{aligned} \rho &= -i \int \frac{d^3\vec{k}}{(2\pi)^3} \frac{d\omega}{2\pi} \, tr \, [\, G(\vec{k},\omega)] \, e^{-i\omega o^-} \\ \vec{I} &= -i \int \frac{d^3\vec{k}}{(2\pi)^3} \frac{d\omega}{2\pi} \, tr \, [\, \vec{\sigma} G(\vec{k},\omega)] \, e^{-i\omega o^-} \end{aligned} \tag{6}$$

and

$$\begin{aligned} \vec{t} &= -i \int \frac{d^2\vec{k}}{(2\pi)^3} \frac{d\omega}{2\omega} \, tr \, [\vec{\tau} G(\vec{k},\omega)] \, e^{-i\omega o^-} \\ P_{ik} &= -i \int \frac{d^3\vec{k}}{(2\pi)^3} \frac{d\omega}{2\pi} \, tr \, [\tau_i \sigma_k \, G(\vec{k},\omega)] \, e^{-i\omega o^-} \end{aligned} \tag{7}$$

the total self-energy (direct and exchange) is

$$\Sigma_{HF} = F_1 \rho + F_2 \sigma^i I_i + F_3 \tau^i t_i + F_4 \tau^i \sigma^k P_{ik} \tag{8}$$

where

$$\begin{aligned} F_1 &= \tfrac{1}{4} [3 f_o - f'_o - g_o - g'_o] \\ F_2 &= \tfrac{1}{4} [5 g_o - f_o - f'_o - g'_o] \\ F_3 &= \tfrac{i}{4} [5 f'_o - f_o - g_o + g'_o] \\ F_4 &= \tfrac{1}{4} [3 g'_o - f_o + f'_o + g_o] \end{aligned} \tag{9}$$

As we are mainly interested in the spin-isospin degree of freedom, we disregard for the moment the spin-spin and isospin-isospin part in Σ_{HF}. If we no insert Σ_{HF} into the Dyson equation we can easily solve for the unknown functions

$$\vec{g}(1,\omega) = \frac{4F}{(F - F_4\, p)(F + F_4\, p)} \tag{10}$$

and

$$P(1,\omega) = \frac{4F_4}{(F - F_4\, p)(F + F_4\, p)} \tag{11}$$

where p is the only non-vanishing component (after rotation in spin-isospin space) of the tensor p_{jk} and $F = \omega - (\epsilon_K - \mu) + i\delta - F_1 N$. With $\tilde{\alpha} = 3f_o - f_o' - g_o - g_o'$ and $\tilde{\beta} = f_o - f_o' - g_o - 3g_o'$, $g(\vec{1},\omega)$ and $P(1,\omega)$ can be integrated with respect to $\vec{1}$, yielding after elimination of μ by means of particle number vonservation the self-consistent equation for the spin-isospin magnetization $M = p/N$

$$\frac{\beta\, \rho}{2\epsilon_F} = \frac{1}{M}\left[(1+M)^{2/3} - (1-M)^{2/3}\right] \tag{12}$$

with $\beta = \tilde{\beta}\,(\frac{d\epsilon_F}{d\rho})_{\rho=\rho_o}$ so that the actual density dependence of the left side is

$$\frac{\beta\, \rho}{2\epsilon_F} = \frac{1}{3}\,\tilde{\beta}\,(\frac{\rho}{\rho_o})^{1/3} \tag{13}$$

where $\tilde{\beta}$ is density independent.

Different magnetization curves are shown in Fig. 5. To decide whether the condensed state $M = 0$ yields lower energy than the normal state $M = 0$ we calculate the

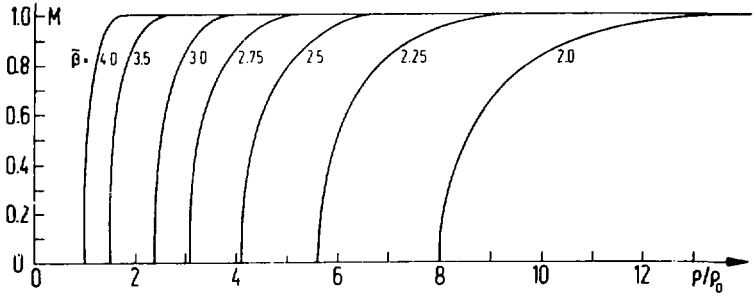

Fig. 5. The density dependence of the spin-isospin magnetization for different values of $\tilde{\beta}$ is depicted.

energy per particle as

$$\frac{E}{N\epsilon_F} = \frac{3}{10}\left[(1+M)^{5/3} + (1-M)^{5/3}\right] + \frac{1}{4}\left[\frac{\alpha\,\rho}{2\epsilon_F} - \frac{\beta\,\rho}{2\epsilon_F}\,M^2\right] \qquad (14)$$

To get lower energy we see that $\beta > 0$ is required. In Fig. 6 we show the actual condensation energy for different values of β. As we neglect spin-spin and isospin-isospin interactions β is essentially given by $\beta = f_o - 3g'_o$. As for normal nuclei ($\rho = \rho_o$) $f_o \approx 1$ and $g'_o \sim 0.7$ there is certainly no phase transition. Nevertheless the momentum dependence of the pion-nucleon interaction induces a renormalization (Migdal, 1978) of g'_o yielding values from $\beta \sim 2$ to $\beta \sim 4$. This momentum dependence induces a periodic magnetization instead of a spatially constant one, i.e. we recover the structure of the pion condensate as a spin-isospin lattice. To decide whether there is really a second minimum in the energy per particle as function of ρ we need the E/A (ρ) curve for the normal nuclear state in order to add the condensation energy. Several results are shown in Fig. 7. For

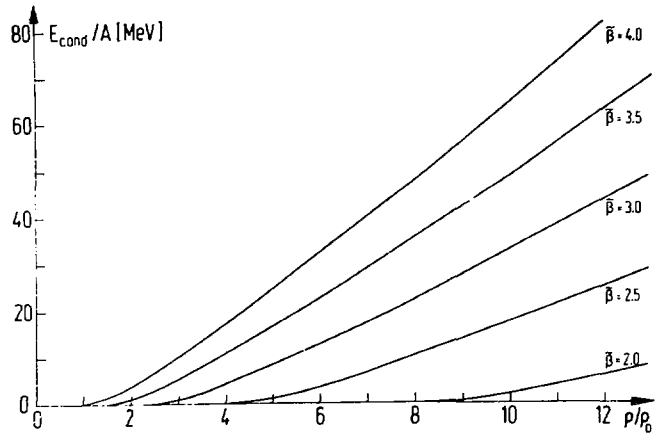

Fig. 6. The condensation energy as function of the density for different values of $\bar{\beta}$.

reasonable values of $\bar{\beta} \sim (2\text{-}4)$ an extreme softening of the equation of state can be observed. At least a van der Waals type of behaviour can be seen, yielding a minimum of the pressure as function of ρ. If the phase transition occurs at rather low density ($\rho/\rho_o \sim 1.5$) a rather broad second minimum may occur allowing extremely high compression of nuclear matter. At reasonable value of $\bar{\beta} \sim 3$ we observe a density isomer at about $\rho/\rho_o \sim 5\text{-}6$ with absolute binding energy of E/A ~ -13 MeV (Fig. 8). The phase transition actually starts at $\rho/\rho_o \sim 2.8$ even lower than the barrier maximum at about -10 MeV. Finally we may summarize that a proper treatment of the spin-isospin phase transition in the framework of the Landau-Migdal Fermi-liquid theory yields a density isomeric state at moderate densities of about $2 \leq \rho/\rho_o \leq 6$ with an energy gain of 20-40 MeV per nucleon. At this low densities the phase transition region (from ρ_{cr}/ρ_o to $\rho(M=1)/\rho_o$ (see Fig. 9)) is rather narrow, so that the condensation can be achieved in a time which is

short compared to the collision time.

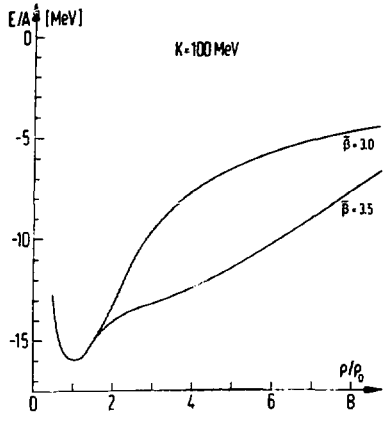

Fig. 7. The nuclear equation of state with spin-isospin condensation shows an extreme flattening at higher densities.

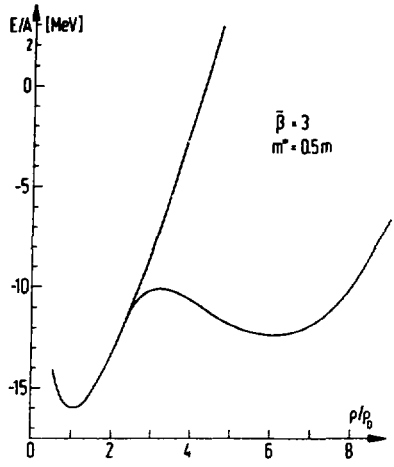

Fig. 8. The equation of state develops a second minimum for an effective nucleon mass $m^* = 0.5\ m$.

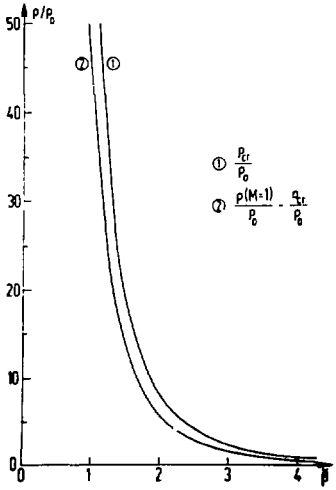

Fig. 9. The critical density and the width of the phase transition are shown as function of $\tilde{\beta}$.

The only possibility to reach such high densities in the lab seems to be violent collisions of heavy ions. This raises the question, whether the high nuclear excitations one expects for these collisions will destroy the ordering effect of this pion condensate. This has been investigated by Ruck, Gyulassy and Greiner. They found that finite size and short time scale are sufficient to allow for pion condensation (Ruck,1976) Gyulassy and Greiner (1977) modified the p-wave part of the pion polarization operator to include the nuclear temperature by a smeared out Fermi distribution of the nucleons (see also the later treatment of Weise and Hecking,1979). They find that the density dependent critical temperature T_c, above which the thermal distributions destroy the ordered spin-isospin lattice lies substantially above that expected from hydrodynamic calculations (see Fig.10).

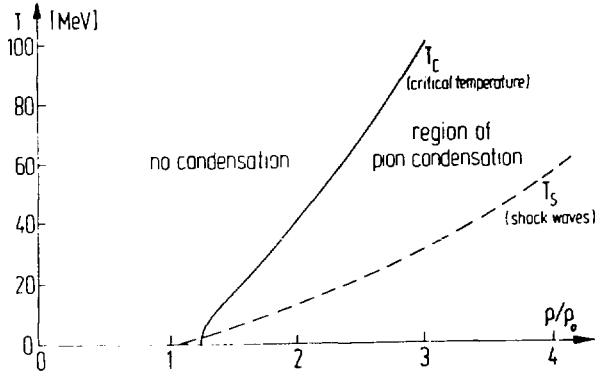

Fig. 10. The critical temperature T_c, above which pion-condensation does not occur. T_s indicates the temperature occurring in shock waves.

As the condensate occurs at finite momentum $k_c \sim 2m_\pi$, the critical distance $R_c \sim k_c^{-1}$ $\sim$ 1 fm. Thus a dense system of dimension $\gtrsim$ 2 fm could support a condensate. The relaxation time of the pion condensate can be estimated from $\tau_{cond}^{-1} = \max|2 \text{ Im } \omega|$, where ω is the complex zero of the pion propagator Δ_π in nuclear matter. This gives $\tau_{cond} \sim 1/5\ \tau_{coll}$ indicating that a condensate can develop during the collision time. The occurrence of a pion condensate is also connected with the critical scattering of nucleons at densities in the vicinity of the phase transition. In fact, the observed strong increase of the n-n scattering (see later) may also be used as an experimental signal for the onset of pion condensation.

Lee (1974) and Wick suggested within the σ-model Lagrangian field theory that the restoration of chiral symmetry can result in very small nucleon rest masses. The practically massless nucleons forming strongly bound nuclei with binding energies of 140-500 MeV/n, i.e. an order of magnitude larger binding effects than in normal nuclear matter. The ground state of this abnormal phase is expected at $\rho \gtrsim$ 2-5 ρ_0. The total energy of the abnormal nucleus consists of the nucleon kinetic energy and a potential energy term arising from the σ-meson field energy. In central collisions of e.g. two Uranium nuclei even the formation of superheavy superdense nuclei seems feasible.

Such an abnormal nucleus can have completely different properties from a normal nucleus: Due to the probably totally different mass defect the atomic mass will not be an integer number. Furthermore, a collapsed (superdense) superheavy nucleus will have interesting atomic properties. Fig. 11 shows the electronic binding energies of collapses superheavy nuclei as function of the nuclear density as calculated by J. Reinhardt. (Stöcker,1978a). One sees that for large Z the binding energ exceeds twice the electron rest mass - an empty electron state will then be filled by an electron from the Dirac Sea, accompanied by the production of positrons without expenditure of energy. This process manifests the spontaneous decay of the neutral vacuum into a charged vacuum. If in a fast nuclear collision collapsed superheavy nuclei are formed, the exotic atomic properties may help in the identification of long lived or even stable collapsed superheavy nuclei via the emission of high energy characteristic X-rays or - better - by searching for sharp resonances in the positron scattering cross section. These observations would yield precise information on the nuclear charge density of an abnormal nucleus.

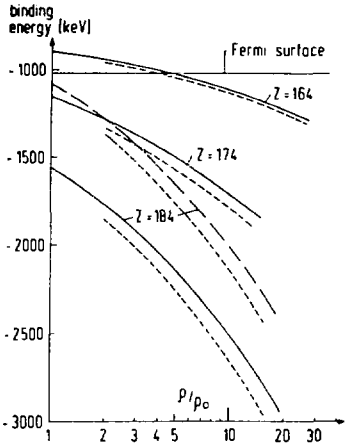

Fig. 11. The electronic binding energy as function of the nuclear density is shown.

6. QUARK MATTER AS A SPECIAL PHASE OF HADRONIC MATTER

The strong compression available in nuclear collisions at very high bombarding energies may serve as a tool to form a new form of matter: If the nuclear matter is so dense that the nucleons overlap strongly it is possible and may be energetically more favourable that not only the nuclei, but also the nucleons desintegrate.

When the nucleons dissolve into their constituents, the partons, which are believed to be quarks, the formation of a multi-quark object is feasible (Collins,1975; Baym,1976; Keister,1976). We will investigate the possible quark phase within the pheonomenological MIT-quark bag model: (Chodos,1974).

One can show that the simple model of a bag - which must be viewed as a volume in space, in which massless quarks move quasi-free - can fit the mass spectrum of

the light hadrons quantitatively quite convincingly, if the following conditions are fulfilled: a) The bag, i.e. the volume in which the quarks move, has a constant positive energy density, which therefore increases infinitely with the bag volume. This bag energy accounts for the quark confining potential, which does not allow the separation of single quarks from each other. b) The zero point motion has to be included for quarks which move within the small volume of a hadron. c) The energy of the quarks is included by solving the Dirac equation for a bound quark state inside the bag. d) Low-order terms in the quark-gluons coupling constant are additionally included to take into account the mutual interactions more realistically.

For our test calculations on the formation of a "Giant Quark Bag" we assumed that the bag energy density constant remains unchanged if the hadronic matter "fuses" into the Giant Quark Bag volume. We neglect the zero point motion, as the GQB is supposed to be much larger than a hadron bag. For the kinetic energy of the quarks we used the free, massless "ultra-relativistic" ($p = 1/\rho \;\; \rho \;\; E_T$) Fermigas model which for zero temperature yields

$$E_{F_Q} = \frac{3}{4} \left(\frac{6\pi^2}{g_Q} \right)^{1/3} \hbar c \;\; \rho_Q^{1/3} \quad . \tag{1}$$

From the quark Fermi energy, the Fermi pressure may easily ba calculated as $P_F = \rho^2 \left. \frac{\partial E}{\partial \rho} \right|_\sigma$ which yields

$$P_{F_Q} = \frac{1}{4} \left(\frac{6\pi^2}{g_Q} \right)^{1/3} \hbar c \;\; \rho_Q^{4/3} \quad . \tag{2}$$

Thus, the fermi energy and -pressure of the quark gas are related

$$P_{F_Q} = \frac{1}{3} \;\; \rho_Q \;\; E_Q \quad . \tag{3}$$

The latter relation does not only hold for T=0, but is actually valid for all temperatures. The interaction of the quarks can be calculated and leads to an effective $\lesssim 50\%$ rise of the density-dependent Fermi energy (Stöcker,1977).

The density-dependent ground state energy of the Giant Quark Bag is then given by

$$E_{BAG} = \sum_Q \left(\frac{B}{\rho_Q} + \frac{3}{4} \left(\frac{6\pi^2}{g_Q} \right)^{1/3} \text{hc} \; (1+\alpha_c) \rho_Q^{1/3} \right). \tag{4}$$

E_{BAG} is depicted in Fig. 12. It is shown, that near the normal ground state of nuclear matter, with the parameters used by Chodos(1974) et al. the GQB energy is approximately $\lesssim 300$ MeV/n above the nuclear matter curve;here we used B = 56 MeV and $\alpha_c = 0.5$. The statical factor g_Q for a quark gas with spin, flavour and colour ($g_Q = 12$) was used. However, for smaller B and α_c, this difference is much smaller and the Quark energy may be lower than that of nuclear matter, already at rather moderate densities, if a rather stiff, i.e. quadratic compression interaction is used for the nucleons.

In our investigation we have up to now not taken into account the density dependence of α_c (Freedman,1978).

$$\alpha_c(k) = \frac{12\pi}{33-2n_f} \;\; \frac{1}{\ln (k^2/\Lambda^2)} \quad .$$

If we replace $k \to k_F$ we induce a density dependence

$$\alpha_c(\rho) = \frac{12\pi}{33-2n_f} \cdot \frac{1}{\ln\left[\left(\frac{6\pi^2}{g}\right)^{2/3} \frac{(\hbar c)^2}{\Lambda^2}\, \rho^{2/3}\right]}$$

i.e. $\alpha_c \to 0$ if $\rho \to \infty$. Detailed calculations by Freedman (1978) et al. show, that $\alpha_c \sim 0.5$ at low baryon densities and $\alpha_c \sim 0.1$ already at $\rho_{nuc} \sim 6\ \rho_o$. We therefore expect to be on the $\alpha_c = 0$ curve at high densities. This density dependence of α_c lowers the phase transision point considerably.

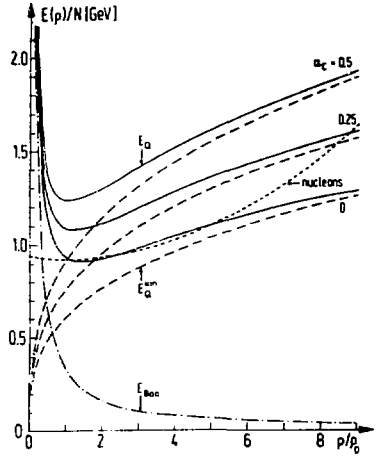

Fig. 12. The energy per nucleon for a quark gas is shown for a bag constant B = 56 MeV and different values of α_c. The nuclear equation of state is shown (dashed curve).

The quark matter equation of state can be put into the relativistic shock equation (3.8) to yield the thermodynamic variables for a dense quark gas when it is formed in a relativistic heavy ion collision.

To solve the relativistic shock equations, the free enthalpy and pressure

$$I = \rho E_F + B + p \tag{5}$$

$$p = p_F - B \tag{6}$$

have to be inserted into equation (3.8), where remaining "undissolved" nucleons are neglected. Then the following equation is obtained:

$$E_F^2 - W_o^2 + p_F \left(\frac{E_F}{\rho} - \frac{W_o}{\rho_o}\right) + B\left(\frac{W_o}{\rho_o} + \frac{E_F}{\rho} + \frac{p_F}{\rho^2}\right) = 0 \quad . \tag{7}$$

Here the last part gives the influence of the Bag itself. Using $p_F = \frac{1}{3} E_F$ for the quark gas, eq. (7) can be solved analytically to yield

$$E_{cm} = \frac{1}{2}\left(\frac{1}{4} W_o \rho/\rho_o + B/\rho + \left(\left(\frac{7}{4} W_o \rho/\rho_o - B/\rho\right)^2 - 3 W_o\left((\rho/\rho_o)^2 - 1\right)\right)^{1/2}\right) \quad (8)$$

From this equation the quark density within the compression zone is obtained as function of the bombarding energy (see Fig. 13). For B=0 this equation reduces to

$$\frac{E_{cm}}{W_o} = \frac{1}{2}\left(\frac{1}{4} \rho/\rho_o + \sqrt{3 + \frac{1}{16}(\rho/\rho_o)^2}\right) \quad (9)$$

These results are also applicable for e.g. Lee-Wick matter and prescribe the upper limit of the compression in the ultra-relativistic regime.

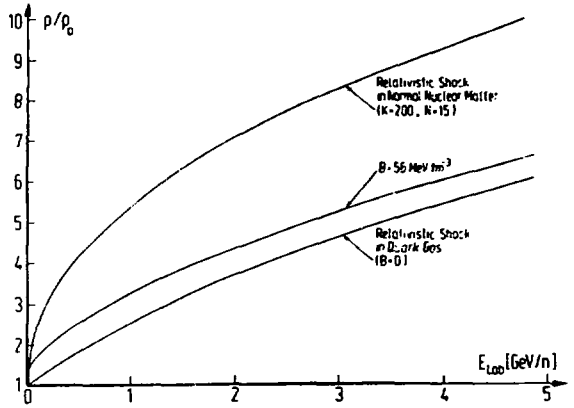

Fig. 13. The actual density achieved in a shock wave in quark matter as function of the bombarding energy.

Due to the large Fermi pressure of the quark gas, its compression increases much slower with the bombarding energy than in the case of nuclear matter. The large ground state energy of the GQB could be responsible for another effect: If at high bombarding energy the nucleons desintegrate and a GQB is formed, the excitation energy of the system mostly has to go into the quark Fermi energy, which can reduce the temperature of the system considerably. Also the distribution of the residual thermal energy over three times as many degrees of freedom will lower the temperature.

In a three-dimensional hydrodynamical test calculation we found that the quark matter is only transiently produced in the collisions of fast nuclei for a very short

time. However, it is possible that part of the quark matter does not immediately recondensate into hadronic matter, but stays within the quark phase for a longer time. This piece of quark matter then expands freely into the state of minimum energy at ρ_{o_Q} . The expansion will approximately follow curves of constant entropy, for which

$$p \cdot V^{4/3} = \text{const and } E \sim \rho^{1/3} \quad \text{(for all T!)} . \tag{10}$$

Such a metastable GQB would have a ground state density different from the nuclear equilibrium density. It can decay by the sudden release of a large amount of energy (~ 300 MeV/n) into a bulk of normal hadronic matter, hopefully a considerable time after the collision: This may open a way of detecting GQB's. The resulting "hadronic nucleus" may have a rather unique structure, e.g. consisting of many resonances.

Furtheron it seems worthwhile to investigate the possibility of condenstion phenomena due to the colour degrees of freedom of the quarks, which mediate a colour quark-quark interaction.

This colour interaction may be written as (Dalitz,1976)

$$U = f(k) \sum_{i=1}^{8} \lambda^i \lambda^i$$

where $$f(k) = 4\pi \alpha_c(k) \frac{1}{k^2}$$

with $$\alpha_c(k) = \frac{12\pi}{33-2n_f} \frac{1}{\ln(k^2/\Lambda^2)}$$

which is the QCD fine-structure constant and n_f = is the number of light flavours. The definite structure of $\alpha_c(k)$ as function of the momentum k is only vaguely known from renormalization group arguments: (Freedman,1978)for $k \to \infty$ it is expected that $\alpha_c \to 0$ (asymptotic freedom at high densities). At low densities α_c should become large (non-perturbative region of colour confinement).

The expression for $\alpha_c(\ )$ given above fits the large k region quite well. The cut-off parameter has been determined from charmonium data to be of the order of $\Lambda \sim$ 300-500 MeV (Richardson,1979). As we treat the quarks in Fermi gas approximation, we replace k by the Fermi momentum k_F thus inducing a density dependent interaction. This corresponds to the assumption that the medium screens the long range quark-quark interaction as in the case of an electron gas.

With the quark propagator

$$G(k,\omega) = \frac{1}{3} [g(k,\omega) + \lambda^i \lambda_i(k,\omega)]$$

we calculate the Hartree-Fock self-energy

$$\Sigma_{HF} = \frac{2}{g} f \rho - \frac{1}{3} f \ d_{iik} C^k$$

$$- \frac{1}{2} [- \frac{4}{3} f \ Cm + \frac{2}{3} f \ d_{iim} \rho$$

$$+ f \ (if_{ikj} + d_{ikj})(if_{jim} + d_{jim}) \ C^k \ ]\lambda^m \ .$$

where f_{ijk} and d_{ikj} are the $SU_c(3)$ structure constants and $C^k(k=1,\ldots,8)$ is the integrated colour density

$$C_k = \frac{2}{3} i \int \frac{d^3k}{(2\pi)^3} \quad \frac{d}{2\pi} \Lambda_k (k,\omega) e^{-i\omega 0^-} \quad .$$

As the colour group $SU_c(3)$ allows to select two diagonal generators e.g. λ_3 and λ_8 (which we call in the following colour-isospin and colour-hypercharge) we investigate e.g. colour condensation in the λ_8-direction. Furthermore we assume the quarks to be massless and treat them as relativistic Fermi gas i.e.

$\varepsilon_F = k_F = (\frac{6\pi^2}{g})^{1/3} \rho^{1/3}$ where g is the factor of statistical degeneracy g=12.

Applying now the method developed in the nuclear context we find the self-consistent equation for the colour magnetization by solving the Dyson equation. For the colour-hypercharge magnetization we find with $F_1 = 1/6 - 3) f$ and $M_8 = (1/2)\ 3\ C_8/\rho$

$$\frac{F_1 \rho}{\varepsilon_F} = \frac{1}{M_8} \quad (1 + \frac{M_8}{2})^{1/3} - (1 - M_8)^{1/3}$$

and the energy

$$\frac{E}{\varepsilon_F N} = \frac{1}{4} [\ 2(1 + \frac{M_8}{2})^{4/3} - (1-M_8)^{4/3}\ ] - \frac{1}{9} \frac{f\rho}{\varepsilon_F} - \frac{1}{6} \frac{F_1 \rho}{\varepsilon_F} M^2 \ .$$

Expanding $(1 \pm M)^{1/3}$ we find the phase transition point as

$$\frac{F_1 \rho}{\varepsilon_F} = \frac{1}{2} \quad .$$

As can be seen from the energy, there is an energy gain through condensation only if $F_1 > 0$, i.e.

$$F_1 = (\frac{1}{6} - 3) 4\pi \alpha_c (k_F) \frac{1}{k_F^2} > 0 \quad .$$

We therefore find that there is no net colour magnitization as long as

$$\alpha_c(k_F) > 0 \quad .$$

Our present knowledge (Freedman,1978) from QCD says that $\alpha_c(k)>0$ at all k. Therefore there should be no phase transition at all. Nevertheless it is well known, that the phase transition from a nucleon gas to a quark gas is very broad with the coexistence of a nucleon and a quark phase. Therefore there may be many-body effects changing $\alpha_c(k)$ to an effective $\alpha_c^{eff}(k)$ during this percolation phase. This $\alpha_c^{eff}(k)$ may have negative domains, thus accomplishing colour condensation. As

$$\frac{F_1 \rho}{\varepsilon_F} \simeq 4 \alpha_c^{eff}(k)$$

already $\alpha_c^{eff} = -\frac{1}{8}$ is sufficient for the colour phase transition to take place. This type of intermediate colour condensate will enhance the nucleon-quark phase transition due to the condensation energy gain, which is (in the condensed region)

$$\frac{E_{cond.}}{Nucleon} = \tilde{\alpha} \left(\frac{\rho}{\rho_o} \right)^{1/3}$$

with $\tilde{\alpha}$= 73 MeV for α_c^{eff} = -0.3. Therefore the nucleon-quark phase transition region at about $5\rho_o$ the actual condensation energy gain is of the order of 125 MeV. We therefore conclude that a phase transition from nucleon to quark matter at densities lower than predicted by bag calculations may be a hint for condensation pheneomena pointing out a deviation from standard QCD. At the phase transition point we expect the well known critical scattering phenomenon (Gyulassy,1977): The scattering cross section is drastically enhanced. This point needs further investigation in the context of quark matter.

THE COMPRESSION AND EXCITATION EXPECTED FROM NUCLEAR SHOCK WAVE CALCULATIONS FOR HIGH ENERGY HEAVY ION COLLISIONS

Let us first look for the results of the one dimensional shock calculations of head-on collisions of equal nuclei, which allow the study of the influence of various parameters of the nuclear equation of state on the reaction, mainly on the compression rates and temperatures reached, but also the shock and flow velocities and on the production of pions and nuclear resonances (Baumgardt,1975; Stöcker, 1978). The compression rate in the rest frame of the compressed matter is shown in Fig. 14. It is found that the compressibility constant is of importance for the compression of the lower energies, where a stiffer equation of state (i.e. larger K-values) results in lower compression. For very high energies, we can neglect the compression energy completely and derive an analytic expression for the asymptotic behaviour of (ρ/ρ_o) asymptotic (E_{LAB}). For an ideal gas $p = 2/3\ \rho\ E_T$ the shock equations reduce to

$$\rho/\rho_o = \frac{1}{2} \left(5 \left(\frac{\gamma_{L+1}}{2} \right)^{1/2} + 3 \right) \qquad (1)$$

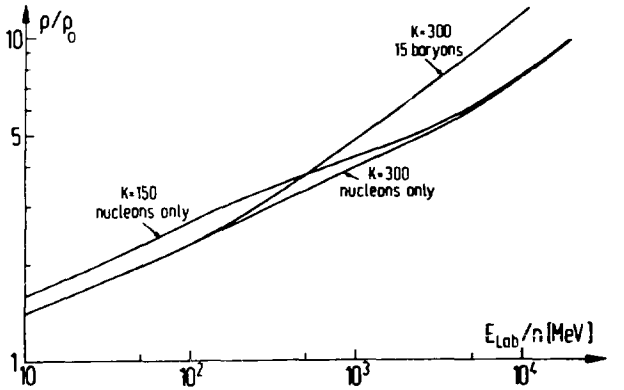

Fig. 14. The compression reached in the rest frame of the compressed matter is shown.

where $\gamma_L = \frac{E_{LAB}}{W_o} + 1$. Therefore, in the relativistic domain, the rest frame compression is not limited to $\rho/\rho_o = 4$ (this was wrongly assumed by various authors (Sobel,1975)) as in the non-relativistic limit ($\gamma_L \simeq 1$), but increases with the square root of the bombarding energy. $\rho/\rho_o = 4$ is reached at $E_{LAB} \simeq 1$ GeV/n, i.e. just where relativistic phenomena become important.

In the ultra-relativistic limit $\gamma \gg 1$, $p = \frac{1}{3}\rho E_T$ one obtains

$$\rho/\rho_o = 4 \cdot \left(\frac{\gamma_L + 1}{2}\right)^{1/2} = 4\ \gamma_{CM} \qquad (2)$$

At the very high energies, the influence of the nucleon resonances dominates. Owing to the increased number of degrees of freedom, the equation of state is softer and therefore higher compression is possible.

Like the compression, the temperature achievable also depends strongly on the nuclear equation of state used. (See Fig. 2). A lower compression constant increases the temperature, as less energy is needed for compression. On the other hand, the inclusion of nucleon isobars decreases the temperature considerably, as the internal excitation goes into the formation of heavy resonances, which means the transformation of thermal energy into additional rest mass. This cooling pheonomenon is what leads to a maximal temperature T^{MAX} in connection with an exponentially increasing hadronic mass spectrum (see later). However, the resonances become important only at densities $\rho/\rho_o \simeq 3$, reached only at relatively high energies. Therefore, the inclusion of resonances is important in the relativistic regime, but may be neglected for moderate energies $E_{LAB} < 400$ MeV/n. At such energies, the feedback of the N^* formation on the system is small and one may consider the $\Delta(3/2,3/2)$ resonance only. In this case the temperature may be calculated for the simple one-phase nucleon gas and from there the resonance excitation can be obtained as in a perturbational treatment. N_Δ/N is then given by the simple formula

$$N_\Delta/N \approx \tau_\Delta\ e^{-E_\Delta/T} = 4\ e^{-\frac{293}{T}} . \qquad (3)$$

We find that thermal pion production is very small for $E_{LAB} \lesssim 400$ MeV/n. This means that copious pion production at low bombarding energies will strongly indicate an exotic phenomenon (see later). The importance of the equation of state for the temperatures attained is seen in Fig. 2, where the temperature obtained in a Fermi gas model is compared to that of a classical ideal gas $E_T = 3/2\ T$ at higher density, the deviations are very large. However, in a relativistic treatment, the Fermion temperature approaches the ideal gas limit for very high temperatures $T \gtrsim 200$ MeV, as then the Pauli principle can be neglected. Fig. 3 shows the influence of the compression constant on the shock velocity in nuclear matter as a function of the shock amplitude ρ/ρ_o in the matter's rest frame: The shock velocity increases with density and with the compression constant. For small amplitudes, the shock velocities tend to the sound velocity C_s/c, of the ground state, which of course is different for different values of K:

$$C_s/c = \left(\frac{\partial p}{\partial e}\right)^{1/2}_{\sigma=\text{const}} = \left(\frac{K}{9\ W_o}\right)^{1/2} \quad \text{for } \rho = \rho_o . \qquad (4)$$

For large amplitudes c_s tends to the velocity of light and the influence of K vanishes. If for the thermal pressure an equation of state (or the gas law) different from an ideal gas is used, i.e. for example $\alpha=1$ instead of $\alpha = 2/3$, $p_T = \rho E_T$ results. The higher internal pressure leads to a much faster increase of $v_s(\rho)$.

Pion Production

To calculate the total pion production rate, one sums over all pions emitted in the decay of the excited resonances and includes the production of the free pion gas. For the strongly compressed state, which is calculated in our model, the formation of temperature-free pions was negligibly small (an order of magnitude down) compared to the Δ-resonance. A comparison with several different model calculations (see Fig. 15) (e.g. pion bremsstrahlung calculation (Vasak,1979), independent nucleon-nucleon collsions (Bertsch,1977), thermal models (Chapline,1973;Heinz, 1978)) does,however, show qualitatively good agreement with the data (Fung,1978). Therefore more refined calculations will be called for interpreting more exclusive experiments. The emission of the pions from the initial, strongly compressed stage during the whole expansion stage, will also increase the number of free pions in the system which is proportional to the volume of the hot matter.

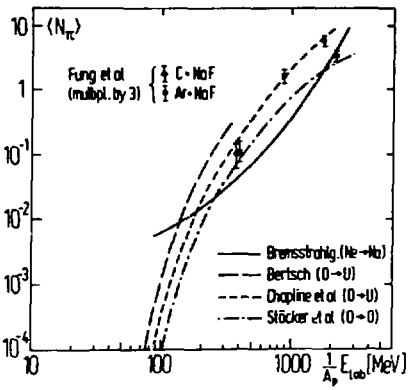

Fig.15. The number of pions produced in a heavy ion collision in different models (see text). Existing experimental results are indicated by points with error bars.

Dependence of the Particle Production on the Nuclear Equation of State.

Within the one-dimensional relativistic shock model, the dependence of the formation of isobars and pions on the nuclear binding energy functional may be investigated by iterative solution of eq.(4.16). In analogy to the influence on the temperature, also the pion production rate strongly reflects the properties density dependence of the compressional energy $E_c(\rho, T=0)$. A soft nuclear equation of state, i.e. small K values, leads to an increasing number of produced particles,as a larger fraction of the internal energy is available for thermal particle production. Thus, the measurement of the rate of increase of the particle production with the bombarding energy may be used to investigate the compression energy $E_c(\rho)$ and the compression constant

$$K_o = 9\,\rho_o^2 \left.\frac{\partial^2 E_c}{\partial \rho^2}\right|_{\rho=\rho_o} \quad \text{and sound velocity} \quad c_s/c = (K/_{9W_o})^{1/2} \qquad (5)$$

experimentally. One can also learn about the thermal properties of the nuclear fluid at high temperatures: Using the ansatz $E_T = 3/2\ T$ for an ideal classical gas yields a much faster increase of the shock temperature with the bombarding energy (see also the next sections).

Influence of the Formation of Abnormal Nuclear Matter on Shock Waves.

In the case that a phase transition into a secondary minimum would occur, these results are drastically changed (Hofmann,1979): Above a critical bombarding energy, the matter is compressed to the critical density ρ_c, at which the pressure does no longer increase with the density. If the pressure $p \sim \partial E_c/\partial \rho$ decreases with increasing density, the matter becomes unstable and collapses with no additional need for external compression into the abnormal superdense state. In the region of decreasing pressure no shock waves can be formed, $(v_s \sim p)$, i.e. the shock phenomena vanish for this region. This can be used as a signal to detect phase transitions experimentally, namely through the disappearance of Mach shock phenomena. It should be noted that this can be used also to detect inflection points in $E_c(\rho)$, where $p_c(\rho)$ decreases, while no secondary minimum is formed! It was shown by Hofmann(1979) that also an equilibrium coexistence of the normal and abnormal phases, which we excluded because of the short collision times we are considering, does not allow for a stable shock front in the phase transition region - nor for a double-shock as postulated by Galitski (1978).

Another effect of the phase transition is also very important: The collapse of the matter into the abnormal state leads to a sudden release of the condensation energy as additional excitation energy. Thus, a phase transition into a density isomeric state will be accompanied by a strong additional heating of the system, which can be used to observe density isomers in heavy ion collisions independent of the disappearance of Mach shock phenomena, namely by strong threshold increase in the excitation function of the particle production rate (pions, resonances, strange particles - see Fig. 16) and of the high energy tails of the particle spectra, which also reflect the temperature of the emitting source.

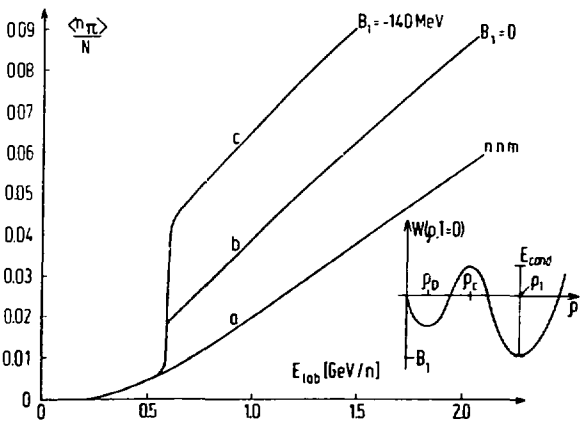

Fig. 16. The influence of a density isomer on the thermal pion production rate is shown.

Expansion and Explosion of the Highly Compressed Matter

The above increase should be observable also when the subsequent expansion of the matter is taken into account. Particles will be emitted during all stages of the reaction from the dense, hot piece of nuclear matter, and mainly from its surface. Two competing processes will lead to the decay of the compressed shock zone: First, the compressed matter will expand isentropically, i.e. with constant entropy. This will result in a collective flow of matter outwards, with the thermal energy per nucleon

$$E_T = \frac{\sigma^2}{2B} \rho^{2/3} \qquad (6)$$

and the temperature

$$T = \frac{\sigma}{B} \rho^{2/3} \qquad (7)$$

diminishing with decreasing density, and the kinetic energy per nucleon increasing because of the expansion $E^{kin} = E_{CM} - (E_T + E_c)$ (see Fig. 17). This process continues until the mean distance between the nucleons is too large to ensure thermal contact and equilibrium: The matter breaks then up into pieces. Possibly these break-up densities are reached at densities where the pressure has a minimum ($\rho/\rho_0 \approx 0.5$) which corresponds to a hydrodynamically unstable situation, where the dilute matter condensates into separate fragments.

In the case that abnormal superdense matter is formed, the system retains at larger temperature as compared to the normal matter case (see Fig. 18). As the isentropic curves show the barrier to the secondary minimum even at large temperatures, a trapping of the matter within the abnormal state is possible for a considerably long time. This is discussed in greater detail in the next sections. Secondly, also the possibility of a rapid explosion of the highly excited shock zone has to be taken into account. Since a considerable fraction of highly energetic particles moves faster than the collective outflow described by isotropic expansion, they can quickly escape from the surface of the shock zone.

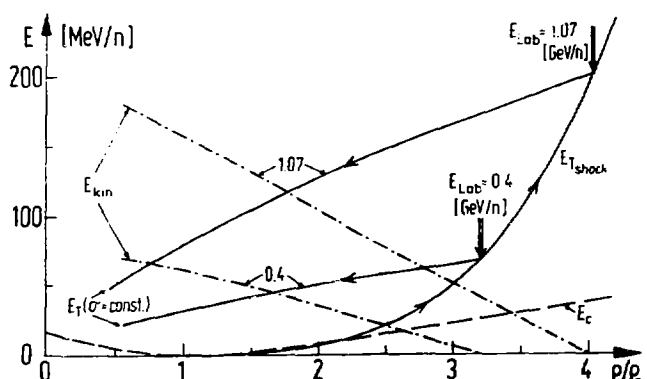

Fig. 17. The reaction kinematics for a heavy ion collision is shown as described in the text.

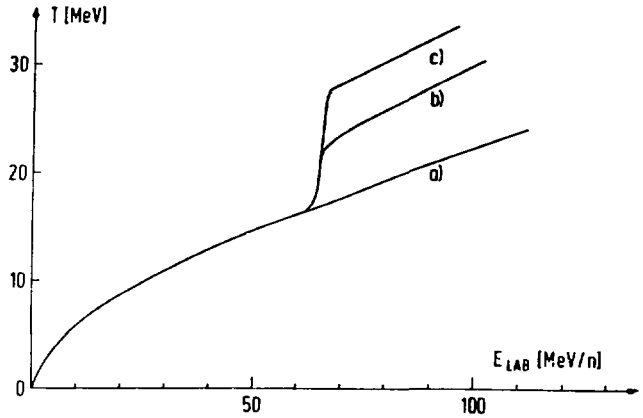

Fig. 18. The energy dependence of the temperature for a) normal nuclear matter, b) density isomer with $B_1 = 0$, c) $B_1 = -140$ MeV.

The vaporization of the surface of the compressed matter (shock zone) will lead to the emission of fast particles, which carry information about the - most interesting- state of highest compression and excitation. Therefore, special emphasis must be given to the observation of the highly energetic radiation components, mainly light, sidewards emitted fragments to learn about the initial compression stage of the reaction. The compressed zone is cooled down via particle radiation, thus slowing down the expansion of the system. The cooling effect, of strong enough, may stabilize an eventually formed abnormal nucleus.

We calculate the expansion of the highly excited matter assuming isentropic expansion of the whole system - the vaporization of the surface of the hot object is presently neglected. Let us, for the sake of simplicity, consider now a pure nucleon Fermigas. Then the thermal energy (6)

$$E_T = \frac{\sigma^2}{2B} \rho^{2/3}$$

for an isentropic expansion (σ= const. t) from the state of highest compression in the shock zone to the lower density can be easily calculated: Because of the expansion, the matter cools down as T, $E_T \sim \rho^{2/3}$. The internal energy $E^* = E_c + E_T$ - compression energy and random thermal motion - is transferred into kinetic energy, namely the directed collective outward flow of the system. Fig.17 shows E_T, E_c, and $E_{kin} = E_{CM} - (E_T + E_c)$ as functions of the density for two different bombarding energies $E_{LAB} = 0.4$ and 1.07 GeV/n. The state of highest compression is approached along the shock adiabate, the thermal energy increasing rapidly with the density. In the expansion stage, however, E_T decreases rather slowly with the density, while the kinetic energy of the collective outflow increases very fast, approximately as

$$E_{kin} = E_{CM} (1 - \rho/\rho_o) \qquad (8)$$

where ρ_o is the shock compression. The kinetic energy of the collective outflow is considerably larger than the internal random motion.
Let us now study the time development of the expansion of a homogeneous density distribution in the non-relativistic one-dimensional case, which can be solved

analytically: One can estimate the time dependence of the density which is in our case $\rho = N/R$ from equation (8)

$$\dot{R}(t) = V_{CM} \left(1 - \frac{R_s}{R(t)}\right)^{1/2} \tag{9}$$

where R_s is the radius of the system in the highly compressed state. Separation of variables and integration yields

$$\frac{1}{V_{cn}} \left\{ R \sqrt{R-R_o} + R_o \ln \left(R + \sqrt{R-R_o} \right) - R_o \ln \sqrt{R_o} \right\} = t \, . \tag{10}$$

Fig. 19 shows the compression- and expansion phase for various cases. One notices that a much lower compression than calculated in the shock model does end up in quite a similar final expansion as the shock calculation, only the initial stages are different (dashed line).

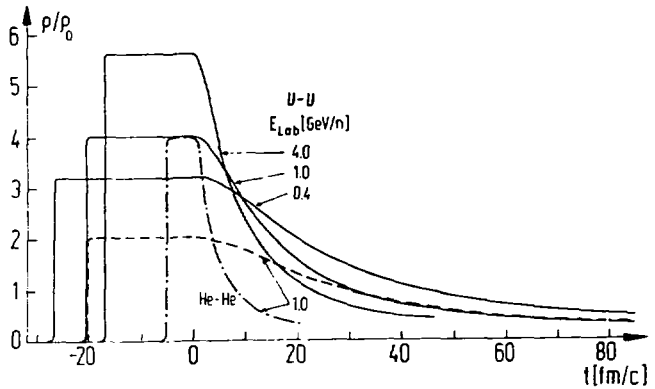

Fig. 19. shows the compression and expansion phase in non-relativistic one-dimensional model.

Another result is the much slower decrease of the density, when a lower bombarding energy is investigated. Finally, the decrease of the density proceeds much faster when collisions of small nuclei are investigated. Therefore, most interesting are central collisions of heavy nuclei, as here the system stays for the longest time in the highly compressed stage $\rho > 2\rho_o$, namely 47 and 36 fm/c for U-U collisions at 0.4 and 1.07 GeV/n. During such a long time, particles (e.g. pions) with v≈0.5 c can travel 24 and 18 fm respectively, much longer distances than they need to leave the highly compressed zone with R ≈ 8 fm. This means that one may even obtain information about the compressed center, when the high energy tails of the particle spectra are studied under 90° in the CM-frame: Here the central compression region can be seen without a shadowing effect from the residual projectile- and target nucleus.

Recently, such an experiment was performed by S. Nagamiya (1979) and collaborators in the bombardment of Na F with Ne-projectiles at various energies.

They measured the spectra of the particles (protons and pions) emitted at 90° in the CM frame. They find an exponential decrease of the particle spectra, from which the temperature of the highly compressed zone can be deduced. Fig. 20 shows the results of their measurements (dots). The solid line represents the shock temperature as obtained (without any fit) from the relativistic shock calculations. A remarkable agreement between the data and the theory is found; thus the experiment seems to indicate that the shock wave model implying strong compression and high excitation may be valid for the description of study theoretically central collisions of fast heavy nuclei. Furthermore, the experiment shows that it is necessary to use a Fermigas ansatz for $E_T(\rho,\sigma)$ - a calculation using a classical ideal nucleon gas with $E_T = 3/2\ T$ yields a linear increase of T(E), which strongly contradicts the experiment.

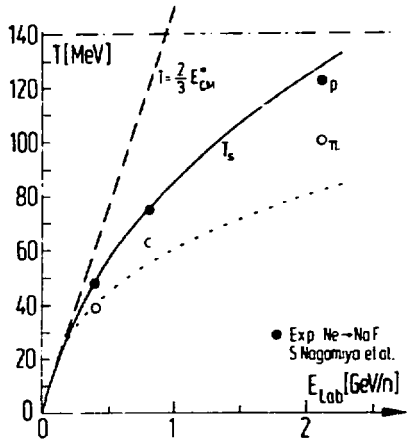

Fig. 20. The proton(full dots) and pion temparatures (open dots) ad deduced from the experiment of Nagamiya et al. compared to the shock calculations for pure nucleon gas (full curve) and including the resonance cooling (dashed curve).

However, the absolute value of the deduced temperature is surprisingly high - one would expect that the matter is cooler due to the resonance - and pion creation. If the curves of Nagamiya (1979) et al. are extrapolated to higher bombarding energies, the limiging temperature (Hagedorn,1965) $T^{Max} \simeq m_\pi c = 140$ MeV may be achieved already for $E_{LAB} \sim 3$ GeV/n, i.e. at heavy ion energies,which are presently only available at the synchro-phasotron in Dubna. The possibility of finding temperatures $T > T^{Max}$ is an exciting task for further experiments. According to

recent papers (Fowler and Weiner,1979; Kapusta,1979) the existence of quark matter would not allow for an exponential mass spectrum of elementary particles and thus a limiting temperature would not exist. Another important feature of the data of Nagamiya is the result that the temperature of the pions is systematically lower than that of the protons. The proton spectra may show up higher energies due to the hydrodynamical outflow of nucleons resulting in an apparently higher temperature. One may also speculate that they arise from a stage cooled because of higher compression energies or finite resonance production, or that the pions are not in a complete thermal equilibrium with the nucleons. Sandoval (1979), Stock, Schroeder and collaborators determined in a streamer chamber experiment the pion production rate in central collisions of Ar on KCl. They measured very large charged particle multiplicities (approximately the sum of the proton numbers of projectile and target) for E_{LAB} = 1-2 GeV/n. They find that the pion multiplicity $\langle m_\pi \rangle$ is of the order of 10-20 per cent of the nucleon multiplicity $\langle m_p \rangle$ increasing approximately linearly with the bombarding energy. Using the temperatures calculated on the basis of the relativistic shock equation, which coincide well with the temperatures measured by Nagamiya, we estimated the number of pions created considering Δ-resonance formation via

$$\frac{\langle m_\pi \rangle}{\langle m_N \rangle} \approx \tau_\Delta \, e^{-E_\Delta/T_s} = 4 \, e^{-E_\Delta/T_s}$$

where τ_Δ = 4 is the statistical factor of the Δ(3/2, 3/2) resonance. In Fig. 21 the data are compared to the calculations. The experimental data are again similar to the results of the shock calculations.

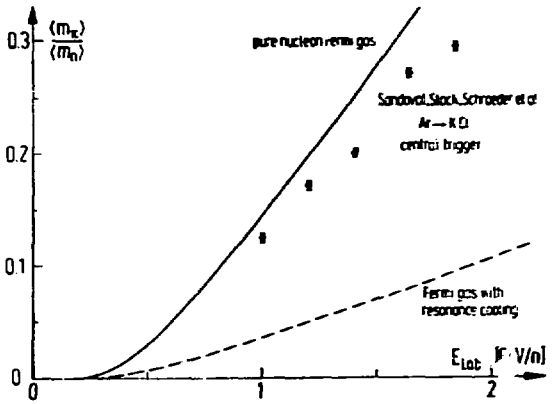

Fig. 21. The pion production rate $\langle m_\pi \rangle / \langle m_N \rangle$ as obtained in the experiment of Sandoval et al. (dots) compared to the shock calculation without resonance cooling (full curve) and including the resonance cooling (dashed curve)

However, again we would expect that the cooling influence of the resonance - and pion formation lowers the temperature, thus leading to a smaller pion production rate than experimentally observed, and to a lower increase of $\langle m_\pi \rangle / \langle m_p \rangle$ with the

bombarding energy (dashed curve). A full relativistic treatment of the resonance production can increase the pion multiplicity obtained in the shock calculation. However, the data point at 1.6 GeV/n is slightly above the straight line. If this result is not due to a statistical error, which cannot be excluded at the moment, an increase of $\langle m_\eta \rangle$ and a change of the slope $\langle m_\pi \rangle$ seems to appear at $E_{LAB} \sim 1.6$ GeV/n. This would be a very exciting result, as it would be interpreted as evidence for phase transition in dense nuclear matter at $\rho/\rho_o \approx 4\rho_o$. From the apparent jump in the temperature one may deduce the condensation energy of the density isomeric state (i.e., the depth of the secondary minimum in E_c as measured from the barrier at E_c (ρ_c)). However, as long as this effect has not been definitely proven by more extended and refined experiments with better statistics and measuring at the lower energies and in smaller energy bins, this remains speculation - which, nevertheless, may be stimulating also for the forthcoming experiments. In conclusion, already from these simple one-dimensional shock calculations it appears that one can learn about the reaction dynamics and the properties of the nuclear equation of state from high energy heavy ion collisions, if the relevent windows, uniquly reflecting the occurrence of interesting or exotic phenomena, are searched carefully.

The Importance of Nuclear Viscosity and Thermal Conductivity

Let us now turn away from the more schematic one-dimensional shock model to more refined nuclear fluid dynamical calculations: Though the solution of the relativistic shock equations allows for an overview of the phenomena and reasonably enables us to obtain values for the various variables considered, it is highly idealised and does not give an answer to the questions concerning the details of a nuclear reaction at high energies. This is only possible by solving the equations of motion for a non-ideal nuclear fluid numerically. The most important feature of a non-ideal fluid is the occurrence of viscous effects and thermal conductivity - therefore at least equations of the Navier-Stokes type have to be solved. A two and three-dimensional relativistic fluid dynamical model is presently under preparation by G. Buchwald, but not yet available. Therefore we concentrate on the influence of the viscosity in a one-dimensional fluid dynamical model. Within this model we can look somewhat deeper into the details of a heavy ion collision, e.g. study the time dependence of the compression and thermal excitation as well as the possibility of formation abnormal superdense states.

To solve the equations of motion - the non-relativistic Navier-Stokes equations in one dimension - we had to incorporate the nuclear potential and the friction tensor into the Euler equations. The Yukawa potential allows for a realistic treatment of the nuclear surface in that a smooth decrease of the density is obtained. For the friction tensor $\vec{S}$ a one dimensional Newtonian form $\vec{S} = -\eta(\vec{\nabla}\cdot\vec{v})^2$ is used. The friction constant is adjusted to $\eta = 10\ \hbar\ \mathrm{fm}^{-3}$, which ensures numerical energy conservation to $E/E_{KIN} \sim 10\%$. The most important advantage of the viscosity is to smooth the otherwise sharp shock fronts obtained in fast collisions to reasonable width. The formation of resonances and pions was not taken into account in these first calculations.

The integration of the equations of motion was done for various bombarding energies. Density isomeric states with different depths and critical densities were also investigated. For normal nuclear matter we first found a rapid increase of the compression rate in the center of mass, followed by a rather stationary stage of constant compression (corresponding to the shock wave model) - and subsequent expansion stage (see Fig. 22a,b). Within that model we can also look for fusion events (see later). The mean thermal energy increases much more slowly - since for hypersonic projectile and target velocities matter not yet reached by the shock stays practically undisturbed in its ground state (see Fig. 22c)

On the other hand, the compression rates and temperatures obtained in the "stationary stage" are in quite good agreement with the result of the shock calculations

(see Fig. 23a,b) The inclusion of thermal conductivity has the consequence that heat energy is transported away from the most strongly compressed regions - this is of great importance for the formation and stabilization of metastable superdense nuclei.

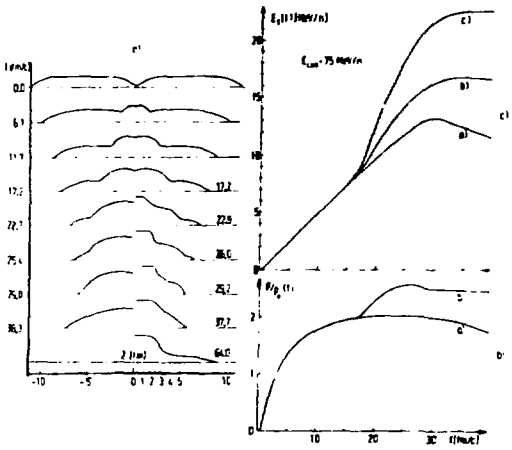

Fig. 22. (a) The density distribution of various stages of a central collision of two equal nuclei E_{lab}=75 MeV/n. The left-hand shows ρ(z) for a normal equation of state K_o=300 MeV/): the second central region quickly expands again. The right-hand side shows the strong density increase in the case of a density isomeric state: a large part of the system stays rather long within the abnormal phase (density isomer at $\rho_c = 2\rho_o, \rho_1 = 2.5\ \rho_o$, $B_1 = 0$).

(b) The central compression $\rho/\rho_o(t)$ increases strongly above the critical density for the production of an isomeric state: compared to the normal nuclear matter (lower curve), the presence of a density isomer leads to the collapse of the nuclear matter into the abnormal superdense phase (upper curve). Thus the matter remains much longer within the strongly compressed state.

(c) The gain of condensation energy leads to a strong increase of the mean thermal energy $E_T(t)$ in the presence of a density isomer (upper curve). Lower curve: normal nuclear matter.

Effectively the thermal conductivity also takes into account particle emission - i.e. for example cooling due to pion - and nucleon evaporation. These investigations are being pursued presently by G. Buchwald (1979) in two- and three-dimensional calculations.

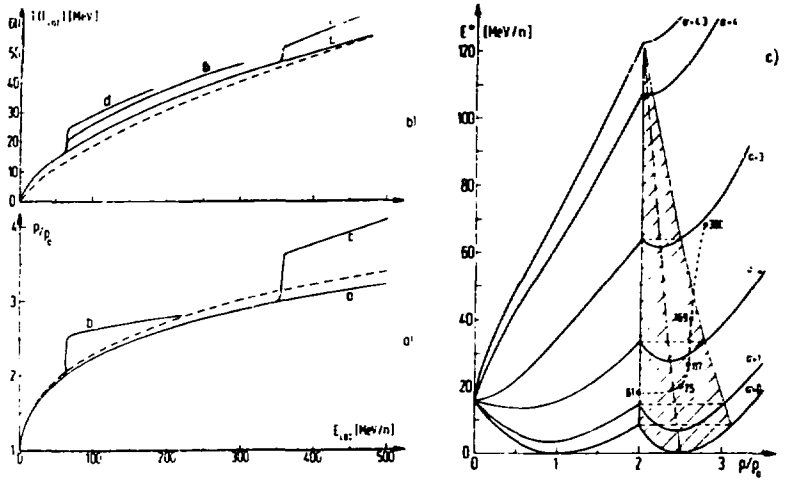

Fig. 23. (a)The central compression ρ/ρ_0 increases smoothly with the bombarding energy up to the critical point for the production of a density isomer.Then the system collapses into the abnormal superdense state:the density increases suddenly.Curve a,normal nuclear matter,dashed curve: result of relativistic shock calculation[4,5]; b,density isomer with $\rho_c/\rho_0=2,\rho_1/\rho_0=2.5,B_1=0$; c,density isomer with $\rho_c/\rho_0=3,\rho_1/\rho_0=4,B_1=0$. (b)Similar to Fig. (a) a threshold increase of the excitation function of the mean temperature $T(E_{LAB})$ reflects the presence of a density isomer. This may be used to detect density isomeric states experimentally(see text).Curve a,normal nuclear matter; b,density isomer with $\rho_c/\rho_0=2,\rho_1/\rho_0=2.5,B_0=0$;c,density isomer with $\rho_c/\rho_0=3,\rho_1/\rho_0=4$, $B_1=0$; d,density isomer with $\rho_c/\rho_0=2,\rho_1/\rho_0=2.5,B_1=-10$ MeV. The rate of increase of T may be used to determine the depth B_1 of the secondary minimum. (c)The expansion of the compressed nuclear system approximately follows the curves $E^*(\rho)=E_c(\rho)+E_T(\rho,T)_\sigma$ of constant entropy σ (=solid lines).These curves still exhibit the secondary minimum for rather high excitations. The shaded area indicates the region for which "fusion" into metastable abnormal states may be possible (see text). The dot-dashed line gives the position of the respective minima os the isentropic curves. The dots mark the state of strongest compression and excitation obtained numerically for the indicated bombarding energies (in MeV/n). The dots within the shaded area actually represent the "numerical fusion events.

Formation of Abnormal Superdense States

Again we find an important effect of a density isomeric state on the thermodynamical variables like ρ and T. When the critical density ρ_c is reached, only a slightly stronger compression results in the collaps of the central compression region into the abnormal state. This also means that the density now becomes

considerably larger than that calculated with an equation of state without density isomer (Fig. 22a, 23a). As the collision time $\tau_{coll} \approx 10^{-22}$ sec is very small compared to the tunnel time τ_{tunnel} necessary to form the equilibrium phase composition, a Maxwell construction for the van der Walls-type equation of state is meaningless during the fast collision process. As a function of the bombarding energy, the compression increases drastically at the threshold for the production of the density isomer (see Fig. 23). Qualitatively the same effects hold for the thermal excitation energy: When the system collapses into the abnormal superdense state, the temperature increases immediately due to the gain of condensation energy (see Fig. 23b). Contrary to the increase of the density, which experimentally is not directly observable, the increase of the temperature may be used to detect the abnormal state: Analogously to the density (see Fig. 23a), the temperature of the system as a function of the bombarding energy shows a drastic increase at the threshold for the formation of the density isomer (see Fig. 23b). As a consequence of the higher temperature, a threshold increase of the high energy parts of the energy spectra of the emitted fragments as well as the pion production rate will reflect the formation of abnormal superdense nuclear matter. On the other hand, fast emission of highly energetic particles can serve as a cooling mechanism for the abnormal nuclear matter. Such mechanisms are not yet included in our model. Thus the formation of metastable, fused superdense nuclei seems feasible for a range of bombarding energies (see Fig.23c).

During the compression stage, the system becomes thermally excited, i.e. a lot of entropy is produced. However, the system starts to expand from the state of highest compression along curves of constant entropy . These curves will exhibit the potential barrier at ρ_c, although the barrier height and density of the secondary minimum become lower for increasing entropy. Therefore, if the energy of the final compression state is smaller than the corresponding isentropic barrier (analogous to the centrifugal barrier), the system can be trapped within a metastable state, from which it may deexcite into the cold density isomeric state via emission of particles from the nuclear surface. Thus, e.g. for U-U collisions, even the production of (meta) stable collapsed superheavy nuclei, which also have very interesting atomic properties, may be feasible. But also at bombarding energies above the fusion region, where the excessive kinetic and thermal energies lead to the decay of the system, it may still remain rather long within the abnormal phase. We find such a behaviour in our model calculations (see Fig. 23c): For the three bombarding energies E_{LAB} = 75, 117, 169 MeV/n, the state of greatest compression lies within the fusion region. Acutally, we could not find a subsequent decay of the formed abnormal system during the time of the calculation (which was considerably longer than the collision time). On the other hand, for energies at 61 MeV/n (which is still undercritical), and 300 MeV/n respectively, we find that the system dissolves again relatively quickly. This apparent energy window for producing "stable" abnormal matter depends, of course, on the location and shape of the barrier between normal and abnormal nuclear matter. Hence our schematic calculations should only be taken as illustration of the physics to be expected, if the equation of state contains exotic features.

In the next paragraph the collisions of two heavy nuclei are studied in a three-dimensional model. This model does not include viscosity and thermal conductivity, but it allows for the theoretical investigation of the modifications due to the three-dimensional case compared to the schematic results obtained here. It especially leads to a decrease of the achievable compression ρ/ρ_0^{Max} as the matter will strongly be pushed to the sides.

8. THREE DIMENSIONAL CALCULATIONS OF HIGH ENERGY COLLISIONS OF EQUAL NUCLEI

To compare the results of the three-dimensional NFD calculations directly to the

relativistic shock calculations and to the one-dimensional non-relativistic Navier-Stokes results, let us go back to the Euler equations (Stöcker,1979). In the presently discussed hydrodynamical calculation, local heating is neglected. This is reasonable approximation, because one can easily estimate the heat energy produced by the strong shocks from the apparent energy loss in the calculations. Comparing the three-dimensional calculations with earlier one-dimensional calculations with the Navier-Stokes equations, we find that this omission has only a minor influence on reaction, but in the decompression phase, the internal pressure is too sm. (the thermal pressure is missing) to ensure the correct expansion velocity. This is not so important for medium energies with moderate thermal excitation but for the higher energies it should be taken into account. The collision of two Zr-nuclei at E_{LAB}=200 and 400 MeV/n was used to investigate the influence of the details of the density isomeric state, which is represented by a parabolic expansion of $E_c(\rho)$ around the secondary minimum. (see Fig.4):

$$E_{c_1}(\rho) = \frac{K_1}{18\rho\rho_1}(\rho - \rho_1)^2 \quad \text{for} \quad \rho > \rho_c = 2\rho_0 \quad .$$

The influence of the density isomer on the reaction is analogous to the results obtained above.

Let us now investigate the dependence of the formation of density isomers and of the compression rate on the mass of the reacting nuclei and on the parameters of the density isomeric state, respectively. To do this we have calculated the reaction Uranium on Uranium at b = 0 fm and 200 MeV/n with the above equation of state. We find only a slight increase of the maximal compression, but generally the same characteristics as in the Zr case. On the other hand, the dependence of the compression on the nuclear equation of state is significant. Lowering the isomeric compression constant $K_1 = 9\,\rho_1^2\partial^2 E_c/\partial^2|_{\rho_1}$ from 3000 MeV to 300 MeV is sufficient to increase the compression from 2.88 to 3.41 at E_{LAB} = 200 MeV/n. Using a density isomer with $\rho_c = 3\,\rho_0, \rho_1 = 4\rho_0$, $E_c(\rho_c)$ = +6 MeV, $E_c = (\rho_1)$= -26 MeV results an even much stronger compression,namely ρ/ρ_c = 4.8 for E_{LAB} = 400 MeV/n. We find that the threshold bombarding energy for the formation of a density isomer as characterized in Fig. 4 is located somewhat below 100 MeV/n. This value is considerably higher than the 60 MeV/n obtained in the one-dimensional Navier-Stokes calculations. This is due to the outflow of matter perpendicular to the collision axis. At 200 MeV/n, the critical impact parameter is b = 7±1 fm, corresponding to an isomer formation cross section of

$$\sigma_{DI} = 1540 \pm \frac{450}{300} \text{ mb} \quad .$$

To compare the nuclear density distributions, as obtained with and without density isomer, directly to the one-dimensional results, Fig. 24 shows cuts through the density distribution along the collision axis ($\rho(z)$, left-hand side) and perpendicular to the collision axis ($\rho(y)$, right-hand side) for a head-on collision of two Zr-nuclei at E_{LAB} = 200 MeV/n. The dashed curves show the density distributions at various times obtained with a normal nuclear equation of state (i.e., no secondary minima in $E_c(\rho)$). The full curves show the analogous results (i.e., the same reaction at the same time) calculated with a density isomeric minimum in $E_c(\rho)$ with a barrier of $E_c(\rho_c)$ = - 8 MeV at a critical density $\rho_c = 2\rho_c$, and the density of the abnormal state at $\rho_1 = 2.5\,\rho_0$ with $E_c(\rho_1)$ = -16 MeV (see Fig. 24).

The upper curves show various stages during the compression phase of the reaction. It is clearly seen that the matter approaching the center of momentum along the z-axis during the reaction is pushed out perpendicular to the collision axis, i.e. along the y-axis. The incident longitudinal momentum is transferred into transverse momentum. This will result in the predominant outflow of matter at center of mass angles of about 90°. This prediction of the hydrodynamical model can be tested experimentally (see below).

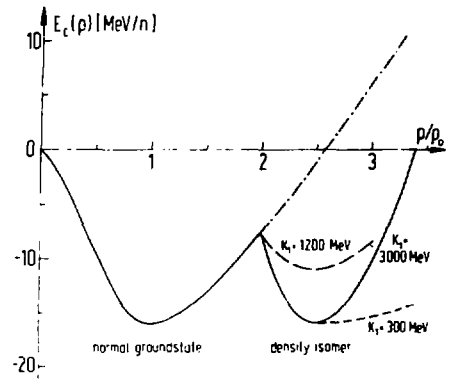

Fig.24 a. The nuclear equation of state used in the three-dimensional calculations shown in Fig.24b.

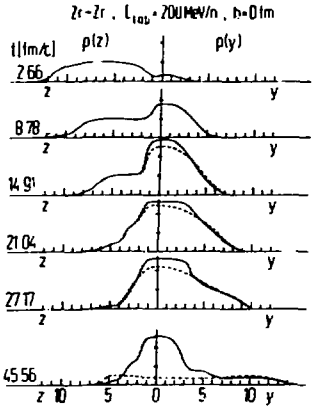

Fig.24 b. The density distributions ρ(z) (left) and ρ(y) (right) of a Zr→Zr head-on collision at E_{LAB}=200 MeV/n resulting from a normal (dashed curves) and densit, isomeric equation of state (full curves) are shown (see text).The curves are to be reflected around the center of mass(y,z=0) respectively.

The perpendicular outflow is stronger in the case of a normal equation of state, while for the density isomeric case the matter is sucked into the isomer, therefore the internal pressure is smaller, resulting in a less pronounced sidewards flow. This may serve as another possibility to detect abnormal nuclear matter experimentally. In analogy to the previously obtained result, the central compression is larger in the presence of the density isomeric state (see Fig. 24). Yet again the most important difference is the following fusion-like "trapping" of the nuclear matter within the abnormal state. While the formation of the superdense matter seems to be rather similar in the two different cases, the decompressed process differs dramatically (lowest curves): For a normal equation of state there only remains a completely dissolved system with very low nucleon density ($\rho/\rho_o \lesssim 0.4$ at t = 40 fm/c, whereas in the isomeric case at the same time a strongly compressed "fused' density isomer surrounded by a dilute atmosphere can be seen. From the low density regimes mainly small reaction fragments will be emitted, i.e. one can expect that central violent collisions result in events with high multiplicities of the emitted fragments. The density isomer may be viewed as a highly excited object moving with the center of mass velocity. The trapping occurs also when the isomeric ground state is energetically less favourable than the normal ground state. This is due to the isentropic expansion of the matter.

We have mentioned already that the occurrence of shock waves in fast central collisions of equal mass nuclei implies a predominant outflow of matter perpendicular to the collision axis. This effect has been predicted very early (Scheid,1968; 1974;1974a; Baumgardt,1976) and constituted one of the earliest predictions in

nuclear shock waves. A recent experiment of the GSI-Marburg-Berkeley collaboration (Wolf and co-workers,1979; Meyer,1979) seems to present evidence for this sidewards splash in the reaction Ar Ca at 1.05 GeV/n.

They detected π^+ in nearly central collisions and measured the pions transverse momenta and rapidity, which is essentially the forward momentum (see Fig. 25). The pion production itself can be viewed as a trigger for centrality. They predominantly find pions emitted with a forward momentum corresponding to the center of mass velocity of the equal mass nuclei, and a rather large sidewards momentum $p_{\perp}/m \approx 0.5$. The maximum in the contour plots is interpreted as a pion emitting source, moving with $v_{source} \sim 0.5c$ to 90° in the CM-frame. This is just what we expect from our calculations. When the compressed, hot matter flows to 90° in the CM-frame. This is just what we expect from our calculations: When the compressed, hot matter flows to 90° in the CM-frame, during the whole expansion stage fast particles will be emitted. Due to the collective flow of the emitting matter the transverse momentum versus rapidity distribution will show up a maximum at the cm rapidity but at finite $p_{\perp}$. This effect will be even more pronounced, as the pions from the initial compressed stage can also escape only under 90° in the CM-frame, because of the shadowing effects of the residual projectile and target nuclei, in the forward-backwards hemisphere. As the velocity and temperature of the pion emitting source are time-dependent, no narrow peak but a broad sidewards bump is expected.

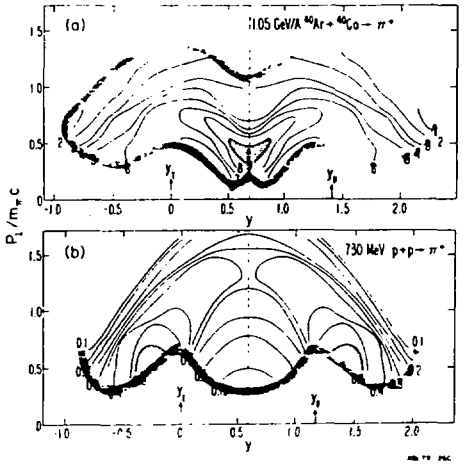

Fig. 25. The rapidity-perpendicular momentum plot of π^+ obtained experimentally in heavy ion collisions shows clearly the sidewards emission of π^+ in contrast to the results for proton-proton collisions where forward-backward emission of π^+ is observed.

From our one-dimensional calculation (see Fig. 19) we can estimate the outflow velocity. During the stage of high compression, the thermal energy is largest - therefore we expect that the thermal pion production occurs mainly in that stage.

For 1 GeV/n and $\rho/\rho_0 > 2$, the outflow kinetic energy increases from E_{kin} = 0-100 MeV/n, corresponding to flow velocities $v/c \lesssim 0.5$. To obtain some more detailed information on this subject, we performed a set of three-dimensional calculations for the case studied experimentally. For these high energy collisions the shock heating has been taken into account properly, as it is most important for the expansion stage. This (accounting for convective heat flow) can be done only by working in the center-of-momentum frame, where the energy per nucleon is the same for all nucleons. Then the the thermal pressure and -energy as well as the temperature can be calculated at each point in space from the discrepancy between the initial and instantaneous energy. However, we remark that the energy density and internal energy vary over all space. The use of a non-relativistic model at bombarding energies $E_{LAB} \sim 1$ GeV/n is not too bad when working in the center of momentum system: Here the kinetic energy per nucleon is only 1/4 of that in the lab, i.e. $E_{CM} \sim 250$ MeV/n and $\gamma_{CM} \sim 1.25$, Therefore, the deviations from a relativistic treatment will be on the order of 25%. This seems to be not too bad for these exploratory investigations. The resulting density contour plots for the reaction Ar Ca are depicted in Fig. 26 for various impact parameters at E_{LAB} = 400 MeV/n. Again it is found that for the central collisions a complete desintegration of the projectile and target appears (normal equation of state). The hot compressed matter is squeezed out into 90° in the center of momentum frame.

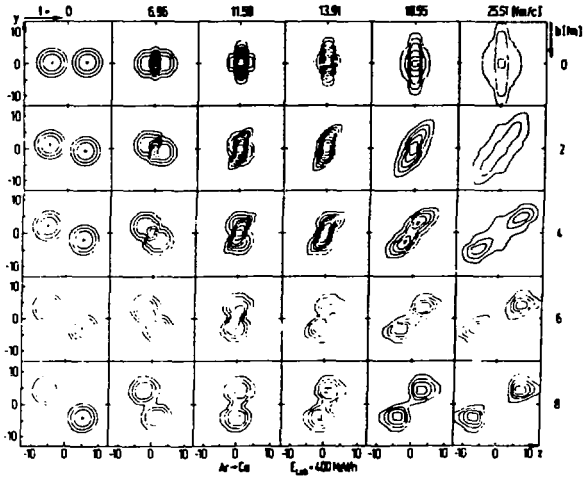

Fig. 26. The density contour plots Ar+Ca are shown at various impact parameters (numbers at the right-hand side) and at various times (indicated on top).

For the more grazing impact parameters the target and projectile are also excited, but they stay rather compact. Therefore we expect that grazing collisions lead to particle evaporation from the target and projectile, which practically maintain their initial velocities. If the impact parameter is lowered, a collective transverse momentum transfer to the whole target and projectile is observed. The nuclei are also much stronger excited - they may not survive the reaction but decay into smaller fragments. For the nearly central collision b = 2 fm, the picture looks like a central collision with a finite rotation energy. One sees that the matter is smashed sidewards with a slight forward-backward asymmetry around 90° in the

center of mass. Also the calculated transverse momentum versus rapidity shows up maxima in the heart-form as is seen in the experiment (Fig. 25). However, as expected, the velocity of the matter (i.e. the pion emitting source) varies continuously in time. For the high temperature stage, where pion production is most probable, then a bump in the transverse momentum distribution appears at

$$P_\perp/_M \approx 0.1 - 0.4 \quad \text{and} \quad P_{II}/_M = \frac{V_{CM}}{c} \pm 0.2 \text{ for } E_{LAB} = 400 \text{ MeV/n}.$$

For 1 GeV/n, qualitatively the same phenomena are found, however, the momentum transfer is larger. The bump is also broader due to the higher excitation energy. For b = 0 collisions we find $P_\perp/_M \approx 0.1 - 0.7$, but a rather narrow $P_{II}/_M$ distribution. If the corrections due to relativistic kinematics are accounted for properly - they lower the velocities by ~20% - we find that the velocity of the sidewards squeezed matter is close to the experimentally determined velocity of the pion emitting source.

In conclusion, the recent measurement of a pion emitting source moving with large transverse momentum to 90° in the center of mass system can be viewed as a further indication for a quasi-hydrodynamic behaviour of nuclear matter in high energy heavy ion collisions. However, the model has to be improved in the future to incorporate consistantly the pion emission process in the calculations.

9. MACH SHOCK PHENOMENA AND THE HIGHLY INELASTIC BOUNCE-OFF EFFECT IN COLLISIONS OF SMALL PROJECTILES WITH HEAVY TARGETS

In the violent reactions of small projectile nuclei with heavy targets, the compression effects reflect in somewhat different phenomena than in the collision of equal mass nuclei. For central collisions, the projectile nucleus penetrating into the target is surrounded by target matter - thus we expect to observe the strongly compressed projectile - which is called the head shock - not directly(Stöcker, 1977a). However, compression- and heat waves (the Mach shock) will travel through the target matter, which allows to study the transport phenomena in nuclear matter (see Fig. 27). This was first predicted by Baumgardt (1975) and Hofmann(1974). When the projectile enters the target with hypersonic velocity (the diving phase), strong local compression and heating of the matter near the contact point occurs. When this head shock continues to interpenetrate the target as a projectile-like object with hypersonic velocity, it pushes matter to the side. This initiates a

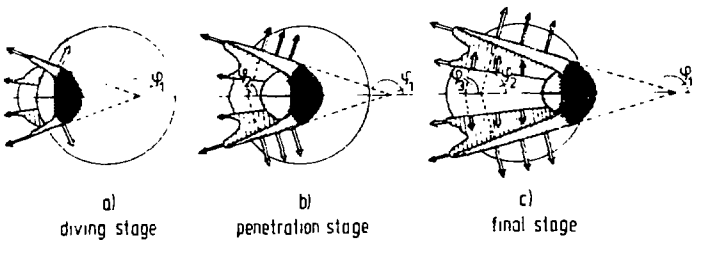

Fig. 27. Various stages of central collision of a light nucleus into a heavier one with the sidewards travelling Mach shock wave are shown schematically.

compression wave which has been called Mach shock wave travelling sidewards through the target matter. This phenomenon allows to study the transport of compressed matter through a region of ground state nuclear matter, namely the residual target nucleus. The nuclear Mach shock wave can be detected experimentally by observing the azimuthally symmetric sidewards emission of matter (predominantly light nuclei) with medium kinetic energy (i.e. significantly higher in energy), much lower than the kinetic energy of the projectile, but different from the evaporation particles. This is discussed below in greater detail. For intermediate impact parameters, the Mach shock phenomenon becomes less pronounced. Here the highly inelastic bounce-off (HIBO) of the projectile from the target is expected to occur; in this process the projectile due to the compression is scattered to the side and is destroyed, transferring a considerable transverse momentum to the residual target nucleus (see the next paragraph).

Recently a series of measurements have been performed at Berkeley and at Dubna (Meyer,1979; Antonenko,1979). They seem to confirm the pioneering experiments of E.Schopper and collaborators (Baumgardt,1975), which have been interpreted earlier as indication for Mach shock waves in relativistic nucleus-nucleus collisions (see later) where this is discussed in detail).

Let us now first discuss the more recent experiments from the GSI-Marburg-Berkeley collaboration (Stock,Gutbrod,Sandoval, Poskanzer et al.,1979). They observe in central collisions of Neon on Uranium a strong sideward emission of nuclear matter, when high multiplicity events with a rather azimuthally symmetric fragment distribution are selected. This is just what has been predicted theoretically if the Mach shock phenomenon appears and strongly supports the earlier measurements of Schopper (Baumgardt,1975; Hofmann,1976). Secondly, in the same reaction strongly φ-asymmetric events with a large momentum transfer on a target-like fragment, accompanied by the 180° correlated explosion of a deflected projectile-like object have been detected (Wolf,1979). This obviously must be interpreted as a highly inelastic bounce-off (HIBO) of the projectile from the target. Our model calculations indicate that these phenomena can be used to detect experimentally the impact parameter in these collisions and to deduce the compression rate in such collisions. This bounce-off is quite analogous to what is seen in Fig. 26 for reactions of equal mass nuclei. We will study theoretically collisions of Neon projectiles with Uranium targets. For the non-relativistic cases let us again use the three-dimensional fluid dynamical model where the same nuclear equation of state and potentials as in the last chapter have been used. Again we work in the equal velocity frame, because of two reasons: First, the local shock heating can most easily be computed in all space within this system. Secondly, the computing time is only half of that when working within the lab frame, because the integration time steps can be doubled.

Results for Central Collisions

First let us investigate theoretically with a normal equation of state the collision of the Ne-projectile with an Uranium target at b = 0 (head-on collision) for E_{LAB}=400 MeV/n. Fig. 28 shows a cut through the scattering plane. Snapshots of the collision are depicted in the form of contour plots of the density in the scattering plane. The density increases by 0.04 fm^{-3} from line to line. The outer line represents 0.02 fm^{-3}, i.e. approximately a tenth of the ground state density ρ_o = 0.17 fm^{-3}. The collision time in fm/c is indicated by the numbers within each plot. The length scale in fm is depicted at the left. Remember that our calculations proceed in the equal velocity frame, therefore the target moves to the left. As the target hits the projectile with hypersonic velocity v_p=0.46 c (while c_s=0.15 c), a head shock zone is formed during the diving phase of the reaction (t~5-8). This strongly compressed and highly excited projectile-like object continues to interpenetrate the target with supersonic velocity, pushing the matter to the side, thus initiating the formation of a sidewards travelling Mach

shock wave within the target nucleus (t~11-20). The density of the matter within the Mach shock decreases with the distance from the head shock, being always considerably smaller than the head shock density. Due to this effect and due to the deceleration of the projectiles, the Mach shock is curved (not a clear cone as in a Mach sound wave). Because of the additional high temperature within the matter, one expects that the emitted matter (mainly light fragments because of the high thermal excitation) will peak strongly, but not too sharply, to the sides. This peak should be narrower, when only α particles or other larger nuclei are investigated, because they carry most clearly the "collective direction" of the Mach-shock wave: They would be destroyed, if they make a temperature collision. Observing them thus means, that they are not temperature-scattered. There are also other reasons for observing the Mach shock in the α-particle window: The pion condensate - a spin-isospin lattice - is expected to be formed in the Mach shock wave and to break up substantially into α-particles. Also, α-particles are expected to be concentrated within the atmosphere of normal nuclei. Because a shock wave would eject mostly the surface particles, again an α-particle window would be predicted.This narrowing of the sidewards Mach shock peak has been first reported experimentally by selecting mainly α-particles in 4π particle track detectors by Schopper and co-workers(Baumgardt,1975). Indeed, also in the above mentioned experiment of the GSI-Marburg-Berkeley collaboration, the predicted sidewards emission of matter has been observed in an electronic experiment measuring the proton angular distribution. However, the sidewards peak of the emitted protons can be seen only, when "central" events are selected, which are identified with high charged-particle multiplicities and azimuthally symmetric charge distributions.For Ne→U at 400 MeV/n the peak position was found at 60° for E_p≈50 MeV and at 50° for E_p≈100 MeV. We calculated the angular distribution of the emitted matter averaging over impact parameters b<4 fm and - because of better statistics - over the calculated currents during the last 25% of the reaction, where the matter expands

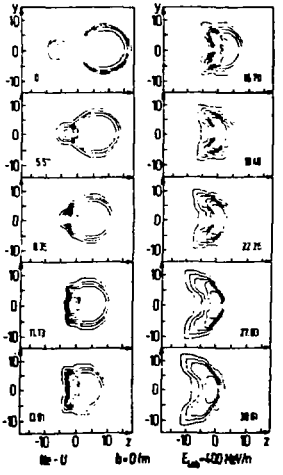

Fig.28. The density contour plots for the collision Ne→U at b=0 fm and E_{LAB}=400 MeV/n as resulting from our three-dimensional calculation.

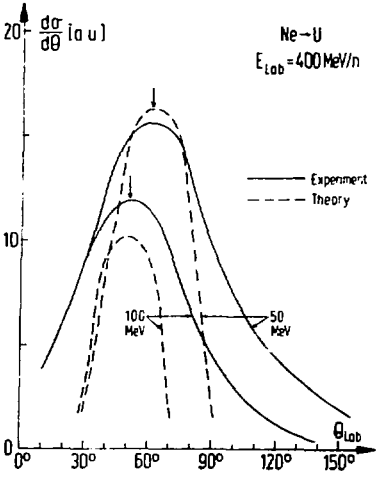

Fig.29. The experimental angular distributions (full curves) are compared to the theoreticall obtained curves (dashed).

and flows apart. Without fitting anything we find peaks in the angular distribution, which are centered at 60° for E_{kin}=50±20 MeV/n and at 50° for E_{kin}=100±10 MeV(see Fig. 29). These are just the same peak positions as found experimentally. In our calculation, for smaller angular bins (±5° instead of ±10°) the peak positions do not change. However, the peaks become rather narrow. The peak is broadened due to the additional thermal smearing, caused by an isotropic Maxwellian distribution of the internal nucleonic velocities. Moreover, not only the peak positions are in good agreement with experiment,but also the relative height of the peaks agree reasonably well. A complete angular distribution for various energies of the observed emission particles in high multiplicity events is shown in Fig.30. It is due to Meyer, Gutbrod, Stock, Sandoval, Poskanzer et al.(Meyer,1979). One can clearly recognize the Mach-shock particles with energies between 10 MeV/n and 2000 MeV/n all peaking around 50°-60° and also the backward directed "diving splash" which is seen for particles with energies around 5-10 MeV/n. The latter is also predicted by fluid dynamics (see Fig. 27) and was already predicted in the very early work by Schopper and co-workers (Baumgardt,1975).

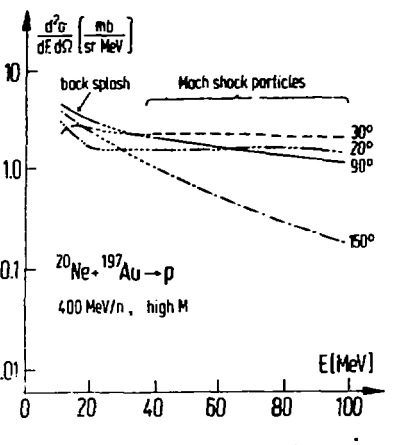

Fig. 30. The experimentally obtained double differential cross section $d^2\sigma/d\Omega dE$ for Ne→Au at 400 MeV/n triggering for the high multiplicities as obtained by Meyer et al. (1979).

The comparison of our theory to the experimental data seems to support the interpretation that compression takes place in high energy heavy ion reaction and that Mach shock waves are formed in central collisions, which can allow for the search of abnormal nuclear matter (see section 10).

Results for Non-Central Collisions

While the central collisions seem to be associated with a total desintegration of target and projectile, in non-central collisions large target- and projectile-like fragments can be observed. We would like to discuss here a new effect occurring in the intermediate impact parameter region, which can be viewed as a highly inelastic

bounce-off (HIBO) of the projectile from the target (Stöcker,1979c). In this process, the projectile is scattered by a compression potential to the side, as is the strongly hit target matter, while a rather large part of the target stays bound. To this heavy target fragment a large transverse momentum is transferred, showing a collective response of the whole fragment to the interaction. This highly inelastic bounce-off can be detected experimentally by measureing a large target fragment with rather large perpendicular momentum in coincidence with many small fragments going into the forward hemisphere, correlated to the target fragment in 180° in the azimuthal angle. The large amount of small, higher energy particles stem from the explosion (nearly complete destruction) of the projectile-like fragment. Fig. 31 shows this bounce-off effect in the Ne U collision at E_{LAB}=400 MeV/n as calculated within our model for three different impact parameters: b = 4,6, and 8 fm. Again, snapshots at various timesteps are taken. One notices that initially, when the target is just hit by the projectile, for the more central b=4 fm collision again a head shock is formed, which additionally also initiates a Mach shock wave in the target. However, as the upper part of projectile and target appear to each other as if they were generally colliding equal nuclei, also a splashing out of matter perpendicular to the collision axis occurs just in analogy to what is seen in the case of a head-on collision of equal nuclei. The bounce-off effect can be viewed as follows: The strong compression potential deflects a considerable part of the projectile to the vacuum. Thus the first group of particles which should experimentally be detected are those deflected fast light fragments (heavy fragments will not survive the high excitation energy). The second group of particles will stem from the compressed direct reaction zone, which will also explode. Thirdly, a rather large residual target fragment, which was not centrally hit, and therefore is not strongly enough disturbed for total desintegration, can survive the reaction. It can get rid off its internal excitation by evaporating off particles. However, during the reaction a considerable amount of transverse momentum is transferred to the whole target-like fragment, while most of the longitudinal momentum is transferred to the exploding direct reaction -(compression) zone, and partly is also carried away by the sidewards deflected residual projectile-like fragment.

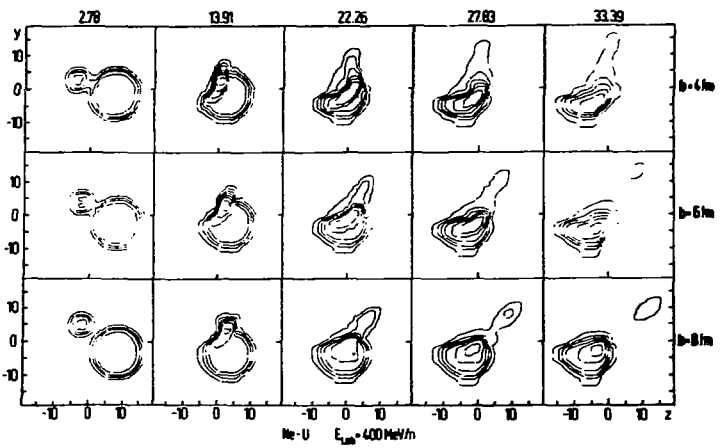

Fig. 31. The density contour plot of the reaction Ne+U at 400 MeV/n for intermediate impact parameters.

For b=6 and 8 fm qualitatively the same picture holds, however, the direct interaction region becomes less compressed with increasing impact parameters, and therefore the interaction between projectile and target is less pronounced (see also Table 1).
The head- and Mach shock become less intense at b=6 fm and can no longer be seen clearly at b=8 fm. A very important feature of the more grazing collision is the change of the scattering angle of the projectile-like fragment to more forward angles with increasing impact parameter (see Fig. 31). It can be viewed as the less pronounced repulsion from a smaller compression potential. We now will show that the dependence of the scattering angle on the impact parameter is of great importance for further analysis of high energy nuclear reaction data, as it can serve as an unique tool to determine the impact parameter of each collision experimentally.

TABLE 1

	b[fm]	0	2	4	6	8
a)	$\langle M_c \rangle$ (E_{kin}>30 MeV) (b) :	37	32	27	21	16
b)	$(\rho/\rho_o)^{max}$ (b) :	2.06	2.02	1.90	1.72	1.34
c)	T^{max}[MeV] (b) :	44	44	44	42	40

The dependence of the mean multiplicity $\langle M_c \rangle$ of high energetic particles, the maximum compression and the maximum temperature on the impact parameter in Ne+U collisions at 400 MeV/n as obtained in the three-dimensional calculations.

As the rate of compression in a reaction does also depend strongly on the impact parameter, the above proposed experiment may be used to determine indirectly the rate of compression achieved in fast nuclear reactions. Therefore, similarly to the Coulomb deflection trajectory used to measure the impact parameter in low energy nucleus collision the measurement of the bounce-off effect can be used for impact parameter measurements in high energy nuclear collisions. To make our discussion more quantative, we define the characteristic variables of the "projectile-like fragment" and "target-like fragment" as the variables at the respective region of maximal density and determine the momenta, energy loss and deflection angle in a late stage of the collision, when the nuclear fragments have split again and thus the investigated variables stay constant in time. The results are plotted in Fig. 32 for the different impact parameters: Fig. 32a shows the dependence of the deflection angle of the projectile-like fragment on the impact parameter b. One notices the increase of the deflection angle ϑ_{LAB}^{defl} with increasing centrality. However, it does not look at all as like elastic scattering of hard spheres, but must be viewed as a highly inelastic reaction with strong mutual interpenetration of projectile and target connected with strong compression and thermalization effects. The diving depth of the projectile into the target can be evaluated approximately from the scattering ange by calculating the effective scattering radius

$$R_{eff} = \frac{b}{\sin\frac{\pi - \vartheta_{LAB}^{defl}}{2}} \qquad (10)$$

of the scattering of a particle by a hard sphere from the scattering angle ϑ_{LAB}.

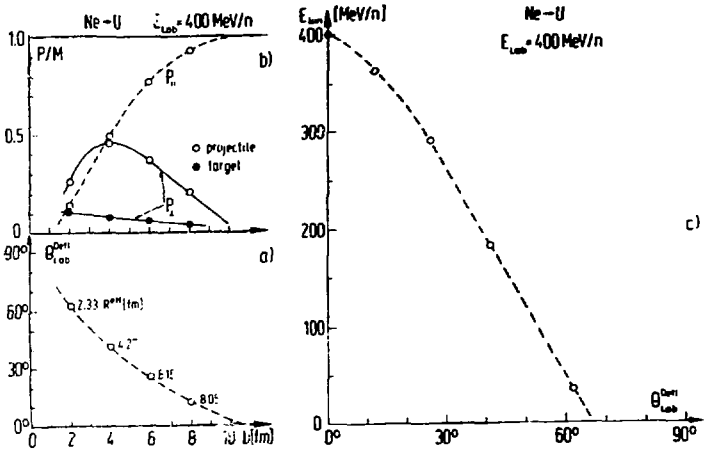

Fig.32. For the collision Ne U at 400 MeV/n we show (a) the dependence of the deflection angle Θ_{LAB} of the projectile-like fragment on the impact parameter b. (c) The forward momentum loss (dashed curve) and sidewards momentum gain (full curve) of the projectile-like fragment (open dots) with decreasing impact parameter and the transverse momentum transfer to the target (full dots). (c) The theoretically obtained deflection function Θ_{LAB} (E_{kin}) is shown.

The numbers in Fig.32a give the effective scattering radius R_{eff} and show that the diving depth d(b) is approximately given by

$$d(b) \simeq (R_T - b) \ . \qquad (11)$$

By measuring Θ_{LAB}^{defl} one may therefore also deduce the interpenetration depth for distinct reactions. The measurement of the deflection angle of the projectile-like fragment, however, can not simply be detected, as the highly excited fragment explodes. Thus one has to measure in coincidence the angles and momenta of all explosion products of thes projectile-like fragment to determine its center-of-mass values. The longitudinal momentum p of the projectile-like fragment is another quantity of interest (see Fig. 32b)): p decreases strongly with increasing centrality and for rather central collision it is only of the order of 10% of the initial momentum. The forward momentum is distributed over many particles and is carried away by the explosion products also of the compressed zone, in which the projectile- and target matter are mixed up and strongly excited. The transverse momentum of the projectile is increasing strongly when b goes from 8 to 6 and 4 fm. It decreases again for b = 2 fm - this is due to the practically complete energy transfer ("sticking") to the dense and hot compression zone (head shock) in the case of nearly central collisions. Actually, the transverse momentum $p_\perp/_M$ of the residual target-like fragment is considerably smaller than $p_\perp/_M$ of the projectile, as the residual target still has a rather large mass compared to the rest of the projectile As the dilute nuclear matter of the direct reaction region expands and still connects the projectile- and target-like fragments, we cannot determine

the mass of the residual target, the only conclusion possible in the moment is that the mass decreases with increasing centrality and is always much smaller than the original target mass. For a more detailed information also the evaporation of particles has to be included in the calculation. It is important to point out that the large momentum transfer on the whole heavy fragment implies a collective response of the whole fragment to the compression potential, which acts between the bounce-off projectile and the target. Therefore, the impact parameter dependence of the transverse momentum transfer is an important information on the compression phenomena. Our theoretically obtained values $0.03 \leq p_{\perp}/_M \leq 0.1$ are in good agreement with the recent data of the GSI-Marburg-Berkeley collaboration (Meyer, 1979). They measured strongly asymmetric events with 180° azimuthal correlation in the scattering plane; for various systems they observe on one side many fast ($E_{kin} > 30$ MeV/n) light particles and, on the other side, a heavy target (e.g. Z=26) at 90° in the lab (i.e. with small forward momentum) with transverse momenta $P_{\perp}/_M$ (e.g. they found values of $p_{\perp}/_M \approx 0.036$, which are in the same region as our results).

In our calculations we obtain practically no longitudinal momentum transfer to the target-like fragment - the same as is observed experimentally. The calculated multiplicities of charges with $E_{kin}>30$ MeV/n depend on the impact parameter (see Table 1). In these experiments it is found that the production of such target-like fragments is predominantly seen for rather high charged particle multiplicities $\langle M_c \rangle \sim 10\text{-}20$ within $E_{kin}>30$ MeV/n. This in our model corresponds to impact parameter $b \sim 6\text{-}8$ fm, when one takes into account the formation of composite particle which we did not discriminate in our $\langle M_c \rangle$ determination from single nucleon. Fig. 32c shows the deflection function of the Neon-like fragment at 400 MeV/n. The kinetic energy loss is larger than 90% of E_{LAB} for $\vartheta \leq 60°$, which corresponds to a rather central collision ($b<2$ fm), but already for $\Theta_{LAB} \approx 30°$ the kinetic energy loss of the projectile-like fragment is of the order of 25%. Contrary to the elastic Coulomb scattering in low energy heavy ion collisions, all scattering processes in the high energy region with impact parameters $b<R_T$ lead to highly inelastic events. By detailed coincidence measurements of these highly inelastic bounce-off effects it will be possible in the future to measure the impact parameter also for collisions at relativistic energies. The various variables, which have to be determined experimentally to deduce the impact parameter, are:
(a) The charged particle multiplicity of fast particles which increases with the centrality. (b) The azimutbal symmetry of the events - symmetry should only appear for very small impact parameters $b \lesssim 2$ fm. (c) The azimuthal asymmetry with 180° correlation in the intermediate impact parameter region. The correlation between the target-like fragment and the exploding projectile-like fragment going hand in hand with the collective response (large perpendicular momentum transfer) of the fragments, the longitudinal momentum loss and the total kinetic energy loss of the projectile-like fragment and the deflection angle of the center of mass of the fast, sidewards pushed particles. From the measuremen of these quantities we can deduce the degree of violence and the diving depth in the reactions, from which not only the impact parameter, but also the compression rates and shock heating can be estimated by comparison with the theory (see our Table 1).
The compression rates obtained are low compared to one-dimensional shock calculations, which at 400 MeV/n yield $\rho/\rho_0^{max} \approx 3.4$. This is largely due to our three-dimensional tratment; the matter pushed to the side can freely expand into the vacuum. To a certain extent this also comes from the smallness of the projectile, which dissolves before the stage of largest compression is reached. For example in U-U collisions, one can reach a rather stationaly stage of constant compression in our calculations. The width of the shock fronts we obtain is of the order 1.5-2 fm, but it depends on the reaction considered. This is more realistic than the infinitely sharp shock fronts used in the simpler model calculations and in a different fluid dynamical approach.

Conclusions

One can split violent collisions of light nuclei with heavy targets into two types, namely nearly central collisions, which exhibit the strong compression phenomena most clearly by the sidewards moving Mach shock wave and very high azimuthally asymmetric fragment distribution with strong sidewards peaks, and the intermediate impact parameter collisions leading to the highly inelastic bounce-off, where the compressed matter acts in analogy to a repulsive spring which releases strong collective transverse momentum transfer. In these 180° correlated events one can learn from the deflection angle and momentum transfer and -loss about the impact parameter and therefore about the compression phenomena in non-central collisions of fast heavy ions. We finally mention, that the results on the deflection function and impact parameter do not depend very sensitively on the equation of state (i.e. compression constant K) used, as long as the nuclear equation of state is normal. If it contains exotic features like density isomers, we expect modifications of the above resulty and even signatures for isomers in the deflection function. Such calculations are presently carried out.

High Density Nuclear Mach Shock Waves and the Search for Density Isomers in Relativistic Collisions

As the Mach shock experiments have not only been carried out at the nonrelativistic energies, but experimental data have been obtained at $E_{LAB} = 4.2$ GeV/n as available in Dubna, we now have to use a relativistic model for interpreting the fast nuclear collisions. We will here investigate the dynamics of a relativistic heavy ion collision in terms of a simplified hydrodynamical model, using a parametrization of the Mach shock geometry similar to the results found in the nonrelativistic calculation. This model allows to study the influence of the nuclear equation of state using the relativistic shock equations. The geometric, thermodynamic- and kinematic variables and their time evolution as obtained in the more schematic calculations are used to yield the mean values of the mentioned variables and of the angular- and energy distribution of the reaction fragments.
In Fig. 33 the typical time evolution as resulting from the calculation is shown. It looks quite similar to those obtained from the full non-relativistic calculations. The calculations are carried out in the lab frame. Mainly three different phases of evolution during the collision can be seen (Baumgardt, 1975).

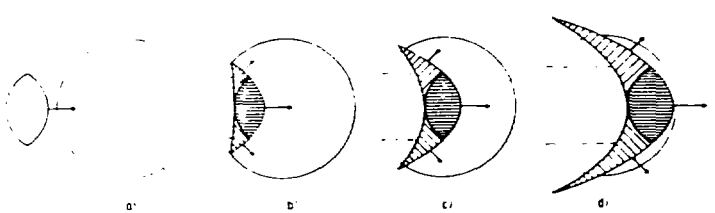

Fig. 33. The geometry of the relativistic Mach shock model is shown for various time steps.

The diving phase: The kinematically contracted projectile enters the target, becomes highly compressed and excited. In the diving process a splashing wave should lead to backward emission of matter.

The penetrating stage: The projectile interpenetrates the target, pushing matter to the side; thus initiating the sidewards travelling strongly compressed Mach shock wave.

The evaporating phase: The projectile- and Mach shock matter leaves the residual target, which now evaporates, while projectile and Mach shock explode because of their very high excitation energies, which correspond to temperatures from 20-60 MeV.

The explosion of the head shock wave which contains at the end of the collision more than double the nucleons of the incoming projectile, is what has been named recently the explosion of the "nuclear fireball" which has been used to explain angular- and energy distributions in non-central high energy heavy ion collisions. It may be possible, that the strongly compressed and highly excited projectile explodes inside the target during the interpenetrating state. This will lead to superstars with enormous multiplicities. In this case the Mach angle will be washed out and cannot be seen. This will be taken into account in a further calculation. As mentioned earlier, the nucleus-nucleus encounters are quantum mechanical processes with corresponding probability distributions. A classical hydrodynamical calculation can therefore be viewed at best as a calculation of the mean values of the quantum mechanical system in the sense of Ehrenfest's theorem. Superimposed to that are always the quantum fluctuations. They lead under the same initial conditions to events with sticking of the projectile and its explosion (superstars), to events with a penetrating superstar and a creation of a Mach shock wave and also to events where the projectile is practically little disturbed by the target (semi-transparency). It is a formidable experimental task to discriminate between these events by making e.g. the proper star-selections.
To restrict the number of degrees of freedom, we parametrize the compression zone by two paraboloids, $z = a_1 r^2 + z_1$, $z = a_2 r^2 + z_2$, which describe the shock front and the backside of the compression zone respectively. The undisturbed part of the target nucleus is described by the part of a spheroid of radius R up to the shock front (paraboloid 1), while the residual nucleus is described by a spheroid up to the backside of the compression zone (paraboloid 2) with a drilled hole of radius F_p in it. The residual nucleus has not yet been incorporated in the present calculations. The projectile (head shock wave) is divided from the Mach shock zone by a third paraboloid $z = -a_1 r^2 + z_2$ (see Fig. 33). Thus the geometry of the system is determined by four variables: a_1, a_2, z_1, z_2. The dynamical variables (energy density, momentum, pressure, temperature, density) are obtained by assuming homogeneous density-, velocity-, and temperature fields in each compression region. Thus for the sake of simplicity we concentrate on the mean values of the physical observables in the different regions as a function of time. The shock equations yield an unique relation between energy, pressure, temperature, velocities, and the rest density in the compression zone. Using these, we can describe the stage of the syster by the four geometrical variables and the density in the Mach- and head shock region. To describe the evolution of the system in time, we need six differential equations for these six variables. These equations are obtained by the conditions that the surface points on the paraboloid have to fulfill the shock equations and that total baryon number A and total energy E are conserved. One has to take into account the correct Lorentz-transformations for the various quantities (density,energy,...) in the different regions.The time evolution of the physical quantities is obtained by simultaneous numerical integration of the six differential equations in time-steps of Δt=0.1 fm/c,which is sufficiently exact to ensure energy- and baryon number conservation better than one percent.

Results of the Schematic Mach-Shock Calculations

The head- and the Mach-shock densities ρ_1 and ρ_2 as a function of time are shown in Fig. 34 for various energies: In the beginning, the projectile is strongly compressed, but this compression is substantially decreased later on. The Mach shock density ρ_2 is about $2\rho_0$ below the Mach shock density ρ_1. The mean compression in the head- and Mach shock (each at t=5 fm/c) is shown in Fig. 35a as function of the bombarding energy. The mean kinetic energy $E_{kin} = ((1-v_f^2)^{-1/2}-1)\ W_o$ of the emitted particles (Fig. 35b) after the collision is smaller than 200 MeV/n for Mach shock particles up to bombarding energies of 5 GeV/n, while it is larger than this experimentally important threshold for the projectile (head shock) at high energies. The temperature in head- and Mach shock just after the collision is shown in Fig. 35c. The fragments from projectile, Mach shock wave and the evaporation residues fall within angular domains relative to the beam axis as shown in Fig. 36.

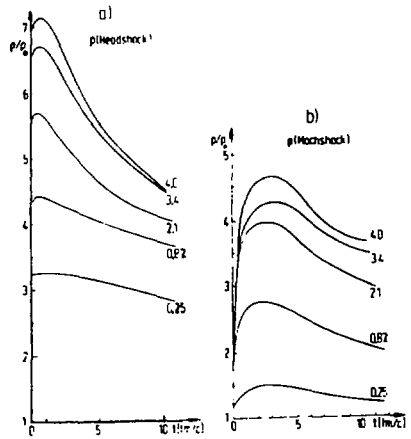

Fig.34. The evoluton of the high densities in the head shock and Mach shock as a function of time.

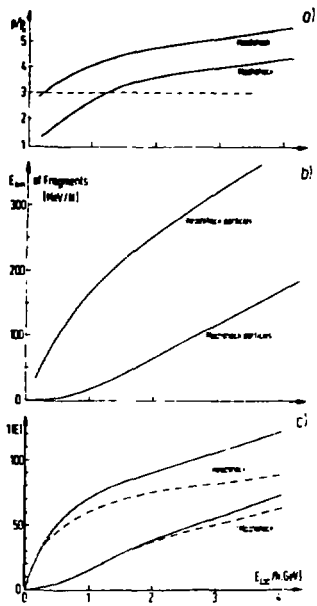

Fig. 35. The density a)kinetic energy of fragments b) and temperature c) of the various compression zones as a function of the incident energy.

As the mean head shock densities are approximately equal to those calculated within the one-dimensional model, we can make use of the latter model to yield the pion production rate, when we take care of the result, that the number of head shock particles is about $2A_p$. The Mach shock angle ϕ is depicted as a function of lab-energy in Fig. 37. It smoothly decreases from about 60 degrees at 0.1 GeV/n to 35 degrees at 4 GeV/n for a normal equation of state. It is smeared out very much because of the temperature in the Mach shock and because of the curvature of the "Mach-"cone". The explosion of the highly excited head shock causes strong emission of fast particles into forward

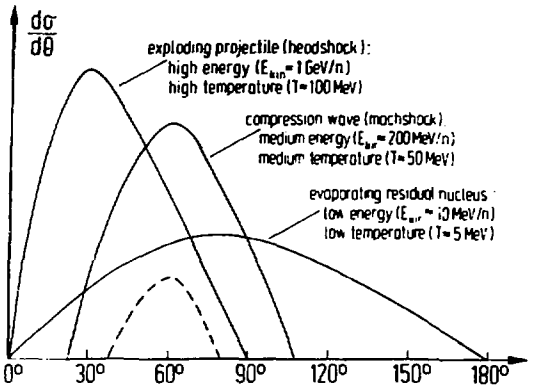

Fig. 36. The fragments of the head- and Mach shock fall into the indicated angular domains. The angular distribution of the evaporation residues is also shown.

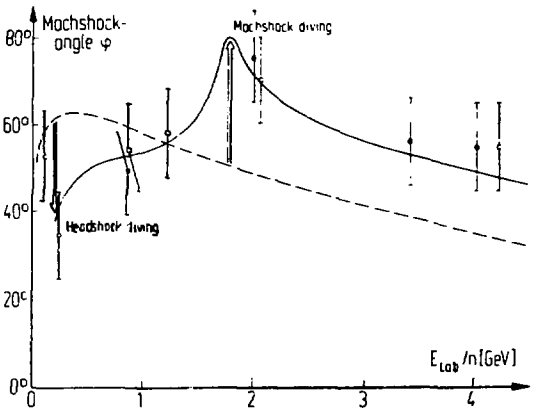

Fig. 37. The Mach-angle φ in dependence of the projectile energy for a normal equation of state (---) and for an equation of state with a density isomer (———).

directions, which may hinder the visibility of the Mach shock peak at small bombarding energies. The energy spectra of the exploding projectiles (head shock) drawn in Fig. 38 were calculated by relativistic addition of the flow velocity and the mean thermal velocity in the head shock after the collision, taking into account the isotropic decay cross section in the rest system of the projectile.

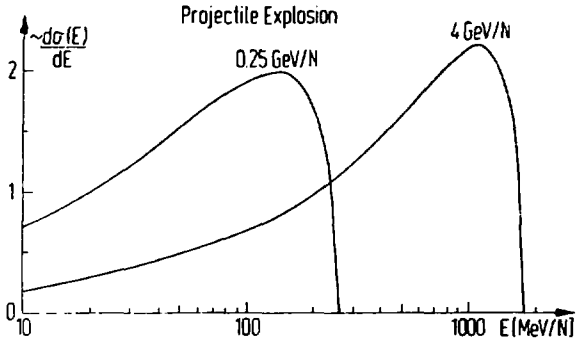

Fig. 38. Energy spectra of exploding projectiles for two different incident energies.

The Influence of a Density Isomer on Mach Shock Waves

If we schematically assume a density isomer at $\rho/\rho_0 \leq 3$, the above picture applies only below $E_{LAB} \approx 0.2$ GeV/n, as then the projectile density reaches the phase transition region, i.e. the region of negative pressure ($p<0$). (See Figs. 39,40). The projectile collapses into the density isomeric state. Thus the "quasi-stable nuclear crystal" can move with rather small dispersion through the surrounding normal nuclear fluid. One may thing of a piece of "nuclear ice" which moves through "nuclear water" - this is important for the appearance of the Mach shock wave, since a water droplet dumping into water produces too high friction and therefore soon damps out the collective motion. This, in fact, can to some extent be seen in the full hydrodynamic calculation (see last section).
As during the phase transition the head shock velocity becomes small, the Mach shock angle φ substantially decreases in this energy region, since the Mach shock moves faster than the collapsing head shock during this time period. The crystallization of the projectile causes a much more pronounced Mach shock peak at higher energy, because the projectile moves with much less friction through the target. At bombarding energies of about 1.5 GeV/n the Mach shock density appraches the critical region: Now the Mach shock matter collapses into the density isomeric state and the Mach shock velocity becomes small, so that the Mach angle now will be substantially increased (see Figs. 37 and 39). It will also be broadened out due to the rapid change in Mach shock velocity within a small density regime. At even higher bombarding energies, the Mach angle shall decrease again as both v_{HS} and v_{MS} tend to the light velocity c at very high densities, so that $\varphi \to 0$ for very high energies. One also may think that higher phase transitions do occur, which may again produce such a characteristic dependence of the Mach angle φ on the bombarding energy.

Comparison of the Calculations with the Experimental Observations

High Density Nuclear Mach Shock Waves (HDNMSW) should be observable in central high energy collisions of light projectiles with heavy targets. The pioneering experiments of Schopper et al. (Baumgardt,1975) supplemented by the theory, have

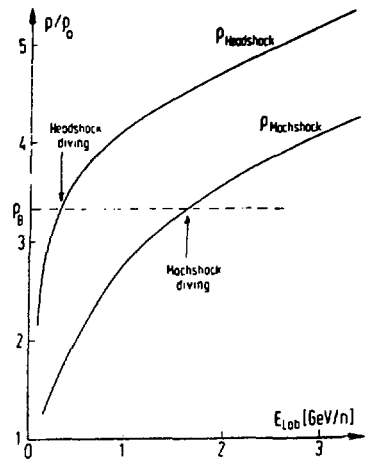

Fig.39. The diving of head shock and Mach shock into a possible second minimum of the equation of state. The head- and Mach shock densities as a function of projectile energy. ρ_B indicates the position of the assumed 2nd minimum in $E_c(\rho)$.

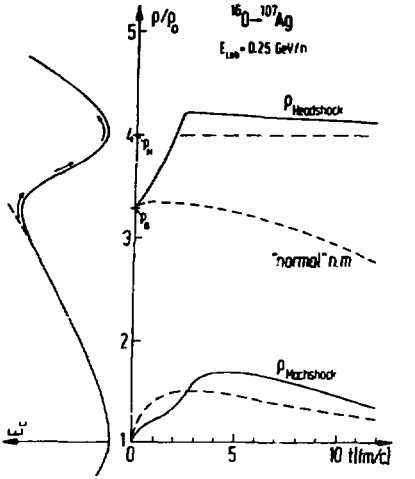

Fig. 40. The time behaviour of head- and Mach shock densities for normal (---) and isomeric nuclear matter (——). Along the ordinate the energy density $E_c(\rho)$ is demonstrated.

set the stage for the criteria to discriminate the Mach shock events from others: 1) In azimuthally symmetric central collisions, which can be identified by very high multiplicities and azimuthally symmetric distributions of the reaction fragments, e.g. by many prong stars in AgCl-detectors or emulsions, a preferential emission angle must be observed. 2) The kinetic energy of these particles will be smaller than 200 MeV/n. It may be decreased to even lower values, if the Mach shock density is in the secondary minimum. 3) The Mach shock peak and the decay of the head shock should predeminantly be seen in the α-particle (or other complex nuclei) channel for three reasons: (a) A pion condensate with a structure of a spin-isospin lattice preferentially decays into nucleons and α-particles as smallest lattice cells. The former can hardly be distinguished from evaporation particles, but the complex fragments can. (b) When the Mach shock wave approaches the nuclear surface, it kicks out the α-particles contained enhanced in the nuclear surface. (c) During the individual collisions of the constituent particles in the high temperature zone of the Mach shock, mainly those α-particles (and heavier clusters) survive, which have not undergone a temperature scattering. Thus the mach angle is conserved by those clusters, while scattered and unscattered nucleons cannot be distinguished. 4) One should find fast pions emitted by highly excited nuclear matter. The occurrence of pion condensation should also lead to a large enhancement of the pion production cross section. 5) Simultaneously to the medium energy sidewards Mach shock peak, a broad high energetic forward peak at $\Theta \sim 40^{\circ}$, stemming from the exploding head shock, will be seen. It may consist of protons and pions mainly because of the extremely high temperatures in the head shock. (see Fig. 38). The head shock particles are ~ in

the mean - of energy and can thus be (partly) discriminated from the Mach shock particles. 6) A nearly isotropic distribution in the lab frame may stem from the residual nucleus with small temperatures and kinetic energies.

In the presence of a density isomer the Mach shock peak should be more clearly pronounced and also should have the above predicted dependence on energy. The experimental data of Schopper et al. (Schopper,1979) which fulfill the above criteria on centrality, energy- and α-particle windows, show a peak in the angular distributions of the reaction fragments. The systematic shift of the preferential angle with energy can be interpreted in comparison with our calculations as indication for a phase transition in dense nuclear matter at $\rho/\rho_o \approx 3\text{-}5$ (see Figs.37 and 41 and figure caption).
Deviations in the prong-angular distribution of multiprong stars have also been seen by the Heckman-group (see Fig. 42). These deviations agree with the peaks seen by Schopper et al. and thus supplement the Mach-shock picture. Also the previously discussed angular distributions obtained by Gutbrod, Stock, Poskanzer et al. (see Figs. 29 and 43) show the peak in the same position as those of Schopper.

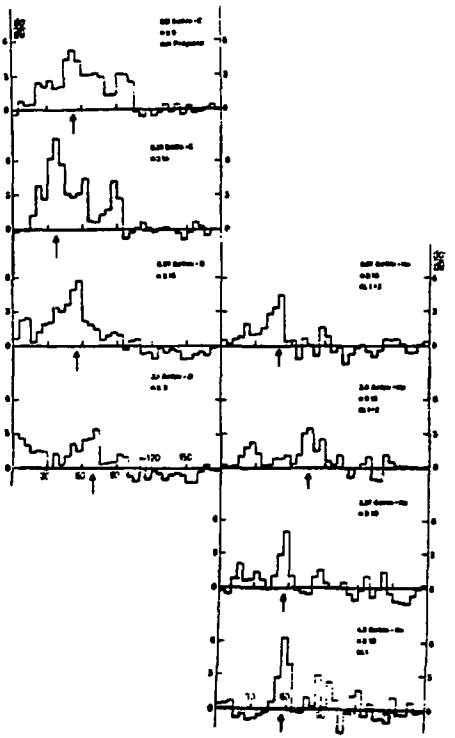

Fig. 41. Angular distribution of prongs for large stars at various energies (after Schopper et al.,1979). The evaporation background had been subtracted. The systematic variation of the peaks can be recognized.

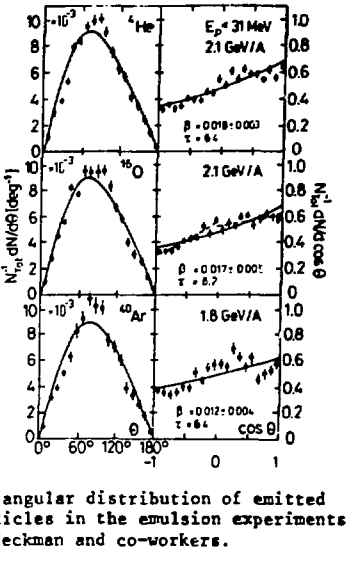

Fig. 42. The angular distribution of emitted particles in the emulsion experiments of Heckman and co-workers.

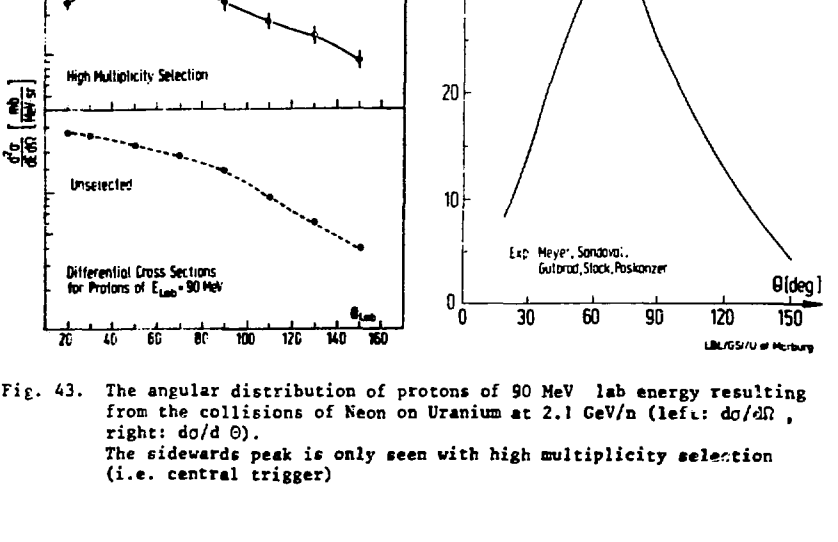

Fig. 43. The angular distribution of protons of 90 MeV lab energy resulting from the collisions of Neon on Uranium at 2.1 GeV/n (left: $d\sigma/d\Omega$, right: $d\sigma/d\Theta$).
The sidewards peak is only seen with high multiplicity selection (i.e. central trigger)

Recently, both Heckman and Schopper have measured the angular distributions of only α-particles coming out of multiple prong stars in emulsion. As was theoretically expected, the α-particle distribution shows the Mach-shock peak much clearer. Also the rapidity plots of the Gutbrod-Stock-Poskanzer-group for various clusters (see Fig. 44) seem to indicate that the heavier particles (e.g. the α-particles) stem from a source of intermediate velocity (the collective Mach shock wave). It is this completion of the picture as well as the additional observation of Schopper (1979) and Baumgardt (private communication) that the velocity of the Mach-shock particles is significantly faster than the velocity of the background particles, which strengthens our confidence in the validity of the Mach-shock model. We predict, that the observation of angular distributions of big clusters out of azimuthally symmetric high multiplicity events will yield well recognizable peaks (Mach shock emission) whose dependence on energy will give us most valuable information about the gross features of the nuclear equation of state.

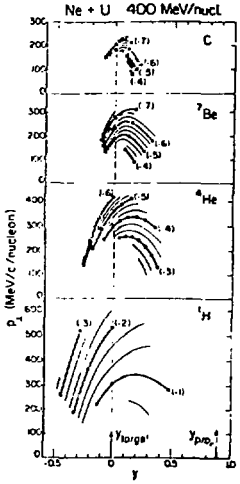

Fig.44. Rapidity plot of the heavier fragments measured by the GSI-LBL-collaboration show emission from medium velocity source.

10. STRONG BOUND PION STATES

In this section we shortly mention a purely speculative phenomenological idea: From the usual description of the pion nucleon interaction by a pseudo-scalar coupling

$$L_{\pi N} = - ig \bar{\psi} \gamma_5 \tau \Psi \vec{\phi}$$

where the pion field couples to the pseudo current

$$\gamma^{\mu}_{5i} = \bar{\psi} \gamma_5 \tau_i \Psi$$

one might expect that for high nuclear densities $\bar{\psi}\gamma^0\psi$ this interaction becomes very strong. Because of the very non-linear interaction between pions and nuclear matter, one does at present know very little about quantitative aspects at high nuclear density. For the low nuclear densities one knows that the pion-nucleon interaction is rather well described by the Kisslinger (Kisslinger,1955) potential. Ericson and Myrer (Ericson,1978) and others have shown that indeed for heavy nuclei (A>200) the Kisslinger potential may lead to bound pion states in the nucleus,the binding energy of the pion increasing with the nuclear density. This is shown qualitatively in Fig. . However, the Kisslinger potential looses its validity at such high densities. Therefore it cannot be definitely concluded that the gap between the π^+- and π^--states will actually approach zero for some critical density ρ_c, as suggested by the figure. For instance a strong repulsive interaction at high pion density (e.g. a ϕ^4 term in the π-Lagrangian) may prevent the two states shown in the figure from approaching each other. Though very little is known about strongly bound pionic states in high density nuclear matter. Such states, eventually leading to "spontaneous" π^+-π^--production i.e. without loss of energy should indeed by an exciting phenomenon if they exist.

Let us - phenomenologically - assume that strongly bound pion states exist in nuclear matter and ask how such states would reveal themselves in relativistic heavy ion collisions. In some test calculations we assumed that the strong collective nuclear force in highly dense nuclear matter leads to a strongly bound pion state with a small effective pionic mass ($m_\pi^{eff} << m_\pi$), which is supposed to arise from the repulsive - interaction. We found that, owing to the strongly bound pionic state the temperature in high energy heavy ion collisions will be reduced substantially at high densities $\rho/\rho_0 \gtrsim 2$ (see Fig. 45). A lot of pions are created in this strongly bound state of rather small energy, thus using up a large amount of the thermal energy of the system. This can lead to a drastic strong cooling even at rather small bombarding energies: These low energetic pionic states can be populated very massively already at relatively low temperature. The sudden reduction of the temperature above the critical bombarding energy necessary for the formation of such a strongly bound state may be detected experimentally as the

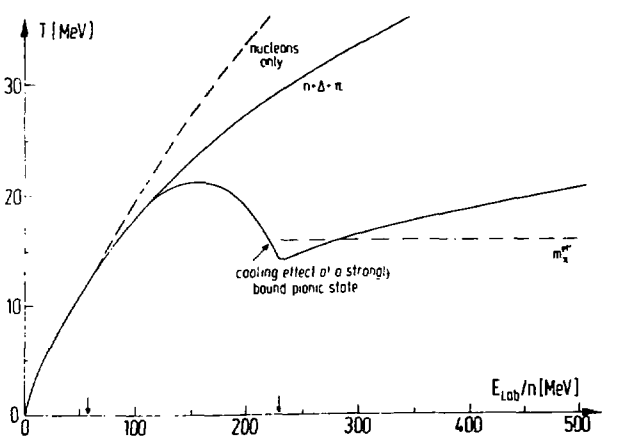

Fig. 45. The presence of a strongly bound pionic state would strongly cool the reaction zone in high energy heavy ion collisions above the critical energy.

evaporation spectra of the reaction products and the mean pion multiplicity strongly depend on the temperature of the compression zone. The pion production rate will be changed additionally because of the following processes: There will be less direct production of free pions as calculated above. However, two step processes, e.g. the excitation of pions from the bound state into the continuum, become important. Also the expansion of the compression zone after the reaction makes the production of free pions, which were originally created in a bound state, feasible.This is so, because of the "adiabatic" extraction of the pions (similar to electron-hole production in intermediate superheavy quasi-molecules) when approaching the upper continuum for smaller densities. Such a process may also lead to a decrease of the limiting temperature in central high energy nuclear collisions.

THE LIMITING TEMPERATURE - THE HADRONIC MASS SPECTRUM

Another important question, which can be raised in connection with high energy nuclear collisions is the search for a "limiting" temperature, as suggested by Hagedorn (1965) to occur in a single n-n collision, and suggested for nucleus-nucleus collisions by us (Scheid,1974; Greiner,1975). In the experimentally determined hadronic mass spectrum one notices a fast (actually nearly exponential) increase of the number of particles (resonances, mesons) with the mass of the particles. Presently, because of the limited accelerator capacities, the particle spectrum is practically only known for masses $m \leq 3$ GeV. However, if the hadronic mass spectrum is assumed to increase exponentially for all masses(which is a consequence of the bootstrap equations) there should exist an upper bound to the temperature which can be reached in high energy particle collisions. This so-called "limiting temperature" T^{Max} originates physically from the fact that hadronic matter with rising thermal excitation prefers to create particles of increasing mass (see Fig. 46). So, instead of increasing the temperature, higher excitation energy

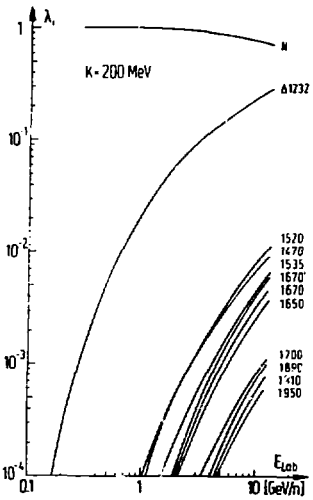

Fig. 46. The probability λ_i for the excitation of various resonances as calculated in the shock model is shown as function of the bombarding energy.

is transformed into mass of heavy particles. This can be seen clearly for the case of nuclear collisions in Fig. 2 , where the lowering of the temperature due to the excitation of resonances is shown (Hofmann,1976). If the number of resonances taken into account is increased, the temperature is substantially decreased compared to the calculation with a lower resonance number. This fact may also be viewed as the distribution of the internal energy over more degrees of freedom, which leads to a lower temperature. With the presently known experimental exponential increase of the hadronic mass spectrum, Hagedorn derived a limiting temperature for hadron-hadron collisions which is of the order of the pion rest mass

$$T^{Max} \approx m_\pi c^2 = 140 \text{ MeV} \quad . \qquad (1)$$

However, according to fluid dynamical calculations one may read such a large temperature only for rather high bombarding energies, $E_{LAB} \geq 10$ GeV/n. The best way to test whether a limiting temperature exists should be in a colliding beam experiment, with the much larger CM-energies available. One can convince oneself that a present CM-energies of the order of 1 GeV/n, it may be difficult to decide experimentally whether the limiting temperature T^{Max} is reached, because of various concurting processes. One indication of a limiting temperature is that the pion production rate no longer increases, as the limiting temperature is reached. However, the decay of the known heavy resonances mainly produces pions, so $\langle n_\pi \rangle$ should nevertheless still increase.

Let us now consider another phenomenon, which may lead to a strong cooling of the nuclear system: According to Huber and Dilling(1978), the excitation energies of the isobaric resonances can be lowered coherently in a nuclear density, the so-called "Giant Isobaric Resonances", where

$$E^{GIR} - E_i^{\text{free } N^*} \approx 50 - 80 \text{ MeV} \; .$$

Such an effect, if it exists, may become even stronger in heavy ion reactions at

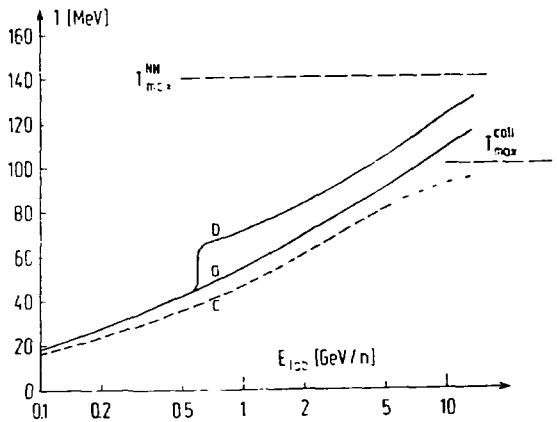

Fig.47. Shows the influence of the lowering of the resonance masses by 140 MeV each (dashed curve c)on the temperature. Curve b was obtained assuming a density isomer of depth ~140 MeV.

high densities, and thus would lead to enhanced transformation of excitation energy into resonance masses, thus lowering the temperature of the system drastically (see Fig. 47). For an exponentially increasing hadronic mass spectrum a coherent lowering of the hadronic masses in the strongly interacting medium should lead to a collective limiting temperature T^{Max}, considerably lower ($T^{Max}_{coll} << T^{Max}_{NN}$) than for the free hadronic masses. Recently, however, it has been shown by different authors (Kapusta,1978; Weiner,1979) that the existence of a quark phase excludes an exponential raise of the hadron mass spectrum and therefore a limiting temperature. In fact there are experimental indications (Friedländer,1979) that there is no limiting temperature.

12. SPECULATIONS ON THE FORMATION OF EXOTIC NUCLEI

The high excitation energy per nucleon achievable in relativistic nuclear collisions may also serve as a tool for the production of exotic pieces of matter like e.g. A^{N*} nuclei, i.e. nuclei which include several nuclear resonances at once of even consist exclusively of nuclear resonances. This would allow the study of the many-particle interaction of N^* with each other. In close analogy, the formation of strange nuclei and even nuclei consisting of strange particles only may be feasible. A number of interesting problems concerning the mutual strange particle interaction have still to be solved. For very large energies, anti-nucleon production becomes feasible, where the total energy for baryon pair production as a collective process is large enough, while the energy per nucleon is still too small ("sub-threshold production"). These opportunities seem very speculative for the moment, however, some preliminary evidence for a strongly enhanced strange particle production process was recently discovered by Sandoval, Stock, Schroeder and coworkers (Sandoval,1979) in a streamer chamber experiment at Berkeley, where they found an order of magnitude increase of the Λ^0 production in RHI-collisions compared to pp-reactions. They measured the proportion $\langle m_{\Lambda^0}\rangle / \langle m_{\pi^-}\rangle$ for the system Ar+K at 1.8 GeV/n and found

$$\langle m_{\Lambda^0} \rangle / \langle m_{\pi^-} \rangle \approx 1.7\% \quad , \tag{1}$$

which is nearly an order of magnitude increase of the strange particle production compared to nucleon-nucleon collisions. This enhanced strange particle production is very exciting, as it points further to a collective production mechanism for heavy baryons. We can estimate the strange particle formation within the one-dimensional shock calculations as presented in section . The thermal excitation probability for a Λ^0 in this model is given by the product of the probability of Kaon production and Λ^0 production

$$\begin{aligned} p &\rightarrow \Lambda^0 + K^+ \\ n &\rightarrow \Lambda^0 + K^0 \end{aligned} \tag{2}$$

$$\frac{\langle m_{\Lambda^0}\rangle}{\langle m_n\rangle} \approx e^{-\frac{E_{\Lambda^0}}{T_s}} \cdot e^{-\frac{m_K c^2}{T_s}} \approx e^{-\frac{674\ \mathrm{MeV}}{T_s}} \quad . \tag{3}$$

The excitation function for Λ^0-production then looks similar to the π-production shown in Fig. 21 , however, with a much smaller value. Inserting the temperature T_s as obtained in the simple shock calculation into equation (3), we find

$$\langle m_{\Lambda^0} \rangle / \langle m_n \rangle \approx 0.0033. \tag{4}$$

Thus, from this rough estimate we obtain

$$\langle m_{\Lambda^0} \rangle / \langle m_{\pi^-} \rangle \approx 2.9\% \tag{5}$$

in reasonable agreement with the preliminary experimental result of Sandoval,Stock, Schroeder and co-workers (Sandoval,1979) and in fact an order of magnitude larger than what has been measured in pp-reactions.

13. SUMMARY AND OUTLOOK

We attempted to demonstrate that Relativistic Heavy Ion physics can open new fields in fundamental research. Very important is the unique opportunity to study the properties of nuclear (hadronic) matter under extreme conditions in fast nuclear collisions: We gave - in our view convincingly - circumstantial evidence for the existence of shock waves, i.e. various high compression and temperature effects in relativistic heavy ion collisions. The once promoted general transparency of nuclear matter at high energies does - as a general effect - not exist. It might only have validity as a quantum-fluctuation, which can, however, be separated experimentall from the strongly interacting nucleus-nucleus encounters.
The high densities which may be achieved in relativistic collisions enable us to search for phase transitions (like pion condensation, density isomers) in nuclear matter and in particular for a transition of baryon into quark matter. These phase transitions themselves amplify because of critical scattering the validity of hydrodynamical and thermodynamical concepts. Therefore we can expect high compression effects to occur even up to bombarding energies of 10 GeV/n and higher. Also the experimental determination of the nuclear compression constant and sound velocity seems feasible. The high thermal excitations allow to study the successive transformation of nuclear matter into highly excited hadronic matter and the search for a limiting temperature. The collective formation of very heavy particles, bulks of strange matter and antimatter are further intriguing possibilities.

There are indications in the Mach-shock experiments of Schopper and Baumgardt (1979) that a phase transition of some kind (perhaps into a density isomeric configuration) might occur between 1.2 and 1.8 GeV/n. To check this out convincingly more refined experiments (excitation functions of α-particle angular distributions from multiplying events, pion production excitation functions) are necessary. Most important in this connection is also the further continuation of these experiments to higher energy up to e.g. 10 GeV/n and even higher energies.

REFERENCES

Anastasio, M.R., and G.E. Brown (1977). Nuc. Phys. A285, 516.
Antonenko, V.G., et al. (1979). Dubna preprint.
Baumgardt, H.G., J.U, Schott, Y. Sakamoto, E. Schopper, H. Stöcker, J. Hofmann, W. Scheid, and W. Greiner (1975), Z.Physik, A237,359.
Baym,G., and S.A. Chin (1976). Phys.Lett.,62B, 241.
Bertsch, G (1977). Phys.Rev.,C15,713.
Bodmer, A.R. (1971). Phys.Rev.,D4, 1601.
Brown, G.E., and W. Weise (1975). Phys.Rep., 22C, 279.
Brown, G.E., and W. Weise (1976). Phys.Rep., 27C, 1.
Buchwald, G. (1979). Thesis, University Frankfurt, unpublished.
Campbell, D.K., R.F. Dashen, J.T. Manassah (1975). Phys.Rev.,D12, 979 and 1010.
Chapline, G.F., M.H. Johnson, E.Teller, and M.S. Weiss (1973). Phys. Rev.,D8,4302.
Chodos, A., R.L. Jaffe, K. Johnson, C.B. Thorn, and V. Weisskopf (1974). Phys.Rev. D9, 3471.
Collins, J.C., and M.J. Perry (1975), Phys.Rev.Lett., 34, 1353.
Dalitz, R.H. (1976). Fundamentals of Quark Models, 17th Scottisch Universities Summer School in Physics, St. Andrews (ed. J.M. Barbour and A.T. Davis).
Ericson, T.E.O., and F. Myhrer (1978). Phys.Lett.,74B, 163.
Feenberg, E., and H. Primakoff (1946). Phys.Rev.,70, 980.
Fowler, G.N. and R.M. Weiner (1979). To be published.

Freedman, B., and L.McLerran (1978). Phys.Rev., D17, 1109.
Friedländer, E. (1979). Private communication.
Fung, S.Y., W. Gorn, G.P. Kiernan, J.J. Lu, Y.T. Oh, and R.T. Poe (1978), Phys.Rev. Lett., 41, 1592.
Galitskii, V.M., and I.N. Mishustin (1978). Phys.Lett., 72B, 285.
Greiner, W. (1975). Talk at the 3rd High Energy Heavy Ion Summer Study, Berkeley, Calif.
Gyulassy, M., and W. Greiner (1977). Ann.Phys., 109, 485.
Hagedorn, R. (1965). Supp. Nuovo Cim., III. 2, 147.
Heinz, U., H. Stöcker, and W. Greiner (1978). Proc. Symp. on Relativistic Heavy Ion Research, GSI, Darmstadt.
Hofmann, J., H. Stöcker, W. Scheid, and W. Greiner (1974). Rep. of the Workshop on BEV/Nucleon Collisions of Heavy Ions, Bear Mountain, New York.
Hofmann, J., W. Scheid, and W. Greiner (1976). Nuovo Cim., 33A, 343.
Hofmann, J., H. Stöcker, M. Gyulassy, W. Scheid, and W. Greiner (1976). Proc. Int. Conf. on Selected Topics in Nuclear Structure, Dubna (USSR)
Hofmann, J., H. Stöcker, U. Heinz, W. Scheid, W. Greiner (1976). Phys.Rev.Lett.,36, 88.
Hofmann, J., B. Müller, and W. Greiner (1979). Phys. Lett., 82B, 195.
Irvine, J.M. (1975). Rep. Prog. Phys., 38, 1385.
Kapusta, J.I. (1979). Nuc. Phys., B148, 461.
Keister, B.D., and L.S. Kisslinger (1976). Phys. Lett., 64I, 117.
Kisslinger, L.S. (1955). Phys. Rev., 98, 761.
Lee, T.D., G.C. Wick (1974). Phys.Rev., D9, 2291.
Maruhn, J.A. (1977). Proc. Conf. on Heavy Ion Collisions, Oak Ridge, Tenn., p.156.
Mattuck, R.D., and B. Johansson (1968). Adv. Physics, 17, 509.
Meyer, W., H. Gutbrod, R. Stock, A. Poskanzer, A. Sandoval, et al. (1978). To be published.
Migdal, A.B. (1967). Theory of Finite Fermi Systems and Applications to Atomic Nuclei. Interscience, New York.
Migdal, A.B. (1972). JETP, 34, 1184.
Migdal, A.B. (1978) Rev. Mod. Phys., 50, 107.
Nagamiya, S., et al. (1979). Phys.Lett., 81B, 147.
Ne'eman, Y. (1974). Physics of Dense Matter (ed. C.J. Hansen), Reidel, Dordrecht, Boston, p. 111.
Richardson, J.L. (1979). Phys. Lett., 82B, 272.
Ruck, V., M. Gyulassy, and W. Greiner (1976). Z. Physik, A277,391.
Sandoval, A., R. Stock, L. Schroeder, et al. (1979). To be published.
Sawyer, R.F., and D.J. Scalapino (1973). Phys. Rev. D7, 953.
Scheid, W., R. Ligensa, and W. Greiner (1968). Phys. Rev. Lett., 21, 1479.
Scheid, W., and W. Greiner (1969). Z.Physik, 226, 365.
Scheid, W., H. Müller, and W. Greiner (1974). Phys. Rev. Lett., 32, 741.
Scheid, W., J. Hofmann, and W. Greiner (1974a). Proc. of the 2nd High Energy Heavy Ion Summer Study, Berkeley, Calif. (ed. L.S. Schroeder), LBL Report No. LBL-3675.
Schopper, E. and H.G. Baumgardt (1979). Priv. communication.
Sobel, M.I., P.J. Siemens, J.P. Bondorf, and H.A. Bethe (1975). Nuc.Phys. A251, 502.
Stanley, H.E. (1971). Introduction to Phase Transitions and Critical Phenomena, Clarendon Press, Oxford.
Stöcker, H., W. Scheid, and W. Greiner (1977). Proc. of the Topical Conf. on Heavy Ion Collisions, Fall Creek Falls State Park, Oak Ridge, USA.
Stöcker, H., J. Hofmann, W. Scheid, and W. Greiner (1977a). Conf. on Nuclear Collisions, Bled, Yugoslavia. Fizika 9, Supp. 4, 671.
Stöcker, H. W. Greiner, and W. Scheid (1978). Z.Physik, A286, 121.
Stöcker, H., J. Reinhardt, J.A. Maruhn, and W. Greiner (1978a). Proc. Workshops on Heavy Ion Physics, Saclay (France).
Stöcker, H., J.A. Maruhn, and W. Greiner (1979). Z. Physik, A290, 297.
Stöcker, H., J.A. Maruhn, and W. Greiner (1979a). Phys. Rep. To be published.
Stöcker, H., J.A. Maruhn, and W. Greiner (1979b). Phys. Lett., 81B, 303.

Stöcker, J.A. Maruhn, and W. Greiner (1979c). To be published.
Vasak, D., B. Müller, and W. Greiner (1979). To be published.
Weise, W., and P. Hecking (1979). To be published.
Wolf, K.L. et al. (1979). Phys. Rev. Lett., 42, 1448.
Wong, C.Y., and T.A. Welton (1974). Phys. Lett., 49B, 243.
Wong, C.Y., J.A. Maruhn, and T.A. Welton (1977). Phys. Lett., 66B, 19.

NUCLEAR PHENOMENA AND THE SHORT DISTANCE STRUCTURE OF HADRONS*

Stanley J. Brodsky
Stanford Linear Accelerator Center
Stanford University, Stanford, California 94305

ABSTRACT

In certain cases, nuclear corrections to hadronic phenomena depend in detail on the nature of quark and gluon interactions, as well as the effects of jet development within the nuclear medium. In this talk I review applications of quantum chromodynamics to fast particle production in nuclear collisions, nuclear form factors, and shadowing in deep inelastic lepton processes. I also discuss a new approach to particle production in hadron-nucleus, nucleus-nucleus and deep-inelastic nuclear reactions from the standpoint of a color-neutralization model.

* Work supported by the Department of Energy under contract number DE-AC03-76SF00515.

I. Introduction

A basic premise of this workshop is that there are aspects of hadronic physics which can only be studied in nuclear collisions. The most dramatic possibility is that novel collective hadronic degrees of freedom or a new phase of hadronic matter will be initiated in central, high-energy heavy-ion collisions.[1] Even if this turns out not to be the case, one can argue that the nucleus is an essential tool for the study of fundamental hadronic mechanisms at distances where the quark and gluon degrees of freedom are relevant.[2]

In this talk I will discuss several topics involving nuclear collisions where one can possibly test and study interesting aspects of quantum chromodynamics (QCD). These include

(A) Hadronic production in hadron-nucleus, lepton-nucleus and nucleus-nucleus collisions.

(B) The question of shadowing in deep inelastic nuclear reactions.

(C) The structure of the nuclear wave function at very short distances and nuclear form factors.

Of course, the advantage of being able to study hadronic mechanisms in close proximity to other quarks and gluons in nuclei has to be counterbalanced by the complexity of the nucleus. By turning to nucleus-nucleus collisions we exactly reverse Feynman's famous analog,[3] in which he compares proton-proton collisions to the smashing together of two delicate watches; it is obviously much simpler to study elementary "gear-gear" interactions, as in e^+e^- collisions. The nucleus-nucleus collision seems to be the analog of the collision of two grandfather clocks, or perhaps

even whole jewelry stores! Despite this, there are fascinating, controversial questions concerning the physics of nuclear collisions which appear to depend in detail on basic mechanisms at the quark and gluon level. This talk touches on only a fraction of these problems, but I hope it will serve to stimulate further experimental and theoretical studies.

II. Hadron Production in Nuclear Collisions

There is now extensive data on hadron production in nuclei from meson, baryon, and lepton beams at laboratory energies up to 200 GeV.[4] The subject is fascinating to theorists, but there is little concensus on the basic particle production mechanisms within the nucleus. This is understandable, since it is not clear we even understand particle production in ordinary nucleon-nucleon collisions! The simplest particle production model consistent with the framework of QCD is the gluon-exchange model of Low[5] and Nussinov.[6]

Let us suppose that two protons interact by the exchange of a single soft gluon (a color octet). This leaves the spectator quarks in each nucleon excited as color octets [see Fig. 1(a)]. The subsequent color neutralization of these two "jets" and the recombination of the gluons and quarks into hadrons is evidentally similar to the particle production mechanism which occurs in $e^+e^- \to q\bar{q} \to$ hadrons.[7] This picture is obviously oversimplified, however in analogy with QED it predicts[7] (a) a uniform central rapidity distribution — expanding as log s (due to the spin-one nature of the gluon) [see Fig. 1(b)], (b) a transverse momentum cutoff (due to hadronic wave function fall-off), (c) a multiplicity distribution

which rises faster than log s (similar to analogous effects in soft photon radiation in QED), and (d) a nearly constant total cross section which depends on the color dipole moment, and hence the size and quark content of the interacting hadrons.

In effect this color-neutralization model leads to final states not so different from the standard multiperipheral model productions, but the underlying mechanisms and time sequence are quite different.

Let us now consider the implications of this picture for a hadron-nuclear collision. Figure 2 illustrates an event where a gluon is exchanged between an incident hadron H and a nucleon N_1 in nucleus A. The quarks and gluons produced in the color-neutralization can subsequently interact and color-excite further nucleons; the figures represents an event where $\nu = 3$ nucleons in A are "wounded." For the average number of wounded nucleons we can use the standard geometrical estimate $\bar{\nu} = A\sigma_{HN}^{inel}/\sigma_{HA}^{inel}$. For simplicity we will first consider the case where one quark of H (and its neutralization cloud) interacts; multiquark interactions will be taken into account later.

The expected multiplicity distribution corresponding to the $\nu = 3$ event of Fig. 2 is shown in Fig. 3(a). We plot the ratio $R_{HA}(y) = [dN/dy]_{HA}/[dN/dy]_{HN}$ (the multiplicity distribution normalized to nucleon-target data) in order to isolate the nuclear effects. The multiplicity distribution ratio for $y < y_A$ reflects the wounding of $\nu = 3$ quarks: $R_{HA}(y) = \nu$. The multiplicity for $y > y_H$ in the projectile region in the simple model is $R_{HA}(y) = 1$; a more detailed model which allows for multi-quark interactions would give $R_{HA}(y) < 1$, reflecting energy-momentum loss. Our analysis here will closely follow the formulation of Ref. (8).

Let us now assume that the rapidity of any of the secondary quarks or gluons which excite N_2 and N_3 in Fig. 2 occur $\frac{-}{}$ on the average — uniformly in rapidity in the central region. (This simple assumption is in fact controversial since it can be argued that the fast constituents produced in the first neutralization tend to be produced outside the nuclear volume. This would bias the secondary interactions toward target rapidities.[9]) Averaging over events then gives the "ramp"-like distribution ratio $R_{HA}(y)$ shown in Fig. 3(b). Analytically, one finds for $y_A < y < y_H$,[8]

$$R_{HA}(y) = \bar{\nu}\left[1 - \left(\frac{y - y_A}{y_C}\right)\right] + \left[1 - \left(\frac{y_H - y}{y_C}\right)^{\bar{\nu}}\right] \qquad (2.1)$$

where $y_C = y_H - y_A \sim \log s$ is the length of the central region. The first term in (2.1) represents the hadrons produced from the $\bar{\nu}$ nuclear excitations. The second term represents the multiplicity produced by the repeated excitation of H and its products. Integrating over the central region gives the ratio,

$$R_{HA} = \frac{N_{HA}}{N_{HN}} = \frac{\bar{\nu}}{2} + \frac{\bar{\nu}}{\bar{\nu}+1} \qquad \left(y_A < y < y_H\right) \qquad (2.2)$$

(The second term $\bar{\nu}/(\bar{\nu}+1)$ gives the mean fraction of the central region populated by H and its products.) Including the fragmentation regions

$$R_{HA} = \left(\frac{\bar{\nu}}{2} + \frac{\bar{\nu}}{\bar{\nu}+1}\right)\frac{\langle n_{CENTRAL}\rangle_{HN}}{\langle n_{TOT}\rangle_{HN}} + \bar{\nu}\,\frac{\langle n_{FRAG}\rangle_{N}}{\langle n_{TOT}\rangle_{HN}} + \frac{\langle n_{FRAG}\rangle_{H}}{\langle n_{TOT}\rangle_{HN}} \qquad (2.3)$$

where $\langle n_{TOT}\rangle_{HN} = \langle n_{CENTRAL}\rangle_{HN} + \langle n_{FRAG}\rangle_{N} + \langle n_{FRAG}\rangle_{N}$. Thus

$$\left(\frac{\bar{\nu}}{2}+\frac{1}{2}\right) \leq R_{HA} \leq \left(\frac{\bar{\nu}}{2}+\frac{\bar{\nu}}{\bar{\nu}+1}\right) \qquad (2.4)$$

where the upper limit is reached for $s \to \infty$. Note that R_{HA} only depends on the projectile cross section through $\bar{\nu} = A\sigma_{HA}^{inel}/\sigma_{HN}^{inel}$. A comparison of this simple prediction with the data of W. Busza et al.[10] is shown in Fig. 4(a). The prediction given in Eq. (2.1) also gives a good representation of the 200 GeV p-A (pseudo-rapidity) data of Azimov et al.[11] in the central region [see Fig. 4(b)]. For $y > y_H$, the data shows that $R_{HA} < 1$, indicating energy-momentum losses for the fast fragments of H; for $y < y_A$ there are indications of cascading in the nuclear target fragmentation region, at least for heavy nuclei.

Let us now turn to nucleus-nucleus collisions $B+A \to X$, and consider the multiplicity ratio (normalized to nucleon-nucleon collisions)

$$R_{BA}(y) = \frac{dN/dy\ (B+A \to X)}{dN/dy\ (N+N \to X)} \qquad (2.5)$$

In virtually all models one expects the ratio in the fragmentation regions ($y \lesssim y_A$, $y \gtrsim y_B$) to equal the number of wounded constituents (nucleons), $W_A = A\sigma_{NB}/\sigma_{AB}$, and $W_B = B\sigma_{NA}/\sigma_{AB}$ in A and B respectively. The interesting question is what $R_{BA}(y)$ looks like in the central region. Several very different possibilities are implies by models in the literature [see Fig. 5(b)]. In the Reggeon-calculus multiple-cut model of Ref. 12, independent (multiperipheral model) chains contained within the projectile wave function are excited and produce multiplicity throughout the central region (subject to overall energy conservation). In the early parton-model approach of Ref. 13, the multiplicity produced due to nuclear excitation occurs only locally in the nuclear target fragmentation region.

The quark-constituent model of Ref. 14 leads to a "3-step" picture since only flat plateau regions are allowed. In the color-neutralization model discussed here, there is no such constraint and the central region smoothly interpolates between the two fragmentation regions.

The calculation of the multiplicity ratio in the color-neutralization model for nucleus-nucleus collisions A+B → X is only slightly more complicated than the nucleus-nucleus case. Notice that each nucleon of A can potentially break-up any nucleon of nucleus B. The average number of times each nucleon in A interacts in B is $\bar{\nu}_B = B\sigma_{NN}^{inel}/\sigma_{BN}^{inel}$. We then find:[8]

$$R_{BA}(y) = \frac{dN/dy\ (B+A)}{dN/dy\ (N+N)} = W_A\left[1-\left(\frac{y-y_A}{y_C}\right)^{\bar{\nu}_B}\right] + W_B\left[1-\left(\frac{y_B-y}{y_C}\right)^{\bar{\nu}_B}\right] \tag{2.6}$$

and the integrated ratio in the central region is

$$R_{BA} \equiv \frac{\langle n\rangle_{B+A}}{\langle n\rangle_{N+N}} = W_A\left[1-\frac{1}{\bar{\nu}_B+1}\right] + W_B\left[1-\frac{1}{\bar{\nu}_A+1}\right] \tag{2.7}$$

There is very little data for nuclear-nuclear collisions. One example is $R_{BA} \cong 3.8$ for $\alpha+A$, $A > 100$ from Eq. (2.7) compared to a ratio of order ~4 from cosmic rays.[15] A comparison of Eq. (2.7) with the model of Bialas, Czyz and Furmanski[14] is shown in Fig. 6. We also note that for $y_{cm} = 0$, Eq. (2.6) predicts

$$\frac{W_A + W_B}{2} \leq R_{AB}\ (y_{cm}=0) \leq W_A + W_B \quad ; \tag{2.8}$$

the ratio is maximal at $y_{cm} = 0$ if A = B.

Having worked out the nucleus-nucleus case, it is simple to generalize the model and allow any or all of the quarks of each nucleon to interact; we simply count "wounded" and interacting quarks rather than nucleons. For example, we can apply Eqs. (2.6) and (2.7) to N-N collisions, taking each nucleon as a "nucleus" with 3 quarks; then

$$W_N = 3\sigma_{qN}/\sigma_{NN} \geq 1 \tag{2.9}$$

and

$$\bar{\nu}_q = 3\sigma_{qq}/\sigma_{qN} \geq 1 \tag{2.10}$$

giving the ratio

$$\frac{dN/dy\ (p+p)}{dN/dy\ (q+q)} = W_N\left[1 - \left(\frac{y - y_A}{y_C}\right)^{\bar{\nu}_q} + 1 - \left(\frac{y_B - y}{y_C}\right)^{\bar{\nu}_q}\right] \tag{2.11}$$

An amusing feature of this result is that $dN/dy(p+p)$ has a bowed distribution, maximal at $y_{cm} = 0$ even if $dN/dy(q+q)$ is flat. This also predicts that $dN/dy(\pi - N)$ is less bowed but is slightly asymmetrical about $y_{cm} = 0$. The previous results for $R_{HA}(y)$ and $R_{AB}(y)$ are unchanged if $\sigma_{qN} = \frac{1}{3}\sigma_{NN}$, $\sigma_{qq} = \frac{1}{3}\sigma_{qN}$ (since they are normalized to N-N collisions); thus one only expects minor changes for the multiplicity ratios for nuclei even if the quark cross sections are screened.

In order to justify the simple counting of quarks as constituents in inelastic reactions, let us consider a meson-nucleus collision where both the quark and antiquark each exchange a color gluon with the target [see Fig. 7]. After two soft gluon-exchanges, the $q\bar{q}$ system can be in either a color octet or color singlet state. If we assume that the resulting hadronic multiplicity is proportional to the color charge (Casimir operators 9/4 and 0 respectively), then the statistical average

over events gives

$$\frac{dN}{dy} \propto \left(\frac{8}{9}\right) \times \left(\frac{9}{4}\right) + \left(\frac{1}{9}\right) \times (0) = 2 \qquad (2.12)$$

i.e., the same result as an incoherent sum. Nevertheless, color coherence implies that the multiplicity distribution will have large fluctuations about the mean.

It is interesting to apply the color neutralization model to deep inelastic lepton scattering on a nuclear target [see Fig. 8]. For large Q^2, the interaction begins with the scattering of a quark in the target along the virtual γ (or W) direction. The particles produced in the color-neutralization of the separated q and qq then can interact and excite additional nucleons in the nucleus.[16] Thus, even though the observed cross section is linear in the nucleon number A, several nucleons can be "wounded" in the deep inelastic process. These expectations can be compared with the inelastic p_{lab} = 150 GeV/c muon-emulsion data shown in Fig. 9(a) from the Cornell, FNAL, Cracow collaboration.[17] The shape of the multiplicity distribution (in pseudo-rapidity η) for incident 150 GeV μ^+ is not very dissimilar from corresponding 60 GeV/c pion-emulsion data! The magnitude of the produced multiplicity in the central region is not quite as large as the pion induced multiplicity, but the data in Fig. 9(b) shows that mean total multiplicity in deep inelastic muon-emulsion collisions is much larger than the corresponding μ-p multiplicity, independent of the value of $\omega = 2q\cdot p/Q^2$. These results give strong evidence that the energy associated with "quark jet" production is effective in producing hadrons in its passage through the nucleus. The similar shapes for dN/dy for μp and πp gives support to the idea that

the same color-neutralization mechanisms are effective in both processes. Further study of particles produced in deep inelastic processes in heavy nuclei, especially the Drell-Yan reaction, $H+A \to \mu^+\mu^- X$, is clearly very important for understanding the basic interactions of q and qq jets in the nuclear medium.

The color-neutralization model presented here, though simple, is based on QCD and should give a reasonable guess on what happens in nucleus-nucleus collisions if such mechanisms are relevant. Although I have done a complete analysis, I believe that this color approach is consistent with generalized Glauber theory; the hadronic multiplicity can be computed from unitarity cuts of the forward scattering amplitude.

In principle, there could be mechanisms operating in high energy nucleus-nucleus collisions which would not occur in hadron-nucleus collisions. For example, the color neutralization of many jets in a single collision could lead to some type of anomalous phenomena, such as an overall excitation or "heating" of the nuclear system. The observables include $dN/dy(A_1+A_2)$, the π/K ratio, charm production, leading particle production, the associated multiplicity in massive lepton pair (on and off resonance), and the rate of η or ψ production or direct photon[18] production, as a hint of anomalous gluon production. I should emphasize that the analysis presented here is only semi-qualitative. However, the basic formulation and results are so simple that they may well be useful as a guide and parametrization of the data.

III. Shadowing in Deep Inelastic Lepton Scattering on Nuclei

It is well known that the photoabsorption cross section for on-shell photons on nuclei at SLAC[19] and Cornell[20] energies is not additive in the nuclear number; empirically $\sigma_{\gamma A} \sim A_{eff}\sigma_{\gamma N}$ where $A_{eff}/A \sim .85 \pm .05$. For virtual photons with $Q^2 \geq 1$ GeV^2, $A_{eff}/A \sim 1$. The central question is what variable controls this "shadowing" phenomena. Two very different points of view have been discussed in the literature.

(A) One can argue that fixed Q^2, $\omega = 2m\nu/Q^2 \to \infty$ electroproduction data connects smoothly to $Q^2 = 0$ photoabsorption physics.[21] This "correspondence principle" argument[22] is reinforced by the fact that for large ω, the photon converts to hadronic matter well before the interaction with the nucleus. Thus one predicts that the cross section is shadowed $\left[\nu W_2^A / A\nu W_2^N < 1\right]$ for sufficiently large ω, independent of the value of Q^2. However, there is a momentum sum rule for the area under νW_{2A} (assuming a conventional gluon-quark momentum fraction balance). Thus as noted by Nicolaev and Zakharov,[13] there must be an "anti-shadowing" region probably at $x = \omega^{-1} = m_\pi/m_N$ where $\nu W_2^A > A\nu W_2^N$ [see Fig. 10(a)]. Such a phenomenon would imply to a new type of dynamical interaction between wee partons within the nucleus.

(B) The alternative view,[8] which I favor, is that for $Q^2 > Q_0^2 \sim 1$ GeV^2, $\nu W_2^A(x) = A\nu W_2^N(x)$ for all $x \lesssim 1$. (In addition for $1 \gtrsim x > A$, there is the standard high momentum tail.) [see Fig. 10(b)] Thus for sufficiently large Q^2, the pointlike interactions of virtual photons in the nucleus are essentially incoherent and additive.

More formally, one can write the total photoabsorption cross section in the spectral form[23]

$$\sigma_{\gamma N}(\nu,Q^2) = C\int \frac{d\mathcal{M}^2\,\mathcal{M}^4}{(\mathcal{M}^2+Q^2)^2}\,\sigma_{e^+e^-}(\mathcal{M}^2)\,\sigma_{\mathcal{M}^2}(\nu,Q^2) \qquad (3.1)$$

where $\mathcal{M}$ is the mass of virtual hadronic state which couple to the photon. The spectrum is computed from the e^+e^- annihilation cross section $\sigma_{e^+e^-}(\mathcal{M}^2)$. In order to obtain Bjorken scaling at large ω [modulo logarithmic scale-breaking] the meson-nucleon cross section must behave as $\sigma_{\mathcal{M}^2}(\mathcal{M},Q^2) \sim (\mathcal{M}^2+Q^2)^{-1}$ for large ν. Notice that only $\mathcal{M}^2 \geq O(Q^2)$ contributes to the $\sigma_{\gamma N} \sim (Q^2)^{-1}$ scaling region. But in this region $\sigma_{\mathcal{M}^2}$ is numerically small, and in the case of nuclei, shadowing of the large Q^2 cross section cannot occur![8] The quark-partons of the nucleus at low x thus act independently and incoherently. Further tests of this idea can also be made using the Drell-Yan process $pA \to \mu^+\mu^- X$.

IV. Short-Distance Processes in Nuclei

One of the most interesting questions which can be analyzed using ordinary nuclei is the study of hadronic matter at high density. Here we will be interested in processes such as nuclear form factors at very large momentum transfer, and fast particle production in nuclear collisions (beyond the usual nucleon kinematic limit) each of which probe the high momentum tail of the nuclear wave function. These reactions are sensitive to the behavior of the quark fields in regions of strong overlap.

There is now extensive data (primarily from H. Steiner et al.[24] at LBL) available for the reactions $A_1 + A_2 \to H + X$ for the collisions of

nuclei such as ^{12}C and ^{4}He, at $E_{lab} \lesssim 2$ GeV/nucleon and the production of systems such as $H = \pi$, p, ^{2}H, ^{3}H, ^{4}He at longitudinal momentum k_L well beyond the nucleon-nucleon kinematic limit. In principle the produced hadron H could have nearly all of the momentum of the beam nucleus, but this is clearly exceedingly rare. The question is how rare? Instead of using standard variables such as k_L/k_{Lmax} or E/E_{max}, it is most convenient to use the "light-cone" fraction[25]

$$x = \frac{k_0 + k_3}{P_0 + P_3} \tag{4.1}$$

where k_0 and k_3 are the energy and longitudinal momenta of H and $P_0 + P_3$ are the energy and momentum of A_1. Notice that x is invariant under boosts along P_3. The invariant phase space is $d^3k/k_0 = d^2k_\perp dx/x$ where $\vec{k}_\perp$ is the transverse momentum of H.

The nuclear momentum space wave function [see Fig. 11(a)] can be written as $\Psi_A(x_a, \vec{k}_{\perp a})$, where by momentum conservation $\sum_a \vec{k}_{\perp a} = 0$, $\sum_a x_a = 1$. Since $k_0 = k_3 + (\vec{k}_\perp^2 + m)/(k_0 + k_3)$ for each constituent, the standard energy denominator is

$$\Delta E \equiv P_0 - \sum_a k_0^a$$

$$\Delta E(P_0 + P_3) = M_A^2 - \sum_a \frac{\vec{k}_{\perp a}^2 + m_a^2}{x_a} \tag{4.2}$$

In the adiabatic limit where the binding energy ϵ vanishes, we have $\vec{k}_\perp^2 \to 0$, $x_a \to m_a/M_A$ and $\Delta E \to 0$. Thus $x_a \sim m_a/M_A$ corresponds to the quasi-elastic peak. For example, for the deuteron

$$\Delta E(P_0 + P_3) = M_D^2 - \frac{M_N^2 + \vec{k}_\perp^2}{x} - \frac{M_N^2 + \vec{k}_\perp^2}{1-x} \qquad (4.3)$$

$$= \begin{cases} M_D^2 - 4M_N^2 - 4\vec{k}_\perp^2 \sim O(M_D\epsilon) & \text{if } x \sim 1/2 \\ M_D^2 - \frac{M_N^2}{0.8} - \frac{M_N^2}{0.2} \sim -2.25\ \text{GeV}^2 & \text{if } x \sim 0.8 \end{cases}$$

Thus, by examining the deuteron wave function in a configuration where one nucleon has 80% of the maximum momentum, the state is probed far off-shell where, in fact, asymptotic freedom perturbative quantum chromodynamic (QCD) calculations should be valid. In this far off-shell regime, the analysis of the high momentum tail of the nuclear wave function clearly involves the synthesis of quark and nuclear physics.

At high energies where cross sections become nearly energy-independent, the reaction $A_1 + A_2 \to H + X$ can be thought of as the materialization of the off-shell wave function[26] [as in Fig. 16]. Thus we expect

$$\frac{dN}{dx}(A_1 + A_2 \to H + X) \equiv \frac{1}{\sigma_{\text{inel}}} \int \frac{d^3\sigma}{d^3k/k_0}\, d^2k_\perp$$

$$= \frac{1}{1-x} \int |\psi(x, \vec{k}_\perp)|^2 \, \Pi\left[d^2k_{\perp a}\right] \Pi\left[dx_a\right] \qquad (4.4)$$

where the integration is over all unobserved momenta, consistent with momentum conservation. (The inverse factor of 1-x arises from the spectators' phase space.) If we use perturbative QCD then the off-shell kinematics for $x \to 1$ requires the repeated iteration of the QCD scale-invariant kernel in order to "stop" each quark spectator in ψ_{A_1}. Each iteration yields an additional $(1-x)^2$ fall-off, and one readily obtains the "spectator quark counting rule",[26,27,28]

$$\frac{dN}{dx}(H/A) \sim C(1-x)^{2n_s-1} = C(1-x)^{6N_s-1} \qquad (4.5)$$

where n_s is the number of quark spectators (originally bound in A) left behind after forming H. For nuclear problems $n_s = 3N_s$, where N_s is the number of spectator nucleons. The constant C is proportional to the wave function at the origin, i.e., the probability amplitude to find all the quarks at the same point. The spectator counting rule can be derived in QCD, with calculable logarithmic modifications arising from the anomalous dimensions of the hadronic wave function. [In addition one finds that[29] (a) the helicity of A and H tend to match as $x \to 1$, (b) additional spin suppression factors of (1-x) can occur in the case of electromagnetic or weak interaction probes,[29,30] and (c) gluon bremsstrahlung in QCD increase the exponent of (1-x) by a log log s term[31] which is proportional to the color charge[32] (Casimir operator) of H. This latter correction does not occur when H is a hadron.] The simple spectator rule[26] gives $dN/dx \sim (1-x)^3$ for q/p, $(1-x)^1$ for q/M, $(1-x)^5$ for p/D, $(1-x)^9$ for q/D for the leading power of the distribution as $x \to 1$. Notice that the prediction $(1-x)^{65}$ for p/C can also be obtained via the sequential fragmentation $(1-x)^{47}$ for α/C convoluted with $(1-x)^{17}$ for p/α. A comparison of the α/C and p/C predictions with the data of Steiner et al.[24] shown in Fig. 12. A systematic comparison of theory and experiment has been given by Blankenbecler and Schmidt.[28] An effective nucleon-constituent model[28] can also be devised to reproduce (4.5).

The recent forward angle data[24] [see Fig. 13] for p/α apparently indicates two components to the fragmentation distribution, possibly reflecting an intermediate regime from $dN/dx\,(p/d) \sim (0.5-x)^5$. The region beyond $x > 0.4$ is fit to $(1-x)^{15}$ and is not inconsistent with

the $(1-x)^{17}$ prediction. Such comparisons could be more definitive if the light-cone variable x were used.

Although the application of quark-gluon dynamics to such relatively low-energy nuclear data may seem radical, I emphasize that it is justified by the fact that quite far off-shell kinematics are really involved.

Perhaps the most dramatic application of short-distance physics to nuclear targets concerns nuclear form factors at large momentum transfer. The elastic form factor F(t) [with $t = q^2 = -Q^2 < 0$] is the probability amplitude that the target system stays intact and unexcited upon deflection from p to p+q in the electromagnetic collision $eA \to eA$. The dimensional counting rule for the (helicity-conserving) form factor[23]

$$F(t) \sim \frac{1}{t^{n-1}} \qquad \left(|t| >> M^2\right) \tag{4.6}$$

(where n is the minimum number of elementary constituents) reflects the fact that the more complex the target, the faster the power-law fall off. From this formula one predicts $tF_\pi(t)$, $t^2G_M^N(t)$, and $t^5F_D(t)$ are each asymptotically constant. The comparison[34,35] with experiment is shown in Fig. 14. The dimensional counting rule can be rigorously derived in QCD, modulo logarithmic modifications (suppression) from the anomalous dimensions of the hadron wave function; e.g., for the nucleon form factor[36] QCD predicts

$$G_M(t) = \frac{\alpha_s^2(t)}{t^2}\left[\sum_{n=0} a_n \log^{-\gamma_n}(-t/\Lambda^2)\right]^2 \left[1 + \mathcal{O}\left(m^2/t\,,\,\alpha_s(t)\right)\right] \tag{4.7}$$

where the γ_n are known positive numbers (amonalous dimensions) and $\alpha_s(t) \sim C/\log(-t/\Lambda^2)$ is the QCD running coupling constant. In general,

the power law reflects the fact that at large t one must pay a penalty of $\alpha_s(t)/t$ to move a constituent from p to p+q. The usual identification of the form factor with the Fourier transform of the static charge distribution is inapplicable to the relativistic regime.

Is it possible that these quark-gluon results can be applied to systems as complex as nuclei? The answer is certainly yes, although the fact that the momentum transfer must be partitioned among the constituent nucleons implies that the momentum transfer required to reach the truly asymptotic regime increases with A.[35]

Nevertheless, the quark concept is useful in the subasymptotic domain where the nucleus can still be regarded as a bound state of nucleons. For example, the deuteron form factor $F_D(t)$ must clearly fall at least as fast as $F_p(t/4)\cdot F_n(t/4)$ since each nucleon must change momentum from $\sim p/2$ to $\sim(p+q)/2$ and stay intact. Thus we should consider the "reduced" form factor $f_D(t)$ defined via[35,37]

$$F_D(t) \equiv F_p(t/4)\, F_n(t/4)\, f_D(t) \tag{4.8}$$

Note that $f_D(t)$ must decrease at large t since it can be identified the probability amplitude for the final state n-p system to remain a ground state deuteron. In fact, the dimensional counting formula (4.6) implies[35,37]

$$f_D(t) \sim \frac{1}{t} \tag{4.9}$$

In general, we can define the reduced nuclear form factor

$$f_A(t) \equiv \frac{F_A(t)}{\prod_{i=1}^{A} F_N(t/A^2)} \tag{4.10}$$

which has the effect of the nucleon form factors removed. By dimensional counting $f_A(t) \sim 1/t^{A-1}$ (as if the nucleons were elementary!), and one expects this result to hold even for moderate values of $|t|$. In contrast, the complete scaling of $F_A(t) \sim t^{1-3A}$ requires very large momentum transfer.[35]

A comparison of the data for $f_D(t)$ with the prediction $t\, f_D(t) \to$ const. is shown in Fig. 15. The asymptotic regime seems to hold for $|t| \geq 1$ GeV^2. Recent data[38] on inelastic electron scattering on deuterons also indicate that the inelastic transfer form factors $\gamma + D \to X$ where m_X^2 is below the pion threshold have a similar behavior. Although, the comparisons with experiment are less decisive, the ^{3}He and ^{4}He high momentum transfer form factors measured at SLAC by Chertok et al.[39] also appear to be consistent with the scaling behavior predicted by Eq. (4.10) [see Fig. 16].

The types of diagram one encounters when computing the deuteron form factor are shown in Fig. 17. Diagram (a) corresponds to a simple "democratic" chain model.[35] Because a single gluon cannot couple to a color singlet, this contribution only is relevant for the part of the nuclear state which contains "mixed color", i.e., does not correspond to a state which can be separated into two color singlet 3 quark systems. The asymptotic form factor for such diagrams behaves as $F_n(t) \sim C/(|t| + m_n^2)^{n-1}$ where $m_n^2 \sim n m_1^2$ and $n = 3A$ for nuclei. For the deuteron state with an ordinary two-nucleon color singlet wave function, the quark interchange diagram of Fig. 17(b) contributes, and gives a contribution of the form of Eq. (4.8) with $f_D(t) \sim C/(|t| + m_0^2)$. This contribution can also be identified with the standard amplitude of Fig. 17(c) where

$T_{np \to np} \propto 1/t^4$ is the off-shell np scattering amplitude at $\theta_{cm} = 90^\circ$. Exchange current (meson-exchange) contributions can also be identified with this amplitude.

In general, one expects that the deuteron ground state consists of a linear combination of a standard color singlet $|np\rangle$ wave function plus a "mixed color" $|6q\rangle$ amplitude. The latter component has a high energy (~270 MeV) in the MIT Bag Model, but it in fact may dominate the high momentum components of the wave function since the np state is suppressed by short range repulsion of the n-p interaction at small distances.[40] Dubokov and Kobushkin[41] have argued that the $|6q\rangle$ mixed color component can account for the anomalous photon polarization seen in $np \to d\gamma$. The $|6q\rangle$ mixed color state is the prototype of new quark matter which, if QCD is correct, must exist within the nuclear wave function. It clearly deserves much more study.

V. Conclusion

As I have outlined in this talk, there now is substantial evidence that the quark and gluon degrees of freedom play a role in phenomena involving ordinary nuclear matter. This evidence is based on the successful predictions based on QCD from

(a) Elastic form factors of nuclei at large momentum transfer,

(b) the tail of the momentum distribution in nuclei observed in fast particle production in nuclear collisions, and, possibly,

(c) the multiplicity distribution observed in nucleon-nucleus and lepton-nucleus scattering.

It is important to explore these phenomena more thoroughly, both by use of higher energy and higher momentum transfer experiments, as well as more theoretical analysis. I should emphasize that the processes (a) and (b) probe amplitudes where quarks are in close proximity, and mixed color states may be playing an important role.

Studies of the final state in deep inelastic processes, especially the Drell-Yan reaction $A+B \to \ell\bar{\ell}X$, inelastic lepton scattering $\ell A \to \ell' X$, and the production of hadrons and jets at large transverse momentum are especially interesting since in such reactions one can study the evolution of colored matter through the nuclear medium.[42] The energy loss patterns of leading particles are particularly interesting.[43] It is also important to determine what are the essential parameters (Q^2 or ω?) which control shadowing of the structure functions and photoabsorption cross section.

Elastic scattering large momentum transfer experiments on nuclei, although difficult, are also of considerable interest. For example, large angle $K^{\pm}$-nucleus scattering can test whether quark interchange mechanisms are dominant.[44] The momentum transfer dependence of such reactions can be predicted using the reduced form factor analysis of Section IV and Ref. 27.

The analysis of nucleus-nucleus collisions which I have presented here is conventional in the sense that I have used only standard features of quark and gluon physics. On the other hand, there could be further surprises as one approaches a new regime of high-energy heavy ion collisions where nuclear matter is forced into new configurations. In any event, we are clearly only at the beginning of the study of high energy processes within the nuclear environment.

ACKNOWLEDGEMENTS

I would like to thank A. Białas, R. Blankenbecler, T. Burnett, B. Chertok, J. Gunion, G. P. Lepage, M. Kühn and I. Schmidt for helpful conversations. The color-neutralization model discussed here is based on an earlier parton model developed in collaboration with J. Gunion and H. Kühn. I would also like to thank M. Gyulassy for inviting me to this workshop.

REFERENCES

1. For a comprehensive review of possible anomalous nuclear phenomena see W. Greiner, report to this conference.
2. Current ideas on the application of quark and gluon physics to nuclear reactions are discussed in A. Białas, FERMILAB-Conf. 79/35 (this conference); N. N. Nikolaev, A. Ya. Ostapchuck and V. R. Zoller, CERN preprint TH-2541; N. N. Nicolaev and S. Pokorski, Phys. Lett. 80B, 290 (1979); and Z. J. Rek and G. Wilk, Phys. Lett. 78B, 333 (1978).
3. R. P. Feynman, "Photon-Hadron Interactions," W. A. Benjamin, Inc., 1972, and unpublished.
4. For recent data and reviews see Ref. 2; T. Ferbel, this conference, W. Busza, Acta. Phys. Pol. B8, 333 (1977); D. Cutts et al., Fermilab-Pub-79/44 (1979); J. E. Elias et al., Fermilab-Pub-79/47 (1979); C. Halliwell, Proc. of the VIII International Symposium on Multiparticle Dynamics, Kaysersberg, France (1977); and W. Busza, Proc. of the VII International Colloquium on Multiparticle Reactions, Tutzing, Germany (1976).
5. F. Low, Phys. Rev. D12, 163 (1975).
6. S. Nussinov, Phys. Rev. Lett. 34, 1286 (1973).
7. S. J. Brodsky and J. F. Gunion, Phys. Rev. Lett. 37, 402 (1976), and Proc. of the VII International Colloquium on Multiparticle Reactions, Tutzing, Germany (1976).
8. S. J. Brodsky, J. F. Gunion and J. Kühn, Phys. Rev. Lett. 39, 1120 (1977).
9. For discussions and references, see A. Białas, Ref. 2.

10. W. Busza, Ref. 4.

11. S. A. Azimov et al., Phys. Lett. B73, 500 (1978). See also N. N. Nikolaev et al., Ref. 2.

12. A. Capella and A. Krzywicki, Phys. Rev. D18, 3357 (1978), Phys. Lett. 67B, 84 (1977).

13. V. I. Zakharov, N. N. Nikolaev, Sov. J. Nucl. Phys. 21, 227 (1975); V. I. Zakharov, Proc. of the 18th International Conference on High Energy Physics, Tbilisi (1976).

14. A. Białas, Fermilab-Conf-79/35-THY (this conference); A. Białas, W. Czyż and W. Furmanski, Acta. Phys. Pol. B8, 585 (1977); A. Białas, Fermilab-Pub-78/75-THY (1978); see also A. Białas and E. Białas, Fermilab-Pub-79/48-THY (1979); A. Białas, M. Blesyzns'i and W. Czyż, Nucl. Phys. B111, 461 (1976).

15. M. F. Kaplan and D. M. Ritson, Phys. Rev. 85, 932 (1952).

16. Note that this differs from the prediction of the parton model of Ref. 8.

17. L. Hand et al., Acta. Phys. Pol. B9, 1987 (1978), Cracow preprint INP-1019/PH (1978). See also H. C. Ballagh et al., Phys. Lett. 79B, 320 (1978), and references therein.

18. L. Mandansky, private communication.

19. W. R. Witzler et al., Phys. Lett. 57B, 201 (1975).

20. J. Eickmeyer et al., Phys. Rev. Lett. 36, 289 (1976); R. Talman, Phys. Rev. D15, 1260 (1977). A complete review of nuclear shadowing is given in T. H. Bauer, R. D. Spital, D. R. Yennie and F. M. Pipkin, Rev. Mod. Phys. 50, 261 (1978); and G. Grammer and J. D. Sullivan, Illinois preprint ILL-TH-77-20 (1977), published in "Electromagnetic Interactions of Hadrons," eds. by A. Donnachie, G. Shaw, Plenum Press.

21. J. D. Bjorken, Acta. Phys. Pol. B2, 5 (1975), and lectures at the DESY Summer Institute (1975). H. Harari, Proc. of the 1971 International Symposium on Electron and Photon Interactions at High Energies, Cornell.

22. J. D. Bjorken and J. B. Kogut, Phys. Rev. D8, 1341 (1973).

23. S. J. Brodsky and J. Pumplin, Phys. Rev. 182, 1794 (1969); V. Gribov, Zh. Eksp. Teor. Fiz. 57, 1306 (1969) [Sov. Phys. JETP 30, 709 (1970)]; S. Brodsky, G. Grammer, G. P. Lepage and J. Sullivan (unpublished).

24. M. C. Lemaire et al., LBL-8453 (1978); H. Steiner, LBL-6756, published in Proc. of the VII International Conference on High Energy Physics and Nuclear Structure, Zurich (1977).

25. See, e.g., S. Weinberg, Phys. Rev. 150, 1313 (1966); L. Susskind and G. Frye, Phys. Rev. 165, 1535 (1968); S. J. Brodsky, R. Roskies and R. Suaya, Phys. Rev. D8, 4574 (1973); M. G. Schmidt, Phys. Rev. D9, 408 (1974); R. Blankenbecler and S. J. Brodsky, Phys. Rev. D10, 2973 (1974) and references therein.

26. R. Blankenbecler and S. J. Brodsky, Ref. 25; J. F. Gunion, UC-Davis preprint UCD-79-4 (1979), and references therein.

27. S. J. Brodsky and B. T. Chertok, Phys. Rev. Lett. 37, 269 (1976); Phys. Rev. D14, 3003 (1976).

28. R. Blankenbecler and I. Schmidt, SLAC-PUB-2010, Proc. of the 8th International Symposium on Multiparticle Dynamics, Kaysersberg, France (1977); Phys. Rev. D15, 3321 (1977).

29. G. R. Farrar and D. R. Jackson. Phys. Rev. Lett. 35, 1416 (1975); S. J. Brodsky and G. P. Lepage, SLAC-PUB-2294 (1979).

30. E. L. Berger and S. J. Brodsky, Phys. Rev. Lett. 42, 940 (1979).

31. See, e.g., Yu. L. Dokshitser, D. I. Dyakanov and S. I. Troyan, SLAC-TRANS-0183 (1978), translated from Proc. of the 13th Leningrad Winter School of Elementary Particle Physics (1978).

32. S. J. Brodsky and G. P. Lepage, Ref. 29.

33. S. J. Brodsky and G. R. Farrar, Phys. Rev. Lett. 31, 1153 (1973) and Phys. Rev. D11, 1309 (1975); V. A. Matveev, R. M. Muradyan and A. V. Tavkheldzie, Lett. Nuovo Cimento 7, 719 (1973).

34. R. G. Arnold, SLAC-PUBS-2334 and 2373 (1979).

35. S. J. Brodsky and B. T. Chertok, Ref. 27.

36. G. P. Lepage and S. J. Brodsky, SLAC-PUB-2348 (1979), to be published in Phys. Rev. Lett.

37. S. J. Brodsky, SLAC-PUB-1497, published in the Proc. of the International Conference on Few Body Problems in Nuclear and Particle Physics, Quebec (1974).

38. F. Martin et al., Phys. Rev. Lett. 38, 1320 (1977); W. P. Schutz et al., Phys. Rev. Lett. 38, 259 (1977).

39. R. G. Arnold et al., Phys. Rev. Lett. 40, 1429 (1978); B. T. Chertok, Phys. Lett. 41, 1155 (1978).

40. V. A. Matveev and P. Sorba, Nuovo Cimento Lett. 20, 435 (1977). See also A. P. Kobushkin, Kiev preprint ITF-77-113E (1977).

41. V. M. Dubovik and A. P. Kobushkin, Kiev preprint ITF-78-85E (1978).

42. A model of particle production at large transverse momentum which takes into account gluon interactions is given by A. Krzywicki, J. Engles, B. Petersson and U. Sukhatme (1979).

43. A. Dar and F. Tagaki, Technion preprint PH-79-28 (1979).

44. S. J. Brodsky and J. Kühn (unpublished).

FIGURE CAPTIONS

1. (a) Simplified representation of particle production in a simple color-gluon exchange model.
   (b) Rapidity distribution of particles produced in a simplified model where hadron production is proportional to the soft gluon distribution [see Ref. 7].
2. Schematic representation of hadron-nucleus interactions in a color excitation/neutralization model. An event where 3 nucleons are "wounded" is shown.
3. (a) Schematic representation of the rapidity distribution of hadrons produced in hadron-nucleus collisions for the "event" of Fig. 2. The distribution is normalized to hadron-nucleon collisions.
   (b) Rapidity distribution ratio obtained after averaging over events of the type of Fig. 2, assuming interactions occur uniformly in rapidity in the nucleus.
4. (a) Comparison of the prediction of Eq. (2.4) with the data of Ref. 10 for the A-dependence of particle production in nuclei.
   (b) Comparison of the prediction of Eq. (2.1) with data for particle production in proton-emulsion collisions (normalized to pp-collisions). The value $\bar{\nu} = 3$ is used. The predictions for the fragmentation regions must be modified to take into account nuclear fragment cascading for $y < y_A$ and energy-momentum loss of fast particle for $y > y_H$. The data are from Ref. 11.
5. Idealized predictions of various models for the rapidity distribution of hadron production in nucleus-nucleus $A + L \to X$ collisions, normalized to nucleon-nucleon collisions (see text).

6. Theoretical predictions for particle production in nucleus-nucleus collisions A + B → X normalized to nucleon-nucleon collisions. The color-neutralization model discussed in Section II (and also in Ref. 8) is compared with the quark-constituent model of Bialas et al., Ref. 14.

7. Schematic representation of sequential gluon exchange for meson collisions. The statistical average over events gives the same result as an incoherent sum of single-gluon exchange events.

8. Schematic representation of particle production in nuclei for deep inelastic lepton scattering.

9. (a) Comparison of particle production for μ^+ emulsion inelastic scattering at $p_{lab} = 150$ GeV/c with hadron-emulsion data (with incident hadron momenta chosen to roughly match the effective virtual photon energy).

   (b) The ratio of muon-nucleus to muon-nucleon multiparticles as a function of $\nu = -q\cdot p_N/q^2$. The data are from Ref. 1.

10. Schematic representation of the ratio of the deep inelastic lepton scattering structure functions $\nu W_2^A/A\nu W_2^N$ illustrating (a) the possibility of shadowing and anti-shadowing region, or (b) the possibility that there is no shadowing for sufficiently large Q^2. Here $x = -q^2/2q\cdot p_N$, $0 < x < A$.

11. (a) Illustration of the momentum-space wave function for a nuclear bound state using the light-cone/infinite momentum frame variables.

    (b) Mechanism for the production of hadrons or sets of quarks or gluons via Pomeron or gluon exchange.

12. Comparison of the spectator counting rule Eq. (4.5) with α and p production in ^{12}C-C collisions at $p_{lab} = 1.05$ GeV/nucleon. The data for the inclusive cross sections are from Ref. 24. A systematic comparison of theory and experiment is given in Ref. 28.

13. Inclusive cross section for $\alpha + C \to p + X$, compared with the p/α and p/d predictions of the spectator counting rule. The data are from Ref. 24.

14. Comparison of the dimensional counting rule $t^{n-1}F(t) \to$ const. ($|t| >> M^2$) with data. The compilation is from Ref. 34 and references therein.

15. The reduced form factor of the deuteron, divided by a monopole form factor. Dimensional counting predicts this ratio should approach a constant at large t. The data are from Ref. 38.

16. Form factor data from Ref. 39 for ^{2}H, ^{3}He and ^{4}He compared to the quark interchange model predictions of Ref. 35.

17. (a) Example of a simple gluon exchange mechanism for the deuteron form factor at large t.

    (b) Quark-interchange contribution to the deuteron form factor.

    (c) Relationship of the deuteron form factor to off-shell n-p scattering.

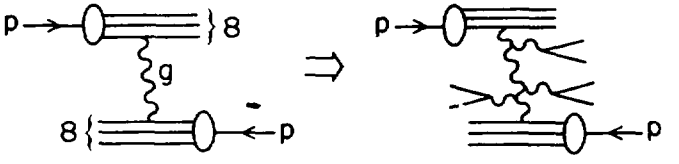

(a)

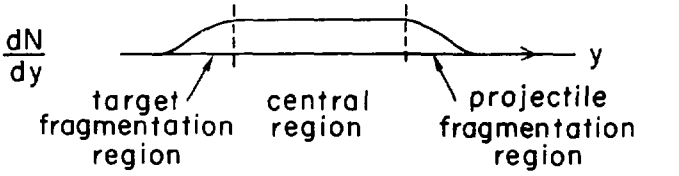

8 - 79

(b)

3673A1

Fig. 1

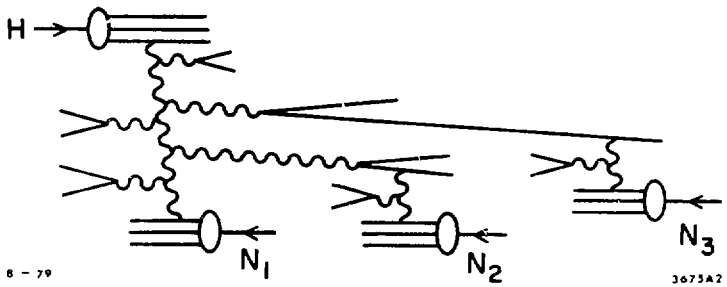

Fig. 2

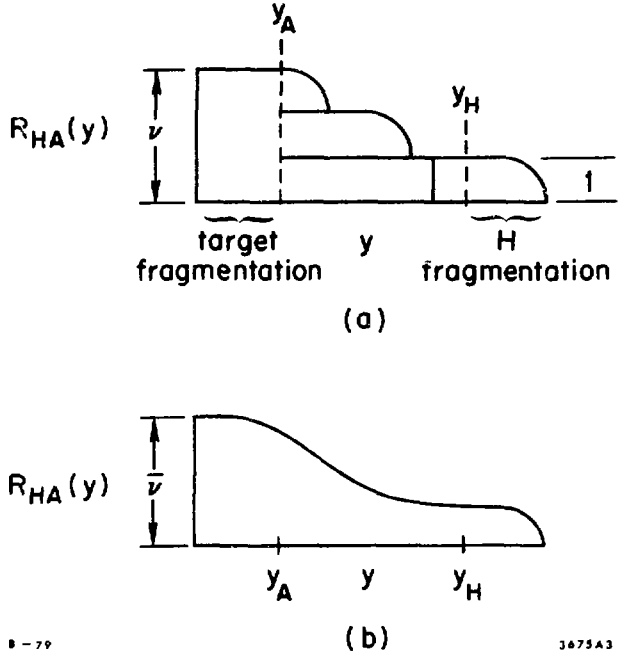
y_A
y_H
$R_{HA}(y)$
ν
1
target fragmentation
y
H fragmentation
(a)
$R_{HA}(y)$
$\bar{\nu}$
y_A
y
y_H
(b)
B-79
3675A3

Fig. 3

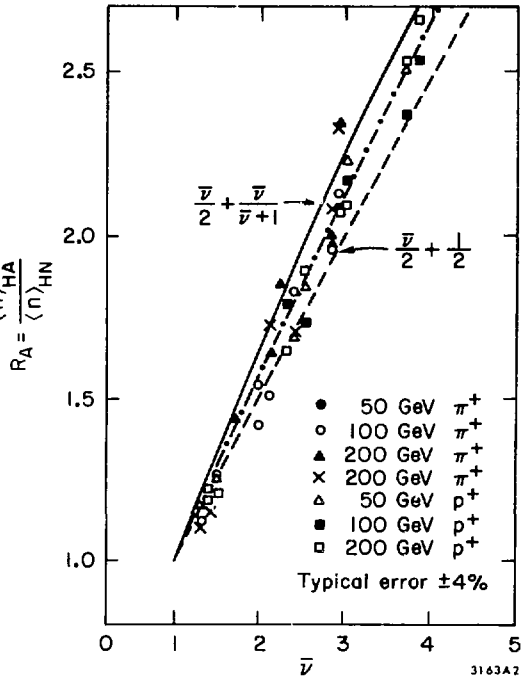
$R_A = \frac{\langle n \rangle_{HA}}{\langle n \rangle_{HN}}$
2.5
2.0
1.5
1.0
0
1
2
3
4
5
$\bar{\nu}$
$\frac{\bar{\nu}}{2} + \frac{\bar{\nu}}{\bar{\nu}+1}$
$\frac{\bar{\nu}}{2} + \frac{1}{2}$
50 GeV π^+
100 GeV π^+
200 GeV π^+
200 GeV π^+
50 GeV p^+
100 GeV p^+
200 GeV p^+
Typical error ±4%
3163A2

Fig. 4a

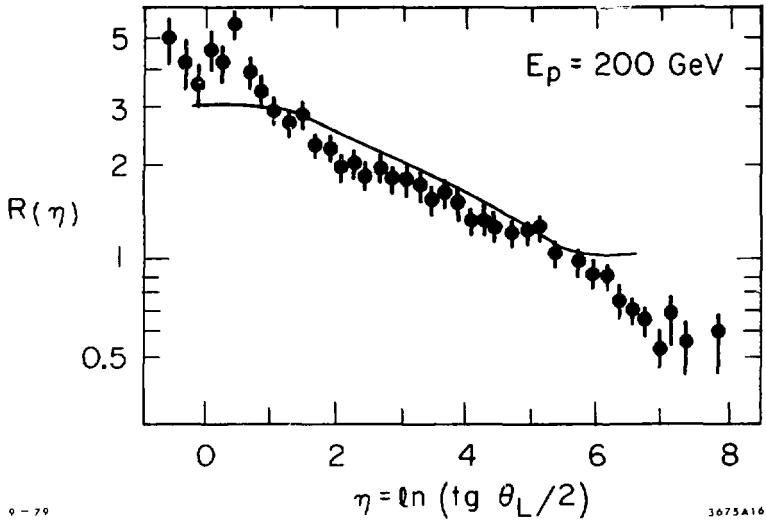

Fig. 4b

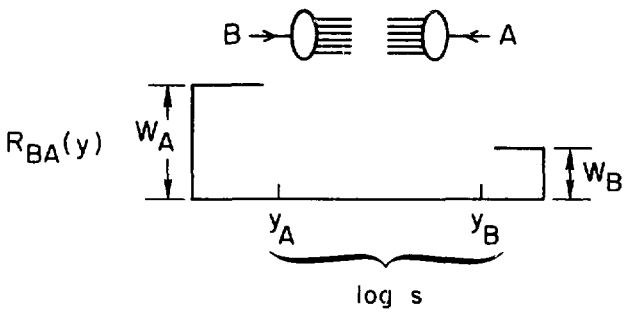

(a)

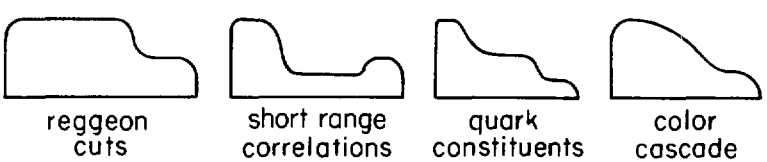

9 - 79

(b)

.675A4

Fig. 5

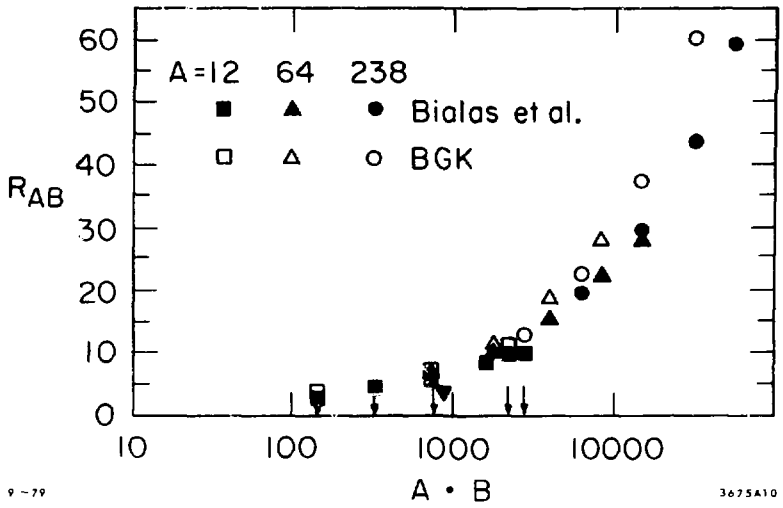
A=12 64 238
Bialas et al.
BGK
R_{AB}
60
50
40
30
20
10
0
10
100
1000
10000
A • B
9-79
3675A10

Fig. 6

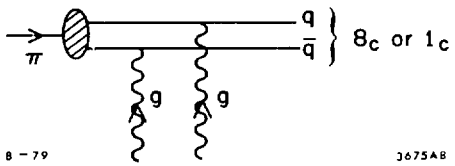

Fig. 7

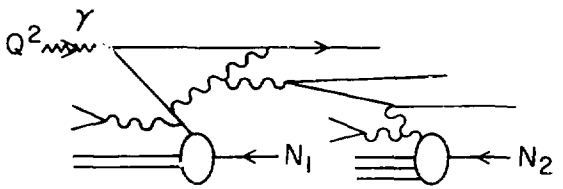

9 – 79 3675A9

Fig. 8

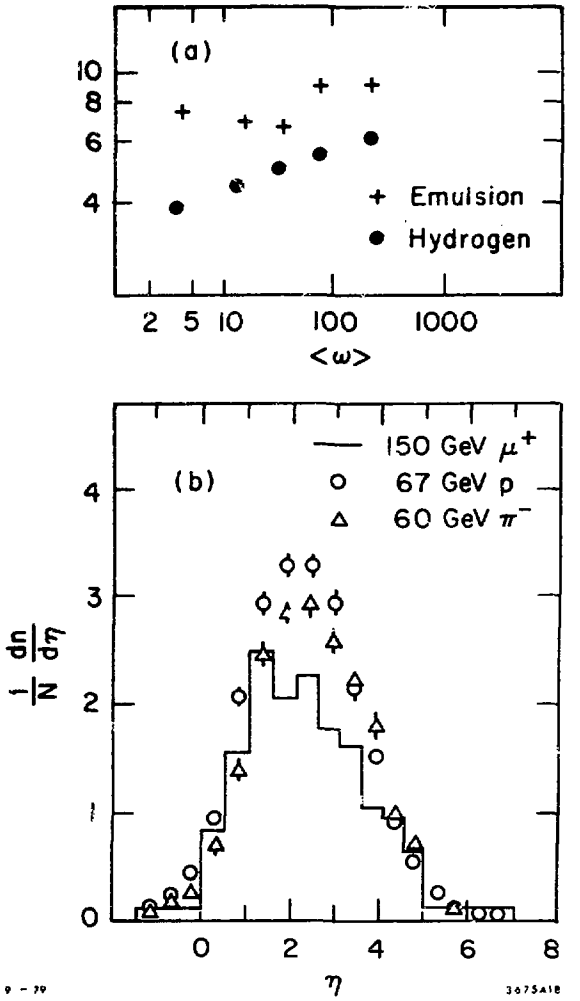
(a)
10
8
6
4
+ Emulsion
● Hydrogen
2 5 10 100 1000
<ω>
(b)
150 GeV μ+
67 GeV p
60 GeV π−
4
3
2
1
0
0 2 4 6 8
η
9 - 79
3675A18

Fig. 9

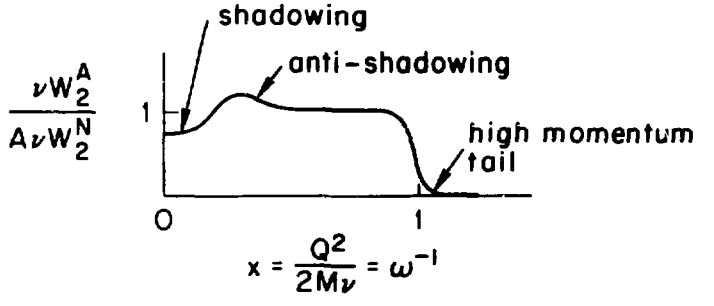

(a)

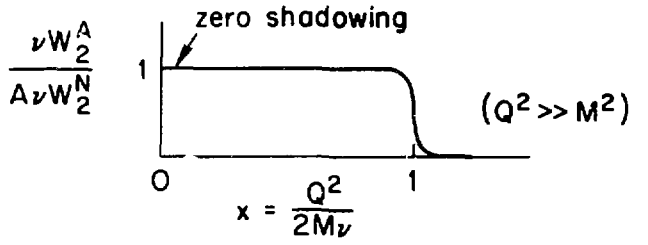

(b)

8-79

3075A7

Fig. 10

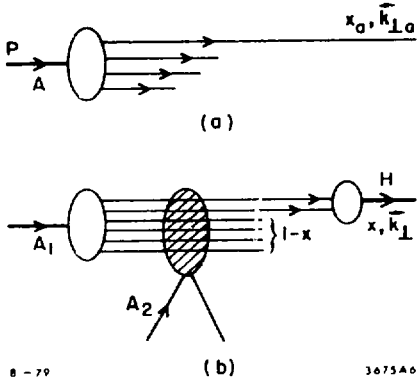

Fig. 11

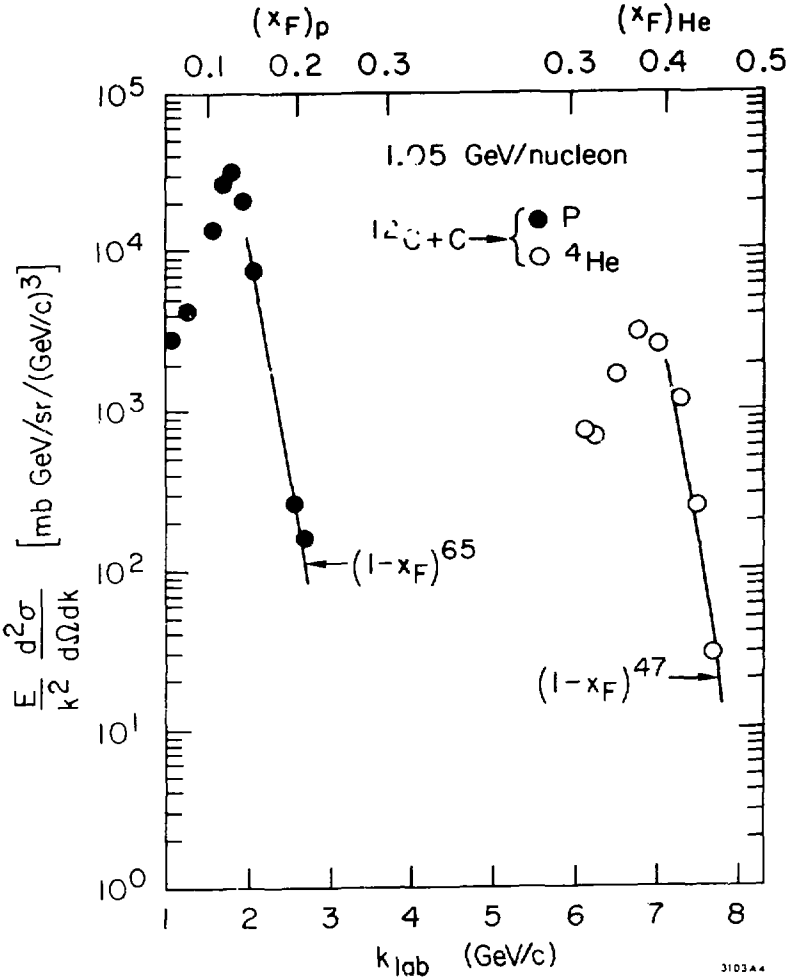
$(x_F)_p$
$(x_F)_{He}$
0.1 0.2 0.3
0.3 0.4 0.5
1.05 GeV/nucleon
$^{12}C + C \rightarrow$ P
^4He
$(1-x_F)^{65}$
$(1-x_F)^{47}$
$\frac{E}{k^2}\frac{d^2\sigma}{d\Omega dk}$ [mb GeV/sr/(GeV/c)^3]
10^5
10^4
10^3
10^2
10^1
10^0
1 2 3 4 5 6 7 8
k_{lab} (GeV/c)
3103A4

Fig. 12

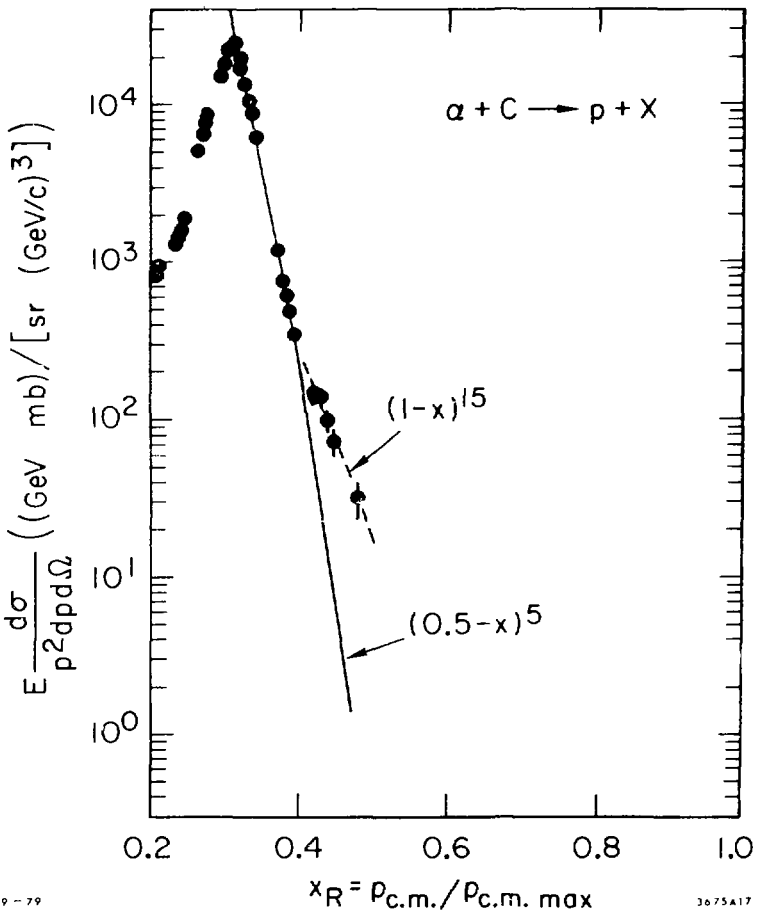
α + C → p + X
$E\frac{d\sigma}{p^2dpd\Omega}$ ((GeV mb)/[sr (GeV/c)^3])
10^4
10^3
10^2
10^1
10^0
$(1-x)^{15}$
$(0.5-x)^5$
0.2
0.4
0.6
0.8
1.0
$x_R = p_{c.m.}/p_{c.m.\ max}$
9-79
3675A17

Fig. 13

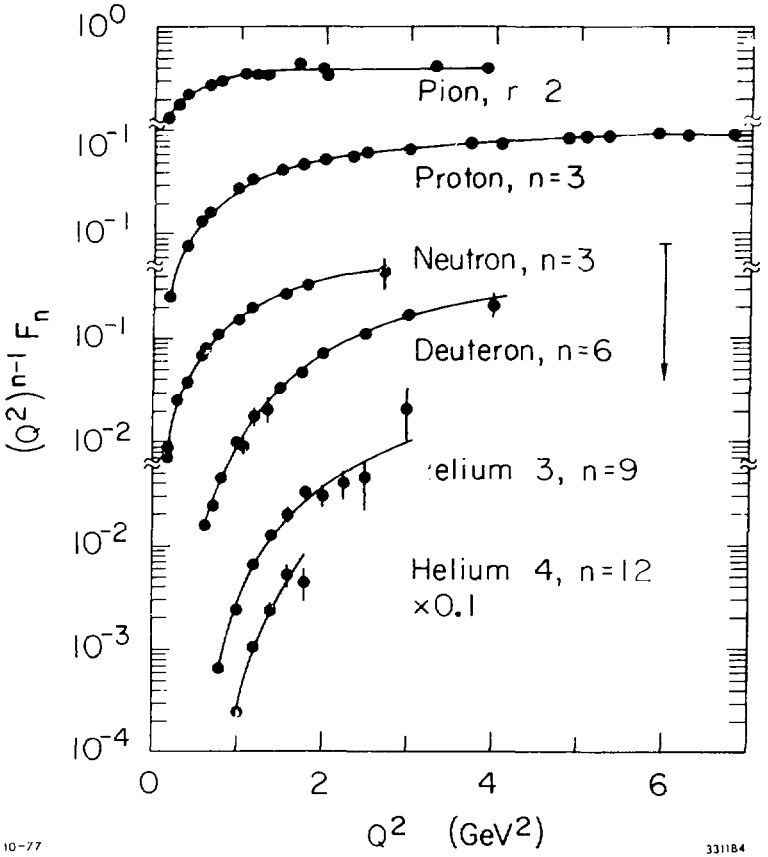
10^0
10^{-1}
10^{-1}
10^{-1}
10^{-2}
10^{-2}
10^{-3}
10^{-4}
$(Q^2)^{n-1} F_n$
Pion, n = 2
Proton, n=3
Neutron, n=3
Deuteron, n=6
elium 3, n=9
Helium 4, n=12
×0.1
0
2
4
6
Q^2 (GeV^2)
10-77
3311B4

Fig. 14

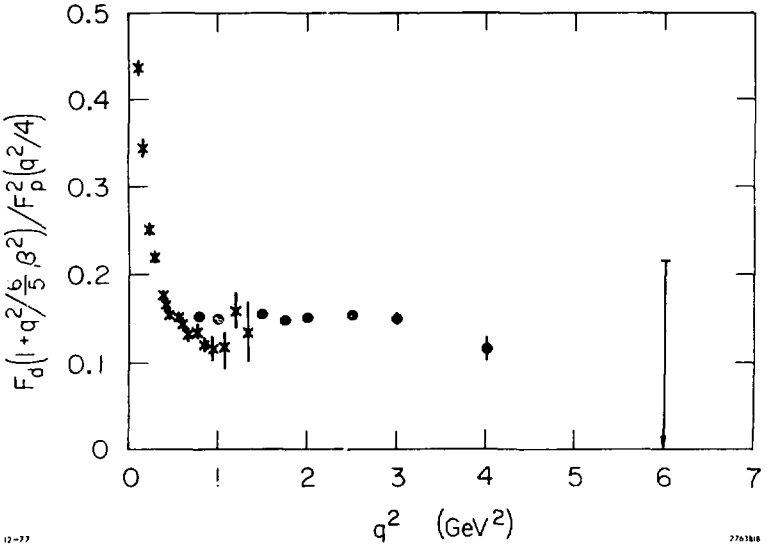
0.5
0.4
0.3
0.2
0.1
0
0
1
2
3
4
5
6
7
$F_d\left(1+q^2/\frac{6}{5}\beta^2\right)/F_p^2(q^2/4)$
q^2 (GeV^2)
12-77
7763B18

Fig. 15

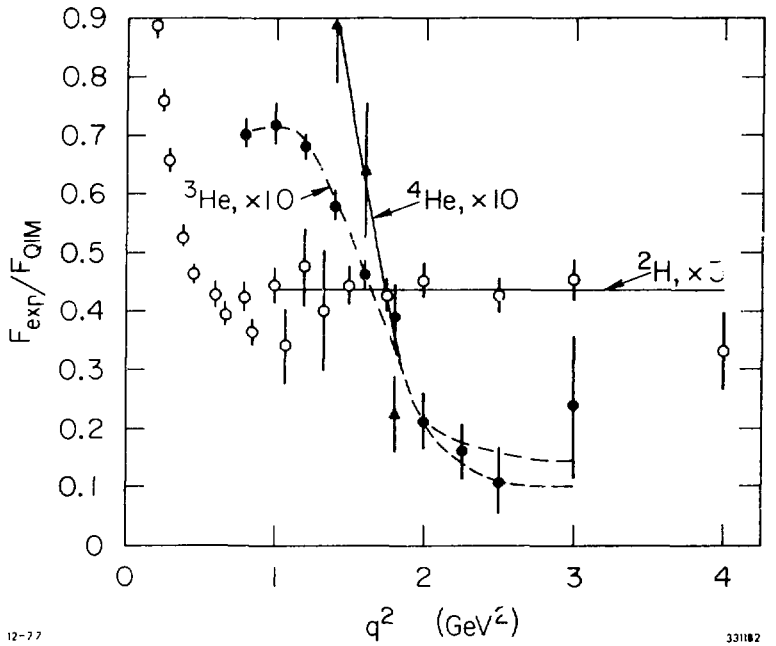
0.9
0.8
0.7
0.6
0.5
0.4
0.3
0.2
0.1
0
F_{exp}/F_{QIM}
^{3}He, ×10
^{4}He, ×10
^{2}H, ×
0
1
2
3
4
q^2 (GeV^2)
12-77
331182

Fig. 16

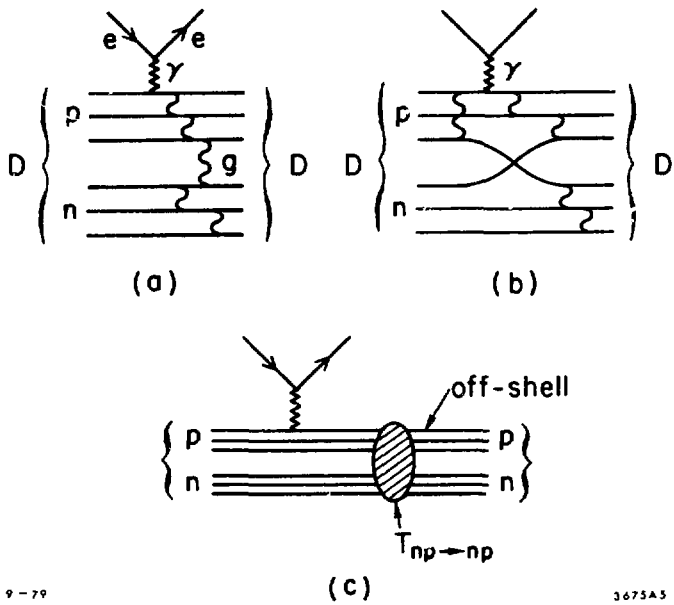

Fig. 17

CRITICAL ANALYSIS OF MODELS FOR HIGH-ENERGY HADRON-NUCLEUS INTERACTIONS

S. A. Azimov, K. G. Gulamov*

and

G. M. Chernov, U. G. Gulyamov†

ABSTRACT

Models of high energy hadron-nucleus interactions proposed recently are critically reviewed and compared with experimental data. An attempt is made to clarify what characteristics and what regions of the phase space are most crucial for different models. Some interesting points where further theoretical and experimental investigations are of importance are discussed.

*Physical Technical Institute, Tashkent 700084, USSR.

†Institute of Nuclear Physics, Ulugbek, Tashkent, USSR.

INTRODUCTION

During the last few years, as a result of increasing interest in the physics of nuclear production, considerable experimental material has been accumulated on inelastic hadron-nucleus (hA) interactions in the range from a few to hundreds of GeV. Although this material is by no means sufficient for answering all the questions of importance, in our opinion, it allows one to draw certain conclusions about the degree of adequacy of some of the numerous model approaches to the subject. Just such an attempt constitutes the main purpose of the present talk.

Theoretical approaches to the problem are such that some of them describe production on nuclei by making use of characteristics of elementary hN collisions a' posteriori, while the othere pretend to explain all types of multiparticle processes. Needless to say, the second class of models is preferable; among them approaches based upon the notions of composite quark-parton structure of elementary particles are of most interest since they allow one to understand the underlying mechanisms of multiple production. As regards phenomenological approaches, it is hard to expect that they would describe the totality of experimental information on nuclear production. These models, as a rule, are far enough from each other in their axiomatics, although they nevertheless have some common general ideas. Below, when considering concrete models and discussing their physical motivations and consequencess for the observables, we shall mainly be interested in the range of their applicability and in the ability to systematize the existing experimental material.

Due to time limitation, preference shall be given to models that are developed enough in the quantitative respect and to experimental data that is, in our opinion, crucial enough for distinguishing between different models. We shall bear in mind that some of the model predictions are of asymptotic nature while the existing data belong to the region of intermediate energies. More complete description of theoretical concepts together with references to many original works of importance not reflected in our talk can be found in earlier reviews.[1-13]

It should be noted that we shall discuss only normal (small $p_\perp$) processes of incoherent production on nuclei constituting the larger part of the production cross section since the coherent reactions and large $p_\perp$ processes will be covered in other talks at this workshop.

The talk is organized as follows. In Section 2 we shall give a brief outline of the ideas that arise when studying ultra-relativistic nuclear collisions and their realization in a few concrete models. In Section 3 the experimental data on one-particle distributions, the leading particle spectra, the nuclear response, and correlation phenomena will be presented and compared to the predictions of models under consideration. Finally, in Section 4 we shall present our main conclusions and suggestions.

MODELS OF MULTIPARTICLE PRODUCTION ON NUCLEI

The Cascade-Evaporation Model

The main assumptions of the model are: 1) the time of realization of intranuclear hN collision is much less than the time interval between two such collisions. This requirement (instantaneous production) is necessary in order to reduce an interaction of a hadron with a

nucleus to a sequence of separate statistically independent intranuclear collisions; and 2) the De Broglie wavelength of particles participating in intranuclear collisions is much less than intranuclear distances. Only in such a case would the picture have quasi-classical features and one might be able to say something about trajectories of particles and two-particle interactions inside the nucleus. In this case an hN interaction is considered to be a superposition of elementary collisions of primary and produced particles with nucleons--the branchy cascade--(see Fig. 1a). In accordance with the model, the process has two stages. During the fast stage, produced particles and recoil nucleons appear as a result of intranuclear collisions, then the slowest particles appear, which are nuclear fragments resulting from the decay of the excited residual nucleus through evaporation. A lot of papers are devoted to concrete calculations with this model; a generalizing monograph[2] is of special interest.

Difficulties that arose when describing cosmic ray data[14] (too fast rise of the multiplicity with E_0 and A) necessitated modification of the model. The purpose was to decrease the total number of intranuclear collisions with the following taken into account:[2] a) absorption of low energy pions within the nucleus; b) the Pauli exclusion principle; c) the existence of leading particles and the related trailing effect, i.e., the decrease of nuclear density after the passage of the fastest leading particles; and d) multiparticle interactions. From a theoretical viewpoint, inclusion of multiparticle interactions, i.e., a lengthy virtual phase, contradicts asumption (1) above and means nothing more than leaving the frameworks of the traditional cascade model. In

regard to the trailing effect there exist two opinions about its significance. In the cascade model this effect plays an essential role.[2] In accordance with the other viewpoint the displacements of recoil nucleons cannot lead to a noticeable decrease of nuclear density during the fast stage of the process for the overwhelming majority of produced particles since velocities of recoils are considerably smaller than those for particles produced. This controversy can probably be resolved by studying nucleus-nucleus (AB) interactions where the trailing effect, if it exists, should manifest itself stronger and not only in the target but in the projectile as well, facilitating its investigation.

Nevertheless, even when accounting for all the above factors, the model cannot describe the stability of the multiplicity of slow particles (particularly, recoil protons) with the primary energy, though it reproduces the multiplicity of relativistic particles (see Fig. 1b). Discrepancies are observed also for a number of other observables in hA interactions. So, if the cascade is forbidden, at least in high energies, it means that assumption (1) above is not fulfilled since assumption (2) works better as the energy increases.

The question arises at what energies and in what regions of phase space does the cascade model work? In order to answer this question it is very attractive to use AB interactions at, say, $p_0 \geq 10$ GeV/c per nucleon. The advantage of AB collisions is that the cascade there should manifest itself stronger than in hA collisions and the choice of P_0 is related to the fact that at lower energies the cascade multiplication of particles produced can effectively be damped due to simple energetic

reasons. The importance of the problem is related to the fact that we don't know which parameter with dimension of length in the theory of strong interactions can be identified with the radius of strong interactions. It is is clear, of course, that its value is comparable in order of magnitude with intranucleonic distances in nuclei. Therefore, disregarding a'priori the off-mass-shell virtual effects is by no means justified even at a few GeV.

The Growth of Longitudinal Distances Essential for Production

The postulate of the cascade model about "instantaneous" production is open to criticism: the decrease of longitudinal momentum transfer (q_L) as E_0 increases leads to spatial sizes of the interaction volume considerably larger than the intranucleonic distances in the nucleus. Also, the Lorentz delay of time at $E_0 \to \infty$ would lead to unlimited growth of realization time of elementary interaction (if the proper time in the c.m.s. $t_0 \neq 0$).

Therefore at sufficiently high energies the notion about the hA interaction as a totality of elementary collisions of free particles should become incorrect and the charcteristics of the interaction must depend on properties of lengthy virtual phase.

These ideas have been discussed already in classic works by Landau and Pomeranchuck[17] who showed that if multiple scatterings during the bremsstrahlung of a relativistic electron in amorphous medium destroy the coherence of the particle field at distances $l < l_f$, then the bremsstrahlung is damped and deviations from the Bethe-Heitler formula should be observed. The length l_f proportional to the photon energy plays the important role in processes of emission of fast particles

and is referred to as the coherence or formation length of the photon (and/or regeneration length of an electron). The meaning of Landau-Pomeranchuk phenomenon (confirmed experimentally[18]) is that if fast electrons, when emitting photons due to multiple scatterings in the medium, could undergo more than one collision on the length $l < l_f$, the emission would be damped.

The growth of longitudinal distances is of importance also in deep-inelastic lepton-hadron scattering.[19] There large distances play an essential role at high p_o; the scaling behavior of electroproduction cross sections corresponds to the version with linear increase in the laboratory frame l_f: $l_f \sim \nu/Q^2$.

An example of a hadronic process where this notion is of primary significance is coherent diffractive production.[20] Here the longitudinal momentum transfer decreases with P_o,

$$q_L \simeq (m_f^2 - m_i^2)/p_o \ , \qquad (1)$$

so that at high p_o production occurs at distances $l_f \gtrsim 1/q_L$ (considerably larger than hadronic sizes) and at the same distances the coherence of amplitudes will be conserved. It is seen from Fig. 3 that at energies presently available the contribution of coherent production increases with energy.[21]

Due to the absence of a rigorous theory of strong interactions it is impossible to perform a model-independent analysis of the character of the growth of formation lengths (and related formation times - t_f) for incoherent production. Most of the models considered below consider

that, for a secondary particle having the energy E and the mass m, one has

$$l_f = \frac{1}{m_o}\frac{E}{m}, \quad t_f = \frac{E}{m} t_o , \qquad (2)$$

where m_o is some characteristic hadronic mass. Due to the rapid decrease of hadronic amplitudes on off-mass-shell, assumption (2) means that secondary particles do not participate in intranuclear collisions at distances $l \lesssim l_f$. Only if we have $l_f < 1$ can one use the usual classical considerations.[23]

The majority of nuclear production models can be separated, crudely speaking, into two groups. In the first group scattering on a nucleus is interpreted as a series of approximately independent (in many important cases this independence is destroyed by the energy-momentum conservation) collisions with single nucleons. In order to elucidate how the presence of a virtual phase is accounted for in such models it is useful to clarify the following points for each concrete model: a) what does interact with intranuclear nucleons, b) what is the cross-section for intranuclear collision, and c) how are we to relate intranuclear interactions with free hN collisions, i.e. what are the characteristics of the final state after the single intranuclear collision.

In the second group of models, the projectile collides with the "tube" of nuclear mater, which is usually considered to be structureless and to behave as an "elementary" particle. In order to come to the point of such models it is necessary to clarify: a) what parameters depend on the characteristics of the final state, b) how are we to

relate the characteristics of hadron-tube interaction to those of hN collision, and c) what are the characteristics of the tube itself.

Landau Hydrodynamic Model (LHM)

Description of multiparticle processes in the LHM[24] is based upon the following assumptions: 1) as a result of high energy interactions a considerable amount of energy is released into the Lorentz-contracted disc, the volume of which, V_{in}, is considerably smaller than that necessary for the observed multiplicity of produced hadrons; 2) since the interaction is strong, the relaxation time is small and it is supposed that the formed hadronic blob is under local statistical equilibrium. The system is considered to be a relativistic fluid characterized by density of energy, pressure, and by distribution of four-velocities of fluid elements; its collective motion is described by equations of relativistic hydrodynamics. The hadronic cluster thus produced undergoes later hydrodynamic expansion; 3) the dynamics of the process is conditioned by both the choice of the equation of state of hadronic matter, $p = f(\Sigma)$, (p and Σ are macroscopic pressure and energy density, respectively) and the boundary conditions imposed on the hydrodynamic equations.

The most remarkable feature of the LHM is the very long time between the moment of formation of the excited hadronic matter and its "materialization" into free particles.

The model was generalized to hA collisions (see, for details[9,10]) by introducing an additional assumption that in this case the projectile interacts collectively with all the nucleons contained in a tube along its path. The radius of cross-section of a tube is σ_{hN}. Since the

realization time for interaction is large, real hadrons of the final state are produced well outside the nucleus. Characteristics of the final state crucially depend on the concrete physical content of three stages of the interaction process--production of excited hadronic matter, its hydrodynamic expansion, and its decay into real particles. So, the choice of the initial volume V_{in} strongly affects the A and E_o dependencies of the average multiplicity, the hydrodynamic expansion determines rapidity distributions of particles produced, transverse momentum distribution depends on the final stage, and so on. It should be noted that the one-dimensional versions of the model usually considered do not take into account the expansion in the transverse direction and lead to factorized inclusive distributions

$$E_o \frac{d^3\sigma}{dp^3} = f(p_\perp, p_\parallel, s) \approx f_\perp(p_\perp, s) f_\parallel(p_\parallel, s), \qquad (3)$$

so that transverse momenta of secondaries are conditioned only by the thermal motion during the final stage of the process. It is quite clear from the above that, strictly speaking, no simple relation exists between the characteristics of hN and hA interactions at the same projectile energy.

The weak ponts of the model are: 1) the classical consideration of the initial stage of the process contradicts the uncertainty relation[25,26] (see also discussion in Refs. 9 and 21); and 2) the model does not take into account the existence of leading particles.

There are two approaches to the leading particles in modern calculations in the frameworks of the LHM. In one, leading particles are produced from the hydrodynamic system (see, e.g., Ref. 28). Such

an approach has some difficulties, for instance, the problem with quantum number conservation. In the second approach leading particles are not included in the composite system, in accordance with the laws of relativistic hydrodynamics, and characteristics of leading particles are adjustable parameters of the theory.[10] It is usually supposed that the hadronic system produced takes the energy kE_o, where k is the inelasticity coefficient.

It should be noted that the region of applicability of the model begins at high enough energies, at least at E_o of an order of magnitude or larger than hundreds of GeV. Therefore it is attractive to extend it to the region of intermediate energies where most of the experimental results have been obtained. Following this idea[29] a model has been proposed (the model of effective target). In such a model a projectile interacts not with the whole tube but with its forward part. The model can be used at energies 5-300 GeV, at lower energies it turns into the cascade model, at higher energies it coincides with the LHM. The main idea is that, in the range 5-300 GeV, a hadron collides in a nucleus with the effective target having the mass

$$M_{eff} = m_N n \sigma_{in} L, \tag{4}$$

where n is the nuclear density, σ_{in} is the inelastic hN cross-section, and the value of the quantity L is the smallest one among two quantities: a) the formation length averaged over the produced particles spectrum

$$\bar{L}_f = c_1 E_o^{1/2} \tag{5}$$

(C_1 is the parameter of the model taken to be 2.4 $fGeV^{-1/2}$) and b) the geometrical length of the tube

$$L_g = 2(R^2 - b^2)^{1/2}, \tag{6}$$

(b is the impact parameter). So, at the energies considered, there exist three regions in the nucleus (Fig. 3). Region I corresponds to the diffuse edge of the nucleus, region II is where the length of tube is shorter than the formation length and, finally, region III is where $L_g > L_f$ is.

Hadron-effective target interaction is considered in the model in full accordance with hydrodynamical estimates

$$\langle n(M_{eff}, E_o)\rangle = \langle n_{pp}(E_o)\rangle \ (M_{eff}/m_n)^{\alpha}, \tag{7}$$

$$\frac{dn}{dy} = \frac{\langle n\rangle}{\sigma(M_{eff})\sqrt{2\pi}} \exp\left[-\frac{(y-y_o(M_{eff})^2}{2\sigma^2(M_{eff})}\right] \tag{8}$$

where $\alpha \simeq 0.65$-0.75. As noted by inventors of the model, its predictions pertain to characteristics of produced particles outside the fragmentation regions, i.e., the leading particles are not taken into consideration.

The Coherent Tube Model (CTM)

The CTM is presently being developed most actively by three groups (Refs. 7,30,31 and references therein). It should be noted, of course, that actually there exist several versions of the model and sometimes calculations performed even by CTM inventors do not agree with each other. The first version of the model,[7,30] the most simple and attractive, has been criticized in many papers and as a result significant modernizations and complications of the model were introduced in papers of the inventors themselves (see, e.g., Ref. 41, 42). In a

recent paper,[31] although the term CTM is used, the phenomenological model considered is much more complicated and multiparameter than earlier versions and is very close in spirit to the statistical-hydrodynamical approach.

Here we briefly discuss the original formulation of the model, its new versions shall be discussed below when considering experimental data. The model is based upon two assumptions:[7] 1) the projectile interacts collectively with all the intranuclear nucleons contained in a tube along the direction of its motion, the tube is considered as a structureless "elementary" particle. For a tube containing i nucleons, the squared total energy in the c.m.s. is

$$s(i) \simeq 2im_nE_o = is, \tag{9}$$

where s is the corresponding quantity for hN collision; 2) quantities not depending on the precise quantum numbers of colliding particles in hN interactions are supposed to be independent of them in h-tube collisions as well. It is assumed for such quantities that an h-tube collision looks like a hN interaction at the same c.m. energy, i.e., at the energy $\sqrt{i}$ times larger than the c.m. energy of the hN collision for the given projectile momentum. Such quantities, as noted in Ref. 7, include the average multiplicity, multiplicity distributions, and inclusive cross-sections for production of particles with normal $p_\perp$.

It has been supposed in the model[7,30] that for fixed A

$$\langle i \rangle = A^{1/3} \tag{10}$$

independent of the type of projectile. Assuming that in hN collisions the multiplicity

$$\langle n \rangle_{hN} \sim s^{\alpha}, \tag{11}$$

where $\alpha \approx 0.25$, and by making use of assumption 2) and Eq. (10) the authors of Ref. 7 obtained for particles produced in hA collisions

$$\langle n_{hA} \rangle \sim (\langle i \rangle s)^{\alpha} = \langle n \rangle_{hN} A^{\alpha/3} \quad . \tag{12}$$

The most attractive feature of the model in comparison, for instance, with the LHM[24] is the claimed possibility of using, for universal characteristics of hA interactions, the same characteristics from hN collisions at energies $\sqrt{i}$ times larger, i.e., the simplicity in calculating of multiplicities and inclusive distributions.

Cluster Type Models

As discussed above, the time of formation of free hadrons in high energy collisions could be very large and one can consider that not the usual hadrons but some hadronic complexes (clusters and fireballs) would propagate through the nucleus after the first intranuclear collision of a projectile. Such consideration constitutes the basis of cluster models. One can note that such an idea had been proposed many years ago in Ref. 33.

In Gottfried's model[3,34] the cascade of energy flux is developed inside the nucleus, the flux being analogous to one-dimensional shock waves in the LHM. In hA collisions under certain postulated conditions this cascade results in production of $\nu+1$ hadronic blobs (Gottfried's hadrons): one fast cluster occupying 2/3 of the full available interval of rapidity and ν slow clusters. Here ν is the number of inelastic intranuclear collisions defined as

$$\bar{\nu} = A\sigma_{inel}^{hN} / \sigma_{prod}^{hA} \quad . \tag{13}$$

Fast Gottfried hadrons take away the main amount of the primary energy decays outside the target, whereas slow parts of the energy flux, which could decay inside the target, do not produce additional particles within the nucleus for energetic reasons. Since the space-time dimensions of the fast hadron on intranucleonic distances are of the same order of magnitude as for usual free hadrons, the cross section for repeated interactions of the fast part of the energy flux with downstream nucleons is taken to be equal to the cross-section of the projectile. Characteristics of the final state in the model are conditioned by decay properties of fast and slow hadrons, which, in turn, are taken from hN interactions. So for the multiplicity the energy flux cascade (EFC) model gives, at presently available energies,

$$R = \langle n\rangle_{hA}/\langle n\rangle_{hN} = 1 + \frac{1}{3}(\langle\nu\rangle - 1) + 0\left(\frac{1}{\ln E_0}\right), \qquad (14)$$

i.e., the contribution from a slow hadron is twice as small as the multiplicity from a fast Gottfried hadron

$$\langle n\rangle_{slow} = (1/2)\langle n\rangle_{fast} \approx (1/3)\langle n\rangle_{hN}.$$

Another type of cluster model is based on the diffractive picture of hN collisions (the hypothesis of limiting fragmentation).[35,36] In these models the first intranuclear collision of a projectile results in production of two fragmentation clusters, the fast cluster being related to the projectile and the slow one related with the recoil nucleon. The fast cluster then undergoes repeated interactions with all downstream nucleons with the same cross-section as a projectile and decays outside the target. In each intranuclear collision the system is reproduced and characteristics of the final state are conditioned

by decay characteristics of clusters, which, in turn, are supposed to be taken from experimental data on hN interactions.

It should be noted that all cluster models suggested so far seem to be rather crude and do not take into account some important effects arising during the passage of hadronic complexes through nuclear matter (see, e.g., Ref. 76).

Models of Multiple Rescatterings

The Fan Diagram Dominance Model. FDDM is most developed in papers by Nikolaev and co-workers (see review, Ref. 11) and is based on the following parton interpretation of the multiperipheral model. A fast hadron before reaching a target produces parton fluctuations with approximately uniform distribution of partons in the rapidity space (Fig. 4). As partons are pointlike objects with cross-section $\sim\pi\lambda\!\!\!^{-2}$, $\lambda\!\!\!^{-}$ being their wavelength, only the slowest, wee partons are capable of interaction with a target, whereas for fast partons it is transparent. So, one can speak about the parton wave function of a fast hadron and the latter can be considered as a multiperipheral ladder of partons having a wee parton. As regards the number of such ladders (or wee partons) the FDDM assumes that as long as we are considering the σ_{hN} to be a pole-dominated contribution, multiladder states can be neglected.

When considering an hA collision, there would arise, in contrast to hN collsions, in accordance with the model, multiple rescatterings related with comparatively slow partons. The first interaction with a nucleon of the target can only be induced by the wee parton of the initial ladder of partons. Due to the interaction the coherence of the initial ladder becomes destroyed and it is possible that some

relatively slow partons from the first ladder emitted near the bottom would turn into hadrons inside the nucleus (as $l_f \sim E$), which, in turn, would produce wee partons of the "second" generation. If such a transition takes place inside the target, one would have secondary interactions with intranuclear nucleons. Therefore one can expect that some low-energy cascading would develop for large nuclear targets. As regards fast partons, they traverse the real nucleus without interactions and the spectra of fast particles would coincide with those from hN collisions. Of course, if one takes into account the energy-momentum conservation at existing moderate energies, then there would be some depletion of spectra of fast particles in nuclear production. Since in Reggeon calculus such a process is described by the so-called fan diagram of Fig. 5, the model is referred to as the fan diagram dominance model. One of the immediate properties of the model is that due to the short-range character of correlations, characteristics of nuclear response would not depend on projectile identity and the cross-section on nuclei should factorize. The data do not show such a behavior and therefore it is necessary to consider other ways of introducing multiple rescatterings inside the nuclear targets.

The Leading Particle Cascade Model. This phenomenological mod (LPCM) is based on the assumption that within the nucleus only the leading particle interacts successively with all the nucleons in its path, whereas for produced particles the target is completely transparent. No rigorous arguments exist justifying such a picture except for the rather intuitive guess that nuclear matter is anisotropic for a high energy particle.[37] The reasons may be related with a very strong

trailing effect, (discussed above in the section on the cascade evaporation model) and with very strong angular collimation of secondaries in high energy interactions. Then the fastest leading particle would interact with downstream nucleons, whereas the particles produced would traverse a target in the region of small densities. This model has a straightforward relation with the Glauber model and corresponds to consideration of diagrams shown in Fig. 6.

There exist theoretical objections to this model[38] related to disregarding inelastic intermediate states. Of course, one can note that recently the Glauber model, including some types of such inelastic screenings and supplemented by the AGK cutting rules, has been developed for inelastic production on nuclei (see review, Ref. 12), but here we shall concentrate on a more probabilistic picture.

In the leading particle cascade model one can easily obtain the following expression for inclusive density of particles in hA interaction[39]

$$\frac{dn^{hA}(y;E_o)}{dy} = \sum_{\nu=1}^{A} p(\nu) \sum_{i=1}^{\nu} \int W(E_i,E_{i-1},i) \frac{dn^{hN}(y-y_o(E_i);E_i)}{dy} dE_i, \quad (15)$$

where $P(\nu)$ is the probability that the leading hadron undergoes exactly inelastic collisions, $dn^{hN}(y-y_o(E_i);E_i)/dy$ is the inclusive density in hN collisions and $W(E_i,E_{i-1},i)$ is the probability that as a result of i-th intranuclear collision the leading particle loses the energy $\Delta E=E_{i-1}-E_i$. The latter is evidently related to the $x = p_l/p_l^{max}$ distribution of the leading hadron in hN collisions, so that for the average $\overline{E}_i$ one has

$$\bar{E}_i = (1 - \bar{k})^{i-1} E_0, \qquad (16)$$

$\bar{k}$ being the average inelasticity coefficient. One may note also that the rapidity shift y_0 reflects the fact that the center of dn^{hN}/dy decreases with decreasing E_i.

It is quite obvious from the above that the cross section for successive interactions of a leader is the same as that for a projectile.

The Capella-Krzywicki Constituent Model. It is assumed in this quasi-eikonal model that the parton wave function of a fast particle contains multiladder configurations (and corresponding wee partons); an interaction between Reggeons (ladders) is being neglected. In hN collisions the contribution of multiladder exchanges playing the role of correction terms is assumed to be small (σ^{hN} is pole dominated), while in collisions with nuclei it rises drastically. No attempt is made in the CKM to seriously consider the projectile fragmentation; it is simply assumed that a multiladder process can be considered as a superposition of "elementary" hN collisions.

So, the model is based on the following intuitive picture. An incident hadron has many (in principle, an infinite number) constituents, each corresponding to a ladder. In hN collisions the contribution comes mainly from interaction of one of the constituents with a nucleon. When passing to hA collisions there arise additional contributions due to interactions of a few constituents with intranuclear nucleons. In fact, projectile consituents interact with all the nucleons along the direction of motion of a projectile, i.e., the quantity controlling the probability that ν constituents are involved in the interaction

with the nucleus coincides with P(ν) defined in the framework of the Glauber model. The main result of the CKM for inclusive production is

$$\frac{dn^{hA}(y;E_o)}{dy} = \sum_{\nu=1}^{A} \nu P(\nu) \int P(E',E_o,\nu) \frac{dn(y-y_o(E');E')}{dy} dE' \qquad (17)$$

The notations are self-explanatory, except for the factor $P(E',E_o,\nu)^{nu}$ which, controlling the energy partition, is taken to correspond to equipartition of primary energy among constituents.

Some comments are in order here. Formally the difference between the LPCM above and the CKM is that the planar vertices of Fig. 4 are substituted by non-planar Mandelstam vertices of Fig. 7b. This results in different formulae for inclusive densities. In the first, model interactions occur successively and any two interactions are separated by some time interval. As regards the second model, here, as shown in a recent analysis,[70] production is dominated by the exchange of Reggeons overlapping in time. So, one can imagine the specific type of collectivity--a projectile interacts simultaneously with several nucleons along its path to the target; indeed, this type of collectivity has nothing to do with that considered when discussing tube models of nuclear production.

The Additive Quark Model. In the AQM a fast hadron, say a proton, is considered to be composed of three spatially separated constituent quarks, each valence quark having a parton cloud. When one of the constituent quarks interacts with a target the others play the role of spectators.

It is well known that the additive quark model explains successfully the static properties of hadrons and dynamic features of hN interactions. It is important to note here that the additive quark model by itself, being the model of symmetry, strictly speaking, does not contain the dynamics of the interaction process; it is necessary to supplement it by some mechanism for quark-quark interaction. It is usually supposed that such an interaction has a multi-peripheral character. When such a picture is applied to hA interactions (see Refs. 11, 43, 44 and Refs. therein), multiple rescatterings of a projectile inside the target arise due to interactions of constituent quarks. If one uses the impulse approximation implying that hN cross-section can be taken as a sum of quark-quark cross-sections ($\sigma^q \simeq 10$mb) and ignores intranuclear cascading, production on the nucleus would be conditioned by an appropriate sum of diagrams shown in Fig. 8 for an incident baryon. The probabilities of such processes occurring can be calculated through the usual optical (or Glauber) formalism for absorption of a particle with the cross-section equal to σ^q.

One can note that after an interaction occurs the constituent quark loses its parton cloud and does not practically participate in further rescatterings, i.e., it has only one related parton ladder. In the models considered[11,12,43,44] contributions of multi-Reggeon exchanges in constituent quark-nucleus interaction are assumed to be small.

It should also be noted that there is the difference in production mechanisms in fragmentation and central regions in the AQM: particles from fragmentation regions are strongly influenced by the spectator

quarks, whereas particles from the central region are produced mainly from the sea.

EXPERIMENTAL DATA AND THEIR COMPATIBILITY WITH MODEL PREDICTIONS

Inclusive "Longitudinal" Distributions of Produced Particles

The main experimentally well-established property of "longitudinal" (rapidity, pseudorapidity, variable $x = p_{\parallel}/p_{\parallel}^{max}$ and so on) distributions of relativistic particles is that the presence of the nuclear target leads to a noticeable decrease of the number of fastest and essential increase of the number of relatively slow produced particles.

Typical examples of the ratio $r(x) = \rho^{hA}(x)/\rho^{hN}(x)$ of inclusive densities $\rho(x) = (1/\sigma)(d\sigma/dx)$ for nuclear and nucleon targets are exhibited in Fig. 9. It should be noted that presentation of data in terms of the normalized density r(x) has the following advantages: 1) this allows one to avoid effects related to the fermi motion of intranuclear nucleons, usually disregarded in analyses at least at $y > 0$ (and/or $\eta > 0$); 2) this allows one to avoid parametrization dependent effects when comparing with theoretical calculations; and 3) this allows one to avoid effects related with the use of pseudorapidity $\eta = \ln\mathrm{ctg}(\Theta/2)$ instead of true rapidity $y = 1/2 \ln(\frac{E+p_{\parallel}}{E-p_{\parallel}})$

It is seen from Fig. 9 that, in the available range of primary energies $E_o \lesssim 400$ GeV, the A dependence of the ratio r(y) changes with y gradually and continuously, without any anomalies expected, for example, in the frameworks of the EFC model. There exists the point y_c, such that $r(y_c) = 1$; it is interesting that it weakly (if at all) depends on A and the number of intranuclear collisions .[45,46] At $y > y_c$, $r(y) < 1$, and the larger y, the stronger the inequality becomes;

this is the effect of "extinction" of fastest particles which will be considered in detail in the section on the projectile fragmentation region. In contrast, at $y < y_c$, $r(y) > 1$ and the smaller y, the stronger the inequality becomes. At minimal y the ratio r(y) is larger than the value $A^{1/3}$ expected in model approaches not taking into account the low-energy cascading.

In Fig. 9a we show, as examples, results of calculations of the ratio $r(\eta)$ performed in the framework of some models previously discussed. One can conclude from the comparison of theoretical calculations with the data that:

1. The FDDM does not describe the data at high energies. It is important to note that the data do not demonstrate the specific limiting behavior of the ratio $r(\eta) \to 1$ at large pseudorapidities predicted by the model (see curve 1 in Fig. 9a) and appear to be due to the noninteracting fast part of the parton ladder. This is seen most clearly from Fig. 10, where p_o-dependence of the difference $y_{max}-\eta_c$ (y_{max} being the kinematical limit of rapidity) is plotted in comparison with model expectations.[47] These data give strong support to models in which fast particles and/or projectile constituents undergo multiple rescatterings. It should be noted that the exact value of this difference seems to be sensitive to concrete assumptions of multiple scattering models (i.e., the energy partition among constituents) and it is of interest to measure it for different projectile particles.
2. Multiple scattering models which do not take into account

the possible low-energy cascading, such as LPCM and CKM, are not consistent with the data at y or $\eta < 1.5$. These, as well as other data discussed below, indicate that in this kinematic region the low-energy cascading does manifest itself most strongly.

3. The most satisfactory description of general features of inclusive distributions can be reached in the frameworks of the AQM and the LHM.

4. As seen from Figs. 9c, d, the inequality $r(y) < 1$ holds for $y > y_c$, not only for the "leading", but for produced particles as well. This important feature of the data will be discussed in more detail in the next section.

Another interesting property of inclusive "longitudinal" distributions of relativistic particles from hA collisions is that they do depend on the nature of a projectile--see an example in Fig. 11. There appears the evident bimodality of pseudorapidity distributions in π-A interactions at 200 GeV/c. An indication exists[46] that the same bimodality of pseudorapidity distributions is seen also in pA interactions but at higher primary energies. The difference of distributions plotted in Fig. 11 and the bimodal structure can be considered as manifestations of different production mechanisms contributing to different kinematic regions of longitudinal variables.

An increase in the number of slow produced particles, when passing from nucleonic to nuclear target, leads to deformation and shift of longitudinal distributions. In Fig. 12 we illustrate such a deformation of η-distributions in π^-A interactions at 200 GeV/c with increasing

number of recoil nucleons (the number of grey particles—n_g) characterizing the thickness of nuclear matter along the path of incident pions.[47] Note that at all n_g η-distributions can be satisfactorily described by the sum of two Gaussians (see also below). Two main peculiarities of the shift of longitudinal distributions are: 1) the centers of rapidity and pseudorapidity distributions shift E_o-independently towards smaller values with increasing A (and ν, and n_g) (see Fig. 13); and 2) the widths (dispersions) of y and η-distributions weakly (if at all) depend on A and ν slowly decreases with n_g. It is important that such behavior of the widths of inclusive distributions is observed for all types of relativistically produced particles (Fig. 14).

The latter observation has direct relation to the adequacy of the CTM to the data. It has been pointed out[48] that the logarithmic growth of widths of longitudinal y- and η-distributions with energy in hN collisions leads, within the CTM, to a logarithmic rise of these widths with A, in contradiction with data of the type plotted in Fig. 14. It should be noted that the CTM is the only model in the field leading to such distributions with dispersions increasing with A (and/or tube mass).

In relation to this observation, it has been suggested by the CTM inventors[41,42] that the target fragmentation products should be eliminated from consideration. In the modified CTM the growth of longitudinal distributions must take place either for separate types of particles produced (for π^- from pA interactions, for instance),[42] or for particles belonging to the central and projectile fragmentation regions.[41] But the data of Fig. 14 do not show the growth of dispersions

for any type of secondary particles and the data of Fig. 15 can be used to conclude that the second way suggested also does not improve the situation. In fact, as is seen from Fig. 15, where the n_g-dependence of the dispersion of the right Gaussians of Fig. 12 corresponding to particle production in the central and projectile fragmentation regions is plotted, the decrease of $\sigma(\eta)$ with n_g takes place also for particles produced outside the target fragmentation region. The same result has been obtained by us for all ensembles of hA interactions in the range 20 to 400 GeV/c. (Let us note, by the way, that the opposite conclusion of Ref. 41 is an artifact of the wrong assumption that the energy transfer to target does not depend on the target mass).

On the other hand one can see from Fig. 14a that the hydrodynamic model[29] quite reasonably describes the data on the n_g-dependence of $\sigma(\eta)$ in this range of energies. The important question arises as to what is the cause of such cardinal divergence of predictions of the CTM and the hydrodynamic model, though both models seem to be very close in the sense that they are based on the common "tube" concepts.

It is well known that in hN collisions the decrease of $\sigma(y)$ with the multiplicity is related with simple phase-space effects (the energy-momentum conservation). Obviously the same is true also for hA interactions. In fact, from the sum rule for the total energy

$$kE_o = \int \frac{1}{\sigma} \frac{d\sigma}{dy} - \text{coshy } m_t dy \ , \qquad (18)$$

by making use, for the sake of simplicity, of the Gaussian approximation for $(1/\sigma)(d\sigma/dy)$ one can easily obtain that

$$\sigma^2_{hA}(y) \approx \text{const} + (\frac{1}{3} - 2\alpha)\ \ln A\ , \qquad (19)$$

where α is the parameter of the approximation $\langle n\rangle_{hA}/\langle n\rangle_{hN} = A^{\alpha}$. One can see from Eq. (19) that $\sigma(y)$ has positive A dependence if $\alpha < 1/6$. In the CTM $\alpha \simeq 1/2$ and therefore $\sigma(y)$ increases with A; in the hydrodynamic model, $\alpha \simeq 0.2$ and $\sigma(y)$ decreases with A. One can note also that the rate of decrease of $\sigma(y)$ grows with α in contrast to the height of y distribution. The latter would increase with A and the rate of increase is larger for larger values of α.

So, we see that the difference between the CTM and the hydrodynamic model lies in the assumption of the models--in the latter one the final state is conditioned not only by larger energy in the c.m.s. than in hN collisions (as in the CTM), but by a larger initial volume as well. One can note that the theoretical critique of the CTM was given in Ref. 49 and the fact that in the CTM the A dependence of the multiplicity contradicts experimental data was also discussed in Refs. 5, 29 and 50.

In a recent paper,[32] an attempt actually has been made to essentially increase the A dependence of tube size; although the term "CTM" is used there, the model considered is considerably more complicated and multiparameter. The author considers four bodies in the final state: a leading hadron, a pionization cluster, an excited knocked out tube and a residual nucleus. The effective number of nucleons in the tube has the A dependence of $A^{\sim 2/3}$ (!) which is equivalent to a huge increase of inelastic hN cross-section (up to $\simeq$120 mb instead of 32 mb for pp interactions). The model predicts that, in contrast to the CTM,

$\sigma(y)$ is a decreasing function of A. It is easy to discover in this model the general tendency to return to old statistical-hydrodynamical concepts, at least for the central pionization region. In fact, the preliminary investigation of statistical consideration for pionization cluster has yet been performed within the model by the same author.[51] Needless to say, in any statistical approach the initial volume plays the decisive role for many observables.

Leading Particles in the Projectile Fragmentation Region

Let us consider in more detail the region of large longitudinal momenta of secondary particles where the main contribution comes from the surviving (leading) particles and products of their fragmentation. This region seems to be sensitive enough to various model assumptions.

Last year, special attention was paid to this region in connection with the experimentally observed weak A dependence of inclusive spectra at large rapidities. Along with very weak A dependence of the average transverse momenta of particles produced and inelasticity coefficients, this observation led to a number of strong hypostheses about the character of the propagation of fast particles through nuclear matter--the hypothesis about the full passivity of the leading particles after the first intranuclear collision, about the transparency of the nucleus for fast particles produced, and so on. These hypotheses were included into many phenomenological models of hA collisions. Of course, since the new more accurate data do not display the A independence of particle spectra in the projectile fragmentation region, the hypotheses above need clarification and the real situation seems to be more complicated.

In fact, as is quite clear already from the data discussed in the previous section, a wide-spread opinion about the coincidence of spectra on nucleonic and nuclear targets at large rapidities is wrong: no region in rapidity exists (except for a point y_c) where the ratio r(y) is A independent. In the range of large rapidities (and/or large momenta) ratio r(y) is less than unity, i.e., the target nucleus absorbs fast particles. This finding, first observed in emulsions, is now well established in most accurate counter experiments. As an example let us consider Fig. 16. It is evident that an increase in the atomic number of the target results in "extinction" of all types of fast secondaries and the degree of this extinction within errors does not depend on the primary energy.

So, it is clear that claims about the full passivity of leading particles inside the nuclear targets are wrong. Also, all the models making use, directly or indirectly, of this assumption and/or leading to $r(y) = 1$ in the projectile fragmentation region for any type of secondary particles are incorrect there, at least at presently available energies (to them one attributes the EFC model, fragmentation models, the FDDM, and some others).

Let us go to the quantitative comparison of model predictions with experimental data in the considered kinematic region.

It is shown in Fig. 17 that the data on spectra of leading protons from pA interactions at 19.2 GeV/c[52] can be reproduced nicely by the Glauber model.[53] Besides, one can learn from this figure how changing the different types of rescatterings contributes to the yield of fast protons. The same conclusion about the compatibility of the LPCM with the data on reaction $pA \to pX$ at 21 GeV/c comes from Ref. 45. The

same model reproduces well the experimentally observed increase of the average transverse momentum of the leading particles passing through the nuclear target. So, one can conclude, the Glauber model reproduces the basic characteristics of leading particles in hA interactions within the existing accuracy of experimental data.

As regards spectra of particles produced in the projectile fragmentation region, the situation in the LPCM is not satisfactory. Inadequacy of the LPCM in this kinematic region for produced particles already follows from the Eq. (15). In fact, bearing in mind that within the LPCM only the first intranuclear collision contributes here, and since the first collision appears in all terms of the sum in Eq. (15), one can easily conclude that for the fastest produced particles r(y) is equal to unity. It is obvious that this circumstance is related to the disregard of various inelastic intermediate states usually discussed when considering inelastic hA cross-sections and processes of diffractive coherent production on nuclei. So, we see that inclusive spectra of produced particles also contain information about the structure of these states which are important for the theory. Within the framework of the Glauber model itself it is difficult to quantitatively account for such intermediate virtual effects; one needs some additional, essentially model-dependent assumptions about both the mechanisms of fragmentation and cross-sections for interactions with downstream nucleons (this is important, for instance, for processes like $pA \to K^- X$, $pA \to \pi^- X$ and so on).

It should be noted that the CKM[40], although leading to $r(y) < 1$ for both the leading the produced particles in the projectile fragmentation

region, also does not contain the detailed consideration of projectile fragmentation in hA collisions.

The additive quark model which makes use of the quark combinatorics in order to describe the spectra of fast particles (both leading and produced, including resonances) lacks this shortcoming. The AQM, being the model of symmetry, contains in itself rules necessary for predicting the composition of particles in the kinematic region under consideration. In Fig. 18 some examples are collected showing a good description of spectra of various types of fast secondaries within the frameworks of the AQM.

As concerns collective models of hA interactions, no reliable quantitative calculations exist for particles belonging to the kinematic region under consideration. Nevertheless, one can note that versions of the LHM in which the "leaders" are included into the hydrodynamic system (see, e.g., Ref. 28) qualitatively reproduce the "extinction" of leading particles with increasing A. Of course, in such models the problem arises, unresolved up to now, with quantum numbers conservation. Besides, another difficulty is related to the uncertainty of how one could describe in these models the growth of transverse momenta of the leading particles since the practical solutions of hydrodynamic equations belong to the one-dimensional case.

In models where the leading particles are not included in the hydrodynamical (or statistical) system, the problem of a detailed description of the behavior of such particles leaves the framework of the models and remains open.

Phenomena in the Target Nucleus Fragmentation Region

Another region of importance where both the differences between theoretical models and the specific properties of nuclear matter could reveal themselves is the region of particles that are relatively slow in the laboratory system. As noted above, the fact that in this region the A dependence of different characteristics of secondaries is most strong seems to be attractive for distinguishing between different models of hA interactions. For example, we have noted above that too strong an A dependence of inclusive distributions at small rapidities cannot be explained by model approaches which completely ignore the possibility of low-energy cascading in high-energy hA collisions.

At present the larger part of information available on recoil protons in hA collisions belongs to the kinematic region $p < 1$ GeV/c (the region of the so-called grey or g-particles in emulsion terminology). It has been shown[57,58] that $\langle n_g \rangle \sim A^{\sim 2/3}$, whereas $\langle \nu \rangle \sim A^{1/3}$, so that the low-energy cascading plays an essential role in formation of protons with momenta $p < 1$ GeV/c. It is very interesting to discuss the data on characteristics of relativistic ($p > 1$ GeV/c) recoil protons from hA interactions that have become available over the last few years.

The presence of appreciable numbers of relativistic protons in hA interactions has been established in emulsion[59] and bubble chamber[60] experiments. Let us consider the main results on the A dependence of the number of knocked out protons versus their momenta.

In Fig. 19a the momentum spectra of protons from inclusive reactions $\pi^- {}^{12}C \to pX$ and $\pi^- p \to pX$ at 40 GeV/c[61] are plotted and compared with each other. It is seen that in the range of considered momenta (hundreds of

MeV/c) the ratio $r(p) = \rho_{\pi^- C}(p)/\rho_{\pi^- p}(p)$ decreases with the momentum of the protons. Hence, at relatively low momenta the A dependence of the number of recoil protons strongly depends on p (see Fig. 20a, where the corresponding p dependence of the parameter $\alpha(p)$ in parametrization $r(p) = \rho_{hA}(p)/\rho_{hN}(p) = A^{\alpha(p)}$ is plotted. Note that here the data on $\pi^- N \to pX$ have been used for normalization).

In Fig. 19b the momentum spectra from reactions $pA \to pX$ and $pN \to pX$ at 21 GeV/c are plotted for recoil protons having 1 GeV/c $\lesssim p \lesssim$ 3 GeV/c.[59] In contrast to the region p < 1 GeV/c, one has for relativistic recoil protons: 1) $\rho_{pA}(p)$ has the same shape as $\rho_{pN}(p)$; 2) the ratio r(p) within errors does not depend on p; 3) a dependence of the number of relativistic recoil protons is practically independent of p (see Fig. 20b), the exponent $\alpha(p)$ has the value $\alpha = 0.26 \pm 0.04$.

It is necessary to point out that protons with momenta $p/p_0 < 0.15$ (this value of p/p_0 corresponds to protons emitted to the backward hemisphere in the c.m.s. of pN collision at 21 GeV/c) can be referred to as recoil protons only conditionally. In fact, in this region there may exist the leading protons undergoing "catastrophic" energy losses and, on the other hand, some recoil protons would pass from this region to the kinematic region of g-particles due to rescatterings within the nucleus. One, of course, may hope that these effects would, at least partially, cancel ech other.

In order to discuss quantitatively the data of Figs. 19 and 20 one needs to know the A dependence of the number of recoil protons in different models, for example, in multiple scattering models. In this case it is easy to show that, if a projectile collides with

nucleons of a nucleus having Z protons and A-Z neutrons and the probability of inelastic charge exchange for a nucleon is q, one would have

$$n_p(hA)\ /n_p(hN) = \sum_{\nu=1}^{A} \nu P(\nu)\ \left[q + (1 - 2q)\ \frac{Z}{A}\right]. \qquad (20)$$

It follows from this formula that if $q < 0.5$ (experimental data on hN interation give $q \simeq 1/3$), the A dependence of the considered ratio would be weaker than the A dependence of $\langle y \rangle$. In particular, for emulsion nuclei under a power law approximation $n_p(pA)/n_p(pN) \sim A^{\alpha}$, the value of the exponent was found to be $\alpha = 0.25$,[59] instead of 1/3 as for $\langle y \rangle$. So, one can conclude, the results of the calculation are in a good agreement with the data of Fig. 20b (in the range 1 GeV/c $\lesssim p \lesssim$ 3 GeV/c).

It is now clear that the rapid increase of $\alpha(p)$ at $p < 1$ GeV/c (Fig. 20a) indicates the presence of other additional mechanisms of formation of protons in that region of momenta; we can attribute them to cascading, cumulative production, evaporation, and so on. It is interesting to note that angular distribution of protons also essentially depends on their momenta: the overwhelming majority of protons having $p > 1$ GeV/c turn out to be emitted to the forward hemisphere in the laboratory system. At $p < 1$ GeV/c an amount of protons emitted to the backward hemisphere (the region kinematically forbidden for hN collisions) rapidly increases with decreasing p.

It is important that the number of fast recoil protons was found to be essentially dependent on the quantum numbers of a projectile. So, in π^+Ne and π^-Ne interactions at 10.5 GeV/c[60] studied in identical experimental conditions, these numbers turn out to be 0.78 and 0.46,

respectively. It is even more interesting that the sensibleness of the yield of nucleons (neutrons and protons) to the quantum numbers of the projectile conserves even in the region of cumulative production.[62]

It is necessary to say that there exists another way to study multinucleon interactions in nuclei. One can also investigate distribution of the total charge of relativistic particles $Q = n_+ + n_-$.[77] The data available for π^-C interactions at 4 (Ref. 78) and 40 (Ref. 77) GeV/c and for $\pi^\pm Ne$ interactions at 25 and 50 GeV/c (Ref. 79) show that: 1) $\langle Q \rangle$ weakly (if at all) depends on E_0; and 2) Q distributions are reproduced satisfactorily within the Glauber model framework.

Finally, it is necessary to discuss important results of very recent experiments on the measurement of polarization of particles (nucleons and Λ-hyperons)[63-66] in the target fragmentation region from hA interactions in a wide range of primary energies (up to 400 GeV). The main results of these experiments are as follows: 1) nucleons and Λ-hyperons from hA interactions turn out to be polarized; and 2) polarization decreases with increasing A and decreasing momenta of nucleons in the nucleus fragmentation region.

The totality of data presented in this section cast doubt on all models of hA interactions in which, as a result of collisions with a projectile, the nucleus as a whole or its part (tube) turns into highly excited state with subsequent decay leading to formation of the final system of nucleons. The data presented do not necessitate inclusion of collective effects for describing phenomena in the target fragmentation region, the only exception being the region of cumulative particles. But the existence of polarizations of cumulative particles,

in our opinion, give the cogent argument indicating that the origin of this collectivity (i.e., the mechanism of formation of cumulative particles) is related not with "large" properties in spatial dimensions objects (like tube), but with local properties of hadronic matter. This means that most probably the short-range effects between intranuclear nucleons and "fluctuons" are responsible for cumulative production of particles.[67,71]

Before ending this section we would like to stress once more that the considered kinematic region is very important for distinguishing between different models simply due to the fact that only intranuclear nucleons are spectators and probes of the production process. Therefore the new, more accurate and definite experimental data in this region are of urgent necessity, especially at higher primary energies and for different projectiles.

Correlations in hA Collisions

When studying hN interactions it has been recognized that sometimes standard characteristics of the process are not sensitive enough to discriminate different models of multiple production; therefore much attention is paid now to the study of multiparticle (correlation) phenomena. The same is true for nuclear production as well.

Two-particle rapidity (or pseudorapidity) correlations among relativistic particles produced in hA collisions have been investigated in a number of papers (see, e.g. review Ref. 58) using correlation functions

$$C_2(y_1, y_2) = \frac{1}{\sigma}\frac{d^2\sigma}{dy_1 dy_2} - \frac{1}{\sigma^2}\frac{d\sigma}{dy_1}\frac{d\sigma}{dy_2},$$

$$R_2(y_1, y_2) = \sigma \frac{d^2\sigma}{dy_1 dy_2} \Big/ \frac{d\sigma}{dy_1}\frac{d\sigma}{dy_2} - 1.$$

The main results obtained from analysis of two-particle correlation functions in hA interactions are as follows:

1. It is observed that there exist positive short-range correlations (similar to those observed in hN collisions) which cannot completely be explained by trivial and kinematic factors. They are present in a wide range of investigated energies (20 to 400 GeV) and probably increase somewhat with E_o.[46]

2. In hA interactions, in qualitative analogy with hN collisions, correlations between pions depend essentially on the signs of charges of pions ($\pi^+\pi^-$, $\pi^-\pi^-$, $\pi^+\pi^-$, ch-ch).[72,73] In particular, correlations between pions with different signs of charge are considerably stronger than for pions with the same sign of charge.

3. Values of the normalized correlation function R_2 decrease considerably with increasing atomic number of the target, the number of g-particles, and ν. It is necessary to point out that the decrease of R_2 has been experimentally observed for many types of particles produced in hA interactions. So, for instance, the values of $R_2(0,0)$ have measured at 0.68±0.18 and 0.34±0.09 for pairs of γ-quanta, and 0.26±0.04 and 0.09±0.8 for $\pi^-\pi^-$ in π^-N and π^- ^{12}C interactions, respectively, at 40 GeV/c (Ref. 73 and 74). Further in a very nice counter

experiment on pA interactions at 400 GeV/c, Ref. 75, it has been observed that in the central region for particles of various species the larger nucleus decreases correlations.

The quantitative calculations of correlation functions in the framework of different models of nuclear production have been performed in two cases:

In the first case, correlation functions were calculated in the framework of the CTM with the Monte Carlo method, as reported in Ref. 46 and 48. It has been shown that in the CTM the function R_2 practically does not depend on A, which disagrees with the data up to 400 GeV/c (see an example in Fig. 21a). The same conclusion has been drawn in Ref. 11, and the observation was also made that the observed A dependence of R_2 is consistent with predictions of multiple scattering models.

In Ref. 41 it has been stressed that within the CTM, R_2 (h-tube) = R_2(hN) only outside the target fragmentation region. We have discussed above that in the central region $R_2(0,0)$ decreases for <u>particles produced</u> in hA interctions even at very high energies (see Fig. 21b for an example of π^-Em interactions at 50 GeV/c.)[72] These results are in obvious disagreement with the CTM predictions.[41] If one assumes that the central region, even at such high energies, contains products of tube fragmentation, this would simply mean that even at the highest FNAL energies the CTM is not yet applicable.

The second case was a very recent paper[68] in which two- and three-particle correlation functions have been calculated in the framework of several multiple scattering models. In all these models, correlations do decrease with A. The authors demonstrate that the models considered

lead to different quantitative results. Therefore it is very instructive to develop investigation of correlation functions in nuclear production. As an example we replotted in Fig. 22 the dependence of $R_2(0,0)$ on A for AQM and the quasi-eikonal model along with experimental results for pEm and π^-Em interactions at 200 GeV/c; it is seen that the data, although not decisive, show better agreement with the predictions of the AQM.

More direct and visual information about the character of correlation relations between produced particles can be obtained from analysis of correlations in the transverse (azimuthal) plane.

In Refs. 45 and 69 the normalized differences

$$\delta_{inc} = \left(\langle n_2\rangle_{\varepsilon>\pi/2} - \langle n_2\rangle_{\varepsilon<\pi/2}\right)/\left(\langle n_2\rangle_{\varepsilon>\pi/2} + \langle n_2\rangle_{\varepsilon<\pi/2}\right) \qquad (21)$$

of associated multiplicities of particles of type 2 in inclusive reactions

$$\left.\begin{matrix} h + N \\ h + A \end{matrix}\right\} \longrightarrow 1 + 2 + X$$

have been considered as a function of species of charged particles 1 and 2, the relative distances among them along the longitudinal axis (for example $\Delta y = |y_1 - y_2|$ or $\Delta\eta = \Delta\eta_1 - \eta_2|$) and for different kinematic regions. The quantity Σ in Eq.(21) is the azimuthal angle among particles 1 and 2 $\Sigma = \arccos$.

The quantity δ_{inc} has a simple meaning; it is the average amount of the transverse momentum of "trigger" particle 1, compensated by one partner particle of type 2. It is easy to calculate δ for the simplest (the so-called global) mechanism of $\vec{p}_{1\perp}$ compensation (for statistical production from one "center", for examle), if one knows

multiplicity distributions of "visible" (for example, charged) and invisible (neutral, for instance) secondary particles.

Figure 23 exemplifies the dependences of δ_{inc} on pseudorapidity of particle 1 (1 and 2 are relativistic particles) in pN and pA interactions at 24 and 67 GeV/c in comparison with a calculation performed in accordance with a statistical-type model that takes into account the presence of invisible (neutral and recoil) particles. One can observe good agreement for N interactions, whereas for pA interactions correlations caused by the conservation of transverse momentum are weaker considerably than in the model. The following is of importance here: 1) the same picture turns out to be conserved up to 400 GeV/c (only the absolute values of δ_{inc} in both interaction classes decrease with E_o and $\langle n \rangle$, and 2) dependence of δ_{inc} on η_1 does not depend on $\Delta\eta$ (for details see Ref. 69), i.e., correlations have a long-range character.

These features of correlation relations between particles in hA interactions seem to be vaguely understood both in purely collective and in cascade type models. The fact that "local" compensation of $\vec{p}_{11}$ does not exist contradicts also such models as the model of independent clusters. Most naturally, although qualitatively, the observed weakening of azimuthal correlations in hA collisions may be reached in models with hadronic constituents.

We would like to note that it seems to be of urgent importance to further investigate correlation phenomena in hA interactions based on more accurate data, especially quantum numbers correlations.

CONCLUSIONS

Let us briefly generalize results of our discussion starting with some trivial remarks.

The models of hA interactions considered above have the following mutual properties:

1. At $A \to 1$ they reproduce (or must reproduce a'priori or a'posteriori) characteristics of elementary hN collisions;
2. they take into account conservation laws, which play an outstanding role in the range of presently available nonasymptotic energies;
3. all of them (with the exception of the cascade model) assume, more or less, the suppression of intranuclear interactions of fast produced particles, though the mechanism of such suppression is different in different models.

These factors, along with the obvious scarcity of precise data, result in the fact that most of the models at first glance describe satisfactorily general trends of standard experimental characteristics and only a detailed analysis including a systematic consideration of a wide variety of experimental material, especially belonging to fine features of the process, could clarify differences in predictions of the models and their adequacy in describing reality. Such an analysis, in our opinion, allows one to conclude the following:

1. With sufficiently high degree of confidence the totality of experimental data already existing allows us to rule out (in the range of accelerator energies) some models of hA interactions which are unable to describe a number of experimental

characteristics of the process. In particular, the following concrete models are examples: a) the cascade model,[2] b) the energy-flux cascade model,[3,34] c) purely diffractive models,[35,36] d) the coherent tube model,[7,41,42] and e) the fan-diagram-dominance model (see Refs. in Ref. 11).

2. Statistical-hydrodynamical and multiple rescatterings approaches (especially those taking into account the composite structure of hadrons) describing a sufficiently large volume of experimental information and having a good adaptability to new data and characteristics can be attributed to the most attractive theoretical approaches to the problem. For all this, the existing concrete realizations of these approaches do not necessarily describe <u>all</u> the experimental data. In particular:
   a) statistical-hydrodynamical approaches do work well in the central region of hA collisions, like in hN interactions; note that this does not contradict microscopic (constituent) models in which production mechanisms are <u>different</u> in the fragmentation and central regions;
   b) difficulties arise in the frameworks of statistical approaches in the projectile fragmentation region, where effects related to the composite structure of hadrons probably play a considerable role (again in the exact analogy with hN collisions);
   c) all the existing models of hA interctions have difficulties in the <u>quantitative</u> description of phenomena in the target nucleus fragmentation region, where the low-energy cascading

and locally collective properties of nuclear matter probably play the considerable role.

It seems to be probable, that the real mechanism of hA interactions should have two or multicomponent character and the contributions of the components depend simultaneously on the atomic number of the target and on the incident beam momentum.

We would like to stress that the present situation with both the volume and accuracy of experimental data available on hA interactions and the degree of the quant· ·ive elaboration of theoretical approaches to the problem is not satisfactory. From the experimental point of view we have no practical information about the cross sections and other characteristics of resonances in nuclear production, about the character of quantum numbers compensation and other fine correlation phenomena, about the composition of secondaries in different kinematic regions, and so on, which undoubtedly would have the decisive role in the construction of a realistic picture of the complicated process of hA interactions.

In conclusion we are glad to express our sincere thanks to A. M. Baldin, V. G. Grishin, O. V. Zhirov, E. M. Levin, G. A. Leksin, N. N. Nikolaev, A. V. Tarasov, and Yu. M. Shabelsky for useful discussions of topics presented in the paper. We are deeply indebted to L. P. Chernova, A. I. Bondarenko, V. Sh. Navotny, and V. I. Petrov for help in data analysis and in preparation of the text.

REFERENCES

1. I. L. Rozental and D. S. Chernavskij, Uspekhi Fiz. Nauk 52, 185, 1954.

2. V. S. Barashenkov and V. D. Toneev, Interactions of High Energy Particles and Atomic Nuclei with Nuclei, Atomizdat, Moscow, 1972.

3. K. Gottfried, CERN Rept., TH-1735, 1973.

4. L. Bertocchi, Report IC/75/67, Trieste, 1975.

5. B. Andersson, Proceedings of the VII International Colloquium on Multiparticle Reactions, Tutzing, 1976, ed. J. Benecke et al. p. 109.

6. K. Zalewski, Multiparti. Production on Nuclei at Very High Energies, Trieste, 1977, ed. G. Bellini et al. p. 145.

7. Y. Afek et al., ibid., p. 591.

8. Meng Ta-Chung, ibid., p. 435.

9. I. L. Rozental, Uspekhi Fiz. Nauk 116, 271 (1975).

10. Yu. P. Nikitin et al., ibid., 121, 3 (1977).

11. N. N. Nikolaev et al., CERN, TH-2541, 1978.

12. Yu. M. Shabelsky, Proc. XIII Winter School of the Leningrad Nuclear Physics Institute, 1978, p. 90.

13. A. Bialas, Proceedings of the IX International Seminar on Multiparticle Reactions, Tabor, 1978, ed. V. Simak et al., p. C1.

14. E. L. Feinberg, Phys. Rept. 5C, 237 (1972).

15. K. G. Gulamov et al., Proc. IV Int. Seminar on Problems of High Energy Physics, Dubna, 1975, p. 233.

16. A. V. Tarasov, Particles and Nclei, 7 (1977).

17. L. D. Landau and I. Ya. Pomeranchuk, in Collected Papers of L. D. Landau, Nauka, Moscow, 1969, papers nr. 75 and 76.

18. M. L. Ter-Mikaelian, High Energy Electromagnetic Processes in Condensed Media, Wiley-Interscience, 1972.

19. B. L. Ioffe, in Problems of Theoretical Physics, Nauka, Moscow, 1972, p. 200.

20. E. L. Feinberg and I. Ya. Pomeranchuk, Nuovo Cim. Suppl., 4, 652 (1956).

21. AGMT collaboration, Nucl. Phys. B137, 37 (1978).

22. BWDKLMT collaboration, Yadrenaya Fizika 29, 105 (1979).

23. F. E. Low, K. Gottfried, Preprint CLNS-382, Ithaca, 1978.

24. L. D. Landau and S. Z. Belenkij, in Collected Papers of L. D. Landau, Nauka, Moscow, 1969, paper nr. 85.

25. D. I. Blokhintsev, ZhETF 32, 350 (1957).

26. A. A. Tyapkin, Particles and Nuclei 8, 543 (1977).

27. M. J. Moravcsik, M. Teper, Preprint OITS-67 1976.

28. N. Masuda and R. M. Weiner, Phys. Rev. D18, 1515 (1978).

29. O. V. Zhirov and E. V. Shuryak, Yadernaya Fizika 28 485 (1978).

30. S. Fredriksson, Nucl. Phys. B111, 167 (1976).

31. F. Takagi, Lett. Nuovo Cim. 14, 559 (1975).

32. F. Takagi, Tohoku University Rept. TU-178/188, 1978.

33. M. Meisowicz, Progress in Elementary Particle and Cosmic Ray Physics 10, 103 (1971).

34. K. Gottfried, Phys. Rev. Lett., 32, 957 (1974).

35. P. M. Fishbane and J. S. Trefil, Phys. Rev. Lett. 31, 734 (1973); Phys. Lett. 51B, 139 (1974).

36. A. Subramanian et al., TIFR-BC-72-12, Bombay, 1972.

37. O. Kofoed-Hansen, Progressive Particle Nuclear Physics, Pergamon Press, 1978, p. 193.

38. L. Caneschi and A. Schwimmer, Proceedings XII Rencontre de Moriond, 1977, v. II, p. 173.

39. S. A. Azimov et al., Z. Phys. A., to be published.

40. A. Capella and A. Krzywicki, Phys. Lett. B67, 84 (1977); preprints LPTPE 77-16, 77-31, 1977.

41. S. Fredriksson and L. Bergstrom, Phys. Lett. 78B, 337 (1978).

42. Y. Afek et al., Phys. Lett. 78B, 329 (1978).

43. V. V. Anisovich et al., Nucl. Phys. B133, 477 (1978).

44. A. Bialas et al., Rept. 944/PH, Krakow, 1977.

45. S. A. Azimov et al., Proceedings V. International Seminar on Problems of High Energy Physics, Dubna, 1978, to be published.

46. AGMT collaboration, Nucl. Phys. B143, 232 (1978).

47. AGMT collaboration, Nucl. Phys. B129 , 205 (1977).

48. S. A. Azimov et al., Phys. Lett. B73, 339 (1978).

49. E. V. Shuryak, Yadernaya Fizika 24, 630 (1976).

50. H. J. Mohring, Report KMU-HEP-7801, 1978.

51. F. Takagi, TU/78/180, 1978.

52. J. Allaby et al., CERN Rept. TH-70-12, 1970.

53. A. v. Tarasov, Ch. Tseren, A. S. Pak, G. Alaverdyan and V. V. Uzhinski, private communiations and to be published.

54. K. Heller et al., Phys. Rev. D16, 2737 (1976)

55. N. N. Nikolaev and A. Ya. Ostapchuk, CERN Rept. TH-2537, 1978.

56. N. N. Nikolaev and S. Pokorski, Phys. Lett. B80, 290 (1979).

57. S. A. Azimov et al., Multiparticle Production on Nuclei at Very High Energies, Trieste, 1977, ed. G. Bellini et al., p. 83.

58. K. G. Gulamov et al., Particles and Nuclei 9, 554 (1978).

59. S. A. Azimov et al., Yadernaya Fizika 8, 933 (1968)., K. G. Gulamov et al., Preprint IYaF, Tashkent, 1979.

60. W. M. Yeager et al., Phys. Rev. D16, 1294 (1977).

61. S. A. Azimov et al., Yadernaya Fizika 23, 987 (1976).

62. Yu. D. Bayukov et al., Preprint ITEF-19, Moscow (1979).

63. G. A. Leksin and A. V. Smirnitski, Preprint ITEF-87 (1977).

64. N. A. Burgov et al., Preprint ITEF-115, Moscow, 1978.

65. P. P. Temnikov et al., JINR P1-12138, Dubna, 1979.

66. R. O. Polvado et al.. Preprint IUHEE-26, Bloomington, 1979.

67. A. M. Baldin, JINR E1-12031, Dubna, 1978; private communications.

68. E. M. Levin et al., Preprint LNPI, Leningrad, 1979.

69. S. A. Azimov et al., Pis'ma v ZhETF 24, 316, 1976.

70. T. Jaroszewich et al., Report INP-1012/PH, Krakow, 1978.

71. L. L. Frankfurt and M.I. Strikman, LNPI 415, Leningrad, 1978.

72. ADLMT collaboration, Pis'ma v ZhETF 24, 107 (1976).

73. N. Angelov et al., JINR P1-10511, Dubna, 1977.

74. N. Angelov et al., JINR P1-10768, Dubna, 1977.

75. D. A. Finley, Ph.D. Thesis, Purdue University, 1978.

76. I. G. Bogatskaya et al., Yadernaya Fizika 26, 1010 (1977).

77. N. Angelov et al., JINR P1-11401, Dubna, 1978.

78. B. S. Yuldashev, private communication.

79. Yu. M. Shabelsky and B. S. Yuldashev, Preprint LNPI, Leningrad, 1979.

80. E. V. Shuryak, private communication.

81. V. Sh. Navotny et al., to be published.

82. T. Ferbel, Invited talk at the VIII International Colloquium on Multiparticle Reactions, Kaiserberg, 1977.

83. S. Backovic and V. G. Grishin, private communication.

84. N. Masuda, Louvain Univ. Rept., 1976.

85. V. G. Grishin, private communication.

86. T. Eichten et al., Nucl. PHys. B44, 333 (1972).

87. A A. Borisov et al., preprint IHEP ONF 78-115, Sepukhov, 1978.

88. S. A. Azimov et al., JINR P1-9021, Dubna, 1975.

89. K. Olimov and S. Lutpullaev, private communication.

FIGURE CAPTIONS

Fig. 1. a) The structure of the final state in the cascade-evaporation model.

b) The energy dependence of multiplicities of different types of secondaries in the hEm interactions; the curves belong to the cascade model.[2]

Fig. 2. The energy dependence of total and topological cross sections in coherent production by protons on emulsion nuclei.[21]

Fig. 3. Three regions in the nucleus corresponding to different lengths of the effective target in the model.[29]

Fig. 4. Fast hadron represented as a parton ladder.

Fig. 5. a) Multiperipheral production process giving the main contribution to the inelastic scatterin on nucleus in the FDDM.

b) The fan diagram of Reggeon calculus.

Fig. 6. Scattering on the nucleus as viewed in the leading particle cascade model.

Fig. 7. a) The multiladder state of a fast hadron.

b) Non-planar Mandelstam diagram for the double scattering.

Fig. 8. Processes contributing to inelastic baryon-nucleus scattering in the additive quark model framework.

Fig. 9. a) $r(\eta)$ as a function of η in p-Em interactions at 24, 50, 200, and 400 GeV/c.[46,57] The solid curves (1) correspond to the FDDM,[11] the broken curves (2) belong to the AQM,[11,55] the chain curves belong to the CKM,[39,40] curve (4) belongs to the LHM,[84] and the dotted curve (5) belongs to the LPCM.[81]

b) y-dependence of $\alpha(y)$ in the parametrization $r(y)=A$ for positively and negatively charged particles from nA interctions at 300 GeV/c.[82]

c) $r(y)$ as a function of y for π^+ and π^- mesons in interactions with several protons $\nu=2$ and 3 at 40 GeV/c. Selection of events with $\nu=2$ and 3 has been performed through the study of distribution of the total charge of the final system of relativistic particles.

Fig. 10. The energy dependence of $y_{max}-\eta_c$ in pEm interactions. The solid curve belongs to the FDDM, the broken line corresponds to multiple rescatterings models.[46]

Fig. 11. Inclusive η-distributions in π^-A and pA interactions in emulsion at 200 GeV/c.[47,57]

Fig. 12. Inclusive η-distributions in π^-A interactions at 200 GeV/c with different n_g values.[47] The curves correspond to the approximation of experimental data by sum of two Gaussians.

Fig. 13. Dependence of $\langle\eta\rangle$ on n_g in pA interactions in emulsion at 24, 50, 67 and 200 GeV/c (from the bottom, respectively).

Fig. 14. a) $\sigma(\eta)$ versus n_g in pA interactions in emulsion at 24, 50, 200 and 400 GeV/c (from the bottom, respectively).[57,46] The curves for 24 and 200 GeV/c belong to the LHM.[80]

b) n_g dependence of $\sigma(y)$ for $\pi^-(0)$, $\pi^+(0)$ and protons (x) in pA interactions at 21 GeV/c.[59] The straight lines show the same for pN interations.

c) $\sigma^2(\pi^-\nu p) - \sigma^2(\pi p)$ for π^+ and π^- mesons as a function of ν in π^{-12}C interactions at 40 GeV/c.[85]

Fig. 15. n_g dependencies of $\langle n\rangle_{fr}$(○), $\langle n_g\rangle - \langle n\rangle_{fr}$(●) and $\sigma(\eta)$ of the right Gaussian of Fig. 12, corresponding to production of particles in the central and projectile fragmentation regions, in π^-Em interactions at 200 GeV/c.

Fig. 16. The ratios of yields of pions and protons produced in pA $4 < \Theta < 6$ interactions at 19.2, 24 and 70 GeV/c[52,86,87] at $4 < \Theta < 6$ mrad in dependence on $x = p_{cm}/p_{cm}^{max}$.

Fig. 17. Spectra of protons from pA interactions at 19.2 GeV/c[52] in comparison with the LPCM predictions.[53] Different curves in Fig. 17a show relative contributions of manifold scatterings. Figures in brackets show the number of inelastic and elastic scatterings, respectively.

Fig. 18. a) The normalized yields of protons and K^+-mesons in pA interactions at 19.2 GeV/c[52] in comparison with the AQM predictions.[55]

b) The same but for Λ-hyperons at 300 GeV/c.[54,56]

Fig. 19. a) Inclusive distributions of protons in π^-C → pX and π^-p X at 40 GeV/c.[88] The curves are Fermi-Dirac distributions;

b) Integral momentum distribution of relativistic recoil (i.e. hving $p < 0$ in the pN c.m.s) protons from pN → pX and pEm → pX at 21 GeV/c.[59]

Fig. 20. The momentum dependence of the $\alpha(p)$ in the parametrization $P_{hA}(\nu)/P_{hN}(p) = A^{\alpha(p)}$ for π^-C interactions[89] and for pEm interactions at 21 GeV/c.[59]

Fig. 21. a) n_g-dependence of the correlators $R_2(\eta_1,\eta_2)$ and $R_2(0,\eta)$ in pEm interactions at 400 GeV/c. Curves belong to the calculations in the CTM framework.[46]

b) $R_2(y_1,y_2)$ for $\pi^-\pi^-$ and ch-ch combinations in π^-Em and π^-p interactions at 50 GeV/c.[72]

Fig. 22. The A-dependence of the $R_2(0,0)$ in pA(a) and π^-A (b) interactions within the AQM (curve 1) and the QEM (curve 2) frameworks. The data points belong to pEm and π^-Em interactions at 200 GeV/c.[68]

Fig. 23. Dependence of δ_{ss} on Δ_1 in pN and pEm interactions at 21 and 67 GeV/c. Curves belong to the statistical model, the broken lines show the experimental average values.

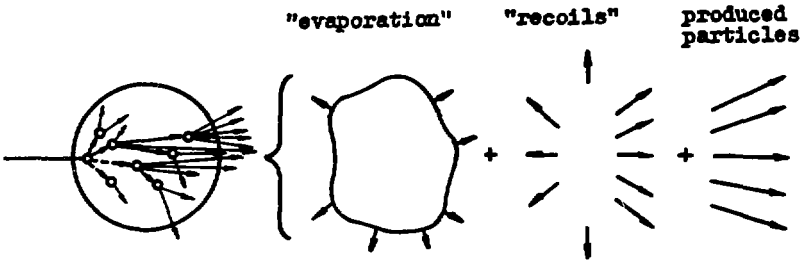

Figure 1a

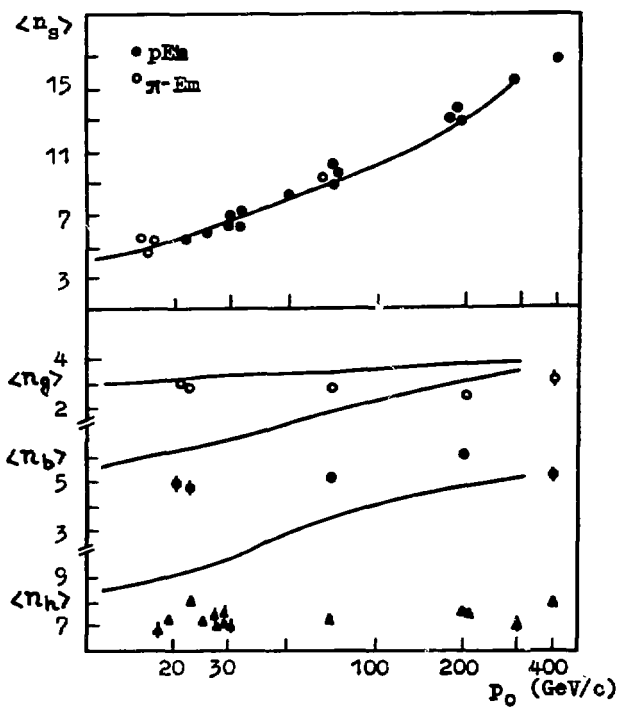

Figure 1b

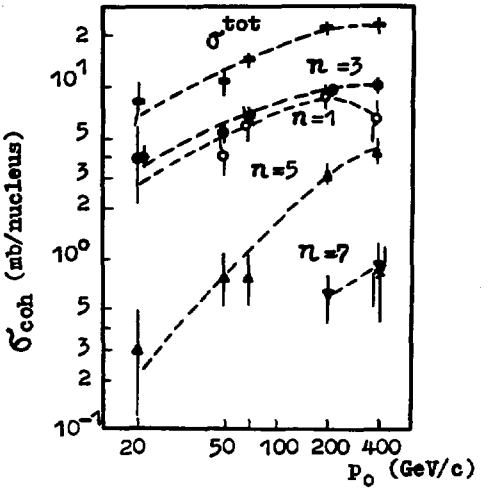

Figure 2

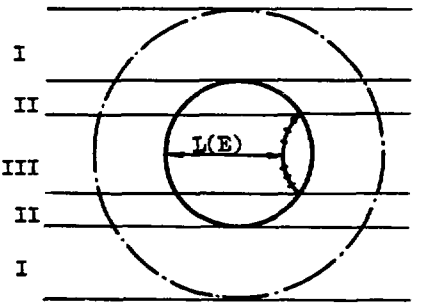

Figure 3

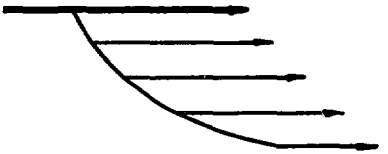

Figure 4

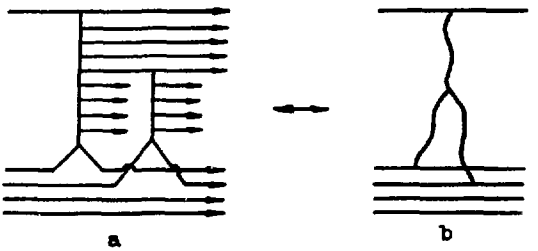

Figure 5

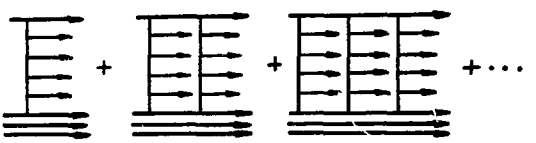

Figure 6

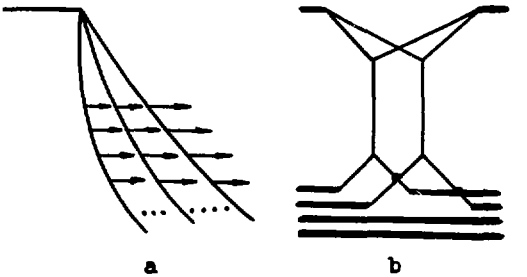

Figure 7

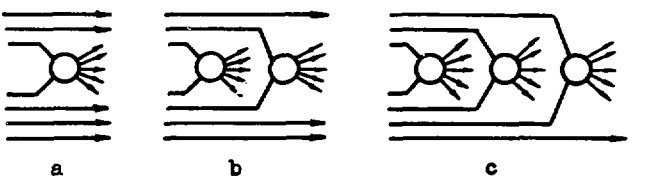

Figure 8

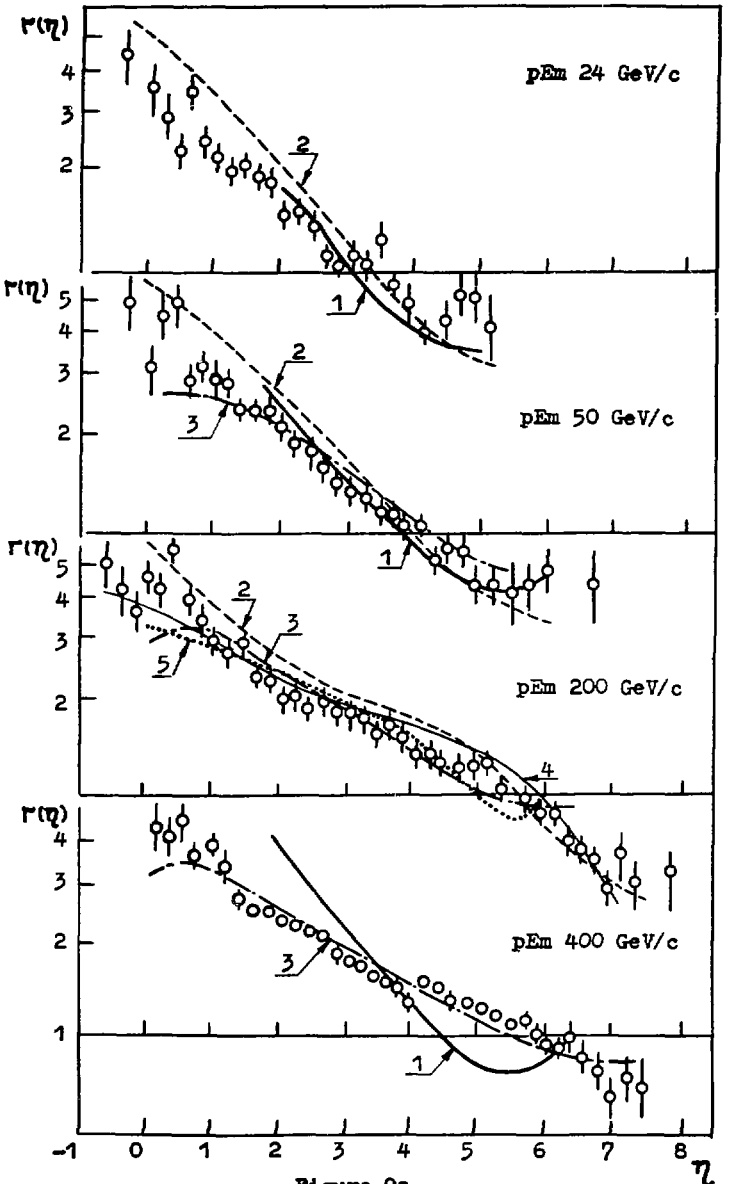

Figure 9a

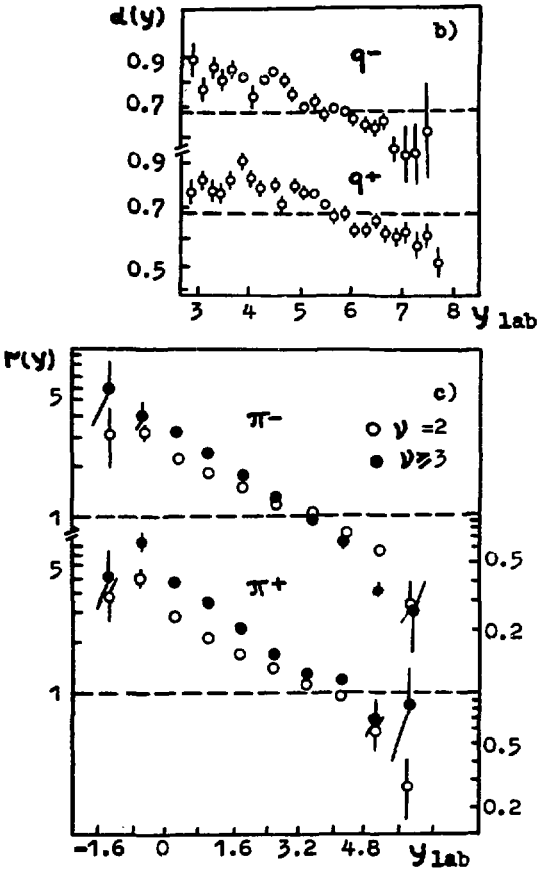
d(y)
b)
q-
q+
0.9
0.7
0.9
0.7
0.5
3
4
5
6
7
8
y lab
r(y)
c)
π-
π+
ν =2
ν≥3
5
1
5
1
0.5
0.2
0.5
0.2
-1.6
0
1.6
3.2
4.8
y lab

Figures 9b,c

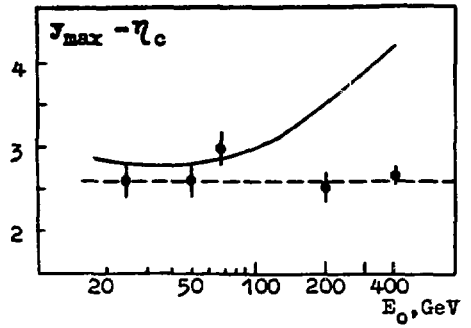

Figure 10

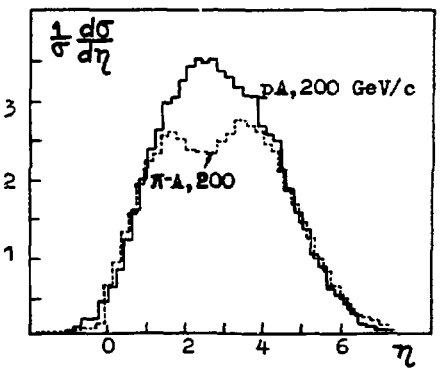

Figure 11

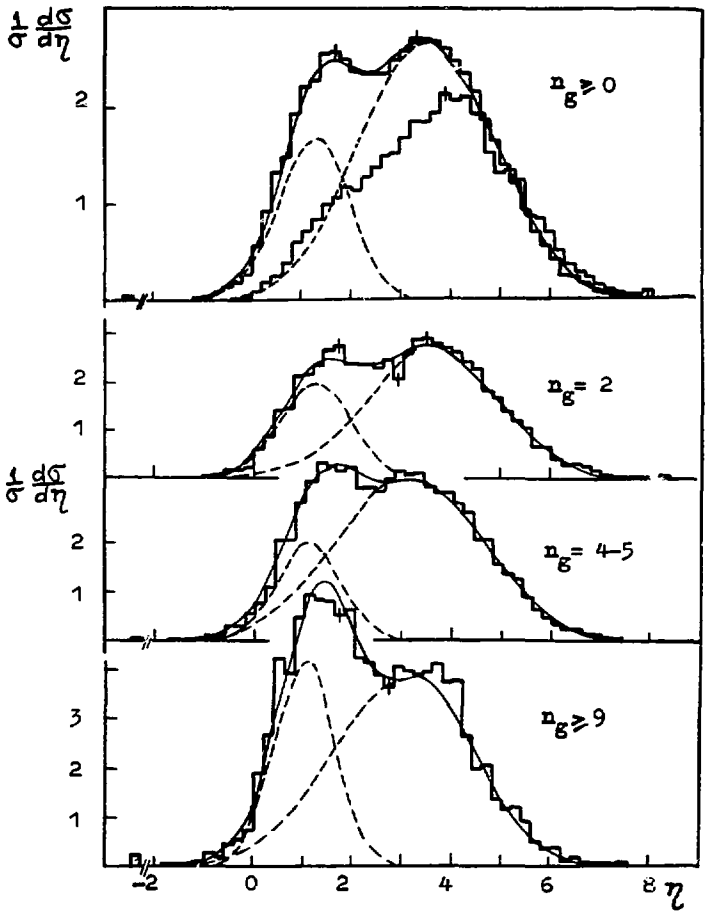
$\frac{1}{\sigma}\frac{d\sigma}{d\eta}$
$n_g \geq 0$
$n_g = 2$
$n_g = 4\text{-}5$
$n_g \geq 9$
η

Figure 12

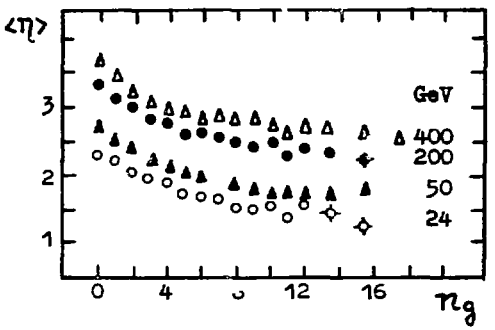

Figure 13

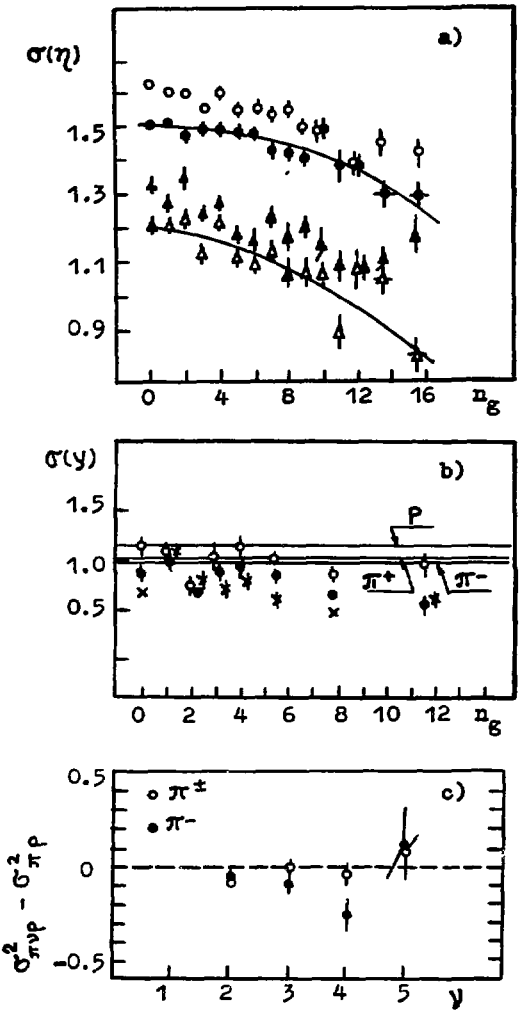
a)
σ(η)
1.5
1.3
1.1
0.9
0
4
8
12
16
n_g
b)
σ(y)
1.5
1.0
0.5
p
π+
π−
0
2
4
6
8
10
12
n_g
c)
0.5
0
-0.5
π±
π−
σ²πνp - σ²πp
1
2
3
4
5
y

Figure 14

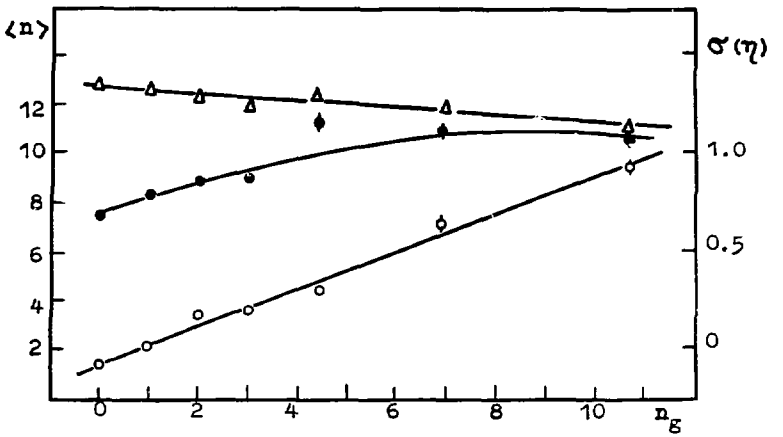

Figure 15

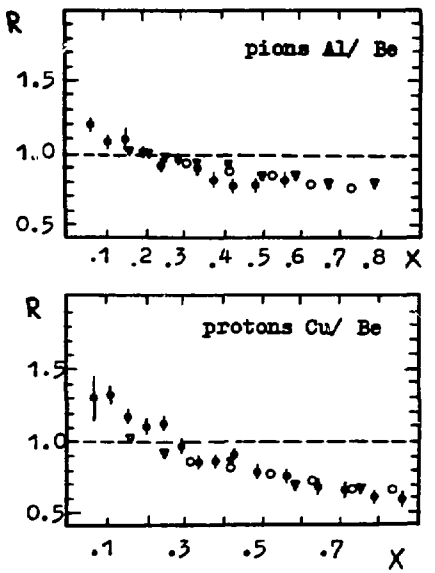

Figure 16

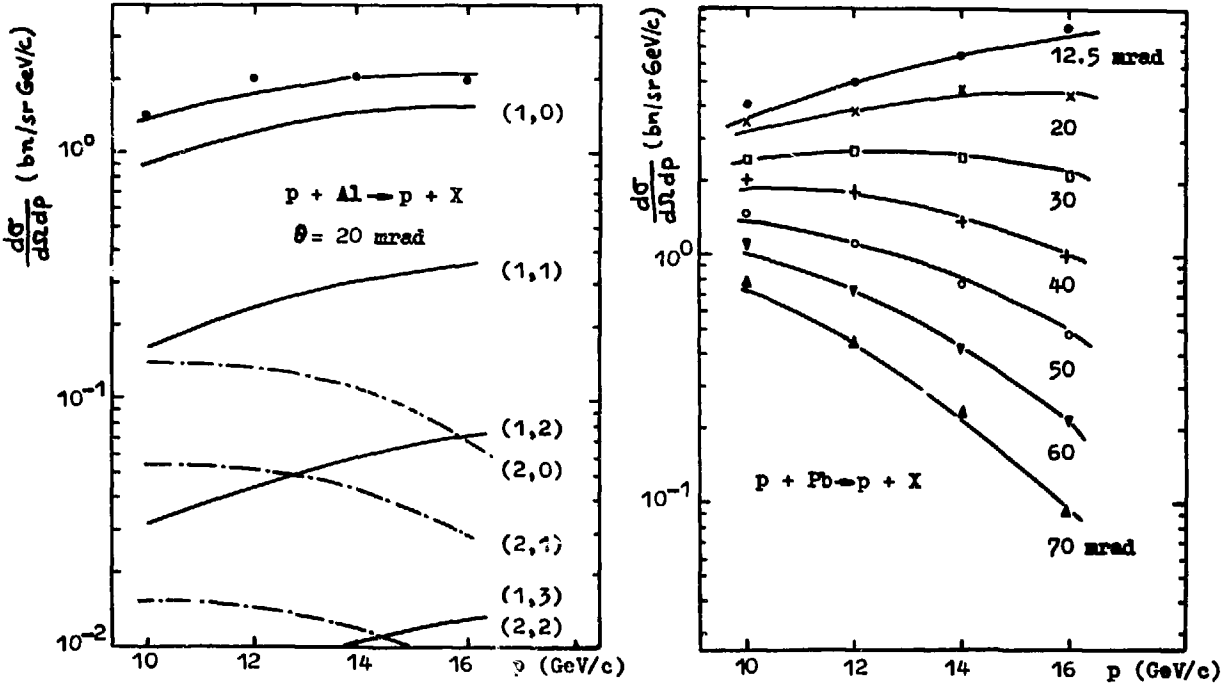
$\frac{d\sigma}{d\Omega dp}$ (bn/sr GeV/c)
10^0
10^{-1}
10^{-2}
p + Al → p + X
θ = 20 mrad
(1,0)
(1,1)
(1,2)
(2,0)
(2,1)
(1,3)
(2,2)
10
12
14
16
p (GeV/c)
$\frac{d\sigma}{d\Omega dp}$ (bn/sr GeV/c)
10^0
10^{-1}
p + Pb → p + X
12.5 mrad
20
30
40
50
60
70 mrad
10
12
14
16
p (GeV/c)

Figure 17

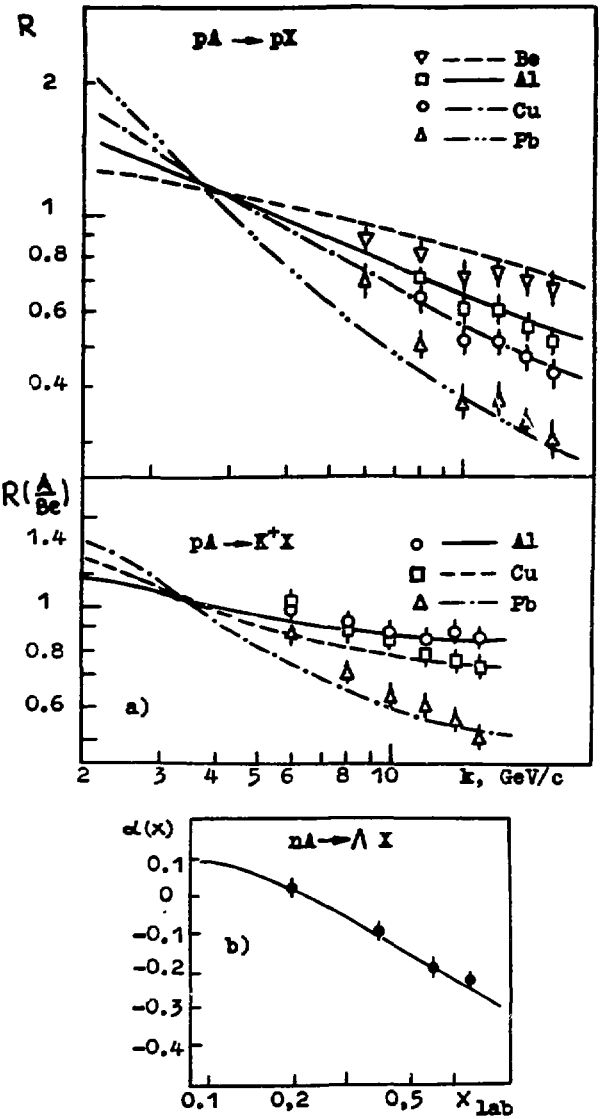
R
pA → pX
Be
Al
Cu
Pb
2
1
0.8
0.6
0.4
R(A/Be)
pA → K⁺X
Al
Cu
Pb
1.4
1
0.8
0.6
a)
2
3
4
5
6
8
10
k, GeV/c
α(x)
nA → Λ X
0.1
0
-0.1
-0.2
-0.3
-0.4
b)
0.1
0,2
0,5
X lab

Figure 18

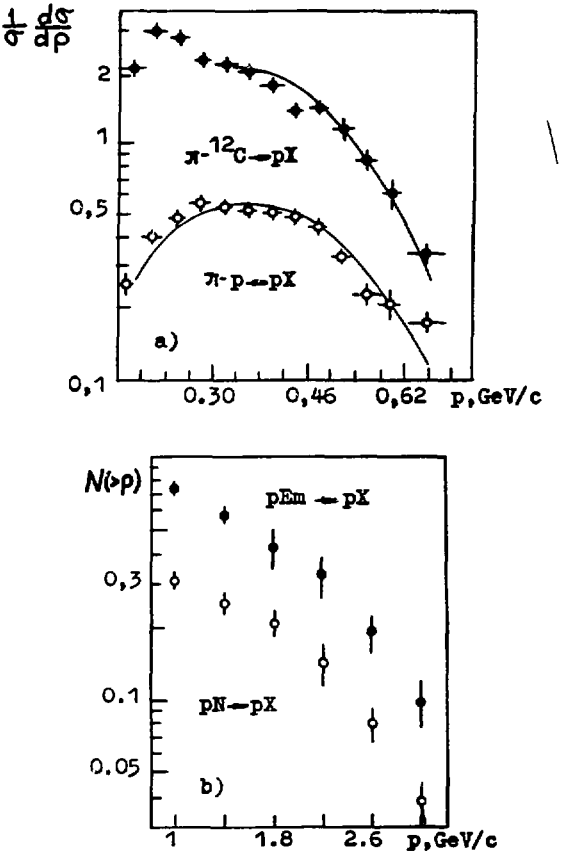
$\frac{1}{\sigma}\frac{d\sigma}{dp}$
2
1
0,5
0,1
$\pi^-{}^{12}C \to pX$
$\pi^- p \to pX$
a)
0.30
0,46
0,62
p,GeV/c
N(>p)
pEm → pX
0,3
0.1
pN → pX
0.05
b)
1
1.8
2.6
p,GeV/c

Figure 19

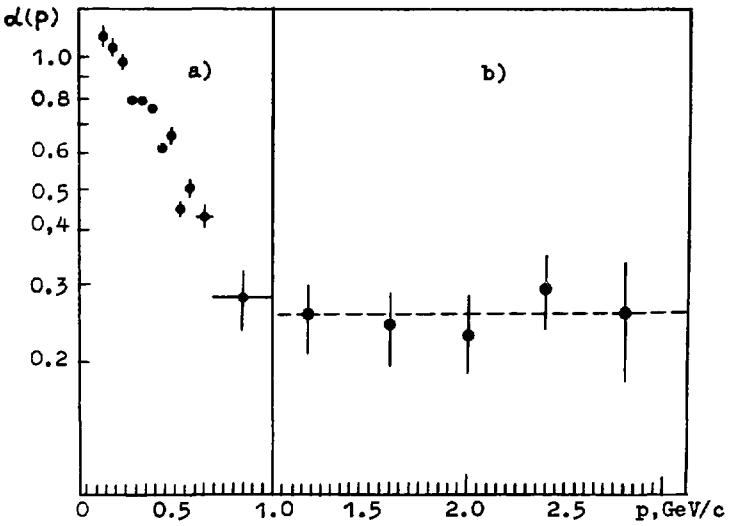

Figure 20

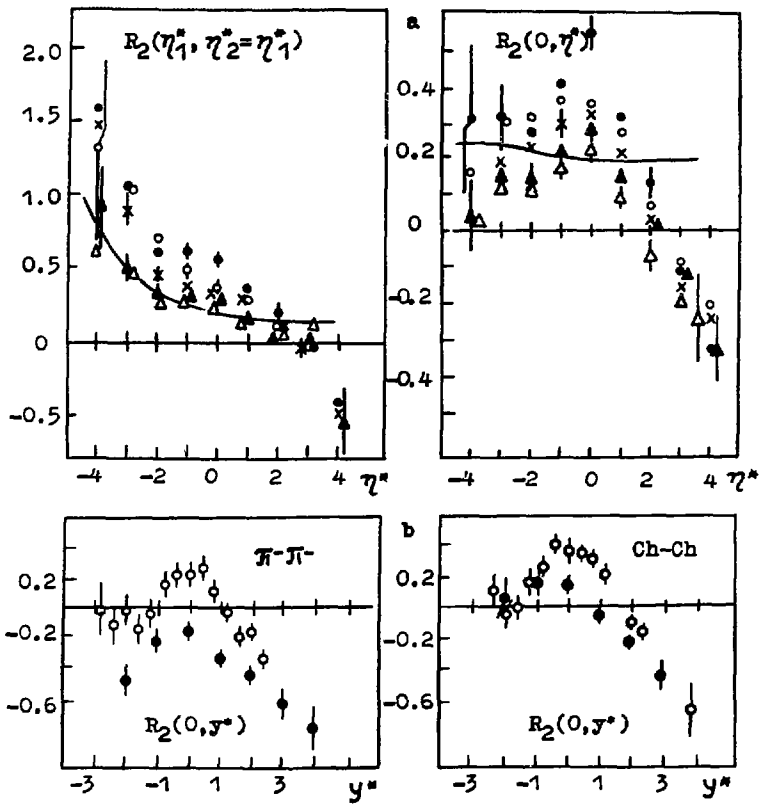

Figure 21

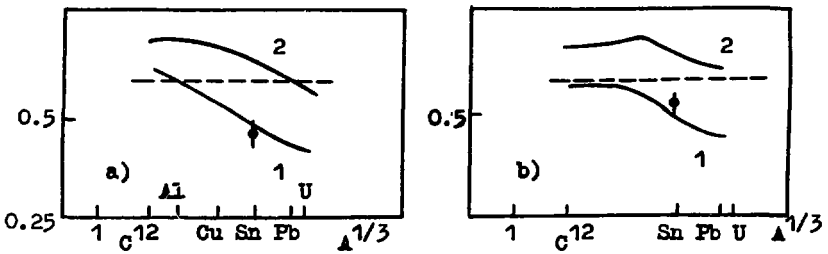

Figure 22

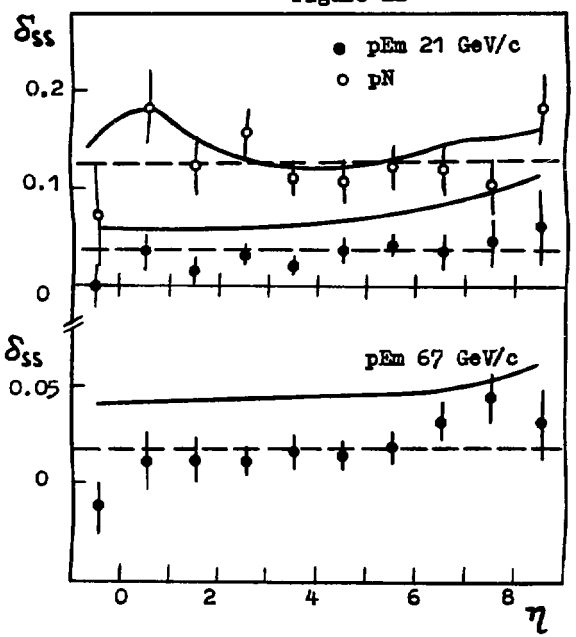

Figure 23

GPO 694-244/101